Reactivity at the membrane interface

HANNAH MARY BRITT

Reactivity at the membrane interface

Hannah Mary Britt

A thesis presented for the degree of
Doctor of Philosophy
April 2018

Supervised by:
Dr. Jackie Mosely & Dr. John Sanderson
Supported by: EPSRC

Chemistry Department
Durham University
United Kingdom

Declaration

The work presented in this thesis is based upon research carried out in the Mosely and Sanderson groups at the Chemistry Department of Durham University between October 2014 and January 2018. All of the work is attributed to the author unless referenced to the contrary in the text. No part of this thesis has been submitted elsewhere for any other degree or qualification at this or any other university.

Abstract

Modulation of internal environment and maintenance of cellular structure and stability are basic requirements to ensure cell survival. These cellular functions are provided by the cell outer membrane, a phospholipid bilayer characterised by the fluid mosaic model. Chemical reactivity at the membrane interface has previously been identified between phospholipids and membrane binding species. Observed reactivity, termed intrinsic lipidation, involves non-enzymatic acyl transfer from phospholipids to a nucleophilic membrane bound molecule. Reactivity has been characterised for membrane active peptides and proteins, and been found influential to the structure and function of both the newly modified species, and the bulk membrane. Research presented within this thesis probes fundamental features of observed intrinsic lipidation reactivity at the membrane interface.

This work has expanded upon previous intrinsic lipidation research, facilitated by the development of informative and robust analytical techniques for the study of reactivity. Optimised TLC has allowed improved routine high throughput reactivity screening, compared to alternative fluorescence and solution state NMR techniques. Informative analysis and mechanistic understanding of intrinsic lipidation has been achieved through LCMS and solid state NMR analysis. Synthetic protocols for preparation of isotopically labelled ^{15}N small molecules, and ^{13}C phospholipids, has facilitated solid state NMR in particular. Biological relevance of peptide intrinsic lipidation has also been probed to determine the role of reactivity in natural function, and disease induction. Biophysical techniques such as CD and tryptophan fluorescence revealed that solution phase intrinsically lipidated melittin adopts an α-helical structure with central proline kink, in contrast to the random coil of unmodified melittin. Furthermore, at µM concentrations, palmitoylated species were shown to undergo spontaneous micelle formation. Disease related behaviour linked to peptide intrinsic lipidation includes moderate antimicrobial activity, and possible induction of amyloid nucleation.

Additionally, this study has identified novel intrinsic lipidation of small molecules *in vitro* utilising chromatographic and ionisation conditions optimised with synthetically prepared standards. Observed for multiple cationic amphiphilic small molecules, intrinsic lipidation was promoted by primary amines in a hydrophilic environment, due to increased proximity between reactive moieties. Small molecule intrinsic lipidation products were shown to exhibit biological relevance, including spontaneous micelle formation, membrane disruption, and phospholipidosis induction. Pharmaceutical propranolol displayed notable intrinsic lipidation *in vitro*, and in Hep G2 cell culture. Initial transesterification from membrane phospholipids produced *O*-acylated propranolol, followed by secondary *N*-acylated propranolol formation by intramolecular *O* to *N* migration. Study of propranolol reactivity has revealed preferential eukaryotic transfer from the *sn*-1 phospholipid backbone position, and reaction kinetics influenced by temperature, pH, and membrane composition.

Acknowledgements

I would like to extend my sincere appreciation to several people, without whom this research would not have been possible. Firstly, thanks to my supervisors Dr. Jackie Mosely and Dr. John Sanderson for the opportunity to undertake this project, and for your guidance and support throughout. Thanks also to past and present members of the Sanderson and Mosely Research groups, particularly Jon, Andy, Vian, Lottie and Chris. Your advice, expertise, and friendship over the last few years have been invaluable. I am also grateful to the Whiting Research group and all those in lab CG 216, for making my time in Durham so enjoyable.

Thanks to Durham University and the Engineering and Physical Sciences Research Council (EPSRC) for providing PhD funding. To Pete Stokes and Dave Parker within the mass spectrometry service, and to the elemental analysis, solution state NMR, and solid state NMR services at at Durham University, for providing sample analysis. Thanks to Gary Sharples and Paul Denny in the Chemistry Department at Durham University, for instructing me in the growth of bacterial and mammalian cell cultures respectively. I am also grateful to Helen Grindley in the Department of Biosciences at Durham University for assistance with electron microscopy, and to Liz Grayson for her fountain of organic chemistry knowledge.

A very special thanks to my parents, I owe everything I have achieved to their unwavering support and encouragement. Finally, to David, for being by my side throughout this amazing journey, and for fuelling it with a constant supply of tea and biscuits.

Contents

Abbreviations

General

AC	Alternating Current
AcOH	Acetic Acid
amu	Atomic Mass Units
ANTS	8-Anilino-1-Naphthalenesulfonic Acid
API	Atmospheric Pressure Ionisation
aq	Aqueous
BEH	Ethylene Bridged Hybrid
Boc	*tert*-Butyloxycarbonyl
Boc_2O	Di-*tert*-Butyl Dicarbonate
CAD	Collisionally Activated Dissociation
CCS	Collision Cross Section
CD	Circular Dichroism
CEM	Chain Ejection Model
CHCA	α-Cyano-4-Hydroxycinnamic Acid
CI	Chemical Ionisation
CID	Collision Induced Dissociation
CL	Cardiolipin
CMC	Critical Micelle Concentration
CRM	Charge Residue Model
CSH	Charged Surface Hybrid

d	Doublet
DBU	1,8-Diazabicyclo(5.4.0)undec-7-ene
DC	Direct Current
DCM	Dichloromethane
DIC	*N*, *N'*-Diisopropylcarbodiimide
DMAP	4-Dimethylaminopyridine
DMF	Dimethylformamide
DPX	*p*-Xylene-Bis-Pyridinium Bromide
DTIMS	Drift Tube Ion Mobility Spectrometry
DTT	Dithiothreitol
EC_{50}	Half Maximal Effective Concentration
ECD	Electron Capture Dissociation
EDG	Electron Donating Group
EI	Electron Ionisation
EIC	Extracted Ion Chromatogram
EID	Electron Induced Dissociation
EM	Electron Microscopy
eq	Equivalents
ESI	Electrospray Ionisation
ESR	Electron Spin Resonance
ETD	Electron Transfer Dissociation
Et	Ethyl
EtOAc	Ethyl Acetate
EtOH	Ethanol
EWG	Electron Withdrawing Group
FA	Formic Acid
FDA	Food and Drug Administration
Fmoc	Fluorenylmethyloxycarbonyl
FRET	Fluorescence Resonance Energy Transfer

FT-ICR	Fourier Transform Ion Cyclotron Resonance
FT-IR	Fourier Transform Infrared Spectroscopy
FWHM	Full Width at Half Maximum
GC	Gas Chromatography
GPC	Glycerophosphocholine
GPI	Glycosyl Phosphatidylinositol
HFIP	Hexafluoro-2-Propanol
HPLC	High Performance Liquid Chromatography
IAA	2-Iodoacetamide
IEM	Ion Evaporation Model
IMS	Ion Mobility Spectrometry
IMMS	Ion Mobility Mass Spectrometry
IPA	Isopropanol
*i*Pr	*iso*-Propyl
IR	Infrared Spectroscopy
J	NMR Coupling Constant
LC	Liquid Chromatography
LD	Linear Dichroism
LDI	Laser Desorption/Ionisation
LCMS	Liquid Chromatography Mass Spectrometry
LUV	Large Unilamellar Vesicle
m	*Meta*
m	Multiplet
MALDI	Matrix-Assisted Laser Desorption/Ionisation
MDS	Molecular Dynamics Simulations
Me	Methyl
MeCN	Acetonitrile
MeOH	Methanol
MIC	Minimum Inhibitory Concentration

MS	Mass Spectrometry
MSMS/MS^n	Tandem Mass Spectrometry
MTBE	Methyl *tert*-Butyl Ether
m/z	Mass to Charge Ratio
NHS	*N*-Hydroxysuccinimide
NMR	Nuclear Magnetic Resonance
NP	Normal Phase
o	*Ortho*
Oleo	Oleoyl (18:1) Moiety
p	*Para*
Palm	Palmitoyl (16:0) Moiety
PBS	Phosphate Buffered Saline
PDA	Photodiode Array Detector
PMA	Phosphomolybdic Acid
ppm	Parts-Per-Million
PTM	Post-Translational Modification
q	Quartet
Q	Quadrupole
QET	Quasi-Equilibrium Theory
QToF	Quadrupole Time-of-Flight
RDB	Ring Plus Double Bonds
RF	Radio Frequency
RP	Reversed Phase
rpm	Revolutions Per Minute
R_s	Resolution
r.t.	Retention Time
s	Singlet
SEC	Size Exclusion Chromatography
SDS	Sodium Dodecyl Sulphate

SM	Sphingomyelin
ssNMR	Solid State Nuclear Magnetic Resonance
SUV	Small Unilamellar Vesicle
t	Triplet
*t*Bu	*tert*-Butyl
t-BuOH	*tert*-Butanol
TEM	Transmission Electron Microscopy
TFA	Trifluoroacetic Acid
THF	Tetrahydrofuran
TIC	Total Ion Chromatogram
TLC	Thin Layer Chromatography
T_m	Transition Temperature
ToF	Time-of-Flight
TWIMS	Travelling Wave Ion Mobility Spectrometry
UPLC	Ultra Performance Liquid Chromatography
UV	Ultraviolet
Vis	Visible
v/v	Volume to Volume Ratio
w_{av}	Average Peak Width
w/v	Weight to Volume Ratio
w/w	Weight to Weight Ratio

Phospholipids

DMPG	1,2-Dimyristoyl-*sn*-glycero-3-phosphoglycerol
DOPC	1,2-Dioleoyl-*sn*-glycero-3-phosphocholine
DOPE	1,2-Dioleoyl-*sn*-glycero-3-phosphoethanolamine
DOPG	1,2-Dioleoyl-*sn*-glycero-3-phosphoglycerol
DOPS	1,2-Dioleoyl-*sn*-glycero-3-phosphoserine
DPPC	1,2-Dipalmitoyl-*sn*-glycero-3-phosphocholine
DPPS	1,2-Dipalmitoyl-*sn*-glycero-3-phosphoserine
OPC	1-Oleoyl-2-hydroxy-*sn*-glycero-3-phosphocholine
OPE	1-Oleoyl-2-hydroxy-*sn*-glycero-3-phosphoethanolamine
OPG	1-Oleoyl-2-hydroxy-*sn*-glycero-3-phosphoglycerol
OPS	1-Oleoyl-2-hydroxy-*sn*-glycero-3-phosphoserine
OPPC	1-Oleoyl-2-palmitoyl-*sn*-glycero-3-phosphocholine
PC	Phosphatidylcholine
PE	Phophatidylethanolamine
PG	Phosphatidylglycerol
PI	Phosphatidylinositol
POPC	1-Palmitoyl-2-oleoyl-*sn*-glycero-3-phosphocholine
POPS	1-Palmitoyl-2-oleoyl-*sn*-glycero-3-phosphoserine
PPC	1-Palmitoyl-2-hydroxy-*sn*-glycero-3-phosphocholine
PS	Phosphatidylserine
SLPE	1-Stearoyl-2-linoleoyl-*sn*-glycero-3-phosphoethanolamine
SLPG	1-Stearoyl-2-linoleoyl-*sn*-glycero-3-phosphoglycerol
SLPS	1-Stearoyl-2-linoleoyl-*sn*-glycero-3-phosphoserine

Amino Acids

Name	3 Letter	1 Letter
Alanine	Ala	A
Arginine	Arg	R
Asparagine	Asn	N
Aspartic Acid	Asp	D
Cysteine	Cys	C
Glutamic Acid	Glu	E
Glutamine	Gln	Q
Glycine	Gly	G
Histidine	His	H
Isoleucine	Ile	I
Leucine	Leu	L
Lysine	Lys	K
Methionine	Met	M
Phenylalanine	Phe	F
Proline	Pro	P
Serine	Ser	S
Threonine	Thr	T
Tryptophan	Trp	W
Tyrosine	Tyr	Y
Valine	Val	V

1 | Literature Review

1.1 Introduction

Cells are the building blocks of life, forming the basis of virtually all living things. Vital to their survival are the many diverse roles carried out by the cell outer membrane. As a protective outer layer, the membrane maintains cell structural integrity and stability, ensuring robustness towards environmental stress. As a physical barrier, the membrane is able to control the entry and exit of substances to the cell. By preventing access of toxic substances, and promoting the uptake of necessary cellular components, the outer membrane ensures that cells thrive. Furthermore, specialised domains within the membrane have unique composition dependent cellular roles. Examples of these roles include control of enzyme activation and membrane transport channels, ultimately regulating cellular pathways. [1,2]

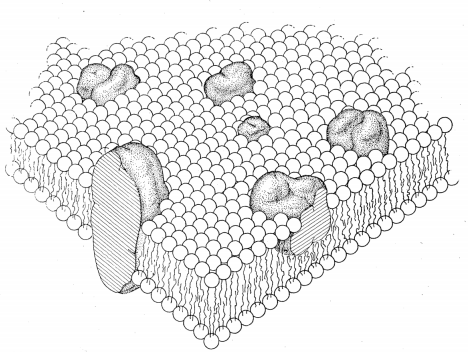

Figure 1.1 The fluid mosaic model of a biological membrane, showing the phospholipid bilayer and globular membrane active peptides/proteins. [3]

In 1972 Singer and Nicolson analysed the available physical and thermodynamic data to characterise cell membrane structure. [3] The resulting fluid mosaic model, Fig. 1.1, describes the membrane as a single-phase dynamic fluid system able to adapt to environmental stresses. The major component of this fluid system is a phospholipid bilayer, spontaneously formed due to innate phospholipid properties. Three regions are present within phospholipids: (i)

phosphate head group; (ii) glycerol backbone; (iii) two fatty acid tails. These regions, Fig. 1.2, give rise to naming nomenclature, exemplified by 1,2-dioleoyl-*sn*-glycero-3-phosphocholine (DOPC). Dioleoyl corresponds to the two oleoyl (18:1) fatty acid chains (green), glycero to the glycerol backbone (red), and phosphocholine to the phosphate head group (blue). A high proportion of electronegative elements combined with its ionic nature makes the phosphate head group hydrophilic in nature. Variation in R_3 modifies head group size and charge, instilling an intrinsic phospholipid positional preference within the membrane. In contrast, fatty acid tails ester linked to the phosphate via a glycerol backbone, are composed of hydrophobic carbon chains. Table 1.1 summarises common fatty acid chain lengths and levels of unsaturation. Acyl chain variation within individual phospholipids, and within the bulk membrane modifies phospholipid bilayer packing and domain formation, impacting physical membrane properties.[4] Within aqueous environments, the balance of phospholipid hydrophobicity and hydrophilicity results in spontaneous formation of multi-phospholipid structures which maximise favourable interactions. Aggregate structures include micelles and vesicles, however curvature and internal cell composition promotes bilayer formation for the cell membrane.[3]

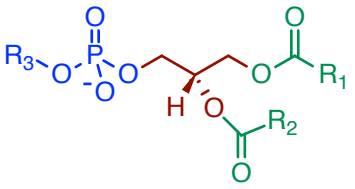

Figure 1.2 Structure of a generic phospholipid: green indicates fatty acid chains where R_1 = acyl chain at *sn*-1 position, and R_2 = acyl chain at *sn*-2 position; red indicates glycerol backbone; blue indicates phosphate head group with variable R_3.

Fatty Acid	Number of Carbons	Number of Double Bonds
Myristoyl	14	0
Palmitoyl	16	0
Stearoyl	18	0
Oleoyl	18	1
Linoleoyl	18	2

Table 1.1 Common fatty acid chain types found as components of phospholipids.

Globular membrane active peptides and proteins are the second cell membrane component presented in the 1972 fluid mosaic model.[3] Despite variation in length and amino acid composition, membrane active peptides are linked by their amphiphilicity, including both a hydrophobic, non-polar region containing alanine-like residues, and a hydrophilic region containing lysine or arginine amino acids. Amphiphilicity allows spontaneous association of membrane active

peptides with a phospholipid bilayer via α-helix formation. Association increases thermodynamic stability by shielding hydrophobic residues from the aqueous environment, whilst simultaneously promoting ionic/polar interactions between water and hydrophilic residues. Whilst some membrane active peptides are unmodified, many undergo post-translational modification to aid in regulation of peptide activity, interactions and localisation.[5] Common modifications include: (i) acylation, i.e. fatty acid substitution on to a nucleophilic amino acid residue; (ii) phosphorylation, i.e. substitution of a phosphate onto serine, threonine or tyrosine; (iii) glycosylation, i.e. substitution of a sugar moiety; (iv) alkylation, i.e. methylation of an oxygen or nitrogen within an amino acid residue side chain.[6] Whilst the key constituents and characteristics remain unchanged, identification of additional cell membrane components has occurred since 1972. Notable examples of this include the presence of cholesterol and glycolipids.[1,7] Furthermore, several other cellular components and external substances such as pharmaceuticals have been observed to undergo transient interactions with the cell membrane.[8,9]

Given the diverse composition and functionality of the cell membrane, it seems unlikely to be a chemically inert structure. Predicted reactivity could result in unidirectional bond formation between membrane components, even with molecules that only transiently interact with the membrane. Any observed reactivity would be expected to greatly influence the structure and properties of molecules involved, and change fundamental understanding of biological pathways. Extrapolating from well characterised solution phase organic chemistry, two such reactions have been identified *in vitro*. The first, intrinsic lipidation of peptides, involves non-enzymatic acyl transfer from phospholipids to membrane-active peptides.[10,11] The second, lipid hydrolysis, produces a lysolipid product via non-enzymatic phospholipid hydrolysis.[12]

Whilst the identification of two novel membrane reactions is important, their power can only be understood and harnessed through further research. Practical challenges and sensitivity limitations have thus far presented barriers to identifying suitable techniques for the study of reactions at the membrane interface, and as such research remains in its infancy. Through developing analytical methods for the study of cell membrane reactivity, it is hoped that further information can be gleaned regarding the biological influence of reactivity at the membrane interface. One focus is understanding reactivity origins and the influence of environmental factors such as membrane composition and physical parameters. Component modification has powerful potential to alter molecular structure, properties and membrane affinity, ultimately impacting upon cellular function. Furthermore, reactivity is predicted to influence bulk membrane properties such as fluidity and curvature, compromising membrane stability and

structural integrity. By studying both causes and consequences of membrane reactivity, the door is opened to both a developed understanding of biological systems, and a means to manipulate them.

1.2 Lysolipid Formation

Lysolipids, Fig. 1.3, are biomolecules similar in structure to phospholipids but with one acyl chain replaced by a hydroxyl group.[13] The remaining acyl chain can be attached to the lysolipid backbone at either the *sn*-1 or *sn*-2 position. Chain migration between the two positions occurs readily, and thus lysolipids exist predominately with the acyl chain in the more stable *sn*-1 position. Biologically, lysolipids adopt a variety of important roles within the cell membrane, including influencing phosphate signalling and regulation of vascular cell function.[14,15] Furthermore, lysolipids have a therapeutic role within drug delivery vehicles, and as detergents for the formulation of numerous commercial products.[16,17]

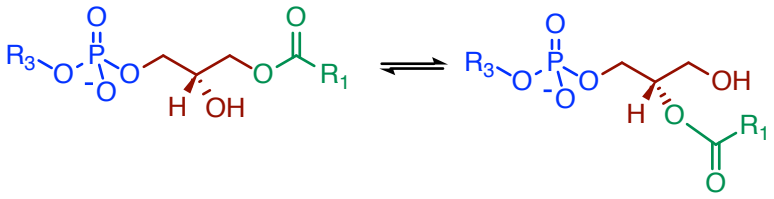

Figure 1.3 Structure of a generic lysolipid: green indicates fatty acid chain in either *sn*-1 or *sn*-2 position; red indicates glycerol backbone; blue indicates phosphate head group with variable R_3.

Phospholipase enzymes are a diverse family of enzymes which produce lysolipids via an enzymatic mechanism of phospholipid hydrolysis.[18,19] Phospholipase-A1 and phospholipase-A2 enzymes cleave the *sn*-1 and *sn*-2 phospholipid acyl chains respectively. Within the cell, phospholipase enzymes are tightly controlled, in order to modulate their activity and subsequent levels of lysolipid production. Cellular lysolipid formation can also proceed through less tightly regulated non-enzymatic mechanisms. Production of lysolipids as a by-product of small molecule or peptide intrinsic lipidation is one example which will be revisited. The aqueous cellular environment provides a further mechanism for lysolipid formation, via solution phase phospholipid hydrolysis.[20] Proceeding as observed for classic organic synthetic hydrolysis, this solution phase mechanism is greatly influenced by local environment. Both acidic and basic pH are known to promote the extent of phospholipid hydrolysis, and to increase the rate of hydrolysis.[21–24] Temperature, membrane composition, and local hydration levels, are also observed to influence solution phase phospholipid hydrolysis.[25,26] Catalytic effects of

proximal biomolecules and membrane binding pharmaceuticals can also promote solution phase phospholipid hydrolysis. Cationic amphiphilic drugs such as raclopride and haloperidol are known to be particularly prolific in causing phospholipid hydrolysis, attributed to their structure and functionalities.[27–29]

Lysolipid formation *in vivo* is tightly controlled, since even low levels cause significant modification to bulk membrane properties and cellular activity.[30,31] Containing a hydrophilic phosphate head group and a single hydrophobic fatty acid chain, lysolipids aggregate in aqueous solution. Above a critical micelle concentration (CMC) in the range of 1 µM, these aggregates are characterised as micelles.[32,33] Micelle forming lysolipids act as detergents within the phospholipid bilayer, disrupting membrane fluidity and curvature.[34] Even minor fluctuations in these membrane properties result in problems for highly tuned membrane activities such as signalling and trafficking. At worst, increased lysolipid levels result in sufficient membrane perturbation such that structural integrity is lost. In this situation, leakage of vital cellular components combined with a diminished barrier to toxic substances ultimately results in cell death.[35]

1.3 Intrinsic Lipidation of Peptides

Post-translational peptide modification within the Golgi apparatus or endoplasmic reticulum is an important biological tool for tuning peptide properties to cellular requirements.[8] Modifications involve peptide folding, amino acid cleavage, or enzymatic covalent attachment of a chemical moiety. Example chemical functionalities include: (i) phosphorylation; (ii) alkylation; (iii) glycosylation; (iv) ubiquitination; (v) lipidation.[6]

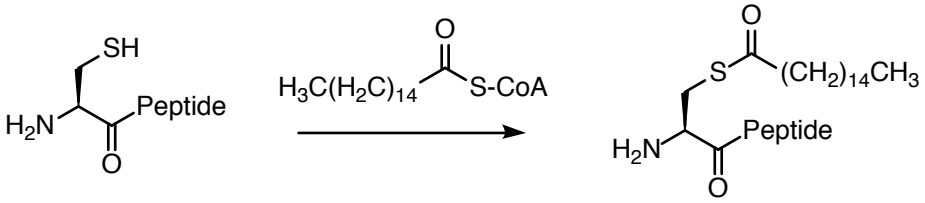

Figure 1.4 Example of post-translational modification of the cysteine residue of a peptide by enzymatic addition of a palmitoyl moeity *in vivo*.

Post-translational lipidation is the addition of one or more acyl chains on to a nucleophilic peptide residue. The process is enzyme mediated and may require a fatty acid analogue to aid transfer.[5] The *N*-terminus and thiolate of cysteine are common post-translational lipidation sites, along with some specific amino acid motifs. Types of post-translational

lipidation, Fig. 1.4, include myristoylation, addition of a saturated 14 carbon acyl chain, and palmitoylation, addition of a saturated 16 carbon chain.[6,36] Approximately 2 % of proteins and peptides synthesised in the human body undergo prenylation, a form of post translational lipidation in which an unsaturated, branched farnesyl (C_{15}) or geranylgeranyl (C_{20}) chain is added.[37] The final form of post-translational lipidation is the *C*-terminal phosphoethanolamine bridge linkage to a glycosyl phosphatidylinositol (GPI) anchor, composed of a glycan sugar group linked through inositol phosphodiester to a lipid moiety.[38]

Post-translational lipidation provides a powerful mechanism for tuning peptides by altering their properties and activity.[5,6] Acyl chain substitution dramatically increases peptide hydrophobicity and affinity for the relatively non-polar phospholipid bilyaer, compared to the aqueous cellular environment. The range of acyl chain modifications available ensures this membrane affinity is tunable and even reversible, such that peptides can undergo selective targetting and adapt to external stimuli. In this way, post-translational lipidation facilitates peptides in their roles of cell signalling and membrane trafficking. Examples of peptides which rely on lipidation mechanisms to facilitate function include membrane localisation of the Src-family of kinases, cellular attachment and protein-protein interaction modulation for the Ras superfamily, and lipid raft formation for signalling and targetting roles.[8,37,38]

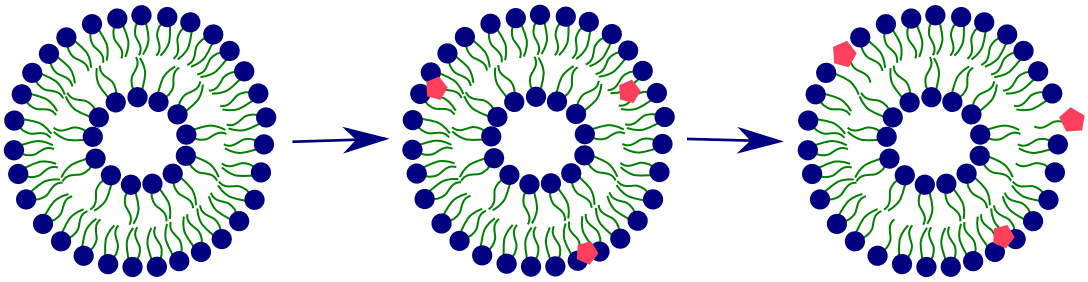

Figure 1.5 Schematic of non-enzymatic peptide intrinsic lipidation. Blue highlights phospholipid head groups; green indicates phospholipid acyl chains; red indicates a membrane active peptide which associates with the membrane and is acylated.[39]

An alternative mechanism for the important process of peptide lipidation is the innate membrane reactivity of intrinsic lipidation, Fig. 1.5. This non-enzymatic process, observed under physiological conditions *in vitro*, promotes lipidation of membrane bound peptides via acyl transfer from membrane phospholipids.[11] Mechanistically, intrinsic lipidation proceeds via the characteristic solution phase pathway described in Scheme 1.1.[39] Initial nucleophilic attack is followed by a series of rearrangements of tetrahedral intermediates, ultimately resulting in lipidated product formation. Key to determining reaction rate is either formation and breakdown of the negatively charged tetrahedral intermediate, or breakdown of the neutral

tetrahedral intermediate. External conditions known to influence these steps are thus believed to be vital in controlling peptide intrinsic lipidation.

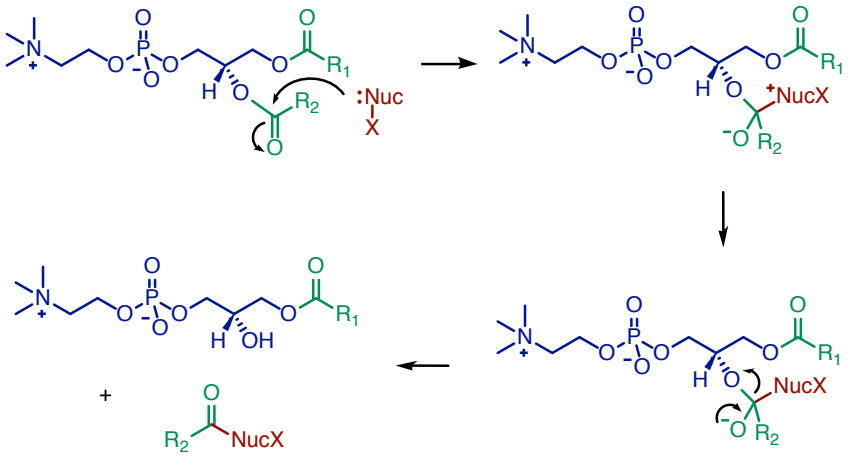

Scheme 1.1 Mechanism of non-enzymatic peptide intrinsic lipidation. Blue highlights phospholipid head group; green indicates phospholipid acyl chains; red indicates the reactive nucleophile of a membrane active peptide.

Mechanistically, intrinsic lipidation creates great complexity, given the numerous potential product combinations. Multi product formation is exemplified even in a simple system, intrinsic lipidation of peptide melittin within a membrane mimic containing only the lipid 1-palmitoyl-2-oleoyl-*sn*-glycero-3-phosphocholine (POPC). In this situation, the phospholipid bilayer contains both parent lipid POPC, and major intrinsic lipidation lysolipid by-products 1-palmitoyl-2-hydroxy-*sn*-glycero-3-phosphocholine (PPC), and 1-oleoyl-2-hydroxy-*sn*-glycero-3-phosphocholine (OPC). Low abundance forms of minor lysolipids, 1-hydroxy-2-palmitoyl-*sn*-glycero-3-phosphocholine, and 1-hydroxy-2-oleoyl-*sn*-glycero-3-phosphocholine, would also be expected. Furthermore, the presence of both unmodified peptide melittin, and multiple forms of modified peptide would be expected. Taking into account the potential for modification at numerous sites (at least 5 in melittin), variation in fatty acid chain types, and potential for up to two rounds of intrinsic lipidation, 50 modified forms of melittin exist.[10] Recent developments suggest the potential for triple lipidation, questioning the assumption that only two rounds of intrinsic lipidation occur, and further adding to product complexity.[40] The diverse range of modified peptide products means that each is observed in low abundance, such that high sensitivity instrumentation is required for visualisation. This sensitivity, along with reaction mixture complexity, creates challenges in the study of intrinsic lipidation, limiting current understanding.

1.3.1 Studying Intrinsic Lipidation of Peptides

Study of peptide intrinsic lipidation is noted to be challenging, however succesful analytical approaches have been developed. Preliminary *in vitro* studies of intrinsic lipidation utilised thin layer chromatography (TLC) to visualise lipid and lysolipid products within the reaction mixture, Fig. 1.6. By measuring spot intensity, TLC allows lipid and lysolipid quantification, facilitating determination of the extent of reactivity.[10] However, use of TLC to monitor peptide intrinsic lipidation requires an extra lyophilisation step, in order to have a sufficient concentration of the lipid and lysolipid for detection. Furthermore, TLC is impractical for identification and quantification of intrinsic lipidation *in vivo*, since lysolipids are found naturally in biological systems and their presence would not confirm reactivity. Study of intrinsic lipidation by TLC is further complicated by background hydrolysis and other means of lysolipid formation both *in vivo* and *in vitro*, which must therefore be considered to modify observed results.[41]

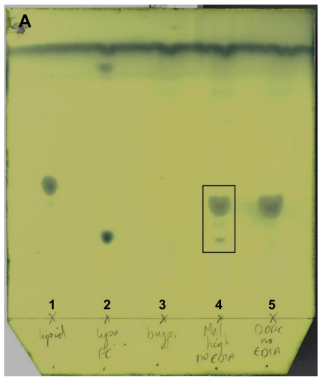

Figure 1.6 TLC analysis of melittin intrinsic lipidation using aluminium-backed silica gel plate, a mobile phase of $CHCl_3$:MeOH:H_2O (6:4:1), and staining with 10 % w/v solution of phosphomolybdic acid (PMA) in EtOH. Rows from left to right: (i) DOPC; (ii) OPC; (iii) Empty; (iv) reaction mixture of DOPC and melittin; (v) DOPC liposomes.[10]

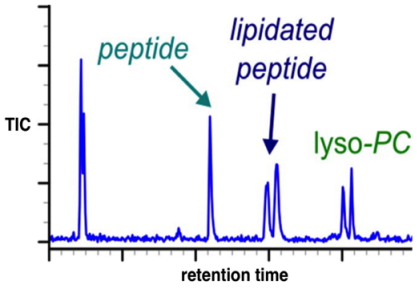

Figure 1.7 Typical chromatogram observed during LCMS analysis of an intrinsic lipidation reaction mixture.[39]

An improved method for the study of peptide intrinsic lipidation *in vitro* is use of LCMS, coupling reversed phase liquid chromatography to mass spectrometry. Optimised detection of peptides and lipid is achievable by electrospray ionisation (ESI) combined with the sensitivity of a high performance Fourier transform ion cyclotron resonance (FT-ICR) mass analyser.[10,11] Gradient optimisation allows predictable chromatograms, Fig. 1.7, with the lipid, parent peptide and modified peptide chromatographically separated. Benefits of this improved method include: (i) visualisation of acylated peptide, a product with no alternative formation pathways to intrinsic lipidation; (ii) mass resolution between transfer of different fatty acid chains; (iii) retention time variation between different acylation positions, with modified peptide residue assignable by tandem mass spectrometry (MSMS), facilitating study of preferential acylation.[39]

The extent of intrinsic lipidation can be quantified by % conversion, using peak modelling to calculate the ratio of modified to unmodified peptide in the LCMS chromatogram, and assuming the sum is a total of 100 % peptide content, Equation 1.1. Whilst easily calculated, this quantification method assumes equivalent ionisation of lipidated peptide and unmodified peptide, the validity of which is unknown without standards. Furthermore, accurate peak area modelling proves challenging for low abundance modified peptide peaks corresponding to multiple acylation steps, assuming peaks are visible at all. Equation 1.2, the Beer-Lambert Law, provides an alternative means of quantifying modified and unmodified peptide containing a tryptophan, tyrosine or phenylalanine residue. UV absorbance at the relevant wavelength is measured during LCMS analysis using a photodiode array (PDA) detector, and required extinction coefficient parameters are known for the relevant amino acids.[11] Unfortunately, accurate quantification by absorbance requires a minimum peptide concentration to reached, a value not fulfilled by acylated peptide under standard experimental conditions for intrinsic lipidation. Altering the peptide:lipid ratio or injection volume to meet this concentration requirement is impractical due to decreased resemblance to natural systems and poor chromatography. An improved method for peptide quantification involves the use of LCMS to generate a calibration curve using a synthetic standard, against which the concentration of the unknown can be determined.[42,43]

$$\%Conversion = \frac{Modified}{(Modified + Unmodified)} \times 100 \tag{1.1}$$

$$\log\left(\frac{I_0}{I}\right) = A = \epsilon c l \tag{1.2}$$

Where $I_0/I = A$ = absorbance; ϵ = molar absorptivity coefficient; c = concentration; l = path length.

Optimised LCMS combined with quantification facilitated further study of peptide intrinsic lipidation. Standard conditions for *in vitro* study of intrinsic lipidation, 37 °C and a 10 mM bicarbonate and 90 mM sodium chloride buffer at pH 7.4, closely mimic natural membrane conditions. Modification of these conditions revealed that high temperature, high salt content, and the presence of bicarbonate promote reactivity, increasing the rate of intrinsic lipidation two fold.[10] Furthermore, optimised LCMS conditions allowed Dods *et al.* to probe selectivity in acylation of peptides with multiple nucleophilic residues.[44] The preference of which nucleophile dominates acyl transfer is found to be peptide specific, with the driving force currently unknown. Potential driving forces include peptide binding orientation, membrane penetration depth, local nucleophile environment, and nucleophile type. Additional selectivity arises from mixed acyl lipids, with preference in the fatty acid chain transferred being down to positioning on the lipid (*sn*-1 vs. *sn*-2 position) or chemical composition. Dods *et al.* probed this selectivity by comparison of two chemically similar phospholipids, POPC and OPPC.[44] Analysis determined fatty acid positioning to be the dominant feature, with transfer from the *sn*-1 position observed to be slightly more prevalent.

1.3.2 Reactivity of Different Membrane Active Peptides

Successful development of TLC and LCMS for the study of peptide intrinsic lipidation *in vitro* allows for further investigation of membrane reactivity. By examining intrinsic lipidation in this way, pathways to understanding biological relevance and therapeutic potential are revealed. Parameters such as innate peptide properties, membrane composition, and environmental conditions are likely to play a role in controlling reactivity rate. As such, further investigation into the influence of these factors upon peptide intrinsic lipidation was carried out *in vitro* using model systems.

Melittin, Fig. 1.8, is a 26 residue membrane active peptide, used as a model for membrane study due to its amphiphilic nature and cationic *C*-terminus.[45] A lytic peptide extracted from honeybee venom, melittin is of particular interest due to its availability, well characterised

structure and properties, similarity to other membrane active peptides, spontaneous membrane association, and intrinsic fluorescence imparted by tryptophan at residue 19. Along with its robustness to physiological conditions, and nucleophilic amino acid residues, these properties made melittin a clear choice for initial study of peptide intrinsic lipidation.[46]

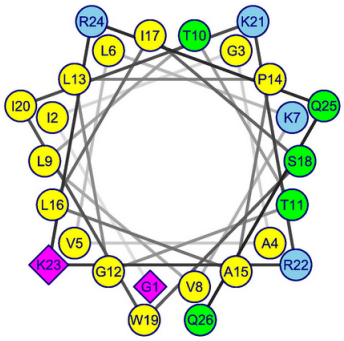

Figure 1.8 Membrane active peptide melittin in the helical wheel structure adopted upon membrane binding. Colours indicate: polar residues (green); basic residues (blue); non-polar residues (yellow); major acylation sites (magenta).

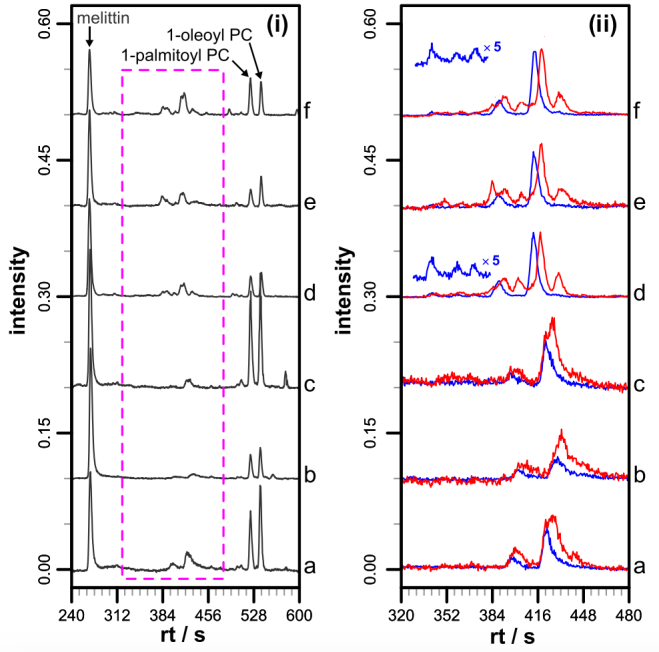

Figure 1.9 LCMS results for acylation of melittin in different conditions: (i) Total ion chromatogram (TIC); (ii) Extracted ion chromatogram (EIC) for palmitoyl melittin (blue) and stearoyl/oleoyl/linoleoyl melittin (red). Conditions shown are all 1:10 peptide:lipid molar ratio, and unless otherwise stated use 90 mM NaCl, 10 mM $NaHCO_3$, pH 7.4 and 37 °C. (a) POPC, no $NaHCO_3$, 72 h; (b) POPC, 20 °C, 150 mM NaCl, 72 h; (c) POPC, no $NaHCO_3$ or NaCl, 48 h; (d) POPC/SLPS (4:1), 72 h; (e) POPC/SLPG (4:1), 48 h; (f) POPC/SLPE (4:1), 72 h.[39]

Melittin undergoes intrinsic lipidation *in vitro* over a broad range of conditions, including physiological conditions, Fig. 1.9.[10] As predicted, the LCMS chromatogram produced a series

of characteristic peaks, the first of which corresponds to unmodified melittin with m/z 949 for triply charged and m/z 712 for a quadruply charged. Modified melittin peaks appear at a later retention time, with the high performance and resolving power of the FTICR mass analyser allowing distinction between transfer of different acyl chain types. Palmitoylated melittin lies at m/z 618, 772, and 1029 for the $[M+5H]^{5+}$, $[M+4H]^{4+}$ and $[M+3H]^{3+}$ respectively, whereas these peaks for myristoylated melittin appear at m/z 612, 765, and 1019. These can be further distinguished from oleoyl, linoleoyl and steareoyl modifications, which due to small mass differences all show peaks at approximate m/z of 623, 778 and 1037.

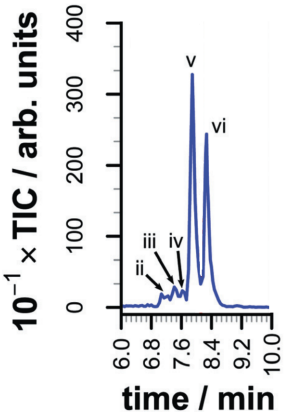

Figure 1.10 Palmitoylated melittin EIC corresponding to modification at: (ii) S18; (iii) K21; (iv) K7; (v) K23; (vi) *N*-terminal.[39]

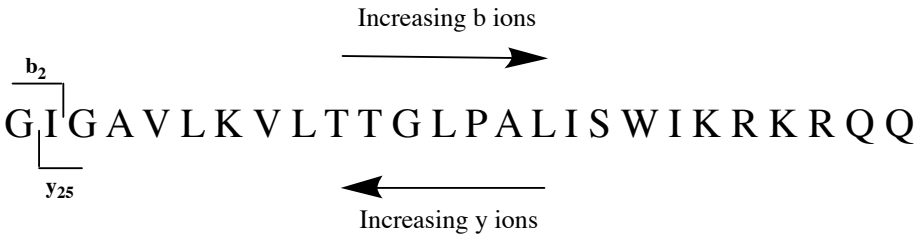

Figure 1.11 Characteristic ions formed by CID MSMS fragmentation of melittin.[47–49]

Optimised chromatographic conditions result in different retention times for acylated melittin modified at different nucleophilic residues. Melittin, Fig. 1.8, has three nucleophilic sites of acylation: (i) ϵ-amino groups of lysine (K) residues at positions 7, 21 and 23; (ii) serine (S) at position 18; (iii) *N*-terminus. Each peak in the group of modified melittin peaks, Fig. 1.10, can be assigned to one of these nucleophiles, with increasing retention time these are: S18, K21, K7, K23 and the *N*-terminus, the final of which has been identified as the most favourable site of acylation. Identification of the modified melittin nucleophiles is possible using tandem mass spectrometry (MSMS). MSMS breaks the peptide apart at the backbone bonds linking amino acids, in order to give a ladder of amino acids from each terminus, Fig. 1.11, one of which will include the mass of amino acid plus the relevant acyl chain. Instability of the $\mathbf{b_1}$

ion, breakage at the first peptide bond from the *N*-terminus, results in observation of this ion being rare, thus the assignment of *N*-terminal acylation is driven by chemical intuition considering the limited nucleophilicity of residue 2, isoleucine.[10]

Validation of intrinsic lipidation as a feasible lipidation alternative to post-translational lipidation requires the process to be general to membrane active peptides rather than melittin specific. Magainin II, Fig. 1.12, is a second well characterised membrane active peptide, extracted from the skin of *Xenopus laevis*, suitable for study of intrinsic lipidation.[50,51] Amphiphilicity aids magainin II in spontaneous helix formation and membrane association from its random coil solution state structure, facilitating the peptide's role in cation channel formation, and antimicrobial activity in concentrations above 2 µM.[52]

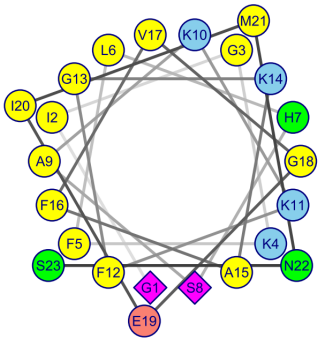

Figure 1.12 Membrane active peptide magainin II in the helical wheel structure adopted upon membrane binding. Colours indicate: polar residues (green); basic residues (blue); acidic residues (red); non-polar residues (yellow); major acylation sites (magenta).

Confirming intrinsic lipidation as a generic process, magainin II is observed to undergo non-enzymatic acylation over a wide range of conditions including physiological conditions, Fig. 1.13.[39] *N*-terminal lipidation is favoured, with secondary acylation sites including: (i) serine residue 8; (ii) lysine residue 4; (iii) histidine residue 7. Variation in relative acylation of serine and lysine between melittin and magainin II provides preliminary indications relating nucleophile reactivity to position and local environment, rather than to chemical type. Additionally, serine 8 resides adjacent to a histidine residue, indicating a potential catalytic effect given speculative observations of histidine acylation and subsequent transfer observed during peptide synthesis.[53]

Further confirmation of intrinsic lipidation as a generic process arises from study of other membrane active peptides *in vitro*. PGLa, Fig. 1.14, is a 21 residue membrane active peptide similar in nature to magainin II, and observed to undergo acylation at the *N*-terminus and at a second position, thought to be serine 4 or lysine 5.[39,54] Helical, with a conformationally

free *N*-terminus confirmed by NMR, membrane bound PGLa is active towards acylation in a more limited range of conditions than melittin or magainin II. Amphiphilic peptides LAK1, LAK3 and penetratin, Table 1.2, require specific conditions for intrinsic lipidation: (i) LAK1 requires POPC:SLPS at a high salt concentration; (ii) LAK3 requires POPC:SLPS (1:1); (iii) penetratin requires POPC at a high salt concentration. Each peptide is observed to have multiple acylation sites, however low abundance of modified peptide prevents information regarding nucleophile preferences from being obtained.[39]

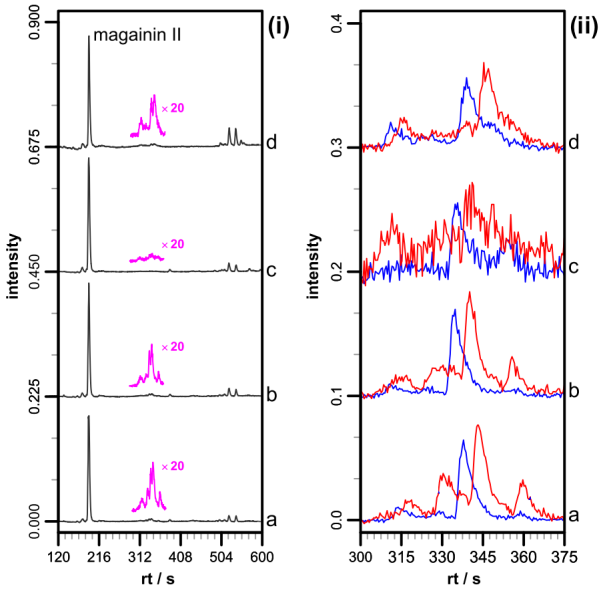

Figure 1.13 LCMS results for acylation of magainin II under different experimental conditions: (i) TIC; (ii) EIC for palmitoyl magainin II (blue) and oleoyl/linoleoyl/stearoyl magainin II (red). Conditions shown are all 1:10 peptide:lipid molar ratio, and unless otherwise stated use 90 mM NaCl, 10 mM $NaHCO_3$, pH 7.4 and 37 °C. (a) POPC/SLPS (1:4), 72 h; (b) POPC/SLPG (1:4), 72 h; (c) POPC/SLPE(1:4), 72 h; (d) 150 mM NaCl, 144 h.[39]

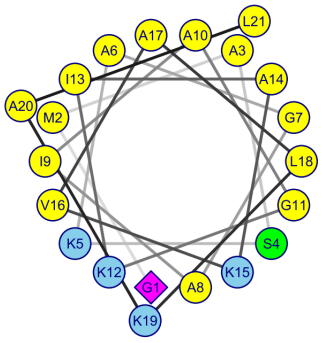

Figure 1.14 Membrane active peptide PGLa in the helical wheel structure adopted upon membrane binding. Colours inducate: polar residues (green); basic residues (blue); non-polar residues (yellow); major acylation sites (magenta).

Upon incubation of six membrane active peptides with biological membrane mimics under physiological conditions, all undergo reactivity with membrane phospholipids *in vitro*. This

intrinsic lipidation reactivity occurs upon a biological timescale, and is therefore relevant to both natural processes and laboratory studies. Novel modified peptides form as a result of reactivity, predicted to have distinct properties and functionalities compared to the unmodified peptides. Preliminary studies indicate preferential nucleophile reactivity, however further work is required in order to confirm the relationship between intrinsic lipidation and nucleophile type, nucleophile environment, neighbouring group effects and pK_a.

Peptide	Amino Acid Sequence
LAK1	KKLALALALALKALALALALKKA
LAK3	KKLALALAKALAKALKLALALAKK
Penetratin	RQIKIWFQNRRMKWKK

Table 1.2 Amino acid sequences of LAK1, LAK3 and penetratin.

1.3.3 Reactivity of Different Membrane Types

Further investigation into the mechanism and reactivity of intrinsic lipidation with respect to its second key component, the phospholipid bilayer, confirms its status as a generic intramembrane reaction *in vitro*.[44] Natural phospholipid bilayers display tremendous complexity, incorporating fatty acid chain types of differing length and saturation, and both zwitterionic and negatively charged phosphate head groups, the structure and size of which instil a positional leaflet preference upon the lipid. The intrinsic complexity of the natural bilayer, combined with the variety of products formed by intrinsic lipidation, results in the requirement of simplified models in order to ensure initial studies probing lipid influence on intrinsic lipidation are beneficial. DPPC membranes provide the simplicity of a single acyl chain type combined with the eukaryotic phosphatidylcholine (PC) head group, however intrinsic lipidation of melittin is not observed in this membrane type. By contrast DOPC, also containing a single type of acyl chain and PC head group, facilitates intrinsic lipidation to a variety of peptides within 24 hours in physiological conditions.[11] Predicted driving forces behind this difference include transition temperature, peptide binding strength and orientation, and curvature, however comparison of these two membrane types only cannot reveal further information.

Dods *et al.* working with melittin utilised a POPC model membrane, incorporating a PC head group characteristic to eukaryotic membranes and two different fatty acid chains for probing positional preferences.[10,39] Further mimicry of the more complex membranes of eukaryotic cells is possible through the inclusion of additional phosphate head group types, with varied fatty acid chains allowing precise tracking of acyl transfer. Phosphatidylserine

(PS), is a small negatively charged phospholipid head group common to the inner leaflet of eukaryotic membranes.[55,56] Cationic membrane active peptide melittin shows increase membrane affinity for PS containing membranes, driven by increased ionic interactions and the decreased conformational freedom they trigger upon binding. Increased peptide binding in this case appears to correlate with increased intrinsic lipidation rate, given that 50 % conversion from melittin to acylated melittin requires 16 days in a POPC membrane, compared to 24 hours for PS containing membranes DOPC:DPPS (4:1) and POPC:SLPS (4:1).[10,44] Of further interest are the acyl transfer characteristics of the DOPC:DPPS membrane, which indicates no palmitoyl transfer from the PS membrane component, whereas for the POPC:SLPS membrane acyl transfer from both components is observable, Fig. 1.15(a). Membrane demixing into a melittin-bound PC membrane and a separate PS phase, observed by deuterium NMR where melittin is bound to a PC:PS membrane in a ratio above 5:1, is one explanation for this characteristic transfer.[46]

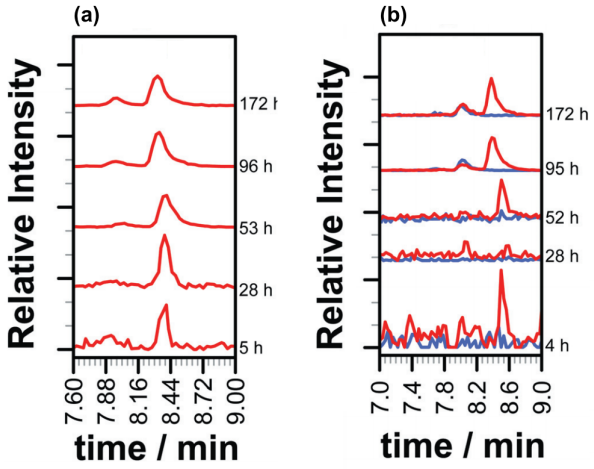

Figure 1.15 EIC showing myristoyl melittin (blue) and oleoyl melittin (red) within (a) DOPC:DPPS (4:1); (b) DOPC:DMPG (4:1); membranes under physiological conditions (1:10 peptide:lipid molar ratio, 90 mM NaCl, 10 mM $NaHCO_3$, pH 7.4 and 37 °C) for 72 hours.[44]

Phosphatidylglycerol (PG), is also a negatively charged phospholipid found in eukaryotic membranes and observed by NMR to undergo demixing with a PC phase in the presence of melittin.[57] Despite reported demixing, both DOPC:DMPG (4:1) and POPC:SLPG (4:1) membranes undergo intrinsic lipidation, Fig. 1.15(b). Acyl transfer is observed from both PC and PG components, indicative of either a mixed membrane or melittin bound to each of the two demixed phases. Further support for the mixed membrane hypothesis arises from the decreased rate of intrinsic lipidation in a PC:PG membrane compared to PC:PS, given that peptides in mixed membranes exhibit decreased conformational freedom and phospholipid

contact. Despite this, correlation of negative charge and intrinsic lipidation rate is again displayed, with DOPC:DMPG (4:1) forming oleoyl melittin in 28 hours and myristoyl in 95 hours, faster than a PC only membrane, Fig. 1.16.[11]

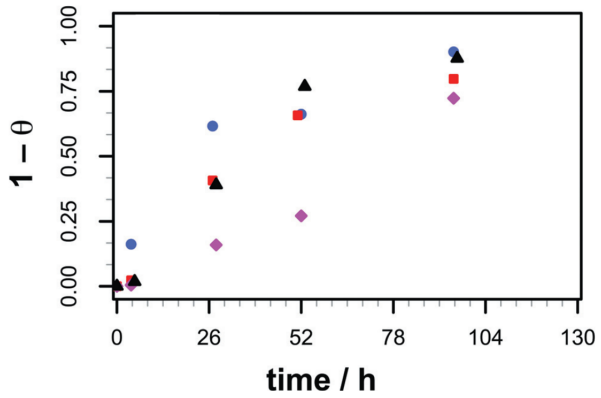

Figure 1.16 A comparison of conversion (1-θ) of melittin to acylated melittin within phospholipid membrane types: POPC (blue circles); OPPC (red squares); DOPC:DMPG (purple diamonds); DOPC:DPPS (black triangles).[44]

Phosphatidylethanolamine (PE), was the final phosphate head group observed in eukaryotic membranes to be tested. Unlike PS and PG, PE head groups are zwitterionic at physiological pH, and thus neutral in charge, limiting the likelihood of ionic interactions between melittin and a PC:PE membrane. Whilst information regarding transfer rate is limited, for a POPC:SLPE (4:1) membrane, modified melittin is observed within 3 hours, with stearoyl and linoleoyl transfer 25 % of palmitoyl and oleoyl transfer, consistent with the 4:1 ratio.[44]

Prokaryotes such as bacteria, fungi and some microbes differ in their membrane composition compared to the eukaryotic PC containing membranes discussed previously.[58] Knowledge of these prokaryotic membranes, and in particular their differences from the membranes of higher eukaryotic organisms, is vital for antimicrobial drug design. Exploitation of differences in intrinsic lipidation is one novel mechanism that could be targeted for antimicrobial design, considering the novel properties of lipidated peptide products, and their potential roles in targeting and signalling. Intrinsic lipidation of two model prokaryotic membrane types was monitored, with the aim of harnessing intrinsic lipidation in such a way that it could be detrimental to bacterial survival.

Gram-negative bacteria, such as *E. coli*, have an outer lipopolysaccharide layer comprised of lipid anchors and specific sugar chains, surrounding a thin peptidoglycan cell wall comprised of a *N*-acetylated muramic acid and *N*-acetylated glucosamine glycan backbone, cross-linked with amino acid chains.[58] Modeling of gram-negative bacteria, Fig. 1.17, is achieved using a

POPE:SLPG (3:1) membrane, containing varied fatty acid chains and a negative PG component to increase binding of cationic model peptide melittin. At physiological conditions *in vitro*, gram-negative membranes did not exhibit intrinsic lipidation of melittin on a biologically relevant timescale, a clear difference compared to eukaryotic membrane models, with antimicrobial potential.[59] The innate increased ionic interactions between melittin and PG have evidently been overcome by other rate-controlling factors driving the reaction. Furthermore, probing of lipid phase and domain formation by incubation of the gram-negative model at 21 °C did not afford acylated melittin on a biological timescale, again pointing to the presence of other reaction driving forces.

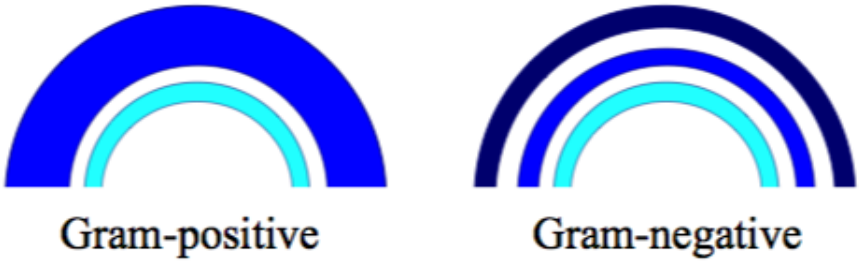

Figure 1.17 Schematic of gram-positive and gram-negative bacteria. Colours indicate: cell membrane (pale blue); peptidoglycan cell wall (mid blue); lipopolysaccharide layer (dark blue).[59]

S. aureus and other gram-positive bacteria, Fig. 1.17, lack the lipopolysaccharide outer membrane associated with gram-negative bacteria. Additionally, the peptidoglycan cell wall of gram-positive bacteria infers increased strength and adaptability due to increased thickness and crosslinking between peptide chains and the glycan backbone. Mimicry of gram-positive bacterial membranes by use of POPE:SLPG (1:3), resulted in increased anionic PG component, expected to favour binding and membrane-affinity of cationic melittin.[56] Intrinsic lipidation *in vitro* was not observable in gram-positive membranes at both physiological (37 °C) and ambient temperatures (21 °C) up to six days.[59] Despite the increased ionic interactions, these observations are in line with those made for gram-negative model membranes, implying membrane binding and lipid phase do not act solely as driving forces of lipidation. However, the natural role of melittin as a lytic peptide must be considered, and thus further focus on intrinsic lipidation of antimicrobial peptides such as magainin II is required prior to the harnessing of intrinsic lipidation for antimicrobial drug design.

1.3.4 Other Influences Upon Intrinsic Lipidation

Successful experimentation confirmed intrinsic lipidation *in vitro* as a process generic to both membrane active peptides and eukaryotic membrane models.[11] However, full understanding of the complex nature of reactivity at the membrane interface required further investigation into potential controlling factors. Introduction of single targeted modifications enabled the impact of individual features upon reactivity to be pinpointed. To this end, modifications were applied to both membrane composition and peptide sequence.

1.3.4.1 Influence of Cholesterol

Cholesterol, Fig. 1.18, is an amphiphilic component of eukaryotic membranes, comprised of a polar OH group and a rigid, hydrophobic, fused ring structure.[7] Cholesterol containing model membranes exhibit altered properties compared to phospholipid only membranes, and provide a more accurate mimic of natural membranes. Physical properties altered by cholesterol insertion into a membrane include: (i) increased uniformity of transition temperatures (T_m), for example the T_m of DOPC (1 °C) is increased in the presence of cholesterol, whereas DPPC with a T_m of 41 °C is made more fluid.[7,60] For mixed acyl systems the impact of cholesterol on T_m is harder to predict, although some systems have been modelled; (ii) decreased membrane binding affinity of amphiphilic peptides, as confirmed by measurement of circular dichroism (CD) and environment dependent tryptophan emission for the model peptide melittin; (iii) structural changes to the membrane upon peptide binding, including membrane degradation and breakage into small, highly curved micelle-like particles.[45,61,62] Given the numerous physical changes to the membrane upon the inclusion of cholesterol, it appears likely that the molecule would also have a major influence upon reactivity of intrinsic lipidation.

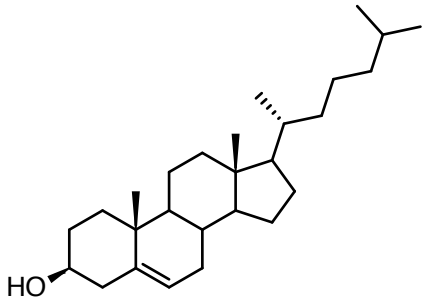

Figure 1.18 The structure of cholesterol.

Natural eukaryotic membranes contain lipid:cholesterol molar ratios between 1:1 and 4:1. Liposomes containing reactive phospholipid DOPC were therefore prepared containing DOPC:cholesterol

(4:1) and DOPC:cholesterol (1:1), in order to examine melittin intrinsic lipidation within these systems.[59] Similarly to DOPC membranes, melittin intrinsic lipidation was observed in DOPC:cholesterol containing membranes under physiological conditions, Fig. 1.19. Reactivity was observed within 24 hours across all systems, suggesting minimum impact of cholesterol upon reaction rate in the presence of DOPC. However, by 72 hours maximum reactivity was observed within the DOPC:cholesterol (4:1) membrane, followed by DOPC:cholesterol (1:1), and finally DOPC. Modification in DOPC only membranes occurs predominantly at the *N*-terminus. However, whilst *N*-terminal modification remains most prevalent upon inclusion of cholesterol, reactivity at additional sites is observed. MSMS confirmed the locations of reactivity as K23, K21, K7, and S18.

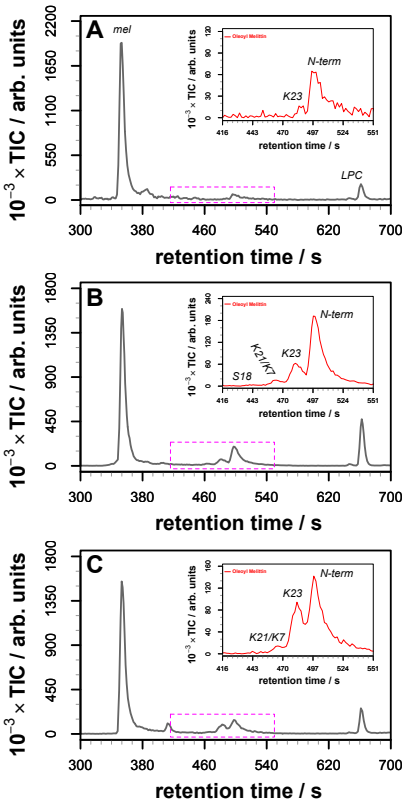

Figure 1.19 TIC for acylation of melittin in membranes containing: (a) DOPC; (b) DOPC:cholesterol (4:1); (c) DOPC:cholesterol (1:1). Inserts show EIC for oleoyl melittin (red). Conditions shown use 1:10 peptide:lipid ratio and incubate in 90 mM NaCl, 10 mM $NaHCO_3$ buffer, pH 7.4 and 37 °C for 72 hours.[59]

Analogous studies were conducted using gel phase phospholipid DPPC, which has a transition temperature of 41 °C, above physiological temperature.[59] Melittin was not observed to undergo intrinsic lipidation in DPPC only membranes, attributed to decreased membrane fluidity. Incorporation of cholesterol into DPPC liposomes caused induction of melittin intrinsic lipidation, Fig. 1.20. Low level product was observed in the DPPC:cholesterol (1:1) system, whereas within DPPC:cholesterol (4:1) liposomes, 30 % conversion to palmitoyl melittin is

observed within 24 hours. In contrast to DOPC containing systems, K23 was observed as the most prevalent site of acylation, followed by the *N*-terminus. Additional minor sites of reactivity, K21 and K7, were observed within the DPPC:cholesterol (4:1) system only.

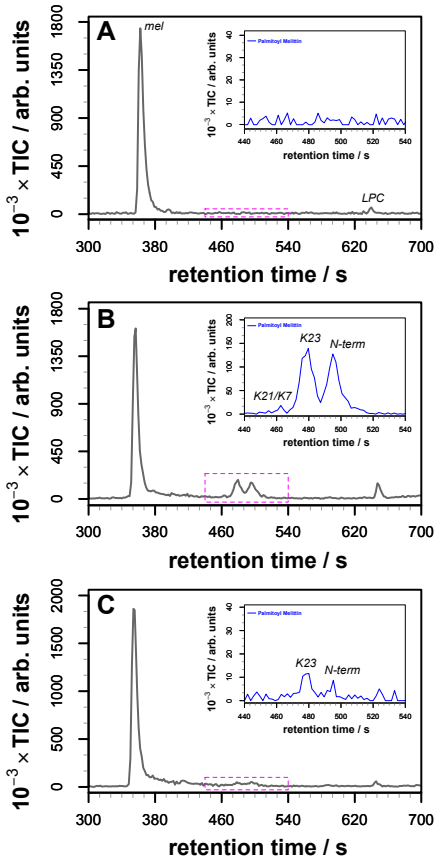

Figure 1.20 TIC for acylation of melittin in membranes containing: (a) DPPC; (b) DPPC:cholesterol (4:1); (c) DPPC:cholesterol (1:1). Inserts show EIC for palmitoyl melittin (blue). Conditions shown use 1:10 peptide:lipid ratio and incubate in 90 mM NaCl, 10 mM $NaHCO_3$ buffer, pH 7.4 and 37 °C for 72 hours.[59]

Additional cholesterol studies used mixed acyl lipid POPC in 1:1 and 4:1 phospholipid:cholesterol molar ratio.[59] Acyl transfer was observed across all systems from 24 hours. Oleoylated melittin was the sole modified product observed from POPC membranes after 24 hours, however cholesterol containing membranes exhibit oleoyl and palmitoyl transfer, indicative of preferential acylation. Later time point 72 hours, Fig. 1.21, revealed palmitoyl and oleoyl transfer across all membrane types. Observed reactivity patterns mimic those noted within DOPC and DPPC systems, with POPC:cholesterol (4:1) exhibiting twice the quantity of modified melittin compared to the POPC:cholesterol (1:1) system. Inclusion of cholesterol was also observed to alter relative product distribution, with K23 acylation favoured in POPC:cholesterol systems, and the *N*-terminus in POPC only.

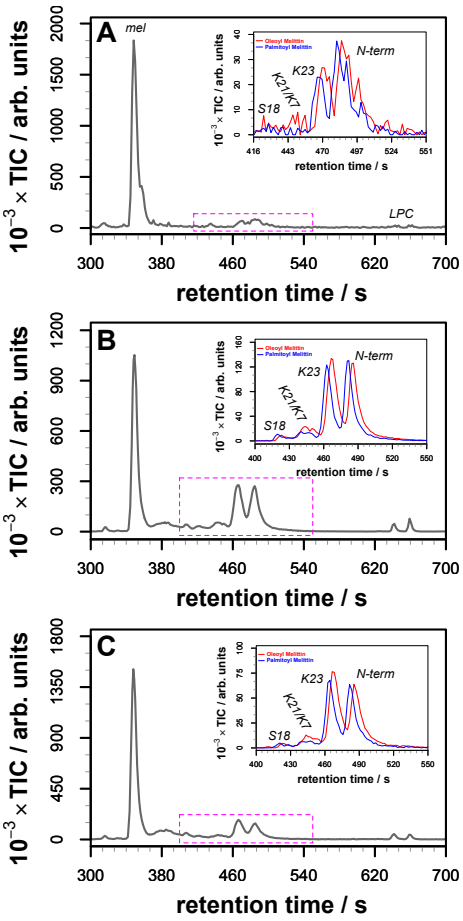

Figure 1.21 TIC for acylation of melittin in membranes containing: (a) POPC; (b) POPC:cholesterol (4:1); (c) POPC:cholesterol (1:1). Inserts show EIC for palmitoyl melittin (blue) and oleoyl melittin (red). Conditions shown use 1:10 peptide:lipid ratio and incubate in 90 mM NaCl, 10 mM $NaHCO_3$ buffer, pH 7.4 and 37 °C for 72 hours.[59]

Membrane affinity, membrane T_m, and membrane disruption alter dramatically upon inclusion of cholesterol within a membrane. However, previous research suggests neither membrane affinity nor T_m are rate determining for intrinsic lipidation.[44] Membrane disruption by cholesterol into highly curved micellar aggregates would be expected to bind membrane active peptides increasingly strongly and in an orientation with increased contact between peptide nucleophiles and phospholipid fatty acid chains, thus aiding intrinsic lipidation.[45,57] Comparisons of small unilamellar vesicles (SUV), Fig. 1.22, highly curved up to 100 nm particles with large unilamellar vesicles (LUV) of > 100 nm in diameter provide a crude test of this theory. Incubation under physiological conditions of DPPC SUVs and LUVs with model peptide melittin yielded no acylation up to 9 days in either case, potentially due to the increased reactivity instilled by increased curvature being too small for detection given the unreactivity of DPPC. Highly reactive DOPC:SLPG (3:1) LUVs yielded both *N*-terminal and K23 acylation of melittin within 4 hours, 23 % conversion within 24 hours, and 49 % within 4 days, including double acylation.[59] By contrast DOPC:SLPG (3:1) SUVs

generated 11 % acylated melittin within 24 hours and 36 % conversion over 4 days, indicative of decreased curvature favouring intrinsic lipidation. However, consideration must be given to the stabilisation of highly curved particles induced by cholesterol, compared to the highly unstable SUVs which merge over time, which may explain such irregularities.[63]

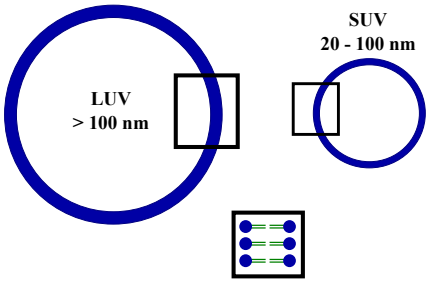

Figure 1.22 Diagram indicating the differences between LUVs (large unilamellar vesicles) and SUVs (small unilamellar vesicles).

1.3.4.2 Influence of the Nucleophile

Differences in rate of intrinsic lipidation are observable between different nucleophiles within a single membrane active peptide, believed to be driven by the surrounding environment altering pK_a and peptide binding orientation with respect to the nucleophile. Melittin, Fig. 1.8, contains three lysine residues of decreasing reactivity: (i) K23, surrounded predominately by hydrophobic residues favouring contact with hydrophobic phospholipid tails; (ii) K21, at a hydrophobic-hydrophilic boundary; (iii) K7, in a hydrophilic region favouring exposure to aqueous cell environment.[10] Influence of surrounding environment upon intrinsic lipidation nucleophiles focused upon four peptides, Fig. 1.23: (i) control peptide 21 containing an *N*-terminal nucleophile only; (ii) peptide 22 containing lysine at position 6 surrounded by hydrophilic arginine residues; (iii) peptide 23 containing lysine at position 7, a hydrophilic-hydrophobic boundary; (iv) peptide 24 containing lysine at position 8 within a hydrophobic environment of leucine residues.

Incubation of peptides 21 to 24 with membrane mimics varying in lipid head group types, and with mixed acyl chains for preference tracking, yielded the intrinsic lipidation results given in Table 1.3.[39,59] Despite complications associated with chromatographic crossover, successful acylation with palmitoyl and oleoyl/stearoyl/linoleoyl was observed for control peptide 21 with a POPC:SLPG (4:1) membrane within 6 days, and peptide 23 with POPC within 5 days, indicative of nucleophiles at a hydrophobic-hydrophilic boundary facilitating acylation due to binding orientation. Unfortunately, the minimal quantities of acylated peptide formed

combined with inconsistency between lipid systems prevent identification of a definitive trend of nucleophile reactivity.

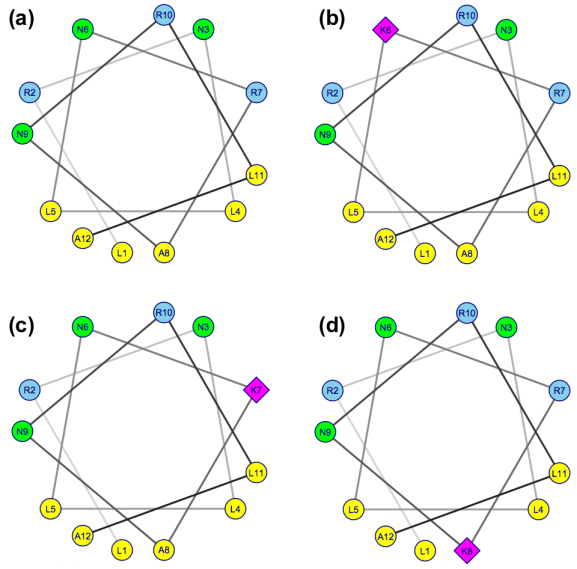

Figure 1.23 The helical wheel structures of peptides: (a) 21; (b) 22; (c) 23; (d) 24. Colours indicate: lysine residues (magenta); hydrophobic residues (yellow); polar, uncharged residues (green); basic residues (blue).

Lipid	Acylation of Peptide 21	Acylation of Peptide 22	Acylation of Peptide 23	Acylation of Peptide 24
POPC	No	No	Yes	No
POPC:Chol (4:1)	No	No	No	No
POPC:SLPG (4:1)	Yes	No	No	No
POPC:SLPE (4:1)	No	No	No	No
POPC:POPS (4:1)	No	No	No	No

Table 1.3 Observed intrinsic lipidation of peptides 21, 22, 23, and 24 within different membrane types. The conditions shown are 1:10 peptide:lipid molar ratio and incubated in 90 mM NaCl, 10 mM $NaHCO_3$ buffer at pH 7.4 and 37 °C for 72 hours.[59]

Nucleophiles of membrane active peptides observed to be involved in intrinsic lipidation include lysine, serine and histidine, however chemical intuition suggests other amino acids also have the relevant functional groups to carry out the role. Peptides containing relevant amino acids, Fig. 1.24, include: sterically unhindered thiolate cysteine (25); highly hindered, hard and moderately electronegative nitrogen containing histidine (28) and tryptophan (29); and weak nucleophile oxygen in sterically unhindered serine (26), slightly hindered threonine (27), and aromatic residue tyrosine (30). Despite low level intrinsic lipidation and

chromatographic crossover, incubation of peptides 26-30 under physiological conditions with a POPC:SLPG (4:1) membrane yielded the rate of acylation 29(W)>27(T)>26(S)>30(Y)>28(H). Peptide 29, containing membrane binding tryptophan, underwent acylation with palmitoyl and oleoyl/stearoyl/linoleoyl chains by day 3 at two locations, determined by MSMS to both be *N*-terminal. Two isomers, *cis* and *trans* caused by peptide membrane binding, were thought to cause these two distinct acylation sites, however testing of this was limited by solubility issues.[59] Noticeably, cysteine containing peptide 25 is not included in the scale of reactivity, since it was observed to undergo both oxidation and dimerisation via disulfide bond formation. Further study showed that use of a reducing agent, dithiothreitol (DTT) to prevent dimerisation only worked for a limited time and was proposed to cleaved sulphur-acyl bonds formed, as indicated by peaks corresponding to loss of thiol esters at *m/z* 743.[64]

Peptide 25
LRNLLNCANRLA

Peptide 28
LRNLLNHANRLA

Peptide 26
LRNLLNSANRLA

Peptide 29
LRNLLNWANRLA

Peptide 27
LRNLLNTANRLA

Peptide 30
LRNLLNYANRLA

Figure 1.24 Sequences of peptides 25 to 30 designed to test the influence of nucleophile type upon intrinsic lipidation. Nucleophile variation is highlighted in green.

Difficulties studying the relationship between different nucleophiles and nucleophile environments, and intrinsic lipidation, result from membrane affinity and solubility limitations. As a result, the impact of individual physical parameters upon intrinsic lipidation rate is prevented, stunting growth of the field of reactions at the membrane interface. Intrinsic lipidation is likely driven by a multitude of factors working together, and in the future these factors must be segregated such that each can be explored and their effects monitored. Extending understanding of intrinsic lipidation in this way may facilitate reaction harnessing in biological organisms, laboratory systems, and pharmaceutical development.

1.4 Intrinsic Lipidation of Small Molecules

Given intrinsic lipidation of membrane active peptides *in vitro*, similar acyl transfer reactions to other nucleophile containing components with membrane affinity might be expected, for example cholesterol or sugars. Small organic molecules have the potential to exhibit such reactivity, providing they have: (i) affinity for biological membranes; (ii) a suitable nucleophilic

group. These criteria are satified by tryptophan-like molecules, containing nucleophilic nitrogen moieties and an indole ring. Indole, Fig. 1.25, exhibits high membrane affinity due to enhanced electrostatic interactions with hydrophilic phospholipid head groups, combined with hydrophobic interactions between the aromatic ring and phospholipid tails.[65–68] Interestingly, the tryptophan-like family includes several known drug molecules targeted to membranes for their disease-related roles. Intrinsic lipidation of small molecules provides analogous functionality to chemical conjugaton with hydrophobic fatty entities, altering hydrophobicity and membrane affinity. Furthermore, lipidated small molecules have been observed to exhibit lytic properties, resulting in membrane degradation and broad-spectrum antibiotic properties against both gram-positive and gram-negative bacteria.[69,70] These physical features facilitate potential therapeutic applications for intrinsic lipidation, without the problems of toxicity, stability and cost associated with peptides.[71,72]

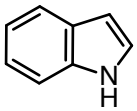

Figure 1.25 The structure of indole.

Phospholipidosis is a lysosomal storage disorder characterised by accumulation of phospholipids in tissues such as the lungs, liver and kidneys.[73] Drug-induced phospholipidosis, in which a drug contributes to this aggregation, is caused by over 50 cationic amphiphillic drug molecules. These drugs, related by structural incorporation of both hydrophobic and a hydrophilic region, cover a variety of different classes, including antidepressants and cholesterol reducing agents.[28,74] Although reversed swiftly by stopping drug administration, problems associated with drug failure and the unknown relationship to drug toxicity make phospholipidosis problematic.[75] Intrinsic lipidation of small organic molecules has potential to be a key stage in drug-induced phospholipidosis, and thus provides a viable target for increased mechanistic understanding and prevention. Preliminary data suggests that the known phospholipidosis inducing drug molecules shown in Fig. 1.26, propranolol **1**, procaine **2** and tetracaine **3**, undergo intrinsic lipidation. However, the influence of this membrane reactivity upon their physical properties and pharmaceutical activity remains largely unknown.[76] Probing the mechanism and rate-determining influences on intrinsic lipidation of small organic molecules is thus of further interest.[77]

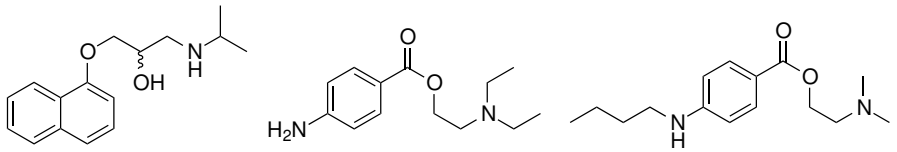

1 **2** **3**

Figure 1.26 Phospholipidosis inducing drug molecules propranolol **1**, procaine **2**, and tetracaine **3**.

Indole based compounds were designed containing an aromatic region and an amine nucleophile, in order to comply with membrane affinity and nucleophile criteria required for intrinsic lipidation.[77] Variation in pK_a, partition coefficient (logP), and distribution coefficient (logD) between these compounds aimed to probe the influence of each of these factors upon intrinsic lipidation. The diversity of these molecules combined with functionality differences provided an ideal initial screen for intrinsic lipidation of small drug molecules. The 84 designed organic small molecules were screened with three membrane types: (i) DOPC, a mimic for eukaryotic membranes; (ii) DOPC:DOPS (4:1), a mimic for viral membranes; (iii) DOPE:DOPG (3:1), a mimic for prokaryotic bacterial membranes. Of key importance for medicinal purposes is selective reactivity between membrane types, particularly selective lipidation within prokaryotic membranes, resulting in the lipidated small molecule having a lytic effect upon the membrane.

Unlike analysis of peptide intrinsic lipidation by LCMS, direct monitoring of lipidated small molecules was not attempted due to low concentrations, small size, and poor ionisation efficiency. Instead, lipidation of small molecules was monitored by the quantity of lysolipid by-product produced compared to a background level of formation. Lysolipids provide a common reaction mixture component, simplifying the screening of a diverse range of small molecules. However, monitoring lysolipid formation is limited by the assumption that intrinsic lipidation of the small molecule is the sole mechanism of lysolipid formation. Furthermore, whilst OPC and OPE lysolipids are quantifiable under the analytical conditions employed, not all lysolipid species are. OPS and OPG for example, produced poor chromatographic peaks and require negative mode ESI ionisation for optimum visualisation.

Preliminary results from high throughput screening of 84 small organic molecules, indicated three categories of molecules: (i) increased lysolipid formation compared to the control sample, indicative of acylated small molecule formation; (ii) decreased lysolipid formation, due to decreased background hydrolysis or a lipidation reaction between lysolipid and the small molecule; (iii) lysolipid levels equal to the control, due to a lack of intrinsic lipidation, or a an equal rate of small molecule acylation with lipid and lysolipid, thus keeping the net quantity

constant. Molecules with high reactivity in prokaryotic PE:PG and PC:PS membranes, combined with low reactivity in eukaryotic PC membranes included compounds **4** (3-aminoindole), **5** (5-aminoindole), **6** ((1H-indazol-7-yl)methanamine) and **7** (3-(2-aminoethyl)-1H-indol-5-ol).[77] These small molecules, Fig. 1.27, are all indoles with free amines, however the amine position and attachment type varies, indicating no clear reactivity trend. A major increase in lysolipid production, 1054 % compared to the background rate, was observed for small molecule **8** (7-amino-4-(1H)-quinolinone) in a PE:PG membrane. Despite this, the result was not reproducible and lipidated small molecule was not observed, indicating either increased lipid degradation induced by compound **8**, or formation by intrinsic lipidation and subsequent hydrolysis of the acylated small molecule, supported by the observation of oleic acid by LCMS.

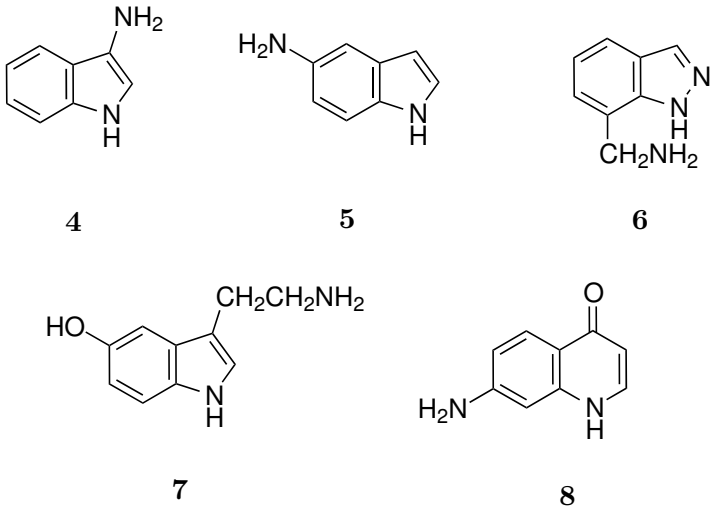

Figure 1.27 Key small organic molecules indicated to be of interest from small molecule intrinsic lipidation studies due to increased lysolipid production.

Considering the potential application of small molecule intrinsic lipidation in antimicrobial or antifungal drug design, candidates were screened for antimicrobial activity against *E. coli* and *S. aureus*.[78] Molecules, Fig. 1.27 and Fig. 1.28, with selective reactivity in PE:PG or PC:PS membranes were chosen: **6** ((1H-indazol-7-yl)methanamine), **8** (7-amino-4(1H)-quinolinone), **9** (6-aminoindole), **10** (1H-benzimidazol-4-amine), and **11** (2-aminomethylbenzimidazole). At concentrations above 10 mM, minor effects upon *E. coli* growth were evident for compounds **6**, **9** and **11**. Simultaneously, complete inhibition of *S. aureus* growth was observed for compounds **8**, **9**, and **10**. Small molecules believed to undergo intrinsic lipidation also have antimicrobial activity, however further work probing the antimicrobial activity of the lipidated small molecules is still required. Additionally, proof of lipidation by visualisation of lipidated small molecules and experimentation of lipidation *in vitro* with *E. coli* and *S. aureus* membrane extracts are necessary for better understanding. Whilst initial screening of small

molecule lipidation *in vitro* has provided promising results, knowledge is still in its infancy and further work is required to develop the method and to gain the understanding required for drug development.

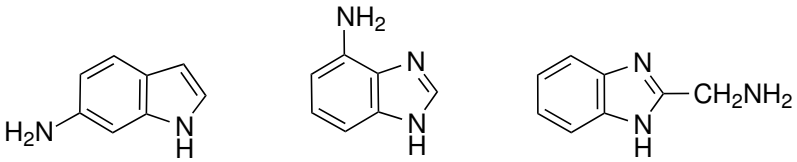

9 **10** **11**

Figure 1.28 Key small organic molecules indicated to be of interest from small molecule intrinsic lipidation studies, and selected for study of antimicrobial activity.

1.5 Conclusions

Knowledge and understanding of the cell membrane has developed considerably since Singer and Nicolson first proposed the fluid mosaic model.[3] Despite these advances, the potential for chemical reactivity within the membrane has been the subject of only limited investigation. Three reactions at the membrane interface have been studied thus far: (i) lysolipid formation; (ii) peptide intrinsic lipidation; (iii) small molecule intrinsic lipidation. Each reactivity is predicted to have distinct implications on cellular activity and membrane integrity.[10,12,77] Understanding membrane reactivity is key to comprehend the fields of drug activity mechanisms, induction of drug side effects and disease, and the therapeutic potential of such reactions. Considerable early stage research is required in order to fully realise the implications and applications of cell membrane reactivity. Challenges in sensitivity and complexity observed during previous study mean new analytical techniques are required. Analysis time, suitability for both *in vitro* and *in vivo* systems, and informative value, are important factors when considering analytical technique selection. Development of suitable analytical techniques for in depth study of membrane reactions would facilitate better understanding of reaction mechanisms and implications. Investigation is required into the role of substrate structure and functionalities, local environment, and membrane composition, upon reactivity. Furthermore, biophysical properties of lysolipids and lipidated reaction products require consideration. The research undertaken within this thesis works to develop methodology for study of reactions at the membrane interface, and to apply this methodology in order to better understand these reactions, and their wider implications.

2 | Instrumentation

In 1912 British physicist J. J. Thomson took the first steps in developing the analytical technique now known as mass spectrometry, when he first observed singly and multiply charged ions. By detecting these ions hitting a photographic plate, Thomson was able to generate a spectrum of mass to charge (m/z).[79,80] Modern day mass spectrometry applies Thomson's work in separating ions by m/z in order to calculate the molecular weight of a species, and thus identify it. However, the field of mass spectrometry has developed significantly since its 1912 origins and is now a far more popular, powerful, and diverse technique.[81]

Major developments in the field of mass spectrometry over the last century include changes in ionisation techniques to accommodate a wider range of molecules, and particularly biomolecules. Most notably, this includes the 2002 Nobel Prize winning work on the advent of electrospray ionisation (ESI) by John Fenn, and Koichi Tanaka's work pioneering soft laser desorption ionisation.[82–87] A further Nobel Prize in the field of mass spectrometry was awarded in 1989 to Hans Dehmelt and Wolfgang Paul for their development of techniques for trapping charged particles, leading to the ion trap mass analyser.[88,89] These developments paved the way for current instrumentation such as the FT-ICR and the Orbitrap mass analysers, which have high mass accuracy and resolving power.[90,91] Furthermore, additional new facets of mass spectrometry have been developed, aiming to provide increased insight into molecular structure. Two such examples are tandem mass spectrometry (MSMS), a technique which fragments precusor ions of interest into smaller product ions, and ion mobility mass spectrometry (IMMS), which separates ions by their mobility through a carrier gas.[92–94]

Modern day mass spectrometers can be seen as hugely complex instruments, however by breaking them down into their constituent parts it is possible to simplify the understanding of how they work and how they can be manipulated for a desired purpose. The first step in analysing a sample by mass spectrometry is the introduction of the sample into the instrument. Direct infusion is possible for samples containing only one species, however more complex

mixtures require separation so that each mixture component is introduced into the mass spectrometer individually. Following sample introduction the usually neutral starting species undergoes conversion into a gas phase ion in a process known as ionisation. Ionisation techniques range from hard ionisation suitable for small stable molecules such as electron ionisation (EI), through to soft techniques such as matrix-assisted laser desorption/ionisation (MALDI) optimal for large biomolecules. Once formed, ions enter the third constituent part of the mass spectrometer, known as the mass analyser. The mass analyser separates the ions based upon their m/z, and directs them onwards to the detector. At the detector, ion abundance is measured and this information is converted into a signal which can provide meaningful data on the sample identity. Several instrumentation examples exist for each constituent part of the mass spectrometer. The optimum configuration required to create an indispensable analytical tool can be determined by the mass range, ionisation potential and complexity of the sample to be studied. For the purposes of this research project, the following instrumentation has been selected:

- Synapt G2-S (Waters Corp., UK), utilised with an ESI source. The mass analyser components include a quadrupole, two T-wave collision cells and a ToF mass analyser connected in series. An ion mobility cell is fitted for ion mobility separation, and an Acquity UPLC for chromatographic separation.
- Autoflex II ToF/ToF (Bruker Daltonics Ltd., UK), a MALDI ionisation source with ToF mass analyser.

2.1 Chromatography

Complex mixtures prove to be challenging mass spectrometry samples, due to issues of ion suppression and spectrum complexity. By preceding mass analysis with a separatory technique, it is possible to introduce components of a complex mixture into the mass spectrometer individually, mitigating these issues. Mass spectrometry compatible separation techniques are required to maintain the integrity of sample components, give consistent and predictable separation, and not to introduce background interference. Chromatography, a technique which separates components in a mixture by partitioning them between two phases, meets this specification.[95,96] Reversed phase liquid chromatography (LC) using an Acquity UPLC (Waters Corp., UK) is the specific technique selected for the separatory analysis carried out within this thesis. Hydrophobic molecules interact strongly with the reversed phase LC

stationary phase and thus are retained for longer than polar molecules, providing separation.

Reversed phase liquid chromatography-mass spectrometry (LCMS) utilises a non-polar chemically modified silica column stationary phase. Several modified stationary phases exist, Table 2.1, with molecular features developed to improve chromatographic separation for specific classes of analytes. A C_{18} column is the classic stationary phase employed for reversed phase LC analysis, whilst more recent developments of the C_8 or C_4 column improve analytical flexibility by decreasing stationary phase hydrophobicity.[96] Phenyl modified stationary phases provide excellent separation for both aromatic small molecules and peptides with a high proportion of aromatic amino acids. The mobile phase adopted for reversed phase LCMS is a polar mass spectrometry compatible solvent in which the analytes studied are soluble. Favourable solvents include water (H_2O), acetonitrile (MeCN), methanol (MeOH) and isopropanolol (IPA). The Acquity UPLC (Waters Corp., UK) affords the user a binary pump such that two miscible solvents can be used simultaneously in a gradient, aiding separation. Factors such as solvent temperature and flow rate are known to be important in order to achieve successful separation of components by LCMS. Furthermore, pH is known to play an important role in ensuring reproducible chromatographic peaks, particularly in the case of zwitterionic species.[97,98]

Column Type	Column Chemistry	Analyte Suitability
C_{18}	C_{18} bonded to silica	All
C_8	C_8 bonded to silica	All
C_4	C_4 bonded to silica	Proteins and large biomolecules
Phenyl	C_6 phenyl bonded to silica	Aromatic and polyaromatic analytes
Amide	Amide bonded to silica	Polar analytes
HILIC	Silica solid core particle	Polar, basic, and water-soluble analytes

Table 2.1 Common stationary phase column chemistries utilised for LCMS.[99]

Achieving good chromatographic separation and quality data requires careful selection of chromatographic parameters such as the nature of the the stationary and mobile phases. Two key features are considered important for judging the success of a separation.[96] The first feature, deemed especially important within an industrial environment, is completing the separation with the minimum time expenditure possible. A short separation time increases the throughput rate of analysis, and provides a more efficient use of materials. The second factor of importance is chromatographic resolution, a measurement of how well differentiated two chromatogram peaks are. Resolution (R_s) between two peaks, defined in Equation 2.1, can be calculated from average peak width (w_{av}) and difference in retention time (Δ r.t.).

These values depend upon three key parameters: (i) efficiency; (ii) selectivity; (iii) retention. It is by altering instrument parameters affecting these three components that improved chromatographic resolution can be achieved. Optimising these parameters is particularly challenging for hydrophobic analytes, due to their strong column retention and subsequent peak broadness.

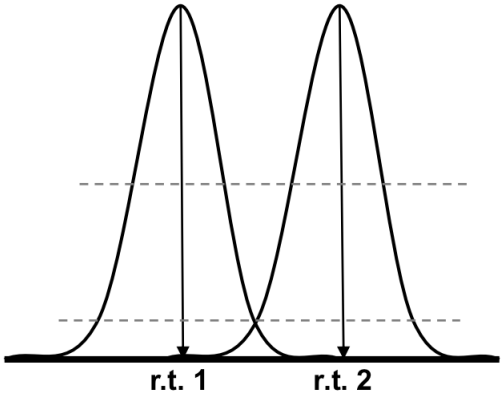

Figure 2.1 Depiction of two resolved peaks in a chromatogram.

$$R_{\mathrm{s}} = \frac{\Delta r.t.}{w_{\mathrm{av}}} \tag{2.1}$$

Where R_{s} = resolution; $\Delta r.t.$ = difference in retention time; w_{av} = average peak width.

2.2 Ion Sources

Ionisation is the conversion of neutral molecules into the more desirable charged ions required for analysis by mass spectrometry. These ions can be manipulated within the mass spectrometer using electric and magnetic fields, thus allowing for separation and detection. Several ionisation techniques exist, some of the most common of which are shown in Fig. 2.2. Correctly matching ionisation method with sample type allows for effective ionisation and quality mass analysis. Factors such as analyte structure, properties and stability can be taken into account in order to inform this decision. Highly energetic ionisation techniques such as EI and chemical ionisation (CI), are termed hard techniques. EI proceeds via electron ejection resulting in formation of a radical cation. These radical cations have increased internal energy, and thus their formation often results in in-source fragmentation of the analyte.[80] Softer ionisation techniques, such as ESI and MALDI, achieve ion formation via protonation/deprotonation or ion attachment.

This mechanism aids in maintenance of an intact molecular ion, proving particularly useful for unstable analytes and biomolecules.[83,100] ESI and MALDI will be further discussed as the most suitable techniques for samples studied within this thesis.

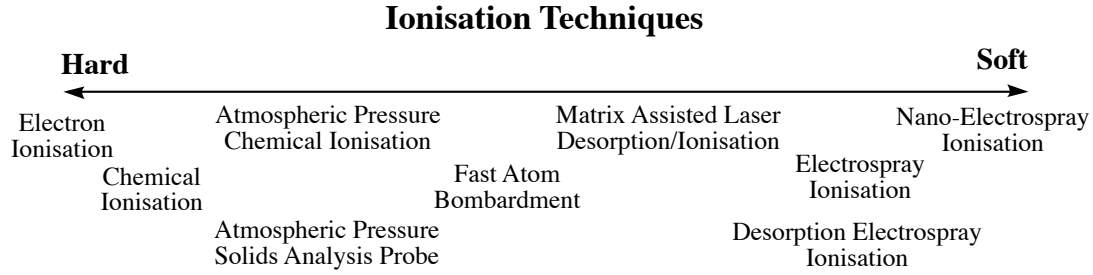

Figure 2.2 Comparison of a selection of currently available ionisation techniques.

2.2.1 Electrospray Ionisation

A favoured ionisation technique within the mass spectrometry community, ESI has wide applicability for molecule types across the pharmaceutical, agricultural and petroleum industries.[83,100,101] The popularity of ESI stems from its soft nature, successfully balancing effective ionisation with minimal in-source fragmentation. Additionally, ESI is an example of atmospheric pressure ionisation (API), a family of ionisation techniques which perform the ionisation process at atmospheric pressure, removed from the rest of the mass spectrometer.[102]

Positive mode ESI utilises protonation or formation of adducts such as Na^+, K^+ or NH_4^+, to form ions. Similarly, negative ESI proceeds via deprotonation or formation of $HCOO^-$, Cl^- or Br^- adducts.[103] The resulting charged ion depends upon the composition of the solution in which the sample is introduced. Since ESI performs well when the sample is introduced from a polar solvent, the technique is often interfaced with chromatography such as LC or size exclusion chromatography (SEC).[84] Chromatography solvents can be prepared to include 0.1 % formic acid (FA) promoting analyte protonation. Alternatively, salt ions can be doped into samples or chromatography solvents to promote adduct formation if desired. Small molecule ionisation via ESI can be limited to singular protonation, however larger biomolecules with multiple potential protonation sites typically present as multiply charged.[83] Multiply charged biomolecules require reduced m/z range compared to single ionisation, facilitating ESI paired with limited range mass analysers e.g. a quadrupole.

ESI proceeds by flowing ions in solution through a capillary needle with an applied voltage and heated N_2 nebulisation gas. This potential difference between the capillary tip and the mass spectrometer creates an electric field, causing positive or negative charge to collect in solution

at the capillary tip. This collection of charge distorts the solution into forming a Taylor cone, Fig. 2.3. At the Taylor Cone tip, an aerosol of droplets containing multiple positive charges is released. This plume of droplets enters a heated inert N_2 atmosphere, designed to shrink the charged droplets via solvent evaporation. As solvent evaporates the charge density of the droplets increases until the Rayleigh limit is reached, Equation 2.2. At this point, Coulomb repulsion exceeds droplet surface tension, resulting in droplet explosion into smaller charged droplets. This process of desolvation and subsequent explosion continues to repeat, forming smaller and smaller droplets.[85,104,105] Finally, ions are completely desorped from the droplets via one of three mechanisms: (i) Ion Evaporation Model (IEM) - solvent evaporation and droplet explosion continue until one analyte ion is lifted from a multi ion droplet; (ii) Charge Residue Model (CRM) - solvent evaporation and droplet explosion continue until one ion surrounded by a layer of solvent remains and the solvent is then evaporated to get a single desolvated ion; (iii) Chain Ejection Model (CEM) - unfolded protein chains migrate to the droplet surface, become charged, and are expelled from the droplet in stepwise fashion starting at the chain terminus. All models are supported by experimentation, with the model adopted thought to depend upon factors such as analyte type, instrument parameters, and solvent. To this end, the CRM is believed to be in effect for hydrophilic molecules, whereas the IEM better supports hydrophobic analytes.[106]

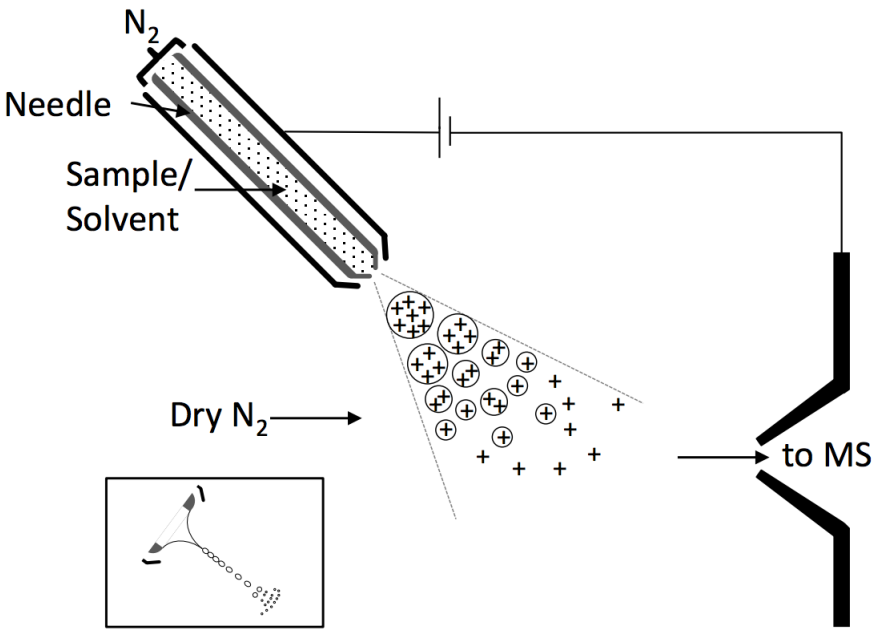

Figure 2.3 Mechanism of ESI ionisation. Inset shows Taylor cone formation.[107]

$$q_{\mathrm{Ry}} = 8\pi^2(\epsilon_0\gamma R^3)^{\frac{1}{2}} \tag{2.2}$$

Where q_{Ry} = charge; ϵ_0 = permittivity of the vacuum; γ = surface tension; R = radius of the spherical droplet.

The instrument utilised for ESI throughout the research presented within this thesis is a Synapt G2-S (Waters Corp., UK). ESI proceeds using a Z-spray ion source, Fig. 2.4, such that the ESI capillary is perpendicular to the sample cone. A gradient in both vacuum and voltage is set between the capillary and the sample cone, pulling desired ions through the source and into the rest of the mass spectrometer. By contrast, neutral molecules and ions of undesired charge are prevented from passing through the sample cone by the perpendicular arrangement of the capillary and the cone.

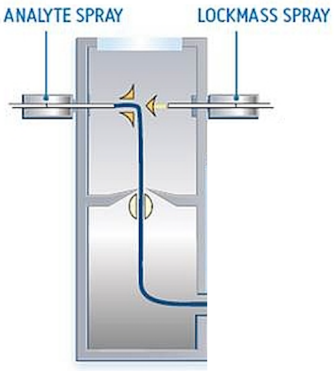

Figure 2.4 ESI source of Waters Synapt G2-S courtesy of Waters Corp., UK.

2.2.2 Matrix-Assisted Laser Desorption/Ionisation

In 1988 Karas and Hillenkamp developed MALDI from laser desorption/ionisation (LDI).[108] Tanaka and team then further developed the technique into what is known today.[86] MALDI is a soft ionisation technique ideal for high molecular weight species such as polymers or biomolecules. Only singly charged ions are produced via protonation, cation attachment, or proton abstraction for all but the largest molecules of m/z higher than 10 kDa, which may multiply charge to a small degree. This single ionisation means that a high mass range analyser is required for pairing with a MALDI ion source. A further drawback is that MALDI is rarely integrated with any chromatographic separation instrumentation, thus ion suppression can be an issue when viualising low abundance or poorly ionising analytes. However, MALDI

has many benefits, including easy sample preparation, and high tolerance of buffers, solvents, salts and solid hydrophobic material in samples.[87,109]

MALDI is characterised by the inclusion of a matrix in order to aid ionisation. Several MALDI matrices have been developed, with the most common and the one selected for this research being α-cyano-4-hydroxycinnamic acid (CHCA).[41] Successful MALDI matrices are characterised by a number of key properties including: (i) ability to absorb at laser wavelength and become excited; (ii) solvent compatibility with analyte; (iii) low sublimation temperature; (iv) suitable proton affinity such that the matrix has the ability to protonate/deprotonate under experimental conditions and then transfer this ionisation to the analyte.

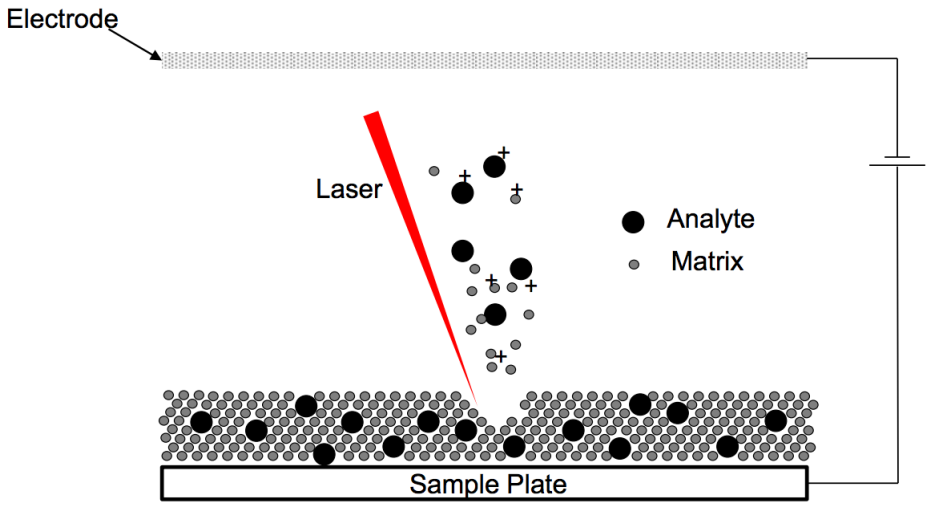

Figure 2.5 MALDI mechanism of ionisation.[107]

Excess matrix is mixed in solution with analyte sample and dried onto a MALDI target plate to form a co-crystalline layer of analyte fully embedded in matrix. A laser beam is pulsed towards the sample irradiating a portion of the sample. In the case of this PhD research, the instrumentation utilised for MALDI-MS is an Autoflex II ToF/ToF (Bruker Daltonics Ltd). This instrument has a 337 nm N_2 laser with 3 ns pulse length and pulse energy of 100 µJ. The laser pulse causes localised rapid heating, triggering desorption of matrix and analyte from the target plate into the gas phase. In addition, the focused laser beams causes excitation of the matrix molecules and subsequent matrix ionisation. Proton transfer from matrix to analyte creates gas phase analyte ions, as indicated by the mechanism in Fig. 2.5. In addition to this mechanism, several other ionisation pathways are likely used in the desorption plume.[110,111]

2.3 Mass Analysers

The mass analyser is the portion of the mass spectrometer following on from the ion source. The role of the mass analyser is to separate gas phase ions by their mass to charge ratio in order to aid detection. Several mass analysers exist, each relying on different principles of separation, which allows the optimum analyser to be selected for the analysis of any given analyte. Several factors are taken into account when choosing a mass analyser, including cost, mass range, scan speed, limit of detection, and time to complete one MS analysis termed the duty cycle. However, there are two factors prioritised above all else when selecting a mass analyser, mass accuracy and resolving power.

Mass accuracy is the difference in m/z measured by the mass analyser compared to the theoretical m/z value.[112] The value is converted into parts-per-million (ppm), Equation 2.3, to give the proposed accuracy of the predicted elemental formula. High accuracy mass analysers allow for the reliable determination of elemental composition, and thus provides more definitive characterisation of the molecule by mass spectrometry. In addition, analysers with high mass accuracy are able to aid in molecule characterisation by distinguishing between ions of the same nominal mass. An example of this is in the case of CO_2 (m/z 43.98928) and CH_3CHO (m/z 44.02567), which both have nominal m/z 44.

$$Accuracy(ppm) = \frac{(Observed(m/z) - Theoretical(m/z))}{Theoretical(m/z)} \times 1000000 \tag{2.3}$$

The second key performance factor utilised when selecting a mass analyser is the resolving power.[80,81] Resolving power is the ability of the analyser to distinguish and separate between ions with a small mass difference. For two overlapping peaks of equal intensity, Fig. 2.6, the resolving power can be defined by Equation 2.4. In this case m is the m/z of the peak and Δm is the mass difference between the two peaks separated by 10 % peak height. Mass resolution of an isolated peak can also be determined, Fig. 2.6. In this case Δm is taken as the peak width at 50 % of the peak height, termed full width at half maximum (FWHM).

$$R = \frac{m}{\Delta m} \tag{2.4}$$

Where R = resolution; m = mass; Δm = difference in mass.

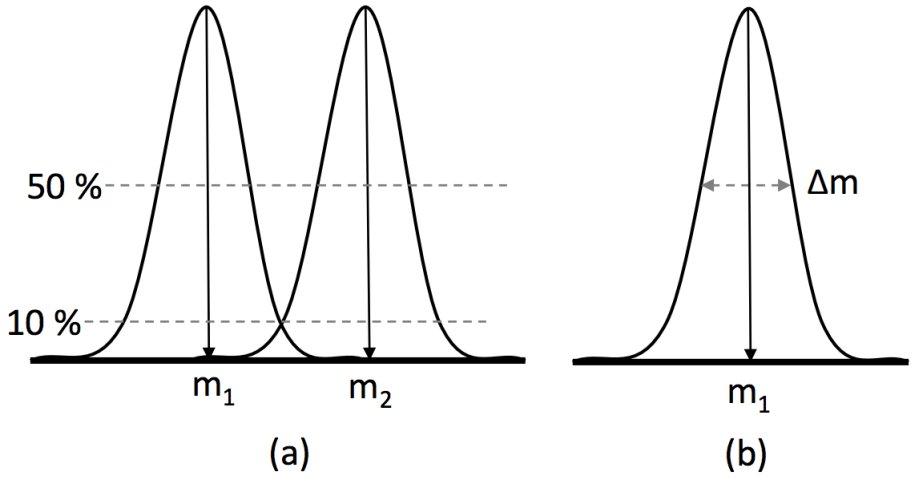

Figure 2.6 Resolving power of a given mass analyser for two overlapping peaks (a) or a single peak (b).[107]

2.3.1 Quadrupole Mass Analysers

A quadrupole is the simplest mass analyser commercially available, being low in resolving power and mass accuracy compared to other available mass analysers, but robust and not requiring high vacuum.[81,113] As such, single quadrupole analysers tend to be employed in small footprint mass spectrometers designed with cost and mobility in mind, rather than power and performance. Alternatively, quadrupoles appear as components of hybrid mass analysers, where several quadrupoles are used together or in conjunction with another analyser type in order to increase performance.[91,114]

Quadrupole mass analysers create a quadrupolar field within a series of parallel rod electrodes, arranged symmetrically around the z axis. A traditional quadrupole utilises four electrode rods to create the quadrupolar field, Fig. 2.7, however analysers with six (hexapole) and eight (octapole) rods have been developed in order to increase the mass range and bandwidth of the analyser. RF and DC voltages are applied to the electrode rods acting in pairs. The DC component (U) applied is identical in magnitude for the electrode pairs, however the two pairs are 180° out of phase. The applied RF voltage is $V\cos(\omega t)$ where V is the amplitude, ω the angular frequency (Hz) and t (s) is time. The alternating RF and DC voltages within the quadrupole analyser create an oscillating electric field. Ions entering the quadrupole are attracted to the electrode rods of opposite charge, thus the oscillating field causes the ions to oscillate through the quadrupole.

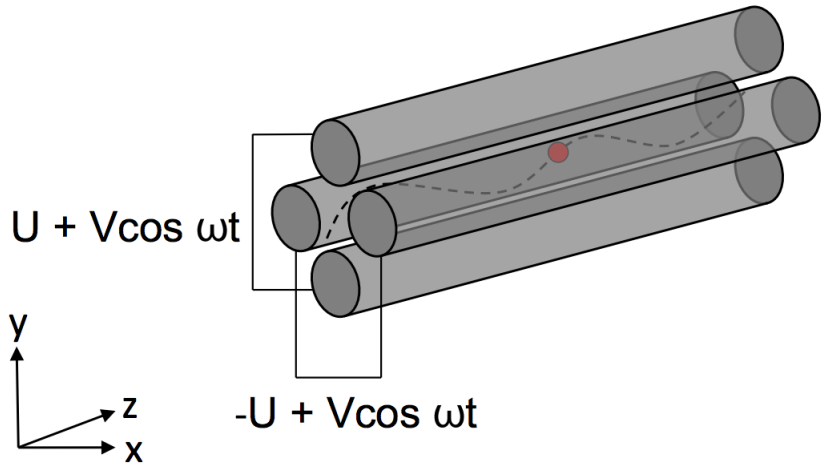

Figure 2.7 Schematic of a quadrupole mass analyser.[107]

$$a_{\mathrm{u}} = \frac{8zeU}{m\omega^2 {r_0}^2} \tag{2.5}$$

Where a_{u} = the x-coordinate of an ion travelling through the quadrupole; z = charge; e = charge of an electron; U = applied DC voltage; m = mass; ω = angular frequency; r_0 = quadrupole radius.

$$q_{\mathrm{u}} = \frac{4zeV}{m\omega^2 {r_0}^2} \tag{2.6}$$

Where q_{u} = the y-coordinate of an ion travelling through the quadrupole; z = charge; e = charge of an electron; V = RF voltage amplitude; m = mass; ω = angular frequency; r_0 = quadrupole radius.

Ion motion and stability within a quadrupole is described by the Mathieu Equations, 2.5 and 2.6.[81] The Matheiu equation describes the parameters q and a as functions of the RF and DC voltages applied to the quadrupole respectively. The equation can be converted into a graphical representation by plotting these two parameters against each other, Fig. 2.8. At the optimum RF:DC ratio, indicated by the blue line in Fig. 2.8, ions are transmitted through the quadrupole with sufficient separation to allow resolution of peaks of differing m/z. Decreasing the RF:DC ratio, shown by the red line in Fig. 2.8, maintains ion transmission, however the resolution decreases as ions of differing m/z are not well separated. Increasing the RF:DC ratio, indicated by the green line in Fig. 2.8, causes instability in the ion trajectories. In this case, ions collide and discharge on the electrode rods of the quadrupole and thus are not

transmitted to the detector.

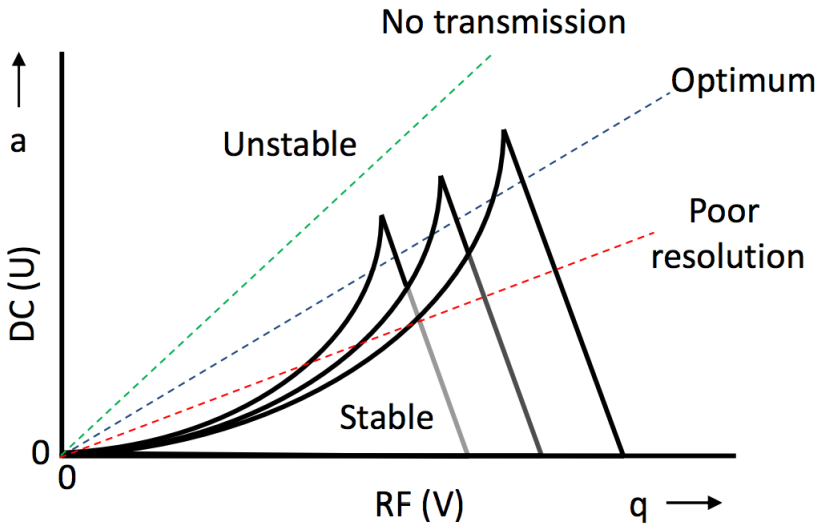

Figure 2.8 Stability profile of a quadrupole mass analyser.[107]

Quadrupole mass analysers are extremely versatile in their capabilities, which can be tuned by manipulating the applied RF and DC voltages. Single ion monitoring is possible by selecting RF and DC components such that only one ion m/z is stabilised and able to traverse the quadrupole. Alternatively, continuous scanning is possible by applying RF and DC voltages in constant ratio but increasing in magnitude. As Fig. 2.8 shows, different m/z ions are stabilised and transmitted as the magnitude increases, allowing for ion separation. Finally, applying an RF voltage only to the quadrupole allows ions of all m/z to transmit without separation. Addition of an inert gas to this region transforms the quadrupole into a collision cell such that fragmentation experiments can be carried out.

2.3.2 Time-of-Flight Mass Analysers

Wiley and McLaren first published a design for the time-of-flight (ToF) mass analyser in 1955.[115] Since this publication ToF analysers have developed into commercial instruments, improving in resolving power and mass accuracy. ToF mass analysers separate ions of differing m/z spatially, by measuring the time taken for ions to move through a fixed distance.[116,117] Ions are expelled from the ion source with an accelerating voltage (V) into a drift region, free from electric or magnetic fields. Ions entering the drift region have a kinetic energy (E_{kin}) as described in Equation 2.7, which is dependent upon their mass (m) and charge (z). Since

velocity (v) is equivalent to the distance travelled (d) in a given time (t), it is possible to further substitute and rearrange Equation 2.7 into Equation 2.8. Given that the mass of an electron (e), accelerating voltage (V), and distance (d) are constants in a ToF analyser, the equation can be further simplified such that m/z is proportional to time^2 (t^2). As a result, ions of low m/z move quickly through the drift tube of a ToF analyser, whereas high m/z ion are much slower resulting in ion separation within the analyser.[118]

$$E_{\text{kin}} = \frac{1}{2}mv^2 = zeV \tag{2.7}$$

Where E_{kin} = kinetic energy; m = mass; v = velocity; z = charge; e = charge on an electron; V = accelerating voltage.

$$\frac{m}{z} = 2eV(\frac{t}{d})^2 \tag{2.8}$$

Where m = mass; z = charge; e = charge on an electron; V = accelerating voltage; t = time; d = distance.

Commercial linear ToF mass analysers contain a linear drift tube region to achieve the desired separation of ions by m/z, Fig. 2.9. These analysers have poor mass accuracy of approximately 200 ppm, and resolution of around 5000 FWHM. Increased ToF analyser resolution is achievable by increasing the distance over which ions separate. However, lengthening the drift tube increases instrument size and quickly becomes impractical. An alternative method for lengthening the drift tube, increasing ToF mass accuracy and resolving power, is to use a reflectron. A reflectron is an ion mirror, which deflects ions hitting it back along the drift tube thus increasing the overall travel distance. An additional benefit is that ions of higher m/z penetrate further into the reflectron, thus experiencing higher voltages and further increasing ion separation. Reflectron ToF mass analysers have mass accuracy of 10 ppm or better with internal calibration, and resolving power of approximately 20,000 FWHM.[117]

MALDI ion sources are particularly well suited for integration with a ToF analyser due to the pulsed laser action providing discrete ion packets. Indeed, the Autoflex II ToF/ToF (Bruker Daltonics Ltd) utilised for MALDI MS throughout this PhD research utilises a ToF mass analyser. The ToF analyser in this particular instrument can be used as a linear ToF analyser when studying analytes of high m/z so as to increase the instrument mass range and improve sensitivity. Alternatively, if analytes of m/z less than 10,000 amu are studied, reflectron mode

can be applied to the ToF increasing resolution and mass accuracy of the resulting data.

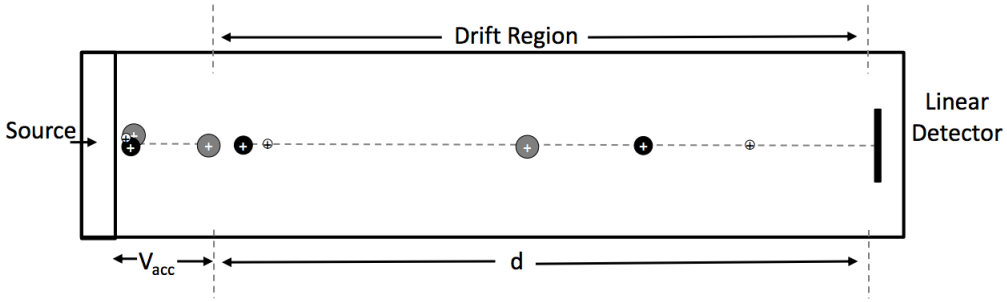

Figure 2.9 Schematic of a linear time of flight (ToF) mass analyser.[107]

2.3.3 QToF Mass Analysers

Mass analyser power and performance can be increased by combining multiple analyser types within one mass spectrometer, termed a hybrid mass analyser.[117,119] One example of this is the Synapt G2-S (Waters Corp., UK) utilised throughout this research. The Synapt G2-S (Waters Corp., UK) contains a QToF mass analyser, a hybrid which combines a quadrupole and a ToF analyser. The quadrupole analyser, labelled in Fig. 2.10, can be utilised to transmit ions in RF only mode, or to isolate a known m/z in single ion monitoring mode for MSMS analysis. In addition, the Synapt G2-S (Waters Corp., UK) contains a ToF mass analyser, labelled in Fig. 2.10. The ToF analyser in the Synapt G2-S (Waters Corp., UK) is preceded by a perpendicular pusher. The pusher uses orthogonal acceleration to convert the continuous stream of ions produced by the ESI ion source into the discrete ion packets required for a ToF analyser.[120] Three reflectron ion mirrors are present in the Synapt G2-S (Waters Corp., UK) ToF analyser. If all three are used, a W ion path configuration is achieved, effectively lengthening the drift tube and improving resolution. Alternatively, the analyser can be used with only one reflectron in which case a V ion path is followed. This pathway instils the mass analyser with less resolving power, however the sensitivity of the instrument is increased due to reduced ion loss.

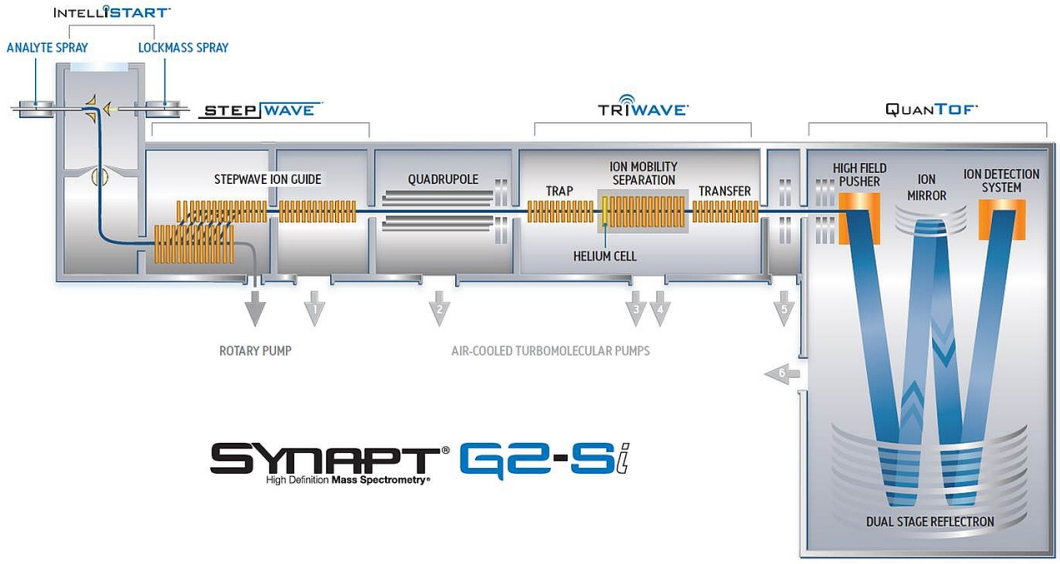

Figure 2.10 Schematic of Waters Synapt G2-S courtesy of Waters Corp., UK.

2.4 Tandem Mass Spectrometry

Tandem mass spectrometry (MSMS) is a technique utilised by mass spectrometrists in order to glean further structural and elemental information about an analyte, enabling improved characterisation.[81,92,94] MSMS proceeds by the selection and isolation of a precursor ion of interest, followed by bond dissociation and thus fragmentation of the precursor ion into product ions and neutral losses. Fragmentation is achieved by increasing the internal energy of the ion using mechanisms such as photodissociation, the introduction of electrons to the trapped ions, or collisions between ions and uncharged molecules. Examples of fragmentations techniques include Collision Induced Dissociation (CID)/Collisionally Activated Dissociation (CAD), Electron Capture Dissociation (ECD), Infrared Multiphoton Dissociation (IRMPD), and Electron Transfer Dissociation (ETD).[121] MSMS analyses are routine across many industries due to their highly informative nature and reproducibility providing a fingerprint for known molecules. Biomarker monitoring and drug test screening are particularly common examples.

MSMS analyses can be carried out such that the two key steps, precursor ion isolation and fragmentation, are separated either by space or by time. Instruments whereby stages are separate events in time, including FT-ICR analysers and Paul traps, are able to perform multiple MSMS cycles such that higher order MS^n spectra can be obtained.[90,91] By contrast, instruments whereby each stage of the process is spatially separated, are limited in the number of MSMS cycles that can be carried out by the physical locations available within

the instrument to perform the required steps.[117] The MSMS analyses carried out throughout this research are performed on the Synapt G2-S (Waters Corp., UK), an MSMS in space instrument. MSMS analyses up to MS^3 are possible utilising the Synapt G2-S (Waters Corp., UK) instrument platform, due to the presence of two T-wave collision cells.[122] These collision cells, termed the trap and transfer respectively, are stacks of ring electrodes with opposing RF voltages applied to adjacent electrodes. Application of a DC voltage to the system creates a travelling wave, propelling ions through a inert buffer gas towards the cell exit. The precursor ion isolation step required prior to these collision cells can be carried out in either the quadrupole, the ion mobility cell, or both. Pseudo-MS^4 analyses are also possible for the Synapt G2-S (Waters Corp., UK), if the initial MSMS cycle is performed by applying a high capillary voltage to unstable ions in the ESI source, resulting in in-source fragmentation.

The Synapt G2-S (Waters Corp., UK) is equipped to perform MSMS analyses using both CID and ETD fragmentation mechanisms. However, since ETD requires multiply charged precursor ions, it is deemed inappropriate for the analyses performed herein. CID MSMS analysis, involves colliding precursor ions of high kinetic energy with neutral inert gas molecules.[123] Inelastic collisions between these two entities allows energy transfer from the gas molecules to the ions, creating a vibrationally excited ion intermediate. This high internal energy redistributes throughout the precursor ion, causing unimolecular dissociation of the weakest bonds within the ion, and thus forming product ions. Quasi-Equilibrium Theory (QET) informs that this redistribution of energy proceed via all available degrees of freedom, and that the bond dissociation is unidirectional thus non-reversible. To this end, instrument parameters are vital in determining the range of product ions formed by CID, and thus their informational value. Altering the DC voltage in the Synapt G2-S (Waters Corp., UK) collision cells can increase the velocity of the ions entering, promoting ion collisions with the gas molecules. Additionally, buffer gas type and pressure are important, with gases of larger cross-sectional area at higher pressure increasing the likelihood of ion collisions. Further, gases of larger cross sectional area transfer more energy in any given collision than a small gas molecule, allowing bond dissociation through higher energy pathways.[119] An example of one such high energy fragmentation pathway is the dissociation of bonds within a stable aromatic structure.

2.4.1 Tandem Mass Spectrometry of Peptides

MSMS is a useful and informative mechanism for peptide sequencing and the elucidation of structural information, whilst maintaining both speed and sensitivity of analysis.[49,114,124,125]

Peptides are predictable in their MSMS fragmentation patterns, with the peptide backbone bonds known to preferentially dissociate. This predictability gives rise to a widely accepted nomenclature for peptide ion fragments, as shown in Fig. 2.11. According to this nomenclature, *N*-terminal fragments are known as **a**, **b**, and **c** product ions, whereas *C*-terminal fragments use the labels **x**, **y**, and **z**.[47] CID favours the formation of **b** and **y** ions which form as a result of amide bond dissociation along the peptide backbone, separating off one amino acid at a time. This fragmentation allows the amino acid sequence of the peptide to be determined, along with the positions of any post-translational modifications (PTM). However, complexity can arise when amino acids of equivalent *m/z* are present in the peptide sequence, such as leucine (L) and isoleucine (I). In this case, increased sequence coverage and fragmentation can be achieved by the selection of a higher charge state precursor ion, which tend to exhibit more instability.[126,127] Alternatively, use of CID in combination with other ion fragmentation mechanisms can prove successful in increasing sequence coverage and ion types.

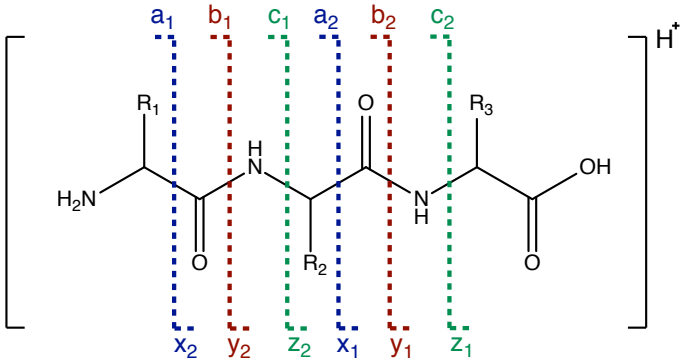

Figure 2.11 Characteristic peptide CID MSMS fragmentation ions.[47]

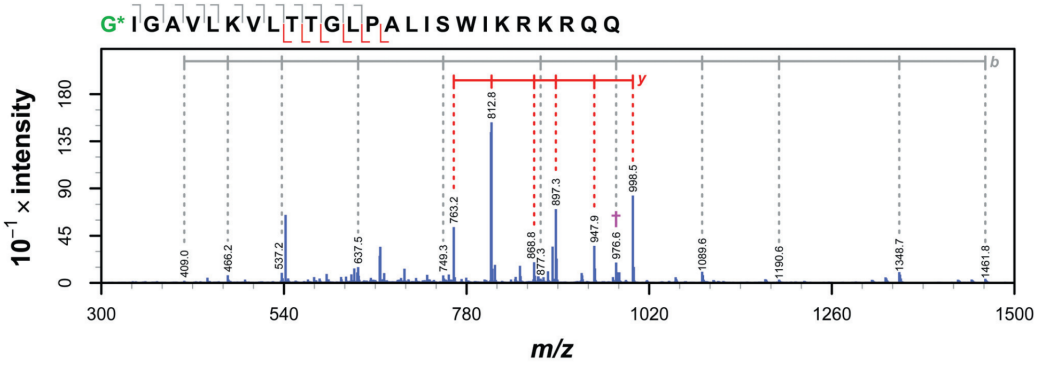

Figure 2.12 CID MSMS of palmitoyl melittin precursor ion *m/z* 772.0 showing key **b** and **y** ions used to distinguish modification position at the *N*-terminus.[44]

Fragmentation of intrinsically lipidated melittin is one example where MSMS of peptides has proved vitally important in relation to this research project in the past. MSMS has been used to determine the location of acyl chain modifications on melittin amino acid side chains. As

Fig. 2.12 shows, observation of **b** and **y** ions in the CID spectrum allows for the position of the modification to be placed within the two *N*-terminal amino acids.[11,44] *N*-terminal $\mathbf{b_1}$ ions are rarely observed in CID spectra due to the relatively small *m/z* and preferential stability of the $\mathbf{b_2}$ ion. Thus observation of the $\mathbf{b_2}$ ion combined with chemical knowledge and intuition must be utilised in order to determine the position of the modification as the *N*-terminal amine.

2.4.2 Tandem Mass Spectrometry of Small Molecules

MSMS of small organic molecules comprises a large proportion of research in the field of mass spectrometry, due to the importance of the technique in providing structural and elemental characterisation information.[100,117,128] Key applications include differentiation of isomers, identification of unknown analytes, biomarker identification, and reaction monitoring. MSMS of known small molecules by the same fragmentation mechanism is highly reproducible, resulting in a fingerprint unique to that molecule. To this end, certain molecule classes have known product ions. For example, CID of a diacyl phospholipid produces a product ion corresponding to the phosphate head group, allowing for identification of phospholipid class.[41] Similarly, sugar rings are observed to fragment depending upon the orientation of groups axial or equitorial to the ring, differentiating between isomers.[129]

Due to significant structural differences between small molecules, their fragmentation patterns are less predictable and systematic than those of peptides. However, it is possible to identify some key trends in product ion formation by MSMS in order to simplify data interpretation.[102] Common cleavages in small molecule MSMS occur at locations in which the charge can be stabilised by the surrounding groups, due to their electron withdrawing or electron donating nature. Weak carbon-heteroatom bonds often dissociate for this reason, since heteroatoms aid in charge stabilisation.[130] In fact, certain species have been identified as having a high probability of being eliminated by MSMS: (i) neutral losses including H_2O, CO_2, NO_2, SO_2, and HX where X is a halide; (ii) radicals such as $OH^{\cdot}$, $CO^{\cdot}$, $NH_2^{\cdot}$, and $X^{\cdot}$; (iii) charged species including PO_3^{3-}.[131,132] It is worth noting that due to the high energy required to separate an electron pair, even electron precursor ions prefer to fragment into even electron product ions rather than radicals. By contrast, highly stable structures such as aromatic rings are unlikely to fragment, and are thus expected to carry through from precursor to product ions. In some cases MSMS results are complicated when bond breakage within a precursor ion results in a subsequent rearrangement of the structure in order to stabilise the product ion.

2.5 Ion Mobility Mass Spectrometry

Ion mobility mass spectrometry (IMMS) is a technique combining mass spectrometry with ion mobility spectrometry.[93,133] Since taking off in popularity in the 1990s, the technique has found applications in a range of fields including proteomics, metabolomics and lipidomics.[94,134–137] Ion mobility spectrometry is a method of separating gas phase ions depending upon their mobility in a carrier gas through a mobility cell. The speed of mobility through the cell is altered by the size and shape of the ions, and thus mobility can be related to the collision cross section (CCS) of the ion.[138,139] Ion mobility provides an added dimension to mass spectrometric analysis, providing both structural information about an ion and an alternative mechanism of separation for ions of similar structure or functionality, for which classic GC or LC separation is challenging.

The Synapt G2-S (Waters Corp., UK) utilises travelling wave ion mobility spectrometry (TWIMS) to achieve ion mobility separation.[122] TWIMS has been utilised in combination with mass spectrometry since 2006, and is best understood from its basis in drift tube ion mobility spectrometry (DTIMS). DTIMS separates ions by introducing them into a helium filled drift tube mobility cell with a constant electric field applied across the cell. Ions travel through the drift tube propelled by the electric field, however they are slowed down by collisions with the gas. Statistically ions of smaller size and shape undergo fewer collisions with gas molecules, and thus are considered to have greater mobility. The combination of propulsion by the field and deceleration by the gas results in an overall velocity specific to that ion. As such, different ions travel through the cell at different velocities, reaching the exit at different times. In this way, ions are separated and their CCS can be calculated from their specific time taken to travel through the mobility cell.

TWIMS uses a similar design to DTIMS, based upon ions moving through a gas filled drift tube.[140] However, instead of a uniform electric field being applied across the whole cell, a TWIMS cell is comprised of a series of stacked ring electrodes of alternating fields. Opposing RF waveforms are applied to adjacent rings, which when combined with the movement of a DC potential from one ring to the next, creates a moving electric field or travelling wave. In portions of the cell with a positive electric field, ions separate based upon their mobility by the same mechanism as is observed for DTIMS. However, improved separation is achieved through the wave formed in the regions with diminished electric field. Ions of high mobility spend more time at the crest of the wave due to their increased velocity, thus "surf" the wave

and move through the cell quickly. By contrast, ions with lower mobility roll over the wave and are carried along, slowing their motion through the mobility cell. Speed and magnitude of the travelling wave can be tuned, affording improved control over ion mobility separation to the user. Following calibration, travel time through the TWIMS mobility cell can be used to calculate ion CCS.

Several examples of IMMS using TWIMS exist which bear relevance to the research presented throughout this thesis. Notably, IMMS has been utilised to separate out complex samples of cellular phospholipids. Unlike traditional LC separation, optimised ion mobility is able to separate phospholipids with only minor structural differences such as *cis* or *trans* nature of a double bond, double bond position, and carbon chain length.[141–144] Further, IMMS has been documented to separate peptides with minor structural variations in PTM location, and even interactions of non-covalently bound drug or co-factors.[8,145,146] Small molecule IMMS is also evident in current literature, with separation of isomers a key focus.[134,135,147] One theme evident throughout all IMMS applications is that optimisation of instrument parameters is vital for successful mobility separation.

3 | Analytical Techniques for Study of Intrinsic Lipidation

3.1 Introduction

Mass spectrometry provides a reliable and informative analytical technique for study of innate reactivity at the membrane interface. Applicable to both peptide and small molecule systems, LCMS facilitates identification and characterisation of acylated reaction products and lysolipid by-products.[39,77] Unfortunately, study of intrinsic lipidation by mass spectrometry also has limitations. The required chromatographic separation of reaction mixture components prior to analysis prevents high throughput study or on-line reaction monitoring. Product quantification, necessary for kinetics determination, proves challenging and requires additional synthetic and analytical steps. Furthermore, mass spectrometry of accurate biological models containing high lipid concentrations prevents visualisation of low abundant products without undesirable side effects, such as column overload or detector saturation. It is therefore desirable to examine alternative analytical techniques, in order to determine their feasibility for study of intrinsic lipidation. The work undertaken within this chapter covers two experimental approaches for study of intrinsic lipidation, with differing desired outcomes. The first approach aimed to investigate methodologies for identifying membrane reactivity through routine high throughput screening of reaction mixtures. The second approach investigated analytical techniques which could be employed for the robust and informative study of more accurate biological models. It was hoped that these methodologies may provide complementary information to mass spectrometry analysis, for example informing on reaction kinetics.

3.2 Routine Reaction Monitoring

Identification and development of analytical techniques for routine monitoring of intrinsic lipidation at the membrane interface was conducted. Desirable techniques exhibit robust and reliable sample analysis in a quick high throughput manner. Techniques adaptable to automated or on-line reaction monitoring provide additional benefits for future exploitation. Ideal analytical methods require minimal sample modification and preparation prior to use, and are applicable to multiple systems including peptides and small molecules. Techniques are not required to be deeply informative, as samples of interest can be taken forward for analysis by mass spectrometry whilst minimising time and solvent wastage. Solution state NMR, fluorescence spectroscopy, and TLC were identified as analytical techniques meeting these requirements. Candidate methods were therefore tested in order to further determine their success and applicability.

3.2.1 Solution State NMR

In principle, solution state NMR provides an efficient and reliable methodology for routine study of intrinsic lipidation. Additional desirable attributes, such as automation and simplistic quantification using peak integrations, can also be attributed to the technique.[148,149] However, solution state NMR monitoring of peptides, small molecules or their acylated analogues within complex biological matrices is impractical due to technique sensitivity limits. Furthermore, peptide and protein NMR is complex to analyse and interpret, preventing high throughput routine analysis.[150–152] Monitoring lysolipid by-product formation by solution state NMR provides a practical alternative for studying intrinsic lipidation. Background phospholipid hydrolysis has previously made lysolipid monitoring an unreliable method for analysing intrinsic lipidation. However, NMR facilitates total speciation, such that lysolipid production attributed to background hydrolysis can be subtracted following quantification of fatty acid by-product. Lysolipid levels resulting from intrinsic lipidation can thus be determined, identifying and quantifying reactivity.[153]

Initially, sensitivity limits of solution state NMR were tested in order to determine applicability of the technique to the study of intrinsic lipidation. Experimental focus was upon confirming whether sufficient proportions of phospholipid, lysolipid and fatty acid exist within reaction mixtures to facilitate solution state NMR study. POPC liposomes, utilised for study of intrinsic lipidation *in vitro*, were prepared in buffer (90 mM NaCl, 10 mM $NaHCO_3$, pH 7.4) at

reaction mixture concentration 0.02 mg mL^{-1}. Modelling intrinsic lipidation and background hydrolysis, liposomes were divided into triplicate portions prior to addition of 5 mol% lysolipid OPC or palmitic acid. Samples were lyophilised and re-suspended in deuterated solvents required for NMR analysis. Selected solvents include $CDCl_3$, MeOD, D_2O, $CDCl_3$:MeOD (1:1) and MeOD:D_2O (1:1). Detection of POPC, or less concentrated counterparts OPC and palmitic acid, by solution state NMR proved impossible under the applied conditions. Solution state NMR was thus deemed insufficiently sensitive for study of intrinsic lipidation, and was not pursued for future routine reaction monitoring.

3.2.2 Fluorescence Spectroscopy

Fluorescence spectroscopy is a diverse biophysical technique with applications in the study of multiple biological systems. Phospholipid aggregates are one such system, with fluorescence spectroscopy providing insights into membrane organisation, structure and dynamics.[7,57,154] Study is facilitated by an extrinsic fluorescent probe exhibiting similar physical characteristics to natural phospholipids, for example a cationic fluorophore with two saturated aliphatic tails. Indirect intrinsic lipidation monitoring of lysolipid reaction by-products has been conducted using rapid fluorescence spectroscopy, with limited success. Liposomes were prepared from fluorescent phospholipid BODIPY PC-A2 (1-O-(6-BODIPY™ 558/568-Aminohexyl)-2-BODIPY™ FL C5-Sn-Glycero-3-Phosphocholine), Fig. 3.1, containing FRET donor-FRET acceptor acyl chains.[153] Reduced FRET was observed in the presence of small molecules, indicative of acyl chain cleavage and lysolipid formation. However, study of intrinsic lipidation by lysolipid abundance is deemed inaccurate without background hydrolysis correction. Furthermore, fluorescent phospholipid analogues are noted to modify membrane structure and dynamics, which may alter behaviour and reactivity at the membrane interface.[154,155] As a result, intrinsic lipidation study using extrinsic fluorescence probes was not considered a suitable method for routine high throughput analysis of intrinsic lipidation.

Harnessing intrinsic molecular fluorescence provides an alternative pathway for fluorescence study of intrinsic lipidation. Aromatic rings, including those within amino acids such as tryptophan and cationic amphiphilic small molecules, exhibit natural fluorescence.[156–158] Their fluorescence wavelength is dependent upon external environment, with hydrophobic environments producing a blueshift in fluorescence wavelength. As a result, emission wavelength of a parent molecule would be expected to differ from that of its increasingly hydrophobic acylated analogue, formed following intrinsic lipidation. Observed emission intensity ratios

could therefore inform upon the presence and extent of species reactivity at the membrane interface.

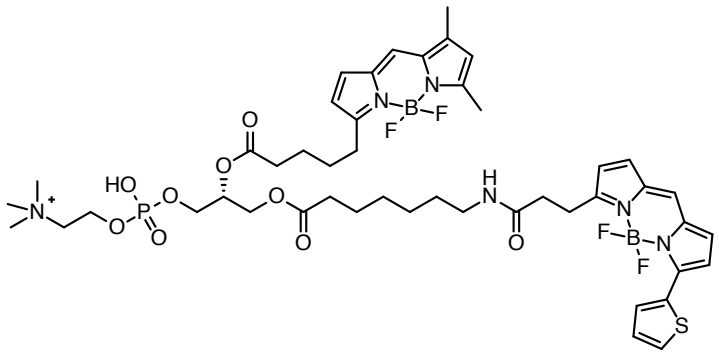

Figure 3.1 Structure of BODIPY PC-A2, containing FRET donor-FRET acceptor acyl chains.

Viability of fluorescence spectroscopy for monitoring intrinsic lipidation was tested using extensively studied model peptide melittin.[159,160] Emission spectra were obtained using a 280 nm excitation wavelength, for unmodified melittin and four synthetically acylated analogues. Acylated peptides containing a palmitoyl or oleoyl acyl chain modification at either the *N*-terminus or K23. Differential emission spectra were observed for modified and unmodified melittin, highlighted by emission maxima presented in Table 3.1, and comparison of melittin and *N*-oleoyl melittin in Fig. 3.2. Acylated peptides all exhibit an emission maximum close to 355.5 nm, blueshifted compared to unmodified melittin at 362.5 nm. Although minor, variation in emission maxima are sufficient to distinguish between modified and unmodified species. However, it is unclear whether the observed blueshift is a direct consequence of lipidation caused by increased peptide hydrophobicity, or a secondary consequence of lipidation, such as folding.

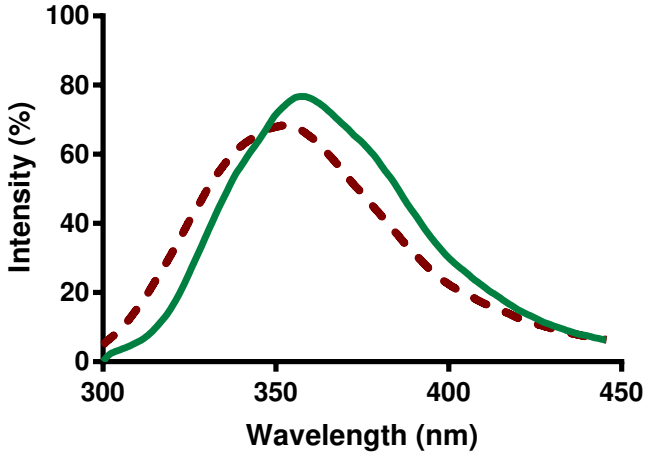

Figure 3.2 Emission of 10 µg mL^{-1} melittin (solid green line) and *N*-oleoyl melittin (dashed red line) in aqueous buffer solution (90 mM NaCl, 10 mM $NaHCO_3$, pH 7.4) following excitation at 280 nm.

Peptide	Emission Maximum (nm)
Melittin	362.5
N-palmitoyl melittin	355.5
K23-palmitoyl melittin	355.5
N-oleoyl melittin	354.5
K23-oleoyl melittin	356.5

Table 3.1 Emission maxima for solution phase melittin analogues based upon tryptophan emission following excitation at 280 nm.

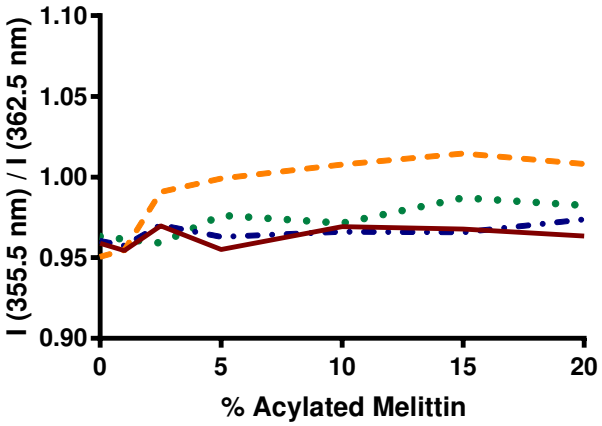

Figure 3.3 I(355.5 nm)/I(362.5 nm) ratio for solution phase melittin upon addition of differing molar % of: *N*-palmitoyl melittin (solid red); K23-palmitoyl melittin (dashed orange); *N*-oleoyl melittin (dotted and dashed blue); K23-oleoyl melittin (dotted green).

The ratio of emission intensities at 355.5 nm and 362.5 nm (I(355.5 nm)/I(362.5 nm)) was calculated for solutions of melittin plus between 0 mol% and 20 mol% acylated melittin, in order to establish a correlation between extent of acylation and I(355.5 nm)/I(362.5 nm) ratio. Despite indications of a slight upward trend, shown in Fig. 3.3, insufficient correlation is observed to utilise in the study of intrinsic lipidation. Consistency in I(355.5 nm)/I(362.5 nm) ratio suggests that fluorescence exhibits inadequate sensitivity to detect the presence of low abundance acylated species. Based upon literature precedent, I(336.0 nm)/I(352.0 nm) ratio was also calculated and compared at different molar ratios of acylated melittin, Fig. 3.4.[45] I(336.0 nm)/I(352.0 nm) ratio is widely employed to measure melittin partitioning in environments of differing polarity, for example binding to a liposome in aqueous solution. I(336.0 nm)/I(352.0 nm) ratio exhibits an initial increase correlating with proportion of acylated peptide, followed by a plateau. Significant initial ratio increases in combination with the observed plateau suggests promotion of melittin folding in the presence of acylated melittin, producing a similar emission blueshift. Small quantities of acylated melittin exhibit power to modify bulk peptide solution, preventing accurate calculation of the proportion of acylated

species from I(336.0 nm)/I(352.0 nm) ratio. Associated data complexity, combined with additional challenges upon inclusion of a membrane, suggest intrinsic fluorescence is unsuitable for routine monitoring of intrinsic lipidation.

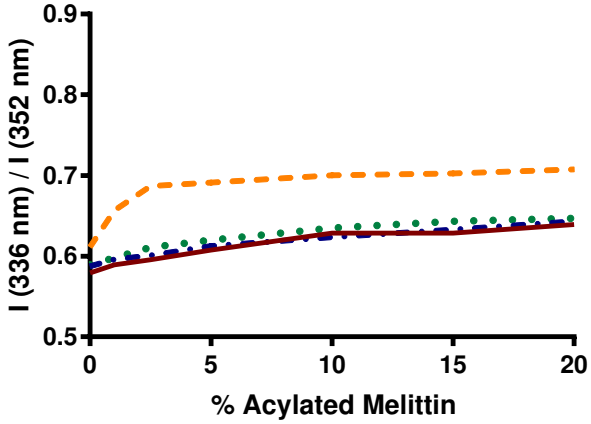

Figure 3.4 I(336.0 nm)/I(352.0 nm) ratio calculated for solution phase melittin upon addition of differing molar % of: *N*-palmitoyl melittin (solid red); K23-palmitoyl melittin (dashed orange); *N*-oleoyl melittin (dotted and dashed blue); K23-oleoyl melittin (dotted green).

3.2.3 Thin Layer Chromatography

Thin layer chromatography (TLC), routinely used for reaction monitoring in organic chemistry, provides an alternative technique for intrinsic lipidation study.[161–163] Normal phase (NP) TLC has been reported for the study of peptide intrinsic lipidation, following optimisation of solvent systems and visualisation techniques.[41] However, TLC study focussed upon monitoring lysolipid, an intrinsic lipidation and phospholipid hydrolysis by-product. Lysolipid origin is indistinguishable by TLC, therefore results are not diagnostic of intrinsic lipidation and are of limited use. Furthermore, a time consuming lyophilisation step was required prior to TLC analysis, preventing swift routine reaction monitoring.

3.2.3.1 Normal Phase TLC

Development of an improved TLC methodology for intrinsic lipidation reaction monitoring requires direct visualisation of acylated products, and minimal sample manipulation prior to analysis. NP TLC cannot facilitate these needs for peptides, however small molecules provide a suitable system. Propranolol **1**, along with synthetically acylated analogues *N*-palmitoyl propranolol **12** and *N*-oleoyl propranolol **13**, were selected in order to further examine this possibility.

Development of suitable NP TLC conditions for the study of small molecule intrinsic lipidation began by identification of a sufficiently sensitive visualisation technique.[163] Stock solutions of propranolol **1**, *N*-palmitoyl propranolol **12** and *N*-oleoyl propranolol **13**, were prepared in MeOH at concentration 1.27 mM. A standard volume (1 µL) of each stock solution was applied to a NP TLC plate, and seven visualisation techniques were tested. Results of the screen, summarised in Table 3.2, revealed three techniques to be unsuitable for further study. Ultraviolet (UV) detection did not enable small molecule visualisation, whilst I_2 revealed only *N*-oleoyl propranolol **13** due to the presence of a carbon-carbon double bond. Coomassie staining produced poorly defined spots, making visualisation unclear and challenging.

Visualisation Technique	Response
UV	No spots observed
PMA	Well defined dark blue spots on pale blue background
Ninhydrin	Well defined orange/yellow spots on white background
Coomassie	Poorly defined white spots on blue background
p-Anisaldehyde	Well defined black spots on pink background
I_2	Yellow spots observed for species containing alkene only
$KMnO_4$	Well defined yellow spots on pink background

Table 3.2 Observed visualisation response from different staining techniques during NP TLC analysis of 1.27 mM stock solutions of propranolol **1**, *N*-palmitoyl propranolol **12**, and *N*-oleoyl propranolol **13**.

Sensitivity of PMA, ninhydrin, *p*-anisaldehyde, and $KMnO_4$ staining at relevant reaction mixture concentrations was tested to determine applicability to NP TLC of intrinsic lipidation. Reaction mixture concentration propranolol **1** (127 µM), was spotted onto a TLC plate in quantities from 1 µL up to 20 µL. Visualisation was observed for all four staining techniques down to 1 µL, equal to 0.03 µg of material, suggesting all exhibit suitable propranolol **1** sensitivity. *N*-palmitoyl propranolol **12** and *N*-oleoyl propranolol **13** solutions were prepared at the lower concentration of 1.27 µM. Concentration mimics 1 % conversion of propranolol **1** into acylated product through intrinsic lipidation. Staining of 1 µL to 20 µL quantities with *p*-anisaldehyde proved unsuccessful, due to poor spot clarity compared to the bright pink background colour. Alternative staining techniques indicated weak staining despite low small molecule concentrations, as summarised in Table 3.3. A 1 µL quantity equates to 0.63 ng of *N*-palmitoyl propranolol **12**, and 0.66 ng of *N*-oleoyl propranolol **13**. Generic stain PMA is determined as the most sensitive staining technique, observing *N*-oleoyl propranolol **13** at 2 µL, compared to 13 µL and 5 µL for ninhydrin and $KMnO_4$ respectively. Direct visualisation of acylated propranolol following 1 % conversion provides an excellent basis for study of small molecule intrinsic lipidation. Sufficient sensitivity suggests no need for lyophilisation prior to

analysis, supporting a routine high throughput analytical method.

Visualisation Technique	*N*-palmitoyl propranolol **12**	*N*-oleoyl propranolol **13**
PMA	2 µL	2 µL
Ninhydrin	10 µL	13 µL
$KMnO_4$	3 µL	5 µL

Table 3.3 Summary of the minimum quantity of 1.27 µM solution of *N*-palmitoyl propranolol **12** or *N*-oleoyl propranolol **13** applied to NP TLC plate required for visualisation under different staining techniques. A 1 µL quantity equates to 0.63 ng of *N*-palmitoyl propranolol **12**, and 0.66 ng of *N*-oleoyl propranolol **13**.

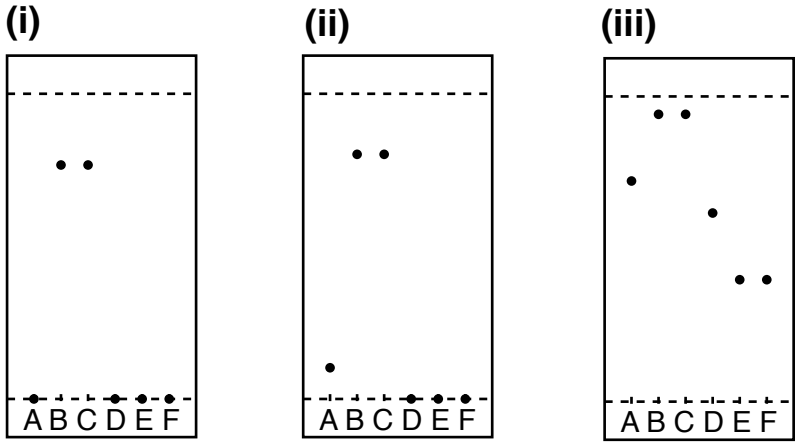

Figure 3.5 NP TLC analysis of small molecule intrinsic lipidation reaction mixture components under three solvent systems: (i) EtOAc:MeOH:$NH_{3\ (14\%\ aq)}$ (98:1:1); (ii) EtOAc:MeOH:$NH_{3\ (14\%\ aq)}$ (38:1:1); (iii) $CHCl_3$:MeOH:H_2O (6:4:1). A = propranolol **1**; B = *N*-palmitoyl propranolol **12**; C = *N*-oleoyl propranolol **13**; D = POPC; E = PPC; F = OPC.

Solvent system optimisation is also required to facilitate study of small molecule intrinsic lipidation by NP TLC. Literature precedent for propranolol **1** TLC reveals three possible solvent systems: (i) Ethyl acetate (EtOAc):MeOH:$NH_{3\ (14\%\ aq)}$ (98:1:1); (ii) EtOAc:MeOH:$NH_{3\ (14\%\ aq)}$ (38:1:1); (iii) $CHCl_3$:MeOH:H_2O (6:4:1).[10,41,164] Propranolol **1** and acylated analogues were studied under these conditions, along with additional reaction mixture components POPC, PPC, and OPC, to identify coelution issues. NP TLC analysis of each solvent system is shown in Fig. 3.5. Phospholipid, lysolipid and propranolol **1** remain on or close to the plate baseline under solvent systems (i) and (ii). Excellent separation between modified and unmodified propranolol **1** is achieved, however overall results are undesirable. Solvent system (iii) exhibits movement and separation of reaction mixture components, although all appear high up the plate. *N*-palmitoyl propranolol **12** and *N*-oleoyl propranolol **13** travel with the solvent front, making visualisation challenging.

Ideal separation was not achieved across three initial solvent systems, therefore system

$CHCl_3$:MeOH:H_2O (6:4:1) was taken forward for further optimisation. Solvent systems of decreased polarity were employed, aiming to retain excellent separation whilst reducing analyte movement up the TLC plate. Modified solvent systems selected were: (i) $CHCl_3$:MeOH:H_2O (12:10:1); (ii) $CHCl_3$:MeOH:H_2O (12:8:1). Results of reaction mixture component separation are depicted in Fig. 3.6, along with initial system $CHCl_3$:MeOH:H_2O (6:4:1) for comparison. Novel solvent systems exhibit excellent separation between propranolol **1** and acylated analogues, combined with distinction between the solvent front and the spots of *N*-palmitoyl propranolol **12** and *N*-oleoyl propranolol **13**. However, clear separation between phospholipid and lysolipid species is evident only under solvent system (ii). Optimum solvent conditions for NP TLC of small molecule intrinsic lipidation were therefore considered to be $CHCl_3$:MeOH:H_2O (12:8:1).

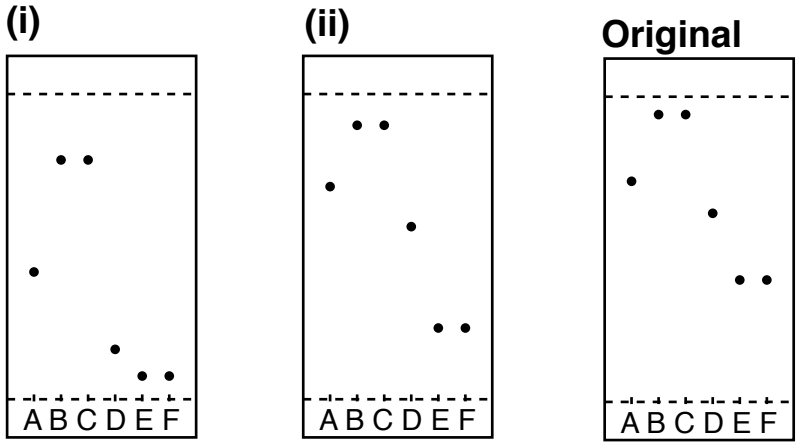

Figure 3.6 NP TLC analysis of small molecule intrinsic lipidation reaction mixture components under two solvent systems: (i) $CHCl_3$:MeOH:H_2O (12:10:1); (ii) $CHCl_3$:MeOH:H_2O (12:8:1); plus original system $CHCl_3$:MeOH:H_2O (6:4:1). A = propranolol **1**; B = *N*-palmitoyl propranolol **12**; C = *N*-oleoyl propranolol **13**; D = POPC; E = PPC; F = OPC.

Optimised solvent system and visualisation method have been determined for study of small molecule intrinsic lipidation by NP TLC. Compared to current mass spectrometry methodology, these conditions facilitate routine, high-throughput reaction monitoring. Additional benefits, compared to previous TLC development, include direct acylated product visualisation down to 1 % conversion, and no lyophilisation requirement prior to analysis. However, whilst optimised conditions are suitable for study of propranolol **1** intrinsic lipidation, they may not apply to small molecules of differing structural and functional features. Testing applicability of conditions to an individual small molecule system would be required prior to analysis of each distinct new molecule.

3.2.3.2 Reversed Phase TLC

Reversed phase (RP) TLC provides an alternative analytical system for routine monitoring of peptide and small molecule intrinsic lipidation through direct product observation.[162,163] RP TLC of peptidic systems was studied using reactive model peptide melittin, in combination with acylated analogues. Correlating with fluorescence studies, acylated analogues utilised were *N*-palmitoyl melittin, K23-palmitoyl melittin, *N*-oleoyl melittin, and K23-oleoyl melittin. 1 µL of 1 mg mL^{-1} stock solution in H_2O was applied to a RP TLC plate for each peptide. Seven visualisation techniques were tested, summarised in Table 3.4, in order to determine stain applicability to study of peptide intrinsic lipidation. Clear, well-defined spots of melittin and acylated analogues were observed for four methods: (i) UV; (ii) ninhydrin; (iii) coomassie; (iv) *p*-anisaldehyde. Furthermore, PMA staining proved successful despite reduced clarity attributed to background interference. Neither I_2 not $KMnO_4$ produced a positive staining result.

Visualisation Technique	Response
UV	Weak glow with well defined spots
PMA	Poorly defined black spots on blue background
Ninhydrin	Well defined yellow/brown spots
Coomassie	Well defined blue spots on white background
p-Anisaldehyde	Well defined purple spots on pink background
I_2	No response
$KMnO_4$	No response

Table 3.4 Observed visualisation response from different staining techniques during RP TLC analysis of 1 mg mL^{-1} stock solutions of melittin, *N*-palmitoyl melittin, K23-palmitoyl melittin, *N*-oleoyl melittin, and K23-oleoyl melittin.

In-depth analysis of stain sensitivity was conducted for the five successful visualisation techniques: (i) UV; (ii) PMA; (iii) ninhydrin; (iv) coomassie; (v) *p*-anisaldehyde. Peptide stock solutions were diluted with H_2O to reaction mixture melittin concentration of 50 µg mL^{-1}. Reaction mixture concentration of acylated melittin is actually predicted to be between 10 and 100 times more dilute than 50 µg mL^{-1}. Using a graduated TLC spotter, peptides were spotted onto a RP TLC plate in quantities from 1 µL up to 20 µL. Visualisation revealed identical staining of melittin and acylated counterparts, attributed to similarities in structure and physical characteristics. Visualisation results, summarised in Table 3.5, indicate a lack of staining sensitivity for all but coomassie. Peptide detection by coomassie is evident down to 4 µL, equivalent to 0.2 µg of material, attributed to increased background contrast provided by the applied destaining step.[165] However, given actual concentrations of acylated peptide are

10 to 100 fold more dilute than $50\,\mu g\,mL^{-1}$, even coomassie detection is insufficiently sensitive for direct study of peptide intrinsic lipidation. Lyophilisation, and subsequent rehydration into a reduced solvent volume, provides a possible answer, however an additional step unfavourably reduces the routine and high throughput nature of analysis.

Visualisation Technique	Minimum Quantity Observed
UV	16 µL
PMA	13 µL
Ninhydrin	13 µL
Coomassie	4 µL
p-Anisaldehyde	14 µL

Table 3.5 Summary of the minimum quantity of $50\,\mu g\,mL^{-1}$ solutions of melittin and acylated melittin applied to RP TLC plate required for visualisation under different staining techniques. A 1 µL quantity equates to 50 ng of peptide.

Development of solvent systems for the study of peptide intrinsic lipidation by RP TLC proved challenging. Multiple applied solvent systems failed to move either melittin or acylated analogues from the TLC baseline. Plate susceptibility towards polar and aqueous solvents suggests that plate silica is insufficiently alkylated to provide suitable analysis of peptide intrinsic lipidation. High performance RP TLC plates, boasting increased alkyl coverage, were purchased as an alternative stationary phase for RP TLC analysis.[166] Increased plate hydrophobicity prevented visualisation by previously optimised aqueous based stains, due to solvent repulsion. Furthermore, plates lack a fluorescent coating, such that UV detection proved impossible. Literature reporting suggests the majority of high performance RP TLC staining techniques to be bespoke and compound specific.[167,168] However, four suitable general staining methodologies were identified:

- PMA in EtOH
- Ninhydrin in *t*-Butanol (*t*-BuOH)
- Ninhydrin in IPA
- Ninhydrin in EtOH

1 µL portions of $1\,mg\,mL^{-1}$ stock solutions in H_2O:EtOH (1:1) of melittin and acylated counterparts were applied to a high performance RP TLC plate. EtOH was required within the stock solution to facilitate application onto the hydrophobic plate. Visualisation was conducted with the four identified high performance RP TLC stains, however insufficient stain sensitivity prevented detection of peptide species.[167,168] Considering TLC analysis was conducted at

stock solution concentration, samples were at least 200 times more concentrated than reaction mixture acylated melittin. Lyophilisation and rehydration are therefore impractical, and RP TLC was not considered viable for routine reaction monitoring of peptide intrinsic lipidation.

Despite minimal success in the study of peptide intrinsic lipidation by high performance RP TLC, the technique may still be applicable to small molecules. In analogous fashion to NP TLC analysis, stain sensitivity was tested using 1.27 mM stock solutions of propranolol **1**, *N*-palmitoyl propranolol **12** and *N*-oleoyl propranolol **13** in MeOH.[167,168] Staining with high performance RP TLC stains revealed successful small molecule visualisation with PMA in EtOH only. Solutions were prepared at reaction mixture concentrations of 127 µM and 1.27 µM, for propranolol **1** and acylated analogues respectively. PMA visualisation of quantities from 1 µL up to 20 µL revealed sufficient stain sensitivity for all species down to 1 µL, equivalent to 0.63 ng of *N*-palmitoyl propranolol **12**, and 0.66 ng of *N*-oleoyl propranolol **13**. Detection is considered ideal for monitoring small molecule intrinsic lipidation through direct product visualisation at 1 % conversion without prior lyophilisation.

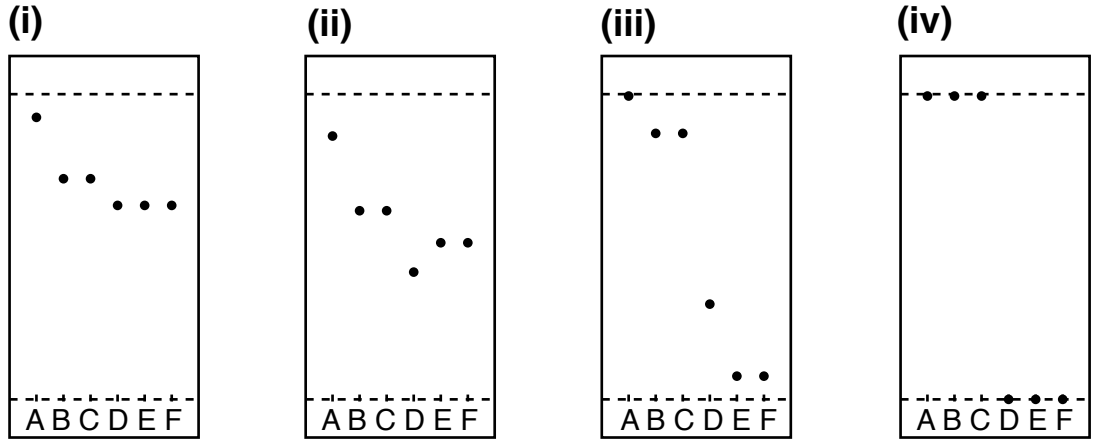

Figure 3.7 High performance RP TLC analysis of small molecule intrinsic lipidation reaction mixture components under four solvent systems: (i) $CHCl_3$:MeOH:H_2O (12:8:1); (ii) $CHCl_3$:MeOH (1:1); (iii) $CHCl_3$; (iv) DCM. A = propranolol **1**; B = *N*-palmitoyl propranolol **12**; C = *N*-oleoyl propranolol **13**; D = POPC; E = PPC; F = OPC.

High performance RP TLC of small molecule intrinsic lipidation also requires development of suitable solvent conditions. Literature precedent suggests four suitable systems: (i) $CHCl_3$:MeOH:H_2O (12:8:1); (ii) $CHCl_3$:MeOH (1:1); (iii) $CHCl_3$; (iv) DCM.[41,165,169] To identify coelution issues, solvent systems were applied to all reaction mixture components, including propranolol **1**, *N*-palmitoyl propranolol **12**, *N*-oleoyl propranolol **13**, POPC, OPC, and PPC. TLC analyses, pictured in Fig. 3.7, suggest DCM is an unsuitable solvent system for intrinsic lipidation study, due to coelution of propranolol **1** and acylated derivatives. Simultaneous baseline retention of phospholipid and lysolipid species further highlights solvent

unsuitability. In contrast, solvent systems (i), (ii), and (iii) facilitate separation of propranolol **1** from acylated analogues. However, poor resolution of multiple species combined with high elution suggest further optimisation is required.

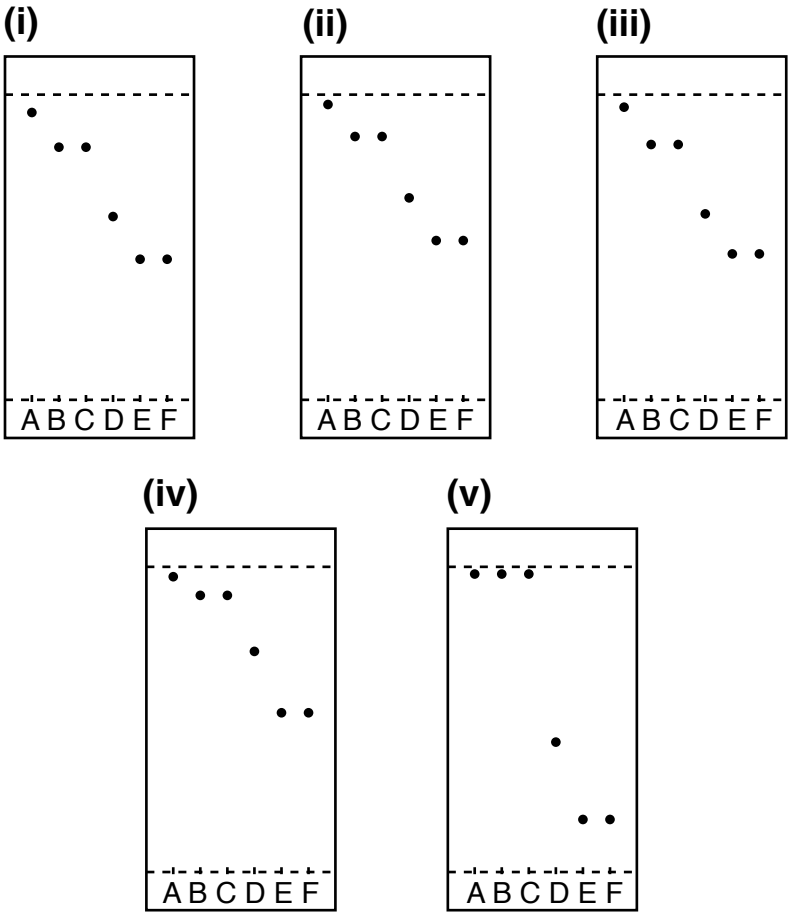

Figure 3.8 High performance RP TLC analysis of small molecule intrinsic lipidation reaction mixture components under five solvent systems: (i) $CHCl_3$:MeOH (6:4); (ii) $CHCl_3$:MeOH (7:3); (iii) $CHCl_3$:MeOH (3:1); (iv) $CHCl_3$:MeOH (8:2); (v) $CHCl_3$:MeOH (9:1). A = propranolol **1**; B = *N*-palmitoyl propranolol **12**; C = *N*-oleoyl propranolol **13**; D = POPC; E = PPC; F = OPC.

Optimisation modified the solvent system $CHCl_3$:MeOH (1:1), aiming to maintain small molecule separation in tandem with reduced movement up the plate, and improved resolution of phospholipid and lysolipid species. Selected solvent systems varied $CHCl_3$:MeOH ratio: (i) $CHCl_3$:MeOH (6:4); (ii) $CHCl_3$:MeOH (7:3); (iii) $CHCl_3$:MeOH (3:1); (iv) $CHCl_3$:MeOH (8:2); (v) $CHCl_3$:MeOH (9:1). High performance RP TLC analyses, shown in Fig. 3.8, indicate excellent separation of phospholipid and lysolipids across all systems, promoted by an increased proportion of $CHCl_3$. However, increased $CHCl_3$ proportion undesirably decreases separation of propranolol **1** from acylated counterparts *N*-palmitoyl propranolol **12** and *N*-oleoyl propranolol **13**. Solvent system $CHCl_3$:MeOH (3:1) facilitates separation of all reaction mixture components, and is thus considered optimum for full small molecule

intrinsic lipidation speciation. However, focussed separation of small molecule components is best achieved by screening with solvent system $CHCl_3$:MeOH (1:1). Solvent system selection dependent upon desired visualisation creates a flexible method of routine reaction monitoring for sensitive study of small molecule intrinsic lipidation.

3.3 In-depth Reaction Monitoring

In-depth study of peptide and small molecule intrinsic lipidation aims to provide insights into reactivity, not obtained through current mass spectrometry methodology. Development of a suitable analytical technique requires identification of an informative methodology, which can provide insight into intrinsic lipidation. Solid state NMR (ssNMR) provides a suitable technique in order to meet the desired outcomes of in-depth monitoring.[170–172] Facilitating continuous speciation, intrinsic structural data, and routine quantification, ssNMR offers potential insights into reaction kinetics and product formation. Furthermore, employment of multiple ssNMR isotopic probes, including ^{31}P and ^{15}N, enables selective visualisation and simplification within complex biological matrices.

Preliminary tests were conducted, in order to determine the feasibility of ssNMR for study of intrinsic lipidation. Reaction mixture concentration ($0.2\,mg\,mL^{-1}$) DPPC liposomes in D_2O prepared by: (i) extrusion; (ii) sonication; were analysed by ^{31}P solid state NMR without success. Comparison to ^{31}P ssNMR standard, phosphoric acid, revealed lack of visualisation could be attributed to a lipid concentration below the detection limit. Liposomes of increased concentration ($2\,mg\,mL^{-1}$) were prepared by both extrusion and sonication, however ssNMR indicated visualisation of sonicated liposomes only. Detection of $2\,mg\,mL^{-1}$ extruded liposomes was prevented by either sample loss during extrusion, or liposome size and physical nature. Additional sonicated DPPC liposomes were prepared at a concentration of $2\,mg\,mL^{-1}$, containing 50 mol% and 5 mol% PPC. Liposomes containing lysolipid aimed to mimic reaction conditions, probing intrinsic lipidation through by-product detection. Visualisation of lysolipid proved successful at 50 mol% and 5 mol% PPC, suggesting suitable sensitivity at the applied concentration for study of intrinsic lipidation.[173]

Initial studies suggest ssNMR monitoring of intrinsic lipidation requires a minimum phospholipid concentration of $2\,mg\,mL^{-1}$. Considering the 1:10 molar ratio of peptide/small molecule:phospholipid employed during study of intrinsic lipidation, high peptide or small molecule concentrations would also be required. Use of increased substrate quantities is

impractical, particularly for peptides, due to being both wasteful and expensive. An alternative experimental approach reduces substrate and phospholipid concentrations required for detection, by employing isotopically labelled analogues. A further benefit of this approach is increased ssNMR sensitivity, facilitated by diagnostic ^{15}N-^{13}C coupling observed only after lipidation. Isotopic labels can be incorporated into small molecules and phospholipids through synthetic preparation.

3.3.1 Isotopically Labelled Small Molecules

Small molecules selected for isotopic labelling, in order to facilitate their study by ssNMR, were propranolol **1** and benzimidazole **11**. Excellent model systems, these small molecules exhibit high propensity towards intrinsic lipidation combined with feasible synthetic preparation and label incorporation. A ^{15}N isotopic label was selected for incorporation into small molecules, positioned at the reactive amine functionality in order to induce the greatest observable shift upon acylation. Development of synthetic methodology was conducted for each small molecule using unlabelled starting materials, then applied to labelled substrates.

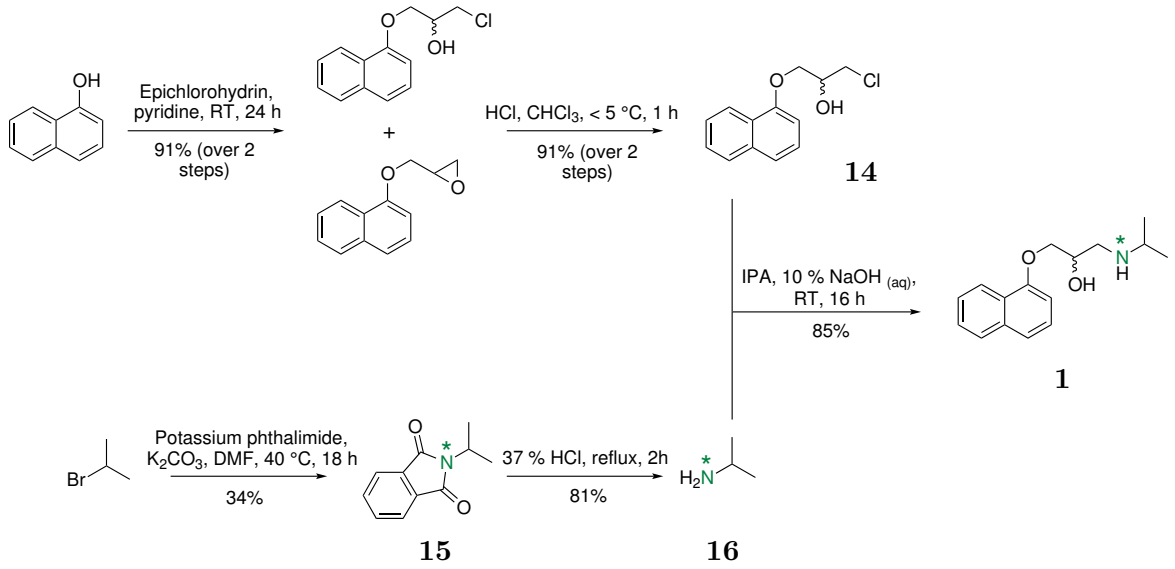

Scheme 3.1 Synthetic protocol for preparation of ^{15}N propranolol **1**. Positioning of ^{15}N label is indicated by **N** and *.

Scheme 3.1 depicts the proposed synthetic protocol for preparation of ^{15}N propranolol **1**, based upon literature precedent.[174] Initial preparation proceeds through substitution of 1-naphthol with epichlorohydrin, resulting in mixed product formation following removal of excess epichlorohydrin by Kugelrohr distillation. Mixed epoxidised and chlorinated products were stirred with HCl in $CHCl_3$ for one hour, in order to drive formation of desired racemic

intermediate **14**. Subsequent reactivity with isopropylamine indicated propranolol **1** formation following TLC monitoring at 16 hours. Excess amine was collected by Kugelrohr distillation, minimising wastage of future labelled material, and desired unlabelled propranolol **1** was isolated by flash column chromatography.

Unlabelled isoproylamine is readily available, however its ^{15}N labelled analogue requires synthetic preparation. Traditional methodology, using ^{15}N ammonia, results in undesirable side product formation, and loss of labelled starting material due to volatility. Alternative methodology, shown in Scheme 3.1, proceeds through formation of ^{15}N isopropylphthalimide intermediate **15** from 2-bromoproprane and ^{15}N phthalimide.[175,176] Subsequent acid cleavage results in formation of the stable HCl salt of ^{15}N isopropylamine **16**, following isolation by freeze drying. ^{15}N isopropylamine **16** reacted with intermediate **14**, successfully resulting in preparation and isolation of ^{15}N propranolol **1**.

The synthetic protocol for preparation of ^{15}N benzimidazole **11** is summarised in Scheme 3.2.[177,178] Successful preparation of unlabelled benzimidazole **11** was achieved, despite slow reaction rate, by refluxing glycine and *o*-phenylenediamine in concentrated HCl for 5 days. However, application of experimental conditions to ^{15}N labelled glycine did not yield labelled benzimidazole **11** formation, even with increased reaction time. Furthermore, troubleshooting did not reveal issues with reaction substrates or conditions. Since reactivity variation cannot be attributed to the presence of a ^{15}N label, the reasons behind this observed lack of reactivity remain a mystery. Inability to optimise reaction conditions on unlabelled substrates prevented further pursuit of ^{15}N benzimidazole **11** synthesis, preventing wastage of expensive labelled material.

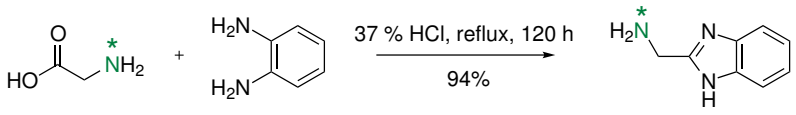

11

Scheme 3.2 Proposed synthetic route for preparation of ^{15}N benzimidazole **11**. Positioning of ^{15}N label is indicated by **N** and *.

3.3.2 Isotopically Labelled Lipids

Preparation of bespoke isotopically labelled small molecules may facilitate ssNMR analysis, however this approach was not deemed practical for all small molecules, or for peptides. Synthesis of ^{13}C labelled phospholipids provides a more versatile alternative to isotopic label

incorporation, facilitating study of intrinsic lipidation by ssNMR. The optimum position for ^{13}C phospholipid labelling is at the carbonyl moiety of reactive ester linkages, facilitating shift observation resulting from acyl transfer. Development of synthetic methodology was conducted for each phospholipid using unlabelled starting materials, then applied to labelled substrates.

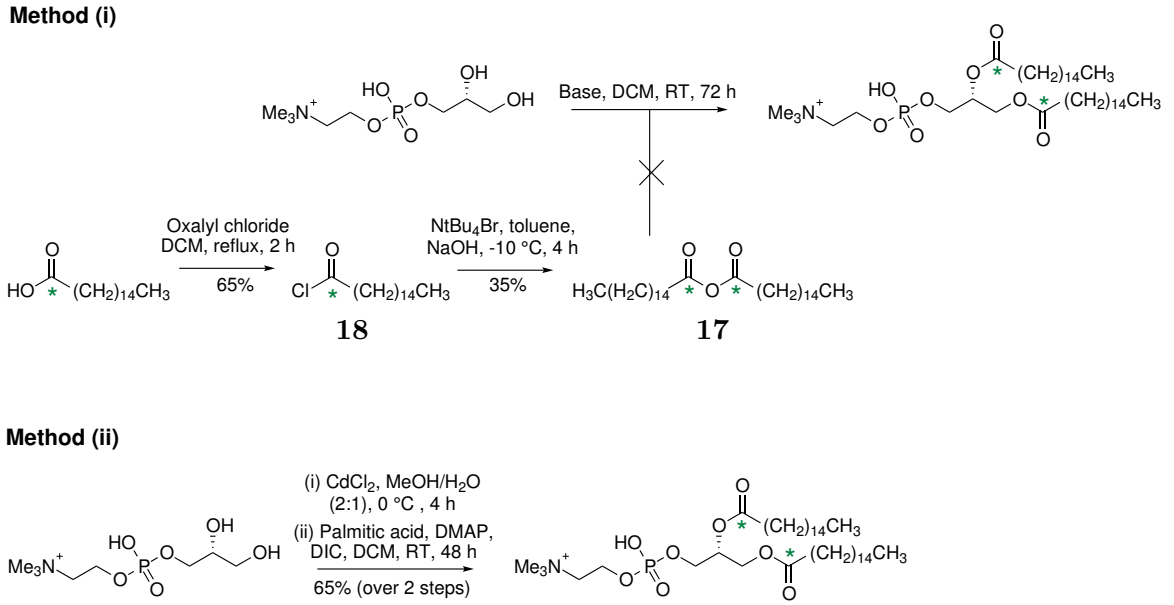

Scheme 3.3 Two proposed synthetic methods for the preparation of ^{13}C labelled DPPC. Positioning of ^{13}C labels are indicated by *.

The simplest phospholipids for synthetic preparation are 1,2-diacyl-*sn*-glycero-3-phosphocholines, containing two identical acyl chains, in combination with a eukaryotic PC head group. Synthetic methodology was therefore developed for production of doubly labelled ^{13}C DPPC based upon literature precedent, as summarised in Scheme 3.3 (i).[179–181] Palmitic anhydride **17** was successfully prepared in high yield from palmitic acid and palmitoyl chloride **18**. However, subsequent conversion from palmitic anhydride **17** into DPPC proved unsuccessful when using either pyridine or 4-dimethylaminopyridine (DMAP) as the base. Employing an alternative literature method, shown in Scheme 3.3 (ii), proved more successful.[182–184] Following glycerophosphocholine (GPC) activation as a GPC-$CdCl_2$ complex, reactivity with 4 equivalents of palmitic acid resulted in production of unlabelled DPPC, purified by trituration. Considering the expense of isotopically labelled molecules, the reduced palmitic acid manipulation prior to reaction with GPC is favourable. Minimising equivalents of palmitic acid from 4 to 2.5 aimed to further prevent wastage of isotopically labelled substrate, however the concurrent reduction in DPPC yield prevented further pursuit. Doubly labelled ^{13}C DPPC was therefore synthesised in high yield and purity by following the synthetic route described in Scheme 3.3 (ii).

The measured DPPC transition temperature of 41 °C places it within the gel phase under physiological conditions, believed to reduce intrinsic lipidation reactivity.[59] Doubly labelled ^{13}C DOPC therefore provides an improved phospholipid for study of intrinsic lipidation by ssNMR. Preparation of unlabelled DOPC was successfully attempted using optimised methodology developed for DPPC synthesis, shown in Scheme 3.4.[182–184] Synthesis was replicated using ^{13}C oleic acid, resulting in formation of doubly labelled ^{13}C DOPC. However, the low product yield of doubly labelled ^{13}C DOPC prevented complete product isolation and characterisation.

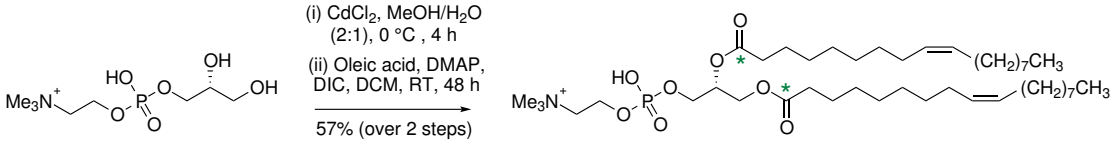

Scheme 3.4 Synthetic route for preparation of ^{13}C labelled DOPC. Positioning of ^{13}C labels are indicated by *.

Isotopically labelled mixed acyl phospholipids are also of interest for the study of intrinsic lipidation by ssNMR, to inform upon preferential acyl chain transfer. Synthesis of mixed acyl phospholipid POPC requires selective *sn*-1 palmitoylation and subsequent *sn*-2 oleoylation. Commercial POPC preparation proceeds by diacyl phospholipid synthesis followed by enzymatic *sn*-2 cleavage. However, this synthetic method is unsuitable for the synthesis of isotopically labelled species due to waste of ^{13}C labelled fatty acids. Scheme 3.5 depicts an alternative synthetic protocol for POPC preparation, exploiting dibutyltin oxide coordination to GPC in order to achieved selective *sn*-1 acylation.[183,185,186] Isolation of lysolipid intermediate **19** from excess tin proved impossible, and therefore was avoided by adopting a one pot synthesis. Oleoyl chloride **20** addition to the reaction mixture resulted in tin displacement, forming POPC, however product characterisation suggests excess tin remains following purification.

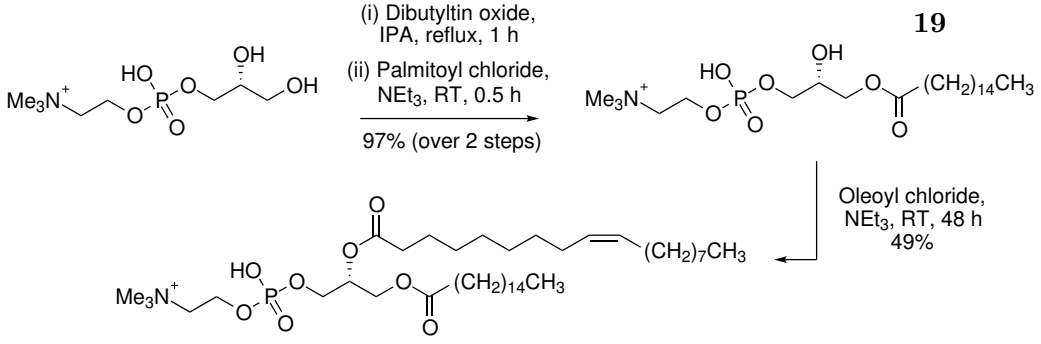

Scheme 3.5 Synthetic method for preparation of mixed-acyl lipid POPC.

Distinguishing between palmitoyl and oleoyl transfer from POPC by ^{13}C ssNMR requires differential acyl chain labelling. Single ^{13}C labelling of acyl chain ester moieties, exhibited in

commercially available products, results in comparable ssNMR shifts, preventing determination of transfer origin. Incorporation of one singly labelled acyl chain, and one doubly labelled acyl chain overcomes this issue. Synthetic preparation of doubly ^{13}C labelled palmitic acid ethyl ester **21** was therefore attempted, following Scheme 3.6 methodology to incorporate labels at positions 1 and 2.[187,188] Ethylbromoacetate **22** preparation was carried out from bromoacetic acid starting material, due to its commercial availability in the doubly ^{13}C labelled form. Bromoacetic acid was converted into acid chloride **23**, then esterified in the presence of excess EtOH. Oxalyl chloride removal *in vacuo* prior to esterification is key in order to prevent formation of oxalic acid ethyl ester, resulting in challenging product purification.[189] Catalyst **24** was simultaneously prepared in high yield and purity, however subsequent reactivity with ethylbromoacetate **22** proved unsuccessful in synthesising intermediate **25**.[190] The adopted synthetic pathway therefore did not proceed further into the synthesis of intermediate **26**, palmitic acid, or their ^{13}C labelled counterparts.

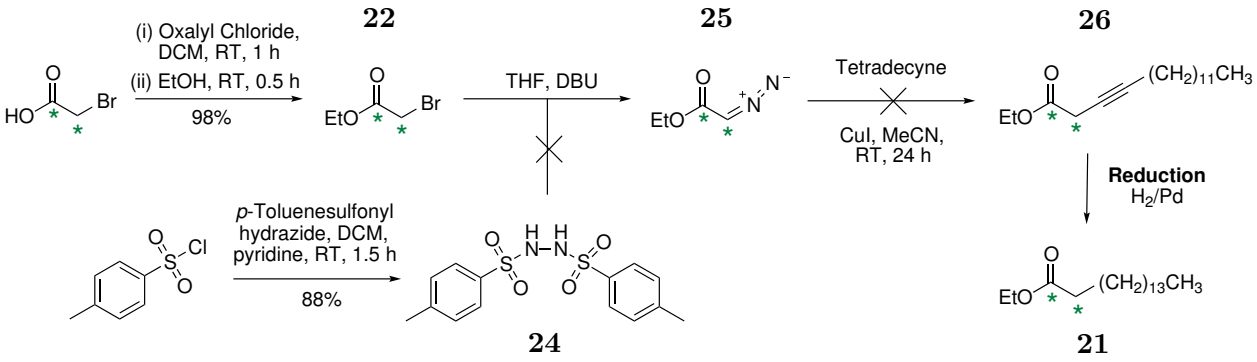

Scheme 3.6 Procedure designed for the synthesis of palmitic acid ethyl ester **21**. Positioning of double ^{13}C labels are indicated by *.

Preparation of doubly labelled ^{13}C oleic acid provides an alternative substrate for synthesis of POPC containing distinguishable acyl chains. Scheme 3.7 presents the proposed synthetic pathway to be adopted, designed with late label incorporation to prevent wastage. Initial coupling of 1-decyne and 1,6-dibromohexane successfully produced intermediate **27** in high yield, following purification by distillation. Subsequent synthesis of intermediate **28** using a modified Reformatsky methodology proved unsuccessful, due to the challenging nature of alkyl bond formation. Suzuki coupling provides an alternative synthetic pathway, requiring preparation of a 1-pinacolborane-7-hexadecyne **29** intermediate.[191–193] Optimisation of palladium catalyst, phosphine derivative and salt content facilitated successful synthesis of intermediate **28** via 1-pinacolborane-7-hexadecyne **29**.[194] Compound purification was complicated by excess B_2pin_2, requiring an ethanolamine wash or vacuum distillation prior to flash column chromatography.

Reduction of the alkyne moiety of intermediate **28** to the *cis* alkene present in oleic acid requires Lindlar's catalyst and H_2. Literature precedent suggested a solvent system of EtOH:hexane, however reduction proved unsuccessful under these conditions, attributed to poor substrate solubility.[195,196] Reduction of intermediate **28** in EtOAc, suitable for solubility and hydrogenation, also proved unsuccessful, returning only starting material. Increased quantities of starting material **28** were required to conduct further optimisation of reduction conditions. However upon repetition of Suzuki protocol, desired product **28** was not produced, preventing further pursuit of doubly labelled ^{13}C oleic acid synthesis.

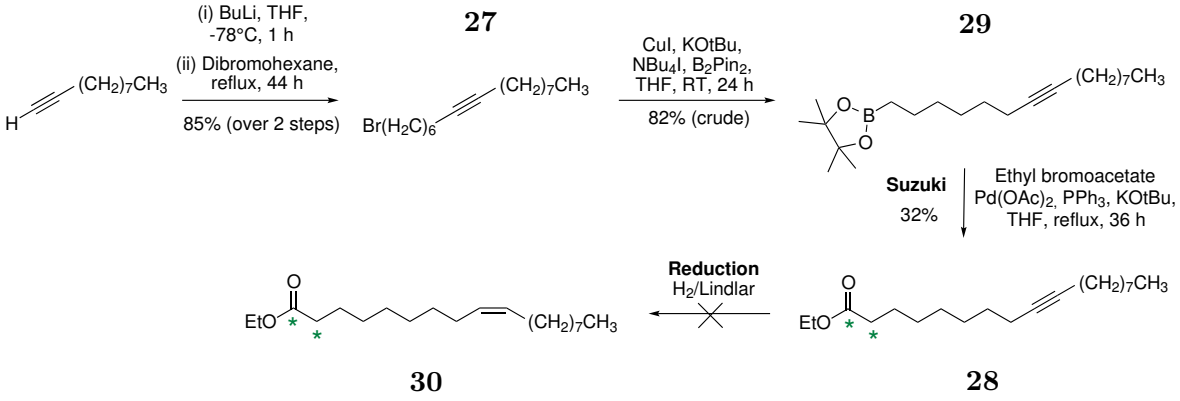

Scheme 3.7 Procedure designed for the synthesis of oleic acid ethyl ester **30**. Positioning of double ^{13}C labels are indicated by *.

3.4 Conclusions

Analytical techniques have been investigated in order to determine their suitability for study of intrinsic lipidation. Desirable techniques provide routine, high throughput reaction mixture screening, in a reliable and accurate fashion. Investigation of solution state NMR and fluorescence spectroscopy deemed these techniques unsuitable for reaction monitoring, due to insufficient sensitivity and complex data interpretation respectively. Reaction monitoring by TLC also proved unsuccessful for peptide intrinsic lipidation, necessitating high performance RP TLC plates requiring insufficiently sensitive visualisation techniques. Development of NP and RP TLC conditions, including visualisation technique and solvent system, proved successful for routine monitoring of propranolol **1** intrinsic lipidation. Validation of TLC conditions is required prior to monitoring intrinsic lipidation of additional small molecules.

ssNMR was identified as an analytical technique with potential to provide robust and informative study of intrinsic lipidation within accurate biological molecules. Complementary to mass spectrometry, ssNMR provides intrinsic structural information, full speciation, and

quantification, ultimately facilitating study of reaction kinetics. Preliminary ssNMR studies suggest that undesirably high concentrations of reaction components are required for analysis, leading to expense and wastage. Isotopic substrate labelling was considered a suitable alternative, facilitating ssNMR analyses at a reduced concentration. Synthetic methodologies for ^{15}N labelled propranolol **1** and benzimidazole **11** preparation were developed, resulting in successful isolation of the former. Furthermore, synthetic preparation of versatile ^{13}C labelled phospholipids was explored, resulting in optimised methodology for preparation of doubly ^{13}C labelled DPPC and DOPC. Synthetic steps were taken towards the challenging synthesis of mixed acyl phospholipid POPC, incorporating doubly labelled fatty acid chains for study of preferential acyl transfer.

4 | Peptide Intrinsic Lipidation

4.1 Introduction

Innate reactivity between membrane active peptides, and phospholipids or lysolipids at the membrane interface, has been characterised *in vitro* as peptide intrinsic lipidation.[10,11] Increased study of peptide intrinsic lipidation has been conducted compared to small molecule and protein analogues, however further investigation is required towards understanding the biological impact of reactivity. Naturally lipidated peptides, formed by enzymatic post-translational modification, exhibit increased hydrophobicity compared to their unmodified counterparts. The resulting increased membrane association serves to benefit the natural roles of lipidated peptides in cell signalling and membrane trafficking.[6,197] Analogous physical properties and biological activities are predicted for peptides lipidated by intrinsic lipidation, compared to enzymatic lipidation. Investigation of acylated peptide properties by employing biophysical techniques aims confirm this theory of analogous behaviour. Furthermore, study of intrinsic lipidation within disease related peptides aims to probe biological behaviour, and establish the therapeutic relevance of intrinsically lipidated peptides.

4.2 Characterisation of Acylated Melittin

Peptides targeted by intrinsic lipidation *in vitro* do not undergo post-translational lipidation, therefore knowledge of their structure and properties following acylation is limited. Lytic peptide melittin is well characterised in solution and membrane bound forms, however its intrinsically lipidated analogues have received little scientific focus.[198] Properties of acylated melittin, in comparison to its unmodified counterpart, were therefore probed in order to better understand their biological relevance. The advent of *N*-stearylated melittin used as a gene transfection vector, serves to highlight the need for improved understanding.[199] Four acylated

melittin analogues were selected for study, *N*-palmitoyl melittin, K23-palmitoyl melittin, *N*-oleoyl melittin and K23-oleoyl melittin. Species mirror the most common acylation sites and fatty acid chains identified during study of intrinsic lipidation within eukaryotic membranes.

4.2.1 Structure of Acylated Melittin

Solution phase melittin adopts a random coil configuration of undefined structure at low concentration, and a tetrameter shielding hydrophobic residues from the aqueous external environment at high concentration.[200–202] Increasingly hydrophobic acylated melittin is predicted to exhibit modified structural behaviour in aqueous solution, shielding the fatty acid chain from the unfavourable external environment. Fatty acid chain chemistry and modification position may influence this solution phase structural behaviour. Biophysical techniques were therefore employed in order to probe the solution phase structure of four acylated melittin derivatives, *N*-palmitoyl melittin, K23-palmitoyl melittin, *N*-oleoyl melittin and K23-oleoyl melittin.

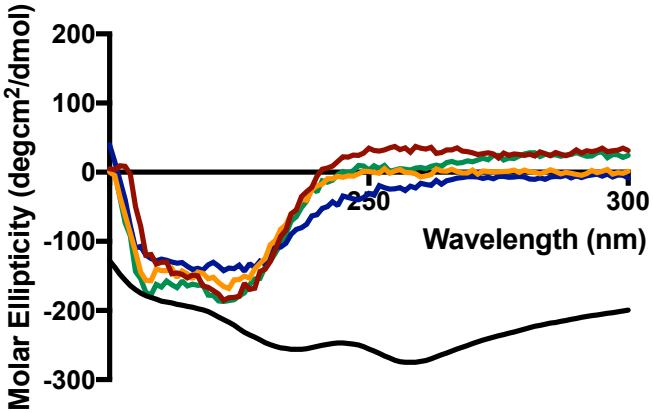

Figure 4.1 CD spectra of solution state melittin (black); *N*-palmitoyl melittin (red); K23-palmitoyl melittin (orange); *N*-oleoyl melittin (blue); K23-oleoyl melittin (green).

Circular dichroism (CD) creates a characteristic spectrum based upon peptide interactions with left circularly polarised light and right circularly polarised light. Comparison to literature standards then facilitates identification of peptide secondary structure.[203,204] CD spectra of four acylated melittin derivatives in aqueous solution, Fig. 4.1, exhibit considerable variation from the random coil of solution phase melittin. Increased negative dichroism at approximately 220 nm suggests acylated melittin derivatives adopt an α-helical conformation in solution. Within error, % helicity is consistent across all forms of acylated melittin, suggesting secondary structure formation occurs irrespective of acyl chain chemistry or position. Comparison to α-helical structures of unmodified melittin suggests the solution phase conformation of acylated

melittin is α-helical with a central kink attributed to the proline residue. However, it is unclear whether bulk peptide structure mimics the individual helices of membrane bound unmodified melittin, or aggregates, mirroring the tetrameric structure observed in solution at high melittin concentrations.[205,206]

The solution phase structure of acylated melittin derivatives can be further probed by employing the intrinsic fluorescence of aromatic amino acid residue tryptophan. Tryptophan emission is susceptible towards external environment, undergoing a blueshift in response to increased local hydrophobicity. Spontaneous melittin helix formation is characterised by a blueshift in maximum tryptophan fluorescence from 352 nm to 336 nm.[45,62] The extent of helix formation can therefore be approximated by the I(336 nm)/I(352 nm) ratio. Analogous tryptophan fluorescence behaviour is predicted for acylated melittin, such that helicity can be determined by the I(336 nm)/I(352 nm) ratio. Fig. 4.2 shows tryptophan emission following excitation at 280 nm for melittin and *N*-acylated analogues. K23-acylated melittin species have been omitted for clarity, however spectra resemble those of their *N*-acylated counterparts. Acylated melittin species exhibit a blueshift in emission maxima compared to unmodified melittin, suggesting tryptophan resides in an increasingly hydrophobic environment. The I(336 nm)/I(352 nm) ratio is presented for solution phase melittin species in Table 4.1. Increased ratios are observed for all acylated species compared to melittin, supporting tryptophan residence in the increasingly hydrophobic environment associated with α-helix formation. The I(336 nm)/I(352 nm) ratio is not observed to be dependent upon either acyl chain chemistry or modification position. Furthermore, the origin of the heightened I(336 nm)/I(352 nm) ratio attributed to *N*-oleoyl melittin remains unclear.

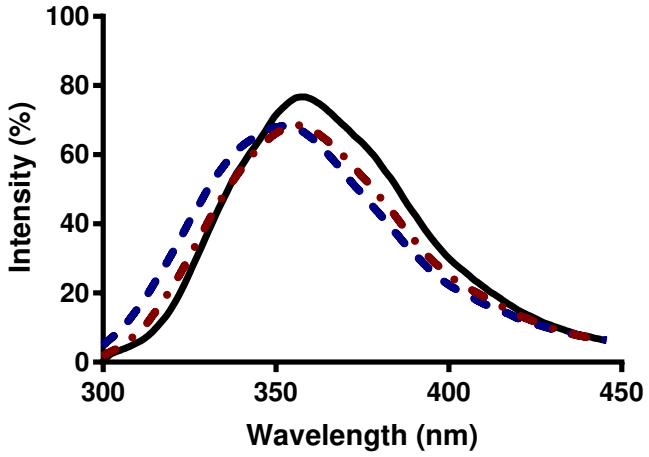

Figure 4.2 Tryptophan emission following excitation at 280 nm for melittin (solid black line); *N*-palmitoyl melittin (dotted and dashed red line); *N*-oleoyl melittin (dashed blue line).

Peptide	Emission Maximum (nm)	I(336 nm)/I(352 nm)
Melittin	362.5	0.67
N-palmitoyl melittin	355.5	0.74
K23-palmitoyl melittin	355.5	0.77
N-oleoyl melittin	354.5	0.86
K23-oleoyl melittin	356.5	0.73

Table 4.1 Emission maxima and I(336 nm)/I(352 nm) ratio for solution phase melittin analogues based upon tryptophan emission following excitation at 280 nm.

Combined CD and trytophan emission data suggest solution phase acylated melittin adopts an α-helical structure. Based upon the constrained nature of secondary amino acid proline, combined with similarities between CD of solution phase acylated melittin and membrane bound unmodified melittin, it is further speculated that the structure contains a kink at proline. Comparison of palmitoyled and oleoylated peptides suggests adopted structure is not influenced by modification position or acyl chain length. However, literature studies suggest that more significant reductions in carbon chain length may favour random coil formation in favour of an α-helix.[207] Similarly, internal acyl chain modifications may exhibit structural differences compared to the *N*-terminal and K23 modified species tested.

4.2.2 Critical Micelle Concentrations for Acylated Melittin

Acylated melittin, comprised of a hydrophobic fatty acid chain and hydrophilic cationic *C*-terminus, can be characterised as amphiphilic. Amphiphilic molecules often aggregate in aqueous solution, in order to promote the maximum number of favourable hydrophobic and hydrophilic interactions. Micelles, depicted in Fig. 4.3, are spherical amphiphilic aggregate structures adopted by detergents, including lysolipids.[208] Micelle formation requires substrate concentrations above a critical micelle concentration (CMC), below which only monomers of undefined structure exist. Naturally lipidated peptides have been reported to undergo micellisation in aqueous solution at concentrations above 0.1 µM.[209,210] Biologically relevant examples are summarised in Table 4.2. Therefore, whilst unmodified melittin does not exhibit micelle formation in aqueous solution, it may be induced by the increased hydrophobicity of acylated melittin analogues.

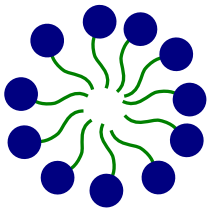

Figure 4.3 Schematic representation of a typical micelle.

Lipidated Peptide	CMC
Arthrofactin	10 µM
Surfactin	70 µM
Pseudofactin II	130 µM

Table 4.2 CMC of known lipidated peptides available from literature sources.[209,210]

Acylated melittin micellisation was studied over the concentration range 100 µM to 1 µM using a Rhodamine 6G assay. Selected due to the cationic nature of melittin, Rhodamine 6G emission at 550 nm is quenched upon micelle formation due to the localised hydrophobic environment.[211,212] Four acylated melittin analogues were tested, *N*-palmitoyl melittin, K23-palmitoyl melittin, *N*-oleoyl melittin, and K23-oleoyl melittin, in order to distinguish CMC variation dependent upon substitution location or acyl chain chemistry. Rhodamine 6G emission in the presence of palmitoylated melittin derivatives, Fig. 4.4, exhibits quenching associated with micelle formation. In the presence of *N*-palmitoylated melittin, Rhodamine 6G emission decreases upon initial peptide addition, indicating immediate micelle formation, and a CMC value of 1 µM or less. In contrast, the observed emission profile in the presence of K23-palmitoyl melittin is reminiscent of literature studies, with an initial plateau followed by a decrease denoting the CMC at 5 µM.[211] Calculated CMC values for palmitoylated melittin derivatives are low compared to the lipidated peptides evidenced in Table 4.2. Observed values fall in a similar concentration range to CMC of lysolipid, for example the CMC of PPC reported in the range 4 µM to 8.3 µM.[213]

Rhodamine 6G emission in the presence of oleoylated melittin derivatives, Fig. 4.5, exhibited different behaviour compared to their palmitoylated counterparts. *N*-oleoyl melittin is not observed to quench Rhodamine 6G emission over the concentration range studied, suggesting lack of micelle formation. Emission of Rhodamine 6G in the presence of K23-oleoyl melittin proves more challenging to interpret. A slight decrease in Rhodamine 6G emission is observed, however it is unclear as to whether this can be attributed to micelle formation, or to background emission variation. Attributing a CMC to K23-oleoyl melittin gives the value 7.5 µM, within the predicted concentration range for palmitoylated melittin and naturally acylated peptides.[209,210]

Furthermore, a K23-oleoyl melittin CMC of 7.5 µM fits with observed lysolipid CMC trends, in which unsaturated species exhibit higher CMC than their saturated counterparts.[33,214] However, attributing the observed decrease in Rhodamine 6G emission in the presence of K23-oleoyl melittin to background variation suggests oleoylated melittin derivatives do not undergo micelle formation. This observed distinction between palmitoylated and oleoylated species can be attributed to the reduced packing ability of unsaturated acyl chains.

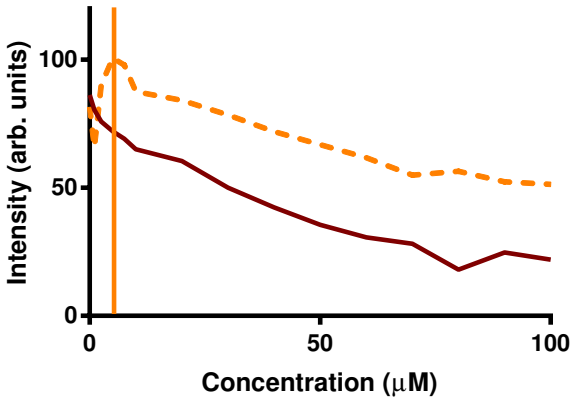

Figure 4.4 Rhodamine 6G emission at 550 nm in the presence of increasing concentrations of *N*-palmitoyl melittin (solid red); K23-palmitoyl melittin (dashed orange). Vertical line denotes the CMC of K23-palmitoyl melittin at approximately 5 µM.

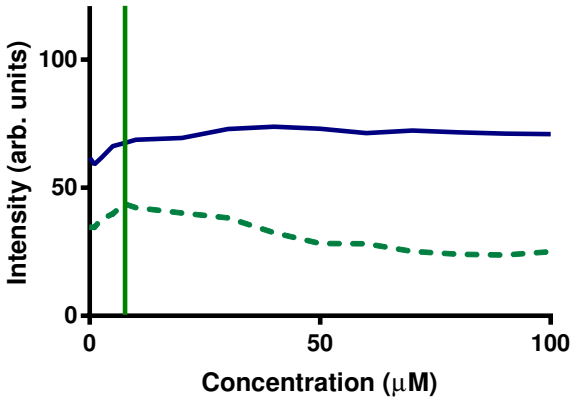

Figure 4.5 Rhodamine 6G emission at 550 nm in the presence of increasing concentrations of *N*-oleoyl melittin (solid blue); K23-oleoyl melittin (dashed green). The vertical line indicates the possible CMC of K23-oleoyl melittin at approximately 7.5 µM.

4.2.3 Antimicrobial Properties of Acylated Melittin

Naturally lipidated peptides exhibit bacterial toxicity associated with membrane disruption caused by their fatty acid substitutions. Toxicity can be quantified by Minimum Inhibitory Concentration (MIC), defined as the minimum concentration required to inhibit microorganism growth. MIC values attributed to lipidated peptides fall within the concentration range of

0.5 µM to 20 µM.[72] Unmodified melittin boasts MIC of 5.6 µM for *S. aureus* and 11.3 µM for *E. coli*, therefore acylated melittin is predicted to exhibit significant bacterial toxicity.[215] This theory was probed by testing the antibacterial activity of four acylated melittin derivatives, *N*-palmitoyl melittin, K23-palmitoyl melittin, *N*-oleoyl melittin, and K23-oleoyl melittin.

The MIC for acylated melittin derivatives were determined against gram-negative *E. coli* following 16 hour incubation with serial peptide dilutions of 32 µM to 0.5 µM.[216] Optical density measurements were used to determine the extent of bacterial growth compared to an untreated control, with complete growth inhibition defining the MIC. Unrestricted bacterial growth was observed in the presence of all acylated melittin analogues at concentrations below 32 µM, suggesting a lack of bacterial toxicity. At 32 µM inhibition was observed for all species, as shown in Table 4.3, with the exception of K23-oleoyl melittin. However, insufficient bacterial growth inhibition was observed to consider this concentration the MIC. Acylated melittin species are therefore noted to exhibit decreased *E. coli* toxicity compared to unmodified melittin, which has an MIC in *E. coli* of 11.3 µM.[215] Bacterial growth relative an untreated control is determined to be 74 % and 77 % for *N*-palmitoyl melittin and K23-palmitoyl melittin respectively, indicating a slight inhibition increase attributed to the *N*-terminal modification. *N*-oleoyl melittin exhibits 84 % *E. coli* growth compared an untreated control, suggesting oleoyl modifications are associated with reduced antimicrobial activity compared to their palmitoylated counterparts, despite increased hydrophobicity.

Peptide	*E. coli*	*S. aureus*
N-palmitoyl melittin	74 %	90 %
K23-palmitoyl melittin	77 %	100 %
N-oleoyl melittin	84 %	100 %
K23-oleoyl melittin	100 %	100 %

Table 4.3 % bacterial growth observed for *E. coli* and *S. aureus* treated with 32 µM acylated melittin analogues. 100 % growth was determine by normalisation to untreated controls.

Analogous studies were conducted in order to determine acylated melittin induced growth inhibition over the concentration range 32 µM to 0.5 µM for gram-positive *S. aureus*. Measured optical densities suggested a lack of bacterial growth inhibition for all acylated peptide derivatives across the concentration range tested, as shown in Table 4.3, with the exception of 32 µM *N*-palmitoyl melittin. *N*-palmitoyl melittin at 32 µM exhibits 90 % *S. aureus* growth compared to an untreated control, highlighting the increased toxicity of this acylated derivative compared to its counterparts. Antimicrobial activity of lipidated melittin in gram-positive bacteria is therefore decreased compared to unmodified melittin, which has a MIC of

5.6 µM.[215] Observed toxicity correlates with *E. coli* data, suggesting *N*-terminal modification and palmitoylation promote antimicrobial activity compared to alternative locations and chain chemistries.

4.3 Amyloid Intrinsic Lipidation

Amyloids are a class of disease-related peptides and proteins observed to undergo aggregation *in vivo*, resulting in the formation of insoluble plaques.[217] Plaques are 10 µm to 200 µm in size, Fig. 4.6 (c), comprising an amyloid fibril core surrounded by other biological entities such as nerve terminals. Cytotoxicity of amyloid plaques is attributed to the involvement of nerve terminals and to plaque structure and insolubility, rather than to the sequence or structure of peptide monomers. Amyloid plaque formation is a hallmark of many degenerative diseases, particularly those associated with the brain or peripheral tissues, such as Alzhiemer's disease. Other diseases attributed to amyloid plaque formation include type 2 diabetes, cystic fibrosis, some forms of emphysema and Parkinson's disease.[218]

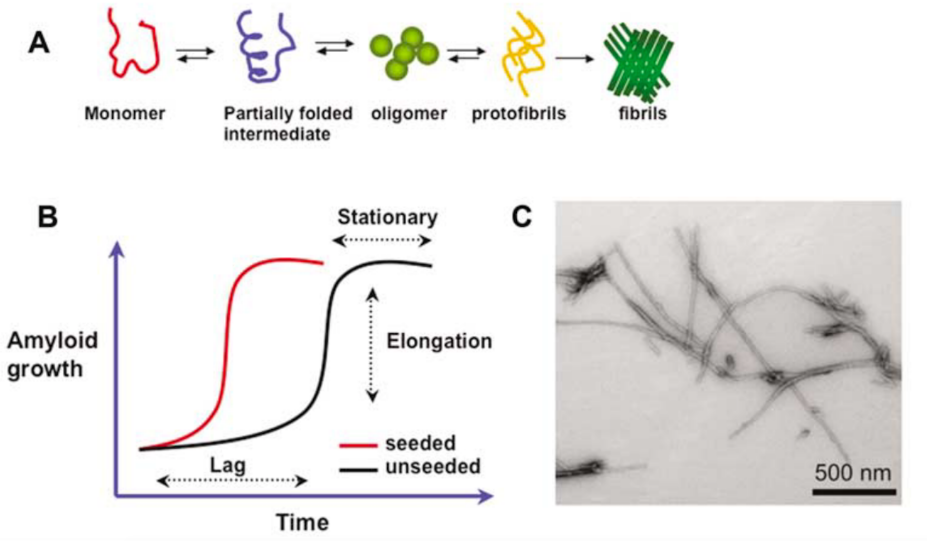

Figure 4.6 (a) The proposed mechanism of amyloid fibril formation, resulting in amyloid plaques linked to degenerative disease induction; (b) Graph showing rate of amyloid assembly; (c) Electron microscopy of typical amyloid fibrils.[219]

Successful treatment of amyloid related diseases requires mechanistic understanding of plaque formation.[9,219] Fig. 4.6 (a) and (b) summarise three key steps involved in plaque formation:

1. Rate-limiting lag phase: monomers undergo folding, unfolding, dimerisation and denaturation, eventually nucleating into small globular amyloidogenic oligomers.

2. Fibril growth phase: amyloidogenic oligomers above a concentration threshold aggregate into an amyloid seed, which then elongates into rod-like filaments. Filaments bundle and intertwine forming first protofibrils then filaments.

3. Saturation: filament elongation ceases and β-sheet filaments form the dense central core of amyloid plaques.

Despite considerable study of the amyloid aggregation process, the trigger for initial amyloid monomer nucleation remains unclear. One theory suggests that protein misfolding exposes novel protein regions normally shielded, inducing aggregation through hydrophobic interactions.[9] Alternative theories include membrane induced proximity facilitating monomer aggregation, or excess peptide accumulation resulting from increased production or reduced clearance.[9] Peptide intrinsic lipidation provides a further possible mechanism for induction of amyloid plaque formation. Synthetic addition of a hydrophobic *N*-terminal membrane anchor analogous to intrinsic lipidation acylation, has been observed to double the rate of amyloid aggregation, shielding the hydrophobic chain from aqueous surroundings.[220,221] Furthermore, intrinsic lipidation induced nucleation is consistent with both the observed lag phase, and the necessity for a catalytic lipid membrane *in vitro* in order to accurately mimic aggregation rates *in vivo*.[219,220] Finally, fluorescent amyloid plaques are formed in the presence of phospholipids comprised of fluorescently labelled acyl chains, suggesting incorporation during fibril formation.[222]

Investigation into the relationship between peptide intrinsic lipidation and amyloid aggregation was probed using three amyloid peptides, Fig. 4.7. Forty amino acid amyloid-β, is formed upon cleavage of APP precursor protein by membrane bound protease β-secretase, and the γ-secretase complex.[9,223,224] Implicated in Alzheimer's disease, the 11-28 residue active region of amyloid-β includes two lysine, one serine and two histidine moieties, primed to undergo intrinsic lipidation. Sixty-seven residue hormone amylin is naturally produced by signal sequence cleavage from proamylin, and subsequence post-translational modification.[225] Implicated in the loss of islet β-cells associated with type 2 diabetes, amylin contains three serine residues capable of intrinsic lipidation within its active region of residues 20-29. β-2 microglobulin, a one hundred nineteen residue component of the major histocompatibility complex, is known to aggregate in joint spaces causing dialysis related amyloidosis.[226] Agregation prone regions of β-2 microglobulin, residues 22–31 and 60–70, contain three lysine residues and one serine prone to intrinsic lipidation reactivity.[227]

(a)

D A E F R H D S G Y **E V H H Q K L V F F A E D V G S N K** G A I I G L M V G G V V

(b)

S N N F G A I L S S

(c)

M S R S V A L A V L A L L S L S G L E A I **Q R T P K I Q V Y S** R H P A E N G K S N F L N C Y V S G F H P S D I E V D L **L K N G E R I E K V E** H S D L S F S K D W S F Y L L Y Y T E F T P T E K D E Y A C R V N H V T L S Q P K I V K W D R D M

Figure 4.7 (a) Amino acid sequence of amyloid-β; (b) Amino acid sequence of amylin; (c) Amino acid sequence of β-2 microglobulin. Active regions are highlighted in green.

Amyloid stock solutions were prepared at 5 µg mL^{-1} in hexafluoro-2-propanol (HFIP) to prevent aggregation during storage.[228] Stock solution portions were incubated under physiological conditions for 72 hours in 1:10 molar ratio with POPC:SLPS (4:1) liposomes. Membrane model selection mimics plaque forming conditions *in vivo*, and facilitates origin of transfer determination through acyl chain diversity. Sample analysis was conducted by MALDI MS on an Autoflex II ToF/ToF (Bruker Daltonics Ltd., UK), rather than standard LCMS with ESI ionisation optimised for study of peptide intrinsic lipidation.[39,40] MALDI instrumentation provides a robust analytical alternative to ESI, compatible with study of amyloid aggregates and increased solvent diversity, which can prove problematic for LCMS.[109,229,230] Neither modified nor unmodified amyloid monomers were observed for amylin, amyloid-β, or β-2 microglobulin following 72 hour incubation with liposomes. Lack of visualisation was considered likely due to amyloid aggregation, preventing sample solubilisation and detection by MALDI MS.

Confirmation of amyloid aggregation under experimental conditions was determined by employing two biophysical techniques, a Thioflavin T fluorescence assay, and electron microscopy (EM).[231] Thioflavin T emission at 485 nm is dependent upon polarity of the dye's external environment.[232–234] Fluorescence is quenched in aqueous solution, therefore increased fluorescence is observed upon amyloid fibril formation providing a hydrophobic environment for Thioflavin T intercalation. Fig. 4.8 shows normalised Thioflavin T emission at 485 nm for amyloids amylin, amyloid-β, and β-2 microglobulin, in solution and in the presence of a lipid membrane. Consistent with monomer detection by MALDI MS, solution phase amyloids do not exhibit the increased Thioflavin T fluorescence indicative of plaque formation, over the time period of study. In contrast, amyloid species in the presence of a lipid membrane

exhibit increased Thioflavin T fluorescence, reaching emission maxima within approximately 15 minutes of incubation. Emission plateaus, indicative of complete amyloid aggregation and dye intercalation, then decreases due to solvent evaporation.

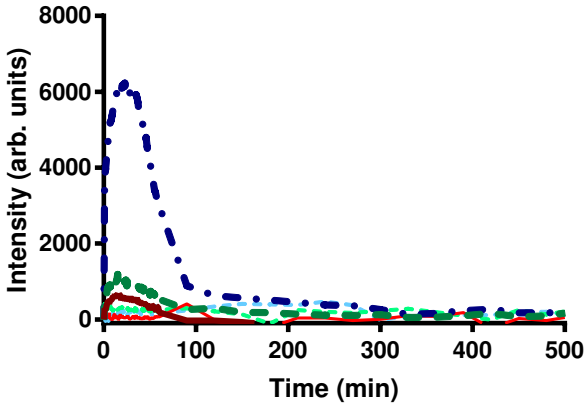

Figure 4.8 Thioflavin T fluorescence at 485 nm under physiological conditions for amylin (solid red), amyloid-β (dashed green), or β-2 microglobulin (dotted and dashed blue) in solution (lighter colours) and in the presence of a POPC:SLPS (4:1) liposomal membrane (darker colours).

Transmission electron microscopy (TEM) provides confirmation of amyloid aggregation in the presence of a lipid membrane through direct visualisation.[235–237] Fig. 4.9 presents one example of plaque formation following 72 hour incubation of amyloid-β with POPC:SLPS (4:1). Fibril length is limited *in vitro* by the initial concentration of amyloid peptide available for aggregation. Combined TEM, Thioflavin T fluorescence, and MALDI MS data support the theory of amyloid aggregation occurring under experimental conditions. Observed aggregation under known peptide intrinsic lipidation conditions serves to support acyl transfer as a possible mechanism for the induction of amyloid nucleation.

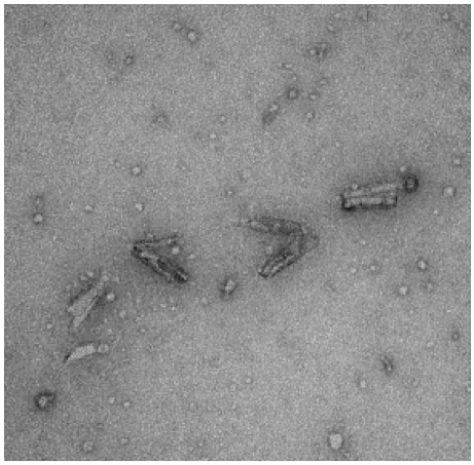

Figure 4.9 TEM of amyloid plaques formed upon 72 hour incubation of amyloid-β with a POPC:SLPS (4:1) lipid membrane under physiological conditions.

Modification to environmental parameters is predicted to aid in the study of amyloid intrinsic lipidation by diminishing amyloid aggregation, and facilitating product visualisation. Literature reports suggest amyloid aggregation can be prevented by employing reduced NaCl concentrations, low temperatures, and by sonicating samples prior to incubation.[228,238] Influence of temperature reduction upon aggregation cannot be tested using a Thioflavin T assay, due to instrument limitations. However, Thioflavin T emission was studied for amyloids in the presence of a lipid membrane using low salt buffer (10 mM $NaHCO_3$ pH 7.4), and following sonication. Amyloid aggregation, indicated by increased Thioflavin T emission, was not observed over 6 hours of study for modified reaction conditions. Aggregation is therefore reduced compared to initial experimental conditions, where emission increase was observed within 15 minutes. Modified experimental conditions were taken forward for 72 hour incubation and MALDI MS analysis, hoping to detect amyloid intrinsic lipidation. However, monomer visualisation was not improved under modified experimental conditions, suggesting amyloid aggregation is slowed by not completely prevented.

Considering the predicted link between intrinsic lipidation and amyloid nucleation, preventing aggregation is likely to simultaneously prevent acyl transfer. Aggregate depolymerisation, and subsequent composition determination, provides an alternative mechanism for the study of amyloid intrinsic lipidation. Aggregates were isolated by centrifugation following 72 hour incubation of amyloids with POPC:SLPS (4:1) liposomes under standard intrinsic lipidation conditions. Amyloid plaques were treated with HFIP, a known depolymerising agent, and analysed directly by MALDI MS.[228] Unmodified monomer and amyloid aggregates were observed for all three amyloid species, suggesting incomplete depolymerisation. Acylated amyloids were not observed, however since this be attributed to either inclusion within remaining aggregates, or to ion suppression, intrinsic lipidation cannot be ruled out.

Literature precedent suggests an alternative method of amyloid depolymerisation is overnight incubation of aggregates at pH 3 in formic acid.[223,224] Isolated amyloid plaques were therefore treated with formic acid and analysed by MALDI MS. Incomplete depolymerisation was observed for all amyloids, characterised by detection of small multi amyloid aggregates. Insufficient depolymerisation occurred to facilitate visualisation of either unmodified or modified amyloid monomers. Determination of intrinsic lipidation reactivity therefore proved inconclusive following formic acid depolymerisation.

Enzymatic digestion provides a third potential mechanism for depolymerisation of amyloid aggregates.[40,223,224,239] Digestion conditions were optimised using monomer β2-microglobulin,

due to its superior size and complexity compared to amylin and amyloid-β. Initial digestion was conducted with trypsin, trypsin:lys C, and pepsin enzymes, in order to determine peptide suitability. Trypsin:lys C was selected for further study, due to increased cleavage at lysine and arginine residues facilitating superior sequence coverage. Cleavage conditions were further modulated as shown in Table 4.4, in order to maximise observed sequence coverage based upon predicted digestion fragments shown in Fig. 4.10. Optimised conditions achieved 96 % β2-microglobulin sequence coverage, as shown in Fig. 4.11, within a 3 hour digestion time. Dithiothreitol (DTT) addition improves sequence coverage from 71 % to 96 % by facilitating amyloid denaturation, whereas iodoacetamide (IAA) addition reduced coverage to 90 %, suggesting cysteine capping is unnecessary. Optimised digestion conditions were applied to monomer amyloid-β, resulting in 100 % sequence coverage as shown in Fig. 4.11. Amylin digestion was not attempted due to lack of relevant lysine or arginine cleavage sites.

Trypsin/LysC:Protein	Time	NH_4HCO_3 Buffer	DTT	IAA	% Coverage
1:40	24 hours	25 mM	Yes	No	20 %
1:40	24 hours	25 mM	Yes	Yes	20 %
1:40	3 hours	50 mM	No	No	71 %
1:40	5 hours	50 mM	No	No	50 %
1:40	3 hours	50 mM	Yes	No	96 %
1:40	3 hours	50 mM	Yes	Yes	90 %
1:40	3 hours	100 mM	No	No	70 %
1:20	3 hours	50 mM	Yes	No	66 %

Table 4.4 Enzymatic digestion conditions employed for study of β2-microglobulin, and resulting sequence coverage determined by LCMS.

Optimised digestion conditions were applied to isolated amyloid aggregates, and analysis conducted by both MALDI MS and ESI LCMS.[240] However, amyloid digestion was not observed in the presence of amyloid plaques, attributed to the insoluble and impenetrable nature of aggregates. Increased digestion times, up to the point of trypsin autolysis, were applied in the hope of facilitating digestion, however this too proved unsuccessful. Enzymatic digestion, along with HFIP and formic acid, was therefore considered unsuitable for aggregate depolymerisation. Inability to disrupt aggregates prevented further study of amyloid intrinsic lipidation, therefore a definitive link between amyloid nucleation and innate acyl transfer remains to be established.

Figure 4.10 Sequence and predicted trypsin:lys C digestion fragments of: (a) β2-microglobulin; (b) amyloid-β.

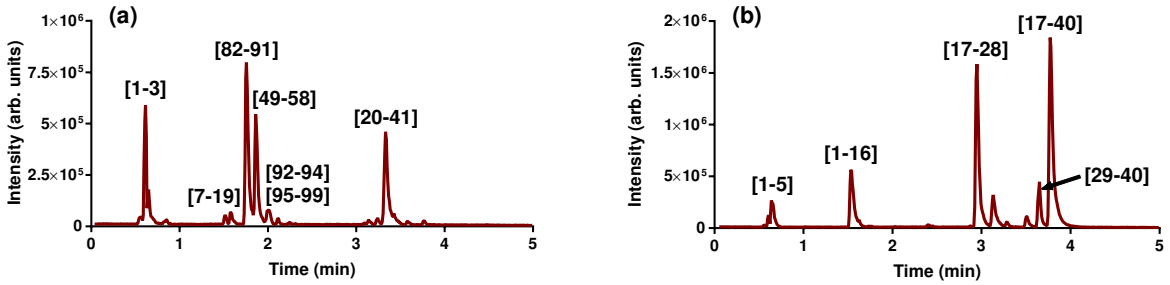

Figure 4.11 TIC of amyloids digested under optimised conditions: (a) β2-microglobulin; (b) amyloid-β.

4.4 Conclusions

Insight into the activities and physical properties of intrinsically lipidated peptides is vital to understanding the biological relevance of innate peptide reactivity. Biophysical techniques have been employed to probe the properties of acylated model peptide melittin, facilitating this understanding. CD and intrinsic tryptophan fluorescence confirm that unlike its unmodified counterpart, acylated melittin exhibits solution phase structure. Predicted to be α-helical with a possible central kink at secondary amino acid proline, structural formation is driven by favourably shielding the hydrophobic acyl moiety from external aqueous environment.

However, it remains unclear as to whether this structure is attributed to monomers or to bulk peptide structure, such as the tetramer adopted by unmodified melittin at high concentrations. Bulk structure was probed by employing fluorescent Rhodamine 6G dye to examine possible micelle formation. Palmitoylated melittin derivatives underwent micellisation, with calculated CMCs of 1 µM and 5 µM for *N*-terminal and K23 modifications respectively. Oleoylated derivatives did not exhibit spontaneous aggregation into micelles, attributed to reduced packing of unsaturated acyl chains. The antimicrobial activity of acylated melittin derivatives was investigated, given the potency of unmodified melittin and similar lipidated peptides. However, only minimal bacterial growth inhibition of *E. coli* and *S. aureus* was observed at 32 µM for acylated melittin. Preferential antimicrobial activity was attributed to palmitoylated and *N*-terminally modified derivatives.

The biological relevance of innate acyl transfer was further probed by investigating links between intrinsic lipidation and disease related peptides. Literature studies suggested intrinsic lipidation could induce the process of amyloid nucleation, ultimately resulting in disease related plaque formation. Significant support for this prediction is attributed to the doubled rate of plaque formation observed for amyloid-β modified with a hydrophobic *N*-terminal anchor. Three amyloids, amylin, amyloid-β, and β2-microglobulin, subjected to peptide intrinsic lipidation conditions, underwent aggregation confirmed by Thioflavin T fluorescence and EM. This observation supports a link between amyloid nucleation and aggregation, however confirmation requires visualisation of acylated amyloid. In an attempt to aid visualisation of acylated amyloid, modified experimental conditions were employed, including reduced salt content, temperature, and sonication. Slowed aggregation was observed under these modified experimental conditions, but not sufficiently eliminated to study acyl transfer. Aggregate depolymerisation and subsequent content analysis was considered a preferable method to facilitate acylated amyloid visualisation. HFIP, formic acid and optimised trypsin:lys C enzymatic digestion were studied, but ultimately proved unsuccessful in complete depolymerisation. Therefore at present a link between intrinsic lipidation and amyloid nucleation can be neither definitively proved nor disregarded.

5 | Small Molecule Intrinsic Lipidation

5.1 Introduction

Small molecule intrinsic lipidation is a non-enzymatic acyl transfer reaction between membrane phospholipids and a small organic molecule.[76,77] The major reaction product from small molecule intrinsic lipidation is the small molecule modified with a hydrophobic acyl chain derived from the membrane. The increased hydrophobicity of the modified small molecule dramatically changes its structure, properties and action. Such modification is particularly important if the small molecule substrate is a pharmaceutical, given the likely resulting changes to activity and side effect induction.

Past research into small molecule intrinsic lipidation has utilised lysolipids, the reaction by-product, as means of studying the reaction.[76,77] Since alternative mechanisms of lysolipid production exist, notably enzymatically *in vivo* and by solution phase hydrolysis, their presence is not diagnostic of small molecule intrinsic lipidation. To definitively prove the existence of small molecule intrinsic lipidation at the membrane interface, direct observation of modified acyl small molecules is necessary. LCMS is the optimum technique for direct observation, due to its informative nature, sensitivity, and robustness towards complex samples. Additional benefits of pursuing LCMS for the study of small molecule intrinsic lipidation include the observed success of the technique for the analysis of peptide intrinsic lipidation, and the ability to tune instrumentation for optimum results.

5.2 Preliminary MS Experiments

Durham University Chemistry Department operates an analytical mass spectrometry service, utilising a QToF Premier (Waters Corp., UK) with ESI source to obtain routine accurate mass data for samples. In the case of complex samples, the instrument can be utilised in combination with an Acquity UPLC (Waters Corp., UK) running a seven minute linear gradient of either H_2O:MeCN or H_2O:MeOH. Initially, it was considered that this validated accurate mass system of moderate sensitivity may be suitable for the study of small molecule intrinsic lipidation, focussing on direct observation of acylated small molecules.

In order to test the instrumentation system described, several test samples were required. Given the complexity of natural biological cell membranes, a model system was deemed more appropriate for initial experiments in order to simplify the resulting data. Use of a model eliminates factors which may cause confusion during data interpretation, including the presence of enzymes, the variety of acyl chain types present within the membrane, and the potential loss of material through solvent extraction steps. Liposomes, Fig. 5.1, also known as large unilamellar vesicles (LUV) were selected for study due to their robustness, simple preparation, the abundance of available research, and their widely accepted similarity to natural membranes.[241] Additionally, since liposomes are single bilayer structures prepared from solution phase phospholipids, their lipid composition can be tuned as desired. In order to assimilate biological conditions, liposomes utilised within this research were prepared via the extrusion method at a diameter of 100 nm and in 10 mM ammonium bicarbonate buffer at pH 7.4.

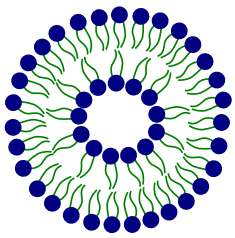

Figure 5.1 A liposome formed of a bilayer of phospholipids. Head groups are shown in blue and acyl chains in green.

Liposomes were prepared at a known concentration containing, for simplicity, only one type of phospholipid, DOPC. DOPC contains oleoyl (18:1) acyl chains at both the *sn*-1 and the *sn*-2 position of the phospholipid backbone. These chains, highlighted purple in Fig. 5.2, are one of the most common acyl chains known to be present in natural cell membranes. In addition,

DOPC contains the PC phosphate head group, highlighted blue in Fig. 5.2, the primary phospholipid head group present in eukaryotic membranes. A eukaryotic model membrane system is deemed appropriate due to the therapeutic relevance of small molecule intrinsic lipidation.

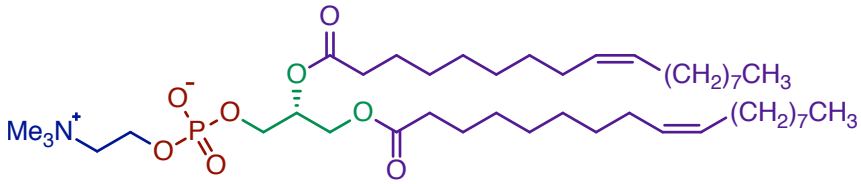

Figure 5.2 Chemical structure of the membrane phospholipid DOPC. Key structural features highlighted: (i) oleoyl chains in purple; (ii) glycerol backbone in green; (iii) phosphate in red; (iv) choline head group in blue.

In order to accurately mimic a natural biological system, the ideal small molecule:lipid molar ratio utilised within this research would be in the range of 1:10000-100000. Unfortunately, samples containing lipid in this excess would require significant dilution in preparation for analysis by mass spectrometry to prevent overloading the chromatography column. This required dilution would therefore reduce the concentration of the modified small molecule injected into the instrument to below the limit of detection. Since visualisation of modified small molecule is key to proving the existence of small molecule intrinsic lipidation, a 1:10 small molecule:lipid molar ratio was utilised. Although the proportion of small molecule is high, this ratio provides the best balance between upper concentration capacity of the instrument and the limit of detection.

Fig. 5.3 details the small molecules selected for the initial study of small molecule intrinsic lipidation. Six cationic amphiphilic small molecules were selected, each containing an amine nucleophile in order to facilitate nucleophilic attack on the phospholipid acyl chains. The small molecules were selected due to their predicted reactivity towards intrinsic lipidation, based on previous research monitoring lysolipid levels in their presence.[77] Further, the small molecules selected cover a range of aromatic moieties and exhibit significant structural variation, in order to ensure the greatest likelihood of observing reactivity. Simultaneously, three cationic amphiphilic commercial pharmaceuticals were selected for study: (i) propranolol **1**; (ii) procaine **2**; (iii) tetracaine **3**. The three pharmaceutical containing samples were at this time prepared by undergraduate student Sanna Appleby.[76]

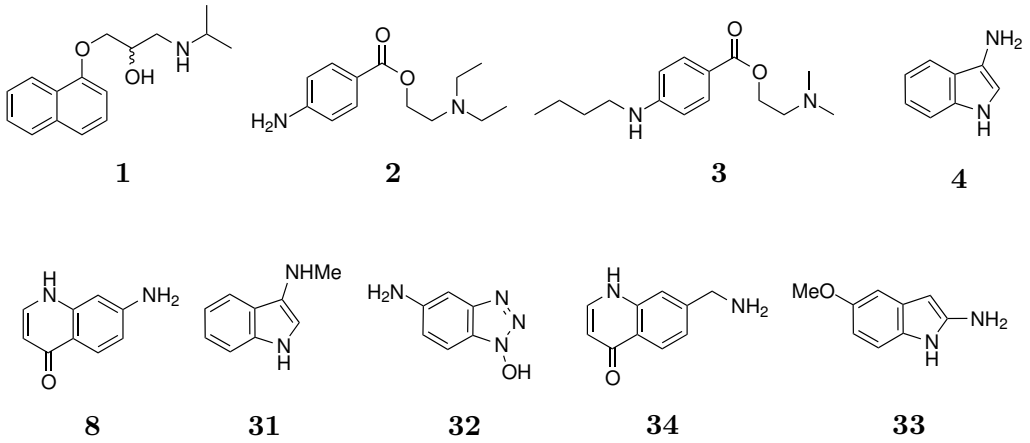

Figure 5.3 Cationic amphiphilic small molecules studied during preliminary screening of small molecule intrinsic lipidation by LCMS on a QToF Premier (Waters Corp., UK).

In accordance with previous research conducted into small molecule intrinsic lipidation, small molecule:phospholipid mixtures were incubated under physiological conditions of pH 7.4 and 37 °C.[77] After 72 hours, samples were centrifuged and vortexed in order to combine and mix the contents. A portion of the sample was diluted in 1:1 H_2O:MeCN to a concentration of small molecule approximated to be 0.1 mg mL^{-1}. Samples were then analysed on a QToF Premier (Waters Corp., UK) with Acquity C_{18} BEH stationary phase, using a five minute linear gradient from H_2O (0.1% formic acid):MeCN (99:1) to H_2O (0.1% formic acid):MeCN (1:99), followed by a four minute organic wash. Analyses were then repeated with a five minute linear gradient from H_2O (0.1% formic acid):MeOH (99:1) to H_2O (0.1% formic acid):MeOH (1:99), followed by a four minute organic wash. Instrument parameters applied to samples were those used as standard for all accurate mass samples analysed by Durham University mass spectrometry service, summarised in the Experimental section of this thesis.

Fig. 5.4 shows one example of the data obtained following analysis of phospholipid:small molecule samples under the standard analytical conditions employed by Durham University mass spectrometry service. Several problems are evident upon analysis of the data, including poor chromatographic resolution and insufficient sensitivity. Particularly problematic is the presence of considerable levels of background interference. Given the low levels of desired modified small molecule product expected, combined with poor ionisation resulting from their increased hydrophobicity, background interference may suppress the signal and prevent visualisation. Overall, it is clear that the instrumentation and conditions utilised for routine analysis of samples by Durham University mass spectrometry service is insufficient for the study of small molecule intrinsic lipidation.

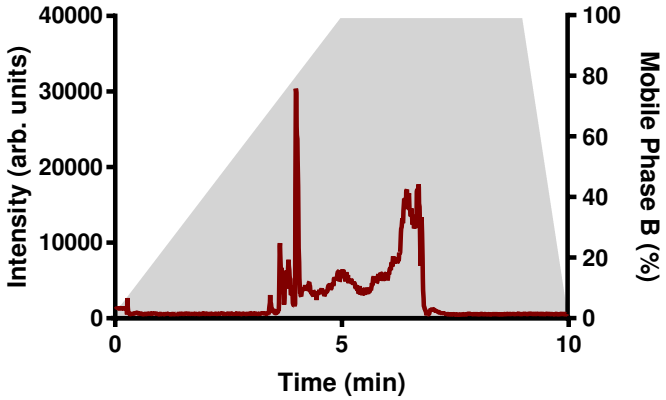

Figure 5.4 Example TIC chromatogram of small molecule incubated for 72 hours with phospholipid, and analysed by LCMS on a QToF Premier (Waters Corp., UK) under non-optimised conditions. No distinct peaks attributed to acylated small molecule or lysolipid species are observed. Analysis was conducted on a BEH C_{18} column (Waters Corp., UK) with the ten minute gradient of mobile phase A (H_2O containing 0.1 % formic acid) and mobile phase B (MeOH) shown in grey.

5.3 Preparation of Synthetic Standards

Bespoke analytical conditions are required in order to successfully develop mass spectrometry for the study of small molecule intrinsic lipidation. Further, given the challenges experienced utilising a QToF Premier (Waters Corp., UK) for the study of small molecule intrinsic lipidation, it is clear that an instrument with high sensitivity, mass accuracy and minimal background interference is required. These criteria, along with other benefits such as increased resolution and the ability to perform IMMS, can be achieved by utilising a Synapt G2-S (Waters, UK) for analysis of small molecule intrinsic lipidation. However, simply performing analysis on an alternative instrument is not sufficient in order to successfully study small molecule intrinsic lipidation. Chromatographic conditions and mass spectrometry instrument parameters require careful tuning in order to improve data quality and analysis.

Optimisation of analytical conditions for the study of small molecule intrinsic lipidation requires experimental standards. Proof of small molecule reactivity at the membrane interface requires visualisation of acylated small molecule, making this the desired standard. These specialised acylated small molecules are unavailable for purchase, and as such organic synthetic techniques were employed for their preparation.[242,243] Propranolol **1**, procaine **2** and tetracaine **3** were selected from the initial intrinsic lipidation screen to undergo synthetic acylation. All three molecules, Fig. 5.5, are readily available as starting materials, hold pharmaceutical relevance, and produce lysolipid in contact with the membrane, suggesting reactivity towards

intrinsic lipidation. Further, all are amphiphilic, containing a hydrophobic ring structure highlighted in red, and a hydrophilic nucleophile containing region, highlighted in green.

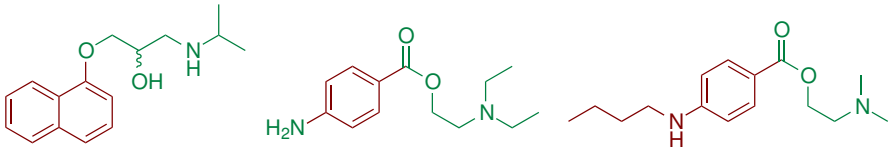

1 **2** **3**

Figure 5.5 Three pharmaceutical molecules selected for acylation in order to develop analytical conditions for the study of small molecule intrinsic lipidation. They are propranolol **1**, procaine **2**, and tetracaine **3**. Hydrophobic regions (red) and hydrophilic regions (green) are highlighted.

Selection of acyl chain types for the preparation of synthetic acylated small molecule standards is also required. Intrinsic lipidation products exhibit an acylation profile mirroring the acyl chain profile of membrane phospholipids. As such, palmitoyl (16:0) and oleoyl (18:1) acyl chains, observed in high abundance within eukaryotic cell membranes, are appropriate choices for synthetic acylation of small molecules. Scheme 5.1 outlines the proposed synthetic strategy for the preparation of six acylated small molecule products. Initially, the desired palmitoyl or oleoyl acid chloride is prepared from the relevant fatty acid by refluxing with oxalyl chloride and anhydrous DCM.[179,244–246] Anhydrous conditions are required in order to minimise hydrolysis of oxalyl chloride and the acid chloride product resulting in diminished yield. Small molecules were then combined with the acid chloride, anhydrous pyridine, and anhydrous DCM to perform the acylation step.[242,243] Four of the six purified products were obtained successfully via this synthetic methodology: (i) *N*-palmitoyl procaine **35**; (ii) *N*-oleoyl procaine **36**; (iii) *N*-palmitoyl tetracaine **37**; (iv) *N*-oleoyl tetracaine **38**.

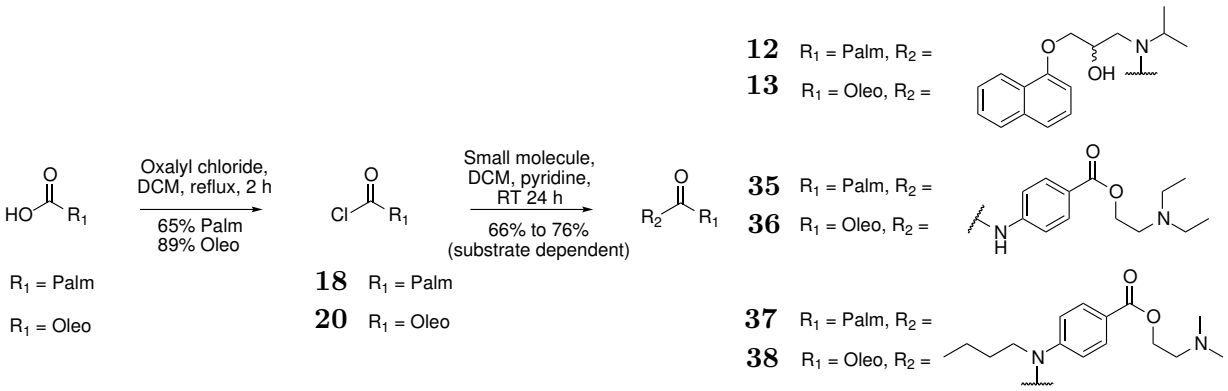

Scheme 5.1 Synthetic protocol for preparation of acylated small molecules: (i) *N*-palmitoyl propranolol **12**; (ii) *N*-oleoyl propranolol **13**; (iii) *N*-palmitoyl procaine **35**; (iv) *N*-oleoyl procaine **36**; (v) *N*-palmitoyl tetracaine **37**; (vi) *N*-oleoyl tetracaine **38**. Palm represents the palmitoyl group $(CH_2)_{14}CH_3$ and oleo represents the oleoyl group $(CH_2)_7CHCH(CH_2)_7CH_3$.

Complex results were obtained following application of the synthetic methodology described in Scheme 5.1 to propranolol **1**. Product purification proved challenging, and the resulting NMR and MS data did not suggest formation of the desired *N*-acylated propranolol products. Improved understanding of the reaction was achieved by repeating the synthetic methodology with a simplified acyl chain. Acetyl chloride, in which the long carbon chain is replaced by a methyl group, was applied to the synthetic methodology in the place of palmitoyl or oleoyl chloride, Scheme 5.2. The improved clarity achieved through the use of acetyl chloride allowed the reaction product, diacetylated propranolol **39**, to be identified. Complexity in the NMR and MS data observed previously is thus attributed to a combination of partial product hydrolysis, unreacted propranolol, and the cis/trans nature of the amide bond in diacylated and *N*-acylated propranolol species.

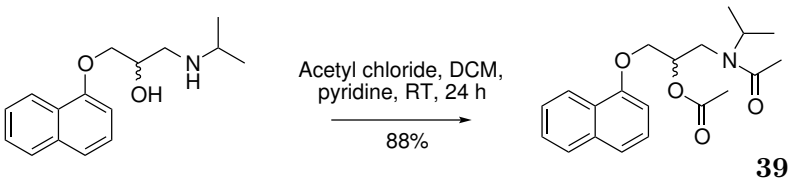

39

Scheme 5.2 Application of original protocol for preparation of *N*-palmitoyl propranolol **12** and *N*-oleoyl propranolol **13** using acetyl chloride. Resulting analysis revealed diacetylated propranolol **39** product formation.

Considering the propensity of propranolol **1** to diacylate in the presence of an acid chloride, a modified synthetic methodology was developed as shown in Scheme 5.3. Initially, formation of diacetylated propranolol **39** is promoted by increasing the number of equivalents of acid chloride from 1.1 to 2.5. Secondly, the *O*-acyl chain is removed by alkaline ester hydrolysis using K_2CO_3 in MeOH.[247] Application of this protocol to propranolol **1**, utilising acetyl chloride as the acid chloride, resulted in successful formation of purified product *N*-acetylated propranolol **40**.

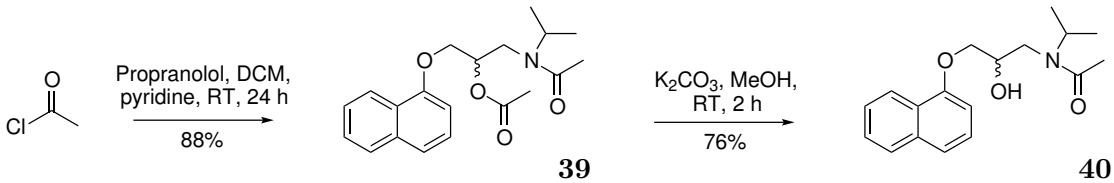

39 **40**

Scheme 5.3 Synthesis protocol for preparation of *N*-acetylated propranolol **40** via diacetylated propranolol **39**. Analogous procedure can be applied to preparation of *N*-palmitoyl propranolol **12** and *N*-oleoyl propranolol **13**.

Given the successful synthesis of *N*-acetylated propranolol **40**, the synthetic methodology was applied to the synthesis of *N*-palmitoyl propranolol **12** and *N*-oleoyl propranolol **13**. The

process progressed via the relevant dipalmitoyled propranolol **41** and dioleoylated propranolol **42** intermediates, ultimately resulting in formation of the desired *N*-acylated products. However, problems were encountered during product purification due to the modified properties of palmitic and oleic acid, byproducts of the ester hydrolysis step, compared to acetic acid.

Palmitic and oleic acid are amphiphilic in nature, resulting in micelle formation in aqueous solution. *N*-palmitoyl propranolol **12** and *N*-oleoyl propranolol **13** are also amphiphilic and likely to form micelles. Within the polar mobile phase required for flash column purification of *N*-acylated propranolol derivatives, mixed micelles are predicted to form. These mixed micelles containing fatty acid and *N*-acylated propranolol prevent separation and purification of the two species. A solution to this problem is presented in Scheme 5.4.[248] Prior to column chromatography the fatty acid is converted into a methyl ester, reducing hydrophilicity of the compound and preventing mixed micelle formation. Desired products *N*-palmitoyl propranolol **12** and *N*-oleoyl propranolol **13** can then be separated from the relevant methyl ester by flash column chromatography.

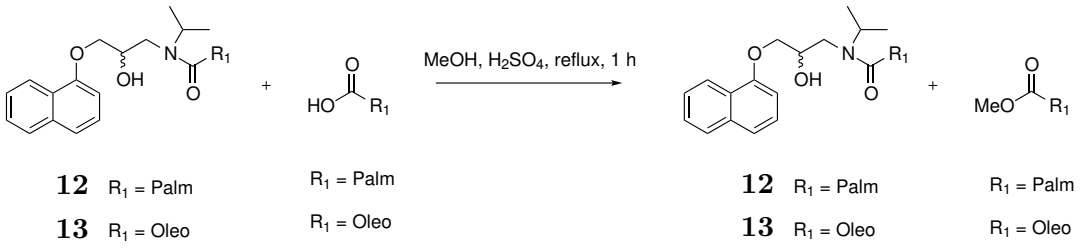

Scheme 5.4 Synthetic method employed to methylate excess fatty acids, facilitating purification of *N*-palmitoyl propranolol **12** and *N*-oleoyl propranolol **13**. Palm represents the palmitoyl group $(CH_2)_{14}CH_3$ and oleo represents the oleoyl group $(CH_2)_7CHCH(CH_2)_7CH_3$.

5.4 Optimisation of ESI Parameters

Armed with synthetic acylated small molecule standards, analytical conditions for the study of small molecule intrinsic lipidation can be developed. ESI was selected as the ionisation technique, due to its reputation for effective ionisation with minimal in-source fragmentation.[105] Optimising ESI instrument parameters allows for efficient ionisation of the hydrophobic acylated small molecules, given their diminished ionisation potential following conversion of an amine in the original small molecule into an amide. The presence of a hydrophobic acyl chain connected via a relatively weak amide bond within the acylated small molecules, means conditions for effective ionisation must be carefully balanced with minimal fragmentation of the desired molecular ion.

Ionisation parameters were optimised by direct infusion of a $0.5\,\mu g\,mL^{-1}$ solution of *N*-palmitoyl procaine **35** in 1:1 H_2O:MeCN into the mass spectrometer at a flow rate of $5\,\mu L/\,min$. The mass spectrum was collected over one minute for each set of conditions, and the resulting data compared in order to determine optimal ionisation parameters. Data quality was determined based upon ion intensity, signal to noise, and level of in-source fragmentation.

Ionisation parameters determined to play major role in analyte ionisation for ESI on a Synapt G2-S (Waters Corp., UK) mass spectrometer are:

- Desolvation gas temperature
- Desolvation gas flow rate
- Source temperature
- Capillary voltage
- Sampling cone voltage
- Source offset voltage

Nitrogen is the desolvation gas utilised within the ESI source throughout the study of small molecule intrinsic lipidation by mass spectrometry. It is selected due to its availability at the necessary purity, inert nature, and stability at high temperatures. The desolvation gas promotes the desolvation of solvated ions released in an aerosol from the capillary needle into gas phase ions. Desolvation gas temperature and flow rate are two vital parameters which can be used to control the desolvation process and modify analyte ionisation. Increased desolvation temperature and increased gas flow rate provide more energy to the gas particles, promoting ion desolvation. However, an increase in desolvation gas energy can also increase collisions between ions and the inert gas, resulting in energy transfer to the ion which is then distributed among all the available degrees of freedom causing bond dissociation. As such, modification to desolvation gas flow rate and temperature were expected to influence ionisation of *N*-palmitoyl procaine **35**. Surprisingly, alterations to the desolvation gas resulted in minimal change to the ionisation profile of *N*-palmitoyl procaine **35**. Optimised values of 350 °C and $600\,L\,h^{-1}$ were selected for desolvation temperature and flow rate respectively, determined by published research into small molecule ESI.[249] Similarly, the source temperature was maintained at 150 °C in accordance with both literature data and compatibility with other instrument users.[40,77]

5.4.1 Capillary Voltage

Capillary voltage is an instrument parameter which describes the voltage applied at the tip of an ESI capillary needle.[81] Voltage application creates a potential difference between the needle and the rest of the mass spectrometer. As a result, selection of correct capillary voltage is vital to ensure charge transfer and motion of ESI droplets formed at the needle tip. Typical positive ESI capillary voltages are in the range of 0.5 to 4.0 kV, however the optimum value is highly dependent upon analyte properties and sample matrix, including solvent. Application of a capillary voltage that is too low prevents development of a Taylor cone at the capillary tip, resulting in formation of large droplets with little horizontal directionality. As a result, droplet desolvation becomes more challenging and sensitivity is reduced, resulting in diminished ionisation. Application of a higher capillary voltage is necessary for certain solvent systems such as those lacking acidic additives or with a high aqueous proportion, due to its corresponding increases in ionisation and sensitivity. However, application of too high a capillary voltage for a given analyte also causes ionisation issues. Major problems include loss of the Taylor cone resulting in rim emission and poor droplet formation, and discharge reducing ionisation stability.[250]

To investigate the effect of capillary voltage upon the ionisation of acylated small molecules a $0.5\,\mu g\,mL^{-1}$ solution of *N*-palmitoyl procaine **35** in 1:1 H_2O:MeCN was direct infused into the mass spectrometer. Data was collected over a one minute period with all parameters kept consistent apart from the capillary voltage, which underwent incremental increases for each analysis. Fig. 5.6 presents the ionisation profile of *N*-palmitoyl procaine **35** at a selection of these capillary voltages. Below 1.0 kV the ion intensity of *N*-palmitoyl procaine **35** is greatly reduced, as indicated by the profile at a capillary voltage of 0.5 kV. The reduction in ionisation results in a corresponding signal to noise decrease, making the capillary voltage inappropriate for the study of intrinsic lipidation. High capillary voltages of 2.0 kV and 2.5 kV exhibit increased ion intensity, however in-source fragmentation to ion *m/z* 193.0736 of molecular formula $C_{10}H_{11}NO_3$ is observed in tandem. Between 1.0 kV and 1.5 kV capillary voltage modification has minimum impact upon ion abundance or fragmentation of *N*-palmitoyl procaine **35**. Considering these observations, and stability issues associated with a high capillary voltages, 1.0 kV was deemed most appropriate for the ionisation of acylated small molecules.[250]

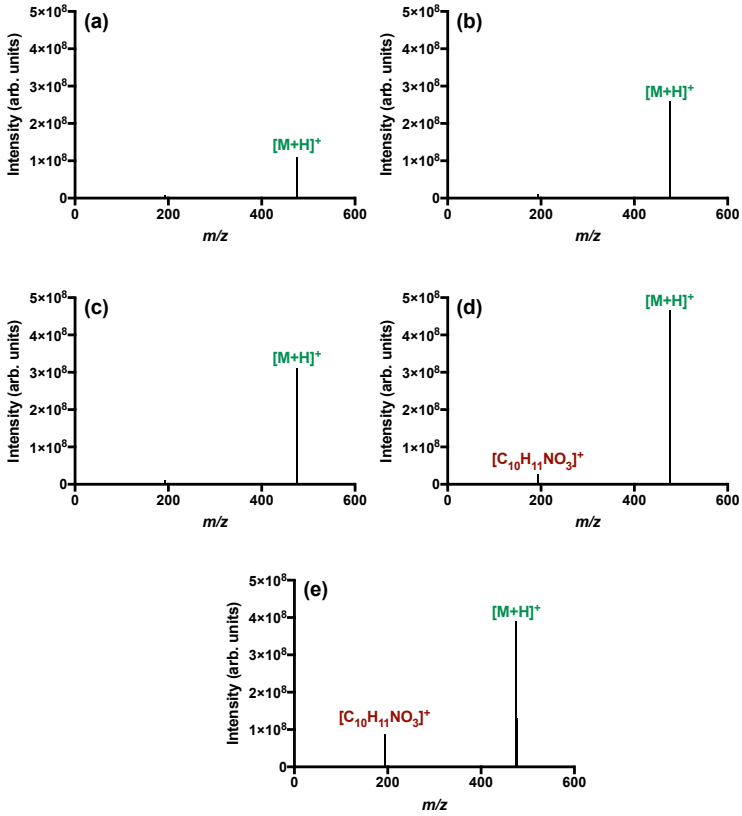

Figure 5.6 Ion profiles of *N*-palmitoyl procaine **35** upon application of differing capillary voltages: (a) 0.5 kV; (b) 1.0 kV; (c) 1.5 kV; (d) 2.0 kV; (e) 2.5 kV.

5.4.2 Sampling Cone Voltage

The sampling cone is an orifice within the ESI source which lies perpendicular to the plume of droplets produced at the capillary needle tip. A voltage in the region of 10 - 100 V is applied to the sampling cone in order to draw ions from the atmospheric pressure region and into the intermediate vacuum region of the mass spectrometer.[81] Voltage application aids in ion transmission, exclusion of unwanted neutral species and declustering of heavily hydrated ions. Selection of an appropriate sampling cone voltage is highly dependent upon analyte type and charge state, with ions of increased mass requiring application of a higher cone voltage. Two key factors are taken into account when tuning the sampling cone voltage for a particular analyte. Firstly, the voltage must be sufficiently high in order to pull the maximum number of ions into the mass spectrometer. Maximising ion transmission results in an increase in instrument sensitivity and aids detection of low abundance or poorly ionising species. However, the increased ion acceleration and transmission associated with a high sampling cone voltage also promotes collisions with molecules of desolvation gas. Inelastic collisions result in increased ion internal energy, causing breakage of weak internal bonds.

This in-source fragmentation process has the undesirable side effect of reducing abundance of the molecular ion, however it can be manipulated for use in MSMS analyses.

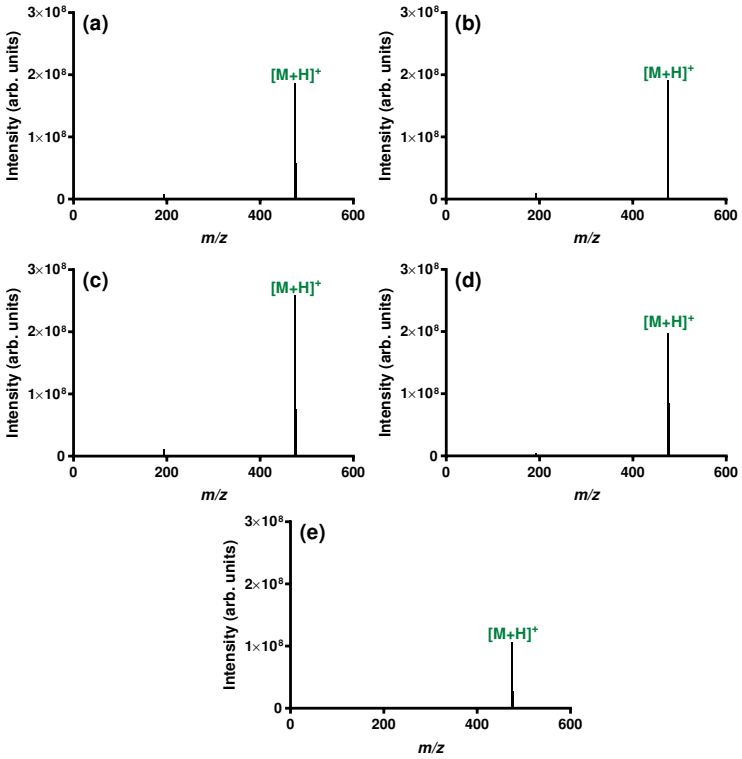

Figure 5.7 Ion profiles of *N*-palmitoyl procaine **35** upon application of differing sampling cone voltages: (a) 30 V; (b) 40 V; (c) 50 V; (d) 60 V; (e) 70 V.

Retaining an intact acylated small molecule molecular ion is vital for detection of small molecule intrinsic lipidation. Prevention of in-source fragmentation at the weak amide bond is vital when selecting an appropriate sampling cone voltage. Mass spectra of *N*-palmitoyl procaine **35** were collected over one minute whilst increasing the sampling cone voltage in 10 V increments. Fig. 5.7 presents the ionisation profiles of *N*-palmitoyl procaine **35** over the region of interest. Across values 30 V to 70 V, the sampling cone voltage promotes transmission of the molecular ion *m/z* 475.3928 with minimal evidence of in-source fragmentation. The maximum molecular ion intensity is reached at a sampling cone voltage of 50 V, therefore this is considered the optimum value for further study.

5.4.3 Source Offset Voltage

Following transmission through the sampling cone into the intermediate vacuum region of the mass spectrometer, ions must continue into the high vacuum region.[81] Ions are pulled down a potential gradient set by the source offset voltage into the StepWave ion transfer,

facilitating entry to the mass analyser region of the mass spectrometer. High source offset voltages increase ion transmission into the mass spectrometer, increasing ion abundance and sensitivity. However, as with a high sampling cone voltage, the increased ion acceleration promotes collisions with gas phase molecules resulting in ion fragmentation.

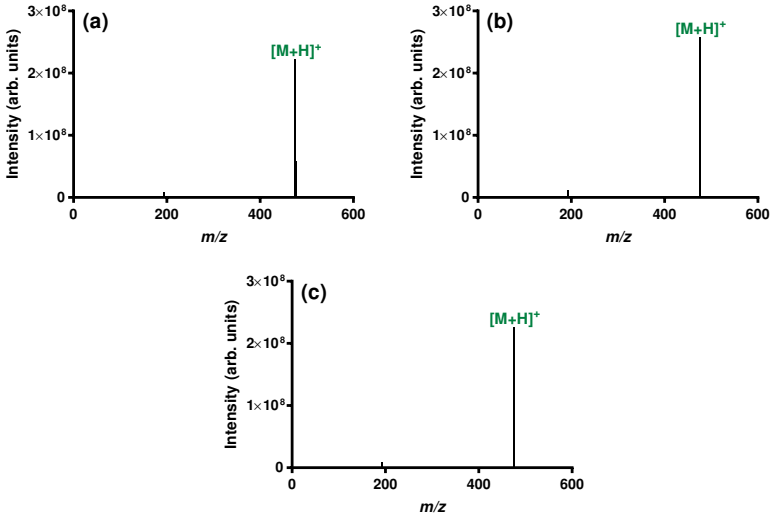

Figure 5.8 Ion profiles of *N*-palmitoyl procaine **35** upon application of differing source offset voltages: (a) 20 V; (b) 30 V; (c) 40 V.

Minimisation of in-source fragmentation at the weak amide bond of *N*-palmitoyl procaine **35** is a key consideration throughout tuning of the ESI source offset voltage. Ionisation profiles obtained over one minute from the direct infusion of *N*-palmitoyl procaine **35** are shown in Fig. 5.8. The source offset voltage was modified over the range of 20 V to 40 V in increments of 10 V. In-source fragmentation of *N*-palmitoyl procaine **35** was not noted to contribute significantly to observed ion profiles across the voltage range tested. Optimum source offset voltage is selected as 30 V based upon its ability to produce the maximum observed ion intensity by facilitating ion transmission.

5.4.4 Summary of Optimised ESI Parameters

Table 5.1 summarises the optimised ESI instrument parameters for the study of *N*-palmitoyl procaine **35**. However, suitability of the parameters for studying acylated small molecules in general, and thus small molecule intrinsic lipidation, must be determined. Utilising the optimised instrument parameters, the five other synthetic acylated small molecule standards were direct infused into the mass spectrometer. These were *N*-oleoyl procaine **36**, *N*-palmitoyl tetracaine **37**, *N*-oleoyl tetracaine **38**, *N*-palmitoyl propranolol **12** and *N*-oleoyl propranolol **13**. Mass spectra for each acylated small molecule standard under optimised condition are

shown in Fig. 5.9. Molecular $[M+H]^+$ ions are observed with good signal to noise for each desired analyte, with additional sodium adduct formation and dimerisation noted for *N*-palmitoyl propranolol **12** and *N*-oleoyl propranolol **13** due to preparation methodology. Low level in-source fragmentation is observed for all species, along with in-source double bond oxidation for *N*-oleoyl procaine **36**. However, observed issues are minimal and successful ionisation of all acylated small molecules cements the optimised parameters as those to be utilised for the study of small molecule intrinsic lipidation.

Parameter	Optimised Value
Capillary Voltage (kV)	1.0
Source Temperature (°C)	150.0
Sampling Cone Voltage (V)	50.0
Source Offset Voltage (V)	30.0
Desolvation Temperature (°C)	350.0
Cone Gas Flow (L/Hr)	60.0
Desolvation Gas Flow (L/Hr)	600.0
Nebuliser Gas Flow (Bar)	6.0

Table 5.1 Optimised positive mode electrospray parameters for mass spectrometry analysis of acylated small molecules.

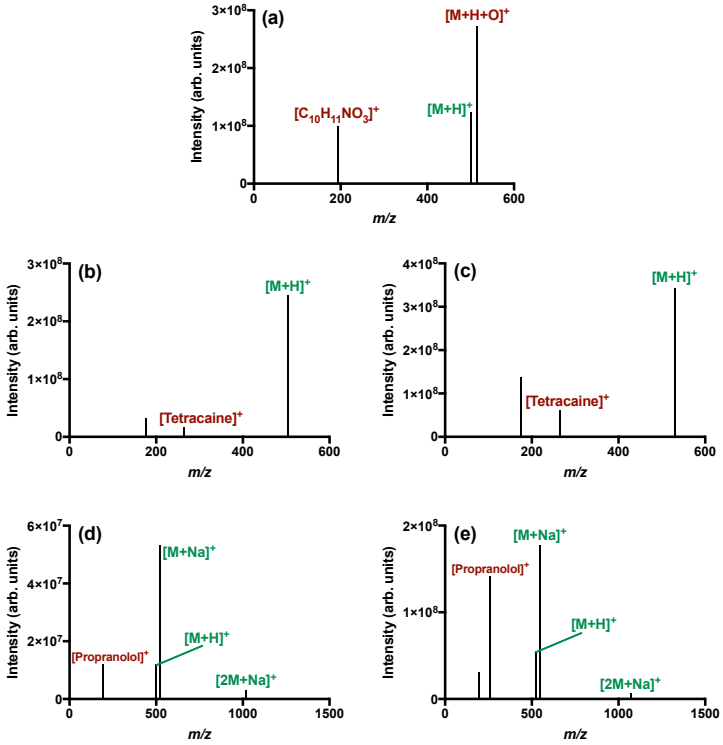

Figure 5.9 Ionisation profiles of synthetically prepared acylated small molecules under optimised instrument parameters given in Table 5.1: (a) *N*-oleoyl procaine **36**; (b) *N*-palmitoyl tetracaine **37**; (c) *N*-oleoyl tetracaine **38**; (d) *N*-palmitoyl propranolol **12**; (e) *N*-oleoyl propranolol **13** .

5.5 Optimisation of Chromatography

Ionisation of hydrophobic small molecules with poor ionisation potential in a complex mixture is challenging. These ions are suppressed in favour of ions corresponding to species with higher abundance or propensity towards ionisation.[106,251] Ion suppression can be avoided by the separation of components in a mixture such that each analyte within the sample is introduced individually into the mass spectrometer. The separation process is carried out by reversed phase LC on an Acquity UPLC (Waters Corp., UK). Reversed phase LC separation can be challenging for hydrophobic analytes due to high column affinity and poor solubility in the polar mobile phase. As a result analyses can be time consuming and exhibit issues with poor peak shape and separation of components. These issues can be avoided by developing optimised chromatography for the system of interest, in this case small molecule intrinsic lipidation.

Development of chromatography for the study of small molecule intrinsic lipidation requires selection of a suitable stationary phase. A BEH C_{18} column (Waters Corp., UK) provides an excellent option due to availability, understanding of the column chemistry, and previous success in the separation of small molecules including hydrophobic analytes.[11,39]

A binary mixture of H_2O (0.1 % formic acid) and MeCN (0.1 % formic acid) was selected as the mobile phase for analysis, given the compatibility with reversed phase LC, solubility of analytes in the solvent, and previous success in small molecule analysis. Building upon previous LC carried out for small molecules, the two solvents ran in a linear gradient at a flow rate of 0.400 mL/ min over a nine minute period.[77] Ensuring parity with ionisation optimisation, procaine **2** was selected as the small molecule utilised to develop chromatography for small molecule intrinsic lipidation. Inclusion of *N*-acylated procaine and lysolipid standards provide a full picture of the predicted contents of a small molecule intrinsic lipidation reaction mixture. As such, 0.5 µg mL^{-1} solutions in 1:1 H_2O:MeCN were prepared for procaine **2**, *N*-palmitoyl procaine **35**, and the lysolipid OPC.

Fig. 5.10 combines the the individual chromatograms for each of the predicted components of procaine lipidation under the chromatographic conditions described. Symmetrical and sharp peaks are observed, suggesting success in this aspect of chromatography. However, poor chromatographic resolution is observed for the peaks corresponding to *N*-palmitoyl procaine **35**, and lysolipid OPC. Given the low abundance of acylated small molecule expected to form through small molecule intrinsic lipidation, and the poor ionisation potential of these

products, such poor resolution was predicted to result in ion suppression issues.

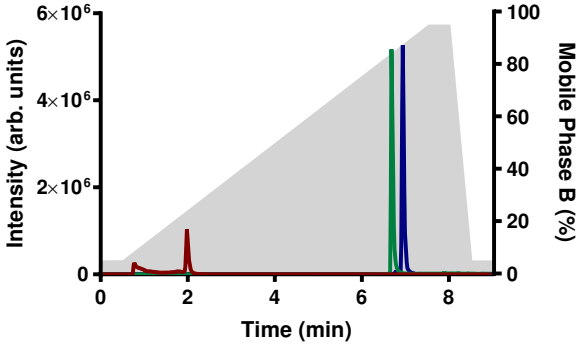

Figure 5.10 Combined traces of procaine **2** (red), *N*-palmitoyl procaine **35** (green), and lysolipid OPC (blue). Analysis was conducted on a BEH C_{18} column (Waters Corp., UK) with the nine minute linear gradient of mobile phase A (H_2O containing 0.1 % formic acid) and mobile phase B (MeCN containing 0.1 % formic acid) shown in grey.

Modification to the linear gradient was attempted in order to improve chromatographic resolution between *N*-palmitoyl procaine **35** and lysolipid by-products, thus avoiding ion suppression. Two modified gradients were developed, each reducing the gradient increase prior to acylated small molecule and lysolipid elution, thus facilitating improved resolution. Fig. 5.11 presents chromatographic traces for species of interest under the two modified gradients highlighted in grey. Improved chromatographic resolution between *N*-palmitoyl procaine **35** and OPC is observed for both new gradients, however the second provides better separation attributed to its extended shallow gradient. Given sharp and symmetrical peak shape is also maintained, modified gradient two was determined to provide optimum chromatographic conditions for study of procaine **2** intrinsic lipidation.

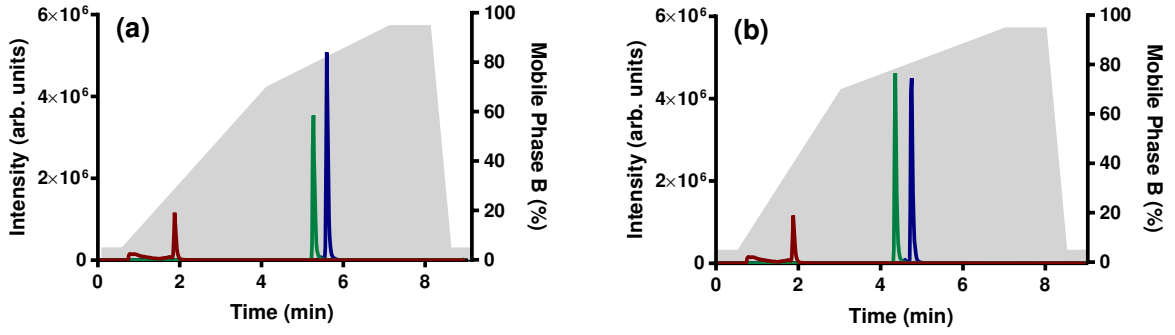

Figure 5.11 Chromatographic traces of procaine **2** (red), *N*-palmitoyl procaine **35** (green), and lysolipid OPC (blue) run on a BEH C_{18} column (Waters Corp., UK): (a) modified gradient one; (b) modified gradient two. Gradients both use mobile phase A (H_2O containing 0.1 % formic acid), and mobile phase B (MeCN containing 0.1 % formic acid) shown in grey.

Validation of the chromatographic conditions developed through the study of procaine **2** is required in order to confirm their suitability for the more general study of small molecule

intrinsic lipidation. One validation mechanism is the analysis of synthetically prepared acylated standards *N*-palmitoyl propranolol **12**, *N*-palmitoyl tetracaine **37**, and *N*-oleoyl procaine **36**. Comparing chromatograms of these acylated small molecules with those of lysolipid OPC, Fig. 5.12, allows for success of the optimised chromatography conditions to be determined. Analysis revealed defined peak shapes and separation between reaction mixture components for all small molecule systems studied, validating the developed chromatography conditions.

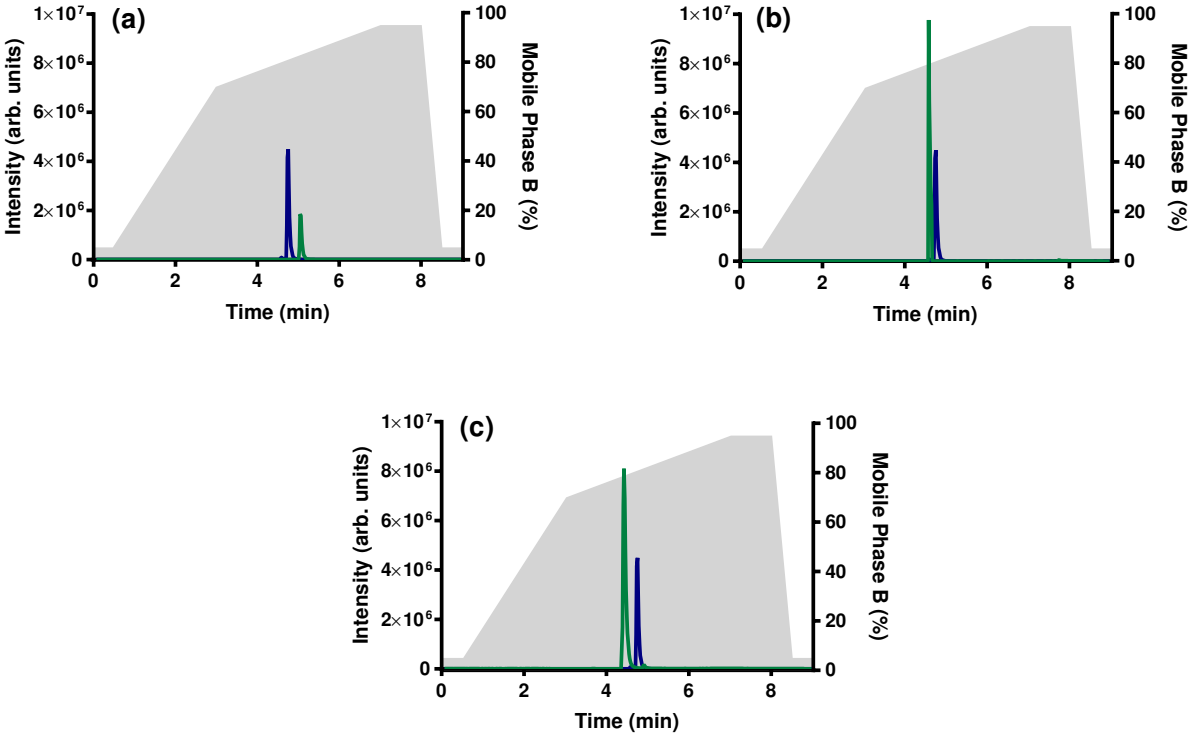

Figure 5.12 Chromatographic traces of lysolipid OPC (blue) synthetically acylated small molecules (green): (a) *N*-palmitoyl propranolol **12**; (b) *N*-palmitoyl tetracaine **37**; (c) *N*-oleoyl procaine **36**. Analysis was conducted using modified gradient two on a BEH C_{18} column (Waters Corp., UK). Mobile phase A (H_2O containing 0.1 % formic acid) and mobile phase B (MeCN containing 0.1 % formic acid) are shown in grey.

Application of optimised chromatography conditions of real small molecule intrinsic lipidation reaction mixtures is necessary to fully validate them. Samples containing DOPC liposomes and small molecule were prepared and incubated under physiological conditions for 72 hours. Fig. 5.13 presents the small molecules selected for this validation process. Propranolol **1**, procaine **2** and tetracaine **3** are included due to their pharmaceutical relevance and key role within the optimisation process. Small molecules **4** and **8** from the original screen of small molecule intrinsic lipidation of the QToF Premier (Waters Corp., UK) are also included. Otherwise, changes have been made to small molecules included within the set due to availability of small molecules, reassessment of potential reactivity, and the necessity of structural and functional diversity to ensure chromatographic validation.

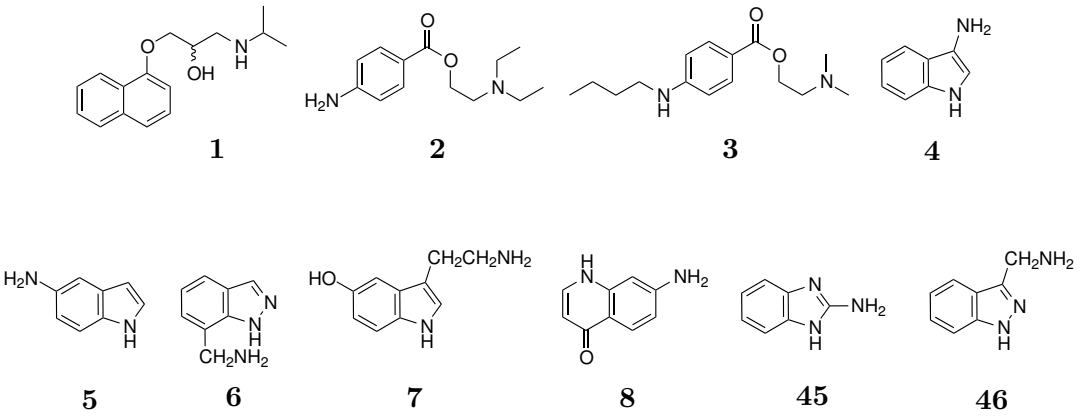

Figure 5.13 Cationic amphiphilic small molecules studied during preliminary screening of small molecule intrinsic lipidation, in an attempt to validate optimised chromatographic conditions.

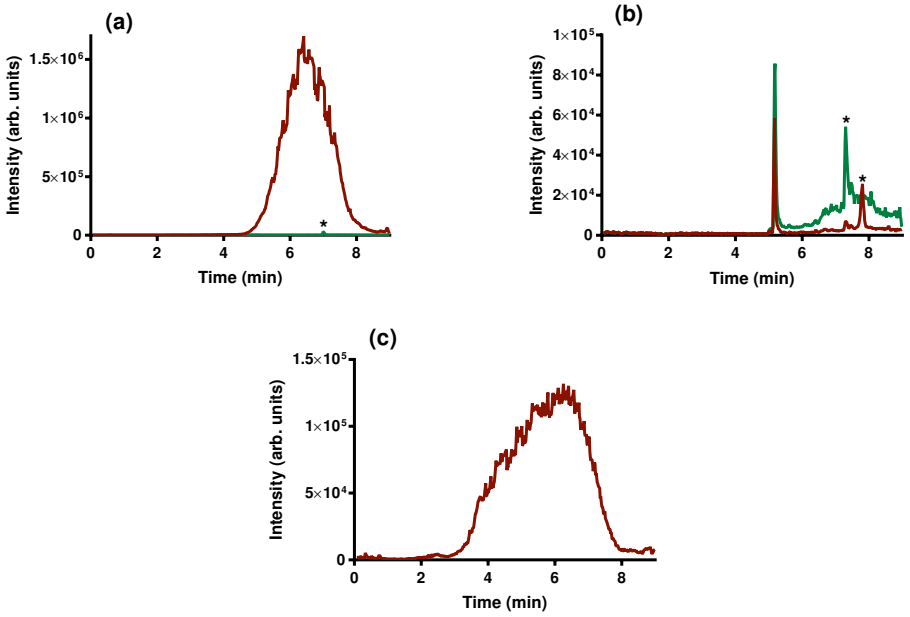

Figure 5.14 Chromatographic traces highlighting key issues associated with analysis of reaction mixtures under optimised chromatographic conditions on a BEH C_{18} column: (a) broad phospholipid peak (red) coelutes with acylated small molecule (*) resulting in ion suppression; (b) retention time fluctuation of second oleoylated propranolol peak (*) between analyses; (c) phospholipid eluting in blank run between analysis indicating column retention.

Validation of the optimised chromatographic conditions proved unsuccessful when faced with this more diverse selection of small molecules. Under the optimised conditions ion suppression of some acylated small molecules is likely, given their observed co-elution with phopholipid, shown in Fig. 5.14 (a). Furthermore, hydrophobic phospholipid present at high concentrations within the samples is retained by the BEH C_{18} column, Fig. 5.14 (c), causing poor peak shape and crossover contamination between samples. Propranolol **1** reaction mixtures exhibit peaks corresponding to the m/z of protonated oleoyl propranolol at two separate retention times. The

later eluting of these peaks coelutes with phospholipid and undergoes significant fluctuations in retention time, Fig. 5.14 (b), making examination challenging under the chromatographic conditions.

Development of chromatography for the study of small molecule intrinsic lipidation proved impossible using a BEH C_{18} column (Waters Corp., UK). Improved chromatography was therefore developed by considering alternative stationary phases with proven records in the separation of hydrophobic or aromatic small molecules. Table 5.2 presents four available columns which fit this criteria, and describes the differences in their column chemistry.[99]

Column Name	Column Chemistry
Acquity CSH C_{18}	Trifunctional C_{18} ligand bonded to a Charged Surface Hybrid (CSH) particle substrate
Acquity BEH Phenyl	Trifunctional C_6 Phenyl, bonded to Ethylene Bridged Hybrid (BEH) substrate
Acquity BEH Shield RP18	Monofunctional embedded polar C_{18}, bonded to Ethylene Bridged Hybrid (BEH) substrate
Acquity BEH C_8	Trifunctional C_8, bonded to Ethylene Bridged Hybrid (BEH) substrate

Table 5.2 Stationary phase column chemistries known to excel in the separation of hydrophobic or aromatic small molecules.[99]

Considering the previous challenges associated with developing chromatography for small molecule intrinsic lipidation utilising acylated standards, a different approach was adopted on this occasion. In an analogous fashion to previously attempted validation experiments, reaction mixtures containing liposomes with either propranolol **1** or compound **46** were prepared. Propranolol **1** was selected due the interesting observation of multiple peaks of oleoylated propranolol *m/z*, one of which elutes at a late retention time. Compound **46** was selected due to the co-elution of acylated product and lysolipid, and its significant structural and functional differences to propranolol **1**. Liposomes were prepared from phospholipid POPC, increasing the diversity of acyl chains available for transfer, and providing a wider variety of acylated small molecule and lysolipid products.

After 72 hours samples were analysed on each of the four stationary phases using first a linear gradient of H_2O:MeCN (both containing 0.1 % formic acid) at a flow rate of 0.400 mL/ min over nine minutes, and then a linear gradient of H_2O:MeOH (H_2O containing 0.1 % formic acid) at a flow rate of 0.400 mL/ min over nine minutes. MeOH was included within the mobile phase in this optimisation step due to the increased solubility of lysolipids and phospholipids in MeOH

compared to MeCN, and the lack of success in previous optimisation attempts. However, MeOH was immediately ruled out as a mobile phase component based on chromatograms resulting from the linear nine minute gradient, Fig. 5.15. Delays were observed in the elution of reaction mixture components across all column types when MeOH was employed as a mobile phase. Delayed elution proved particularly problematic for hydrophobic analytes, including acylated small molecules, resulting in an undesirable increase in run time, coelution, and reduced peak quality.

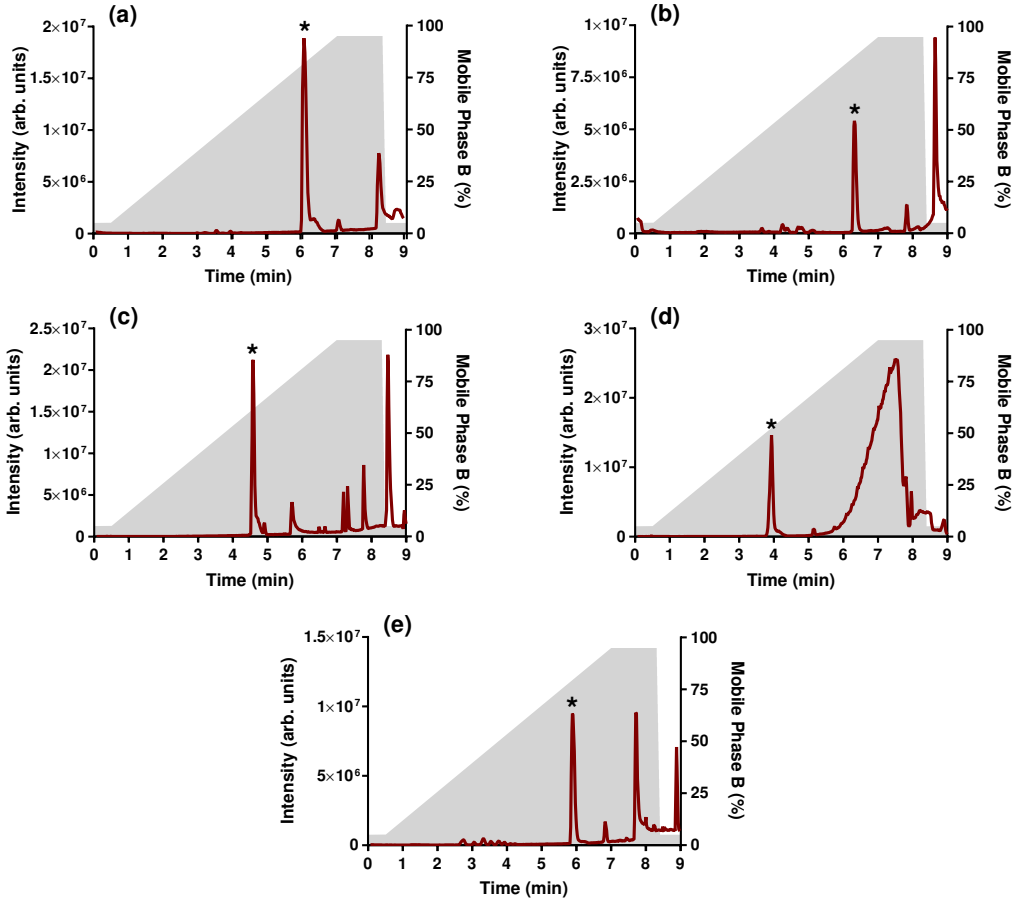

Figure 5.15 Examples of propranolol **1** reaction mixtures with POPC analysed on five stationary phase types: (a) Acquity BEH C_{18}; (b) Acquity CSH C_{18}; (c) Acquity BEH Phenyl; (d) Acquity BEH Shield RP18 ; (e) Acquity BEH C_8. Mobile phase conditions shown in grey employed a 9 minuted linear gradient of H_2O(0.1 % formic acid):MeOH. * indicates the peak corresponding to propranolol **1**, the earliest eluting species in the mixture.

Fig. 5.16 and Fig. 5.17 show chromatograms of propranolol **1** and compound **46** reaction mixtures respectively, using a nine minute linear H_2O:MeCN gradient. The Acquity CSH C_{18} (Waters Corp., UK) stationary phase provides little improvement compared to its Acquity BEH C_{18} (Waters Corp., UK) counterpart, exhibiting similar issues in separating mixture components and retention of phospholipids. Both the Acquity BEH C_8 (Waters Corp., UK) and Acquity BEH Shield RP18 (Waters Corp., UK) stationary phases give improved separation

of components compared to the Acquity BEH C_{18} (Waters Corp., UK) column, however issues remain with lipid retention and peak broadening. By contrast, the Acquity BEH Phenyl (Waters Corp., UK) stationary phase designed for aromatic small molecules achieves excellent component separation. Further, the Acquity BEH Phenyl (Waters Corp., UK) column consistently elutes phospholipid in a distinct peak even at high concentrations, minimising co-elution and preventing contamination between samples.

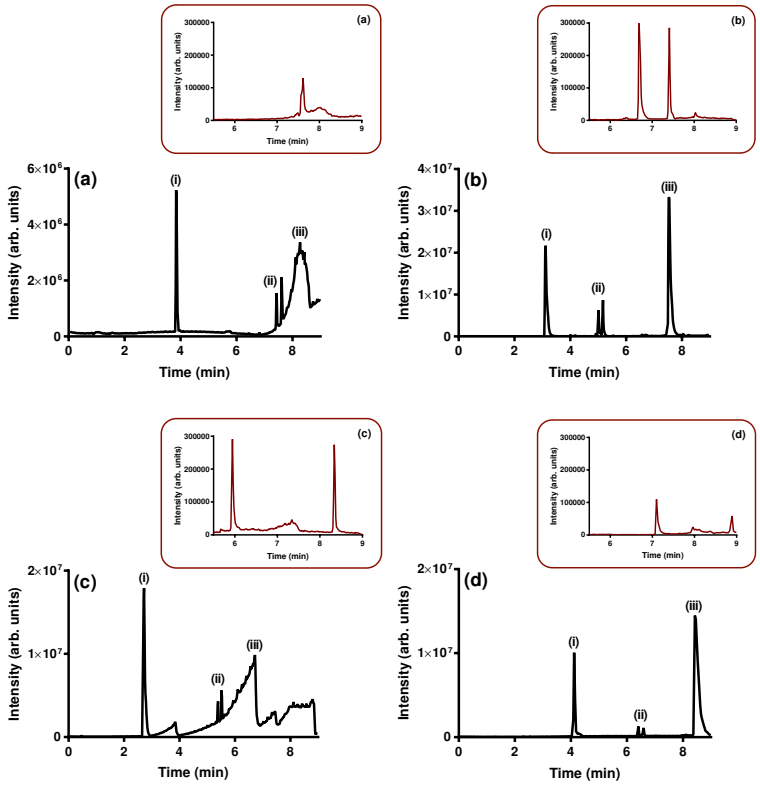

Figure 5.16 TIC (black) of propranolol **1** reaction mixture with POPC, analysed on four stationary phase types: (a) Acquity CSH C_{18}; (b) Acquity BEH Phenyl; (c) Acquity BEH Shield RP18 ; (d) Acquity BEH C_8. Mobile phase conditions used a 9 minuted linear gradient of H_2O:MeCN (both containing 0.1 % formic acid). Key species highlighted: (i) propranolol **1**; (ii) lysolipids PPC and OPC; (iii) POPC. Insets show EIC (red) for m/z 524.4, corresponding to protonated oleoyl propranolol **1** intrinsic lipidation products.

The Acquity BEH Phenyl (Waters Corp., UK) with a nine minute linear H_2O:MeCN gradient clearly provided superior chromatographic results compared to other stationary and mobile phases. No further modifications to the linear gradient were deemed necessary, due to the elution and separation of all reaction components. As such, these conditions were considered suitable for the study of small molecule intrinsic lipidation, and were taken forward for this purpose.

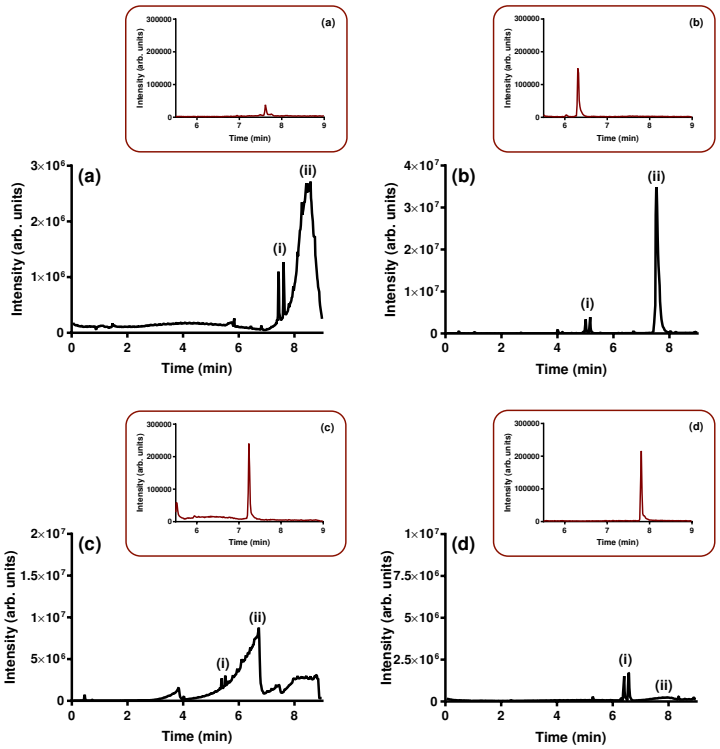

Figure 5.17 TIC (black) of compound **46** reaction mixture with POPC, analysed on four stationary phase types: (a) Acquity CSH C_{18}; (b) Acquity BEH Phenyl; (c) Acquity BEH Shield RP18 ; (d) Acquity BEH C_8. Mobile phase conditions used a 9 minuted linear gradient of H_2O:MeCN (both containing 0.1 % formic acid). Key species highlighted: (i) lysolipids PPC and OPC; (ii) POPC. Insets show EIC (red) for m/z 412.3 corresponding to protonated oleoyl compound **46** intrinsic lipidation products.

5.6 Proving Small Molecule Intrinsic Lipidation

5.6.1 Pharmaceutical Small Molecules

Development of LCMS parameters for the study of small molecule intrinsic lipidation centred upon direct observation of acylated small molecules. In comparison to previous analysis monitoring lysolipid by-product, these conditions allow for small molecule reactivity at the membrane interface to be proved. Propranolol **1**, procaine **2** and tetracaine **3**, are the small molecules selected to provide proof of small molecule intrinsic lipidation. Acylated standards of all three have been synthesised, providing predictable retention times under the developed chromatographic conditions and aiding identification. DOPC liposomes were selected for the study due to their mimicry of eukaryotic membranes. DOPC contains a single acyl chain type (oleoyl) such that acylated product formation is limited to the oleoylated products, maximising the abundance and minimising complexity.

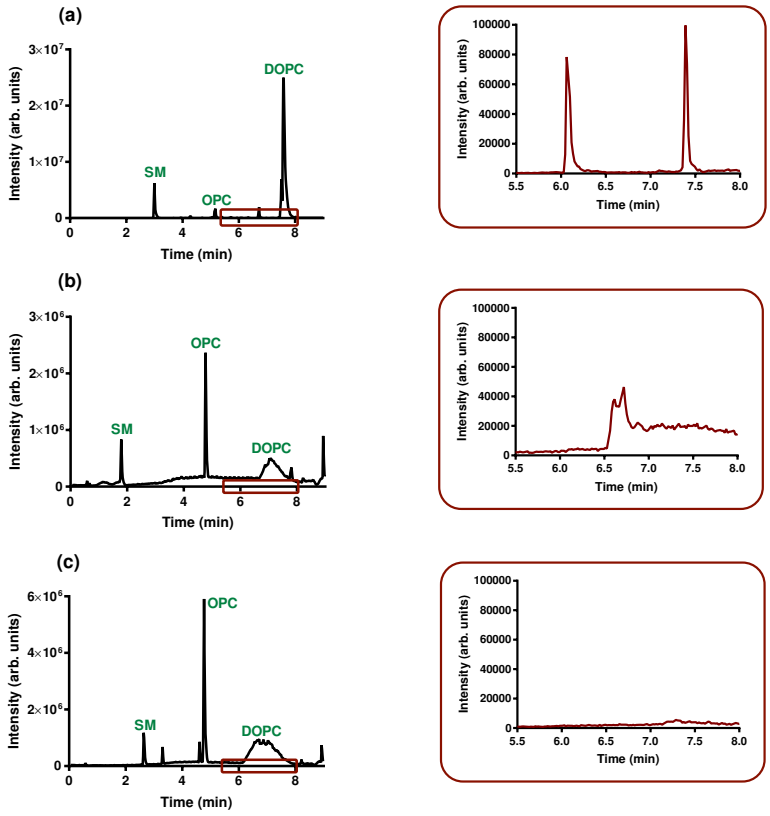

Figure 5.18 TIC corresponding to DOPC liposomes incubated for 72 hours under physiological conditions with: (a) propranolol **1**; (b) procaine **2**; (c) tetracaine **3**. The inserts show EIC for *m/z* of relevant protonated oleoylated products.

After 72 hours, mass spectrometry confirmed the presence of phospholipid, lysolipid and the relevant small molecule in each reaction mixture, Fig. 5.18. Study of the relevant retention time windows for acylated products did not yield a result for either procaine **2** or tetracaine **3**. As shown by the extracted ion chromatograms, Fig. 5.18 inserts, neither *N*-oleoyl procaine **36** or *N*-oleoyl tetracaine **38** were present. From this it can be concluded that under the conditions tested procaine **2** or tetracaine **3** are unreactive towards intrinsic lipidation.

The reaction mixture containing small molecule propranolol **1** contains two chromatographically distinct peaks attributed to the *m/z* of oleoylated propranolol. These two peaks, Fig. 5.18 (a) insert, correspond to products eluting at 6.1 min and 7.4 min. As Table 5.3 shows, accurate mass attributes both peaks to the molecular formula $C_{34}H_{54}NO_3$ with a ring-plus-double bonds (RDB) value of 8.5. This information aligns with that expected of protonated oleoylated propranolol, suggesting one or both peaks may be a result of small molecule intrinsic lipidation of propranolol.

Retention Time (min)	Observed m/z	Molecular Formula	RDB	Error (ppm)
6.1	524.4095	$C_{34}H_{54}NO_3$	8.5	-0.2
7.4	524.4092	$C_{34}H_{54}NO_3$	8.5	0.4

Table 5.3 Peaks observed in propranolol reaction mixture with DOPC under physiological conditions, determined to be of nominal m/z 524, attributed to protonated oleoylated propranolol.

Although accurate mass confirms that the chromatographic peaks at retention times 6.1 min and 7.4 min can both be attributed to the molecular formula $C_{34}H_{54}NO_3$, further confirmation is necessary to prove that the species are derived from the parent small molecule propranolol **1**. CID MSMS was performed on each of the two peaks, with the resulting data presented in Fig. 5.19. The presence of ions at m/z 260.1646 and m/z 260.1645 for the peaks at retention times 6.1 min and 7.4 min respectively, can be attributed to the molecular formula $C_{16}H_{22}NO_2$ with errors of -1.9 ppm and -2.7 ppm. This formula corresponds to the molecular ion of propranolol **1**. Additional ions at nominal m/z of 183 and 155 correspond to propranolol **1** product ions reported in the literature.[128,252,253]

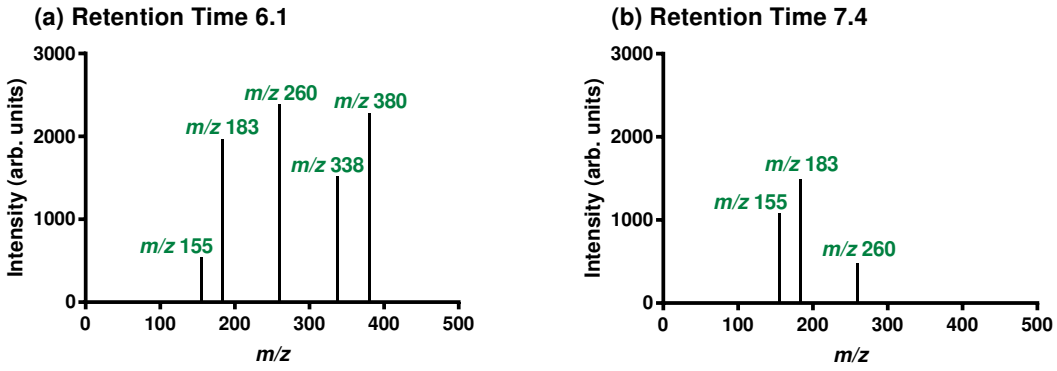

Figure 5.19 CID MSMS carried out at two chromatographic peaks representing nominal m/z 524, attributed to protonated oleoylated propranolol.

The species associated with peaks at retention times 6.1 min and 7.4 min are both propranolol derived with the molecular formula $C_{34}H_{54}NO_3$. The peak at retention time 7.4 min matches the retention time of synthetically prepared *N*-oleoylated propranolol **13**, and is attributed to this species. The peak at retention time 6.1 min was attributed to an alternative oleoylated propranolol species, hypothesised to be *O*-oleoylated propranolol **47**. Investigation into the nature and relationship of these species will be pursued in Chapter 6 of this thesis, including complete analysis of the associated MSMS data presented in Fig. 5.19. The formation of oleoylated propranolol species observed in the reaction mixture are only possible as a result of non-enzymatic reactivity with the membrane. Considering this, the observation provides the

first definitive proof of the existence of small molecule intrinsic lipidation.

Despite the observed reactivity of propranolol **1** with a DOPC membrane, there is a lack of reactivity for procaine **2** and tetracaine **3**. One mechanism predicted to increase reactivity involves increasing the proportion of small molecule bound to the phospholipid membrane by promoting electrostatic attraction. Given the cationic amphiphilic nature of all three small molecules, increased binding can be achieved by modification of the liposome composition to include negatively charged phospholipids. A DOPC:DOPS (4:1) phospholipid mixture is utilised to prepare one set of liposomes, mimicking the composition of a viral membrane. DOPS contains a negatively charged PS phosphate head group, highlighted blue in Fig. 5.20, and two oleoyl fatty acid chains. The second set of liposomes provide a model of a bacterial cell membrane, contain a mixture of DOPE:DOPG (3:1).[254] DOPE and DOPG contain the PE and PG phosphate head groups, which are zwitterionic and negatively charged in nature respectively.

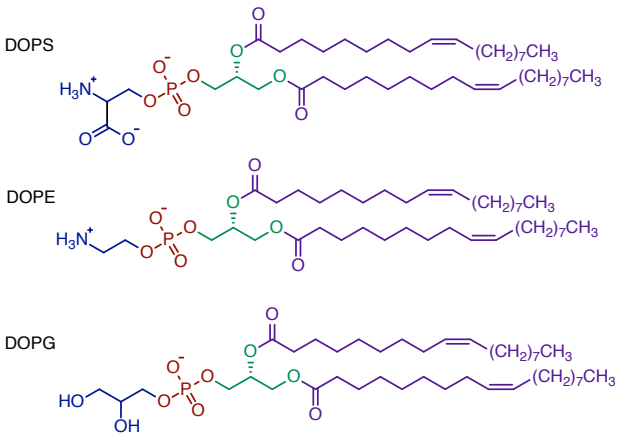

Figure 5.20 Chemical structure of the membrane phospholipids DOPS, DOPE and DOPG. Key structural features highlighted: (i) oleoyl chains in purple; (ii) glycerol backbone in green; (iii) phosphate in red; (iv) head group in blue.

Propranolol **1** undergoes intrinsic lipidation resulting in formation of two distinct oleoylated products in both DOPC:DOPS (4:1) and DOPE:DOPG (3:1) membranes. The two products are determined by retention time and MSMS analysis to be equivalent to those observed within a DOPC only membrane. This reactivity confirms that intrinsic lipidation is possible in models of eukaryotic, prokaryotic and viral membranes irrespective of composition. By contrast, procaine **2** and tetracaine **3** were not observed to undergo intrinsic lipidation in any of the three membrane types. This occurs despite the increased electrostatic attraction between the cationic amphiphilic small molecules and negatively charged phospholipids.

Limited available research into small molecule intrinsic lipidation provokes challenges in understanding the unreactive nature of procaine **2** and tetracaine **3**. However, it is possible to speculate on the reasons behind this lack of reactivity by considering key small molecule properties, Table 5.4.[255,256] Determined in liposomal membrane (DMPC)-water systems at pH 7.4, logD values take into account membrane partitioning for both ionised and unionised forms of small molecule species. Procaine **2** and tetracaine **3** exhibit logD values of 1.00 and 2.35 respectively, indicating a decreased preference for membrane binding compared to reactive propranolol **1**.[255] Furthermore, under physiological conditions membrane association is promoted to a greater extent for the ionised unreactive forms of procaine **2** and tetracaine **3**, compared to propranolol **1**.[255] Consideration of pK_a values for procaine **2**, tetracaine **3**, and propranolol **1**, Table 5.4, further supports the observation that the predominant species at physiological pH are unreactive ionised forms. Reduced binding affinity combined with similarly unfavourable speciation, provides insight into the unreactive nature of procaine **2** and tetracaine **3** compared to reactive propranolol **1**.

Small Molecule	pK_a	logD (pH 7.4)	Polar Surface Area (Å^2)
Propranolol **1**	9.53	2.63	41.49
Procaine **2**	8.49	1.00	55.56
Tetracaine **3**	9.04	2.35	41.57

Table 5.4 Physical properties attributed to propranolol **1**, procaine **2**, and tetracaine **3**.[257] logD values were determined using a liposomal membrane (DMPC)-water system at pH 7.4 and 21 °C.[255] These and all future reported pK_a values correspond to the calculated pK_a of the conjugate acid of the most basic site.

In addition to pK_a and logD values, membrane binding orientation is predicted to influence a small molecule's ability to undergo intrinsic lipidation. Fortunately, interactions of procaine **2** and tetracaine **3** with the cell membrane have been studied extensively, due to the role of membrane penetration depth and orientation in their anaesthetic activity. Boulanger *et al.* determined that both procaine **2** and tetracaine **3** have multiple composition dependent binding sites and orientations within the cell membrane, each of which has a distinct binding strength.[258] However, combined NMR, linear dichroism (LD) and molecular dynamics simulations (MDS) studies reveal one favoured binding orientation per compound, Fig. 5.21.[256,259,260] Tetracaine **3** penetrates the membrane deeply upon binding, burying its reactive amine nucleophile within the hydrophobic bilayer region. The lack of tetracaine **3** reactivity may therefore be accounted for by insufficiently close proximity between the reactive amine and a phospholipid ester linkage. Procaine **2** penetrates the membrane less deeply upon binding, lying in

the hydrophilic head group region of the bilayer. However, the reactive amine of procaine **2** does not penetrate the ester containing bilayer region, preventing proximity between the two. Membrane fluidity is altered upon small molecule binding, modulating local hydration levels predicted to have an effect upon intrinsic lipidation through the catalytic activity of H_2O.[11,261]

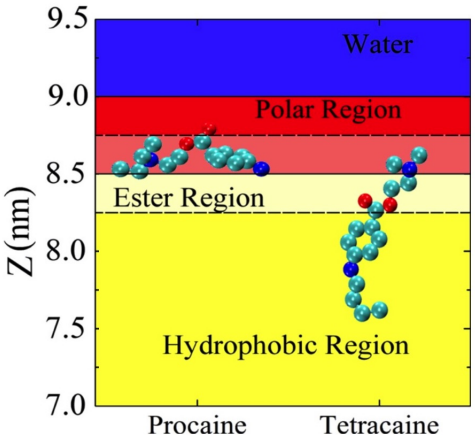

Figure 5.21 MDS modelling predictions for the predominant membrane binding orientation of procaine **2** and tetracaine **3**.[256]

Several small molecule and membrane characteristics are speculated to influence small molecule intrinsic lipidation of procaine **2** and tetracaine **3**. It is possible to predict the influence of some factors, such as membrane composition, pK_a, logD and small molecule binding orientation. However, the extent of the contribution of each factor towards the small molecule intrinsic lipidation reactivity is unknown. In summary, small molecule intrinsic lipidation is a highly complex process dependent upon several variables, and significant work remains in order to develop a clear understanding of the reaction.

5.6.2 Other Small Molecules

Propranolol **1** reactivity provides proof of small molecule intrinsic lipidation. However it remains to be discovered whether this is a unique property of one small molecule or a more generic process. Investigation into this was pursued using the cationic amphiphilic small molecules shown in Fig. 5.22, studied previously without success during chromatographic optimisation. Under optimised analytical conditions each small molecule was screened for the presence of intrinsic lipidation reaction product in combination with DOPC, DOPC:DOPS (4:1) and DOPE:DOPG (3:1) bilayers.

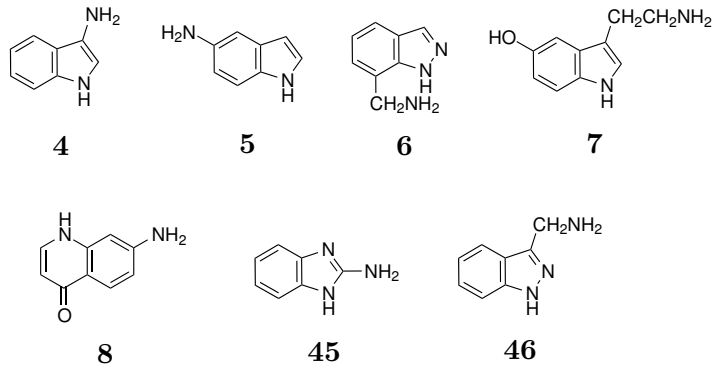

Figure 5.22 Cationic amphiphilic small molecules used to investigate whether small molecule intrinsic lipidation is a generic process.

Table 5.5 summarises observations of acylated product formation for each small molecule tested in the three membrane types. Small molecules **4**, **8** and **7** either do not undergo small molecule intrinsic lipidation or have product levels below the instrument limit of detection. Four of the seven small molecules, **5**, **45**, **46** and **6** exhibited formation of acylated product, confirmed by accurate mass. Where intrinsic lipidation products were observed, formation was consistent across all membrane systems tested in all but the case of compound **5**. This observation may suggest the role of membrane composition is minimised in controlling small molecule intrinsic lipidation, however without quantification of products this cannot be said with certainty. These results prove a stark contrast to past research monitoring intrinsic lipidation via lysolipid by-product formation, supporting the belief that monitoring of lysolipid is not a reliable mechanism for studying small molecule intrinsic lipidation.

Small Molecule	Oleoylated Product Molecular Formula	Oleoylated Product Theoretical m/z	DOPC Observed Error (ppm)	PC:PS Observed Error (ppm)	PE:PG Observed Error (ppm)
4	$C_{26}H_{41}ON_2$	397.3219	-	-	-
5	$C_{26}H_{41}ON_2$	397.3219	-2.3	-	-4.0
45	$C_{25}H_{40}ON_3$	398.3173	-1.8	-3.8	-2.8
46	$C_{26}H_{42}ON_3$	412.3328	-2.7	-4.9	-3.2
6	$C_{26}H_{42}ON_3$	412.3328	-1.7	-2.9	-0.7
8	$C_{27}H_{41}O_2N_2$	425.3168	-	-	-
7	$C_{28}H_{45}O_2N_2$	441.3481	-	-	-

Table 5.5 Protonated oleoylated products formed by small molecule intrinsic lipidation observed by LCMS within different membrane types: (i) DOPC; (ii) PC:PS is DOPC:DOPS (4:1); (iii) PE:PG is DOPE:DOPG (3:1).

Observation of oleoylated product formation for small molecules **5**, **45**, **46** and **6** confirms

that small molecule intrinsic lipidation is general process. As such, other cationic amphiphilic small molecules of greater structural and functional diversity were tested to look for evidence of intrinsic lipidation. The small molecules in Fig. 5.23 were combined with eukaryotic, viral and prokaryotic membrane models and analysed by mass spectrometry. Table 5.6 summarises the results of this screening process. Oleoylated product formation was observed for five small molecules, compounds **49**, **50**, **52**, **58**, and **59**. Membrane composition was not observed to modify the propensity of a small molecule towards intrinsic lipidation for compounds **49**, **58**, and **59**, given the comparable results between liposome types. However, membrane selectivity was observed for compound **50**, exhibiting reactivity in a DOPC membrane only, and compound **52**, exhibiting reactivity in both DOPC and DOPC:DOPS (4:1) membrane systems. These observations suggest preferential eukaryotic reactivity irrespective of increased electrostatic attraction associated with prokaryotic model systems. Further study is required in order to determine whether this observed selective reactivity is small molecule specific, a result of low product abundance, or a general feature of small molecule intrinsic lipidation.

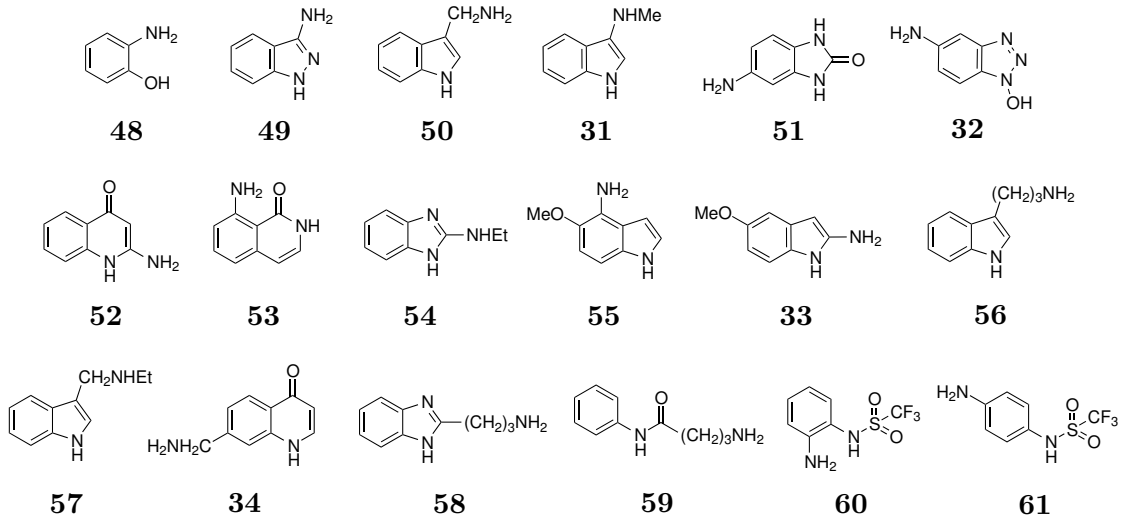

Figure 5.23 Cationic amphiphilic small molecules used to investigate whether small molecule intrinsic lipidation is a generic process.

Small Molecule	Oleoylated Product Molecular Formula	Oleoylated Product Theoretical m/z	DOPC Observed Error (ppm)	PC:PS Observed Error (ppm)	PE:PG Observed Error (ppm)
48	$C_{24}H_{40}O_2N$	374.3059	-	-	-
49	$C_{25}H_{41}ON_3$	399.3250	-5.8	-4.3	-5.3
50	$C_{27}H_{43}ON_2$	411.3375	-8.3	-	-
31	$C_{27}H_{44}ON_2$	412.3454	-	-	-
51	$C_{25}H_{40}O_2N_3$	414.3121	-	-	-
32	$C_{24}H_{40}O_2N_4$	416.3151	-	-	-
52	$C_{27}H_{41}O_2N_2$	425.3168	-3.8	-2.6	-
53	$C_{27}H_{42}O_2N_2$	426.3246	-	-	-
54	$C_{27}H_{44}ON_3$	426.3484	-	-	-
55	$C_{27}H_{43}O_2N_2$	427.3325	-	-	-
33	$C_{27}H_{44}O_2N_2$	428.3403	-	-	-
56	$C_{29}H_{47}ON_2$	439.3688	-	-	-
57	$C_{29}H_{47}ON_2$	439.3688	-	-	-
34	$C_{28}H_{44}O_2N_2$	440.3403	-	-	-
58	$C_{28}H_{46}ON_3$	440.3641	-4.3	-4.3	-4.5
59	$C_{28}H_{47}O_2N_2$	443.3638	-5.2	-3.6	-2.3
60	$C_{25}H_{40}O_3N_2SF_3$	505.2712	-	-	-
61	$C_{25}H_{40}O_3N_2SF_3$	505.2712	-	-	-

Table 5.6 Protonated oleoylated products formed by small molecule intrinsic lipidation observed by LCMS within different membrane types: (i) DOPC; (ii) PC:PS is DOPC:DOPS (4:1); (iii) PE:PG is DOPE:DOPG (3:1).

Probing the physical parameters associated with all cationic amphiphilic small molecule studied facilitates examination of factors controlling intrinsic lipidation reactivity. Table 5.7 provides available pK_a, logP and logD values for the small molecules screened for intrinsic lipidation, with reactive species highlighted in green. pK_a values corresponding to reactive species are not indicative of a trend, spanning a range of 3.72 up to 11.91. Despite the low pK_a of compound **8** increasing the proportion of reactive neutral amine at physiological pH, there is no indication of reactivity. By contrast, compound **58** is active towards intrinsic lipidation despite its pK_a of 11.91 minimising the proportion of available reactive species. Similarly, no trend between intrinsic lipidation reactivity and either logP or logD value is observed. Even compounds with similar logP and logD values, such as **51** and **52** differ in their propensity towards membrane reactivity. Unfortunately, properties and membrane binding activity of small molecules within this study are poorly characterised compared to their pharmaceutical counterparts. As a result, information regarding membrane binding orientation and membrane

penetration depth is unavailable. Considering the variation in physical parameters observed between reactive species, these factors may play a vital role in modulating intrinsic lipidation of small molecules.

Small Molecule	pK_a	logP	logD (pH 7.4)
4	5.31	1.55	1.53
5	4.94	0.85	0.85
45	6.93	1.15	0.72
46	8.16	0.83	-0.61
6	8.99	-1.19	-1.01
8	2.58	-0.40	-0.40
7	9.52	0.54	-2.04
48	4.74	0.50	0.49
49	3.72	1.46	1.46
50	10.48	1.61	-1.27
31	0.61	1.54	1.54
51	5.61	0.20	0.17
32	7.25	-0.20	-0.58
52	3.79	0.14	0.14
53	3.12	0.50	0.50
54	7.26	2.94	1.37
55	3.96	1.22	1.22
33	4.16	1.17	1.17
56	10.63	1.81	-1.18
57	10.86	2.28	-0.75
34	9.00	1.08	-0.52
58	11.91	1.68	-0.97
59	9.85	0.89	-1.63
60	4.85	2.01	0.31
61	2.98	1.99	0.69

Table 5.7 Physicochemical properties of small molecules screened for intrinsic lipidation calculated using ChemAxon.[262] Reactive small molecules are highlighted in green.

5.7 Conclusions

Small molecule intrinsic lipidation is characterised by an acyl transfer reaction from a membrane phospholipid to a small organic molecule. Previous research has attempted to study the reaction through monitoring of lysolipid, a reaction by-product.[77] Given that lysolipid formation is not diagnostic of reactivity, a novel approach seeks to monitor the acylated small molecule product directly by mass spectrometry. Unfortunately, visualisation of acylated small molecules is

analytically challenging due to their hydrophobicity and poor ionisation potential. As a result, bespoke analytical conditions are required beyond those utilised routinely within Durham University mass spectrometry service.

Successful development of mass spectrometry for the study of small molecule intrinsic lipidation requires instrument parameters to be tuned using acylated small molecule standards. Organic synthetic methodologies facilitated the preparation of *N*-palmitoyl procaine **35**, *N*-oleoyl procaine **36**, *N*-palmitoyl tetracaine **37**, and *N*-oleoyl tetracaine **38** standards. *N*-palmitoyl propranolol **12** and *N*-oleoyl propranolol **13** were also prepared synthetically despite technical challenges resulting from micelle formation during purification.

Preparation of synthetic acylated small molecules facilitated the optimisation of ESI parameters for their study. Capillary voltage, sample cone voltage and source offset voltage proved key parameters in balancing maximum ionisation with minimum in-source fragmentation. In addition, synthetic standards aided the development of chromatographic conditions for the study of small molecule intrinsic lipidation. Initial conditions utilised a H_2O:MeCN gradient on a BEH C_{18} (Waters Corp., UK) stationary phase. However, these conditions exhibited issues with co-elution and contamination when faced with real reaction mixtures containing increasingly diverse small molecules. Modification of the stationary phase to a BEH Phenyl column (Waters Corp., UK) resolved these issues, ultimately resulting in successful optimisation of chromatographic conditions.

Definitive proof of small molecule intrinsic lipidation *in vitro* occurred through the observation of acylated propranolol using the bespoke analytical conditions developed. Two intrinsic lipidation products of propranolol **1** were confirmed by accurate mass and MSMS in the presence of eukaryotic, viral and prokaryotic model membranes. Screening of a more structurally and functionally diverse family of small molecules revealed nine further small molecules able to undergo intrinsic lipidation. This observation serves as proof that intrinsic lipidation *in vitro* is a general process and not unique to propranolol **1**. However, it is noted that not all cationic amphiphilic small molecules undergo intrinsic lipidation upon binding the membrane. Factors such as logP, pK_a, membrane composition, and binding orientation, are predicted to play a role in this. Without further research it is impossible to determine the extent to which each factor has an effect, and whether there are additional factors in play.

6 | Propranolol Intrinsic Lipidation *in vitro*

6.1 Introduction

James W. Black discovered propranolol **1** in 1964, a drug in the β blocker family found to affect the heart and circulatory system.[263,264] Prescribed either orally or intravenously, propranolol **1** treats a range of conditions including high blood pressure, angina and migraines. The subject of the 1988 Nobel Prize in Medicine, propranolol **1** is considered to be both safe and effective, featuring on the World Health Organisation's List of Essential Medicines.[265] Despite its popularity within the pharmaceutical industry, study of propranolol **1** has revealed poorly understood promiscuous behaviour.[158,258,266–268] This behaviour, linked to propranolol's **1** lipid solubility, raises questions about the drug's safety, mechanism of activity, and side effects.

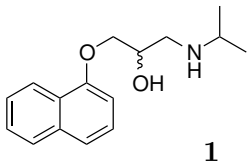

1

Figure 6.1 The structure of β blocker propranolol **1**.

Cationic amphiphilic in nature, propranolol **1** has a logD value at physiological pH 7.4 of 2.63, promoting membrane binding.[269] Interactions between propranolol **1** and the cell membrane are observed to impact the membrane structure and composition.[28,157,268,270] Increases in membrane fluidity, disorder and curvature occur upon propranolol **1** binding, impacting not only the local area but the bulk membrane. Bulk membrane modifications influence the activity of membrane bound components. Thus propranolol **1** binding is observed to alter enzymatic activity and block sodium ion channels.[261] Anaesthetic behaviour of propranolol

1 has also been linked to interactions with the cell membrane, given similar mechanisms of action observed for anaesthetics such as procaine **2** and tetracaine **3**.[256,261] Phospholipidosis, a major but poorly understood side effect of propranolol **1** and other drugs, is linked to the cell membrane. A lysosomal storage disorder, phospholipidosis is characterised by phospholipid accumulation in tissues.[73,74,271]

Small molecule intrinsic lipidation is one membrane-drug interaction which may play a role in the promiscuous behaviour of propranolol **1**. Preliminary studies presented in Chapter 5 of this thesis observe formation of acylated propranolol derivatives in the presence of a membrane mimic. This non-enzymatic acyl transfer is attributed to an innate reactivity between propranolol **1** and phospholipids. Further investigation is required in order to determine the significance of this reactivity. This includes characterisation of product nature and quantity, influence upon the physiochemical properties of propranolol **1**, and impact of environmental factors.

6.2 Products of Propranolol Intrinsic Lipidation

Mass spectrometry reveals the presence of two propranolol **1** derived products upon incubation of propranolol **1** with a DOPC phospholipid membrane under physiological conditions. Accurate mass information obtained using a Synapt G2-S (Water Corp., UK) mass spectrometer, attributes the molecular formula $C_{34}H_{54}NO_3$ to both propranolol **1** derived species. Based on the molecular formula, these species are hypothesised to be oleoylated propranolol formed via acyl transfer from the membrane. CID MSMS supports this theory, revealing product ions attributed to both intact propranolol **1** and known propranolol **1** MSMS fragments. However, the two propranolol **1** derived products are clearly chemically and structurally distinct, given their chromatographic differences. As shown in Fig. 6.2, the retention times attributed to the two products are 6.1 min and 7.4 min respectively.

Considering both the analytical data obtained and the solution phase reactivity of propranolol **1**, the nature of the two propranolol **1** derived species can be hypothesised. Propranolol **1** contains two nucleophilic functionalities able to perform intrinsic lipidation, an alcohol and a secondary amine. Accordingly, the two products are predicted to be the ester *O*-oleoyl propranolol **47** and the amide *N*-oleoyl propranolol **13**, shown in Fig. 6.3. Confirmation that these are the observed propranolol **1** derived species can be achieved by comparison to their synthetically prepared analogues.

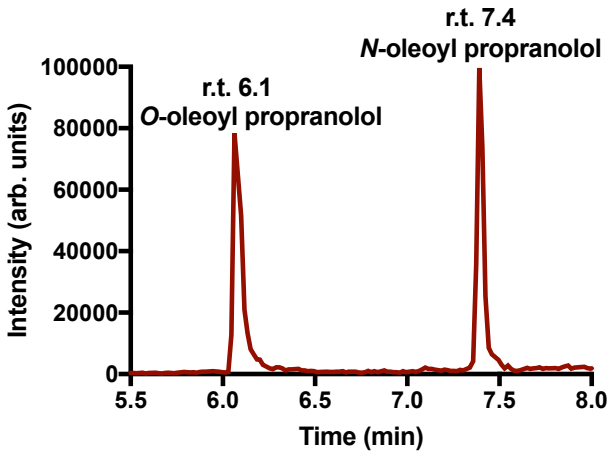

Figure 6.2 EIC for *m/z* 524.4102 attributed to the molecular formula $C_{34}H_{54}NO_3$, within a reaction mixture of propranolol **1** with DOPC phospholipid membrane under physiological conditions.

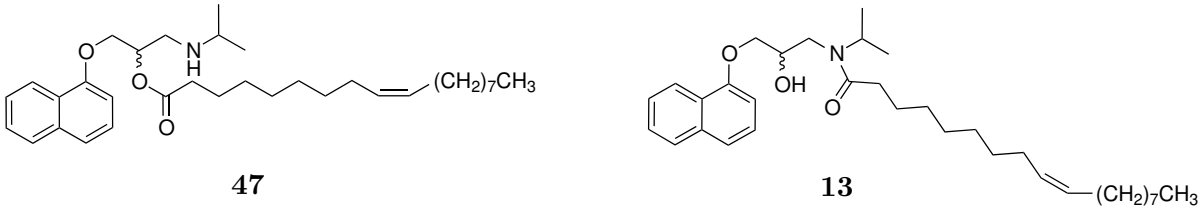

Figure 6.3 The two predicted products of propranolol **1** intrinsic lipidation: (i) *O*-oleoyl propranolol **47**; (ii) *N*-oleoyl propranolol **13**.

6.2.1 *O*-Acylated Propranolol

Confirmation of *O*-oleoyl propranolol **47** as a propranolol **1** derived intrinsic lipidation product requires comparison to a synthetic standard of the molecule. Accordingly, synthetic methodology for the preparation of *O*-oleoyl propranolol **47** is presented in Scheme 6.1.[179,244,245,272] *O*-palmitoyl propranolol **62** can also be synthesised via this methodology. Preparation of both species allows the influence of acyl chain type upon analytical parameters such as retention time and MSMS fragmentation to be determined. Palmitoyl and oleoyl are the preferred acyl chains due to their synthetic availability, and commonality to eukaryotic cell membranes.

The initial step in the preparation of an *O*-acylated propranolol species is synthesis of *N*-Boc propranolol **63**. Boc protection of propranolol **1** under standard conditions acts to shield the amine moiety and prevent future reactivity. *N*-Boc propranolol **63** is then exposed to the relevant acid chloride, palmitoyl chloride **18** or oleoyl chloride **20**. Stirring under argon in anhydrous DCM and pyridine results in formation of the intermediates *N*-Boc-*O*-palmitoyl propranolol **64** and *N*-Boc-*O*-oleoyl propranolol **65**.

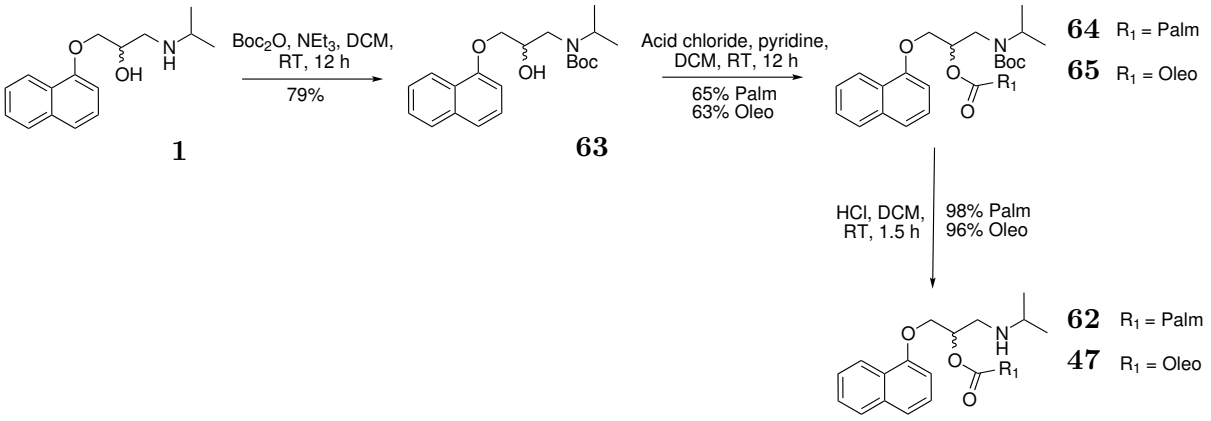

1 **63**

Scheme 6.1 Synthetic protocol for preparation of *O*-acylated propranolol derivatives *O*-palmitoyl propranolol **62** and *O*-oleoyl propranolol **47**. Palm represents the palmitoyl group $(CH_2)_{14}CH_3$ and oleo represents the oleoyl group $(CH_2)_7CHCH(CH_2)_7CH_3$.

The final synthetic step is cleavage of the Boc protecting group from the *N*-Boc-*O*-palmitoyl propranolol **64** and *N*-Boc-*O*-oleoyl propranolol **65** intermediates. Boc removal must proceed whilst preventing loss of the desired product through secondary reactions. Product loss can occur as a result of either propranolol **1** formation via ester hydrolysis, or via *O* to *N* acyl chain migration, producing *N*-acylated propranolol. Traditional conditions for Boc cleavage utilise trifluoroacetic acid (TFA) in DCM, followed by by-product removal *in vacuo*.[272] Acidic conditions combined with limited time in solution prevent unwanted hydrolysis or migratory side reactions. As a result, the TFA salts of *O*-palmitoyl propranolol **62** and *O*-oleoyl propranolol **47** were successfully synthesised. However, the presence of large non-natural TFA counter ion modifies properties of the *O*-acylated propranolol TFA salts compared to the *O*-acylated propranolol products of intrinsic lipidation. These modifications cause analytical problems, particularly chromatographically, resulting in isolation of products as their TFA salts being deemed undesirable.

Boc cleavage can also be performed using HCl, resulting in the formation of a chloride salt product with increased biological relevance. *N*-Boc-*O*-palmitoyl propranolol **64** and *N*-Boc-*O*-oleoyl propranolol **65** were stirred with HCl in ethyl acetate (EtOAc), and the organic layer washed with 10 % HCl solution to remove aqueous soluble impurities. Despite the acidic conditions maintained throughout, the increased time in solution resulted in migratory side reactions. As a result, the final products were identified as *N*-palmitoyl propranolol **12** and *N*-oleoyl propranolol **13** rather then the desired *O*-acylated counterparts. HCl in DCM provides an alternative HCl based Boc cleavage methodology, whilst allowing impurities to be removed *in vacuo* rather than through an aqueous work up. This synthetic route promotes

product solubility, reduces time in solution, and maintains acidic conditions for the prevention of intramolecular *O* to *N* migration or hydrolysis reactions. As a result, purified HCl salts of the desired products *O*-palmitoyl propranolol **62** and *O*-oleoyl propranolol **47** were isolated.

The identities of *O*-palmitoyl propranolol **62** and *O*-oleoyl propranolol **47** were determined through characterisation by accurate mass MS, IR, ^{1}H and ^{13}C NMR. The species were then analysed by MS under the conditions developed for the study of small molecule intrinsic lipidation. 3 µL of a 1 µg mL^{-1} solution of either *O*-palmitoyl propranolol **62** or *O*-oleoyl propranolol **47** in 1:1 H_2O:MeCN was injected into the LC of the mass spectrometer at time point zero. Retention times of 6.0 min and 6.1 min were observed for *O*-palmitoyl propranolol **62** and *O*-oleoyl propranolol **47** respectively. As indicated in Fig. 6.4, this provides sufficient chromatographic separation to distinguish between the two chemically similar species. *O*-palmitoyl propranolol **62** produces a molecular ion at *m/z* 498.3961 corresponding to the correct molecular formula $C_{32}H_{52}NO_3$ with an error of 2.8 ppm. *O*-oleoyl propranolol **47** produces a molecular ion at *m/z* 524.4111 corresponding to the molecular formula $C_{34}H_{54}NO_3$ with an error of 1.3 ppm. Neither species produces ions attributed to in-source fragmentation, adduct formation or dimerisation under the ionisation conditions tested.

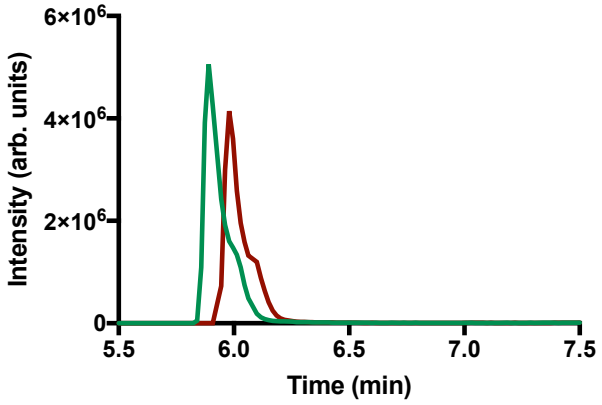

Figure 6.4 EIC for *O*-acylated propranolol species *O*-palmitoyl propranolol **62** (green) and *O*-oleoyl propranolol **47** (red) analysed by LCMS under optimised conditions.

CID MSMS of *O*-acylated propranolol derivatives provides increased structural information and a characteristic fingerprint for comparison with propranolol intrinsic lipidation products. Table 6.1 presents the product ions resulting from CID MSMS of the molecular $[M+H]^+$ ions of *O*-palmitoyl propranolol **62** and *O*-oleoyl propranolol **47**. Notably, product ions are consistent for both *O*-acylated propranolol species, irrespective of acyl chain. The low energy required for dissociation of the weak ester bond makes loss of the acyl chain favourable, preventing its retention within product ions. This favourable loss of the acyl chain also

prevents the formation of product ions associated with fragmentation at the oleoyl double bond, a phenomenon observed in similar species.

Theoretical *m/z*	Molecular Formula	Accuracy *O*-palmitoyl propranolol **62** (ppm)	Accuracy *O*-oleoyl propranolol **47** (ppm)	RDB
74.0606	C_3H_8NO	-5.4	1.4	0.5
98.0970	$C_6H_{12}N$	1.0	0.0	1.5
116.1075	$C_6H_{14}NO$	-1.7	0.0	0.5
155.0861	$C_{12}H_{11}$	-2.6	-1.9	7.5
157.0653	$C_{11}H_9O$	-1.9	-2.5	7.5
183.0810	$C_{13}H_{11}O$	-1.6	-2.2	8.5
218.1181	$C_{13}H_{16}NO_2$	-3.7	-6.4	6.5
260.1651	$C_{16}H_{22}NO_2$	-2.3	-1.9	6.5

Table 6.1 MSMS fragments observed from CID MSMS of protonated *O*-palmitoyl propranolol **62** *m/z* 498.3961 and protonated *O*-oleoyl propranolol **47** *m/z* 524.4111.

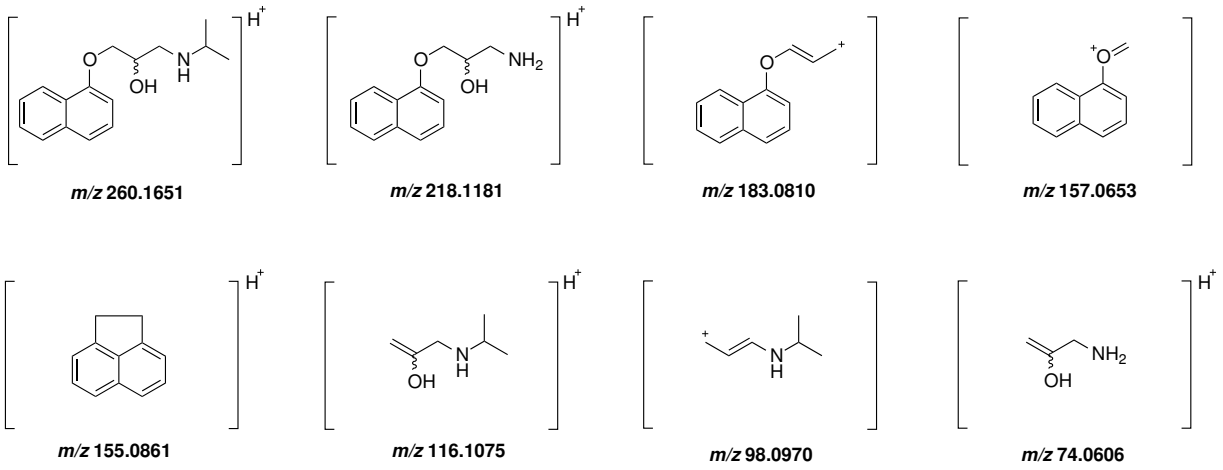

Figure 6.5 Predicted CID MSMS ion assignments for *O*-acylated propranolol derivatives **47** and **62**.

Considering the labile nature of the acyl chain, it is unsurprising that all product ions resulting from CID MSMS of *O*-palmitoyl propranolol **62** and *O*-oleoyl propranolol **47** are derived from parent drug propranolol **1**.[128,252,253] In fact, the product ion at *m/z* 260.1651 corresponds to the molecular formula $C_{16}H_{22}NO_2$, which is attributed to propranolol **1**. Further product ions are a result of the dissociation of weak bonds within propranolol **1** producing favourable neutral losses, for example H_2O or an isopropyl (*i*Pr) moiety. Predicted cleavages resulting in formation of these ions are presented in Fig. 6.5. One product ion is of particular interest, *m/z* 155.0861 corresponding to the molecular formula $C_{12}H_{11}$. Formation of this ion is only

possible through bond dissociation combined with a gas phase rearrangement. The driving force for this rearrangement is presumed to be the increased stability of the resulting ion, attributed to its aromaticity.[132]

It could be argued that the product ions resulting from CID MSMS of *O*-palmitoyl propranolol **62** and *O*-oleoyl propranolol **47**, are not greatly informative. However, they do prove that the species are propranolol **1** derived. In addition, the product ions provide a characteristic fingerprint of fragmentation from a known precursor ion, allowing for comparison with propranolol intrinsic lipidation products. Whilst it is acknowledged that further structural information may be gleaned from complimentary fragmentation techniques such as EID, this is considered unnecessary since the information obtained is sufficient for the requirements.

6.2.2 *N*-Acylated Propranolol

N-oleoyl propranolol **13** is hypothesised to be the second product of propranolol **1** intrinsic lipidation within a DOPC membrane. Confirmation of this hypothesis requires comparison of reaction mixture species with synthetically prepared *N*-acylated standards. Preparation of both *N*-oleoyl propranolol **13** and *N*-palmitoyl propranolol **12** has been described in Chapter 5 of this thesis, for the development of analytical conditions for the study of small molecule intrinsic lipidation. The identity of the species, shown in Fig. 6.6, have been confirmed by accurate mass MS, IR, and ^{1}H and ^{13}C NMR characterisation.[247] These analyses also confirm product purity, revealing no residual propranolol **1** or *O*-acylated propranolol impurities.

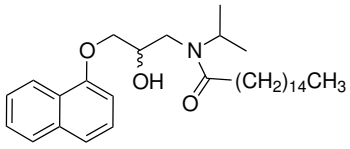

12

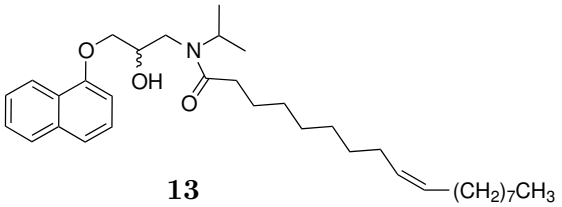

13

Figure 6.6 Structure of *N*-palmitoyl propranolol **12** and *N*-oleoyl propranolol **13**.

Samples containing 1 µg mL^{-1} solution of either *N*-palmitoyl propranolol **12** or *N*-oleoyl propranolol **13** in 1:1 H_2O:MeCN were prepared. A small volume (3 µL) of each sample was injected into the LC of the mass spectrometer and analysed under the conditions developed for study of small molecule intrinsic lipidation. Analysis of *N*-palmitoyl propranolol **12** produced the chromatogram depicted in Fig. 6.7, containing a single major product peak at retention time 7.3 min. The ion *m/z* 498.3949 corresponds to that peak, and is attributed to the

molecular formula $C_{32}H_{52}NO_3$. The accuracy of this formula is 0.8 ppm, well within the 4.0 ppm accuracy limit of the Synapt G2-S (Waters Corp., UK). This molecular formula supports attribution of the *m/z* 498.3949 ion to the $[M+H]^+$ molecular ion of *N*-palmitoyl propranolol **12**. Ions corresponding to other adducts, dismerisation or in-source fragmentation were not observed.

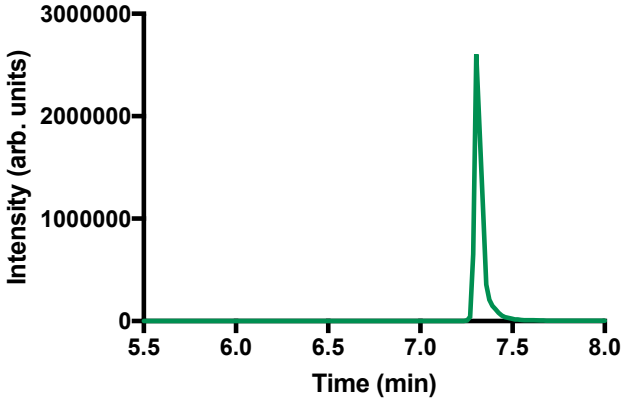

Figure 6.7 EIC of *m/z* 498.4 corresponding to protonated *N*-palmitoyl propranolol **12**.

Observed *m/z*	Molecular Formula	Accuracy (ppm)	RDB
74.0609	C_3H_8NO	+2.7	0.5
98.0970	$C_6H_{12}N$	-2.0	1.5
116.1073	$C_6H_{14}NO$	-2.6	0.5
155.0860	$C_{12}H_{11}$	-0.6	7.5
157.0653	$C_{11}H_9O$	-0.6	7.5
183.0808	$C_{13}H_4O$	-1.1	8.5
218.1178	$C_{13}H_{16}NO_2$	-2.3	6.5
260.1648	$C_{16}H_{22}NO_2$	-1.2	6.5
312.2896	$C_{19}H_{38}NO_2$	-2.2	1.5
354.3364	$C_{22}H_{44}NO_2$	-2.5	1.5
480.3835	$C_{32}H_{50}NO_2$	-0.6	8.5

Table 6.2 MSMS fragments observed following CID of protonated *N*-palmitoyl propranolol **12**.

CID MSMS of *N*-palmitoyl propranolol **12** was carried out in order to obtain a reproducible fingerprint of the species for comparison with propranolol intrinsic lipidation products. Product ions resulting from this fragmentation are presented in Table 6.2. Similarly to CID MSMS of *O*-acylated propranolol derivatives, the majority of product ions observed can be attributed to propranolol **1**.[128,252,253] The characteristic parent drug product ion is present at *m/z* 260.1648 with molecular formula $C_{16}H_{22}NO_2$. Further characteristic propranolol **1** fragments observed include ions of *m/z* 183.0808 corresponding to loss of both amine and alcohol moieties, and the

rearrangement product at *m/z* 155.0860. This result is unsurprising considering the relatively weak nature of the internal *N*-palmitoyl propranolol **12** amide bond. Dissociation is favourable under CID MSMS condition, and thus a high proportion of product ions exhibit acyl chain loss.

Three unique CID MSMS product ions of *N*-palmitoyl propranolol **12**, in which the acyl chain is maintained have been identified. Molecular formulae attributed to these ions are given in Table 6.2, and their predicted structures, based upon favourable bond dissociation, are presented in Fig. 6.8. Product ion *m/z* 480.3835 corresponds to the molecular formula $C_{32}H_{50}NO_2$, most likely a result of the loss of H_2O from *N*-palmitoyl propranolol **12**. The other two product ions *m/z* 354.3364 and 312.2894 correspond to the molecular formulae $C_{22}H_{44}NO_2$ and $C_{19}H_{38}NO_2$ respectively. Fragmentation is predicted to occur at the weak ether bond linking the naphthol oxygen to the backbone of propranolol **1**, resulting in a neutral loss of the stable aromatic species. The two product ions differ in the presence of the amine bound *i*Pr group, primed for dissociation via a weak carbon-heteroatom bond destabilised by the proximal amide. These two species are analogous to propranolol **1** product ions *m/z* 116.1073 and 74.0609, but with the acyl chain retained. The presence of these three ions provides a distinction between the MSMS fingerprints of *N*-palmitoyl propranolol **12** and *O*-palmitoyl propranolol **62**, aiding intrinsic lipidation product determination.

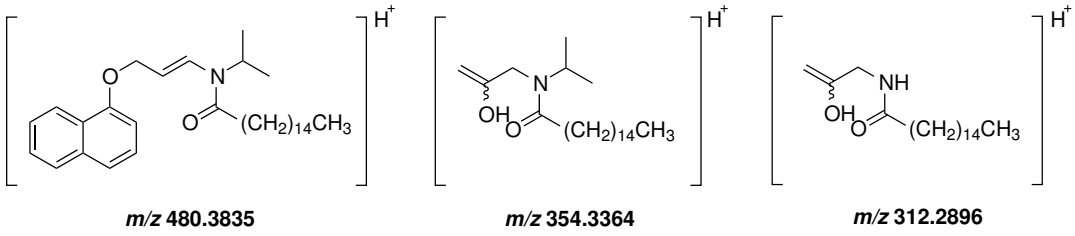

Figure 6.8 Predicted CID MSMS ion assignments for *N*-palmitoyl propranolol **12**.

The analytical experiments carried out on *N*-palmitoyl propranolol **12**, were applied to synthetically prepared *N*-oleoyl propranolol **13** for comparison. Fig. 6.9 depicts the chromatogram resulting from this analysis, with the major product peak at retention time 7.4 min. The ion attributed to this peak is of *m/z* 524.4102, attributed to the molecular formula $C_{34}H_{54}NO_3$ with an error of 0.6 ppm. The molecular formula corresponds to the $[M+H]^+$ peak of *N*-oleoyl propranolol **13**, with no observation of in-source fragmentation or adduct formation.

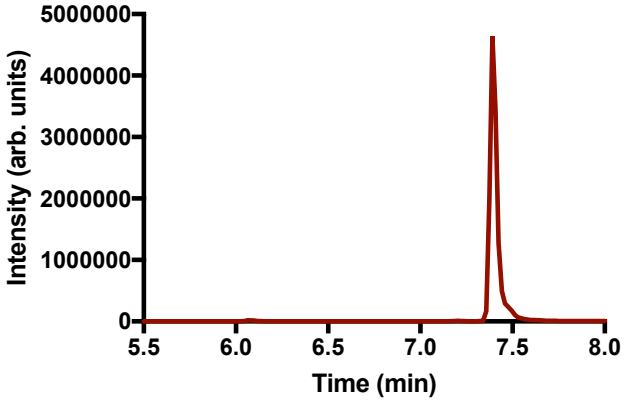

Figure 6.9 EIC of *m/z* 524.4 corresponding to protonated *N*-oleoyl propranolol **13**.

Observed *m/z*	Molecular Formula	Accuracy (ppm)	RDB
74.0603	C_3H_8NO	-10.8	0.5
98.0959	$C_6H_{12}N$	-11.2	1.5
116.1074	$C_6H_{14}NO$	-0.9	0.5
155.0859	$C_{12}H_{11}$	-0.6	7.5
157.0654	$C_{11}H_9O$	+0.6	7.5
183.0808	$C_{13}H_4O$	-1.1	8.5
218.1173	$C_{13}H_{16}NO_2$	-4.1	6.5
260.1645	$C_{16}H_{22}NO_2$	-2.7	6.5
338.3053	$C_{21}H_{40}NO_2$	-1.8	2.5
380.3523	$C_{24}H_{46}NO_2$	-1.3	2.5
506.3989	$C_{34}H_{52}NO_2$	-1.0	9.5

Table 6.3 MSMS fragments observed following CID of protonated *N*-oleoyl propranolol **13**.

CID MSMS of *N*-oleoyl propranolol **13** was also performed, resulting in formation of the product ions detailed in Table 6.3. The majority of fragmentation can be attributed to known propranolol **1** product ions, corresponding to amide bond dissociation.[128,252,253] Two of these product ions, *m/z* 98.0970 and 74.0609, exhibit low mass accuracy to their assigned molecular formulae, with values of -11.2 ppm and -10.8 ppm respectively. Increased error (ppm) is attributed to the low observed *m/z* of these species, with error conversion into atomic mass units (amu) producing acceptable error values of 0.0010 and 0.0003 for *m/z* 98.0970 and 74.0609 respectively. Unique product ions of *N*-oleoyl propranolol **13** are observed at *m/z* 506.3989, 380.3523, and 338.3053. Predicted structures for these species, featured in Fig. 6.10, mirror those observed in the CID MSMS profile of *N*-palmitoyl propranolol **12**, in which the acyl chain is retained. Molecular formula $C_{34}H_{52}NO_2$ corresponds to loss of H_2O, $C_{24}H_{46}NO_2$ to loss of the 1-naphthol ring, and $C_{21}H_{40}NO_2$ to loss of both the 1-naphthol ring and an

*i*Pr moiety. No additional product ions attributed to cleavage at the oleoyl double bond were observed, despite this being a known phenomenon.[273] This is likely due to preferential dissociation of one of multiple carbon-heteroatom bonds with lower dissociation energy.

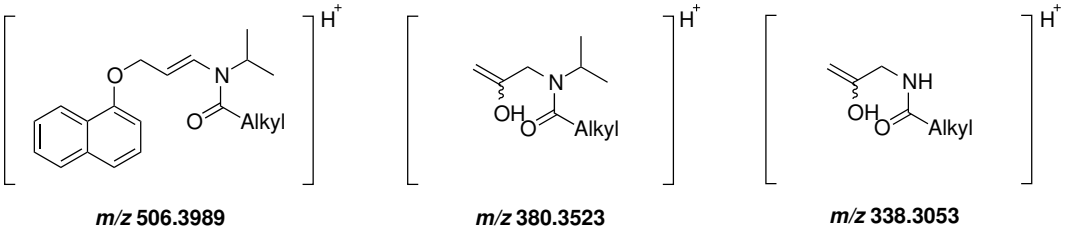

Figure 6.10 Predicted CID MSMS ion assignments for *N*-oleoyl propranolol **13**.

6.2.3 Diacylated Propranolol

Considering that both the alcohol and amine moieties of propranolol **1** participate in intrinsic lipidation individually, resulting in the formation of *N*-acylated propranolol and *O*-acylated propranolol species. Logic dictates that it may also be possible for both nucleophilic moieties within a single molecule to react, resulting in formation of a diacylated propranolol species. Observations from solution phase chemistry support this hypothesis, since propranolol **1** preferentially forms diacylated propranolol in the presence of an acid chloride, rather than a singly acylated species.[247,274] In order to determine whether diacylated propranolol is formed by intrinsic lipidation, synthetic standards are required for comparison. Standards are particularly important given that observation of diacylated propranolol derivatives by mass spectrometry is challenging, due to their hydrophobicity, insolubility in standard LCMS solvent systems, and poor ionisation. Dipalmitoyl propranolol **41** and dioleoyl propranolol **42**, depicted in Fig. 6.11, were available for this purpose, having been isolated as intermediates in the preparation of their corresponding *N*-acylated propranolol analogues.

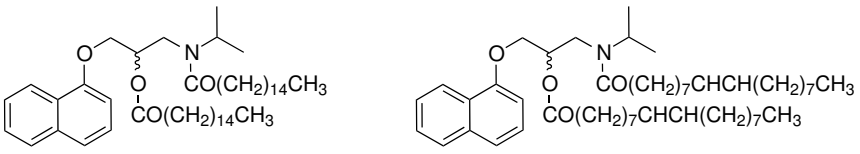

41 **42**

Figure 6.11 Structures of dipalmitoyl propranolol **41** and dioleoyl propranolol **42**.

Solutions at concentration 1 µg mL^{-1} of either dipalmitoyl propranolol **41** or dioleoyl propranolol **42** in 1:1 H_2O:MeCN were prepared for the study of diacylated propranolol analogues. A 3 µL portion of these samples was injected into the mass spectrometer for analysis under

the conditions developed to study small molecule intrinsic lipidation. Success of the chromatographic conditions were considered initially, since the hydrophobicity of diacylated propranolol species increases their column retention. Under the optimised nine minute chromatographic gradient, dipalmitoyl propranolol **41** and dioleoyl propranolol **42** eluted at retention times of 8.7 min and 8.8 min respectively, Fig. 6.12 (a). These retention times place elution within the aqueous post gradient wash phase of the chromatogram, with mobile phase conditions of 95:5 H_2O (0.1 % formic acid):MeCN (0.1 % formic acid). Late elution is concerning, since observation may be prevented by minor fluctuations in mobile or stationary phase, or by complex biological matrices which delay elution. An extended ten minute gradient added 0.5 minutes to both the aqueous wash (95:5 H_2O (0.1 % formic acid):MeCN (0.1 % formic acid)) and the preceding organic wash (5:95 H_2O (0.1 % formic acid):MeCN (0.1 % formic acid)). Under the extended gradient, retention times of 8.6 min and 8.7 min were observed for dipalmitoyl propranolol **41** and dioleoyl propranolol **42** respectively, Fig. 6.12 (b). Within the organic wash, these retention times are sufficiently early to ensure elution irrespective of chromatographic fluctuations. As a result, the more robust ten minute gradient was utilised for all future study of small molecule intrinsic lipidation.

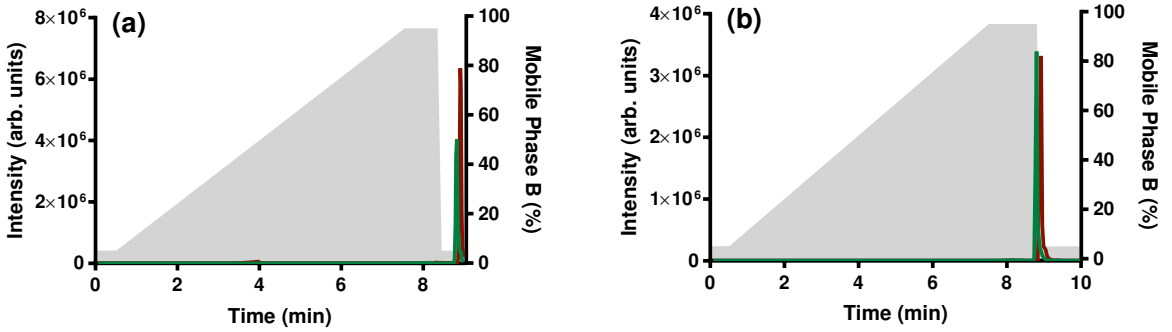

Figure 6.12 EIC of dipalmitoyl propranolol **41** *m/z* 736.6 (green) and dioleoyl propranolol **42** *m/z* 788.7 (red) using gradients: (a) optimised conditions determined in Chapter 5; (b) extended ten minute gradient. Analysis was conducted using a BEH Phenyl column (Waters Corp., UK). Mobile phase A (H_2O containing 0.1 % formic acid) and mobile phase B (MeCN containing 0.1 % formic acid) are shown in grey.

Ionisation of hydrophobic diacylated propranolol species also causes concern, given the loss of primary ionisation sites from propranolol **1** following acyl transfer. Fig. 6.13 depicts the observed ion profile attributed to the major chromatographic peak at retention time 8.6 min during analysis of dipalmitoyl propranolol **41**. Several ionic species related to dipalmitoyl propranolol **41** are observed, and these are summarised in Table 6.4. The ions of *m/z* 736.6249 and 758.6068 are determined to be the $[M+H]^+$ and $[M+Na]^+$ ions of dipalmitoylated propranolol **41**. Sodium adduct formation despite low sodium availability occurs due to

interactions between sodium ions and the naphthol aromatic ring.[275] In dipalmitoyl propranolol **41**, this interaction becomes more favourable due to a lack of available protonation sites. Proton and sodium bound dimers are also observed in low abundance. These species, of *m/z* 1472.2426 and 1494.2242, form due to the poor ionisation potential of dipalmitoyl propranolol **41** making adduct sharing more favourable.[276,277] A final ion observed in the ion profile of dipalmitoyl propranolol **41** is attributed to in-source fragmentation. At *m/z* 480.3844, this ion is also observed during CID MSMS of *N*-palmitoyl propranolol **12**, and is attributed to loss of the palmitoyl ester group.

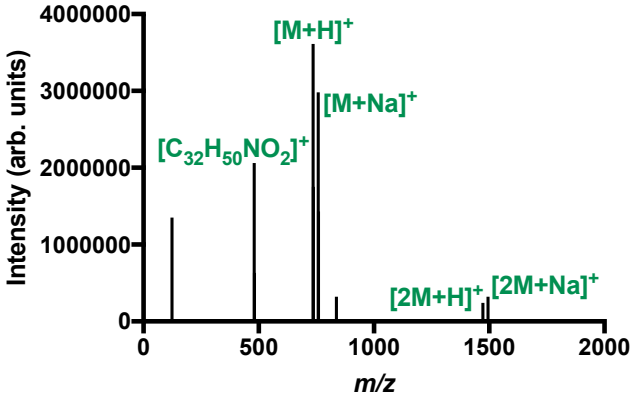

Figure 6.13 Positive mode ESI ion profile of dipalmitoyl propranolol **41**. Ions of interest are labelled.

Observed *m/z*	Molecular Formula	Accuracy (ppm)	RDB	Assignment
480.3844	$C_{32}H_{50}NO_2$	0.4	8.5	-
736.6249	$C_{48}H_{82}NO_4$	0.7	8.5	$[M+H]^+$
758.6068	$C_{48}H_{81}NO_4Na$	0.7	8.5	$[M+Na]^+$
1472.2426	$C_{96}H_{193}N_2O_8$	1.2	16.5	$[2M+H]^+$
1494.2242	$C_{96}H_{192}N_2O_8Na$	0.9	16.5	$[2M+Na]^+$

Table 6.4 Observed ions and relevant assignments from ESI MS of dipalmitoyl propranolol **41**.

Ionisation of a single chemical species which results in the formation of multiple ionic species, as is the case for dipalmitoyl propranolol **41**, spreads the total ion abundance. The reduced abundance of each individual ion may cause visualisation issues at low concentrations. Several options exist in order to overcome this issue, including minimising in-source fragmentation by modifying ionisation parameters, altered acid selection favouring protonation, and doping sodium into samples to promote sodium adduct formation in favour of protonation. Unfortunately, none of these options are viable for the study of small molecule intrinsic lipidation due to the complex multi species reaction mixture. Instead, data mining for all known ions

attributed to dipalmitoyl propranolol **41** at retention time 8.6 min in intrinsic lipidation reaction mixtures will be required in order to identify product formation.

Solvent System	$[M+H]^+$ (%)	$[M+H]^+$:$[M+Na]^+$
MeCN	75	1:0.88
MeCN:H_2O (9:1)	61	1:1.02
MeCN:H_2O (1:1)	50	1:1.11
MeCN:DCM (10:0.01)	83	1:0.77
MeCN:H_2O:DCM (9:1:0.01)	100	1:0.76
MeCN:H_2O:DCM (1:1:0.01)	66	1:0.92
MeCN:DCM (10:0.1)	79	1:0.90
MeCN:H_2O:DCM (9:1:0.1)	90	1:0.81
MeCN:H_2O:DCM (1:1:0.1)	87	1:0.76

Table 6.5 Comparison of dipalmitoyl propranolol **41** derived ions observed following sample preparation in different solvent systems. $[M+H]^+$ (%) is normalised relative to the highest observed $[M+H]^+$ peak.

Solubility of hydrophobic dipalmitoyl propranolol **41** in the polar mobile phase associated with reversed phase LC must also be considered. Precipitation resulting from low solubility has the potential to both damage instrumentation and limit analytical results. Samples of dipalmitoyl propranolol **41** at a concentration of 1 µg mL^{-1} were prepared in nine different solvent systems. Ratios of H_2O:MeCN were varied between the systems, given the increased analyte solubility in organic solvents. DCM was added to some solvent systems in order to determine whether its positive effects on analyte solubility outweighed any negative effects on ESI due to volatility or immiscibility. Samples were direct infused into the mass spectrometer at a flow rate of 0.4 µL/ min, and scan data collected over 1 minute. Solvent system success was determined based upon maximising intensity of the $[M+H]^+$ ion and minimising $[M+H]^+$:$[M+Na]^+$. The ratios of $[M+H]^+$ to other ionic species associated with dipalmitoyl propranolol **41** were not considered as they remained unchanged between solvent systems. The solvent screen results, presented in Table 6.5, show increased $[M+H]^+$ ionisation in solvent systems with an increased proportion of organic solvent MeCN. Inclusion of DCM in the solvent system does not provide a predictable trend in $[M+H]^+$ intensity. The three preferred solvent systems are MeCN:H_2O:DCM (9:1:0.01), MeCN:H_2O:DCM (9:1:0.1) and MeCN:H_2O:DCM (1:1:0.1). Since injection of a largely organic solvent into the initial aqueous chromatographic conditions is undesirable, MeCN:H_2O:DCM (1:1:0.1) is considered the preferred solvent system for future use.

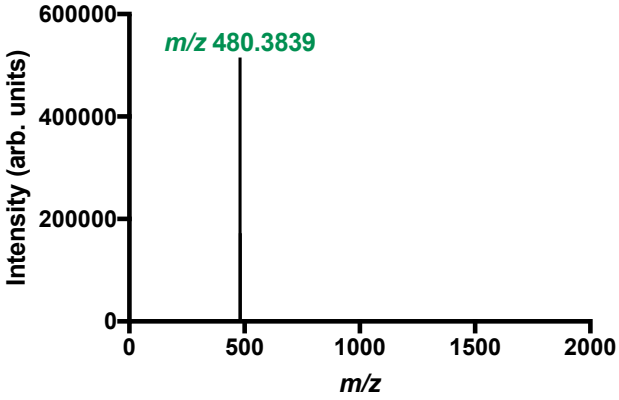

Figure 6.14 CID MSMS of dipalmitoyl propranolol **41** using precursor ions $[M+H]^+$ *m/z* 736.6249 or $[M+Na]^+$ *m/z* 758.6068.

Dipalmitoyl propranolol **41** was subjected to CID MSMS for characterisation and comparison purposes. Both the $[M+H]^+$ ion of *m/z* 736.6249 and the $[M+Na]^+$ of *m/z* 758.6068 were selected as precursor ions. Variation in adduct type and location can modify bond dissociation by CID MSMS, resulting in differing fragmentation patterns. However, as shown in Fig. 6.14, both the $[M+H]^+$ and $[M+Na]^+$ precursor ions fragment into a single major product ion. The sole product ion, *m/z* 480.3839, is attributed to the same ionic species formed by in-source fragmentation of dipalmitoyl propranolol **41**. The production of this ion by CID MSMS is testament to its stability, which can be attributed to resonance charge stabilisation. Hoping to glean further structural and functional information, CID MSMS was carried out using the precursor ion *m/z* 480.3844. The product ions, summarised in Table 6.6, correspond to known propranolol **1** fragments. Conspicuously absent is a peak at *m/z* 260, corresponding to the molecular ion of propranolol **1**. However, considering the nature of the precursor ion this is unsurprising, since the ester group including the alcohol moiety of propranolol **1** has already been lost.

Theoretical *m/z*	Molecular Formula	Accuracy (ppm)	RDB
155.0863	$C_{12}H_{11}$	1.3	7.5
157.0651	$C_{11}H_9O$	-1.3	7.5
183.0810	$C_{13}H_{11}O$	0.0	8.5

Table 6.6 Observed ions following CID MSMS of dipalmitoyl propranolol **41** derived precursor ion *m/z* 480.3844.

Analysis of dioleoyl propranolol **42** under optimised small molecule intrinsic lipidation conditions produces a chromatographic peak at retention time 8.7 min. Mirroring observations for dipalmitoyl propranolol **41**, several ionic species are present under that chromatographic peak.

The ions, depicted in Fig. 6.15, correspond to the ionic species $[M+H]^+$, $[M+Na]^+$, $[2M+H]^+$ and $[2M+Na]^+$. In-source fragmentation resulting in loss of the dioleoyl propranolol **42** ester group produces the ion of m/z 506.3991. Three additional ionic species of high intensity are observed, corresponding to m/z 396.2531, 678.5083 and 700.4902. Molecular formulae for these ionic species have been determined, however beyond that their identities have not been established. Fragmentation and rearrangement involving at least one oleoyl double bond is predicted as the cause, given the lack of equivalent species observed in the ion profile of dipalmitoyl propranolol **41**.

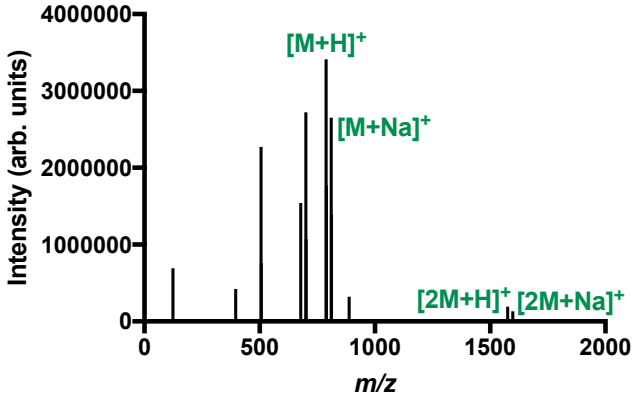

Figure 6.15 Positive mode ESI ion profile of dioleoyl propranolol **42**. Ions of interest are labelled.

Observed m/z	Molecular Formula	Accuracy (ppm)	RDB	Assignment
396.2530	$C_{25}H_{34}NO_3$	-2.0	9.5	-
506.3991	$C_{34}H_{52}NO_2$	-1.4	9.5	-
678.5083	$C_{41}H_{66}N_4O_4$	0.2	11.0	-
700.4901	$C_{41}H_{65}N_4O_4Na$	0.4	11.0	-
788.6539	$C_{52}H_{86}NO_4$	2.3	11.0	$[M+H]^+$
810.6351	$C_{52}H_{85}NO_4Na$	3.5	11.0	$[M+Na]^+$
1576.2990	$C_{104}H_{171}N_2O_8$	0.3	20.5	$[2M+H]^+$
1598.2795	$C_{104}H_{170}N_2O_8Na$	3.7	20.5	$[2M+Na]^+$

Table 6.7 Observed ions and relevant assignments from ESI MS of dioleoyl propranolol **42**.

Solvation of dioleoyl propranolol **42** in different solvent systems, and the influence upon $[M+H]^+$ ion intensity and $[M+H]^+$:$[M+Na]^+$ ratio was considered. The results, summarised in Table 6.8, project similar conclusions to those made in the study of dipalmitoyl propranolol **41** solubility. Ion ratios beyond $[M+H]^+$:$[M+Na]^+$ were largely unaffected by solvent system, an increased proportion of MeCN resulted in increased $[M+H]^+$ intensity, and the effects of DCM were varied. In summary, the results support the observation that MeCN:H_2O:DCM (1:1:0.1)

is the optimum solvent system to be used for diacylated propranolol sample preparation.

Solvent System	$[M+H]^+$ (%)	$[M+H]^+$:$[M+Na]^+$
MeCN	51	1:0.93
MeCN:H_2O (9:1)	61	1:0.85
MeCN:H_2O (1:1)	26	1:1.37
MeCN:DCM (10:0.01)	87	1:0.70
MeCN:H_2O:DCM (9:1:0.01)	100	1:0.59
MeCN:H_2O:DCM (1:1:0.01)	62	1:0.87
MeCN:DCM (10:0.1)	87	1:0.69
MeCN:H_2O:DCM (9:1:0.1)	75	1:0.75
MeCN:H_2O:DCM (1:1:0.1)	77	1:0.74

Table 6.8 Comparison of dioleoyl propranolol **42** derived ions observed following sample preparation in different solvent systems. $[M+H]^+$ (%) is normalised relative to the highest observed $[M+H]^+$ peak.

Precursor ions $[M+H]^+$ *m/z* 788.6539 and $[M+Na]^+$ *m/z* 810.6351 were selected for CID MSMS of dioleoyl propranolol **42**. As shown in Fig. 6.16, both precursor ion species fragmented into a single product ion of *m/z* 506.3994. This resonance stabilised ion, also a product of *N*-oleoyl propranolol **13** CID MSMS, is attributed to loss of the ester moiety. Given the limited information available from CID MSMS of either molecular ion, CID MSMS using a *m/z* 506.3994 precursor ion was attempted. Multiple product ions were observed, summarised in Table 6.9. However, no unique product ions were observed, all could be attributed to known propranolol **1** fragments. The absence of a propranolol **1** molecular ion due to loss of the ester group prior to precursor ion isolation, was once again noted.

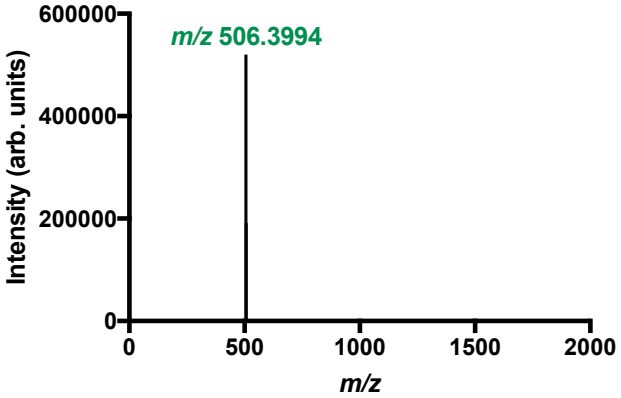

Figure 6.16 CID MSMS of dioleoyl propranolol **42** precursor ions $[M+H]^+$ *m/z* 788.6539 and $[M+Na]^+$ *m/z* 810.6351.

Theoretical *m/z*	Molecular Formula	Accuracy (ppm)	RDB
155.0863	$C_{12}H_{11}$	2.1	7.5
157.0651	$C_{11}H_9O$	0.3	7.5
183.0810	$C_{13}H_{11}O$	0.1	8.5

Table 6.9 Observed ions following CID MSMS of dioleoyl propranolol **42** derived precursor ion *m/z* 506.3994.

Analysis of dioleoyl propranolol **42** under optimised intrinsic lipidation analytical conditions produced some unidentified ions through in-source fragmentation. Molecular formulae for these species were determined in Table 6.7, however CID MSMS may aid in further structural and functional characterisation. Accurate mass information suggests that two of these ionic species, *m/z* 678.5085 and 700.4901 are the protonated and sodiated adducts of the same chemical species. Sodiated adduct *m/z* 700.4901 was selected as the precursor ion for CID MSMS due to its increased ion intensity compared to protonated adduct *m/z* 678.5085. Product ions are presented in Table 6.10 along with their corresponding molecular formulae, and the predicted structures are given in Fig. 6.17. Product ion *m/z* 183.0800 has been observed throughout previous CID MSMS of propranolol **1** and its derivatives, attributed to loss of both the ester and amide moieties. Similarly, product ion *m/z* 242.1551 can be attributed to dissociation of the amide bond combined with loss of the ester moiety. Neither species attributed to these product ions provides information regarding the structure of precursor ion *m/z* 700.4901. The product ion of *m/z* 506.3989 was characterised during CID MSMS of *N*-oleoyl propranolol **13**, and is attributed to loss of the ester moiety. Observation of this product ion indicates that the aromatic ring and amide moiety of dioleoyl propranolol **42** are retained throughout in-source fragmentation into ions *m/z* 678.5085 and 700.4901. Observation of this product ion thus suggested that the in-source fragmentation is located within the ester bound oleoyl chain. Considering the molecular formula $C_{41}H_{65}N_4O_4Na$ of precursor ion *m/z* 700.4901 and its protonated analogue *m/z* 678.5085, the relevant in-source dissociation is located at the ester bound oleoyl double bond. This theory is supported by additional in-source fragmentation and CID MSMS product ion *m/z* 396.2530, Fig. 6.17, wherein the same dissociation is observed at the double bond of the amide bound oleoyl chain, following loss of the ester moiety.

Theoretical m/z	Molecular Formula	Accuracy (ppm)	RDB
183.0810	$C_{13}H_4O$	5.4	8.5
242.1545	$C_{16}H_{20}NO$	2.5	7.5
396.2539	$C_{25}H_{34}NO_3$	2.2	9.5
506.3998	$C_{34}H_{52}NO_2$	1.8	9.5

Table 6.10 Observed ions following CID MSMS of dioleoyl propranolol **42** in-source fragment m/z 700.4901.

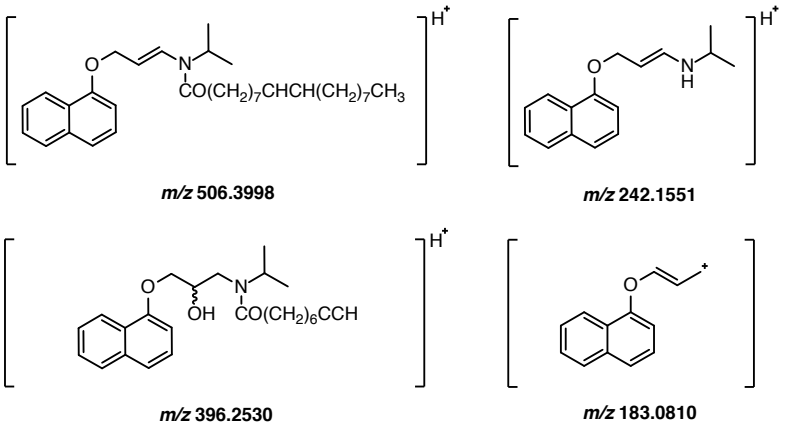

Figure 6.17 Predicted structures of ions observed following CID MSMS of dioleoyl propranolol **42** in-source fragment m/z 700.4907.

6.2.4 Reaction Mixture Products

Synthetic standards of potential propranolol **1** intrinsic lipidation products have been synthesised and characterised under the analytical conditions developed in Chapter 5 of this thesis to study the reaction. By comparing the oleoylated synthetic standards with a reaction mixture containing propranolol **1** and DOPC liposomes, the chemical nature of propranolol **1** intrinsic lipidation products can be determined. Fig. 6.18 compares chromatograms of the reaction mixture, synthetic *O*-oleoyl propranolol **47**, and synthetic *N*-oleoyl propranolol **13**. Retention times suggest that the two reaction mixture species correspond to *O*-oleoyl propranolol **47** eluting at retention time 6.1 min, and *N*-oleoyl propranolol **13** eluting at 7.4 min. Comparison of CID MSMS product ions for each species, Fig. 6.19, confirms this observation. *O*-oleoyl propranolol **47** and *N*-oleoyl propranolol **13** have been succesfully determined as the products of propranolol **1** intrinsic lipidation.

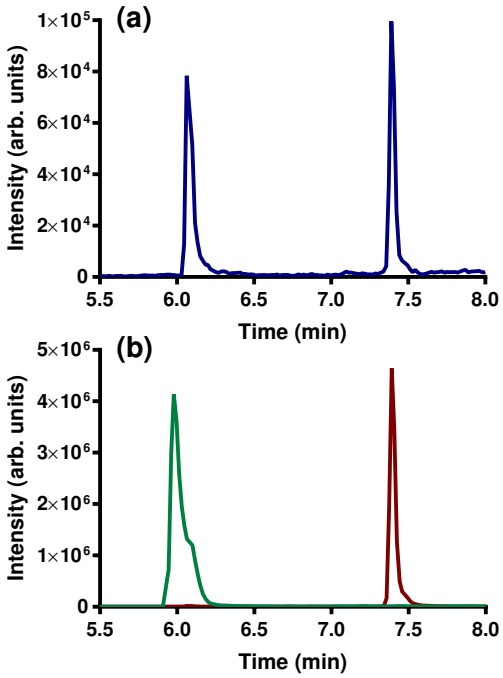

Figure 6.18 EIC corresponding to oleoylated propranolol species observed: (a) in propranolol **1** reaction mixture with DOPC (blue); (b) during analysis of *O*-oleoyl propranolol **47** (green) and *N*-oleoyl propranolol **13** (red).

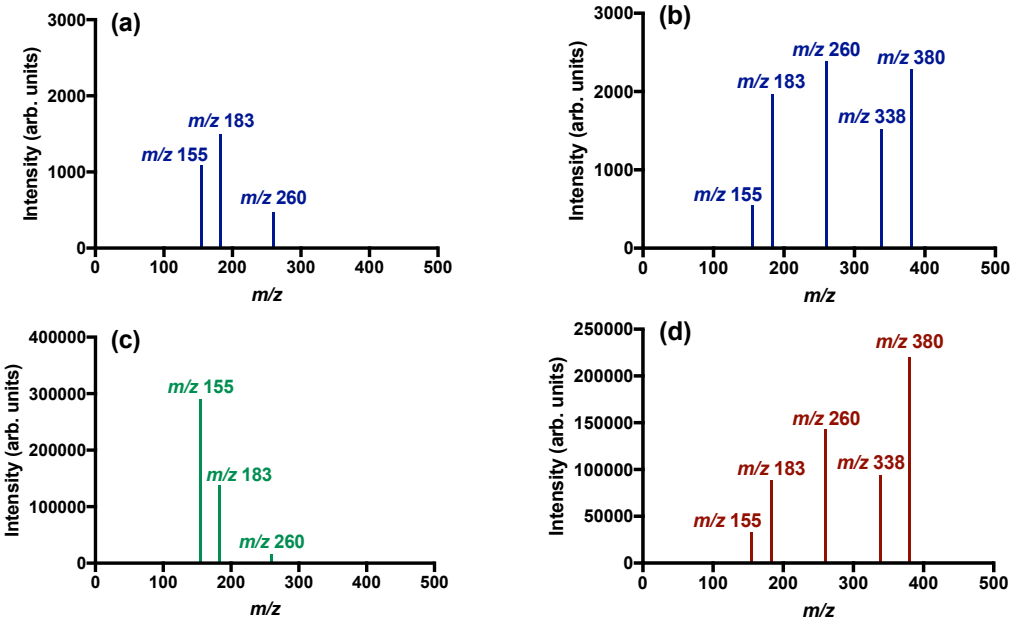

Figure 6.19 CID MSMS corresponding to oleoylated propranolol species observed: (a) in propranolol **1** reaction mixture with DOPC at retention time 6.1 min (blue); (b) in propranolol **1** reaction mixture with DOPC at retention time 7.4 min (blue); (c) during analysis of *O*-oleoyl propranolol **47** (green); (d) during analysis of *N*-oleoyl propranolol **13** (red).

Dioleoyl propranolol **42** is an additional potential intrinsic lipidation product of propranolol **1** in the presence of a DOPC membrane. Retention time and ionic species associated with dioleoyl propranolol **42** have been determined using a synthetic standard. However, no

evidence of dioleoyl propranolol **42** formation via intrinsic lipidation has been observed. One possible explanation is that dioleoyl propranolol **42** forms in low abundance, below the limit of detection for the analytical instrumentation, preventing visualisation. Alternatively, dioleoyl propranolol **42** production may proceed at a slow rate, such that the species is not formed within the 72 hour time period studied. However, it is also possible that dioleoyl propranolol **42** may simply not be an intrinsic lipidation product. A secondary acylation step may prove impossible in the modified membrane binding orientation adopted following primary acylation. Modified orientation could result in reduced proximity between nucleophilic moieties and the phospholipid ester linkages, preventing reactivity.

6.3 Quantifying Propranolol Intrinsic Lipidation

Products of propranolol **1** intrinsic lipidation have been successfully characterised through comparison with synthetically prepared standards. The two major product types, *O*-acylated propranolol and *N*-acylated propranolol, are chemically and structurally distinct. This distinction is mirrored in their properties, and in their response to analytical conditions. Understanding the relationship between these two products over a variety of conditions is vital in order to understand the mechanistic details of propranolol **1** intrinsic lipidation. Quantification of intrinsic lipidation product formation provides an accurate and informative method of increasing this understanding.[42,43] Further, product quantification paves the way towards understanding the influence of environmental factors upon intrinsic lipidation. By determining the proportion of each acylated propranolol product present under various conditions, the influence of factors such as temperature, pH, and membrane composition can be determined.

6.3.1 Preparation of Calibration Curves

Quantification is a challenging area within the field of mass spectrometry.[42,43] Variation between molecules greatly influences both their elution time and ionisation potential and as a result, the analytical response. Quantification of species irrespective of ionisation differences requires preparation of a calibration curve for each molecule studied. Calculation of chromatographic peak area at a variety of concentrations can be used to prepare a dose-response curve, allowing for future concentration determination. The synthetically prepared standards of propranolol **1** intrinsic lipidation products allows for this calibration approach

to be adopted. For each synthetic standard, a 1000 ng mL^{-1} solution in H_2O:MeCN (1:1) was prepared with accuracy and precision. The solutions were then subjected to seven 1:1 serial dilutions with H_2O:MeCN (1:1). The concentration range covered by these dilutions, 1 µg mL^{-1} to 7.8 ng mL^{-1}, is sufficient for all possible reaction mixture components. Each concentration point was prepared and analysed in triplicate by mass spectrometry to ensure accurate analytical responses were obtained.

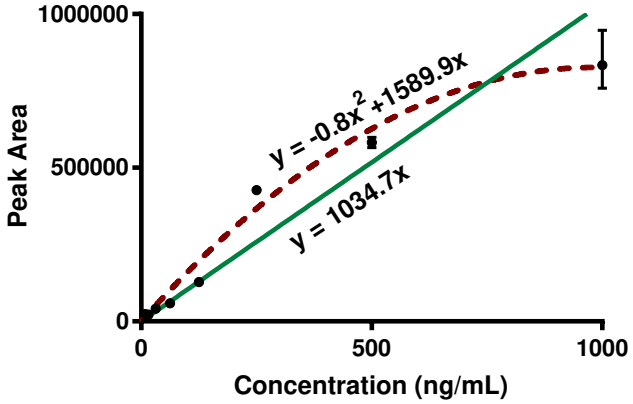

Figure 6.20 Chromatographic peak area response observed for varying concentrations of propranolol **1**. These and all future reported errors are calculated through analysis of triplicate samples, as detailed in the Experimental of this thesis. Trend fitting at 125 ng mL^{-1} and below shown by the solid green line. Trend fitting at 250 ng mL^{-1} and above shown by the dashed red line.

The concentration dependent analytical response of propranolol **1** over the concentration range of 1 µg mL^{-1} to 7.8 ng mL^{-1} is presented in Fig. 6.20. Determination of the concentration for a given chromatographic peak area requires this calibration curve data to be fitted to an equation. However, trend fitting proves challenging in the case of propranolol **1**. At concentrations of 125 ng mL^{-1} and below, the data can be fitted with a positive linear trend line described by Equation 6.1:

$$y = 1034.7x \tag{6.1}$$

Indicated by the solid green linear trend line in Fig. 6.20, Equation 6.1 fits the experimental data at 125 ng mL^{-1} and below with a reasonable R^2 value of 94.8 %. However, at concentrations of 250 ng mL^{-1} and above, this linear trend is poorly maintained, and fluctuations in chromatographic peak area are observed, leading to increased error. The observed change in analytical response at high concentrations is attributed to instrument saturation and difficulties with modelling tailing chromatographic peaks. As a result, trend fitting the calibration data

of propranolol **1** at high concentrations requires application of a polynomial curve described by Equation 6.2:

$$y = -0.8x^2 + 1589.9x \tag{6.2}$$

Exhibiting a slightly reduced R^2 value of 93.2 %, trend fitting of Equation 6.2 is represented by the dashed red line in Fig. 6.20. Intrinsic lipidation reaction mixture concentrations of propranolol **1** fall within this curved, high error portion of the calibration data, in order to ensure visualisation of low abundance acylated intrinsic lipidation products. As a result, interpretation of propranolol **1** concentration using this curve must take into account the associated error. It may not be possible to distinguish between small reductions in propranolol **1** concentration attributed to intrinsic lipidation, however application to the detection of incorrect sample preparation and dilution remains informative.

Fig. 6.21 presents average chromatographic peak areas for *N*-palmitoyl propranolol **12** and *N*-oleoyl propranolol **13** over the concentration range $1\,\mu g\,mL^{-1}$ to $7.8\,ng\,mL^{-1}$. The trends in peak area for both species can be modelled over the entire concentration range with a positive linear gradient passing through the origin. Instrument saturation resulting in a drop in response at higher concentrations is not observed, due to the poor ionisation efficiency of *N*-palmitoyl propranolol **12** and *N*-oleoyl propranolol **13** compared to propranolol **1**. An associated reduction in error is also observed, with consistent peak areas observed across the three samples prepared at each concentration. Trend fitting for *N*-palmitoyl propranolol **12** was achieved as shown by the solid green line in Fig. 6.21, by Equation 6.3 with an excellent R^2 value of 99.6 %:

$$y = 167.3x \tag{6.3}$$

Similarly *N*-oleoyl propranolol **13** trend fitting was achieved, shown by the red dashed line in Fig. 6.21. The resulting trend, exhibiting an R^2 value of 99.9 %, is described by Equation 6.4:

$$y = 242.9x \tag{6.4}$$

Shallow gradients are observed for trends associated with both *N*-palmitoyl propranolol **12** and *N*-oleoyl propranolol **13**, attributed to loss of a primary propranolol **1** ionisation site following

conversion from an amine to an amide. Poor ionisation efficiently is further highlighted by challenges in quantification at concentrations of 7.8 ng mL^{-1} and below, signifying the limit of quantification for *N*-acylated propranolol derivatives. *N*-oleoyl propranolol **13** exhibits a steeper gradient than *N*-palmitoyl propranolol **12**, suggesting increased ionisation and charge stabilisation are facilitated by the oleoyl double bond.[132]

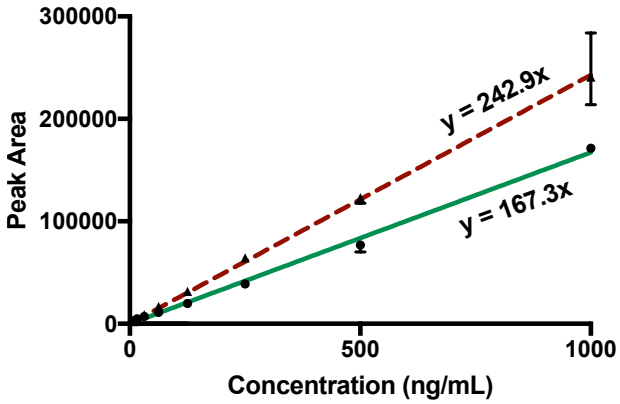

Figure 6.21 Chromatographic peak area response observed for varying concentrations of *N*-palmitoyl propranolol **12** (circles) and *N*-oleoyl propranolol **13** (triangles). Trend fitting for *N*-palmitoyl propranolol **12** shown by the solid green line, and *N*-oleoyl propranolol **13** by the dashed red line.

Analytical response over the concentration range 1 µg mL^{-1} to 7.8 ng mL^{-1} was also determined for *O*-palmitoyl propranolol **62** and *O*-oleoyl propranolol **47**. The propensity of *O*-acylated propranolol derivatives to hydrolyse or migrate in solution increases the challenge in generating calibration data for these species.[278] Swift preparation and immediate analysis of each individual sample was required to ensure neither *O* to *N* migration nor hydrolysis affected the resulting data, shown in Fig. 6.22. Data fitting revealed linear trends and reduced error for both *O*-palmitoyl propranolol **62** and *O*-oleoyl propranolol **47**, indicating improved peak shape compared to propranolol **1**, and no instrument saturation. The linear trend of R^2 value 99.9 % associated with *O*-palmitoyl propranolol **62**, shown by the solid green line in Fig. 6.22, is described by Equation 6.5:

$$y = 498.5x \tag{6.5}$$

Trend fitting associated with *O*-oleoyl propranolol **47**, shown by the red dashed line in Fig. 6.22, is described by Equation 6.6 with excellent R^2 value 99.9 %:

$$y = 731.7x \tag{6.6}$$

The fitted gradients indicate a reduced ionisation potential of *O*-palmitoyl propranolol **62** and *O*-oleoyl propranolol **47** compared to propranolol **1**. However, ionisation of *O*-palmitoyl propranolol **62** and *O*-oleoyl propranolol **47** is increased compared to their *N*-acylated propranolol counterparts, due to their retention of the favourable amine protonation site. As a result, the limit of quantification for *O*-acylated propranolol derivatives lies below that of $7.8\,\mathrm{ng\,mL^{-1}}$ attributed to *N*-acylated derivatives. *O*-oleoyl propranolol **47** exhibits increased ionisation compared to *O*-palmitoyl propranolol **62**, attributed once again to the oleoyl double bond. Differences in calibration data obtained for propranolol **1** and its acylated derivatives indicates the importance of generating calibration curves for the quantification of propranolol **1** intrinsic lipidation.

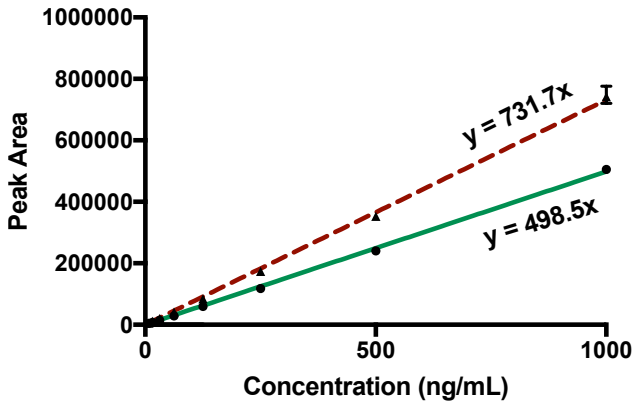

Figure 6.22 Chromatographic peak area response observed for varying concentrations of *O*-palmitoyl propranolol **62** (circles) and *O*-oleoyl propranolol **47** (triangles). Trend fitting for *O*-palmitoyl propranolol **62** shown by the solid green line, and *O*-oleoyl propranolol **47** by the dashed red line.

6.3.2 Relationship Between *O*-Acylated and *N*-Acylated Propranolol

Generation of calibration data for the quantification of propranolol **1** intrinsic lipidation products, unleashes great potential for better understanding the observed reactivity between propranolol **1** and the membrane. One aspect of reactivity that can be better understood via quantification is the relationship between the two products of propranolol intrinsic lipidation, *O*-acylated propranolol and *N*-acylated propranolol. Under standard solution phase conditions employed for organic synthesis, the two acylated species are deeply intertwined.[278–280] The alcohol functionality of the hydrochloride salt of propranolol **1** acts as the primary nucleophile

in the presence of anhydrides and *N*-hydroxysuccinimide (NHS) esters, forming *O*-acylated propranolol.[243,247] However, *O*-acylated propranolol is highly unstable, such that competing hydrolysis and intramolecular rearrangement swiftly deplete the product. For example, in pH 7.4 aqueous solution at room temperature, *O*-acetyl propranolol **66** is fully converted into *N*-acetyl propranolol **40** and propranolol **1** within 50 minutes.[278] Intramolecular *O* to *N* migration is the most favourable mechanism of *N*-acyl propranolol formation at physiological pH, due to amine protonation diminishing its nucleophilic activity. However in the presence of a base and a reactive acid chloride electrophile direct amine reactivity is possible, resulting in formation of diacyl propranolol and *N*-acyl propranolol species.[243,247] Based upon these solution phase observations, a relationship between *O*-acylated propranolol and *N*-acylated propranolol derivatives was proposed, predicting the propranolol **1** intrinsic lipidation pathway summarised in Fig. 6.23 (a). Propranolol **1** intrinsic lipidation was predicted to proceed through initial transesterification, forming primary product *O*-acylated propranolol. Unstable *O*-acylated propranolol then decomposes into secondary intrinsic lipidation product *N*-acylated propranolol through intramolecular *O* to *N* migration, described by rate constant k_1. Simultaneously *O*-acylated propranolol hydrolyses back into propranolol **1** with rate constant k_2. Fig. 6.23 (b) serves to highlight further complexity associated with this proposed pathway of propranolol **1** intrinsic lipidation, by separating propranolol **1** derived species by ionisation state and membrane association.

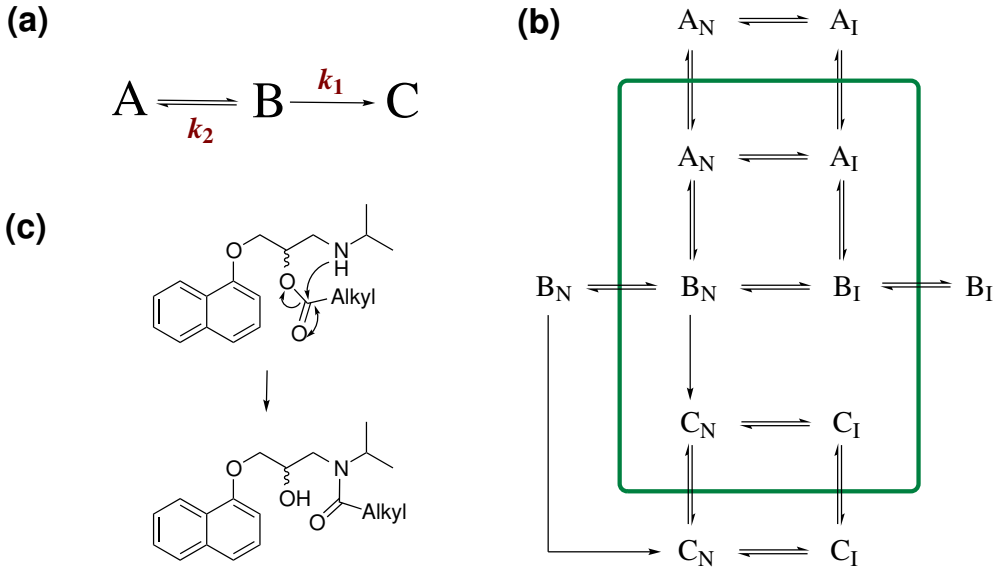

Figure 6.23 Predicted pathway for propranolol **1** intrinsic lipidation: (a) simplistic overview; (b) complete overview including all steps in the pathway. **A** represents propranolol **1**, **B** *O*-acylated propranolol derivatives, and **C** *N*-acylated propranolol derivatives. Subscript N indicates the neutral form, and I the ionised form. Inside the green box are membrane bound species, outside are in solution; (c) curly arrow mechanism of *O* to *N* migration.

Analysing the behaviour of *O*-acylated propranolol and *N*-acylated propranolol within the confines of a membrane allowed determination of the accuracy of the pathway for propranolol **1** intrinsic lipdation proposed in Fig. 6.23. Reaction mixtures containing a 1:10 molar ratio of relevant acylated propranolol derivative to membrane phospholipid were incubated under physiological conditions. Portions of the reaction mixture were taken over a time period up to 144 hours, and analysed under optimised MS conditions for small molecule intrinsic lipidation. Chromatographic peak areas corresponding to propranolol **1** derived species were calculated, and the relative product concentrations determined using calibration data presented in Section 6.3.1. DOPC liposomes were utilised for incubation with *O*-palmitoyl propranolol **62** and *N*-palmitoyl propranolol **12**, and DPPC liposomes for *O*-oleoyl propranolol **47** and *N*-oleoyl propranolol **13**. Selection of membrane phospholipids comprised of opposing acyl chain type to those of the small molecule allows for determination of acyl chain origin. Two preparation methods were utilised in order to combine phospholipids with the relevant propranolol **1** derivatives. The first combined an aqueous solution of the relevant acylated small molecule species with solution phase phospholipid liposomes prepared by the extrusion method. The second involved preparation of a thin dried film of combined phospholipid and small molecule, followed by hydration and liposome preparation by the extrusion methodology. Comparison of the two preparation methods allows for the impact of lag time associated with membrane binding, upon variation in hydrolysis and *O* to *N* rate to be determined.

An overview of the resulting data reveals some key trends observed for all four acylated propranolol **1** derivatives. Comparable results were obtained for both of the preparation methods tested, indicating negligible *O* to *N* migration or hydrolysis during the lag time associated with membrane binding. This observation is unsurprising considering the hydrophobic nature of the species and their associated logD values at physiological pH, presented in Table 6.11, likely aiding in swift membrane association. Additionally, at time point zero all reaction mixtures contained a small proportion (< 9 %) of unmodified propranolol **1**. Formation is attributed to hydrolysis following synthetic purification or during reaction mixture preparation. Further, in reaction mixtures containing *O*-palmitoyl propranolol **62** or *O*-oleoyl propranolol **47**, some of the Boc protected analogue remained. The presence of the Boc-protected analogue is attributed to insufficient deprotection time during *O*-palmitoyl propranolol **62** and *O*-oleoyl propranolol **47** synthesis. However, the peak area associated with the Boc protected species remains constant and thus is not considered problematic.

Species	LogD (pH 7.4)
Propranolol **1**	2.6
O-palmitoyl propranolol **62**	7.7
N-palmitoyl propranolol **12**	8.7
O-oleoyl propranolol **47**	8.2
N-oleoyl propranolol **13**	9.2

Table 6.11 LogD values for propranolol derivatives at pH 7.4 calculated using ChemAxon.[262]

Reaction mixtures containing *N*-palmitoyl propranolol **12** in the presence of a DOPC membrane, and *N*-oleoyl propranolol **13** in the presence of a DPPC membrane were analysed. Over the 144 hours studied no modification to the analytical profile of *N*-palmitoyl propranolol **12** was observed, Fig. 6.24, indicating small molecule stability within the membrane. *N*-oleoyl propranolol **13** was observed to undergo hydrolysis, Fig. 6.24, however the observed rate is slow, with less than 10 % reduction in *N*-oleoyl propranolol **13** concentration over the 144 hour time period studied. Furthermore, formation of diacylated propranolol was not observed for either *N*-palmitoyl propranolol **12** or *N*-oleoyl propranolol **13**, suggesting a lack of reactivity between membrane phospholipids and *N*-acylated propranolol derivatives. This observation supports previous indications that double intrinsic lipidation of propranolol **1** does not occur, attributed to unfavourable nucleophile position within the binding orientation of the singly acylated species. The observed stability and robustness of membrane bound *N*-acylated propranolol derivatives is consistent with solution phase studies, and supports the pathway of propranolol **1** intrinsic lipidation proposed in Fig. 6.23.

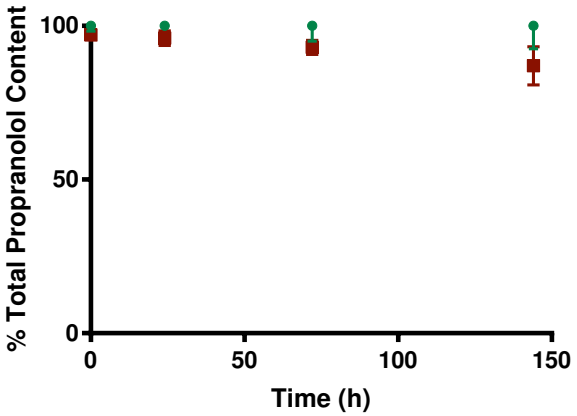

Figure 6.24 Quantity of *N*-palmitoyl propranolol **12** present in a DOPC membrane (green circles), and *N*-oleoyl propranolol **13** present in a DPPC membrane (red squares) under physiological conditions over 144 hours.

By contrast, membrane bound *O*-palmitoyl propranolol **62** and *O*-oleoyl propranolol **47** do

not exhibit stability under physiological conditions. As shown in Fig. 6.25, the proportion of total propranolol **1** content attributed to *O*-palmitoyl propranolol **62** decreases exponentially from 99 % to less than 1.5 % over 144 hours. In parallel, the proportion of *O* to *N* migration product *N*-palmitoyl propranolol **12**, fitted by the dashed line in Fig. 6.25, increases from 0 % up to 84 % of the total propranolol **1** derived content. The proportion of hydrolysis product propranolol **1** also increases from 1 % to approximately 15 % of the total propranolol **1** derived content, as shown by the dotted and dashed line in Fig. 6.25. Decomposition of *O*-palmitoyl propranolol **62** can therefore be attributed to simultaneous non-reversible hydrolysis and *O* to *N* migration reactions. These observed changes in the nature of propranolol **1** derived content are consistent with solution phase observations, and the pathway of propranolol **1** intrinsic lipidation proposed in Fig. 6.23.

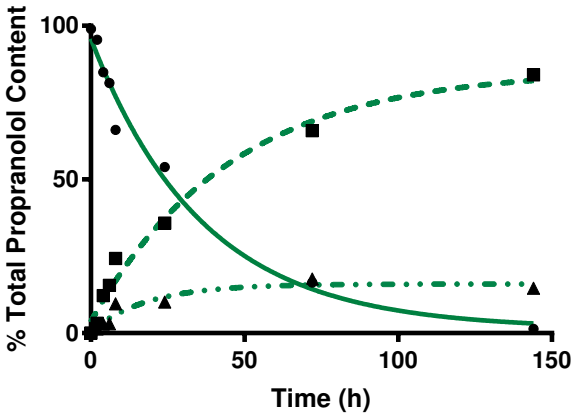

Figure 6.25 Analysis of propranolol **1** derived species present upon incubation of *O*-palmitoyl propranolol **62** with a DOPC membrane under physiological conditions over 144 hours: (i) *O*-palmitoyl propranolol **62** experimental data points are indicated by circles, and fitting by the solid line; (ii) *N*-palmitoyl propranolol **12** experimental data points are indicated by squares, and fitting by the dashed line; (iii) propranolol **1** experimental data points are indicated by triangles, and fitting by the dotted and dashed line. Error bars are omitted for clarity.

Further understanding of the mechanism of propranolol **1** intrinsic lipidation can be achieved by considering the relative rates of *O* to *N* migration and hydrolysis. *O*-palmitoyl propranolol **62** decomposition within the membrane displays first-order kinetics, and thus can be considered using the rate equation defined in Equation 6.7:

$$[\mathbf{62}] = [\mathbf{62}]_0 e^{-k_{\text{obs}}t} \tag{6.7}$$

Where [**62**] = concentration of *O*-palmitoyl propranolol **62**; $[\mathbf{62}]_0$ = concentration of *O*-palmitoyl propranolol **62** at time point 0; k_{obs} = observed rate constant; t = time.

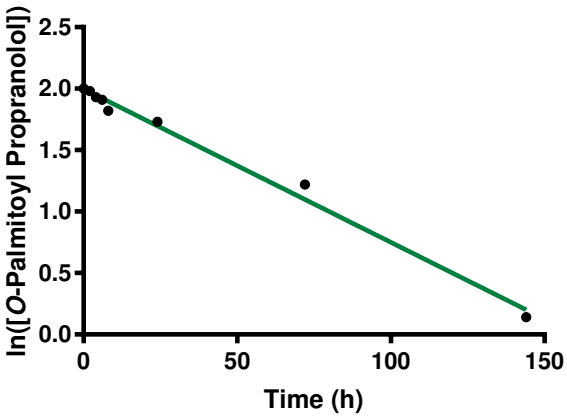

Figure 6.26 Plot of ln([*O*-palmitoyl propranolol **62**]) present in a DOPC membrane under physiological conditions over 144 hours. Circles indicate experimental data, and the trend is fitted with the solid green line.

Plotting relevant time and concentration parameters in a semi-log plot, as demonstrated in Fig. 6.26, facilitates data fitting with a linear trend. The resulting trend gradient is equal to the observed rate constant (k_{obs}), determined to be $12.5 \times 10^{-3}\,\mathrm{h}^{-1}$. Given that *O*-palmitoyl propranolol **62** decomposition is attributed to both hydrolysis and intramolecular migration, this observed rate constant (k_{obs}) can be further defined as the sum of the rate constant of *O* to *N* migration (k_1) and the rate constant of hydrolysis (k_2). Given the consistent ratio between the two decomposition products over time, rate constants for *O* to *N* migration (k_1) and hydrolysis (k_2) also remain consistent.[278] As a result these rate constants can be determined by Equations 6.8 and 6.9 respectively:

$$k_1 = k_{\mathrm{obs}}[\mathbf{12}]/([\mathbf{12}] + [\mathbf{1}]) \tag{6.8}$$

Where k_1 = rate constant for intramolecular *O* to *N* migration; k_{obs} = observed rate constant; [**12**] = concentration of *N*-palmitoyl propranolol **12**; [**1**] = concentration of propranolol **1**

$$k_2 = k_{\mathrm{obs}} - k_1 \tag{6.9}$$

Where k_2 = rate constant for hydrolysis; k_{obs} = observed rate constant; k_1 = rate constant for intramolecular *O* to *N* migration.

The rate constant attributed to formation of propranolol **1** by hydrolysis (k_2) was therefore determined to be $2.7 \times 10^{-3}\,\mathrm{h}^{-1}$. By contrast an increased k_1 value of $9.8 \times 10^{-3}\,\mathrm{h}^{-1}$ was calculated for formation of *N*-palmitoyl propranolol **12**. Respective rate constants indicate *O* to *N* migration as the primary form of membrane bound *O*-palmitoyl propranolol **62**

decomposition under physiological conditions, resulting in build up of stable *N*-palmitoyl propranolol **12**.

Equivalent experiments conducted utilising *O*-oleoyl propranolol **47** revealed a similar analytical response to those of *O*-palmitoyl propranolol **62**, as depicted in Fig. 6.27. The proportion of total propranolol **1** derived content attributed to *O*-oleoyl propranolol **47** decreased from 91 % to less that 4 % over the 144 hours studied. However, unlike *O*-palmitoyl propranolol **62** decomposition, increased propranolol **1** formation was not observed, indicating that *O*-oleoyl propranolol **47** decomposition cannot be attributed to hydrolysis. This observation is due to either a lower propensity of *O*-oleoyl propranolol **47** towards hydrolysis, or to reduced aqueous availability within the gel phase DPPC membrane. Decomposition of *O*-oleoyl propranolol **47** is wholly attributed to non-reversible *O* to *N* acyl chain migration. This is reflected in the increased proportion of *N*-oleoyl propranolol **13** from 0 % up to 87 % over 144 hours, as shown by the dashed line in Fig. 6.27.

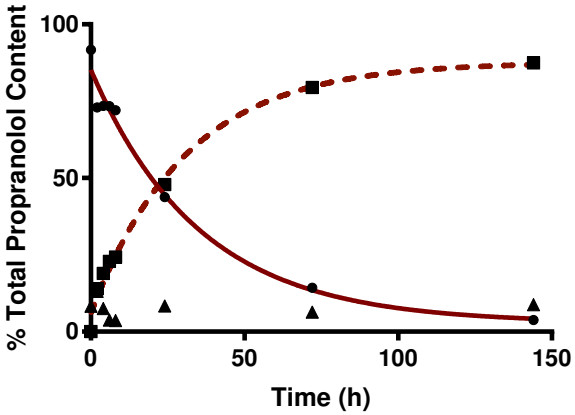

Figure 6.27 Analysis of propranolol **1** derived species present upon incubation of *O*-oleoyl propranolol **47** with a DPPC membrane under physiological conditions over 144 hours: (i) *O*-oleoyl propranolol **47** experimental data points are indicated by circles, and fitting by the solid line; (ii) *N*-oleoyl propranolol **13** experimental data points are indicated by squares, and fitting by the dashed line; (iii) propranolol **1** experimental data points are indicated by triangles. Error bars are omitted for clarity.

O-oleoyl propranolol **47** decomposition within the membrane also displays first-order kinetics, and can be considered using the rate equation defined in Equation 6.10:

$$[\mathbf{47}] = [\mathbf{47}]_0 e^{-k_{\text{obs}}t} \tag{6.10}$$

Where [**47**] = concentration of *O*-oleoyl propranolol **47**; $[\mathbf{47}]_0$ = concentration of *O*-oleoyl propranolol **47** at time point 0; k_{obs} = observed rate constant; t = time.

Plotting relevant experimental parameters and fitting the data with a linear trend, Fig. 6.28, allows determination of an observed rate constant (k_{obs}) for *O*-oleoyl propranolol **47** decomposition of $9.5 \times 10^{-3}\,\mathrm{h}^{-1}$. As previously demonstrated in Fig. 6.27, *O*-oleoyl propranolol **47** decomposition proceeds via intramolecular *O* to *N* migration only. Therefore, the rate constant attributed to *O* to *N* migration (k_1) is equal to k_{obs}, with a value of $9.5 \times 10^{-3}\,\mathrm{h}^{-1}$.

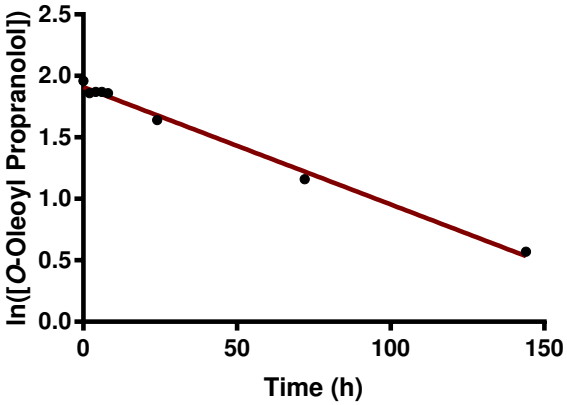

Figure 6.28 Plot of ln([*O*-oleoyl propranolol **47**]) present in a DPPC membrane under physiological conditions over 144 hours. Circles indicate experimental data, and the trend is fitted with the solid red line.

Intramolecular *O* to *N* migration is the predominant method of *O*-palmitoyl propranolol **62** and *O*-oleoyl propranolol **47** decomposition in the presence of a membrane under physiological conditions. Migration has been characterised in solution under neutral and basic environmental conditions, however variation upon introduction of a membrane must be considered.[280,281] The presence of the neutral form of *O*-acylated propranolol species is presumed as an *O* to *N* migration requirement both in solution and in the presence of a membrane. Considering the reported decrease in $\mathrm{p}K_\mathrm{a}$ associated with *O*-acylation of propranolol **1**, an increased proportion of the neutral species would be present under physiological conditions to facilitate migration.[278] Additionally, consideration must be given to the location of *O* to *N* migration. Membrane bound *O*-acylated propranolol may have flexibility and freedom to allow *O* to *N* migration, or alternatively the process may be limited to the solution phase. Based upon available data, it is unclear as to which of these proposed *O* to *N* migration locations is relevant. Considering relative solution phase rates of hydrolysis compared to *O* to *N* migration at physiological pH, hydrolysis would be expected to dominate, supporting localisation of *O* to *N* migration within the membrane.[278] Furthermore, given the hydrophobicity of *O*-acylated propranolol and associated heightened logP, limited neutral solution phase species would be available to facilitate migration. However, without knowledge of the impact of acylated propranolol upon membrane integrity, it is unclear as to whether the membrane even remains intact following

intrinsic lipidation. Micellisation or membrane disruption may provide sufficient flexibility to aid intramolecular *O* to *N* migration whilst retaining phospholipid aggregate structure.

Compiling the results of stability studies of membrane bound acylated propranolol **1** derivatives provides insight into the mechanism of propranolol **1** intrinsic lipidation. Observations support the predicted pathway of propranolol **1** intrinsic lipidation proposed previously in Fig. 6.23. Experimentation suggests that *O*-acylated propranolol species are the primary kinetic products of propranolol **1** intrinsic lipidation. *O*-acylated propranolol formation via intrinsic lipidation can be reversed through general acid or general base catalysed hydrolysis. However, the resulting formation of propranolol **1** is slow within the membrane under physiological conditions and does not comprise the primary pathway of *O*-acylated propranolol decomposition. This observation is at odds with solution phase behaviour at pH 7.4, whereupon *O*-acylated propranolol derivatives containing saturated acyl chains up to 10 carbons exhibit 90 % hydrolysis to propranolol **1** following decomposition.[278] The difference is attributed to reduced accessibility of water or hydroxide ions within the membrane compared to in solution. Instead, *O*-acylated propranolol derivatives decompose via an intramolecular rearrangement in the form of an *O* to *N* acyl chain migration. The resulting *N*-acylated propranolol derivatives are thermodynamically stable products, and remain intact within the membrane over the relevant time period for intrinsic lipidation. Rate constants for *O* to *N* migration (k_1) are determined to be $9.8 \times 10^{-3}\,\mathrm{h}^{-1}$ and $9.5 \times 10^{-3}\,\mathrm{h}^{-1}$ for *O*-palmitoyl propranolol **62** and *O*-oleoyl propranolol **47** respectively. Whilst similar between the two species, these rate constants differ significantly from the value of $4.0\,\mathrm{h}^{-1}$ attributed to *O*-acetyl propranolol **66** in solution under physiological conditions. The reduced *O* to *N* migration rate may be due to a combination of diminished small molecule mobility within the membrane bound state, and steric considerations of the long acyl chains. Furthermore, it is considered unlikely that the amine of propranolol **1** reacts directly with membrane phospholipids. Rather, it is increasingly likely that *N*-acylated propranolol derivatives form solely via *O* to *N* migration. This assumption is supported by the fact that at physiological pH the majority of the amine exists in a protonated form, making nucleophilic activity challenging. Additional support is provided by the membrane bound orientation of ionised propranolol **1**, the primary species present under physiological conditions, described in Fig. 6.29 in accordance with neutron diffraction and NMR studies.[267] The cationic ammonium moiety of ionised membrane bound propranolol **1** is localised within the phosphate head group region, facilitating favourable electrostatic interactions. Within this orientation the amine of propranolol **1** is not sufficiently proximal to a phospholipid ester linkage, an issue predicted during the study of procaine **2** and tetracaine **3** to be problematic for the

progression of intrinsic lipidation. By contrast, ionised propranolol's **1** alcohol is located in close proximity to the phospholipid ester linkage when membrane bound, a prime position to facilitate intrinsic lipidation at this position. Neutral membrane bound propranolol **1**, a minor contributor to total propranolol **1** content under physiological conditions, penetrates further into the membrane in accordance with the pH piston theory. Under basic environmental conditions promoting neutral species formation, membrane binding orientation places the amine moiety proximal to phosphate ester linkages, such that these conditions could facilitate direct formation of *N*-acylated propranolol.

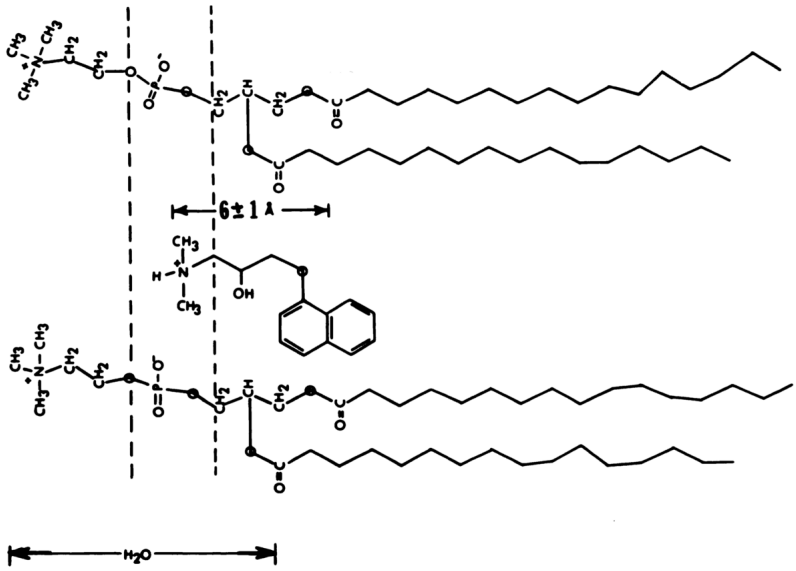

Figure 6.29 Membrane binding orientation of ionic propranolol **1** within a neutral DMPC membrane as determined by neutron diffraction, and in accordance with the pH piston theory.[267]

Temperature modification is predicted to influence the rate of both intramolecular *O* to *N* acyl chain migration, and hydrolysis of *O*-acylated propranolol, thus modifying intrinsic lipidation rate and product distribution. As major decomposition pathways of *O*-acylated propranolol, influence of temperature upon both reactions can be studied via the stability of *O*-acylated propranolol derivatives. Analogous experiments to those conducted for membrane bound *O*-palmitoyl propranolol **62** and *O*-oleoyl propranolol **47** at 37 °C were therefore conducted at 4 °C and 57 °C. Quantification of propranolol **1** derived species within each sample provides a mechanism for determining the extent of decomposition at these temperatures. Decomposition can then be further subdivided into the relative contributions from each of intramolecular *O* to *N* acyl chain migration, and hydrolysis.

Reduction in temperature from 37 °C down to 4 °C is accompanied by a parallel drop

in decomposition for both *O*-palmitoyl propranolol **62** and *O*-oleoyl propranolol **47**. As demonstrated in Fig. 6.30, following 144 hours of study 75 % of *O*-palmitoyl propranolol **62** and 40 % *O*-oleoyl propranolol **47** remains stabilised within the membrane. Decomposition via hydrolysis is considered negligible at 4 °C, since proportion of propranolol **1** does not increase beyond low level fluctuations attributed to instrument error. Reduced *O*-acyl hydrolysis is due to a combination of lower molecular energy preventing the activation energy barrier being overcome, and the presence of less fluid membrane limiting water availability. Decomposition is therefore attributed wholly to intramolecular *O* to *N* migration, however this is also slowed by the temperature decrease. After 144 hours only 20 % of total propranolol **1** derived content is attributed to *N*-palmitoyl propranolol **12**, and 53 % to *N*-oleoyl propranolol **13**, as shown in Fig. 6.30.

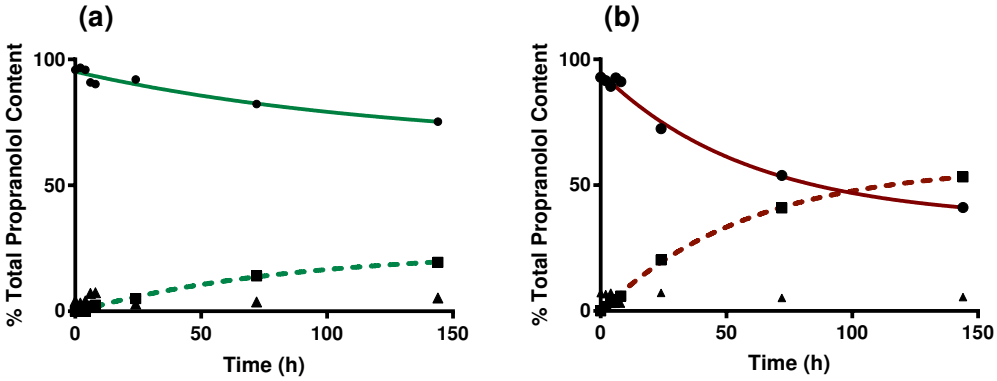

Figure 6.30 Analysis of propranolol **1** derived species present upon incubation at 4 °C for 144 hours: (a) *O*-palmitoyl propranolol **62** with a DOPC membrane; (b) *O*-oleoyl propranolol **47** with a DPPC membrane. Species presented include: (i) *O*-acylated propranolol experimental data points are indicated by circles, and fitting by the solid line; (ii) *N*-acylated propranolol experimental data points are indicated by squares, and fitting by the dashed line; (iii) propranolol **1** experimental data points are indicated by triangles. Error bars are omitted for clarity.

Plotting relevant time and concentration parameters in a semi-log plot, Fig. 6.31, reveals that the rate of *O*-palmitoyl propranolol **62** and *O*-oleoyl propranolol **47** decomposition at 4 °C follows standard first order kinetics. Therefore, decomposition can be described using the Equations 6.11 and 6.12:

$$[\mathbf{62}] = [\mathbf{62}]_0 e^{-k_{\text{obs}}t} \tag{6.11}$$

Where [**62**] = concentration of *O*-palmitoyl propranolol **62**; $[\mathbf{62}]_0$ = concentration of *O*-palmitoyl propranolol **62** at time point 0; k_{obs} = observed rate constant; t = time.

$$[\mathbf{47}] = [\mathbf{47}]_0 e^{-k_{\text{obs}}t} \tag{6.12}$$

Where [**47**] = concentration of *O*-oleoyl propranolol **47**; $[\mathbf{47}]_0$ = concentration of *O*-oleoyl propranolol **47** at time point 0; k_{obs} = observed rate constant; t = time.

In accordance with Equations 6.11 and 6.12, fitting the experimental data can be achieved with linear trends, as demonstrated by Fig. 6.31. Observed rate constants (k_{obs}), equal to trend gradients, were determined to be $0.7 \times 10^{-3}\,\text{h}^{-1}$ and $2.6 \times 10^{-3}\,\text{h}^{-1}$ for *O*-palmitoyl propranolol **62** and *O*-oleoyl propranolol **47** respectively. Considering the lack of hydrolysis at 4 °C, under these conditions k_{obs} is equivalent to k_1 the rate constant for *O* to *N* migration. Strikingly, at 4 °C k_1 for *O*-oleoyl propranolol **1** is three times that of *O*-palmitoyl propranolol **1**. This observation is attributed to membrane disruption associated with the oleoyl double bond, increasing fluidity and flexibility of molecular movement, compared to the rigid saturated palmitoyl moiety.[1,28,282] Observed k_1 values at 4 °C are considerably reduced compared to 37 °C, as highlighted in Table 6.12. Decreased temperature, and the corresponding reductions in molecular energy and membrane fluidity act to facilitate this slowed rate of *O* to *N* migration.

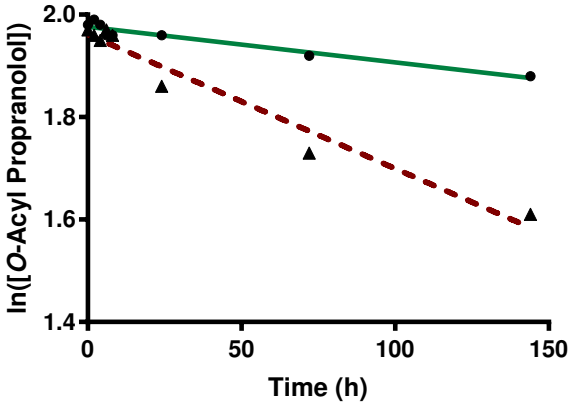

Figure 6.31 Plot of: (i) ln([*O*-palmitoyl propranolol **62**]) present in a DOPC membrane at 4 °C over 144 hours with circles indicating experimental data, and the trend fitted with the solid green line; (ii) ln([*O*-oleoyl propranolol **47**]) present in a DPPC membrane at 4 °C over 144 hours with triangles indicating experimental data, and the trend fitted with the dashed red line.

Temperature (°C)	*O*-Palmitoyl Propranolol **62**	*O*-Oleoyl Propranolol **47**
4	$0.7 \times 10^{-3}\,\text{h}^{-1}$	$2.6 \times 10^{-3}\,\text{h}^{-1}$
37	$9.8 \times 10^{-3}\,\text{h}^{-1}$	$9.5 \times 10^{-3}\,\text{h}^{-1}$

Table 6.12 Rate constants (k_1) for intramolecular *O* to *N* migration determined for *O*-palmitoyl propranolol **62** and *O*-oleoyl propranolol **47** at 4 °C and 37 °C.

Analysis of membrane bound *O*-palmitoyl propranolol **62** and *O*-oleoyl propranolol **47** stability

over 144 hours was also conducted at 57 °C. Unfortunately study of DPPC bound *O*-oleoyl propranolol **47** at 24 hours and beyond proved impossible due to poor spectrum quality. However, experimental data confirms that decomposition of *O*-palmitoyl propranolol **62** and *O*-oleoyl propranolol **47** is dramatically increased at 57 °C compared to 37 °C and 4 °C, Fig. 6.32. *O*-palmitoyl propranolol **62** is completely depleted prior to analysis at 144 hours, and *O*-oleoyl propranolol **47** is reduced to less than 56 % of total propranolol **1** content within 8 hours. Intramolecular *O* to *N* migration is the major decomposition pathway, with *N*-palmitoyl propranolol **12** and *N*-oleoyl propranolol **13** making up 44 % and 39 % of their respective samples within 8 hours. Hydrolysis resulting in increased propranolol **1** is also observed in both systems tested, as shown in Fig. 6.32.

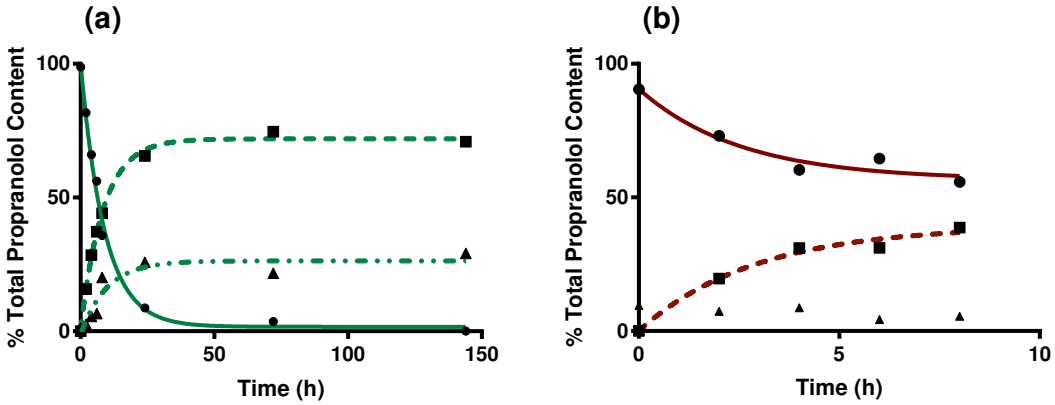

Figure 6.32 Analysis of propranolol **1** derived species present upon incubation at 57 °C for 144 hours: (a) *O*-palmitoyl propranolol **62** with a DOPC membrane; (b) *O*-oleoyl propranolol **47** with a DPPC membrane. Species presented include: (i) *O*-acylated propranolol experimental data points are indicated by circles, and fitting by the solid line; (ii) *N*-acylated propranolol experimental data points are indicated by squares, and fitting by the dashed line; (iii) propranolol **1** experimental data points are indicated by triangles, and fitting by the dotted and dashed line. Error bars are omitted for clarity.

Considering the available information it has proved impossible to fit experimental data, shown in Fig. 6.32, obtained beyond 24 hours to standard rate laws. However, plotting relevant time and concentration data obtained over the initial 8 hours of study, Fig. 6.33, suggests that initial decomposition can be described by first order kinetics. Observed rate constants (k_{obs}) are therefore described by the previously defined Equations 6.11 and 6.12. Trend fitting reveals k_{obs} values of $52.2 \times 10^{-3}\,\mathrm{h}^{-1}$ and $23.7 \times 10^{-3}\,\mathrm{h}^{-1}$ for *O*-palmitoyl propranolol **62** and *O*-oleoyl propranolol **47** at 57 °C. Since decomposition proceeds via both *O* to *N* migration and hydrolysis, these observed rate constants can be further subdivided into their constituent rate constants. Rate constants for migration (k_1) are defined using Equations 6.13 and 6.14:

$$k_1 = k_{obs}[\mathbf{62}]/([\mathbf{62}] + [\mathbf{1}]) \tag{6.13}$$

Where k_1 = rate constant for *O* to *N* migration; k_{obs} = observed rate constant; [**62**] = concentration of *O*-palmitoyl propranolol **62**; [**1**] = concentration of propranolol **1**.

$$k_1 = k_{obs}[\mathbf{47}]/([\mathbf{47}] + [\mathbf{1}]) \tag{6.14}$$

Where k_1 = rate constant for *O* to *N* migration; k_{obs} = observed rate constant; [**47**] = concentration of *O*-oleoyl propranolol **47**; [**1**] = concentration of propranolol **1**.

k_1 values of $40.5 \times 10^{-3}\,h^{-1}$ and $19.3 \times 10^{-3}\,h^{-1}$ were determined for *O*-palmitoyl propranolol **62** and *O*-oleoyl propranolol **47** respectively. Observed values are increased compared to observed k_1 values at 4 °C and 37 °C, summarised in Table 6.13. Increased mobility associated with both the liquid phase bulk membrane and membrane bound *O*-acylated propranolol species aids in intramolecular *O* to *N* migration at higher temperatures. Furthermore, an increased proportion of solution phase species present at higher temperatures may facilitate *O* to *N* migration.[153] *O*-palmitoyl propranolol **62** exhibits an increased k_1 value compared to *O*-oleoyl propranolol **47**, in similar fashion to the observed pattern at 37 °C. This increased rate constant may be attributed to differences in activation energies, or to the reduced steric bulk of *O*-palmitoyl propranolol **62** compared to *O*-oleoyl propranolol **47**.

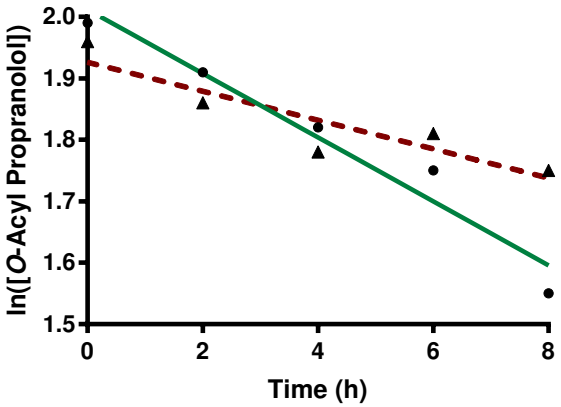

Figure 6.33 Plot of: (i) ln([*O*-palmitoyl propranolol **62**]) present in a DOPC membrane at 57 °C over 8 hours with circles indicating experimental data, and the trend fitted with the solid green line; (ii) ln([*O*-oleoyl propranolol **47**]) present in a DPPC membrane at 57 °C over 8 hours with triangles indicating experimental data, and the trend fitted with the dashed red line.

Temperature (°C)	*O*-Palmitoyl Propranolol **62**	*O*-Oleoyl Propranolol **47**
4	$0.7 \times 10^{-3}\,h^{-1}$	$2.6 \times 10^{-3}\,h^{-1}$
37	$9.8 \times 10^{-3}\,h^{-1}$	$9.5 \times 10^{-3}\,h^{-1}$
57	$40.5 \times 10^{-3}\,h^{-1}$	$19.3 \times 10^{-3}\,h^{-1}$

Table 6.13 Rate constants (k_1) for intramolecular *O* to *N* migration determined for *O*-palmitoyl propranolol **62** and *O*-oleoyl propranolol **47** at 4 °C, 37 °C, and 57 °C.

Intramolecular *O* to *N* migration is the primary mechanism of *O*-acylated propranolol decomposition at 57 °C, however decomposition by hydrolysis is also relevant. Contribution of the rate constant for hydrolysis (k_2) to k_{obs} can be calculated using Equation 6.15:

$$k_2 = k_{\text{obs}} - k_1 \tag{6.15}$$

k_2 = rate constant for hydrolysis; k_{obs} = observed rate constant; k_1 = rate constant for intramolecular *O* to *N* migration.

k_2 values for *O*-palmitoyl propranolol **62** and *O*-oleoyl propranolol **47** at 57 °C were determined to be $11.6 \times 10^{-3}\,h^{-1}$ and $4.4 \times 10^{-3}\,h^{-1}$ respectively. The calculated k_2 value for *O*-palmitoyl propranolol **62** is significantly higher than that of *O*-oleoyl propranolol **47** at 57 °C, suggesting increased hydration and membrane fluidity. However, both k_2 values are heightened compared to data obtained at 4 °C and 37 °C, summarised in Table 6.14, where hydrolysis is only observed for DOPC bound *O*-palmitoyl propranolol **47** at 37 °C. Increased hydrolysis rate is testament to the increased molecular motion, hydration and fluidity achieved through an increase in temperature.

Temperature (°C)	*O*-Palmitoyl Propranolol **62**	*O*-Oleoyl Propranolol **47**
4	$0.0\,h^{-1}$	$0.0\,h^{-1}$
37	$2.7 \times 10^{-3}\,h^{-1}$	$0.0\,h^{-1}$
57	$11.6 \times 10^{-3}\,h^{-1}$	$4.4 \times 10^{-3}\,h^{-1}$

Table 6.14 Rate constants (k_2) for hydrolysis determined for *O*-palmitoyl propranolol **62** and *O*-oleoyl propranolol **47** at 4 °C, 37 °C, and 57 °C.

Having analysed the behaviour of *O*-acylated propranolol derivatives at varying temperatures it was possible to employ the experimental data in order to determine further kinetics information. Hydrolysis was not observed across all systems tested, therefore further data interpretation is impossible, however activation energies for intramolecular *O* to *N* migration can be calculated by employing the Arrhenius Equation 6.16:

$$k_2 = Ae^{\frac{E_a}{RT}} \tag{6.16}$$

Where k_2 = rate constant for intramolecular O to N migration; A = pre-exponential factor; E_a = activation energy; R = gas constant; T = temperature.

Plotting relevant temperature and rate constant parameters, shown in Fig. 6.34, reveals activation energies of 19.5 kJ mol^{-1} and 9.6 kJ mol^{-1} for intramolecular migration of O-palmitoyl propranolol **62** and O-oleoyl propranolol **47** respectively. The higher activation energy associated with O-palmitoyl propranolol **62** migration explains the increased variation in k_2 observed for this species over the temperature range tested, shown previously in Table 6.13. Furthermore, activation energy variation suggests that intramolecular migration is more challenging in O-palmitoyl propranolol **62** than O-oleoyl propranolol **47**, which may explain the increased likelihood of decomposition by hydrolysis within this system, highlighted by rate constants previously presented in Table 6.14.

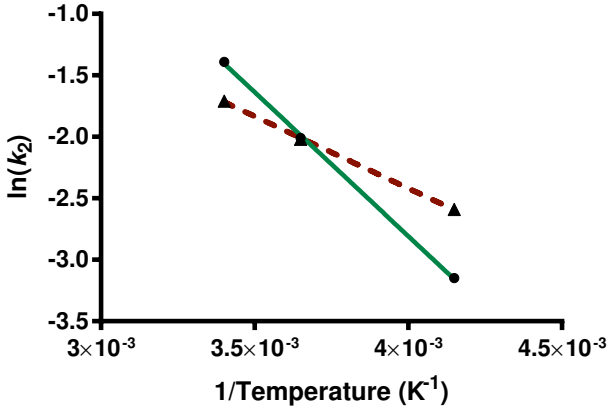

Figure 6.34 Arrhenius plot utilising rate constants of O to N migration (k_2) for: (i) O-palmitoyl propranolol **62** in a DOPC membrane with circles indicating experimental data, and the trend fitted with the solid green line; (ii) O-oleoyl propranolol **47** in a DPPC membrane with triangles indicating experimental data, and the trend fitted with the dashed red line.

6.3.3 Reactivity Under Physiological Conditions

Quantification of intrinsic lipidation products, combined with the newly developed understanding of the pathway of propranolol **1** intrinsic lipidation, provides a useful tool for further examining membrane reactivity of propranolol **1**. Reactivity *in vitro* under physiological conditions provides a biologically relevant starting point. In depth examination of propranolol **1** reactivity within different membrane models provides a route towards understanding reactivity preferences related to phospholipid head group and acyl chain composition. A developed

understanding of propranolol **1** intrinsic lipidation *in vitro* is vital in order to unravel the biological and pharmaceutical potential. Furthermore, such investigation is expected to aid in directing the future study of propranolol **1** intrinsic lipidation, with particular focus *in vivo*.

Initially, comparison of propranolol **1** intrinsic lipidation within three different membrane models was attempted. Model membranes were prepared containing phospholipid compositions of DOPC, DOPC:DOPS (4:1), and DOPE:DOPG (3:1) in order to mimic eukaryotic, viral and prokaryotic membranes respectively. Whilst previous analysis shown in Chapter 5 of this thesis indicated reactivity differences between these membrane types, it was hoped that quantification could provide a more definitive comparison. Application of calibration data to the analytical response within each membrane type provides concentration data for propranolol **1** derived species.

Total oleoylated propranolol product concentration ([*O*-oleoyl propranolol **47**] plus [*N*-oleoyl propranolol **13**]) following a 72 hour incubation of propranolol **1** with each membrane type is presented in Table 6.15. Concentration results are obtained as an average of samples prepared and analysed in triplicate. Comparison reveals 68.7 ng mL^{-1} of oleoylated propranolol product formed in the presence of a DOPC membrane, equivalent to 12 % of the total propranolol **1** derived content of the mixture. Modification of the membrane to contain DOPC:DOPS (4:1) dramatically reduces the oleoylated product concentration to 3.6 ng mL^{-1}, just under 2 % of the total propranolol **1** content. The observed reduction in reactivity is counter-intuitive considering the increased membrane binding affinity of cationic amphiphilic propranolol **1** to a negatively charged PS membrane.[270] Considering the increased electrostatic attraction, reduced reactivity can be attributed to a slightly altered membrane binding orientation of propranolol **1** within these negatively charged membranes, enhancing favourable electrostatics but reducing alcohol proximity to the phospholipid ester linkages. Further binding orientation modifications may arise as a result of inherent membrane asymmetry and domain formation, given that PS containing phospholipids preferentially inhabit the membrane inner leaflet *in vivo*.[1,283,284] Propranolol **1** rich domain formation within the inner leaflet is a potential outcome of this asymmetry, a phenomenon observed for other cationic amphiphilic drugs binding to negatively charged membranes.[27,285]

Membrane Composition	Total Oleoyl Propranolol Concentration ($ng\,mL^{-1}$)	Total Oleoyl Propranolol as % Total Propranolol Content
DOPC	68.7	12.1
DOPC:DOPS (4:1)	3.6	1.6
DOPE:DOPG (3:1)	16.3	3.1

Table 6.15 Comparison of the total concentration of oleoyl propranolol (*O*-oleoyl propranolol **47** plus *N*-oleoyl propranolol **13**) after 72 hours under physiological conditions within three membrane types.

The prokaryotic model membrane DOPE:DOPG (3:1) resulted in a total oleoylated product concentration of $16.3\,ng\,mL^{-1}$, as shown in Table 6.15, corresponding to just over 3 % of the propranolol **1** derived species. Reduced reactivity compared to the DOPC membrane model supports the determination that increased propranolol **1** membrane binding affinity does not guarantee increased intrinsic lipidation. However, increased reactivity compared to DOPC:DOPS (4:1) suggests more favourable membrane properties such as a lack of domain formation, altered position of the negative charge, or more favourable binding orientation.

Analysis of intrinsic lipidation product formation in eukaryotic, viral and prokaryotic membrane models after 72 hours can be further separated into the component species, as shown in Table 6.16. Interesting differences are evident when comparing the proportion of *O*-oleoyl propranolol **47** and *N*-oleoyl propranolol **13** between systems. After 72 hours, DOPC and DOPE:DOPG (3:1) membranes exhibit an increased proportion of *N*-oleoyl propranolol **13** compared to *O*-oleoyl propranolol **47**. This observation is attributed to initial reactivity at the alcohol moiety of propranolol **1**, followed by an intramolecular *O* to *N* migration. By contrast, the DOPC:DOPS (4:1) membrane exhibits increased levels of *O*-oleoyl propranolol **47** compared to *N*-oleoyl propranolol **13**. Insufficient *O*-oleoyl propranolol **47** production, or reduced rate of *O* to *N* migration compared to *O*-oleoyl propranolol **47** intrinsic lipidation, may cause this. However, it is worth noting that product concentrations within the DOPC:DOPS (4:1) membrane are close to the limit of quantitation. Instrument error associated with these values is thus significant, resulting in reduced confidence in the reported relative proportions of *O*-oleoyl propranolol **47** and *N*-oleoyl propranolol **13**.

Membrane Composition	*O*-oleoyl propranolol **47** as % Total Propranolol **1** Content	*N*-oleoyl propranolol **13** as % Total Propranolol **1** Content
DOPC	3.0	8.9
DOPC:DOPS (4:1)	1.0	0.6
DOPE:DOPG (3:1)	0.9	2.1

Table 6.16 Comparison of the proportion of *O*-oleoyl propranolol **47** and *N*-oleoyl propranolol **13** as % of total propranolol **1** content after 72 hours under physiological conditions within three membrane types.

Study of propranolol **1** intrinsic lipidation under physiological conditions after 72 hours provides informative data regarding the reaction. However, more detailed information can be gleaned through analysis of reaction mixtures at regular time points. As a result, portions of propranolol **1** reaction mixture with each membrane model were taken and analysed in triplicate at time points of 2, 4, 6, 8, 24, 72, 144, and 216 hours. To negate for error associated with fluctuation in sample dilution prior to analysis, values are normalised and reported as a percentage of total unmodified plus modified propranolol **1** content. Data describing total oleoylated propranolol content in each membrane type over the time period studied is presented in Fig. 6.35. Preliminary inspection suggests an increase in oleoylated product formation over time for each membrane composition up to 72 hours. However, later time points 144 and 216 hours indicate a decrease in observed oleoylated product proportion for all membrane types. Data normalisation combined with performance of experiments in triplicate prevents this decrease in oleoylated product being attributed to dilution or sample preparation error. Furthermore, chemical modification of the oleoylated product, such as diacylation or acyl chain oxidation, which may contribute to oleoylated product depletion have been investigated and eliminated as likely causes. Hydrolysis of *O*-acylated propranolol derivatives has been noted previously in Section 6.3.2, providing a possible explanation or the observed decrease in oleoylated product proportion. However, observed oleoylated product depletion at later time points is better attributed to the known instability and loss of structural integrity within liposome membrane models beyond 120 hours.[241] This instability may be further exaggerated by the attainment of a critical mass of oleoylated propranolol derivative, such that further reactivity is prevented and hydrolysis is promoted. Considering this observed complexity in later time points, analyses conducted at 144 and 216 hours were not taken forward for further study.

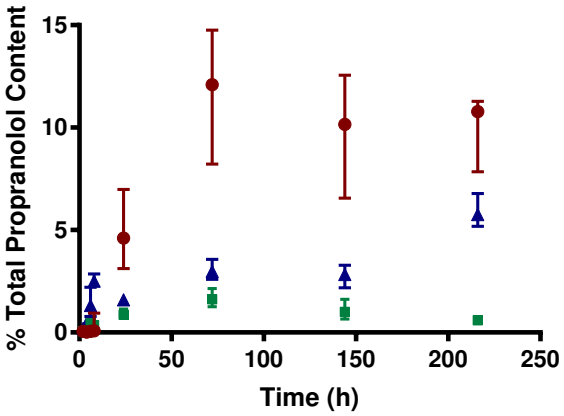

Figure 6.35 Comparison of total oleoyl propranolol product over time period up to 216 hours (9 days) within three membrane types: (i) DOPC shown by red circles; (ii) DOPC:DOPS (4:1) shown by green squares; (iii) DOPE:DOPG (3:1) shown by blue triangles.

Closer inspection of membrane models DOPC, DOPC:DOPS (4:1) and DOPE:DOPG (3:1), under physiological conditions over the first 8 hours of study, indicates oleoylated product formation within 2 hours, Fig. 6.35. *O*-oleoyl propranolol **47** is the sole contributor to total oleoylated product at this time point, as shown in Table 6.17, and continues to be over the initial 8 hours of study. Considering observation of *O*-oleoyl propranolol **47** only and the lack of ester hydrolysis determined previously, the rate constant attributed to transesterification would be equal to the observed rate constant over the first 2 to 8 hours of study. Relevant plots were therefore prepared, Fig. 6.36, in order to determine rate equation order as zero order (Fig. 6.36 (a)), first order (Fig. 6.36 (b)), or second order (Fig. 6.36 (c)). However, following analysis of the resulting data it remained unclear as to which order of reaction was most relevant. Given challenges in observation and quantification of oleoylated product at these early time points, with low abundance causing issues for both instrument detection and peak modelling, the observed issues in rate constant determination are unsurprising. Furthermore, results are complicated by potential variation in transesterification rate over time, evidenced by reduced DOPC reactivity compared to viral and prokaryotic systems over the first 2 to 8 hours, a trend reversed at 72 hours as demonstrated in Table 6.15. These considerations act to explain some of the discrepancies in oleoylated product content observed during this time period, such as a perceived decrease over time.

	Total Oleoylated Product = *O*-Oleoyl Propranolol **47**		
Time (h)	DOPC	PC:PS	PE:PG
2	0.06	0.06	0.19
4	0.02	0.11	0.46
6	0.05	0.46	1.32
8	0.08	0.36	2.51

Table 6.17 Comparison of the proportion of oleoyl propranolol equal to *O*-oleoyl propranolol **47** as % of total propranolol **1** content over the first 8 hours of study plus under physiological conditions within three membrane types: (i) DOPC; (ii) DOPC:DOPS (4:1); (iii) DOPE:DOPG (3:1).

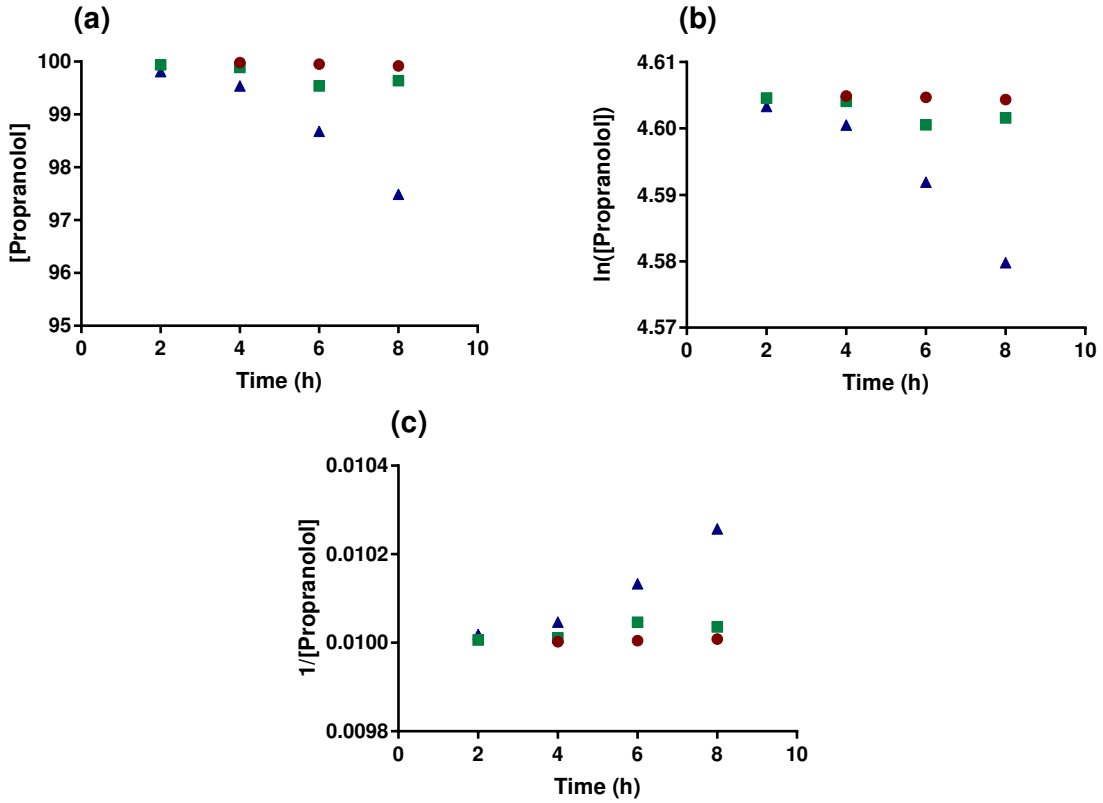

Figure 6.36 Plots prepared for the determination of rate equation order within DOPC (red circles), DOPC:DOPS 4:1 (green squares) and DOPE:DOPG 3:1 (blue triangles) membrane models: (a) zero order; (b) first order; (c) second order.

Between 24 hours and 72 hours, analytical results obtained from the study of propranolol **1** incubation under physiological conditions with three membrane models, prove most informative. A linear increase in proportion of total oleoylated propranolol product is evident for each membrane type, as shown in Fig. 6.37. The gradient attributed to each increase represents the rate of oleoylated product formation, Table 6.18, however care must be taken considering the low number of data points available. The steepest gradient of $0.17\,h^{-1}$, attributed to

the fastest rate of oleoylated propranolol formation, is credited to the eukaryotic DOPC membrane. The prokaryotic model DOPE:DOPG (3:1) exhibits the second fastest rate with a gradient of $0.04\,h^{-1}$, and the viral model DOPC:DOPS (4:1) the slowest rate with a gradient of $0.02\,h^{-1}$. Variation in rate of oleoylated product formation presents a clear preference towards propranolol **1** intrinsic lipidation in a eukaryotic membrane model, despite reduced electrostatic attraction compared to DOPC:DOPS (4:1) and DOPE:DOPG (3:1) membranes. It is impossible to attribute the increased reactivity of the eukaryotic DOPC membrane to a single factor, such as binding orientation, hydration levels and nucleophile properties. This conclusion highlights the complex nature of intrinsic lipidation, and supports the assumption that numerous factors contribute to reactivity. Further, analysis of the rate of oleoylated product formation must be considered in light of the broader and more complex picture of propranolol **1** intrinsic lipidation. Several distinct reactions contributed to the production of total oleoylated propranolol content. These reactions, which include transesterification, hydrolysis, and intramolecular *O* to *N* migration, each have a unique associated rate constant. It is unclear as to whether these individual rate constants remain consistent over time or are altered by environmental factors such as membrane integrity or accumulation of a critical proportion of oleoylated product.

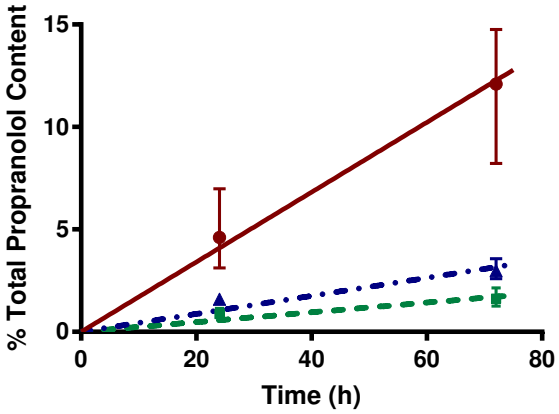

Figure 6.37 Comparison of total oleoyl propranolol product over time period up to 72 hours within three membrane types: (i) DOPC shown by red circles and modelled with a solid red line; (ii) DOPC:DOPS (4:1) shown by green squares and modelled by a green dahsed line; (iii) DOPE:DOPG (3:1) shown by blue triangles and modelled by a blue dotted and dashed line.

Membrane Type	Rate (h^{-1})
DOPC	0.17
DOPC:DOPS (4:1)	0.02
DOPE:DOPG (3:1)	0.04

Table 6.18 Comparison of the rate of oleoyl propranolol formation within three membrane types, determined from gradients of trend fitted data shown in Fig. 6.37.

Separation of total oleoylated product proportion into its contributing species, *O*-oleoyl propranolol **47** and *N*-oleoyl propranolol **13**, aids in understanding the relative rates of formation. Despite variation in absolute quantities over 72 hours, Fig. 6.38 indicates that the three membrane models exhibit similar trends. As previously demonstrated in Table 6.17, *O*-oleoyl propranolol **47** production via transesterification from a membrane phospholipid, is observed within two hours. *O*-oleoyl propranolol **47** production then continues to increase before starting to plateau as a result of competitive *O* to *N* migration. Considering both the observed plateau in *O*-oleoyl propranolol **47** concentration reached over time, and the determination of *O* to *N* migration as the primary mechanism of *O*-oleoyl propranolol **47** decomposition, the rate of initial intrinsic lipidation via transesterification is predicted to be comparable to the rate of *O* to *N* migration.

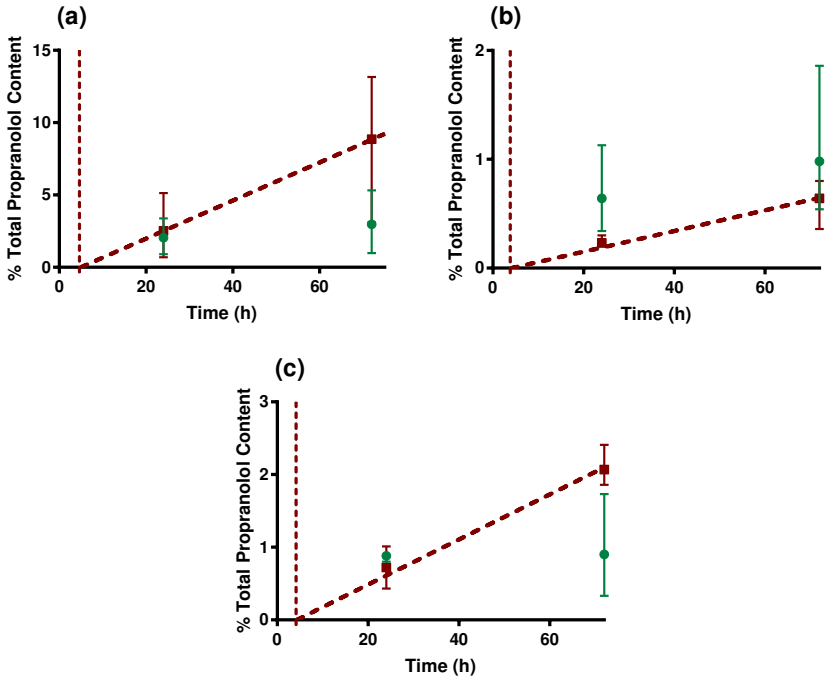

Figure 6.38 Comparison of concentrations of *O*-oleoyl propranolol **47** (experimental data as green circles) and *N*-oleoyl propranolol **13** (experimental data as red squares and trend fitted by dashed red line) products over time period 24 and 72 hours within three membrane types: (a) DOPC; (b) DOPC:DOPS (4:1); (c) DOPE:DOPG (3:1).

In contrast to *O*-oleoyl propranolol **47**, production of *N*-oleoyl propranolol **13** is characterised by an initial lag phase followed by a linear increase, shown in Fig. 6.38. The lag phase is attributed to time designated for the accumulation of *O*-oleoyl propranolol **47**, required prior to *N*-oleoyl propranolol **13** formation via *O* to *N* migration. Extrapolating the rate of *N*-oleoyl propranolol **13** production back from 24 hours, the lag phase can be estimated to last approximately 4 to 5 hours, as highlighted by dashed vertical lines in Fig. 6.38. However, at

experimental time points close to this, 6 and 8 hours, *N*-oleoyl propranolol **13** is not observed by MS due to low abundance ($<1\,\mathrm{ng\,mL^{-1}}$) preventing detection. This observation further supports the issues raised previously, associated with validity of results obtained by mass spectrometry at the limit of instrument detection. The subsequent linear increase in *N*-oleoyl propranolol **13**, irrespective of precursor concentration, indicates both a consistent rate of formation and stability of *N*-oleoyl propranolol **13**. The gradient associated with the linear increase in *N*-oleoyl propranolol **13** can be correlated with rate of its production. In a now familiar trend, the membrane model DOPC exhibits the fastest rate of product formation, followed by DOPE:DOPG (3:1), and then DOPC:DOPS (4:1). It is unclear whether this rate of *N*-oleoyl propranolol **13** formation continues indefinitely until no precursor propranolol **1** or *O*-oleoyl propranolol **47** remains, or whether production is capped at a critical proportion of *N*-oleoyl propranolol **13**.

Propranolol **1** intrinsic lipidation under physiological conditions clearly differs between model membranes containing phospholipids with differing phosphate head groups. Reactivity variation between membranes containing different acyl chain types is also of interest. In particular, investigation of preferential transfer of an acyl chain, either due to chemical composition or position on the phosphate backbone, is required. Phospholipids POPC and OPPC, which contain the same acyl chain moieties in alternate positions on the phosphate backbone, provide an excellent means of probing preferential transfer. Additionally, both POPC and OPPC contain a eukaryotic PC phosphate head group, optimising both predicted reactivity towards intrinsic lipidation, and pharmaceutical relevance.

Comparison of total palmitoylated product and total oleoylated product observed within POPC and OPPC membranes following 72 hours under physiological conditions, is presented in Table 6.19. Liposomes containing POPC produced an increased quantity of palmitoylated product, whereas liposomes containing OPPC present with increased oleoylated product. These observations correspond to preferential transfer of the acyl chain at the *sn*-1 position of the phosphate backbone. Acyl transfer dictated by backbone position rather than chemical nature highlights the importance of membrane binding orientation, and suggests reactivity facilitated by increased proximity between the alcohol of propranolol **1** and the *sn*-1 position of the phosphate backbone.[267] An alternative interpretation is that increased lability promotes transesterification at the *sn*-1 position over the *sn*-2 position.

Membrane Composition	Total Palmitoyl Propranolol Concentration ($ng\,mL^{-1}$)	Palmitoyl Propranolol (%)	Total Oleoyl Propranolol Concentration ($ng\,mL^{-1}$)	Oleoyl Propranolol (%)
POPC	100.7	36.8	49.8	18.2
OPPC	13.3	5.4	20.9	8.5

Table 6.19 Comparison of the total concentration of palmitoyl propranolol (*O*-palmitoyl propranolol **62** plus *N*-palmitoyl propranolol **12**) and the total concentration of oleoyl propranolol (*O*-oleoyl propranolol **47** plus *N*-oleoyl propranolol **13**) after 72 hours under physiological conditions within POPC and OPPC membrane types.

Differences in total acylated product formation, the sum of palmitoylated product plus oleoylated product, are also evident between POPC and OPPC membrane types, Table 6.19. Intrinsic lipidation within a POPC membrane attributes 55 % of the total propranolol **1** derived species to acylated propranolol, compared to 14 % within an OPPC membrane. The reason for this variation is unclear, but is hypothesised to be due to either minor differences in propranolol **1** binding orientation, or to membrane fluidity variation considering the transition temperatures of -2 °C and -9 °C for POPC and OPPC respectively. The conversion level of 55 % observed within the POPC membrane contrasts with earlier observations for lipidation reactions in DOPC (Chapter 5) which suggested that acylated propranolol production is capped at a final critical concentration.

In parallel to experiments conducted to test the influence of phosphate head group upon propranolol **1** intrinsic lipidation, regular reaction monitoring was executed utilising POPC and OPPC membranes. Analysis of total palmitoylated propranolol and total oleoylated propranolol at time points of 2, 4, 6, 8, 24, 72, 144 and 216 hours, is presented in Fig. 6.39. Observations discussed during comparison of eukaryotic, viral, and prokaryotic membrane models regarding data complexity at time points of 144 and 216 hours also hold for the POPC and OPPC models tested. The validity of results obtained at early time points, 8 hours and prior, is also noted here given that low abundance causes instrumental challenges, and thus results exhibit significant error. Despite these caveats, preferential *sn*-1 transfer is evident for both membrane compositions as early as 2 hours into the study. The preference is maintained for both membrane compositions throughout the time period up to 72 hours. Application of linear trend fitting to data presented in Fig. 6.39 at time points up to 72 hours informs upon the relative reaction rates, summarise in Table 6.20. Gradients of formation up to 72 hours for the species associated with *sn*-1 acyl transfer are steeper than those of their *sn*-2

counterparts, indicating a faster associated rate. Beyond 72 hours, at time points 144 and 216 hours, preferential transfer becomes less obvious, attributed to an increased lysolipid contribution to membrane composition and associated variation in intrinsic lipidation rate.

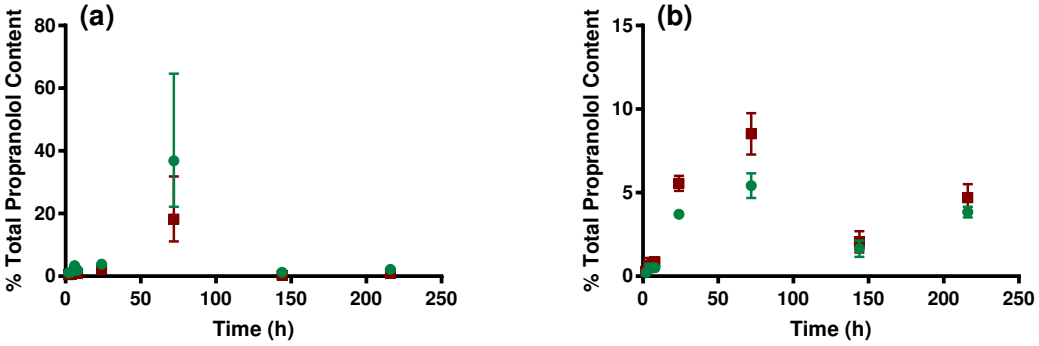

Figure 6.39 Comparison of concentrations of total palmitoyl propranolol (green circles) and total oleoyl propranolol (red squares) intrinsic lipidation products formed under physiological conditions over a time period up to 216 hours (9 days) within two membrane models: (a) POPC; (b) OPPC.

Membrane Composition	Rate *sn*-1 Transfer (h^{-1})	Rate *sn*-2 Transfer (h^{-1})
POPC	0.48	0.24
OPPC	0.13	0.08

Table 6.20 Rates of *sn*-1 and *sn*-2 transfer within POPC and OPPC membrane systems under physiological conditions. Rates were calculated as the gradient of plots of relevant product concentration vs. time up to 72 hours.

Data presented in Table 6.21 separates total palmitoylated product and total oleoylated product formed within POPC and OPPC membranes after 72 hours under physiological conditions into the constituent *O*-acylated and *N*-acylated species. Preferential *sn*-1 transfer is exhibited for both POPC and OPPC membranes within both *O*-acylated and *N*-acylated propranolol species. Irrespective of membrane composition and acyl chain chemistry, the *N*-acylated propranolol analogue is identified as the major reaction product. The variation between *O*-acylated propranolol and *N*-acylated propranolol concentration is striking, with the latter present at four to eight times the abundance. This observation is consistent with the behaviour of propranolol **1** within DOPC and DOPE:DOPG (3:1) membrane models, previously presented in Table 6.16.

Membrane Composition	% *O*-palmitoyl propranolol **62**	% *N*-palmitoyl propranolol **12**	% *O*-oleoyl propranolol **47**	% *N*-oleoyl propranolol **13**
POPC	4.1	32.8	2.1	16.1
OPPC	1.0	4.4	1.3	7.2

Table 6.21 Comparison of the % of *O*-palmitoyl propranolol **62**, *N*-palmitoyl propranolol **12**, *O*-oleoyl propranolol **47**, and *N*-oleoyl propranolol **13** after 72 hours under physiological conditions within POPC and OPPC membranes.

Separation of acylated propranolol **1** derivatives into constituent species can also be achieved utilising by performing reaction monitoring at regular time points, as demonstrated in Fig. 6.40. Production of *O*-palmitoyl propranolol **62** and *O*-oleoyl propranolol **47** within the POPC membrane, Fig. 6.40 (a) and (b), increases initially from time point zero before reaching a plateau. Comparison to data obtained for DOPC suggests a similar mechanism of action, in which the rate of transesterification is similar to rate of *O* to *N* migration. By contrast, proportion of *O*-palmitoyl propranolol **62** and *O*-oleoyl propranolol **47** within an OPPC membrane exhibits an initial increase followed by a fall, Fig. 6.40 (c) and (d). The decrease observed between 24 and 72 hours suggests that rate of *O* to *N* migration plus hydrolysis outstrips rate of transesterification. An increased rate of breakdown of the *O*-acylated products may be attributed to facilitation of intramolecular transfer or hydrolysis by an increase in membrane fluidity, or binding orientation of the small molecule.

As shown in Fig. 6.40, *N*-palmitoyl propranolol **12** and *N*-oleoyl propranolol **13** formation follows a pattern in both POPC and OPPC membranes which mimics observations in DOPC, DOPC:DOPS (4:1), and DOPE:DOPG (3:1) systems. By considering palmitoylated and oleoylated species together, Fig. 6.41, and fitting the data as shown by the dashed red lines, an initial lag phase of 4 to 6 hours was determined to precede *N*-acylated propranolol **1** formation within POPC and OPPC membranes. This lag phase facilitates the required build up of *O*-palmitoyl propranolol **62** and *O*-oleoyl propranolol **47** prior to *O* to *N* migration. Lag phase length calculated by data extrapolation is further supported by analytical detection of *N*-palmitoyl propranolol **12** and *N*-oleoyl propranolol **13** at time points of 4 and 6 hours for OPPC and POPC respectively. Following the lag phase, proportions of *N*-palmitoyl propranolol **12** and *N*-oleoyl propranolol **13** increase steadily in a linear fashion within both membrane types. Further highlighting preferential acyl transfer, the rate of *N*-acylated product formation is notably increased for species containing the acyl chain transferred from the *sn*-1 position on the phosphate backbone, Fig. 6.40.

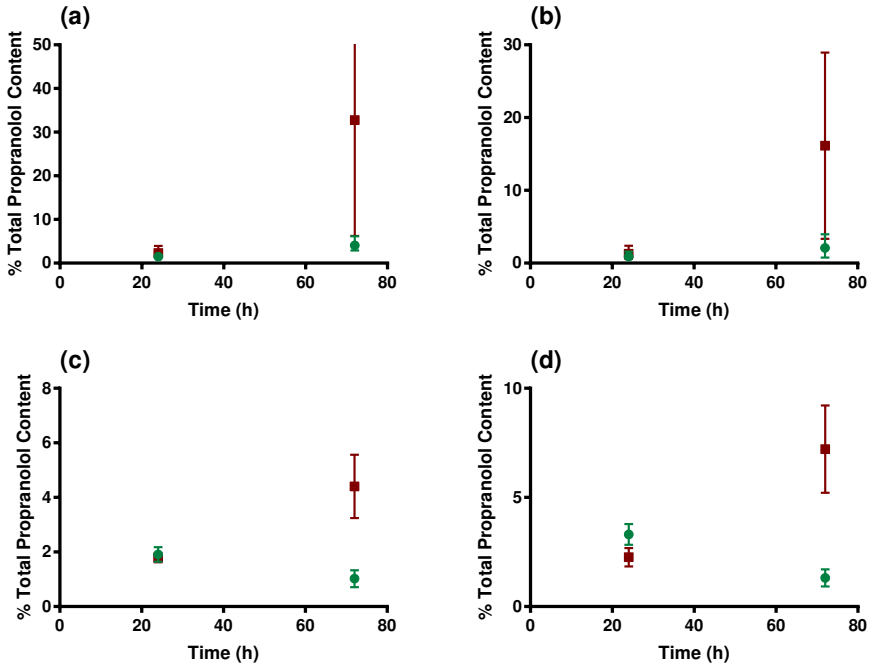

Figure 6.40 Comparison of the proportion of total *O*-acyl propranolol (green circles), and *N*-acyl propranolol (red squares) studied under physiological conditions over time period 24 to 72 hours within membrane models: (a) *O*-palmitoyl propranolol **62** and *N*-palmitoyl propranolol **12** within a POPC membrane; (b) *O*-oleoyl propranolol **47** and *N*-oleoyl propranolol **13** within a POPC membrane; (c) *O*-palmitoyl propranolol **62** and *N*-palmitoyl propranolol **12** within an OPPC membrane; (d) *O*-oleoyl propranolol **47** and *N*-oleoyl propranolol **13** within an OPPC membrane.

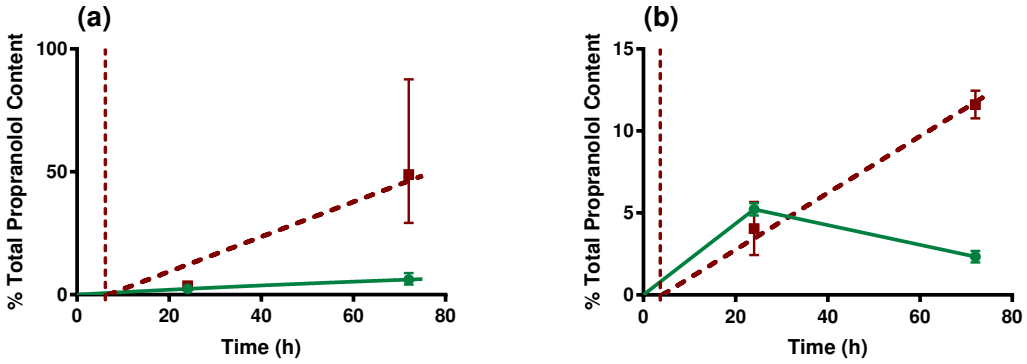

Figure 6.41 Comparison of the proportion of total *O*-acyl propranolol (experimental data as green circles and trend fitted by solid green line), and *N*-acyl propranolol (experimental data as red squares and trend fitted by dashed red line) studied under physiological conditions over time period 24 to 72 hours within membrane models: (a) POPC; (b) OPPC. Dashed lines indicate end of *N*-acyl propranolol lag phase.

The kinetics of propranolol **1** intrinsic lipidation under physiological conditions across all membrane types can be summarised into a discrete series of observations. The primary step of propranolol **1** intrinsic lipidation is an initial transesterification reaction forming *O*-acylated propranolol. Production of *O*-acylated propranolol can be described as a logarithmic curve,

indicating at initial increase in product followed by a plateau. The plateau is attributed to a competing intramolecular *O* to *N* migration reaction occurring at a similar rate to transesterification. Migratory product *N*-acylated propranolol forms at a steady linear rate following an initial 4 to 6 hour lag phase at 37 °C. In addition, two forms of preferential intrinsic lipidation reactivity were observed under physiological conditions. Eukaryotic membrane mimic DOPC, containing a PC phosphate head group, exhibits the highest observed levels of intrinsic lipidation. Acylated product quantities are increased compared to viral and prokaryotic membranes, despite their increased electrostatic attraction to cationic amphiphilic propranolol **1**. Furthermore, preferential transfer of the acyl chain located at the *sn*-1 position on the phosphate backbone, compared to the *sn*-2 position, is observed irrespective of acyl chain chemistry. Consideration of membrane binding orientation and proximity between reactive moieties can explain these observations of preferential intrinsic lipidation.[267]

6.4 A Kinetic Model for Propranolol Intrinsic Lipidation

Quantification of the products of propranolol intrinsic lipidation has aided in developing understanding of propranolol **1** reactivity at the membrane interface under physiological conditions. Enhanced clarity of the mechanisms which facilitate product formation, and identification of preferential acyl chain transfer has been achieved. Application of these principles and quantification techniques to intrinsic lipidation systems, whilst varying environmental factors, provides a mechanism for studying reaction kinetics. Variation of parameters such as temperature, pH, and form of the lipid aggregate, can determine how these factors impact upon propranolol **1** reactivity. Understanding the impact of chemical and environmental parameters upon reaction rate and product formation, provides a means of reaction control. Potential future exploitation of propranolol **1** intrinsic lipidation relies upon the ability to successfully command and manipulate reactivity. Determination of industrial and biological relevance of propranolol **1** intrinsic lipidation is also aided by an improved grasp of the reaction kinetics.

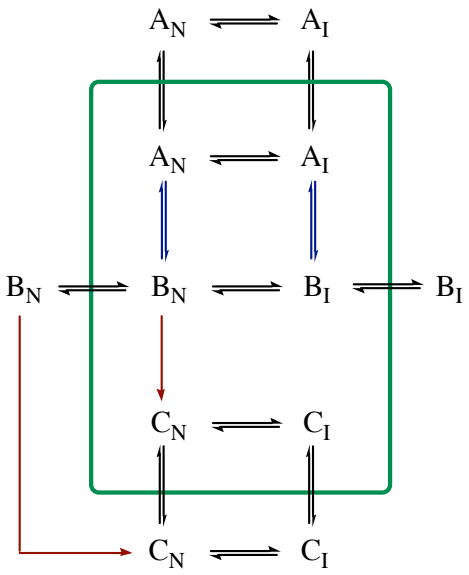

Figure 6.42 Summary of the relevant steps required for consideration of propranolol **1** intrinsic lipidation reaction kinetics. **A** represents propranolol **1**, **B** *O*-acylated propranolol derivatives, and **C** *N*-acylated propranolol derivatives. Subscript N indicates the neutral form, and I the ionised form. Inside the green box are membrane bound species, outside are in solution. Blue arrows highlight transesterification steps, and red intramolecular *O* to *N* migration.

Prior to considering the impact of altered environmental parameters upon propranolol **1** intrinsic lipidation kinetics, the complexity of the process must be noted. Subdivision of the reaction into relevant steps, each with distinct associated rate constants, is shown by differential colouring in Fig. 6.42. Several reaction steps can proceed via either the ionised (I) or the neutral (N) form of propranolol **1**, which cannot be distinguished by mass spectrometry. Clarity can be obtained by considering each step in Fig. 6.42 individually as follows:

1. Association of propranolol **1** with the membrane - Environmental pH relative to the pK_a of propranolol **1** (9.42) determines the proportion of neutral to ionic species. Ionic propranolol **1** exhibits a temperature dependent decreased logP value compared to the temperature independent logP of its neutral counterpart.[153] Neutral and ionic propranolol **1** species also vary in membrane binding orientation in accordance with the pH piston theory.[255]

2. Transesterification (highlighted blue in Fig. 6.42) - Reversible transesterification is expected to proceed irrespective of membrane bound propranolol **1** ionisation state. Comparable solution phase transesterification reactions suggest pH dependent acid and base catalysed transesterification pathways exist.

3. Acid-base equilibrium of *O*-acylated propranolol - *O*-acylated propranolol species exhibit

decreased pK_a values compared to propranolol **1**, increasing the proportion of neutral species available at pH 7.4. Simultaneously, the hydrophobicity of *O*-acylated propranolol species promotes the membrane bound state.[278]

4. Hydrolysis of *O*-acylated propranolol - Hydrolysis has been determined as a minor pathway of *O*-acylated propranolol decomposition in the presence of a membrane. Hydrolysis can proceed via acid or base catalysed pathways providing sufficient aqueous content surrounds the species.[274]

5. Intramolecular *O* to *N* migration (highlighted red in Fig. 6.42) - Migration is the major pathway for *O*-acylated propranolol decomposition in the presence of a membrane. Neutral *O*-acylated propranolol is required as the precursor species to allow the amine functionality to accept an acyl chain. Currently it is unclear whether *O* to *N* migration proceeds in solution only, within the membrane bound state, or both.

Simplification of propranolol **1** intrinsic lipidation aids in probing the reaction kinetics. To this end, the following assumptions have been drawn from literature data and previously discussed experiments:

- Based upon evidence from control experiments, minor side reactions such as phospholipid hydrolysis and oxidation are considered to have a negligible impact upon the overall reaction process of intrinsic lipidation.

- Membrane phospholipids, utilised in a ten fold molar ratio compared to propranolol **1**, are considered to be in excess for purposes of kinetics studies.

- Diacylation of propranolol **1** via the intrinsic lipidation pathway does not occur.

- Under conditions studied, intrinsic lipidation does not occur at significant levels between propranolol **1** and lysolipid. Lysolipids are present solely following phospholipid hydrolysis, thus abundance levels are low over the relevant time period.

- *N*-acylated propranolol species are stable thermodynamic reaction products, remaining membrane bound upon formation due to associated hydrophobicity.

6.4.1 Influence of Temperature

Reaction kinetics for both solution phase and biological systems are known to be greatly altered by environmental temperature. Increased temperature provides reactive molecules with higher energy, aiding their ability to overcome the activation energy barrier to reaction participation. Further, higher energy levels increase molecular motion, facilitating the collisions between reactive species required for solution phase reactivity. Influence of temperature upon propranolol **1** intrinsic lipidation is predicted to be more complex than upon standard solution phase reaction kinetics. Increased molecular energy within the phospholipid bilayer favours an increasingly fluid and mobile membrane system, with heightened hydration levels. It is unclear how increased membrane fluidity will impact the proximity between the phospholipid ester linkage and the alcohol of membrane bound propranolol **1**, however penetration is predicted to be similar assuming no modification to membrane phase or propranolol **1** ionisation. Proximity between reactive moieties is required for propranolol **1** intrinsic lipidation to successfully proceed via transesterification. Further, within a heavily hydrated membrane, hydrolysis of both *O*-acylated propranolol and membrane phospholipids is expected to be promoted. Favoured hydrolysis compared to transesterification or intramolecular *O* to *N* migration would diminish formation of acylated propranolol derivatives. Determining how these factors are balanced, and the resulting impact upon propranolol **1** intrinsic lipidation requires study of the reaction at temperatures above and below physiological conditions of 37 °C.

Examination of propranolol **1** intrinsic lipidation at varying temperature was conducted by combining propranolol **1** with a phospholipid membrane at 4 °C, 37 °C, and 57 °C. Reaction mixture analysis was conducted under optimised LCMS conditions at time points of 24, 72 and 144 hours. Time points beyond this range were not investigated during the course of this study due to challenges associated with reaction mixture stability, and instrument detection limitations. Eukaryotic DOPC, viral DOPC:DOPS (4:1), and prokaryotic DOPE:DOPG (3:1) membranes were tested in order to investigate the effect of temperature upon reaction rate in the presence of different phosphate head groups associated with different membrane models. POPC and OPPC were also tested in order to determine whether preferential *sn*-1 acyl chain transfer observed at 37 °C is maintained despite changes in temperature.

The dependence of propranolol **1** intrinsic lipidation at different temperatures can be examined by considering total acylated product formation. Total acylated product is defined as the sum of *O*-palmitoyl propranolol **62**, *O*-oleoyl propranolol **47**, *N*-palmitoyl propranolol **12**, and

N-oleoyl propranolol **13**. Total acylated product formation within each membrane type studied following 72 hours is presented in Fig. 6.43 at 4 °C, 37 °C and 57 °C. Increased acylated product formation, indicative of the extent of propranolol **1** intrinsic lipidation, is evident for each membrane type upon temperature increase. Reactivity is promoted by increased molecular energy available at higher temperatures, aiding in overcoming the activation energy barrier for the preliminary transesterification step required for propranolol **1** intrinsic lipidation. Increased molecular mobility attributed to higher temperatures is not noted to reduce reactivity by disrupting the proximity of reactive moieties. One notable exception to these observations is within the POPC membrane, Fig. 6.43 (b), where 55 % conversion to acylated product is observed at 37 °C, compared to 45 % at 57 °C. At 37 °C substantial differences in peak area of acylated products were observed between each of the triplicate samples analysed. Identification of anomalous results therefore proves challenging, resulting in increased error and reduced confidence in the data at this time point. Consequently, the value of 55 % attributed to total acylated product within a POPC membrane at 37 °C may be higher than the true value. Alternatively, propranolol **1** intrinsic lipidation within a POPC membrane may be favoured at 37 °C compared to 57 °C. Unfavourable disruption to key reactivity factors such as proximity of reactive moieties or membrane binding orientation may occur within the POPC membrane at 57 °C, resulting in reduced propranolol **1** intrinsic lipidation.[267]

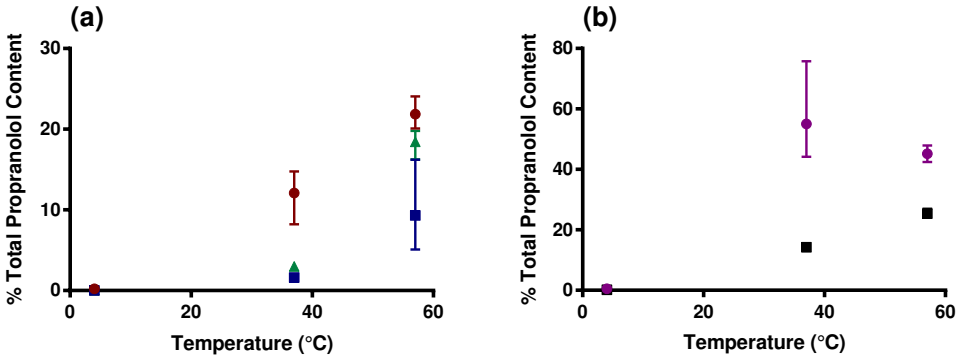

Figure 6.43 Total acylated product formed at varying temperatures (4 °C, 37 °C and 57 °C) within 72 hours at pH 7.4, in the presence of five membrane systems: (a) DOPC (red circles), DOPC:DOPS 4:1 (blue squares) and DOPE:DOPG 3:1 (green triangles) ; (b) POPC (purple cicles) and OPPC (black squares).

Total acylated product formation can also be utilised to determine the extent of propranolol **1** intrinsic lipidation with varying temperature at time points of 24 and 144 hours, summarised in Table 6.22 and Table 6.23 respectively. Increased total acylated product, indicative of increased propranolol **1** intrinsic lipidation, is observed at higher temperatures across all membrane types. Promotion of reactivity at higher temperatures at 24 hours and 144 hours,

attributed to increased ability to overcome the activation energy barrier of transesterification, supports the observations made following analysis at 72 hours.

	Total Acylated Product (%)		
Membrane Type	4 °C	37 °C	57 °C
DOPC	0.2	4.6	20.6
DOPC:DOPC (4:1)	0.0	0.9	5.2
DOPE:DOPG (3:1)	0.0	1.6	12.4
POPC	0.0	6.0	28.7
OPPC	0.0	9.3	23.6

Table 6.22 Proportion of total acylated product formed after 24 hour incubation at varying temperatures (4 °C, 37 °C, and 57 °C) within five membrane types.

	Total Acylated Product (%)		
Membrane Type	4 °C	37 °C	57 °C
DOPC	0.2	10.2	56.8
DOPC:DOPC (4:1)	0.1	1.0	20.9
DOPE:DOPG (3:1)	0.1	2.8	22.2
POPC	0.7	1.6	47.5
OPPC	0.5	3.7	65.4

Table 6.23 Proportion of total acylated product formed after 144 hour incubation at varying temperatures (4 °C, 37 °C, and 57 °C) within five membrane types.

Preferential reactivity at temperatures greater than 37 °C can be determined by comparison of the proportion of total acylated product formed by propranolol **1** intrinsic lipidation. To this end, eukaryotic membrane model DOPC, viral model DOPC:DOPS (4:1), and prokaryotic model DOPE:DOPG (3:1) were examined at 4 °C and 57 °C. Under physiological conditions the observed order of reactivity towards propranolol **1** intrinsic lipidation, reported in Section 6.3.3, is eukaryotic, followed by prokaryotic, and finally viral. Presented in Fig. 6.43, this observed reactivity trend is retained at 4 °C and 57 °C following 72 hours incubation. Further, the trend is also noted following analysis of samples incubated at 4 °C and 57 °C at 24 and 144 hours, as shown in Table 6.22 and Table 6.23. Conservation of this reactivity trend occurs despite temperature variation, and the associated modifications to membrane phase and fluidity. These membrane modifications may be expected to level subtle differences between the three membrane systems, such as domain formation and propranolol **1** binding orientation. However, given retention of the reactivity trend upon temperature variation, sufficient differences between the three membrane types as related to propranolol **1** intrinsic lipidation, must remain.

Investigation of the impact of temperature change upon the preferential *sn*-1 acyl chain transfer observed at 37 °C, was also conducted. Investigation was facilitated by comparison of POPC and OPPC membranes, phospholipids comprised of identical acyl chain moieties in opposing backbone positions. Fig. 6.44 presents total palmitoylated product and total oleoylated product observed for each membrane type following 72 hour incubation at 4 °C, 37 °C, and 57 °C. Preferential *sn*-1 transfer, palmitoyl for POPC and oleoyl for OPPC, is observed for both membrane compositions at 4 °C and 57 °C. This preference is noted despite the low abundance of palmitoylated and oleoylated products formed by propranolol **1** intrinsic lipidation at 4 °C. Preferential *sn*-1 transfer at 4 °C and 57 °C after 72 hours is attributed to increased proximity between the alcohol of membrane bound propranolol **1** and the phospholipid *sn*-1 ester linkage, compared to the *sn*-2 linkage.

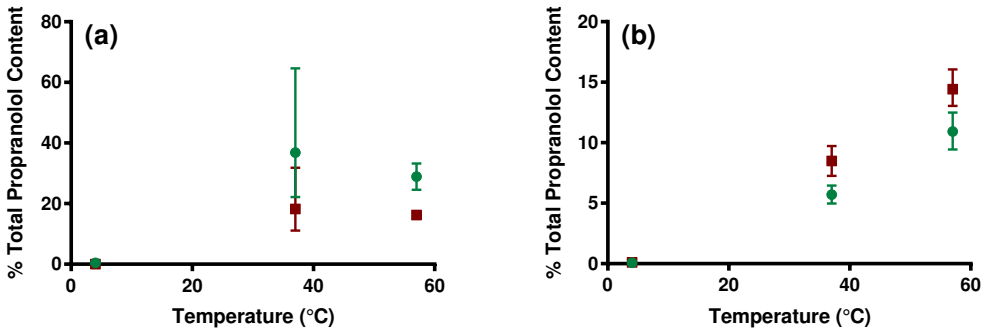

Figure 6.44 Total palmitoylated product (green circles) and total oleoylated product (red squares) formed by propranolol **1** intrinsic lipidation after 72 hours at varying temperatures (4 °C, 37 °C and 57 °C) in the presence of: (a) POPC membrane; (b) OPPC membrane.

Preferential *sn*-1 acyl chain transfer persists at 57 °C within both POPC and OPPC membranes at the additional time points of 24 and 144 hours, as highlighted in Table 6.24. However, more complex results are observed upon comparison of total palmitoylated product and total oleoylated product formed at 4 °C after 24 and 144 hours. Following a 24 hour incubation at 4 °C, neither palmitoylated propranolol nor oleoylated propranolol are observed analytically for POPC or OPPC membranes, Table 6.25. Lack of product observation prevents determination of preferential acyl chain transfer, and is attributed to reduced intrinsic lipidation reactivity at low temperatures combined with altered product distribution. Insufficient molecular energy to overcome reaction activation energy, combined with reduced molecular mobility, can explain observed reactivity limits. Analysis of samples incubated at 4 °C for 144 hours with a POPC membrane suggest retention of preferential *sn*-1 acyl chain transfer. However, this preferential *sn*-1 transfer is not reflected within an OPPC membrane following 144 hours at 4 °C, Table 6.25. By contrast, increased *sn*-2 transfer results in slightly higher levels of palmitoylated propranolol

compared to oleoylated propranolol. Observed differences in preferential acyl chain transfer may be attributed to the low levels of propranolol **1** intrinsic lipidation at 4 °C, resulting in product abundance at the limit of instrument detection and thus increasing the associated error. Alternatively, preferential *sn*-1 transfer may be replaced by either preferential *sn*-2 transfer or a distinction based upon acyl chain chemistry. A change in transfer preference at low temperature is possible within the confines of the less fluid membrane present at 4 °C, particularly considering the increased activation energy attributed to palmitoyl chain migration in Section 6.3.2.

Membrane Type	Time (hours)	Palmitoylated Product (%)	Oleoylated Product (%)
POPC	24	18.1	10.6
OPPC	24	9.5	14.1
POPC	144	29.9	17.7
OPPC	144	28.8	36.5

Table 6.24 Proportion of total palmitoylated product and total oleoylated product formed at 57 °C within POPC and OPPC membranes after 24 and 144 hours.

Membrane Type	Time (hours)	Palmitoylated Product (%)	Oleoylated Product (%)
POPC	24	0.0	0.0
OPPC	24	0.0	0.0
POPC	144	0.6	0.1
OPPC	144	0.3	0.2

Table 6.25 Proportion of total palmitoylated product and total oleoylated product formed at 4 °C within POPC and OPPC membranes after 24 and 144 hours.

Analysis has been conducted to determine the influence of temperature upon propranolol **1** intrinsic lipidation rate and reactivity preferences. Temperature has also been determined to influence the rate of intramolecular *O* to *N* migration within acylated propranolol species. Combining these two phenomena, it is possible to determine the influence of temperature upon the relative product distribution of *O*-acylated and *N*-acylated propranolol formed by intrinsic lipidation. Lowering environmental temperature from 37 °C to 4 °C results in formation of *O*-oleoyl propranolol **47** as sole intrinsic lipidation product within DOPC, DOPC:DOPS (4:1) and DOPE:DOPG (3:1) membranes over the time period studied, Fig. 6.45. Lack of *N*-oleoyl propranolol **13** formation is attributed to a diminished *O* to *N* migration rate at 4 °C. *O*-oleoyl propranolol **47** formation at 4 °C is first observed at 24 hours within the eukaryotic DOPC membrane, and at 72 hours within the viral and prokaryotic systems. Following initial formation, a slow increase in *O*-oleoyl propranolol **47** is observed within DOPC:DOPS (4:1)

and DOPE:DOPG (3:1) membrane models, supporting a low rate of initial transesterification and minimal *O* to *N* migration.

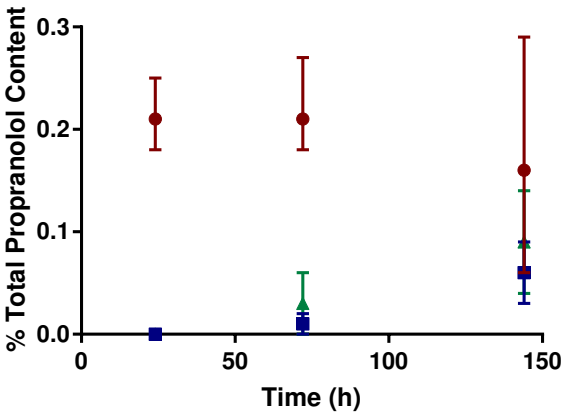

Figure 6.45 Total oleoylated product equal to *O*-oleoyl propranolol **47** only, formed over time at 4 °C and pH 7.4 in the presence of DOPC (red circles), DOPC:DOPS 4:1 (blue squares) and DOPE:DOPG 3:1 (green triangles) membrane systems.

Study of acylated product formation at 4 °C within POPC and OPPC membranes, Fig. 6.46, can also offer insight into the kinetics of propranolol **1** intrinsic lipidation. Acylated product formation is observed within both membrane systems from 72 hours, however unlike other membrane systems studied at 4 °C, both *O*-acylated propranolol and *N*-acylated propranolol species contribute. *N*-palmitoyl propranolol **12** is noted as the sole *N*-acylated species in both POPC and OPPC membrane systems. Increased rate of *O* to *N* migration for *O*-palmitoyl propranolol **62** compared to *O*-oleoyl propranolol **47** could explain this observation. However, previously determined rate constants for migration (k_1) of $0.7 \times 10^{-3}\,\mathrm{h}^{-1}$ and $2.6 \times 10^{-3}\,\mathrm{h}^{-1}$ for *O*-palmitoyl propranolol **62** and *O*-oleoyl propranolol **47** respectively do not support this theory. Alternatively, the presence of *N*-palmitoyl propranolol **12** as sole *N*-acylated product may suggest preferential transesterification of the palmitoyl moiety compared to the oleoyl moiety at 4 °C. Despite low product abundance, it has been determined that *N*-palmitoyl propranolol **12** formation within POPC and OPPC systems proceeds at 4 °C as observed under physiological conditions. An initial lag phase of 45 to 50 hours, highlighted by the vertical line in Fig. 6.46 (b), increased compared to 4 to 6 hours at 37 °C, is followed by an increase in *N*-palmitoyl propranolol **12** concentration. Within the OPPC membrane the increase in *N*-palmitoyl propranolol **12** concentration occurs more steadily, as shown by the dashed line in Fig. 6.46 (b). By contrast, in the presence of the POPC membrane the increase seems initially fast but then plateaus, suggestive of rate variation. Simultaneously, production of *O*-palmitoyl propranolol **62** and *O*-oleoyl propranolol **47** is observed to progress linearly within POPC and OPPC membranes at 4 °C, as shown by the solid green lines in Fig. 6.46.

Data extrapolation suggests transesterification commences at time point zero, with the lack of observed product at 24 hours attributed to the low abundance of acylated product, less that 0.05 % (<1 ng mL^{-1}).

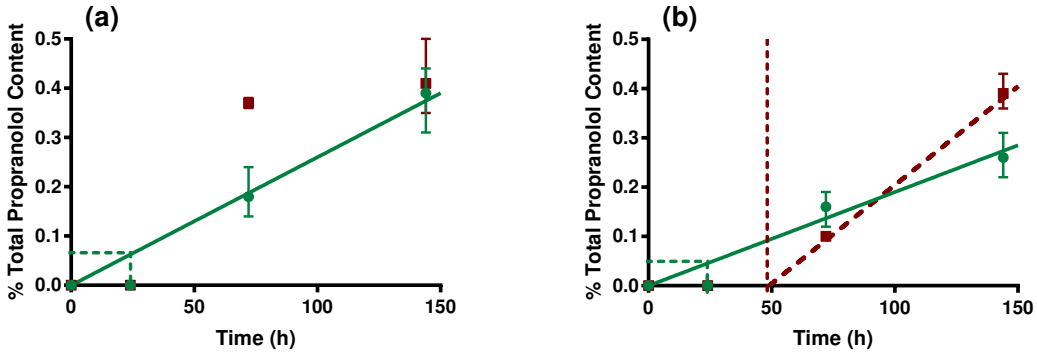

Figure 6.46 Total *O*-acylated product (experimental data as green circles and trend fitted with a solid green line), and total *N*-acylated product (experimental data as red squares and trend fitted with a dashed red line), formed from propranolol **1** at 4 °C in the presence of: (a) POPC membrane; (b) OPPC membrane. The box indicates the proportion of *O*-acylated product at 24 hours, below the limit of instument detection. The vertical line indicates end of *N*-acylated derivative lag phase.

Increasing environmental temperature from 37 °C to 57 °C is also predicted to influence the distribution of *O*-acylated and *N*-acylated products of propranolol **1** intrinsic lipidation. Similar trends in product formation at 57 °C are observed for membranes containing a PC phosphate head group, as shown in Fig. 6.47. Unlike at 4 °C and 37 °C, *N*-acylated propranolol production at 57 °C does not exhibit a lag phase on the scale of the time period studied. Data extrapolation shown by the red dashed lines in Fig. 6.47, suggests *N*-acylated propranolol formation commences within minutes of time point zero, suggesting no requirement for prior *O*-acylated propranolol accumulation. *N*-acylated product concentration proceeds to increase linearly within DOPC and OPPC systems, Fig. 6.47 (a) and (c), with slope gradient providing a means of formation rate comparison. At 57 °C the rate of *N*-acylated propranolol formation by intramolecular *O* to *N* migration is increased compared to at 37 °C, as shown in Table 6.26. *O*-acylated propranolol formation within PC membranes at 57 °C also differs from the logarithmic curve observed under physiological conditions. As shown in Fig. 6.47, an initial increase in *O*-acylated propranolol formation over 24 hours at 57 °C is followed by a steady decrease in concentration at later time points of 72 and 144 hours. Decreasing concentration is indicative of a faster rate of *O*-acylated propranolol decomposition by *O* to *N* migration compared to *O*-acylated propranolol formation by transesterification.

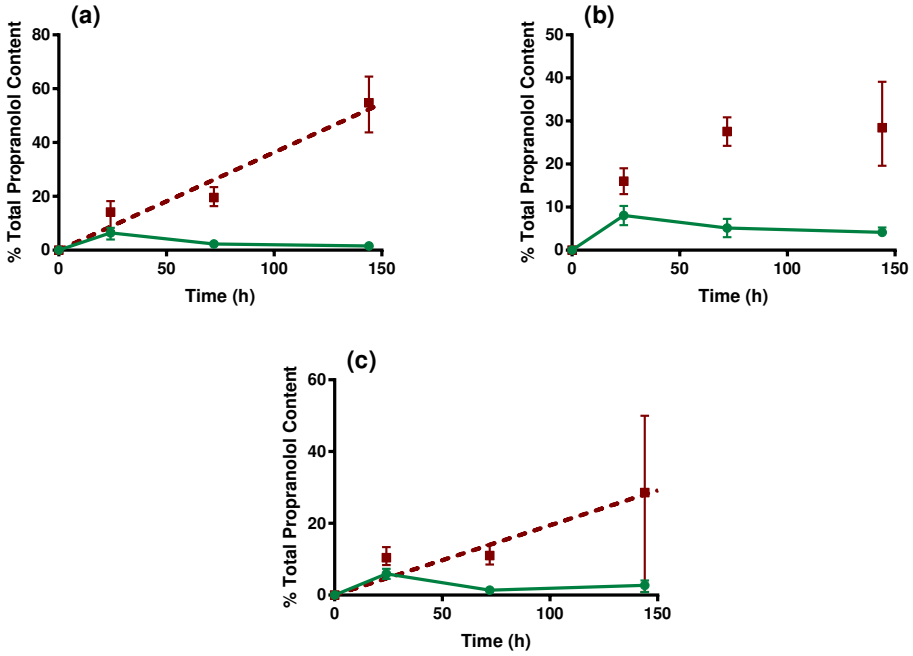

Figure 6.47 Total *O*-acylated product (experimental data as green circles and trend fitted with a solid green line), and total *N*-acylated product (experimental data as red squares and trend fitted with a red dashed line), formed at 57 °C in the presence of: (a) DOPC; (b) POPC; (c) OPPC.

Membrane Type	Rate at 37 °C (h^{-1})	Rate at 57 °C (h^{-1})
DOPC	0.13	0.36
OPPC	0.17	0.19

Table 6.26 Comparison of the rate of *N*-acyl propranolol formation within two membrane types at 37 °C and 57 °C.

Study of *N*-oleoyl propranolol **13** production at 57 °C within viral DOPC:DOPS (4:1) and prokaryotic DOPE:DOPG (3:1) membranes reveals similar results to those observed for PC membranes, Fig. 6.48. *N*-oleoyl propranolol **13** formation commences within minutes of time point zero in the prokaryotic membrane, indicating a diminished lag phase compared to at physiological temperatures. Viral membrane DOPC:DOPS (4:1) exhibits a 5 hour lag phase prior to *N*-oleoyl propranolol **13** production, consistent with the reduced membrane reactivity. *N*-oleoyl propranolol **13** concentration increases linearly up to 144 hours within the viral membrane model, Fig. 6.48 (a), whereas concentration increases and then plateaus in the presence of DOPE:DOPG (3:1), shown in Fig. 6.48 (b). *O*-oleoyl propranolol **47** concentration at 57 °C does not exhibit a significant decrease over time within viral and prokaryotic membranes, in contrast to PC membranes. A logarithmic curve is observed for *O*-oleoyl propranolol **47** production within the viral membrane at 57 °C. Analogous to observations under physiological conditions, this trend suggests similar reaction rates for

transesterification and *O*-oleoyl propranolol **47** decomposition. At 57 °C, contributions from both hydrolysis and *O* to *N* migration have previously been shown to influence decomposition in approximately a 1:4 ratio. Within the prokaryotic membrane insufficient data points exist to determine whether *O*-oleoyl propranolol **47** concentration is best characterised by a linear decrease or a logarithmic curve. Consequently, transesterification rate must be similar or lower than rate of *O*-oleoyl propranolol **47** decomposition by hydrolysis and migration pathways.

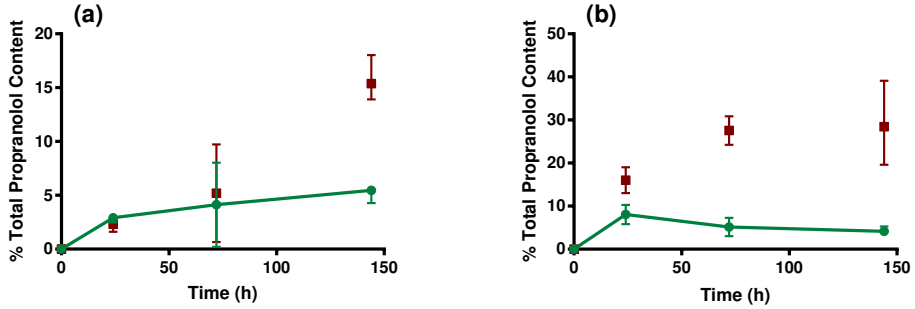

Figure 6.48 Total *O*-acylated product (experimental data as green circles and trend fitted with a solid green line), and total *N*-acylated product (experimental data as red squares), formed at 57 °C in the presence of: (a) DOPC:DOPS (4:1); (b) DOPE:DOPG (3:1).

The influence of temperature upon the reaction kinetics of propranolol **1** intrinsic lipidation can be summarised into key findings. Increased temperature is observed to increase the rate of both preliminary intrinsic lipidation step transesterification, and secondary intramolecular *O* to *N* migration. Consequently, higher levels of total acylated intrinsic lipidation product are evident across all membrane types upon temperature increase from 4 °C through to 57 °C. Temperature is also observed to modify product distribution, with higher temperatures favouring thermodynamic product *N*-acylated propranolol over kinetic product *O*-acylated propranolol. Increased energy availability, aiding in molecular mobility and membrane fluidity at high temperatures is believed to facilitate this distribution. Additionally, higher temperatures provide further energy to aid in overcoming the required activation energy barrier, promoting reactivity. Vital reactivity parameters, membrane binding orientation and proximity of reactive moieties, are not predicted to be negatively influenced by increased temperature, as had been speculated. Preferential reactivity trends noted at 37 °C are broadly retained at 4 °C and 57 °C. Included in these are favourable *sn*-1 acyl chain transfer, and favourable eukaryotic reactivity compared to viral and prokaryotic analogues.

6.4.2 Influence of pH

Modification to propranolol **1** intrinsic lipidation kinetics can be achieved by altering the environmental parameter of pH from physiological conditions. Predicting the effect of modified pH upon intrinsic lipidation reactivity is challenging due to the complex nature of the multi-step reaction. Fundamentally, environmental pH alters the proportion of ionised to neutral propranolol **1** available for membrane association. Altered ratio of ionised to neutral propranolol **1**, affects the rate of the preliminary membrane binding step required to facilitate propranolol **1** intrinsic lipidation.[158] Furthermore, altered proportion can modify propranolol **1** membrane penetration and binding orientation, influencing proximity of reactive moieties, and nucleophilicity of the alcohol and amine residues.[267] Nucleophilicity changes would present as a modified rate of intrinsic lipidation, altering rate of both transesterification and intramolecular *O* to *N* migration. *O*-acylated propranolol decomposition by hydrolysis can in principle be influenced by pH if the decomposition is subject to general acid or base catalysis, ultimately altering intrinsic lipidation product stability and distribution.[278,280] Consideration must also be given to phospholipid hydrolysis modulation by environmental pH and potentially by either neutral or ionised propranolol **1** analogues. Resulting modified lysolipid proportion within the bulk membrane impacts propranolol **1** reactivity towards intrinsic lipidation, membrane disruption and possible micelle formation.[31]

Considering the appreciable and complex influence of pH upon the multi-step process of intrinsic lipidation, experiments were designed to probe reactivity beyond physiological conditions. Buffer solution of 10 mM ammonium bicarbonate adjusted with formic acid to pH 4.30 was prepared in accordance with mobile phase preparation guidelines.[286] Intrinsic lipidation reaction mixtures were incubated within this pH 4.30 buffer at 37 °C using five membrane types. Eukaryotic DOPC, viral DOPC:DOPS (4:1), and prokaryotic DOPE:DOPG (3:1) for comparison of membrane models, POPC and OPPC to study preferential acyl transfer. Triplicate sample analysis was conducted following incubation times of 24, 72 and 144 hours. Reaction mixture constituents were quantified according to the previously defined methodology presented in Section 6.3.1.

Propranolol **1** intrinsic lipidation is not observed within eukaryotic, viral or prokaryotic membrane models following 24 or 72 hour incubation at pH 4.30, Table 6.27. The slow acid catalysed transesterification rate reported for commercial biodiesel production likely applies to the transesterification step of intrinsic lipidation.[248,287] Combined with increased acid

catalysed hydrolysis suggested by the literature, *O*-oleoyl propranolol **47** formation may be non-existent or transient, preventing analytical observation.[278,280] Further, at pH 4.30 the predominant forms of propranolol **1** and *O*-oleoyl propranolol **47** are their ionised analogue. Amine protonation reduces nucleophilicity and makes the process of intramolecular *O* to *N* acyl chain migration unfavourable. Analysis of samples incubated for 144 hours at pH 4.30, Table 6.27, indicate *N*-oleoyl propranolol **13** concentrations of $<0.5\,\mathrm{ng\,mL^{-1}}$ across all membrane models despite lack of *O*-oleoyl propranolol **47**. Direct nucleophilic amine activity is unlikely given its protonated nature, instead the theory of transient *O*-oleoyl propranolol **47** formation is supported. Competing transesterification and acid catalysed hydrolysis form low level transient *O*-oleoyl propranolol **47**. Slow *O* to *N* migration proceeds within the neutral analogue of this transient species, resulting in formation of stable *N*-oleoyl propranolol **13**. Alternative theories such as acid catalysed oxidation or hydrolysis of the double bound resulting in modified product formation have been discounted due to lack of analytical observation. Further support is derived from intact double bond retention within parent phospholipid and lysolipid species at pH 4.30. Insufficient product quantities prevented an accurate comparison between models to determine preferential transfer.

	O-Oleoyl Propranolol **47** (%)			*N*-Oleoyl Propranolol **13** (%)		
	Time 24 h	Time 72 h	Time 144 h	Time 24 h	Time 72 h	Time 144 h
DOPC	0.0	0.0	0.0	0.0	0.0	< 0.1
DOPC:DOPS (4:1)	0.0	0.0	0.0	0.0	0.0	< 0.1
DOPE:DOPG (3:1)	0.0	0.0	0.0	0.0	0.0	< 0.1

Table 6.27 Comparison % total propranolol **1** content attributed to *O*-oleoyl propranolol **47** and *N*-oleoyl propranolol **13** at pH 4.3 in the presence of three membrane models: (i) DOPC; (ii) DOPC:DOPS (4:1); (iii) DOPE:DOPG (3:1).

Membranes containing two distinct acyl chain chemistries, such as POPC and OPPC, exhibit interesting intrinsic lipidation reactivity differences at pH 4.30. Oleoyl transfer proceeds in a similar fashion to the DOPC membrane, as shown in Table 6.29, with *N*-oleoyl propranolol **13** the sole intrinsic lipidation product at concentrations of $<0.5\,\mathrm{ng\,mL^{-1}}$ following 144 hours. This observation is attributed to transient *O*-oleoyl propranolol **47** formation followed by *O* to *N* migration. Similarly, palmitoyl transfer to either the alcohol or amine moiety is not definitively observed following 24 or 72 hour incubation, as shown in Table 6.28. The slow transesterification rate combined with decreased *O* to *N* migration within the protonated

species can explain this observation. However, at 144 hours the proportion of total propranolol **1** content attributed to *O*-palmitoyl propranolol **62** was calculated to be 4.0 % (24.9 ng mL^{-1}) for POPC, and 4.9 % (24.5 ng mL^{-1}) for OPPC. Observed across triplicate samples, this sudden increase in *O*-palmitoyl propranolol **62** content cannot be attributed to sample contamination or dilution error. The sudden concentration jump is justified by either continuous *O*-palmitoyl propranolol **62** build up, which was below instrument detection limit at earlier time points, or by a sudden environment induced increase in transesterification rate as time progresses. In tandem, *O*-palmitoyl propranolol **62** decomposition by acid catalysed hydrolysis and *O* to *N* migratory pathways must be decreased compared to those of the oleoylated analogue.

	O-Oleoyl Propranolol **47** (%)			*N*-Oleoyl Propranolol **13** (%)		
	Time 24 h	Time 72 h	Time 144 h	Time 24 h	Time 72 h	Time 144 h
POPC	0.0	0.0	4.0	0.0	0.0	0.0
OPPC	0.0	0.0	4.9	0.0	0.0	0.0

Table 6.28 Comparison % total propranolol **1** content attributed to *O*-palmitoyl propranolol **62** and *N*-palmitoyl propranolol **12** at pH 4.3 in the presence of two membrane models: (i) POPC; (ii) OPPC.

	O-Oleoyl Propranolol **47** (%)			*N*-Oleoyl Propranolol **13** (%)		
	Time 24 h	Time 72 h	Time 144 h	Time 24 h	Time 72 h	Time 144 h
POPC	0.0	0.0	0.0	0.0	0.0	< 0.1
OPPC	0.0	0.0	0.0	0.0	0.0	< 0.1

Table 6.29 Comparison % total propranolol **1** content attributed to *O*-oleoyl propranolol **47** and *N*-oleoyl propranolol **13** at pH 4.3 in the presence of two membrane models: (i) POPC; (ii) OPPC.

Study of propranolol **1** intrinsic lipidation kinetics under basic conditions, above the pK_a of the propranolol **1** ammonium, also provides valuable reactivity information. Under basic conditions propranolol **1** predominantly adopts the neutral form, expected to enhance base catalysed transesterification and intramolecular *O* to *N* migration. Preparation of a 10 mM ammonium bicarbonate buffer solution adjusted to pH 10.4 using aqueous ammonia.[286] For comparability to studies at pH 4 and pH 7, environmental temperature of 37 °C and use of five model membranes were retained.

Propranolol **1** intrinsic lipidation at pH 10.4 is evident across all five membrane models from primary analysis at time point 24 hours through to final analysis at 144 hours, Fig. 6.49. After 144 hours between 12 % and 52 % of the total propranolol **1** derived content can be attributed to acylated species. In the presence of all membrane systems studied, acylated product formation exhibits an initially sharp increase in intrinsic lipidation, followed by a subsequent reduction in rate after 24 hours. This variation in rate is attributed to reduced propranolol **1** content combined with modified membrane composition and characteristics. Reactivity trends noted at physiological pH are retained at pH 10.4, with eukaryotic model DOPC indicating increased reactivity compared to prokaryotic and viral counterparts, Fig. 6.49 (a). Furthermore, in line with observations made under physiological conditions, total reactivity is heightened within the POPC membrane at pH 10.4 compared to the OPPC membrane, Fig. 6.49 (b). Despite comparability in observed trends, overall reactivity differences are evident between intrinsic lipidation at pH 7.4 and pH 10.4. Gradients of total acylated product formation for DOPC, DOPC:DOPS (4:1), and DOPE:DOPG (3:1) membranes are steeper at pH 10.4 than pH 7.4, indicating increased rate of intrinsic lipidation. For example, at pH 10.4 the gradient of total acylated product concentration over time within the DOPC membrane is $0.38\,h^{-1}$, more than twice that of gradient $0.17\,h^{-1}$ observed at pH 7.4. The increased rate of intrinsic lipidation under basic conditions is attributed to base catalysis of the transesterification step of intrinsic lipidation increasing its rate, combined with enhanced nucleophilicity of the reactive moieties within propranolol **1**. Diminished *O*-acylated propranolol decomposition by the hydrolysis pathway in favour of *O* to *N* migration is known at basic pH in solution, which may also aid in enhancing intrinsic lipidation product retention within the membrane.[278,280]

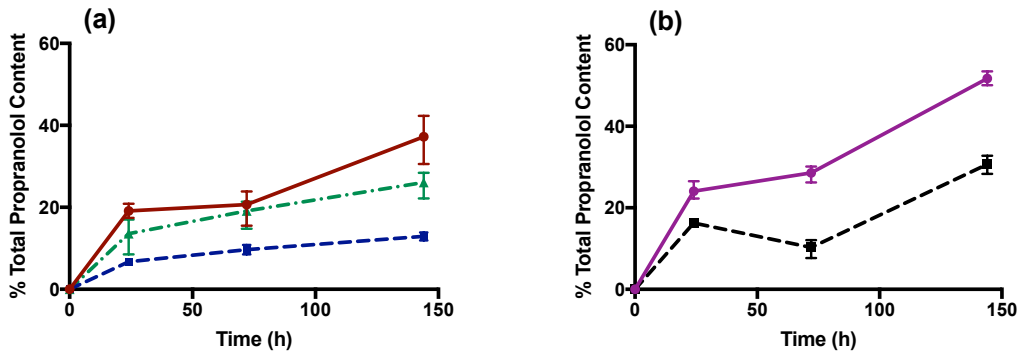

Figure 6.49 Total acylated product formed at pH 10.4 and 37 °C within 72 hours, in the presence of five membrane systems: (a) DOPC (experimental data as red circles and connected with a solid red line), DOPC:DOPS 4:1 (experimental data as blue squares and connected with a blue dashed line line) and DOPE:DOPG 3:1 (experimental data as green triangles and connected with a dotted and dashed green line); (b) POPC (experimental data as purple circles and connected with a solid purple line) and OPPC (experimental data as black squares and connected with a dashed black line).

Dividing total acylated product proportion within POPC and OPPC systems into its respective palmitoylated and oleoylated constituents provides further insight into reactivity differences within multi-acyl phospholipid membranes. Following 24 hour incubation at pH 10.4, Table 6.30, preferential *sn*-1 acyl chain transfer occurs, correlating with observations at physiological pH. Proximity between the *sn*-1 ester linkage on the phosphate backbone and the alcohol of membrane bound propranolol **1** could explain this preference. However, comparison of palmitoylated to oleoylated product ratio after 144 hours incubation at basic pH, Table 6.30, indicates increased palmitoylated propranolol within both POPC and OPPC membranes. Preferential palmitoyl transfer has been noted previously within temperature related kinetics studies of intrinsic lipidation, and at acidic pH. Attribution of preferential palmitoyl transfer to modification of oleoylated product by double bond hydrolysis, oxidation and diacylation, or to instrument concentration limitations, can be disproved and discounted. Rather, a concious modification in preferential transfer must occur as the intrinsic lipidation progresses under these conditions, catalysed by changes in rates of the relevant steps or by variation in environmental conditions. Study of the palmitoylated product distribution may aid in providing further insight.

Membrane Composition	P:O Ratio at 24 hours	P:O Ratio at 144 hours
POPC	16.3 : 7.8	35.2 : 16.5
OPPC	6.8 : 9.5	16.1 : 14.5

Table 6.30 Comparison of the total palmitoylated product (P) to total oleoylated product (O) ratio within POPC and OPPC membranes after 24 hours and 144 hours at pH 10.4 and 37 °C.

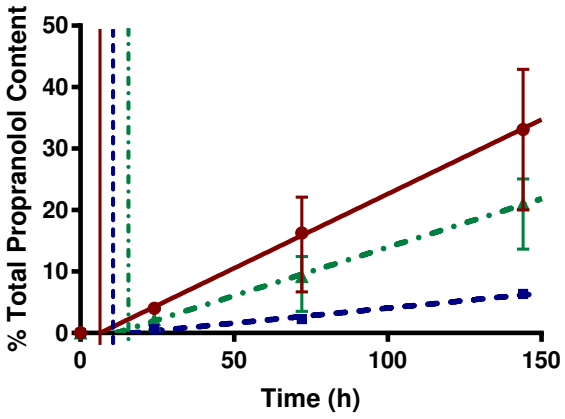

Figure 6.50 *N*-oleoyl propranolol **13** formation over 144 hours at pH 10.4 and 37 °C within DOPC (experimental data as red circles and fitted with a solid red line), DOPC:DOPS 4:1 (experimental data as blue squares and fitted with a blue dashed line line) and DOPE:DOPG 3:1 (experimental data as green triangles and fitted with a dotted and dashed green line) membranes. Vertical lines indicate end of lag phase.

The distribution of *O*-acylated and *N*-acylated propranolol **1** intrinsic lipidation products is also altered by environmental pH. Fig. 6.50 shows the formation of *N*-oleoyl propranolol **13** within eukaryotic, viral and prokaryotic membrane models at pH 10.4. Analogously to observations made at physiological pH, *N*-oleoyl propranolol **13** concentration increases linearly over time following an initial lag phase. Extrapolation of available data determines the lag phase lengths as approximately 6 hours, 17 hours, and 12 hours for DOPC, DOPC:DOPS (4:1), and DOPE:DOPG (3:1) systems respectively. *N*-oleoyl propranolol **13** lag phase length across all systems at pH 10.4 is increased compared to the 4 to 6 hours observed at physiological pH. This increased lag time may be accounted for by a requirement for increased *O*-oleoyl propranolol **47** concentrations prior to commencement of *O* to *N* migration. Alternatively, *O* to *N* migration may not proceed when *O*-oleoyl propranolol **47** is membrane bound or within certain binding orientations, slowing *N*-oleoyl propranolol **13** formation at basic pH where the neutral species is predominantly membrane associated. Furthermore, under basic conditions increased neutral membrane bound propranolol **1** may facilitate direct amine reactivity. Amine proximity to the phospholipid ester linkages within the binding orientation of the neutral species is expected to aid in direct reactivity. Overall the physiological pattern of reactivity, eukaryotic followed by prokaryotic and finally viral, is retained for *N*-oleoyl propranolol **13** at pH 10.4.

N-palmitoyl propranolol **12** and *N*-oleoyl propranolol **13** concentrations within POPC and OPPC membranes under basic conditions are shown in Fig. 6.51. Acyl chain transfer from the *sn*-1 position proceeds through a lag phase of less than one hour and approximately 4 hours for POPC and OPPC respectively, followed by linear increases of differing rates. Given comparable migratory rate constants for palmitoyl and oleoyl moieties at 37 °C, preferential transfer must result from favourable *sn*-1 reactivity at the transesterification step producing an increased quantity of the relevant *O*-acylated precursor. Ultimately increased *sn*-1 precursor availability results in an increased concentration of the relevant *N*-acylated analogue. Transfer of *sn*-2 position acyl chains within POPC and OPPC membrane systems proceeds as a linear increase in relevant product concentration following a lag phases 7 to 8 hours. Differences in lag phase length support a hypothesis that *O*-acylated precursor availability is vital in determining migratory rate and *N*-acylated species concentration.

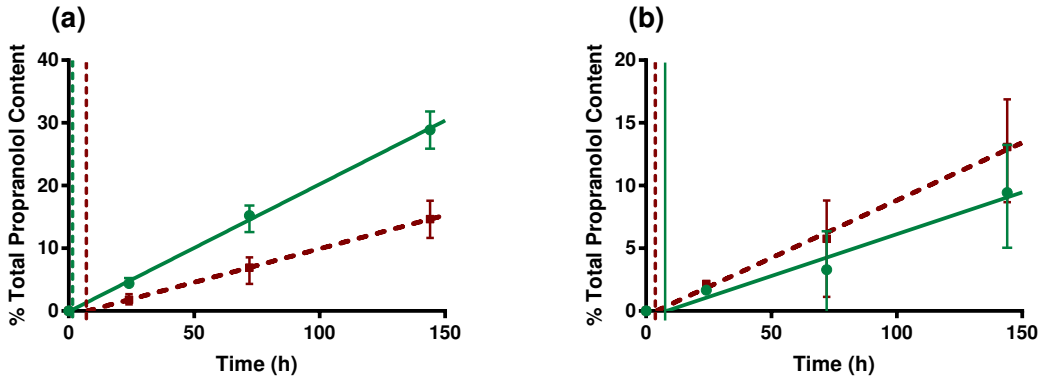

Figure 6.51 *N*-palmitoyl propranolol **12** (experimental data as green circles and fitted with a solid green line) and *N*-oleoyl propranolol **13** (experimental data as red squares and fitted with a dashed red line) formation over 144 hours at pH 10.4 and 37 °C within membrane systems of: (a) POPC; (b) OPPC. Vertical lines indicate end of lag phase.

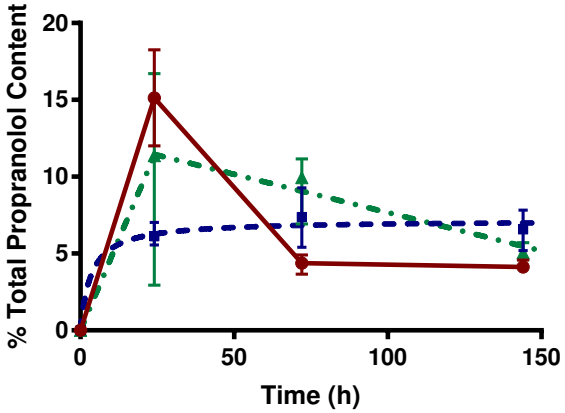

Figure 6.52 *O*-oleoyl propranolol **47** formation over 144 hours at pH 10.4 and 37 °C within membrane systems of DOPC (experimental data as red circles and connected with a solid red line), DOPC:DOPS 4:1 (experimental data as blue squares and fitted with a blue dashed line line) and DOPE:DOPG 3:1 (experimental data as green triangles and fitted with a dotted and dashed green line).

O-oleoyl propranolol **47** concentration within viral membrane model DOPC:DOPS (4:1) increases and plateaus over 144 hours at pH 10.4, Fig. 6.52. The plateau, also observed at physiological pH, indicates comparable rates of *O*-oleoyl propranolol **47** formation and decomposition. By contrast, *O*-oleoyl propranolol **47** concentration within eukaryotic and prokaryotic systems under basic conditions shows an initial increase over 24 hours, followed by reduction to steady state concentrations. Also notable at high temperatures, reduction in *O*-oleoyl propranolol **47** concentration is characteristic of a faster rate of ester decomposition compared to formation. Given previous observations that membrane bound *O*-oleoyl propranolol **47** decomposition proceeded by *O* to *N* migration only under physiological conditions, this is presumed as the mechanism. Increased migration rate at pH 10.4 compared to pH 7 can be attributed to an increased proportion of neutral *O*-oleoyl propranolol **47** under basic

conditions compared to physiological pH, facilitating acyl chain acceptance by the amine functionality.

O-oleoyl propranolol **47** formation within POPC and OPPC membranes at pH 10.4 proceeds in an analogous fashion to within the DOPC membrane Fig. 6.53. An initial concentration increase is followed by a reduction to a steady state concentration, indicating a higher rate of *O* to *N* migration compared to transesterification. *O*-palmitoylated propranolol **62** concentration presents with a different trend, increasing to time point 24 hours, decreasing at 72 hours, and subsequently increasing again at final time point 144 hours. The final concentration increase at 144 hours in OPPC results in the previously discussed loss of preferential *sn*-1 transfer in favour of palmitoyl chain transfer. Determining the underlying causes of the observed trend in *O*-palmitoylated propranolol **62** concentration under basic conditions is challenging, especially given that only three data points are available. Varied rate of formation or decomposition over the time period studied provides the most likely explanation. *O*-palmitoyl propranolol **62** decomposition by the hydrolysis pathway not utilised by *O*-oleoyl propranolol **47** potentially varies depending upon partition coefficients and membrane hydration levels. These parameters alter as the reaction progresses, changing the concentration and nature of membrane bound species, and disrupting the bulk membrane. Lysolipid concentration, upon general base catalysed hydrolysis of phospholipids, also increases as reaction time progresses. Intrinsic lipidation reactivity between lysolipids and propranolol **1** may occur, altering rate of *O*-palmitoyl propranolol **62** formation.

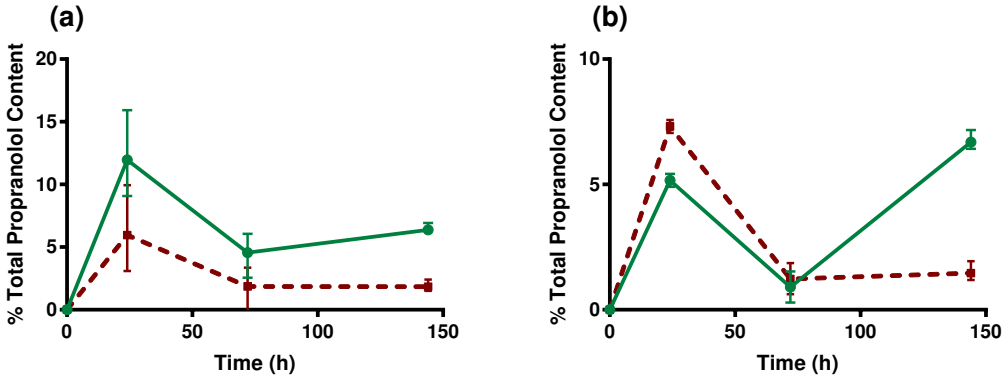

Figure 6.53 *O*-palmitoyl propranolol **62** (experimental data as green circles and connected with a solid green line) and *O*-oleoyl propranolol **47** (experimental data as red squares and connected with a dashed red line) formation over 144 hours at pH 10.4 and 37 °C within membrane systems of: (a) POPC; (b) OPPC.

The influence of pH alteration upon rate of propranolol **1** intrinsic lipidation and product distribution can be summarised as follows. pH reduction from neutral 7 to acidic 4.3 diminishes

intrinsic lipidation reactivity, producing *N*-oleoyl propranolol **13** as sole reaction product after 144 hours within oleoylated systems. Observations are attributed to an increased proportion of ionised species within the reaction mixture, reducing base catalysis, membrane affinity, nucleophilicity and amine availability for *O* to *N* migration. Combined with increased acid catalysed hydrolysis of *O*-acylated intermediates, only transient low level formation occurs preventing successful analysis. Low product abundance prevents identification of trends in preferential transfer under acidic conditions. Conversely, at basic pH 10.4 an increased proportion of neutral reactive propranolol **1** derived species are present, aiding in intrinsic lipidation progression. As a result, total intrinsic lipidation product formation is increased under these conditions compared to physiological pH. Furthermore, reactivity trends in which eukaryotic membranes exhibit heightened reactivity compared to prokaryotic and viral membrane systems are retained despite pH modification. Rate of intramolecular *O* to *N* migration is faster than transesterification at pH 10.4 across most systems, despite increased lag time compared to physiological pH, attributed to availability of the neutral amine. However, *O*-palmitoyl propranolol **62** concentration variation over the time period of study indicates rate fluctuations for relevant formation and decomposition processes as a result of environmental changes.

6.4.3 Influence of Membrane Composition

Mimicry of natural membranes containing only diacyl phospholipids provides an informative model for the study of propranolol **1** intrinsic lipidation. Whilst this model allows characterisation of acyl transfer from diacyl phospholipids to propranolol **1**, analogous non-enzymatic reactivity between propranolol **1** and lysolipids has been overlooked. Lysolipid products of phospholipid hydrolysis and propranolol **1** intrinsic lipidation contain a single ester-linked acyl chain with a potential propensity to undergo similar transfer reactions.[30,31,173] Probing transfer of this single acyl chain *in vitro* will provide insight into intrinsic lipidation kinetics, and improved understanding of reactivity *in vivo* by more accurately mimicking natural membrane composition.[32,34]

Self assembly of lipid species into organised structures within an aqueous environment depends upon both innate species properties and molecular geometry. Diacyl phospholipids are known to adopt a bilayer structure within aqueous environments, promoting favourable hydrophobic interactions between fatty acid chains. In contrast, lysolipids self-assemble into micelles under aqueous conditions, providing their concentration is higher than their associated

CMC.[208,211] CMC, the lowest concentration of lysolipid required to facilitate micelle formation, is dependent upon lysolipid properties. Within the µM concentration range, lysolipid CMC is inversely proportional to acyl chain length and level of saturation.[33,214] Propranolol **1** binding strength and orientation differs between bilayer and micellar structures, predicted to result in corresponding changes to intrinsic lipidation reactivity.[288,289] Further, differences in hydration levels and membrane curvature associated with micelles compared to bilayers, may impact intrinsic lipidation.[208,211]

Study of propranolol **1** intrinsic lipidation by lysolipids was facilitated by hydration and vigorous mixing of a dried lysolipid film, resulting in micelle preparation. PPC and OPC lysolipids, with CMC values of 4.0 µM to 8.3 µM, and 4.0 µM respectively, were selected for study due to incorporation of the eukaryotic PC head group, and either a palmitoyl or oleoyl acyl chain.[33,214] Propranolol **1** was added to micelles in a 1:10 small molecule:lysolipid molar ratio, and the mixture incubated under physiological conditions. Sample analysis under optimised chromatographic and ionisation conditions was conducted at 24, 72 and 144 hours, and mixture components quantified using calibration curves of synthetic standards. Anomalous data points and dilution error were identified through study of each sample in triplicate.

Propranolol **1** intrinsic lipidation by PPC and OPC lysolipids was studied by determination of total acylated propranolol **1** product content, compared to analogous reactivity within DPPC and DOPC liposomes. Total acylated product is considered representative of rate of propranolol **1** intrinsic lipidation within each membrane type. Evidenced in Fig. 6.54, total acylated propranolol **1** product is increased at all studied time points within PPC and OPC micelles compared to corresponding DPPC and DOPC bilayers. At 144 hours, 64 % of total propranolol **1** derived content can be attributed to acylated species in the presence of PPC, and 55 % in the presence of OPC. In contrast, figures determined in the presence of DPPC and DOPC bilayers are 49 % and 15 % respectively. In addition to the observed increase in propranolol **1** intrinsic lipidation by lysolipids compared to diacyl phospholipids, the two exhibit differing production trends. Total acylated product formation within DPPC and DOPC bilayers increases over the time period studied, however within PPC and OPC micelles this initial linear increase tails off by 144 hours. Evidenced by the curvature in Fig. 6.54, the observed trend variation suggests initial swift propranolol **1** intrinsic lipidation by lysolipids, followed by a rate decrease over time.

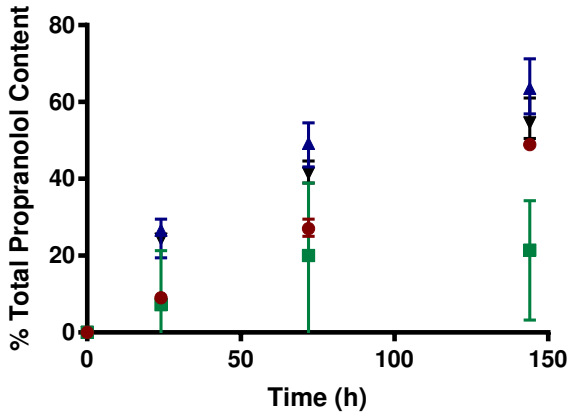

Figure 6.54 Total acylated product formation under physiological conditions in the presence of DPPC (red circles), DOPC (green squares), PPC (blue triangles), and OPC (black inverted triangles) membrane systems.

Despite intrinsic lipidation reactivity differences between phospholipid bilayers and lysolipid micelles, both palmitoyl containing systems exhibit increased reactivity compared to their oleoyl containing counterparts, Fig. 6.54. Corresponding preferential palmitoyl transfer has previously been noted during the study of peptide intrinsic lipidation by lysolipids.[40] However, intrinsic lipidation within DPPC membranes has not been observed prior to this study, attributed to DPPC's high transition temperature producing a gel phase bilayer at physiological temperatures.[59] The resulting reduction to hydration levels and penetration of membrane active species, are anticipated to have negative effects on the rate of intrinsic lipidation in gel phase DPPC bilayers. As a result, the reason for increased non-enzymatic palmitoyl transfer to propranolol **1** within both PPC and DPPC systems compared to oleoyl containing counterparts is unclear. However, tightened packing of saturated palmitoyl chains compared to kinking of unsaturated oleoyl chains, provides a potential mechanism for increased reactivity by increasing the proximity between reactive moieties.[282]

Beyond study of propranolol **1** intrinsic lipidation within lysolipid micelles by monitoring total acylated product content, product distribution should also be considered. *O*-acylated propranolol decomposition by intramolecular *O* to *N* migration increases 30 fold within a cationic dodecyltrimethylammonium bromide micelle compared to solution phase decomposition.[288] Increased decomposition is attributed to increased polarisation of the carbonyl bond within micelle associated *O*-acylated propranolol. Accordingly, altered carbonyl polarisation within *O*-acylated propranolol bound to zwitterionic PPC or OPC micelles, could potentially impact *O* to *N* acylated product distribution following initial intrinsic lipidation by transesterification. Fig. 6.55 depicts *O*-acylated propranolol and *N*-acylated propranolol concentrations within PPC and OPC systems up to 144 hours. Similar product distribution and reactivity profiles

are observed for intrinsic lipidation within both PPC and OPC micelles, in line with their comparable physical properties.

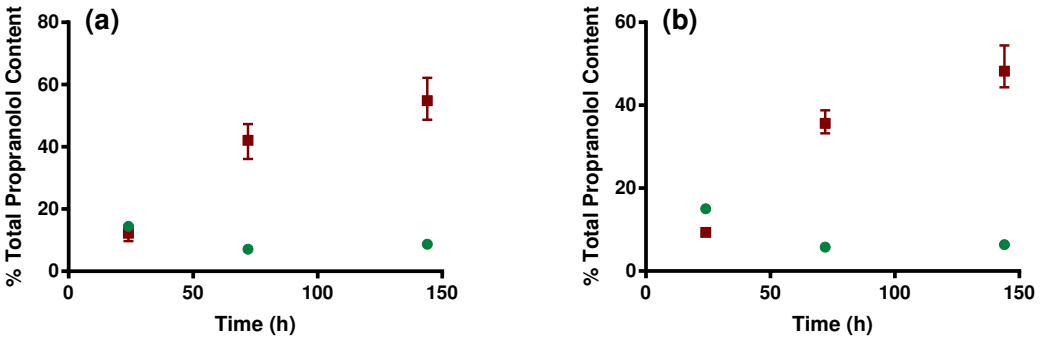

Figure 6.55 *O*-acylated propranolol (green circles) and *N*-acylated propranolol (red squares) product distribution under physiological conditions up to 144 hours within micelles containing: (a) PPC; (b) OPC.

Formation of *N*-acylated propranolol within micellar systems commences following an initial lag phase, in analogous fashion to DOPC and DPPC bilayer systems. Lag phase length is calculated as between 14 hours to 15 hours within PPC and OPC, compared to the 4 to 6 hour lag phase observed within bilayer systems under physiological conditions. *N*-acylated propranolol concentration within micellar systems then increases over 144 hours, following a logarithmic curve rather than the linear increase associated with bilayer systems. Both observations are consistent with a changing rate of *N*-acylated propranolol formation by *O* to *N* migration within micelles over the time period studied. *O*-acylated propranolol concentration within PPC and OPC micelles is also affected by the variation in rate of decomposition by *O* to *N* migration, compared to rate of formation by transesterification. As shown in Fig. 6.55, *O*-acylated propranolol concentration initially increases up to 24 hours, due to species formation with minimal decomposition. *O*-acylated propranolol concentration then decreases to steady state as rate of *O* to *N* migration eclipses rate of transesterification, before finally plateauing as rate of formation and rate of decomposition become comparable.

Significant variation in propranolol **1** intrinsic lipidation reactivity and product distribution *in vitro* is noted between phospholipid containing bilayers and lysolipid containing micelles. However, increased biological relevance and mechanistic understanding can be achieved by moving from the study of single component membranes to complex mixtures.[1,3] Notably, preparation of mixtures containing both micellar lysolipids and bilayer forming phospholipids introduces interesting phase behaviour, predicted to impact intrinsic lipidation reactivity. NMR, electron spin resonance (ESR), and spectrophotometry provide insight into the structure and phase behaviour within these combined lipid systems, dependent upon the species involved and

relative quantities.[31,173,290] Lipid mixtures containing 95:5 molar ratio of phospholipid:lysolipid were prepared containing DPPC:OPC and DOPC:PPC. At this molar ratio under physiological conditions, studies indicate the DPPC:OPC phase behaviour is 100 % bilayer, whilst the DOPC:PPC mixture is > 95 % bilayer in nature.[32] Lysolipids PPC and OPC act as detergents within the bilayer at 5 mol%, resulting in minor disruption and increased fluidity. For comparison, lipid mixtures containing 5:95 molar ratio of DPPC:OPC and DOPC:PPC were also studied. Primarily containing lysolipid, literature suggests that these lipid mixtures have 0 % bilayer content under physiological conditions, instead adopting a micellar structure with inserted intact diacyl phospholipids.[32] Pairing lipid species containing differing acyl chains aids in determining the origin of acyl chain transfer, and informing on relative rates of intrinsic lipidation for each species within the system.

Comparison of intrinsic lipidation reactivity within systems of differing phase behaviour can be evaluated by considering total acylated propranolol **1** product formation. Table 6.31 presents this data for lipid mixtures containing DPPC and OPC following 72 hour incubation under physiological conditions. Total acylated product concentration decreases from 27.1 ng mL^{-1} to 13.1 ng mL^{-1} upon introduction of 5 mol% OPC into a DPPC membrane. Decreased product formation is attributed to reduced DPPC reactivity within the disrupted OPC containing bilayer compared to the intact DPPC bilayer. Increased membrane fluidity and the resulting altered proximity of reactive moieties is predicted to play a role in reducing DPPC reactivity. Lysolipid OPC reactivity remains unchanged, with scaling from 5 mol% to 100 mol% predicting a total acylated product concentration of 42.2 ng mL^{-1}, comparable to the observed value of 41.1 ng mL^{-1}. In contrast, addition of 5 mol% DPPC into an OPC micelle increases total acylated product concentration from 41.4 ng mL^{-1} to 50.5 ng mL^{-1}. Transfer from both lysolipid and phospholipid components within the disrupted micelle is increased compared to single component systems. Oleoyl transfer from lysolipid OPC increases from 41.4 ng mL^{-1} to 45.2 ng mL^{-1}. Scaling DPPC transfer from 5 mol% to 100 mol% produces a total palmitoylated product concentration of 107.2 ng mL^{-1} compared to 27.1 ng mL^{-1} observed within the DPPC only bilayer. Differential propranolol **1** binding strength and orientation, combined with increased structure associated with DPPC inclusion in the micelle, are predicted to facilitate the observed increase in reactivity.

Mixture	Palmitoyl Propranolol (%)	Oleoyl Propranolol (%)
DPPC	27.1	-
DPPC:OPC (95:5)	11.0	2.1
DPPC:OPC (5:95)	5.4	45.2
OPC	-	41.4

Table 6.31 Proportion of total propranolol **1** content attributed to palmitoylated propranolol and oleoylated propranolol within DPPC:OPC mixtures after 72 hours incubation under physiological conditions.

Analogous studies were conducted monitoring total acylated propranolol **1** production within DOPC:PPC lipid mixtures. Table 6.32 summarises the resulting data following 72 hour incubation under physiological conditions. Total acylated product concentration is decreased from $20.0\,\mathrm{ng\,mL^{-1}}$ to $9.0\,\mathrm{ng\,mL^{-1}}$ upon addition of 5 mol% PPC into a DOPC bilayer. Reduced reactivity is attributed to both transfer from phospholipid DOPC, down from $20.0\,\mathrm{ng\,mL^{-1}}$ to $6.8\,\mathrm{ng\,mL^{-1}}$, and transfer from lysolipid PPC, which with scaling to 100 mol% is down from $49.2\,\mathrm{ng\,mL^{-1}}$ to $43.0\,\mathrm{ng\,mL^{-1}}$. Attributed to lysolipid induced bilayer disruption and subsequent changes to phase behaviour and propranolol **1** binding, reduced reactivity is consistent with observations made for the corresponding DPPC:OPC (95:5) mixture. Decreased total acylated product concentration is also observed upon introduction of 5 mol% DOPC into a PPC micelle. Reduced intrinsic lipidation is attributed to diminished acyl transfer from the lysolipid PPC component within the disrupted micelle. Transfer from phospholipid DOPC is increased within the DOPC:PPC (5:95) system, scaling transfer from 5 mol% to 100 mol% results in $71.2\,\mathrm{ng\,mL^{-1}}$ of oleoylated product.

Mixture	Palmitoyl Propranolol (%)	Oleoyl Propranolol (%)
DOPC	-	20.0
DOPC:PPC (95:5)	6.8	2.2
DOPC:PPC (5:95)	3.6	24.4
PPC (0:100)	49.2	-

Table 6.32 Proportion of total propranolol **1** content attributed to palmitoylated propranolol and oleoylated propranolol within DOPC:PPC mixtures after 72 hours incubation under physiological conditions.

Discussion thus far has eluded to modified acyl chain transfer rates within lipid systems of differing phase. Consideration of palmitoyl to oleoyl ratio, and comparison to the molar ratio of lipid system components, provides further insight. Table 6.33 presents the normalised ratios of palmitoylated product concentration to oleoylated product concentration for DPPC:OPC and

DOPC:PPC systems at 95:5 molar ratio. Assuming comparable rate constants and reaction order for each species, the predicted product ratio would be 19:1 for acyl chain transferred from phospholipid:acyl chain transferred from lysolipid. Evidently, the observed product ratios differ from the predicted 19:1 ratio indicating differing reactivity rates between the species. Heightened lysolipid reactivity rate compared to phospholipid transfer rate results in an increased proportion of lysolipid derived acylated propranolol **1** product. However, it is noted that the ratio of phospholipid derived product to lysolipid derived product varies across the time period studied, indicative of variation in relative reaction rates. Palmitoyl:oleoyl ratio within the DPPC:OPC (95:5) system decreases from 7:1 to 5:1, whilst within the DOPC:PPC (95:5) system the ratio increases from 1:3 to 1:5. A consistent intrinsic lipidation rate has previously been observed within phospholipid bilayer systems, however the phenomenon of rate variation over time has been described for intrinsic lipidation within lysolipid micelles. As a result, variation in the palmitoyl to oleoyl ratio is attributed to changes in rate of lysolipid reactivity over time, due to modified bilayer characteristics upon increasing concentration of acylated propranolol **1** product.

Time	P:O Ratio for DPPC:OPC	P:O Ratio for DOPC:PPC
24	7.2 : 1.0	1.0 : 2.7
72	5.2 : 1.0	1.0 : 3.2
144	5.3 : 1.0	1.0 : 5.3

Table 6.33 Palmitoylated propranolol (P) to oleoylated propranolol (O) ratio observed under physiological conditions within mixed membranes containing 95:5 ratio of either DPPC:OPC or DOPC:PPC.

Analogous data regarding palmitoyl to oleoyl ratio within DPPC:OPC and DOPC:PPC systems of molar ratio 5:95, is presented in Table 6.34. The predicted product ratio based upon molar ratio of system components is 1:19 for acyl chain transferred from phospholipid:acyl chain transferred from lysolipid. The observed ratios are decreased from the predicted value, indicating increased rate of phospholipid reactivity compared to lysolipid reactivity. This observation is in agreement with previous studies comparing intrinsic lipidation rate in lysolipid micelles containing phospholipid, suggesting acyl transfer from phospholipids is promoted by the presence of lysolipid within the system studied.[40] Variation in ratio of palmitoylated product to oleoylated product over time is observed within these micellar systems. Palmitoyl:oleoyl ratio within the DPPC:OPC (5:95) system increases from 1:5 to 1:10, and the DOPC:PPC (5:95) system from 3:1 to 8:1. Consistent with observation made within DPPC:OPC (95:5) and DOPC:PPC (95:5) systems, ratio variation is attributed to

a altered reaction rate of lysolipids with propranolol **1** over time due to modified micellar characteristics.

Time	P:O Ratio for DPPC:OPC	P:O Ratio for DOPC:PPC
24	1.0 : 5.5	2.8 : 1.0
72	1.0 : 8.4	6.9 : 1.0
144	1.0 : 10.2	8.1 : 1.0

Table 6.34 Palmitoylated propranolol (P) to oleoylated propranolol (O) ratio observed under physiological conditions within mixed membranes containing 5:95 ratio of either DPPC:OPC or DOPC:PPC.

6.5 Conclusions

Subject of the 1988 Nobel Prize in Medicine, propranolol **1** is a widely prescribed blockbuster pharmaceutical, employed to treat a range of conditions including high blood pressure, angina and migraines.[263,264] Understanding the behaviour of propranolol **1** and its interactions within the body, is vital to determine the impact of the drug upon human health and well being. Propranolol **1** intrinsic lipidation *in vitro* is a previously undiscovered action of propranolol **1** occurring upon interaction of the drug with a cell membrane. This non-enzymatic mechanism modifies drug properties and bulk membrane characteristics, ultimately predicted to impact a range of important cellular and pharmaceutical processes.

Successful organic synthesis of predicted products of propranolol **1** intrinsic lipidation has facilitated study of this membrane reactivity *in vitro*. Analytical characterisation of synthetic *O*-acylated propranolol, *N*-acylated propranolol, and diacylated propranolol by optimised mass spectrometry reveals *O*-acylated propranolol and *N*-acylated propranolol as intrinsic lipidation products. Furthermore, the two species were determined to be related by an intramolecular *O* to *N* migratory rearrangement, resulting in the following proposed mechanism for propranolol **1** intrinsic lipidation. Initial propranolol **1** reactivity proceeds by a transesterification reaction from membrane phospholipids to the alcohol functionality, forming kinetic product *O*-acylated propranolol. Subsequent *O* to *N* migration promotes formation of the secondary thermodynamic reaction product, *N*-acylated propranolol.

Quantification of propranolol **1** intrinsic lipidation reaction products has also been facilitated by the preparation of synthetic standards. Under physiological conditions quantification indicates over 50 % conversion of propranolol **1** into acylated derivatives is possible through innate membrane reactivity. High levels of conversion indicate significant biological and

pharmaceutical relevance of propranolol **1** intrinsic lipidation. Two instances of preferential transfer have been identified under physiological conditions: (i) increased reactivity within eukaryotic PC membrane models compared to prokaryotic (PE:PG) or viral counterparts (PC:PS); (ii) preferential *sn*-1 transfer from the phospholipid backbone compared to transfer from the *sn*-2 position. Furthermore, in addition to innate reactivity between propranolol **1** and diacyl phospholipids, analogous reactivity with lysolipids has been observed. An increased acyl transfer rate is observed for lysolipids compared to diacyl phospholipids, with lysolipids capable of promoting transfer from diacyl phospholipids within mixed lipid systems. Finally, product quantification combined with temperature and pH variation has provided insight into the influence of these environmental factors upon reactivity kinetics and product distribution. Temperature increase has been observed to promote both the rate of propranolol **1** intrinsic lipidation, and the rate of intramolecular *O* to *N* migration, ultimately resulting in up-regulation of the formation of *N*-acylated propranolol derivatives. Increased pH exhibits similar effects on propranolol **1** intrinsic lipidation, promoting reactivity and formation of *N*-acylated species. These observations are attributed to an increased proportion of the neutral form of propranolol **1**, facilitating both intramolecular *O* to *N* migration, and direct amine reactivity with phospholipids. Conversely, intrinsic lipidation is only rarely observed to proceed under acidic conditions, due to protonation of reactive moieties preventing reactivity. Notably, preferential eukaryotic and *sn*-1 reactivity observed under physiological conditions are largely maintained upon variation of these environmental parameters.

7 | Small Molecule Intrinsic Lipidation *in cellulo*

7.1 Introduction

Small molecule intrinsic lipidation, and in particular intrinsic lipidation of propranolol **1**, has been well characterised *in vitro* (Chapter 6). Analytical simplification makes *in vitro* study desirable, however true investigation of the biological relevance of intrinsic lipidation requires use of an increasingly complex cellular system. Study of intrinsic lipidation *in cellulo* aims to determine the feasibility of innate reactivity within the complex confines of a biological system, filled with competing propranolol **1** binding sites and enzymatic reaction pathways. Observed reactivity *in cellulo* would provide validation that the process is both biologically and pharmaceutically relevant, warranting further investigation.

7.2 Development of Analytical Conditions

Study of small molecule intrinsic lipidation *in cellulo* creates an analytical challenge of increased difficulty compared to *in vitro* liposomal systems. Membrane complexity, particularly the presence of multiple acyl chain types, would result in an increased variety of low abundance acylated intrinsic lipidation products. Chromatographic separation of these products, combined with sufficient ionisation at low abundance, would be required in order to definitively distinguish and characterise the species. Furthermore, increased lipid and lysolipid diversity *in cellulo* creates a challenging sample medium, requiring suitable analytical conditions for the separation of lipid species from desired products. Achieving analytical separation of lipid species provides the added benefit of characterising cellular lipid profile under the influence of intrinsic lipidation.

Optimised analytical conditions for the study of small molecule intrinsic lipidation *in vitro* did not translate to the study of reactivity *in cellulo*, given the added analytical challenges. Considerable coelution of lipid species and acylated small molecules, highlighted in Fig. 7.1, result in ion suppression of low abundance species and significantly reduce data quality. Renewed optimisation of both chromatographic and ionisation parameters was therefore required in order to facilitate study of intrinsic lipidation within biological systems. Considering that phospholipids and lysolipids are the major components of membrane systems *in cellulo*, synthetic standards of these species were obtained (Avanti Polar Lipids Inc.) in order to aid in optimisation.

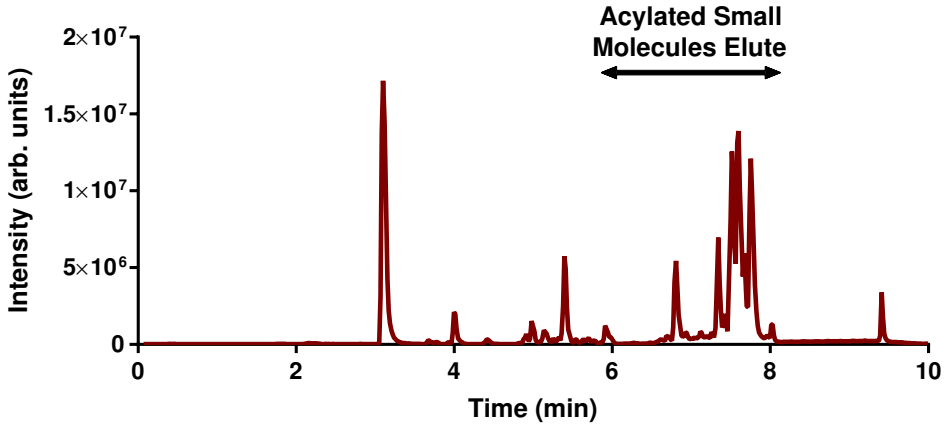

Figure 7.1 TIC of complex bovine liver extract analysed under optimised analytical conditions for the study of small molecule intrinsic lipidation. Elution of phospholipid species during the retention time window attributed to acylated small molecules resulting in ion suppression is highlighted.

7.2.1 Optimisation of Positive ESI Parameters

Literature studies suggest that optimised analysis of neutral PC and PE phospholipids is conducted using ESI mass spectrometry in positive ionisation mode.[291,292] Optimisation was therefore conducted using a Synapt G2-S (Waters Corp., UK) mass spectrometer fitted with Z-spray ESI source. Phospholipid POPC, Fig. 7.2, was selected as the optimisation analyte, being readily availability and containing the neutral PC head group in combination with biologically common palmitoyl and oleoyl acyl chains. POPC stock solution at concentration $0.5\,\mu g\,mL^{-1}$ in IPA:H_2O:MeCN (2:1:1), was directly infused into the mass spectrometer at a flow rate of $5\,\mu L/\,min$. Mass spectra were collected over one minute, and compared based upon molecular ion intensity, signal to noise ratio, and level of in-source fragmentation.

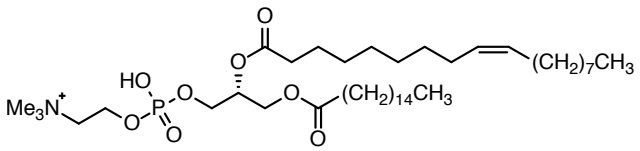

Figure 7.2 The structure of zwitterionic phospholipid POPC.

Three key instrument parameters were identified to facilitate optimisation of phospholipid ESI:

- Capillary voltage
- Sampling cone voltage
- Source offset voltage

Additional instrument parameters, including source temperature, desolvation temperature, and desolvation gas flow, remained unchanged throughout the optimisation process. These parameters were considered to have reduced impact upon phospholipid ionisation, and maintaining their consistency with other methodologies was considered useful for future analyses.

Capillary voltage describes the voltage applied at the tip of the ESI capillary needle, creating a potential difference between the needle and the rest of the mass spectrometer.[81] Correct voltage selection aids in aerosol formation, desolvation, and ion motion through the mass spectrometer. Initial analytical conditions, based upon optimised parameters for acylated small molecule ionisation, used a capillary voltage of 1.0 kV. Under these conditions, visualisation of desired POPC molecular ion $[M+H]^+$ was observed at *m/z* 760.5870 corresponding to molecular formula $C_{42}H_{83}NO_8P$ with 0.04 ppm. In-source fragmentation was not observed, however sodium adduct $[M+Na]^+$ and proton bound dimer $[2M+H]^+$, were noted at *m/z* 782.5642 and 1520.1693 respectively. Observation of the undesired $[M+Na]^+$ species was attributed to the presence of environmental sodium, combined with increased POPC affinity for sodiation compared to protonation.[276] Dimerisation likely occurs due to high POPC concentration combined with poor ionisation potential of the hydrophobic species.[277]

Table 7.1 presents the relative ion intensities of protonated and sodiated POPC species utilising five different capillary voltages in the range 1.0 kV to 3.0 kV. Increased capillary voltage result in both a desirable increase in $[M+H]^+$ intensity, and an undesirable increase in $[M+H]^+$:$[2M+H]^+$ ratio. Therefore, protonation is determined to be favoured by selection of a higher capillary voltage. In contrast, $[M+H]^+$:$[M+Na]^+$ ratio reaches a minimum at

2.0 kV, suggesting increased undesirable $[M+Na]^+$ formation at capillary voltages both above and below this value. Appropriate capillary voltages for ionisation of neutral phospholipids were therefore determined as 2.0 kV and 2.5 kV. A 2.0 kV capillary voltage was selected for future phospholipid analysis, due to problematic discharge being widely reported at high ESI capillary voltages.[250]

Capillary Voltage (kV)	$[M+H]^+$	$[M+H]^+$:$[2M+H]^+$:$[M+Na]^+$
1.0	$2.37x10^7$	1 : 0.16 : 0.73
1.5	$8.07x10^7$	1 : 0.13 : 0.35
2.0	$2.25x10^8$	1 : 0.20 : 0.24
2.5	$2.34x10^8$	1 : 0.25 : 0.28
3.0	$1.76x10^8$	1 : 0.26 : 0.30

Table 7.1 Ion intensity for $[M+H]^+$ of POPC at *m/z* 760.5870, and ratio of $[M+H]^+$ to undesirable ion alternatives $[2M+H]^+$ and $[M+Na]^+$ at varying capillary voltages.

Sampling cone voltage aids in transmission of ions from the ESI capillary needle through the ionisation source and towards the instrument mass analyser.[81] Higher sampling cone voltages increase transmission and therefore ion abundance, however the associated increase in ion kinetic energy can result in unwanted inelastic collisions and in-source fragmentation. Results of sampling cone voltage modification from the original value of 50 V to 30 V and 70 V are presented in Table 7.2. Intensity of POPC molecular ion *m/z* 760.5870 drops upon alteration of the sampling cone voltage. At 30 V reduced ion intensity is attributed to a reduced number of ions being pulled through the sampling cone. At 70 V the change is associated with reduced $[M+H]^+$ transmission in favour of $[M+Na]^+$ ions, combined with preferential fragmentation of the $[M+H]^+$ species due to its lower dissociation energy compared to $[M+Na]^+$. This theory is based upon the observed change in $[M+H]^+$:$[M+Na]^+$ ratio from 4:1 at sampling cone voltage 50 V to 2:1 at sampling cone voltage 70 V. As a result, sampling cone voltage for future phospholipid study by ESI in positive mode was selected to be 50 V.

Sampling Cone Voltage (V)	$[M+H]^+$	$[M+H]^+$:$[2M+H]^+$:$[M+Na]^+$
30	$1.61x10^8$	1 : 0.20 : 0.33
50	$2.25x10^8$	1 : 0.20 : 0.24
70	$1.09x10^8$	1 : 0.17 : 0.49

Table 7.2 Ion intensity for $[M+H]^+$ of POPC at *m/z* 760.5870, and ratio of $[M+H]^+$ to undesirable ion alternatives $[2M+H]^+$ and $[M+Na]^+$ at varying sampling cone voltages.

Source offset voltage defines the voltage difference applied in order to transmit ions from the

ESI source into the StepWave ion transfer, and onwards to the analyser region of the mass spectrometer.[81] Analogously to sampling cone voltage, high source offset values promote ion transmission but may inadvertently cause in-source fragmentation of ions in tandem. Table 7.3 presents the results of POPC ionisation using three distinct source offset voltages, 20 V, 30 V and 40 V. Optimum $[M+H]^+$ intensity of 2.25x10^8 is observed using a source offset voltage of 30 V. Furthermore, both the $[M+H]^+$:$[2M+H]^+$ ratio and $[M+H]^+$:$[M+Na]^+$ ratio favour desired ion $[M+H]^+$ at 30 V to a greater extent than at 20 V and 40 V. In-source fragmentation of POPC was not observed for any of the source offset voltages tested. Consideration of the observed results suggests 30 V to be the optimum source offset value for future study of phospholipids by positive ESI.

Source Offset Voltage (V)	$[M+H]^+$	$[M+H]^+$:$[2M+H]^+$:$[M+Na]^+$
20	1.13x10^8	1 : 0.24 : 0.67
30	2.25x10^8	1 : 0.20 : 0.24
40	1.24x10^8	1 : 0.22 : 0.57

Table 7.3 Ion intensity for $[M+H]^+$ of POPC at *m/z* 760.5870, and ratio of $[M+H]^+$ to undesirable ion alternatives $[2M+H]^+$ and $[M+Na]^+$ at varying source offset values.

Parameter	Optimised Value
Capillary Voltage (kV)	2.0
Source Temperature (°C)	150.0
Sampling Cone Voltage (V)	50.0
Source Offset Voltage (V)	30.0
Desolvation Temperature (°C)	350.0
Cone Gas Flow (L/Hr)	60.0
Desolvation Gas Flow (L/Hr)	600.0
Nebuliser Gas Flow (Bar)	6.0

Table 7.4 Optimised positive mode ESI parameters for ionisation of neutral phospholipids such as POPC.

Optimised positive ESI parameters for the study of neutral PC and PE phospholipids have been successfully developed, as summarised in Table 7.4. Parameters mirror those optimised for the study of acylated small molecules, with the exception of capillary voltage. Analysis of additional neutral phospholipids and synthetically prepared acylated small molecules under these conditions resulted in successful visualisation of all species. Ionisation of acylated small molecules was observed to be comparable to ionisation using previously optimised small molecule intrinsic lipidation parameters. As a result, these newly optimised positive ESI parameters will be taken forward for future study of small molecule intrinsic lipidation and

lipid profiling within complex biological systems.

7.2.2 Optimisation of Negative ESI Parameters

Phospholipids containing negatively charged PS or PG phosphate head groups are better suited to ESI analysis in negative mode, rather than positive mode.[291,292] Negative mode ESI parameters have not previously been developed during the study of intrinsic lipidation, therefore optimisation is required. Phospholipid POPS, Fig. 7.3, was selected as the optimisation analyte in order to create parity with the optimisation of positive mode ESI parameters. POPS is comprised of biologically relevant palmitoyl and oleoyl acyl chains, in combination with a eukaryotic PS head group. POPS stock solution at a concentration of $0.5\,\mu g\,mL^{-1}$ in IPA:H_2O:MeCN (2:1:1) was directly infused at a flow rate of $5\,\mu L/\,min$ into the ESI source of a Synapt G2-S mass spectrometer (Waters Corp., UK). Mass spectra were collected over a one minute time period and compared upon modification of capillary voltage, sampling cone voltage, and source offset voltage.

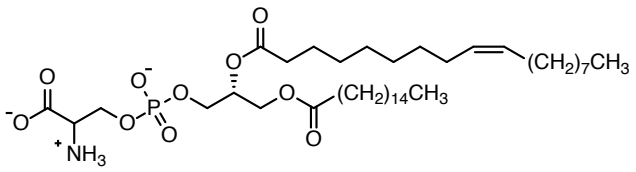

Figure 7.3 The structure of negative phospholipid POPS.

Negative mode ESI optimisation was undertaken building on a base of available ionisation parameters developed for the study of small molecules by another instrument user. POPS analysis resulted in observation of the $[M\text{-}H]^-$ ion at *m/z* 760.5146 corresponding to molecular formula $C_{40}H_{75}NO_{10}P$ with 2.28 ppm error. Neither adduct formation nor in-source fragmentation of POPS was observed under these conditions. However, two contaminant ions were observed at *m/z* 181.0642 and 265.1490, the later of which can be attributed to plasticiser tributylphosphate.[293] Table 7.5 summarises $[M\text{-}H]^-$ ion intensity values, the sole available distinguishing factor, upon application of capillary voltages from 1.0 kV to 3.0 kV. Ion intensity reaches a maximum at capillary voltage 2.5 kV, resulting in selection of this voltage for future phospholipid ESI in negative mode.

Capillary Voltage (kV)	$[M-H]^-$
1.0	$5.70x10^6$
1.5	$6.95x10^7$
2.0	$1.91x10^8$
2.5	$2.77x10^8$
3.0	$1.60x10^8$

Table 7.5 Ion intensity for $[M-H]^-$ of POPS at *m/z* 760.5146, at varying capillary voltages.

Table 7.6 summarises POPS $[M-H]^-$ ion intensity upon application of sampling cone voltages from 20 V to 50 V. Intensity of the molecular ion at *m/z* 760.5146 reaches a maximum at sampling cone voltage 30 V. Considering neither in-source fragmentation nor adduct formation are observed under the instrumentation parameters studied, it is unclear as to why ion intensity at 30 V exceeds that of higher sampling cone voltages known to promote ion transmission. Despite this, an optimised sampling cone voltage of 30 V was selected for future phospholipid study by negative mode ESI.

Sampling Cone Voltage (V)	$[M-H]^-$
20	$2.53x10^8$
30	$3.15x10^8$
40	$2.33x10^8$
50	$2.77x10^8$

Table 7.6 Ion intensity for $[M-H]^-$ of POPS at *m/z* 760.5146, at varying sampling cone voltages.

Negative mode ESI source offset voltage was also altered in order to determine the influence upon POPS ionisation. Given the observed lack of adduct formation or in-source dissociation even at high voltages, POPS $[M-H]^-$ ion intensity was used to select the optimum source offset value. Table 7.7 summarises *m/z* 760.5146 ion intensity for source offset values of 20 V to 40 V, with a maximum of $3.15x10^8$ observed at 30 V. Further negative mode ESI of phospholipids was therefore conducted using an optimised 30 V source offset voltage.

Source Offset Voltage (V)	$[M-H]^-$
20	$1.68x10^8$
30	$3.15x10^8$
40	$1.72x10^8$

Table 7.7 Ion intensity for $[M-H]^-$ of POPS at *m/z* 760.5146, at varying source offset values.

Optimised negative ESI parameters for the study of negatively charged PS and PG phospholipids have been successfully developed, as summarised in Table 7.8. These newly optimised ESI parameters will be taken forward for future study of negative lipid profiling within complex biological systems.

Parameter	Optimised Value
Capillary Voltage (kV)	2.5
Source Temperature (°C)	150.0
Sampling Cone Voltage (V)	30.0
Source Offset Voltage (V)	30.0
Desolvation Temperature (°C)	350.0
Cone Gas Flow (L/Hr)	60.0
Desolvation Gas Flow (L/Hr)	600.0
Nebuliser Gas Flow (Bar)	6.0

Table 7.8 Optimised negative mode ESI parameters for ionisation of negatively charged phospholipids such as POPS.

7.2.3 Optimisation of Chromatographic Conditions

Analysis of complex biological systems by mass spectrometry can be aided by the application of suitable chromatographic conditions. In fact, liquid chromatography can ultimately determine the success of analysis in the context of biological systems. Optimised chromatography separates mixture components, minimising ion suppression and ensuring successful identification and characterisation of all species within the mixture. Considering that optimised chromatography for the study of small molecule intrinsic lipidation *in vitro* has been shown not to translate to study *in cellulo*, a novel chromatographic approach is needed.

Development of chromatography for the study of small molecule intrinsic lipidation and lipid profiling *in cellulo* can be performed using a synthetic biological model. Synthetic standards of lysolipids and phospholipids were obtained and combined at concentrations of $0.5\,\mu g\,mL^{-1}$ to create a lipid mixture. Standards selected, Table 7.9, cover a variety of phospholipid classes including neutral PC and PE phospholipids observed in positive mode ESI, and PS and PG phospholipids observed by negative ESI. Chromatographic separation of phosphate head group classes within both lysolipid and phospholipid species is vital for successful analysis. Furthermore, lysolipids such as PPC and OPC, and phospholipids such as DOPG and SLPG, were included within the lipid mixture to ensure chromatographic separation of species differing in their acyl chain chemistry. POPC and OPPC, comprised

of the same acyl chains in opposing backbone positions, were also incorporated into the lipid mixture, in order to determine whether chromatographic resolution of these structurally similar species proved possible.

Species	Observation Mode	$[M+H]^+$	$[M-H]^-$
PPC	Positive	496.3403	-
OPC	Positive	522.3560	-
OPE	Both	480.3090	478.2934
OPG	Negative	-	509.2879
DOPC	Positive	786.6013	-
POPC	Positive	760.5856	-
OPPC	Positive	760.5856	-
DOPE	Both	744.5543	742.5387
DOPG	Negative	-	773.5333
SLPG	Negative	-	773.5333
DOPS	Negative	-	786.5285
POPS	Negative	-	760.5129

Table 7.9 Mixture of phospholipid and lysolipid standards employed in order to optimise chromatography for the study of intrinsic lipidation and lipid profiling in complex biological systems.

Chromatographic conditions for study of lipid species were derived from the application note "Lipid Separation using UPLC with Charged Surface Hybrid Technology" (Waters Corp., UK).[294] The methodology utilises UPLC on a CSH C_{18} column (Waters Corp., UK) at 55 °C to separate components of lipid extracts, which include both phospholipids and lysolipids. Unusual mobile phases of high organic content are employed during analysis, due to the hydrophobicity of lipid species increasing column retention and preventing solvation in MeCN or H_2O. Mobile phase A was therefore prepared as MeCN:H_2O (6:4) with 10 mM ammonium formate and 0.1 % formic acid, and mobile phase B IPA:MeCN (9:1) with 10 mM ammonium formate and 0.1 % formic acid. Analysis of the prepared mixture of lipid standards under these chromatographic conditions, in both positive and negative ESI modes, proved successful. Chromatograms presented in Fig. 7.4 highlight the desirable peak shapes and excellent separation of all species irrespective of head group class or acyl chain type. POPC and OPPC prove the exception to this observation, coeluting due to structural similarities. Lysolipid species elute between 1 min and 4 min, as shown in Fig. 7.4, whereas phospholipid species elute later between 10 min and 14 min separated by head group class. Despite the observed analytical success, it was noted that the chromatographic conditions employed contained considerable dead time in which species did not elute. This dead time was determined as

prior to 2 min, between 3 min to 10 min, and after 15 min. Undesirable dead time results in a considerable 20 minute analysis time per sample, reduction of which would both increase throughput and minimise solvent wastage.

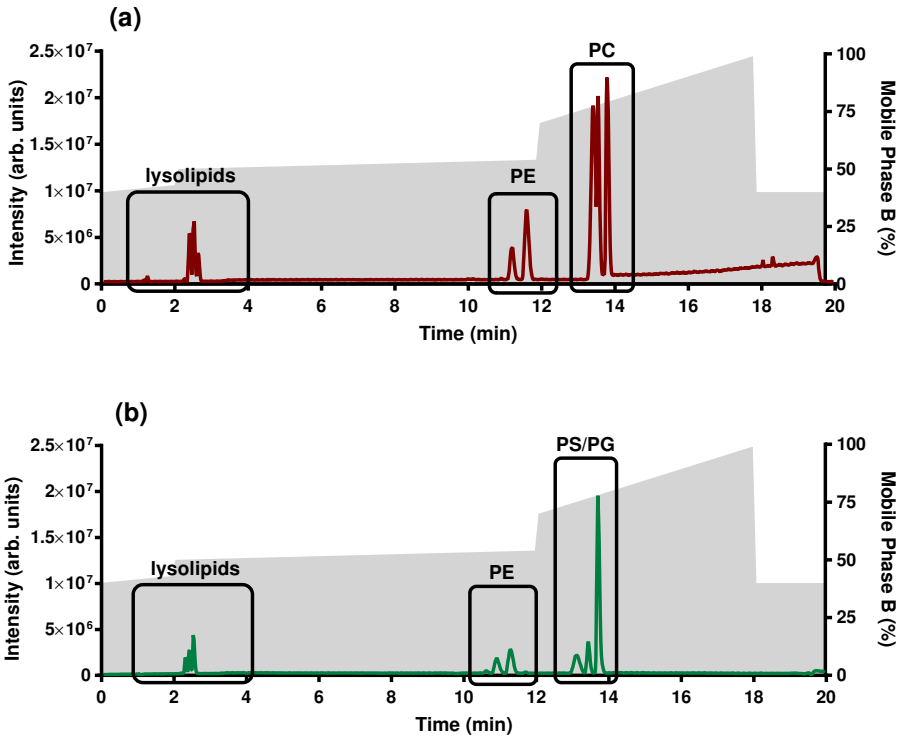

Figure 7.4 Analysis of standard lipid mixture under chromatographic conditions described in "Lipid Separation using UPLC with Charged Surface Hybrid Technology" (Waters Corp., UK) with % of mobile phase B (IPA:MeCN (9:1) with 10 mM ammonium formate and 0.1 % formic acid) shown in grey: (a) positive mode shown in red; (b) negative mode shown in green.[294]

Modifications to initial chromatographic conditions were carried out stepwise, in hopes of achieving excellent peak shape and separation within a shorted time period. Modified gradient one focussed upon reduction of dead time prior to 2.0 minutes. An initial mobile phase ratio of 50:50 (A:B) was therefore selected in favour of the 60:40 (A:B) ratio utilised under preliminary chromatographic conditions. Resulting chromatograms retain excellent peak shape and resolution for phospholipid species eluting between 8 min and 12 min, as shown in Fig. 7.5 (a). However, chromatographic modifications are observed within the first 5.0 minutes of analysis, affecting lysolipid separation only. Under modified conditions dead time at the start of analysis is reduced by only 0.5 min, resulting in a time period of 1.5 min prior to analyte elution. Furthermore, as shown by comparison of Fig. 7.5 (b) and (c), chromatographic resolution of lysolipids is completely lost using both positive and negative mode ESI under the modified conditions. Modified gradient one was thus determined to be unsuccessful in reducing analysis time whilst retaining resolution, and initial mobile phase conditions of 60:40

(A:B) were applied to all future analyses.

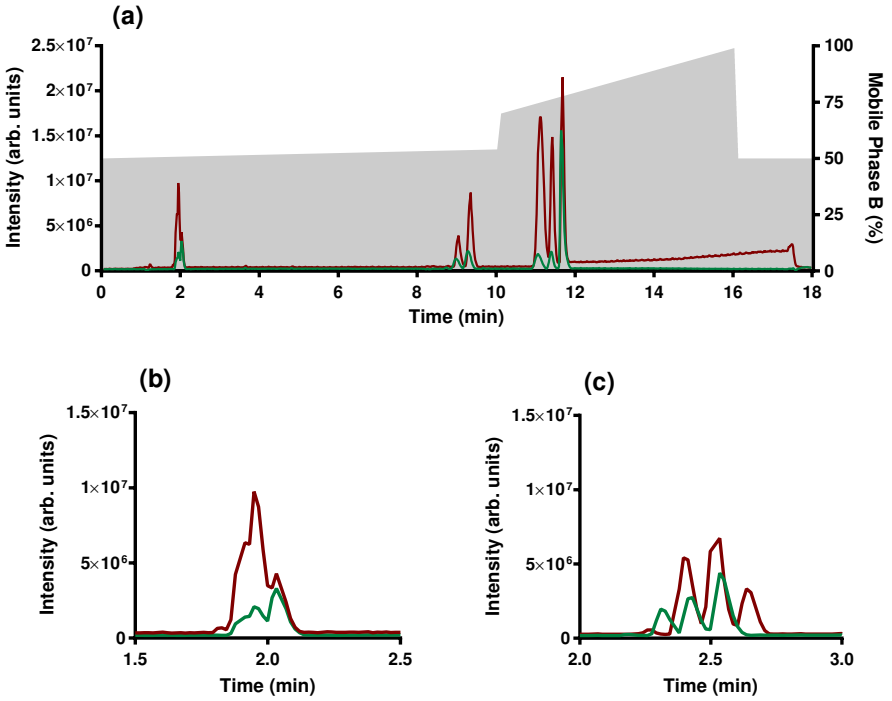

Figure 7.5 Analysis of standard lipid mixture under modified chromatographic gradient one: (a) TIC with positive mode shown in red, negative mode shown in green, and % of mobile phase B (IPA:MeCN (9:1) with 10 mM ammonium formate and 0.1 % formic acid) shown in grey; (b) lysolipids eluting under modified gradient one exhibiting loss of resolution; (c) lysolipids eluting under initial chromatographic conditions.

Dead time between 3 min and 10.5 min was the second chromatographic issue tackled by gradient alteration. Modified gradient two attempted to overcome this issue by reducing the time period taken for mobile phase composition to change from 50:50 (A:B) to 46:54 (A:B). Under initial chromatographic conditions this change occurs over the time period 2.1 min to 12 min, whereas modified gradient two reduces this time period by 5 min such that the change occurs over 2.1 min to 7 min, as shown in Fig. 7.6 (a). Reduction of dead time in this fashion decreases analysis time and increases sample throughput. Lysolipid elution of both neutral and negative classes between 2 min and 3 min is unchanged upon gradient modification. Phospholipid elution in shifted from between 11 min to 13 min to the earlier retention time of 9.0 minutes, as shown in Fig. 7.6 (a). However, under these chromatographic conditions phospholipid species coelute irrespective of class and acyl chain type. This observation is highlighted by comparing phospholipid elution under modified gradient two, shown in Fig. 7.6 (b), with elution under the initial gradient, shown in Fig. 7.6 (c). As a result, modified gradient two was not considered feasible for the analysis of small molecule intrinsic lipidation within complex biological samples.

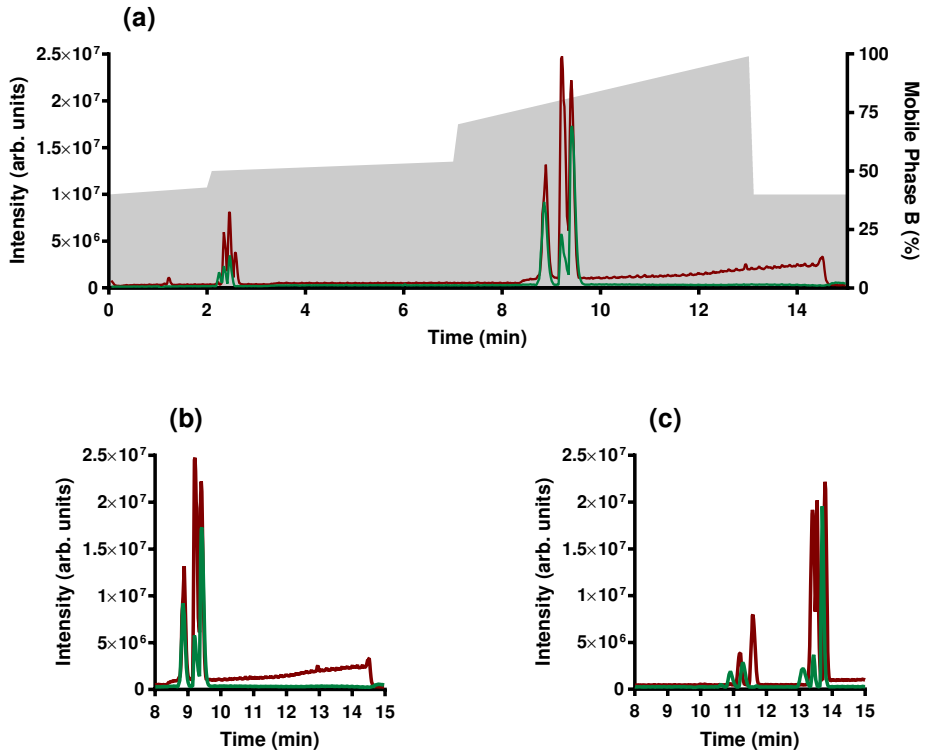

Figure 7.6 Analysis of standard lipid mixture under modified chromatographic gradient two: (a) TIC with positive mode shown in red, negative mode shown in green, and % of mobile phase B (IPA:MeCN (9:1) with 10 mM ammonium formate and 0.1 % formic acid) shown in grey; (b) phospholipids eluting under modified gradient two exhibiting loss of class separation; (c) phospholipids eluting under initial chromatographic conditions.

Modified gradient three attempted to retain the shortened run time of modified gradient two in combination with the excellent chromatographic separation observed under initial analytical conditions. Decreased rate of mobile phase change over the time period immediately prior to and throughout phospholipid elution was applied to modified gradient two in order to achieve this, Fig. 7.7 (a). Modified gradient two undergoes a gradient change of 30:70 (A:B) to 1:99 (A:B) over the time period 7.1 min to 13 min. Modified gradient three alters this gradient change, instead undergoing 30:70 (A:B) to 20:80 (A:B) over the time period of 7.1 min to 10 min, followed by 20:80 (A:B) to 1:99 (A:B) over 10 min to 11 min. Further reduction in run time was achieved by a reduced organic wash period from 2 min in duration to 1 min. Despite modification, chromatographic separation of phospholipids by modified gradient three largely mirrors that of modified gradient two, Fig. 7.7 (b) and Fig. 7.7 (c). Minor resolution increases are observed for PC phospholipids, however complete separation of classes achieved under initial chromatographic conditions and evidenced for comparison in Fig. 7.7 (d), remains elusive. Considering these elution problems, the dead time between 3 min and 10.5 min observed under initial analytical conditions is noted to be vital for phospholipid

separation. Phospholipid separation during this time period occurs as analytes travel through the column, ultimately resulting in chromatographic resolution upon elution. Retention of this separatory period was therefore maintained for future analyses despite the associated increase in run time.

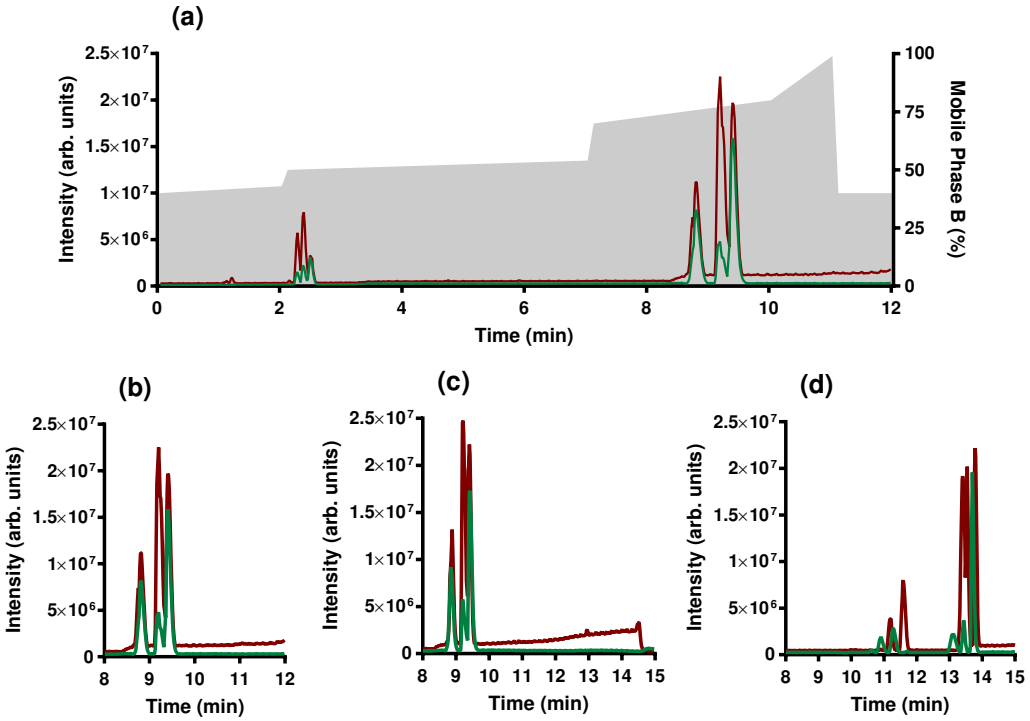

Figure 7.7 Analysis of standard lipid mixture under modified chromatographic gradient three: (a) TIC with positive mode shown in red, negative mode shown in green, and % of mobile phase B (IPA:MeCN (9:1) with 10 mM ammonium formate and 0.1 % formic acid) shown in grey; (b) phospholipids eluting under modified gradient three exhibiting loss of class separation; (c) phospholipids eluting under modified gradient two exhibiting loss of class separation; (d) phospholipids eluting under initial chromatographic conditions.

Chromatographic resolution of phospholipids is noted to be excellent under initial conditions, attributed to the dead time between 3 min and 10.5 min. However, there remains room for improvement. Modified gradient four builds upon original chromatographic conditions, aiming to improve separation by decreasing the rate of mobile phase change immediately prior to and throughout phospholipid elution. Mobile phase ratio changes from 30:70 (A:B) to 1:99 (A:B) over the time period 12.1 min to 18 min under initial conditions. Modified gradient four substitutes this mobile phase ratio change with a change of 30:70 (A:B) to 15:85 (A:B), as shown in Fig. 7.8, reducing the rate of mobile phase change within equivalent run time. Resulting chromatographic changes were observed between 10 min and 15 min during phospholipid elution, as shown in Fig. 7.8. Elution of earlier phospholipids, for example the PE class at 11 min, remains unchanged under the new chromatographic conditions. However, later

eluting PC, PS, and PG species exhibit increased class and acyl chain separation as a result of application of the modified gradient. In summary, chromatographic results for modified gradient four are comparable to those observed under initial chromatographic conditions, providing a suitable alternative for analysis.

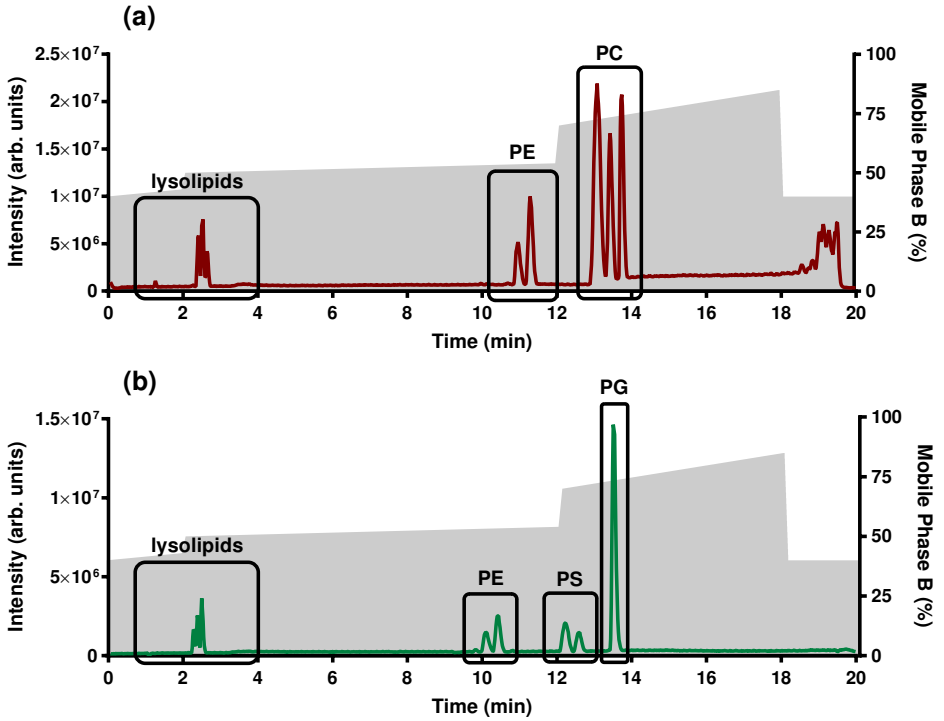

Figure 7.8 Analysis of standard lipid mixture under modified chromatographic gradient four with % of mobile phase B (IPA:MeCN (9:1) with 10 mM ammonium formate and 0.1 % formic acid) shown in grey: (a) positive mode shown in red; (b) negative mode shown in green.

Two sets of suitable chromatographic conditions for the study of small molecule intrinsic lipidation within biological systems have been identified using a mixture of lipid standards. The two analytical methods are matched in their capacity to separate lipid species, run time, and solvent usage. As a result, the initial gradient was selected for future study, due to its robust and reliable nature combined with a proven record of successful applications.[294] However, prior to further study two addition analytical challenges were noted in relation to chromatographic development. Firstly, sensitivity of the Synapt G2-S (Waters Corp., UK) instrument requires solvent qualities above and beyond those available commercially at HPLC/UPLC grade. Reduced solvent quality results in severe contamination of analyses conducted using positive ESI mode, resulting in suppression of desirable analytes. IPA distillation to remove low boiling impurities was therefore conducted upon commercial solvent prior to use within a mobile phase system. Furthermore, repeated analyses resulted in the observation of peak broadening particularly for negatively charged phospholipid species. Broadening was ultimately

determined to be dependent upon mobile phase pH, which underwent fluctuations due to solvent evaporation and poor ammonium formate solubility in IPA. Issues were overcome by regular determination and adjustment of mobile phase pH to values of 4.5 and 6.2 for A and B respectively, resulting in consistent peak shapes and retention times.

7.3 Intrinsic Lipidation in *E. coli* Extracts

Prior to study of small molecule intrinsic lipidation *in cellulo*, optimised analytical conditions were tested utilising an alternative biological system. Study of this alternative system aimed to confirm successful method development, whilst providing insight into intrinsic lipidation within a system of increased complexity compared to simple liposomes. Merging *in vitro* study with increased molecular diversity, the alternative system selected comprised extrusion prepared liposomes constructed from commercially available cell extracts. The first of these extracts, polar *E. coli* extract, was obtained through $CHCl_3$:MeOH extraction of *E. coli* B (ATCC 11303), followed by acetone precipitation and further extraction with diethyl ether.[295] Resulting *E. coli* extract liposomes contain PE, PG and cardiolipin (CL) species, whilst incorporating a diverse range of fatty acyl chain types. Additional biological features, including peptides and proteins, are not contained within the extract, providing increased simplicity compared to a true cellular system.

Understanding of *E. coli* extract lipid content is required in order to facilitate successful study of small molecule intrinsic lipidation within the liposomal system. Employing optimised analytical conditions, extract lipid profiling was conduced by both positive and negative mode ESI. Polar *E. coli* extract contains predominantly PE, PG and CL species, Fig. 7.9, resulting in data obtained using negative mode ESI being most informative. Negative mode scans were combined over the retention time window of lysololipid elution between 1.0 to 6.0 minutes, and phospholipid elution between 13.0 minutes and 20.0 minutes. Ions exceeding the intensity threshold of $1x10^5$ were isolated and assigned through comparison with the LIPID MAPS Gateway.[296] Following removal of anomalies not observed across duplicate analyses, and those exhibiting error of > 4.0 ppm, the lipid profile presented in Table 7.10 was obtained.

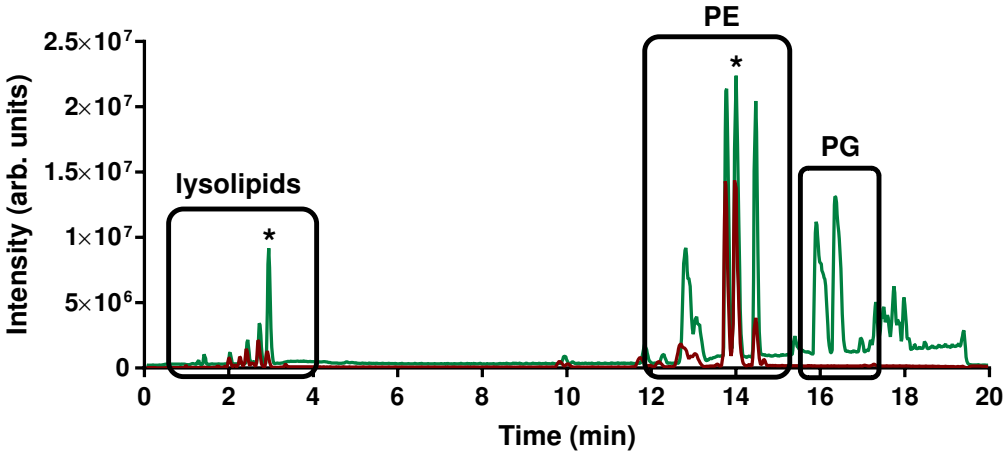

Figure 7.9 TIC of phospholipid and lysolipid species identified within *E. coli* extract including positive mode ESI (red) and negative mode ESI (green). * indicate internal standards LPC(17:0) eluting at 2.9 min and PC(17:0) eluting at 14.2 min.

Twenty-seven distinct phospholipid species were identified as components of polar *E. coli* extract. Content was attributed to 61 % PE class phospholipids and 39 % PG class phospholipids, comparable to the reported distribution of 67 % PE and 23 % PG.[295,297] Percentage discrepancy is attributed to lack of CL observation, reported as 9.8 % of total lipid content, due to increased structural diversity of CL species and corresponding low abundance. CL, found in most bacterial membranes, is a dimeric diphosphatidylglycerol lipid containing a glycerol backbone and four distinct acyl moieties. Furthermore, comparison of the observed lipid profile with available literature data suggests the absence of six phospholipid species contained within the extract, (32:1) PE, (33:1) PE, (36:2) PE, (33:1) PG, (34:1) PG, and (36:1) PG.[297] High abundance ions corresponding to nominal masses of these phospholipid species are observed, however mass accuracy prevents their assignment as the species in question. Literature analysis was conducted using Autoflex I (Bruker Daltonics Ltd., UK) instrumentation with external calibration, exhibiting 50-100 ppm accuracy, thus discrepencies can be explained by diminished literature accuracy compared to the Synapt G2-S (Waters Corp., UK) instrumentation employed herein.[297,298]

Observed *m/z*	Theoretical *m/z*	Error (ppm)	Assignment
452.2743	452.2782	3.6	LPE(16:0)
464.2751	464.2782	3.6	LPE(17:1)
478.2907	478.2939	3.6	LPE(18:1)
660.4620	660.4610	1.5	PE(30:1)
686.4742	686.4766	3.5	PE(32:2)

690.5097	690.5079	2.6	PE(32:0)
693.4714	693.4712	0.3	PG(30:0)
716.5262	716.5236	3.6	PE(34:1)
720.4960	720.4973	1.8	PE(36:5)‡
721.5034	721.5025	1.2	PG(32:0)
730.5397	730.5392	0.7	PE(35:1)
735.5152	735.5181	3.9	PG(33:0)
746.5138	746.5130	1.1	PE(38:6)‡
748.5286	748.5286	0.0	PE(38:6)† / PE(38:5)‡
749.5318	749.5338	2.7	PG(34:0)
762.4703	762.4715	1.6	PE(37:7(OH))
772.4933	772.4923	1.3	PE(39:8)
777.4683	777.4712	3.7	PG(37:7)
798.6023	798.6018	0.6	PE(40:2)
804.5884	804.5912	3.5	PE(42:6)† / PE(42:5)‡
805.6296	805.6328	4.0	PG(39:0)†
811.5496	811.5494	0.2	PG(39:4)
817.5013	817.5025	1.5	PG(40:8)
852.6826	852.6851	2.9	PE(45:3)† / PE(45:2)‡
873.6237	873.6226	1.3	PG(42:2(OH))
922.7305	922.727	3.8	PE(49:3)
1101.9003	1101.9043	3.6	PG(58:0(OH))

Table 7.10 Phospholipid and lysolipid species identified within *E. coli* lipid extract.[295] † indicates the presence of alkyl ether substituent; ‡ indicates the presence of alkenyl ether (plasmalogen) substituent.

Fatty acid distribution within *E. coli* extract includes saturated and unsaturated acyl moieties of varying carbon chain length.[299,300] Five plasmalogen species, common to anaerobic bacteria, are also observed within the PE lipid content of the system.[301] Biosynthesised within peroxisomes, plasmalogenic lipids contain an alkenyl ester functionality at their *sn*-1

position. Further acyl chain insight can be gleaned from the presence of three lysolipids with the lipid profile, LPE (16:0), LPE (17:1) and LPE (18:1). Considering abundance and successful visualisation, these acyl chains are predicted to be most common within polar *E. coli* extract. Observation of 16:0 (palmitoyl) and 18:1 (oleoyl) acyl chains is unsurprising considering their reported abundance within *E. coli* extract, summarised in Table 7.11. In contrast, presence of the 17:1 fatty acid chain is not reported within *E. coli* extract fatty acid distribution. Consequently, this is assumed to be a misassignment by LIPID MAPS, and the species observed is analogous cyclopropyl bacterial fatty acid cyclo 17:0.[296]

Fatty Acid	*E. coli* PE (%)	*E. coli* PG (%)	*E. coli* CL (%)
14:0	1.5	1.6	2.2
15:0	0.0	1.2	4.8
16:0	33.6	43.6	33.3
16:1	9.3	7.4	10.2
17:0	17.7	0.5	1.4
cyclo 17:0	0.0	26.8	27.0
18:0	0.0	1.4	0.0
18:1	34.1	9.8	14.4
19:0	3.8	0.0	5.3
cyclo 19:0	0.0	5.6	2.2
Unknown	0.0	0.0	1.4

Table 7.11 Fatty acid distribution of *E. coli* lipid extract.[295]

7.3.1 Propranolol Reactivity

Following characterisation of lipid content within polar *E.coli* extract, study of small molecule intrinsic lipidation within the system was conducted. Propranolol **1**, studied significantly *in vitro*, was incubated in 1:10 drug:lipid molar ratio with *E. coli* extract liposomes, based upon an average phospholipid molecular weight of 719.3020. Incubation proceeded for 72 hours under physiological conditions prior to analysis under optimised analytical conditions designed for study of small molecule intrinsic lipidation within complex biological systems. Potential acylated propranolol **1** products of intrinsic lipidation were predicted based upon the known fatty acid distribution, and data screened for the presence of these species.

Multiple acylated propranolol **1** derivatives were observed upon incubation with *E. coli* extract, as summarised in Table 7.12. CID MSMS performed upon species of sufficient abundance confirmed these to be *O*-acylated derivatives, rather than their *N*-acylated counterparts.

Product assignment is consistent with the hypothesised pathway of propranolol **1** intrinsic lipidation at physiological pH. Initial reactivity proceeds through transesterification from the phospholipid ester onto the alcohol moiety of propranolol **1**, resulting in formation of an *O*-acylated species. Subsequent *N*-acylated intramolecular migration products are not observed within *E. coli* extract, indicating either a lack of migration within more complex biological systems, or increased acyl chain diversity combined with poor ionisation potential of *N*-acylated species preventing visualisation.

Fatty Acid Transferred	Theoretical *m/z*	Observed *m/z*	Error (ppm)	R.T. (min)
14:0	470.3634	470.3617	3.7	4.1
15:0	484.3791	-	-	-
16:0	498.3947	498.3956	1.8	5.4
16:1	496.3791	496.3805	2.9	4.3
17:0	512.4104	-	-	-
cyclo 17:0	510.3947	510.3960	2.5	5.1
18:0	526.4260	526.4290	5.8	5.6
18:1	524.4104	524.4106	0.4	5.1
19:0	540.4417	-	-	-
cyclo 19:0	538.4260	538.4264	0.7	6.9

Table 7.12 Acylated propranolol **1** derivatives observed following optimised LCMS analysis of propranolol **1** incubation under physiological conditions with liposomes prepared from *E. coli* extract.

O-acylated propranolol **1** derivatives corresponding to all known *E. coli* fatty acid chains are observed, with the exceptions of 15:0, 17:0, and 19:0. Low abundance of 15:0 and 19:0 acyl chains within *E. coli* extract explains their lack of observable transfer, however lack of 17:0 transfer is surprising considering it comprises 17.7 % of PE fatty acid content. Taken in tandem with the observation of abundant cyclo 17:0 transfer despite 0.0 % contribution to PE fatty acid content, two theories can be predicted. The first theory suggests preferential acyl chain transfer from PG and CL components of *E. coli* liposomes in favour of PE content, due to increased proximity induced by electrostatic interactions between negative phospholipids and cationic propranolol **1**. Alternatively, as supported by literature studies, reported PE fatty acid content is incorrect such that *E. coli* contains 17.7 % cyclo 17:0 rather than linear 17:0.[137,297,302] In addition to cyclo 17:0, *O*-acylated propranol **1** derivatives present in highest abundance result from transfer of 16:0 and 18:1 acyl moieties. This observation is consistent with fatty acid distribution data, in which 16:0 appears in greatest abundance, and 18:1 as second and third most common for PE, and PG/CL components respectively. Further predicted acyl chain transfers, 14:0, 16:1, and 18:0 are assigned based upon accurate mass

and retention time data alone, due to low abundance preventing CID MSMS analysis.

Extracted ion chromatograms (EIC) for major *O*-acylated propranolol **1** derivatives formed by intrinsic lipidation within *E.coli* extract liposomes, are presented in Fig. 7.10. Observed retention times reflect known patterns of acyl chain retention exhibited by lysolipids and other acylated species.[11,40] Increased carbon chain length and associated hydrophobicity results in a corresponding retention time increase, indicated by retention times of 14:0, 16:0 and 18:0 acyl chains as 4.1 min, 5.4 min, and 5.6 min respectively. Unsaturation is observed to decrease analyte retention, exemplified by 16:0 and 16:1 acyl chains of retention time 5.4 min and 4.3 min respectively, and 18:0 and 18:1 acyl chains at 5.6 min and 5.1 min respectively. Retention time comparison for cyclopropyl derivatives is not possible due to lack of linear counterparts. Intrinsic lipidation product ratios based upon observed chromatographic peak area have not been determined due to known ionisation efficiency differences between acylated propranolol **1** derivatives evidenced in Chapter 6 of this thesis.

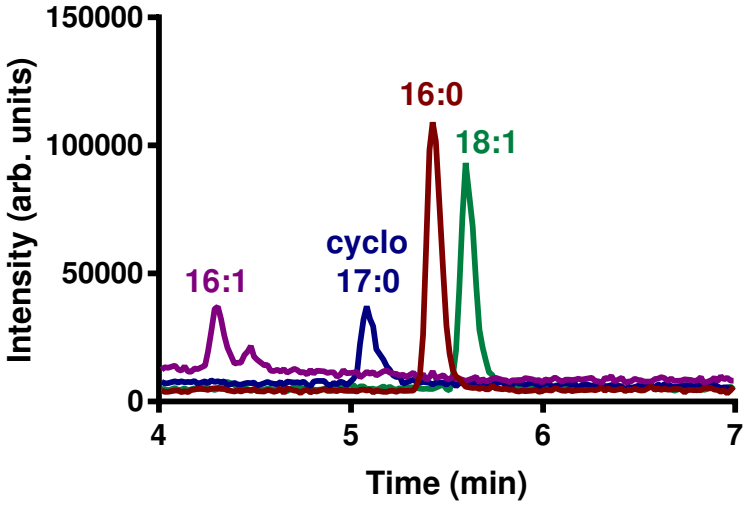

Figure 7.10 EIC for major acylated propranolol **1** derivatives observed following LCMS analysis of propranolol **1** incubation under physiological conditions with liposomes prepared from *E. coli* extract.

Small molecule intrinsic lipidation observed within *E. coli* liposomes has the capacity to alter bulk membrane lipid profile. Optimised analytical conditions provide lipidomics of *E. coli* PE and PG species using negative mode ESI, which can be compared with the untreated *E. coli* profile given in Table 7.10. Lack of cellular proteins allows observed changes to be attributed directly to the action of propranolol **1**, rather than phospholipase or head group exchange enzymes. Comparison of lipid profiles for untreated and propranolol **1** treated *E. coli* indicates similarities between the two, with an identical majority of observed phospholipids. Five phospholipid species were observed in untreated liposomes but not noted to be present

upon propranolol **1** treatment, these were PG(33:0), PE(37:7(OH)), PG(39:4), PE(49:3), and PG(58:0(OH)). Phospholipid loss can be attributed to reduced abundance below the prescribed threshold for LIPID MAPS assignment following either intrinsic lipidation or hydrolysis.[296] Furthermore, nine additional phospholipid species not found in untreated samples were identified within propranolol **1** treated *E. coli* liposomes, summarised in Table 7.13. The origin of these additional species remains unclear, however their presence can be explained by either low level abundance fluctuations close to the limit of instrument detection, or to increased lipid solubility in the presence of propranolol **1**.

Observed *m/z*	Theoretical *m/z*	Error (ppm)	Assignment
634.4489	634.4453	2.2	PE(28:0)
705.4685	705.4712	3.8	PG(31:1)
756.5560	756.5549	1.5	PE(37:2)
758.5713	758.5705	1.1	PE(37:1)
764.5198	764.5236	3.5	PE(38:5)
772.5841	772.5862	2.7	PE(38:1)
779.5842	779.5807	0.3	PG(36:0(OH))†
807.4835	807.4818	2.1	PG(38:7(OH))
815.6155	815.6171	2.0	PG(40:2)† / PG(40:1)‡

Table 7.13 Additional phospholipid species identified within *E. coli* lipid extract upon treatment with propranolol **1**. † indicates the presence of alkyl ether substituent; ‡ indicates the presence of alkenyl ether (plasmalogen) substituent.

Lysolipid abundance provides a further distinguishing feature between propranolol **1** treated and untreated *E. coli* extracts. LPE(16:0), LPE(cyclo 17:0), and LPE(18:1) lysolipids are observed in both treated and untreated samples, whilst lysolipid LPG(18:1) is observed in propranolol **1** treated samples only. Despite similar speciation, lysolipid abundances differ between treated and untreated samples, as evidenced by semi-quantification using internal standard LPC(17:0). Normalised peak areas, presented in Table 7.14, show a slight lysolipid increase in response to propranolol **1** treatment, corresponding with *in vitro* observations using liposome systems. Upregulation of phospholipid hydrolysis in the presence of propranolol **1** combined with lysolipid production through intrinsic lipidation facilitate this increase in lysolipid concentration within the bulk membrane, decreasing membrane integrity.[27]

Lysolipid	Untreated Peak Area	Treated Peak Area
LPE (16:0)	2.48	2.58
LPE (cyclo 17:0)	0.05	0.07
LPE (18:1)	0.08	0.09

Table 7.14 Chromatographic peak areas attributed to the three lysolipids present in *E. coli* lipid extract: (i) untreated; (ii) treated with propranolol **1** in 1:10 small molecule:lipid molar ratio. Peak areas are normalised and presented as % of internal standard LPC(17:0) chromatographic peak area.

7.3.2 2-Aminomethylbenzimidazole Reactivity

Study of benzimidazole **11** intrinsic lipidation within *E. coli* extracts was also conducted. Benzimidazole **11** was selected due to availability, combined with observed high levels of intrinsic lipidation within membrane models *in vitro*. Acylated product characterisation *in vitro* suggests formation of a single benzimidazole **11** intrinsic lipidation product, resulting from reactivity of the free primary amine. Single product formation reduces product diversity compared to propranolol **1**, simplifying analysis by mass spectrometry. Following incubation for 72 hours under physiological conditions, reaction mixtures were screened for acylated **11** derivatives predict by *E. coli* fatty acid distribution.

Observed acylated **11** derivatives, summarised in Table 7.15, reflect a similar pattern of acyl chain transfer as described for propranolol **1**. Low abundance 18:0 and cyclo 19:0 acyl chains, where transfer is observed to propranolol **1** but not benzimidazole **11**, are the exception to this. High abundance transfer of 16:0, and 18:1 acyl chains to benzimidazole **11** is observed, reflecting recorded fatty acid distribution. Furthermore, abundant transfer of cyclo 17:0 is noted, whilst linear 17:0 is not, supporting previous suggestions of errors in reported fatty acid distribution, or preferential transfer from PG and CL species. Transfer of 14:0 and 16:1 acyl chains is noted based upon retention time and accurate mass, since low abundance prevents CID MSMS confirmation. Observed reactivity of the 14:0 acyl chain is interesting considering transfer is not noted for fatty acyl chains of similar or higher abundance, such as 18:0 and 19:0. Preferential positioning of 14:0 acyl chains, or favourable transfer of shorter chain lengths could explain this observation, however further data would be required for confirmation.

Fatty Acid Transferred	Theoretical m/z	Observed m/z	Error (ppm)	R.T. (min)
14:0	358.2858	358.2861	0.7	3.7
15:0	372.3015	-	-	-
16:0	386.3171	386.3167	1.1	5.0
16:1	384.3015	384.3017	0.6	4.0
17:0	400.3328	-	-	-
cyclo 17:0	398.3171	398.3166	1.4	4.7
18:0	414.3484	-	-	-
18:1	412.3328	412.3318	2.4	5.3
19:0	428.3641	-	-	-
cyclo 19:0	426.3484	-	-	-

Table 7.15 Acylated benzimidazole **15** derivatives observed following LCMS analysis of benzimidazole **15** incubation under physiological conditions with liposomes prepared from *E. coli* extract.

EIC for acylated derivatives of benzimidazole **11**, formed by intrinsic lipidation with *E. coli* extract, are shown in Fig. 7.11. Despite reduced product diversity compared to study of acylated propranolol **1** species, known patterns of acyl chain retention are observed. Increased carbon chain length from 14:0 to 16:0 results in a corresponding retention time increase from 3.7 min to 5.0 min. Inclusion of a double bond into the acyl chain structure reduces product retention, as exhibited by acyl chains 16:0 and 16:1 having retention times of 5.0 min and 4.0 min respectively. Intrinsic lipidation product ratios were not calculated based upon observed chromatographic peak area, due to predicted ionisation efficiency variation between acylated benzimidazole **11** derivatives.

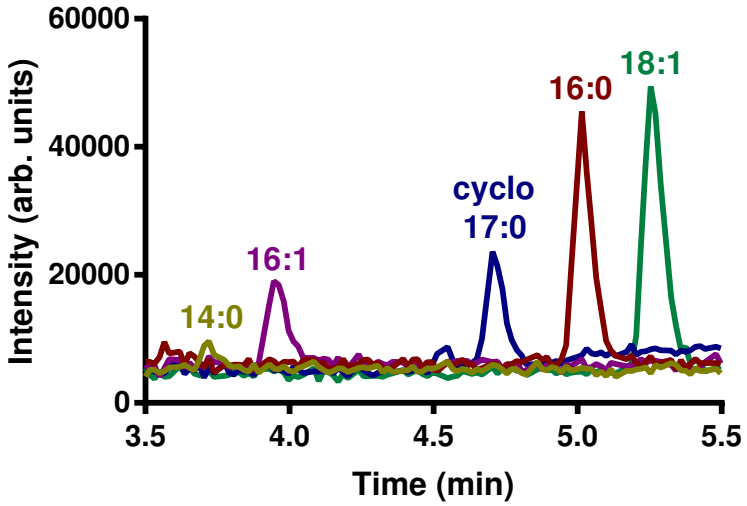

Figure 7.11 EIC for acylated benzimidazole **11** derivatives observed following LCMS analysis of benzimidazole **11** incubation under physiological conditions with liposomes prepared from *E. coli* extract.

Optimised analytical conditions facilitate lipid profile comparison between untreated and benzimidazole **11** treated *E. coli* extracts. Lipidomics of treated samples reveal a majority of shared lipid species with untreated and propranolol **1** treated *E. coli*, corresponding to the lipid profile given in Table 7.10. However, seven phospholipid species observed in the untreated membrane were lost upon benzimidazole **11** treatment, these were PE(30:1), PE(35:1), PG(33:0), PE(38:6)‡, PE(37:7(OH)), PE(49:3), and PG(58:0(OH)). Three species, PG(33:0), PE(49:3), and PG(58:0(OH)), correspond to species also lost following propranolol **1** treatment, and attributed to reduced abundance following intrinsic lipidation or hydrolysis. Furthermore, eight additional phospholipid species, not found in untreated samples, were identified within benzimidzole **11** treated *E. coli* liposomes, summarised in Table 7.16. Three of the additional species, PE(28:0), PE(37:2), and PG(40:2)† / PG(40:1)‡, were also observed upon treatment of *E. coli* extract with propranolol **1**. The origin of these additional species remains unclear, however their presence can be explained by either low level abundance fluctuations close to the limit of instrument detection, or to increased lipid solubility in the presence of benzimidazole **11**.

Observed *m/z*	Theoretical *m/z*	Error (ppm)	Assignment
634.4442	634.4453	1.7	PE(28:0)
676.4927	676.4923	0.6	PE(31:0)
687.4239	687.4242	0.4	PG(30:3)
756.5558	56.5549	1.2	PE(37:2)
771.5162	771.5181	2.5	PG(36:3)
793.4692	793.4661	3.9	PG(37:7(OH))
802.506	802.5028	3.5	PE(40:8(OH))
815.6155	815.6171	1.6	PG(40:2)† / PG(40:1)‡

Table 7.16 Additional phospholipid species identified within *E. coli* lipid extract upon treatment with benzimidazole **11**. † indicates the presence of alkyl ether substituent; ‡ indicates the presence of alkenyl ether (plasmalogen) substituent.

Lysolipid abundance was noted to vary in propranolol **1** treated *E. coli* liposomes, therefore similarly modified lysolipid adundance was predicted in benzimidazole **11** treated systems. Abundance was determined for major lysolipid species LPE(16:0), LPE(cyclo 17:0), and LPE(18:1), through chromatographic peak area modelling and normalisation using internal standard LPC(17:0). As summarised in Table 7.17, lysolipid abundance was noted to be slightly upregulated in benzimidazole **11** treated *E. coli* compared to untreated systems. Corresponding to observations made *in vitro* using simple liposomal systems, lysolipid upregulation can be attributed to increased phospholipid hydrolysis combined with benzimidazole **11**

intrinsic lipidation. Variation in bulk membrane lysolipid concentration impacts membrane stability and integrity, with significant disruption known to result in leakage of intracellular contents and ultimately cell death.[30,31,35]

Lysolipid	Untreated Peak Area	Treated Peak Area
LPE (16:0)	2.48	2.73
LPE (cyclo 17:0)	0.05	0.07
LPE (18:1)	0.08	0.20

Table 7.17 Chromatographic peak areas attributed to the three lysolipids present in *E. coli* lipid extract: (i) untreated; (ii) treated with benzimidazole **11** in 1:10 small molecule:lipid molar ratio. Peak areas are normalised and presented as % of internal standard LPC(17:0) chromatographic peak area.

7.4 Intrinsic Lipidation in Liver Extracts

Propranolol **1** and benzimidazole **11** exhibit intrinsic lipidation reactivity in the presence of liposomes prepared from polar *E. coli* extract. However, study *in vitro* using simple eukaryotic and prokaryotic models suggests both small molecules undergo preferential eukaryotic reactivity. Merging *in vitro* study with increased molecular diversity, intrinsic lipidation within liposomes prepared from polar liver extract was compared to the equivalent *E. coli* derived system. Polar liver extract was obtained through $CHCl_3$:MeOH extraction of bovine liver tissue, followed by acetone precipitation and further extraction with diethyl ether.[303] Resulting liver extract liposomes contain PC, PE, PI and cholesterol species, whilst incorporating a diverse range of fatty acyl chain types. Additional biological features, including peptides and proteins, are not contained within the extract, providing increased simplicity compared to a true cellular system.

Optimised analytical conditions facilitated successful study of small molecule intrinsic lipidation within liver extract through lipid profile determination. Combined analyses by positive and negative mode ESI provided insight into chromatographically resolved PC, PE and PI species present within polar liver extract, Fig. 7.12. Scans were combined over the retention time windows of lysololipid elution between 1.0 min to 6.0 min, and phospholipid elution between 13.0 min and 20.0 min. Ions exceeding the intensity threshold of $1x10^5$ were isolated and assigned through comparison with the LIPID MAPS Gateway.[296] Following removal of anomalies not observed across duplicate analyses, and those exhibiting error of > 4.0 ppm, the lipid profile presented in Table 7.18 was obtained. Unrealistic assignments attributed to

acyl chain species known to be absent within eukaryotic liver cells were also removed.

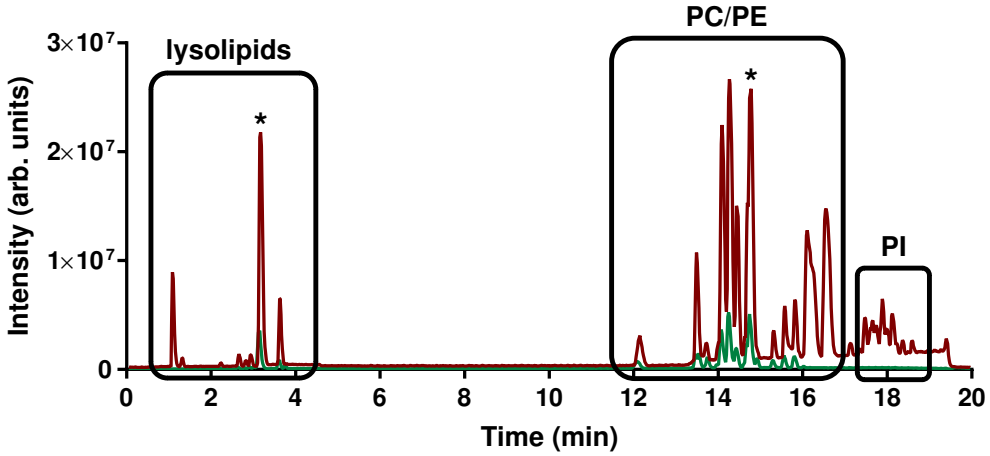

Figure 7.12 TIC of phospholipid and lysolipid species identified within Hep G2 cells including positive mode ESI (red) and negative mode ESI (green). * indicate internal standards LPC(17:0) eluting at 3.2 min and PC(17:0) eluting at 14.9 min.

Observed *m/z*	Theoretical *m/z*	Error (ppm)	Assignment
438.2988	438.2979	2.1	LPE(16:0)‡
452.2762	452.2772	2.2	LPE(16:1)
466.3274	466.3292	3.9	LPE(18:0)‡
478.2938	478.2928	2.1	LPE(18:2)
482.3228	482.3241	2.7	LPE(18:0)
502.2926	502.2928	0.4	LPE(20:4)
508.3756	508.3762	1.2	LPC(18:0)‡
518.3239	518.3241	0.4	LPC(18:3)
544.3383	544.3398	2.8	LPC(20:4)
546.3540	546.3554	2.6	LPC(20:3)
568.3392	568.3398	1.1	LPC(22:6)
597.3057	597.3035	3.7	LPI(18:2)
601.3324	601.3348	4.0	LPI(18:0)
690.5065	690.5069	0.6	PE(32:1)
694.5036	694.5018	2.6	PC(28:0(OH))
698.5127	698.5119	1.1	PE(34:4)† / PE(34:3)‡
718.5381	718.5382	0.1	PE(34:1)

738.5423	738.5432	1.2	PC(34:4)‡
748.5272	748.5276	0.5	PE(38:6)‡
748.6210	748.6215	0.7	PC(34:0)†
750.5461	750.5432	3.9	PE(38:6)† / PE(38:5)‡
756.5531	756.5538	0.9	PC(34:3)
756.5930	756.5902	3.7	PE(38:2)‡
768.5548	768.5538	1.3	PE(38:4)
770.6049	770.6058	1.2	PC(36:3)† / PC(36:2)‡
772.5859	772.5851	1.0	PE(38:2)
784.4915	784.4912	0.4	PE(40:10)
790.5955	790.5957	0.3	PE(38:1(OH))
808.5826	808.5851	3.1	PC(38:5)
828.5161	828.5174	1.6	PE(42:10(OH))
828.6099	828.6113	1.7	PC(38:3(OH))
830.5680	830.5695	1.8	PC(40:8)
832.6788	832.6790	0.2	PE(42:0)
837.5488	837.5488	0.0	PI(34:1)
842.6614	842.6634	2.4	PC(40:2)
845.5183	845.5175	0.9	PI(35:4)
846.6953	846.6947	0.7	PC(40:0)
850.5942	850.5957	1.8	PC(40:6(OH))
853.6163	853.6165	0.2	PI(36:0)†
856.7183	856.7154	3.4	PC(42:2)†
862.6303	862.6321	2.1	PC(42:6)
863.5669	863.5644	2.9	PI(36:2)
869.5526	869.5539	1.5	PI(38:6)† / PI(38:5)‡
884.7485	884.7467	2.0	PC(44:2)†
885.5472	885.5488	1.8	PI(38:5)
887.5615	887.5644	3.3	PI(38:4)

889.5770	889.5801	3.5	PI(38:3)
891.5959	891.5957	0.2	PI(38:2)
905.6475	905.6478	0.3	PI(40:2)† / PI(40:1)‡
915.5927	915.5957	3.3	PI(40:4)
931.5306	931.5331	2.7	PI(42:10)

Table 7.18 Phospholipid and lysolipid species identified within polar bovine liver lipid extract.[303] † indicates the presence of alkyl ether substituent; ‡ indicates the presence of alkenyl ether (plasmalogen) substituent.

Fatty Acid	Liver PC (%)	Liver PE (%)	Liver PI (%)
16:0	14.0	5.0	0.0
16:1	0.0	0.1	0.0
18:0	33.0	33.7	46.0
18:1	17.0	9.8	8.0
18:2	12.0	10.9	6.0
18:3	0.0	0.8	0.0
20:3	8.0	4.1	13.0
20:4	7.0	19.5	17.0
22:6	0.0	2.1	0.0
Unknown	9.0	14.0	10.0

Table 7.19 Fatty acid chain distribution of bovine liver lipid extract.[303]

Fifty-one distinct lipid components were observed following analysis of bovine liver extract. Species can be subdivide into thirty-eight phospholipid components, and thirteen lysolipid components. Phosphate head groups observed cover the classes PC, PE, and PI in accordance with available data dictating the mixture contains 42 % PC, 26 % PE, and 10 % PI/lyso PI. Additional recorded components include 5 % cholesterol, a known sterol component of eukaryotic membranes unable to undergo intrinsic lipidation with small molecules, and 17 % other lipid species including neutral lipids. Saturated and unsaturated acyl chain types are represented within liver extract, in addition to both hydrolysed and plasmalogen moieties.[300,301,303] Plasmalogen presence within both PC and PE lipid classes is known within liver cells, however proportions are usually low at <1 % PC and < 4 % PE within sheep liver. Lysolipid species provide insight into specific acyl chains present, which include 16:0, 16:1, 18:0, 18:2, 18:3, 20:3, 20:4, and 22:6. Observed acyl chains reflect those attributed to liver membrane lipids within available literature data, Table 7.19, with the exception of the 18:1

chain.

7.4.1 Propranolol Reactivity

Study of propranolol **1** intrinsic lipidation, facilitated by lipid profile determination, was conducted using polar bovine liver extract. Under physiological conditions, propranolol **1** was incubated for 72 hours in 1:10 drug:lipid molar ratio with liver extract liposomes, based upon an average phospholipid molecular weight of 756.3360. Screening for predicted acylated propranolol **1** derivatives was conducted following analysis under optimised conditions designed for study of small molecule intrinsic lipidation within complex biological systems.

Table 7.20 summarises acylated propranolol **1** derivatives observed upon incubation with liver extract. CID MSMS performed upon species of sufficient abundance confirmed these to be *O*-acylated derivatives, rather than their *N*-acylated counterparts. Absence of *N*-acylated species is attributed to either reduced intramolecular migration, or poor ionisation of the multiple low abundant species. Product assignment is consistent with both the predicted pathway of propranolol **1** intrinsic lipidation, and reactivity observations made during study of propranolol **1** intrinsic lipidation within *E. coli* extract.

Fatty Acid Transferred	Theoretical *m/z*	Observed *m/z*	Error (ppm)	R.T. (min)
16:0	498.3947	498.3947	0.0	5.4
16:1	496.3791	-	-	-
18:0	526.4260	526.4276	3.0	7.4
18:1	524.4104	524.4099	0.9	5.6
18:2	522.3947	522.3951	0.7	4.6
18:3	520.3791	-	-	-
20:3	548.4104	548.4109	1.0	5.0
20:4	546.3947	546.3932	2.8	2.6
22:6	570.3947	-	-	-

Table 7.20 Acylated propranolol **1** derivatives observed following LCMS analysis of propranolol **1** incubation under physiological conditions with liposomes prepared from bovine liver extract.

Predicted *O*-acylated propranolol **1** derivatives not observed upon incubation with liver extract include transfer of 16:1, 18:3, and 22:6 acyl chains. Minor membrane components, these chain chemistries are attributed solely to PE class phospholipids in low proportions of 0.1 %, 0.8 %, and 2.1 % respectively. Their low abundance explains their lack of observable transfer, with acylated small molecule quantities predicted to fall below the limit of instrument detection. All

additional acyl chain chemistries attributed to liver extract are represented in the formation of acylated propranolol **1** derivatives, however 20:4 transfer is based upon accurate mass and retention time only due to poor ion intensity preventing CID MSMS. Relatively poor 20:4 transfer combined with abundant transfer of other moieties, particularly 16:0, 18:0, and 18:1, suggests observed transfer patterns correlate with PC fatty acid content. Preferential transfer from PC class lipids is likely due to the increased ratio of PC species (42 %) compared to PE (26 %) and PI (10 %) counterparts. However, absolute quantification of differential transfer could be determined based upon peak area comparisons, due to known differences in ionisation efficiencies for acylated propranolol **1** derivatives.

Fig. 7.13 presents EIC for *O*-acylated propranolol **1** derivatives formed by intrinsic lipidation within liver extract liposomes, with the exception of low abundant 20:4 transfer. Observed retention times reflect known patterns of acyl chain retention exhibited by lysolipids and other acylated species. Reduced retention due to shorter carbon chain length or increased unsaturation is evidenced by acyl chains 16:0 and 18:0 at retention times of 5.4 min and 7.4 min respectively, and chains 18:0, 18:1 and 18:2 at retention times 7.4 min, 5.6 min and 4.6 min respectively. Retention times of 16:0 and 18:1 acylated propranolol **1** formed within liver extract liposomes are consistent with corresponding products formed within *E. coli* extract. However, 18:0 acylated propranolol **1** exhibits markedly different retention between the two, observed at 5.6 min within *E. coli* and 7.4 min within liver extract. Observed differences suggests an incorrect assignment attributed to *E. coli*, due to increased mass accuracy error and lack of 18:0 transfer observed within the analogous benzimidazole system.

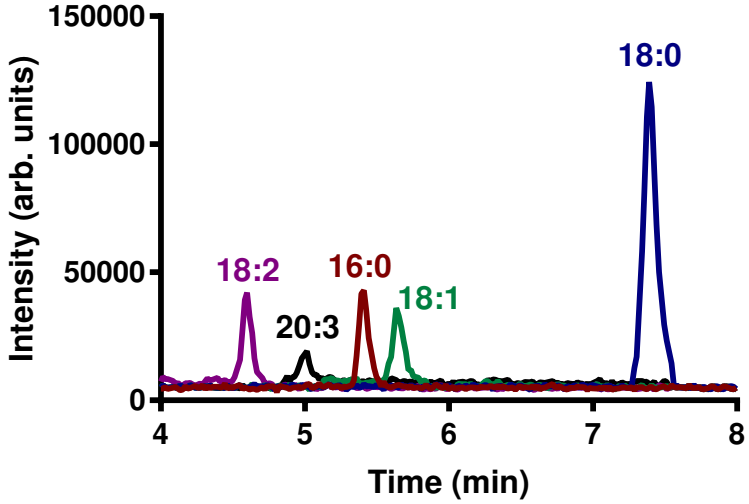

Figure 7.13 EIC for acylated propranolol **1** derivatives observed following LCMS analysis of propranolol **1** incubation under physiological conditions with liposomes prepared from bovine liver extract.

Lipid profile modifications to liver extract liposomes upon treatment with small molecule propranolol **1** for 72 hours were determined using optimised analytical conditions. Lack of cellular proteins allows observed changes to be attributed directly to the action of propranolol **1**, rather than phospholipase or head group exchange enzymes. The observed lipid profile of propranolol **1** treated liver liposomes resembles that of the untreated control, retaining thirty of the thirty-eight phospholipids. Eight phospholipids covering PC, PE and PI classes observed within untreated liver extract, were not observed during analysis of propranolol **1** treated extract. Increased phospholipid hydrolysis combined with intrinsic lipidation reactivity likely diminished these species such that abundance falls below the prescribed threshold for LIPID MAPS assignment.[296] Simultaneously, eleven additional lipid species, summarised in Table 7.21, were identified during analysis of propranolol **1** treated liver extract. The origin of these species is unclear, however sufficient safeguards have been implemented to ensure the observed increase in phospholipid diversity is real. Low level abundance fluctuations close to the limit of instrument detection, or increased lipid solubility in the presence of propranolol **1** provide possible explanations.

Observed *m/z*	Theoretical *m/z*	Error (ppm)	Assignment
610.4445	610.4443	0.32	PE(26:0(OH))†
643.3405	643.3453	2.12	PI(20:0)
648.4622	648.4599	3.5	PC(26:1)
710.4755	710.4756	0.1	PE(34:5)
764.5213	764.5225	1.6	PE(38:6)
798.6392	798.6371	2.6	PC(38:3)† / PC(38:2)‡
818.6633	818.6634	0.1	PC(38:0)
874.7305	874.726	0.7	PC(42:0)
886.7617	886.7623	0.7	PC(44:1)†
951.6877	951.6896	2.0	PI(42:0)
995.7169	995.7158	1.1	PI(44:0(OH))

Table 7.21 Additional phospholipid species identified within bovine liver lipid extract upon treatment with propranolol **1**. † indicates the presence of alkyl ether substituent; ‡ indicates the presence of alkenyl ether (plasmalogen) substituent.

7.4.2 2-Aminomethylbenzimidazole Reactivity

For comparison with propranolol **1** and the *E. coli* system, benzimidazole **11** intrinsic lipidation was also studied using bovine liver extract. Incubation proceeded for 72 hours under physiological conditions prior to analysis under optimised analytical conditions designed for study of small molecule intrinsic lipidation within complex biological systems. Potential

acylated benzimidazole **11** products of intrinsic lipidation were predicted based upon the known fatty acid distribution, and data screened for the presence of these species. In contrast to propranolol **1**, only a single acylated form of benzimidazole **11** is predicted.

Acylated benzimidazole **11** derivatives formed within liver extract liposomes, Table 7.22, mirror acylated propranolol **1** derivatives. Lack of 16:1, 18:3, and 22:6 acyl chain transfer is once again attributed to their status as only minor acyl chain components of PE class liver lipids. Favourable acyl chain transfer from more abundant PC phospholipids compared to PE and PI counterparts is exemplified by considerable formation of 16:0, 18:0 and 18:1 acylated benzimidazole **11** products. Furthermore, low level transfer of 18:2, 20:3 and 20:4 acyl chains are noted, resulting in formation of additional intrinsic lipidation products.

Fatty Acid Transferred	Theoretical *m/z*	Observed *m/z*	Error (ppm)	R.T. (min)
16:0	386.3171	386.3167	1.1	5.0
16:1	384.3015	-	-	-
18:0	414.3484	414.3489	1.1	6.7
18:1	412.3328	412.3313	3.6	5.3
18:2	410.3171	410.3168	0.8	4.3
18:3	408.3015	-	-	-
20:3	436.3328	436.3323	1.1	5.0
20:4	434.3171	434.3159	2.9	3.6
22:6	458.3171	-	-	-

Table 7.22 Acylated benzimidazole **11** derivatives observed following LCMS analysis of benzimidazole **11** incubation under physiological conditions with liposomes prepared from bovine liver extract.

EICs for chromatographically observable acylated benzimidazole **11** derivatives are presented in Fig. 7.14. Observed retention times mirror known patterns, with reduced carbon chain length and increased unsaturation resulting in earlier product elution. Comparable product retention times are observed within liver extract as those attributed to products within *E. coli*, supporting product identification. Examples include 16:0 benzimidazole **11** eluting at 5.0 min in both liver liposomes and in *E. coli* extract. Similarly, 18:1 benzimidazole **11** consistently elutes at the retention time 5.3 min within both liver and *E. coli* systems.

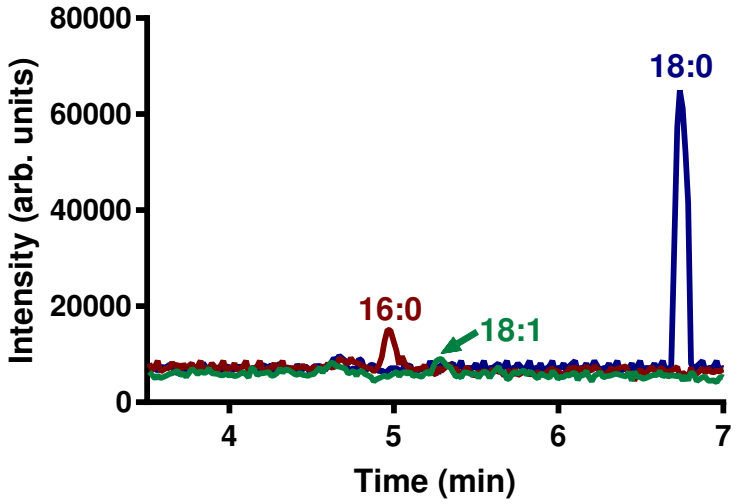

Figure 7.14 EIC for acylated benzimidazole **11** derivatives observed following LCMS analysis of benzimidazole **11** incubation under physiological conditions with liposomes prepared from bovine liver extract.

Observed m/z	Theoretical m/z	Error (ppm)	Assignment
621.3045	621.3035	1.6	LPI(20:4)
672.4593	672.4599	0.9	PC(28:3)
710.4723	710.4756	1.0	PE(34:5)
753.4553	753.4549	0.5	PI(28:1)
764.5245	764.5225	2.6	PE(38:6)
792.6466	792.6477	1.34	PC(36:0(OH))†
799.4929	799.4967	2.4	PI(30:0(OH))
806.6251	806.6270	2.4	PC(36:0(OH))
835.5323	835.5331	1.0	PI(34:2)
839.5637	839.5644	0.8	PI(34:0)
874.7299	874.726	1.34	PC(42:0)
959.6192	959.6219	2.8	PI(42:4(OH))

Table 7.23 Additional phospholipid species identified within bovine liver lipid extract upon treatment with benzimidazole **11**. † indicates the presence of alkyl ether substituent; ‡ indicates the presence of alkenyl ether (plasmalogen) substituent.

Lipodomics studies reveal the influence of benzimidazole **11** treatment upon the lipid profile of bovine liver extract. Optimised analysis suggests retention of the majority of lipid species observed within untreated and propranolol **1** treated liver systems. However, two lysolipid species plus twelve of the thirty-eight phospholipid species were not visualised during analysis of benzimidazole **11** treated samples. Four of the species lost compared to untreated liver extract were also absent in the lipid profile of propranolol **1** treated liposomes. Increased lysolipid abundance, consistent with observations *in vitro* and in *E. coli* extract, suggests that

phospholipid hydrolysis reduces abundance of phospholipid species such that they fall below the required threshold. In tandem, twelve novel lipid species not attributed to untreated liver extract were observed in benzimidazole **11** treated samples, Table 7.23. Four species, PC(42:0), PE(38:6), PI(28:1), and PE(34:5), are also observed within propranolol **1** treated liver extract. Similarities between propranolol **1** and benzimidazole **11** treated liver extracts suggest they employ analogous mechanisms to modify lipid profile.

7.5 Intrinsic Lipidation in Hep G2 Cells

Optimised analytical conditions for the study of lipidomics and small molecule intrinsic lipidation within complex biological systems have been validated using polar *E. coli* and liver extracts. Furthermore, cellular extracts have provided insight into acylated product formation and distribution within complex systems, applicable to study of intrinsic lipidation *in cellulo*. Hep G2 cells provide a suitable study medium for moving reactivity monitoring *in cellulo*, enabling biological relevance of intrinsic lipidation to be explored. A well characterised human liver cancer cell line, Hep G2 cells provide a comparable system to the eukaryotic bovine liver cell extract studied in liposomal form. Selection of the Hep G2 cell line is attributed to their use in the study of drug induced phospholipidosis, a side effect linked to intrinsic lipidation.[73,74]

Additional experimental steps are required to facilitate study of intrinsic lipidation *in cellulo*, compared to liposomal systems. Cell viability and survival is required over the 72 hour time period of study to ensure successful analysis. Concentration of small molecule propranolol **1** must therefore be selected accordingly. Approximately 20000 cultured cells were added to each well of a sterile 96-well plate, then left to adhere overnight at 37 °C in 5 % CO_2 and 95 % humidity. Propranolol **1** stock solution in H_2O was added to triplicate cell samples at 30 µM, along with ten further serial dilutions down to final concentration 29 nM. Following 72 hours, cell growth compared to an untreated control was determined by visual study. Cell survival was observed across all samples, however at a propranolol **1** concentration of 30 µM cell number was reduced by approximately 30 % compared to untreated counterparts. Successful analysis of intrinsic lipidation products is facilitated by increased abundance relative to other cellular species. Considering both cell viability and analytical requirements, a propranolol **1** concentration of 30 µM was selected for study of intrinsic lipidation *in cellulo*.

Analysis of intrinsic lipidation *in cellulo* requires a second additional experimental step

compared to study in liposomal systems. Isolation of small molecule and lipid components from Hep G2 cells is required prior to sample analysis, in order to minimise sample complexity and ensure visualisation of intrinsic lipidation products. Isolation requires development of a robust and reproducible method of cellular extraction. Optimised extraction conditions were determined by comparison of an *in vitro* POPC and propranolol **1** reaction mixture under different extraction conditions. Three extraction solvents were tested in accordance with the literature:

- $CHCl_3$
- $CHCl_3$:MeOH (2:1) aka the Folch method[304]
- Methyl *tert*-butyl ether (MTBE)[305]

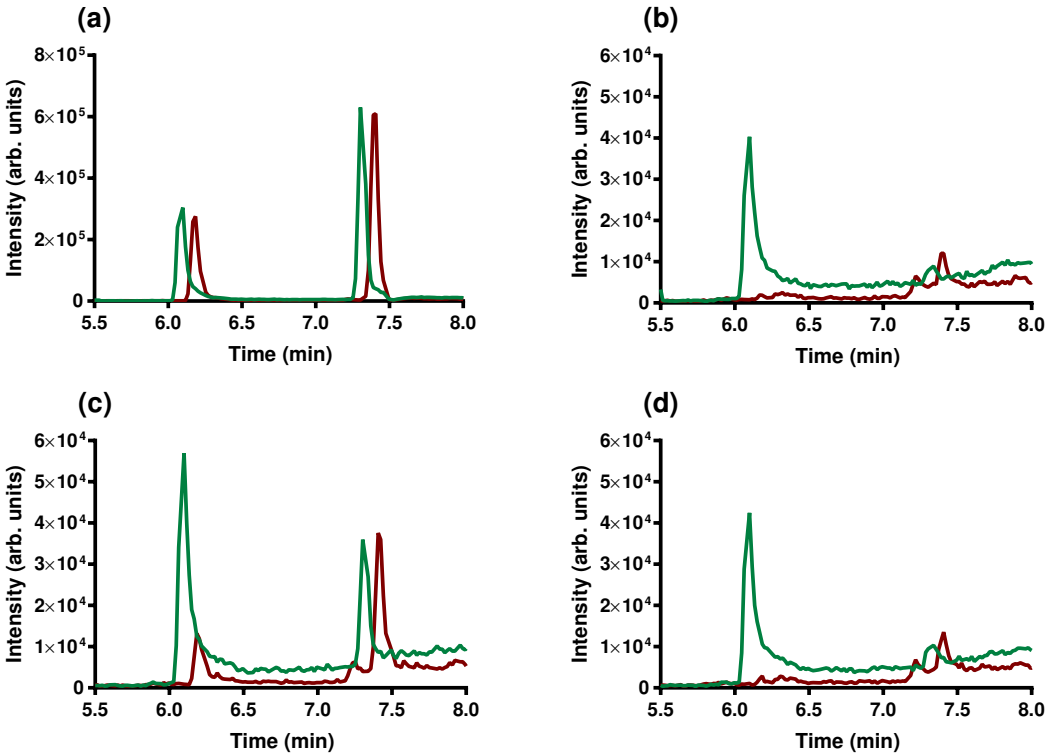

Figure 7.15 EIC comparing palmitoylated propanolol species (green) and oleoylated propranolol species (red) before and after extraction: (a) no extraction; (b) $CHCl_3$ extraction; (c) $CHCl_3$:MeOH (2:1) extraction; (d) MTBE extraction.

Comparable extraction of phospholipid POPC and small molecule propranolol **1** was exhibited under all extraction conditions, resembling analysis conducted prior to extraction. However, as shown in Fig. 7.15, differential extraction of acylated small molecules is noted between experimental conditions. Neither $CHCl_3$ not MTBE, Fig. 7.15 (b) and (d) respectively, successfully extracted these low abundant species, particularly *N*-acylated derivatives, as

denoted by their absence in the relevant EIC. In contrast, the Folch method, Fig. 7.15 (c), exhibits EIC comparable to those obtained prior to extraction, albeit with some loss of oleoylated species. Successful extraction was noted for lysolipids, in addition to both *O*-acylated and *N*-acylated propranolol **1** derivatives. Successful extraction of acylated propranolol **1** derivatives is vital to ensure study of intrinsic lipidation *in cellulo* can be conducted reliably. As a result $CHCl_3$:MeOH (2:1) was selected as the optimum solvent for extraction of Hep G2 cells prior to intrinsic lipidation analysis.

Lipid profiling of Hep G2 cells was conducted, facilitated by optimised extraction methodology and analytical conditions. Positive and negative mode ESI analysis was required to ensure Hep G2 cell lipid diversity was captured, Fig. 7.16. However, literature reports suggest diacylglycerophospholipids, especially PC and PE classes, to be the major cellular components.[306,307] Summarised in Table 7.24, thirty-four phospholipid species and three lysolipids were identified within Hep G2 cells. Identified phospholipids comprise chromatographically resolved 11 % PS, 27 % PE, 30 % PC, and 32 % PI head group classes, Fig. 7.16, varying from reported figures of 4 % PS, 24 % PE, 47 % PC, and 7 % PI. Furthermore, literature studies report an additional 6 % PG and 12 % sphingomyelin (SM) content not observed during these lipid profiling attempts for unknown reasons. Differential % calculation methods, for example % of the total number of observed species versus % weight, accounts for some of the observed variation. However, PI content presents the most startling contrast between observed and reported lipid classes, attributed to either a reduced abundance of multiple PI species or differences in cellular preparation.

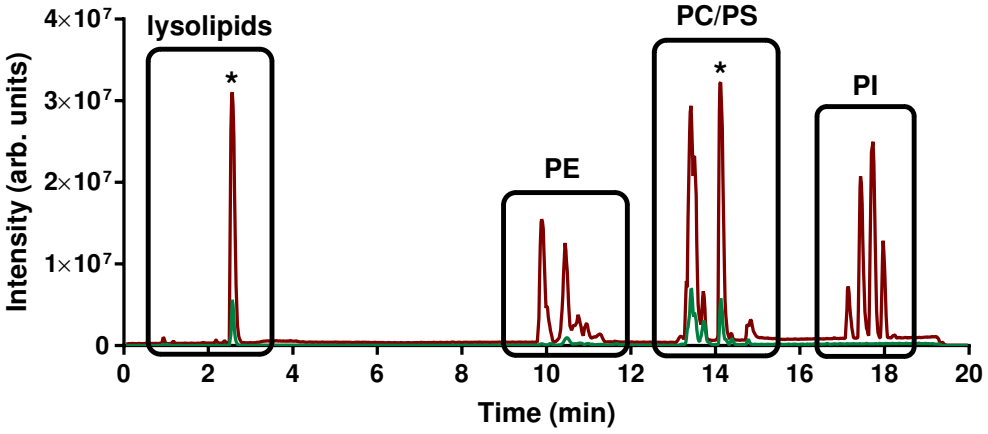

Figure 7.16 TIC of phospholipid and lysolipid species identified within Hep G2 cells including positive mode ESI (red) and negative mode ESI (green). * indicate internal standards LPC(17:0) eluting at 2.5 min and PC(17:0) eluting at 14.1 min.

Observed m/z	Theoretical m/z	Error (ppm)	Assignment
454.2918	454.2928	2.2	LPE(16:0)
482.3234	482.3241	1.5	LPE(18:0)
502.2926	502.2928	0.3	LPE(20:4)
680.4845	680.4861	2.4	PE(30:0(OH))
708.4623	708.4599	3.4	PE(34:6)
722.5305	722.5331	3.6	PC(30:0(OH))
728.4844	728.4861	2.3	PE(34:4(OH))
728.5236	728.5225	1.5	PC(32:3)
732.5518	732.5538	2.7	PC(32:1)
736.5463	736.5487	3.3	PE(34:0(OH))
738.5084	738.5069	2.0	PE(36:5)
746.6082	746.6058	3.2	PC(34:1)†
748.5247	748.5276	3.9	PE(38:6)‡
754.5399	754.5382	2.3	PC(34:4)
760.4916	760.4912	0.5	PE(38:8)
772.4771	772.4770	0.1	PS(34:3(OH))
776.6183	776.6164	2.4	PE(38:0)
784.5821	784.5851	3.8	PC(36:3)
790.5396	790.5382	1.8	PE(40:7)
794.5720	794.5695	3.1	PE(40:5)
806.5726	806.5695	3.8	PC(38:6)
810.5984	810.6008	2.9	PC(38:4)
813.5496	813.5488	1.0	PI(32:0(OH))†
822.5671	822.5654	2.1	PS(40:5)†
832.6467	832.6437	3.6	PS(40:0)†
834.6035	834.6008	3.2	PC(40:6)
837.5468	837.5488	2.4	PI(34:1)

853.6168	853.6165	0.4	PI(36:0)†
855.4987	855.5018	3.6	PI(36:6)
860.6177	860.6164	1.5	PC(42:7)
860.6713	860.6739	3.0	PC(40:1(OH))
860.6757	860.6750	0.8	PS(42:0)†
863.5659	863.5644	1.7	PI(36:2)
881.5176	881.5175	0.1	PI(38:7)
885.5453	885.5488	4.0	PI(38:5)
887.5651	887.5644	0.8	PI(38:4)
889.5801	889.5801	0.0	PI(38:3)
911.5610	911.5644	3.7	PI(40:6)
929.5779	929.5750	3.1	PI(40:5(OH))
931.5313	931.5331	1.9	PI(42:10)
951.5598	951.5593	0.5	PI(42:8(OH))
959.5664	959.5644	2.1	PI(44:10)

Table 7.24 Phospholipid and lysolipid species identified within Hep G2 cells. Species highlighted in green are unique to treated cells; species highlighted in pink are unique to untreated cells; † indicates the presence of alkyl ether substituent; ‡ indicates the presence of alkenyl ether (plasmalogen) substituent.

Lipidomics of untreated Hep G2 cells were compared to analogous data obtained following incubation for 72 hours with 30 µM propranolol **1**. Comparable lipid profiles are observed for PC, PE and PS classes between the treated and untreated systems. Fifteen previously characterised lipid species are not observed following propranolol **1** treatment, highlighted pink in Table 7.24. Lost lipid components, which include one PC, one LPE, and two PE species, are dominated by eleven high molecular weight PI phospholipids. The theory of multiple low abundant PI species fits with reduced PI species visualisation as they fall below the required abundance threshold for analysis. Alternatively, the observed reduction in PI content can be attributed to a cellular response following propranolol **1** treatment. Five novel lipid species, highlighted green in Table 7.24, are attributed solely to propranolol **1** treated cells. Lipid proportions are therefore modified to 16 % PS, 36 % PE, 44 % PC, and 12 % PI,

resembling more closely reported values.

Lysolipids LPE(16:0), LPE(18:0), and LPE(20:4) are observed in the lipid profile of untreated and propranolol **1** treated Hep G2 cells. Preferential observation of LPE in favour of LPC formed from the more abundance PC lipid class, suggests an innate preference in either enzymatic formation, hydrolysis, or retention within the membrane. Semi-quantification using internal standard LPC(17:0) enables variation in lysolipid abundance to be determined, as shown in Table 7.25. Abundance of all lysolipid species are increased in propranolol **1** treated cell compared to untreated. Propranolol **1** intrinsic lipidation combined with increased background hydrolysis likely contribute to the observed increase in lysolipid abundance, as noted *in vitro*. Lysolipid upregulation is observed despite tightly controlled regulation of membrane composition employed by cells in order to maintain their structure and integrity.

Lysolipid	Untreated Peak Area	Treated Peak Area
LPE (16:0)	0.03	0.06
LPE (18:0)	0.08	0.12
LPE (20:4)	0.37	0.44

Table 7.25 Chromatographic peak areas attributed to the three lysolipids present in Hep G2 cells: (i) untreated; (ii) treated with propranolol **1** in 1:10 small molecule:lipid molar ratio. Peak areas are normalised and presented as % of internal standard LPC(17:0) chromatographic peak area.

Consideration of the reported Hep G2 fatty acid distribution summarised in Table 7.26, suggests observed lysolipids do not reflect fatty acid abundances.[308] Lysolipids containing 18:1 and 16:1 fatty acid chains are not observed, despite their high reported abundances of 39 % and 12 % respectively. Lysolipids are observed corresponding to the approximately 16 % of Hep G2 fatty acid content attributed to second most abundant species 16:0, and also to the less abundant 18:0 and 20:4 moieties, appearing at 8 % and 6 % respectively. Lack of correlation between lysolipid observation and fatty acid distribution supports the proposed theory of preferential formation or retention during membrane turnover. Within the complex cellular system, membrane composition is vital to a plethora of biological processes, and thus is predicted to be tightly regulated preventing undesirable phospholipid modification and lysolipid build up.

Fatty Acid	Hep G2 (%)
14:0	1.0
16:0	16.4
16:1	12.3
18:0	8.0
18:1	38.8
18:2	5.0
18:4	1.3
20:3	2.4
20:4	6.0
20:5	1.2
22:5	0.7
22:6	2.7

Table 7.26 Fatty acid chain distribution of Hep G2 cell line.[308]

Fatty Acid Transferred	Theoretical *m/z*	Observed *m/z*	Error (ppm)	R.T (min)
14:0	470.3634	470.3637	0.6	2.88
16:0	498.3947	498.3965	3.6	3.77
16:1	496.3791	496.3762	5.8	3.34
18:0	526.4260	526.4283	4.3	4.86
18:1	524.4104	524.4106	0.4	3.88
18:2	522.3947	522.3917	5.8	1.76
18:4	518.3634	518.3622	2.4	1.76
20:3	548.4104	548.4078	4.7	3.70
20:4	546.3947	-	-	-
20:5	544.3791	-	-	-
22:5	572.4104	-	-	-
22:6	570.3947	-	-	-

Table 7.27 Acylated propranolol **1** derivatives observed following LCMS analysis of propranolol **1** incubated under physiological conditions for 72 hours with Hep G2 cells.

Hep G2 cell lipid profiling facilitates understanding of propranolol **1** intrinsic lipidation *in cellulo*. Potential acylated propranolol **1** products of intrinsic lipidation can be predicted using the reported fatty acid composition of Hep G2 cells, and extracts screened for these species. Observed ions, attributed by accurate mass and retention time data to acylated propranolol **1** derivatives, are summarised in Table 7.27. Observed errors are occasionally above instrument recommendations of 4.0 ppm due to reduced ion intensity, requiring careful consideration of assignment accuracy. Sufficient ion abundance facilitated CID MSMS of two species, products resulting from 16:0 and 18:1 transfer, Fig. 7.17. Characterisation confirms the products to

be *O*-acylated propranolol **1** derivatives, in agreement with observations made during cell extract study. Additional acylated species are thus also presumed to be *O*-acylated derivatives, with either reduced rate of intramolecular *O* to *N* migration or poor ionisation preventing visualisation of *N*-acylated counterparts.

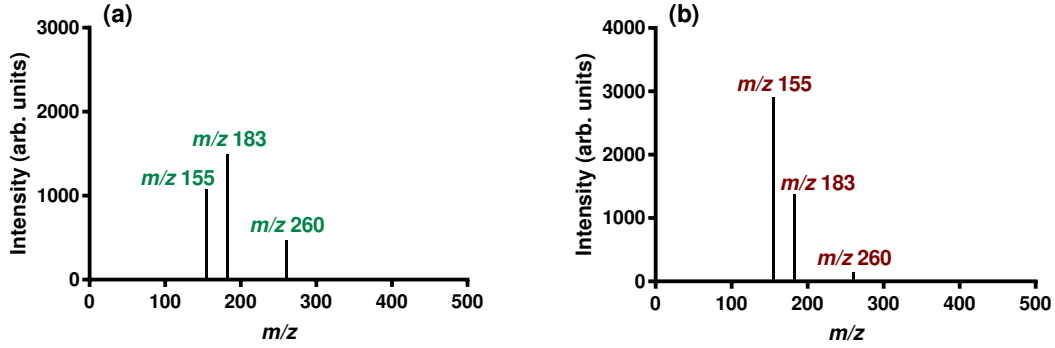

Figure 7.17 CID MSMS carried out to determine identity of acylated products of propranolol **1** intrinsic lipidation in Hep G2 cells: (a) parent ion *m/z* 498.3961 attributed to $[M+H]^+$ of *O*-pamitoyl propranolol **62**; (a) parent ion *m/z* 524.4111 attributed to $[M+H]^+$ of *O*-oleoyl propranolol **47**;.

Eight distinct *O*-acylated propranolol derivatives are observed to form within Hep G2 cells, Table 7.27. Transfer of 16:0 and 18:1 acyl chains represent the most abundant product species, reflecting their position as the most abundant fatty acids within Hep G2 cells at 16.4 % and 38.8 % respectively. Beyond this, observed products do not mirror reported fatty acid abundance, either due to incorrect reporting or low species abundance combined with differing ionisation efficiencies. Preferential transfer of shorter carbon chain lengths is observed irrespective of fatty acid distribution, suggesting acyl chain chemistry influences transfer within Hep G2 cells. Preferential acyl chain transfer could also be attributed to lipid class and propranolol **1** localisation within the asymmetric cellular membrane, however insufficient phospholipid speciation is available to confirm this supposition. EIC for observed acylated products are shown in Fig. 7.18. Known patterns of acyl chain elution dictated by chain length and unsaturation are observed, supporting correct species assignment. Two low abundant species are excluded for Fig. 7.18, 18:2 and 18:4 acylated propranolol **1** derivatives, both of which are assigned a retention time of 1.8 min, Table 7.27. Identical retention suggests either incorrect species assignment, or insufficient product separation prior to early elution.

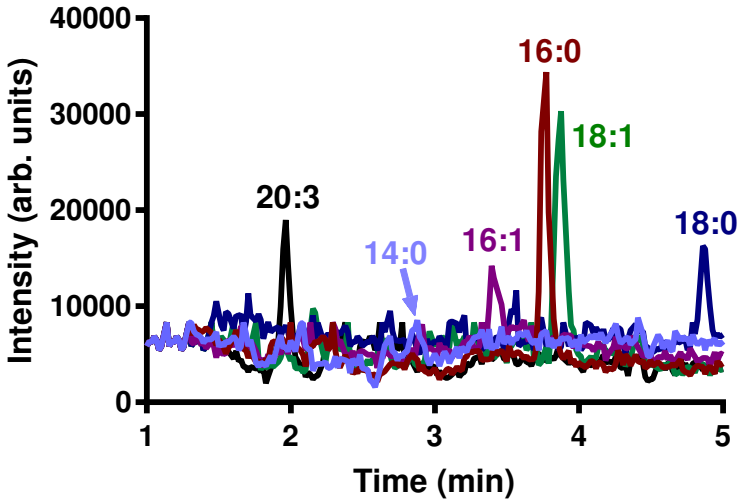

Figure 7.18 EIC for acylated propranolol **1** derivatives observed following LCMS analysis of propranolol **1** incubated under physiological conditions for 72 hours with Hep G2 cells.

7.6 Conclusions

Instrument optimisation has facilitated the study of complex biological systems by mass spectrometry, ensuring high quality informative data. Ionisation of phospholipid species POPC and POPS has been studied using positive and negative mode ESI respectively. Modification of parameters including capillary voltage, sampling cone voltage and source offset, enabled the development of optimised phospholipid conditions. Successful application of optimised ionisation parameters to the detection of acylated small molecules ensures conditions are suitable for study of lipidomics and small molecule intrinsic lipidation within complex biological systems. Chromatographic conditions have also been developed using a mixture of lipid standards, ensuring chromatographic resolution between phospholipids of varying head group classes and acyl chain types. Component separation and lipid solubility were aided by application of a highly organic solvent mixture including IPA. Regular monitoring of mobile phase pH proved vital in preventing elution time inconsistencies and peak broadening.

Employing optimised analytical conditions, small molecule intrinsic lipidation was studied within complex biological systems. Reactive small molecules propranolol **1** and benzimidazole **11** were examined following 72 hour incubation with liposomes prepared from commercial cell extracts. Diverse acylated small molecule products were characterised within both prokaryotic *E. coli* extract, and eukaryotic bovine liver extract. Observed acylated products reflect the fatty acid profile of systems studied, supporting a non-enzymatic transfer mechanism. Propranolol **1** intrinsic lipidation was also studied *in cellulo* using the Hep G2 liver cancer

cell line, resulting in the first evidence of intrinsic lipidation *in cellulo*. Acylated propranolol **1** products were predicted and identified in accordance with reported cellular fatty acid content. CID MSMS confirmed products to be *O*-acylated species rather than the *N*-acylated analogues formed *in vitro* via intramolecular migration. Preferential acyl chain transfer was noted *in cellulo*, favouring shorter carbon chain lengths. Proof of innate intrinsic lipidation *in cellulo* highlights the biological and pharmaceutical relevance of membrane reactivity.

Lipid profile modifications resulting from small molecule intrinsic lipidation were also monitored under the optimised analytical conditions developed. *E. coli* and liver extract liposomes exhibit increased lipid diversity across a range of classes following treatment with either propranolol **1** or benzimidazole **11**. Furthermore, systems exhibit heightened lysolipid levels in the presence of small molecules, correlating with *in vitro* observations. Membranes containing high proportions of lysolipid are known to exhibit modified membrane characteristics and reduced structural integrity. Analogous lipid profiling of propranolol **1** treated Hep G2 cells suggest phospholipid and lysolipid species are retained in similar abundance to untreated cells. Cellular regulatory mechanisms are predicted to modulate membrane composition in the presence of disruptive propranolol **1**, ensuring cell survival.

8 | Expanding Small Molecule Horizons

8.1 Introduction

Optimised analytical conditions provide proof of innate *in vitro* reactivity between small molecules and membrane phospholipids, termed intrinsic lipidation. Furthermore, intrinsic lipidation has been identified as a general process, affecting multiple membrane binding small molecules rather than being the unique property of a single small molecule. Understanding small molecule intrinsic lipidation as a generic process requires increased understanding of two key areas:

1. Reactivity in relation to structural and functional small molecule features
2. The biological and pharmaceutical impact of reactivity

Increased knowledge of these two areas provides a mechanism for the application of intrinsic lipidation reactivity to the drug development process. Structural and functional prediction of the likelihood of small molecule intrinsic lipidation for a drug candidate allows early identification, ultimately saving time and money. Understanding the relationship between intrinsic lipidation and drug activity or side effect induction provides insight into the severity of patient outcomes following treatment with a drug candidate exhibiting reactivity. Alternatively, understanding of intrinsic lipidation could provide a mechanism for tuning reactivity within a drug candidate, harnessing the process to obtain desirable biological or pharmaceutical results.

8.2 Investigating Reactivity

Despite the definition of small molecule intrinsic lipidation as a generic process, not all membrane binding small molecules exhibit reactivity. Diminished reactivity is observed despite the cationic amphiphilic nature of some small molecules, known to facilitate membrane binding and nucleophile availability.[28,65–68] Subtle structural and functional characteristics must therefore play a role in controlling reactivity. Identifying structural and functional trends influencing small molecule intrinsic lipidation is challenging considering the diverse range of molecules tested thus far. An alternative approach subdivides small molecules into reactivity families for study. Each reactivity family differs by a single structural or functional feature, providing insight into the distinct role of that feature in influencing reactivity.

Cationic amphiphilic small molecules contain two distinct functional regions: (i) a hydrophobic aromatic ring; (ii) a hydrophilic region containing a protonated amine at physiological pH. Reactivity family design incorporated modifications to both regions, including modifying the aromatic ring, differing nucleophile type, and altering nucleophile position relative to the aromatic ring. Reactivity comparison between small molecules within a reactivity family requires quantification, due to differing ionisation efficiencies between small molecule species. The initial *in vitro* screen for small molecule intrinsic lipidation under physiological conditions discussed during Chapter 5 of this thesis, served to further highlight this need. Absolution quantification of acylated small molecules through calibration is unrealistic given time constraints and the multiple syntheses required. Introduction of a single acylated synthetic standard at known concentration into all samples provides an alternative semi quantitative approach. Addition of a standard with similar characteristics and ionisation efficiency to the acylated products of interest facilitates conversion approximation, eliminating dilution and instrumentation issues.[42,43] Study of reaction mixtures in triplicate further aids in anomaly identification, ensuring consistent results.

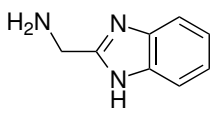

11

Figure 8.1 Compound **11**, selected as the small molecule core for preparation of an acylated synthetic standard.

Semi quantification of small molecule intrinsic lipidation was achieved by preparation of an acylated synthetic standard based upon core small molecule **11**, Fig. 8.1. Selection of compound **11** was based upon high levels of observed reactivity during preliminary intrinsic lipidation studies discussed during Chapter 5 of this thesis, combined with simplicity and flexibility of synthesis from readily available starting materials. Scheme 8.1 presents the proposed synthetic route for the preparation of an oleoylated standard of compound **11**, to be known as compound **67**.[177,178] Synthetic acylation with an oleoyl moiety provides the best ionisation efficiency mirror for acylated small molecules formed by intrinsic lipidation within dioleoyl phospholipid membranes. Preparation of compound **11** in high yield and purity was achieved despite slow reaction rate by refluxing glycine and *o*-phenylenediamine in concentrated HCl for 5 days. An alternative literature methodology for the preparation, boasting high product yield in the shorter reaction time of two hours, proved unsuccessful.[309] Compound **67** was prepared through reaction of compound **11** with acid chloride **20** under anhydrous conditions.[310] Purification of compound **67** by flash column chromatography yielded a yellow oil to be utilised as a synthetic semi quantification standard.

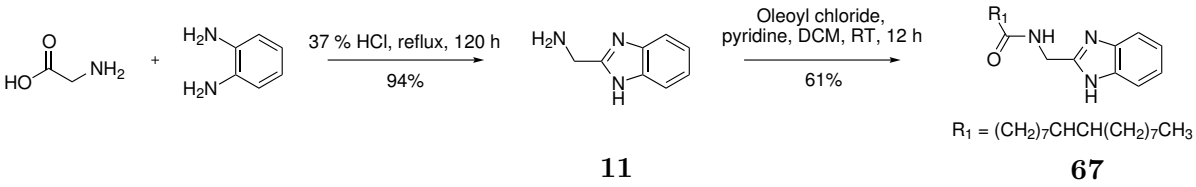

11 **67**

Scheme 8.1 Synthetic protocol for the preparation of acylated standard **67**.

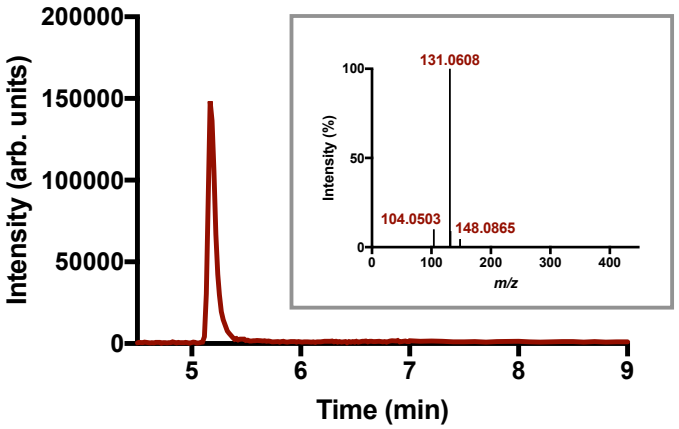

Figure 8.2 TIC of synthetically prepared acylated standard **67** under optimised LCMS conditions. Inset shows fragmentation pattern following CID MSMS of the molecular ion of acylated standard **67** of m/z 412.3324.

Stock solution of synthetic acylated standard **67** at concentration 1 µg mL^{-1} was prepared in MeCN:H_2O (1:1), and studied under optimised intrinsic lipidation analytical conditions.

Analysis revealed a chromatographic peak at retention time 5.2 min corresponding to singly charged ion *m/z* 412.3324, Fig. 8.2. Ion *m/z* 412.3324 can be attributed to molecular formula $C_{26}H_{42}N_3O$ with 0.9 ppm error, corresponding to the $[M+H]^+$ ion of acylated standard **67**. CID MSMS of molecular ion *m/z* 412.3324 revealed fragmentation into low abundance ion *m/z* 148.0865 of molecular formula $C_8H_{10}N_3$, corresponding to the $[M+H]^+$ ion of precursor small molecule **11**. Major CID MSMS product ion *m/z* 131.0608 can be attributed to molecular formula $C_8H_7N_2$ with 0.9 ppm error. Combined with a RDB value of 6.5, this product ion is predicted to result from cleavage at the CH_2-N bond proximal to the amide functionality.

8.2.1 Modification to Hydrophobic Regions

Successful synthesis and analysis of acylated standard **67** provides methodology for semi quantitative study of reactivity families, designed to probe the influence of a single feature upon intrinsic lipidation. Reactivity family one focussed on modification to the hydrophobic portion of cationic amphiphilic small molecules, altering the aromatic ring. This aromatic modified reactivity family, Fig. 8.3, was compiled from available small molecules in order to avoid further synthetic preparation. Six aromatic ring types are represented within the family: (i) benzene ring **68**; (ii) naphthol ring **69**; (iii) indoles **4** and **5**; (iv) imidazoles **49** and **70**; (v) benzimidazoles **45** and **71**; (vi) triazole **72**. Beyond aromatic variation, highlighted red in Fig. 8.3, small molecules within the family consistently contain a ring bound nucleophilic amine, highlighted green. Selection of a reactive amine in favour of an alcohol or thiol moiety is due to prevalence in marketed pharmaceuticals, proven reactivity record, and favourable matching with the electrophilic phospholipid ester. Indole, imidazole and benzimidazole rings are doubly represented within the reactivity family, localising the nucleophilic amine at differing positions relative to the hydrophilic nitrogen rich portions of these particular aromatic rings.

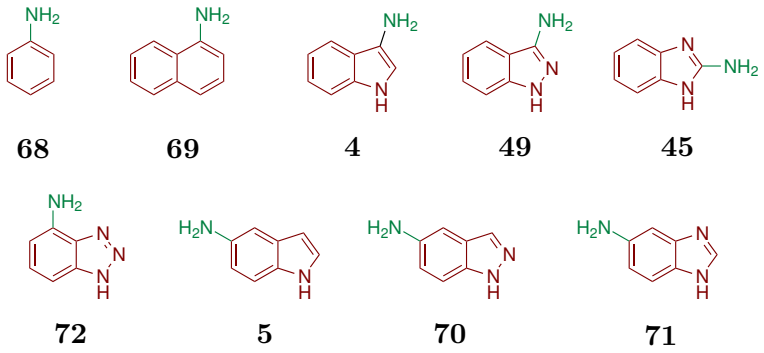

Figure 8.3 Family of small molecules prepared to study the influence of ring type upon small molecule intrinsic lipidation.

Reactivity family members were incubated under physiological conditions for 72 hours in triplicate with three liposomal membrane models, eukaryotic (DOPC), viral (DOPC:DOPS 4:1), and prokaryotic (DOPE:DOPG 3:1). Following addition of 1.25 µL of acylated standard **67** stock solution, samples were analysed under optimised chromatographic and ionisation conditions. Analyses did not reveal acylated product formation above the limit of instrument detection for any members of reactivity family one. Predicting the reasons behind this observed lack of reactivity is challenging due to the complexity of small molecule intrinsic lipidation. Family members exhibit differing physical parameters including pK_a, logP and logD values summarised in Table 8.1. However despite variation in logD from 0.23 (compound **71**) to 2.13 (compound **69**), and in pK_a from 3.00 (compound **72**) to 6.93 (compound **45**), lack of reactivity is retained for all small molecules studied. The sole consistent family feature, positioning of the nucleophilic amine directly on the aromatic ring, provides one theory to explain lack of reactivity. MDS and linear dichroism (LD) studies predict deep membrane penetration for small molecules within reactivity family one, even those comprised of a heterocyclic aromatic ring.[156,158] Residing with the hydrophobic bilayer region, and with limited flexibility, reactive amine moieties would be expected to have limited proximity to phospholipid ester linkages in order to facilitate intrinsic lipidation.

Small Molecule	pK_a	logP	logD (pH 7.4)
68	4.64	1.14	1.14
69	4.13	2.13	2.13
4	5.31	1.55	1.53
49	3.72	1.46	1.46
45	6.93	1.15	0.72
72	3.00	0.96	0.96
5	4.94	0.85	0.85
70	3.74	0.65	0.65
71	6.10	0.28	0.23

Table 8.1 Calculated physicochemical properties of small molecules in reactivity family one, studied to determine the influence of aromatic ring type upon intrinsic lipidation.[262]

8.2.2 Modification to Hydrophilic Regions

Investigating the impact of a modified hydrophobic aromatic ring region upon intrinsic lipidation reactivity resulted in limited success. Theory suggests the lack of reactivity is due to membrane binding orientation, combined with limited motion of the hydrophilic nucleophile. Accordingly, it can be concluded that the aromatic region of cationic amphiphilic small

molecules plays only a minor role in controlling intrinsic lipidation. As a result, attention was turned to modification of the hydrophilic region of membrane binding small molecules in order to understand the relationship between molecular structure, functionality, and intrinsic lipidation. Given the heightened complexity within the hydrophilic region compared to its hydrophobic counterpart, modifications to this area require further subdivision. Three families form the basis of study, investigating nucleophile position on the aromatic ring, nucleophile displacement from the aromatic ring, and nucleophile type.

8.2.2.1 Nucleophile Displacement

Limited nucleophile flexibility may be one possible cause of diminished reactivity observed during the study of reactivity family one. Further investigation of this theory can be achieved by modifying nucleophile displacement from the aromatic ring, through altered carbon linker length. Resulting changes to nucleophile movement and membrane bound orientation are predicted to aid in promoting intrinsic lipidation by facilitating proximity of reactive functionalities. Reactivity family two, Fig. 8.4, aims to probe this theory by building upon two unreactive small molecules present in reactivity family one. Unreactive indole **4** undergoes a linker length increase of one carbon in compound **73**, and three carbons in **56**. Similarly, benzimidazole **45** is joined by counterparts **11** and **58**, with linker lengths of one and three carbons respectively. Indole and benzimidazole cores were selected as a subset of reactivity family one due to time constraints and compound availability.

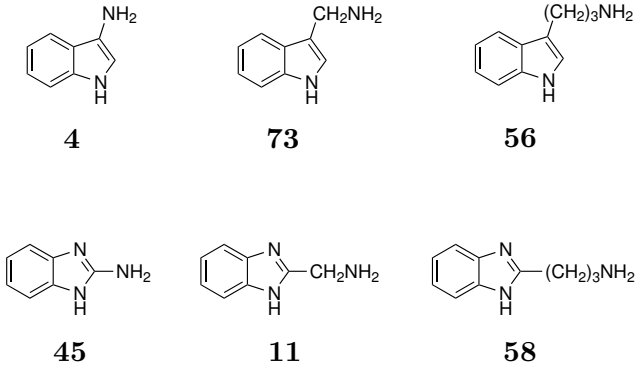

Figure 8.4 Family of small molecules prepared to study the influence of nucleophile displacement upon small molecule intrinsic lipidation.

Reactivity family members were incubated under physiological conditions for 72 hours in triplicate with three liposomal membrane models, eukaryotic (DOPC), viral (DOPC:DOPS 4:1), and prokaryotic (DOPE:DOPG 3:1). Following addition of 1.25 µL of acylated standard

67 stock solution, samples were analysed under optimised chromatographic and ionisation conditions. Exception to the addition of acylated standard **67** is applied in the case of benzimidazole **11**, in which the desired intrinsic lipidation product is identical to the synthetic acylated standard. Samples containing compound **11** were analysed both with and without addition of acylated standard **67**, in order to distinguish between innate reactivity and the internal standard.

Intrinsic lipidation is not observed for small molecules **4**, **73** and **56**, containing an indole core. Mirroring observations made during the study of reactivity family one, benzimidazole **45** similarly does not exhibit acylated product formation. However, analysis of benzimidazole **11** containing a single carbon linker, reveals a chromatographic peak at retention time 5.2 min corresponding to *m/z* 412.3328 with 0.0 ppm error. Molecular formula $C_{26}H_{42}N_3O$ attributed to this ion is consistent with oleoylation of benzimidazole **11** by intrinsic lipidation. Furthermore, analysis of benzimidazole **58** containing a three carbon linker, reveals a chromatographic peak at retention time 5.2 min corresponding to *m/z* 440.3630 with -1.4 ppm error. Corresponding molecular formula $C_{28}H_{46}N_3O$ suggests that this represents the molecular ion of intrinsic lipidation product oleoylated benzimidazole **58**. CID MSMS of the two oleoylated benzimidazole species results in dissociation of the amide bond, producing analogous spectra to that of acylated standard **67**, presented in Fig. 8.2. Intrinsic lipidation of benzimidazoles **11** and **58** in comparison to unreactive **45**, supports the hypothesis that nucleophilic flexibility aids in promoting reactivity by facilitating proximity of reactive functionalities. Reactivity is observed despite negative logD values at physiological pH, Table 8.2, indicating reduced membrane affinity of benzimidazoles **11** and **58** compared to their unreactive counterpart benzimidazole **45**. Furthermore, increased pK_a values of 12.24 and 11.91, attributed to benzimidazoles **11** and **58** respectively, suggest species exist in predominantly in the ionised form, expected to limit reactivity. These observations, combined with the unreactive nature of indole species **73** and **56**, suggests the relationship between nucleophile displacement and intrinsic lipidation reactivity is not straightforward. Reduced logD values combined with a predicted increase in membrane penetration of indoles compared to benzimidazoles, may provide a barrier to direct reactivity of nucleophilic amine residues, which cannot be overcome by increased nucleophile displacement.[156] Alternatively, solution phase chemistry predicts that acylation of benzimidazole species follows distinct pathway compared to their indole counterparts. Application of solution phase observations to membrane studies suggests intrinsic lipidation proceeds via initial reactivity of nitrogen within the aromatic heterocycle, followed by swift intramolecular rearrangement into the observed product.[311,312] This mechanism adds

complexity to the benzimidazole intrinsic lipidation compared to indole counterparts, and provides an explanation for observed reactivity variation.

Small Molecule	pK_a	logP	logD (pH 7.4)
4	5.31	1.55	1.53
73	10.16	1.88	-1.04
56	10.63	1.81	-1.18
45	6.93	1.15	0.72
11	12.24	0.87	-0.25
58	11.91	1.68	-0.97

Table 8.2 Calculated physicochemical properties of small molecules in reactivity family two, studied to determine the influence of aromatic ring type upon intrinsic lipidation.[262]

Chromatographic peak areas corresponding to oleoylated benzimidazole products of intrinsic lipidation within DOPC liposomes are presented in Table 8.3. Normalisation of peak areas as a percentage of internal synthetic standard peak areas are also presented. Resulting analysis concludes that the relationship between nucleophile displacement from a benzimidazole ring, and reactivity towards intrinsic lipidation is not proportional. Despite containing a three carbon linker of increased flexibility, benzimidazole **58** exhibits a 14 % normalised peak area corresponding to acylated product, compared to 45 % for benzimidazole **11**, containing a single carbon linker. Explanation for this observation can be derived if the increased linker length of benzimidazole **58** facilitates penetration of the nucleophilic amine into the hydrophilic bilayer region. Favourable electrostatic interactions within this region retain the nucleophile such that proximity to reactive phospholipid ester linkages is reduced. Alternatively, assuming benzimidazole acylation proceed by an intramolecular migration pathway, decreased product formation could be attributed to altered migration rate.

Small Molecule	Acylated Small Molecule Peak Area	Proportion of Internal Standard
45	0	0 %
11	2895.39	45 %
58	1460.00	14 %

Table 8.3 Raw peak area data, and normalised peak area as a proportion of internal standard peak area, for acylated derivatives of reactivity family two members. Data based upon LCMS analysis following 72 hour incubation under physiological conditions with a DOPC membrane.

Benzimidazoles **11** and **58** undergo intrinsic lipidation within viral DOPC:DOPS (4:1) and prokaryotic DOPE:DOPG (3:1) membrane systems, in addition to eukaryotic DOPC. Nor-

malised peak areas relative to an internal standard corresponding to acylated product are presented for each membrane system in Table 8.4. Increased reactivity of benzimidazole **11** compared to increasingly flexible **58** is retained between membrane systems studied. However, differing membrane dependent reactivity patterns are evident between the two benzimidazole species. Compound **11** maximum reactivity within the eukaryotic DOPC membrane, followed by DOPC:DOPS (4:1), and lest reactive DOPE:DOPG (3:1). In contrast, compound **58** exhibits reduced reactivity within the DOPC membrane compared to the equally reactive DOPC:DOPS (4:1) and DOPE:DOPG (3:1) systems. Reactivity differences are hypothesised to result from molecule specific alterations to intrinsic physical properties such as logP and binding orientation, in the presence of negatively charged phospholipids.

Membrane Composition	Peak Area Acylated **11**	Peak Area Acylated **58**
DOPC	45 %	14 %
DOPC:DOPS (4:1)	29 %	19 %
DOPE:DOPG (3:1)	23 %	19 %

Table 8.4 Normalised peak area, reported as a proportion of internal standard peak area, for oleoylated derivatives of benzimidazoles **11** and **58**. Data based upon LCMS analysis following 72 hour incubation under physiological conditions with membrane systems: (i) DOPC; (ii) DOPC:DOPS (4:1); (iii) DOPE:DOPG (3:1).

8.2.2.2 Nucleophile Position

Observed small molecule intrinsic lipidation of benzimidazoles **11** and **58** is facilitated by a nucleophilic amine localised close to hydrophilic ring nitrogens. Insight into structural influences on intrinsic lipidation can be achieved by probing preservation of reactivity upon nucleophile relocation to alternative ring positions. Given the unavailability of suitable benzimidazole species, a family of chemically similar imidazole species, Fig. 8.5, provide an alternative canvas for study. These indazoles exhibit similar hydrophobicity/hydrophilicity balance, intramolecular migratory activity, and nucleophile displacement, as the reactive benzimidazole species. Furthermore, study is simplified by similar physical properties attributed to all indazole species within the family, including logP, logD, and pK_a values summarised in Table 8.5. Reactivity family three indazoles differ by nucleophilic amine localisation, small molecule **46** is substituted at position 3, **74** at position 4, and subsequently compounds **75**, **76** and **6** at positions 5, 6, and 7 respectively.

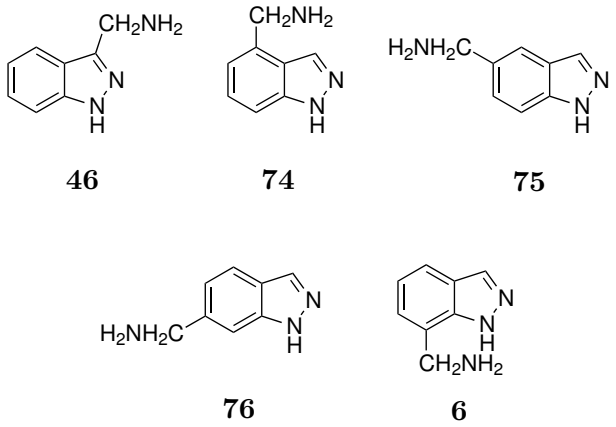

Figure 8.5 Family of small molecules prepared to study the influence of nucleophile position upon small molecule intrinsic lipidation.

Small Molecule	pK_a	logP	logD
46	8.16	0.83	-0.61
74	8.78	1.09	-0.94
75	8.91	0.96	-1.12
76	8.89	1.09	-0.98
6	8.99	1.19	-1.01

Table 8.5 Calculated physicochemical properties of reactivity family three small molecules, predicted to influence small molecule intrinsic lipidation.[262]

Reactivity family members were incubated under physiological conditions for 72 hours in triplicate with three liposomal membrane models, eukaryotic (DOPC), viral (DOPC:DOPS 4:1), and prokaryotic (DOPE:DOPG 3:1). Following addition of 1.25 µL of acylated standard **67** stock solution, samples were analysed under optimised chromatographic and ionisation conditions. Intrinsic lipidation of reactivity family three indazoles was observed for all species irrespective of membrane composition. Table 8.6 summarises retention time and accurate mass data for the observed oleoylated products of intrinsic lipidation, corresponding to molecular formula $C_{26}H_{42}N_3O$. Mass error of < 4.5 ppm is noted for observed products, consistent with instrument accuracy considering low species abundance. Chromatographic analysis suggests comparable retention times for all oleoylated product species, unsurprising considering their structural and function similarities. Retention time similarities within the small molecule family are reflected within analysis of the relevant parent indazoles.

Small Molecule	R.T. (min)	Observed *m/z*	Error (ppm)	Molecular Formula	RDB
46	6.3	412.3321	-1.7	$C_{26}H_{42}N_3O$	7.5
74	6.2	412.3310	-4.4	$C_{26}H_{42}N_3O$	7.5
75	6.4	412.3332	-3.2	$C_{26}H_{42}N_3O$	7.5
76	6.2	412.3311	-4.1	$C_{26}H_{42}N_3O$	7.5
6	6.5	412.3318	-2.4	$C_{26}H_{42}N_3O$	7.5

Table 8.6 Analytical data corresponding to molecular ions of oleoylated derivatives of compounds **46**, **74**, **75**, **76** and **6**, formed by intrinsic lipidation.

Small Molecule	Acylated Product Peak Area	Proportion of Internal Standard
46	700.00	3 %
74	490.00	2 %
75	333.33	4 %
76	416.67	6 %
6	1929.05	25 %

Table 8.7 Raw peak area data, and normalised peak area as a proportion of internal standard peak area, for acylated derivatives of reactivity family three members. Data based upon LCMS analysis following 72 hour incubation under physiological conditions with a DOPC membrane.

Despite observed intrinsic lipidation of all family three indazoles, the extent of reactivity differs between species. Differential reactivity is highlighted by absolute and normalised peak areas of acylated small molecule products of intrinsic lipidation, presented in Table 8.7. Indazole **6** exhibits heightened reactivity levels within the DOPC membrane compared to other family members, with a normalised peak area of 25 %. Substituted at position 7, indazole **6**'s nucleophile is localised on the hydrophilic ring face, facilitating membrane bound proximity to phospholipid ester linkages. Indazole **76**, substituted at position 6, exhibits the second highest normalised product peak area at 6 %. Nucleophile localisation within compound **76** is at a hydrophobic/hydrophilic ring interface, lowering reactivity compared to indazole **6**. Further family reactivity can be characterised by the trend **75** > **46** > **74**. However, normalised peaks areas for these species are comparable due to limited product abundance, thus the observed trend may prove inaccurate. Low reactivity of species **74** and **75** is unsurprising considering their nucleophile localisation on the hydrophobic indazole face, penetrating the hydrophobic tail bilayer region and reducing phospholipid ester proximity. Diminished reactivity of indazole **46** proves more surprising considering the proximity of substitution position 3 to hydrophilic ring nitrogens. Hypothetically, this observation could be explained by assuming indazole membrane binding occurs such that ring position 3 is oriented away from the phospholipid

head groups and glycerol backbone. This proposed orientation would also facilitate indazole **6** reactivity, however literature data to support or disprove the theory is unavailable.

Reactivity family three species also undergo intrinsic lipidation within viral DOPC:DOPS (4:1) and prokaryotic DOPE:DOPG (3:1) liposomal systems, with normalised peak areas presented in Table 8.8. The observed relationship between membrane composition and reactivity is consistent across the indazoles studied, with increased reactivity observed within the prokaryotic membrane, followed by the viral, and finally the eukaryotic. Favourable intrinsic lipidation within prokaryotic model systems proves particularly interesting, providing a possible mechanism of action for previously described antimicrobial activity of these small molecules. Increased reactivity in the presence of negatively charged membrane lipids can be attributed to a number of factors including modified membrane properties, altered indazole logP, or binding orientation changes. Furthermore, the relative reactivity rates of family three indazoles remains largely consistent across the three membrane systems studied. Indazole **6**, substituted at position 7, consistently exhibits the highest reactivity levels, followed by indazole **76**, substituted at position 6. Indazoles **46**, **74** and **75** indicate similarly low reactivity levels across the membrane systems studied, although their relative reactivity order is membrane specific. Reactivity observations made within viral and prokaryotic membranes serve to support the theory that membrane bound indazoles orient with the hydrophilic face proximal to phospholipid ester linkages, whilst directing substituents at ring positions 3, 4, and 5 towards the hydrophobic bilayer region.

Small Molecule	Peak Area DOPC	Peak Area PC:PS	Peak Area PE:PG
46	3 %	7 %	10 %
74	2 %	9 %	16 %
75	4 %	8 %	12 %
76	6 %	13 %	17 %
6	25 %	61 %	108 %

Table 8.8 Normalised peak area, as a proportion of internal standard peak area, for acylated derivatives of reactivity family three members. Data based upon LCMS analysis following 72 hour incubation under physiological conditions three membrane systems: (i) DOPC; (ii) DOPC:DOPS (4:1); (iii) DOPE:DOPG (3:1).

8.2.2.3 Nucleophile Type

Small molecule reactivity families studied thus far have adopted an amine functionality as the nucleophilic residue primed to undergo intrinsic lipidation. Reactivity family four,

Fig. 8.6, based upon a core of reactive benzimidazole **11**, probes the influence of different nucleophilic functionalities upon intrinsic lipidation reactivity. Benzimidazoles **77** and **78** contain nucleophilic alcohol and thiol functionalities respectively, in place of the reactive amine of benzimidazole **11**. The alcohol functionality is both a poor nucleophile and poor match to the hard phospholipid ester compared to an amine, predicting a reduction in intrinsic lipidation reactivity. Thiol reactivity is less predictable, as despite being a highly reactive nucleophile compared to an amine, the soft thiol nature provides a poor match to the electrophilic phospholipid carbonyl. Furthermore, the added capability of thiols to undergo disulphide bond formation may provide a further challenge to intrinsic lipidation reactivity. Additional members of reactivity family four, benzimidazoles **79**, **80**, **81** and **82** retain an amine nucleophile with methyl, ethyl, propyl and isopropyl substitutions respectively. Modification of the reactive nucleophile from a primary to secondary amine introduces steric hindrance as a barrier to reactivity.

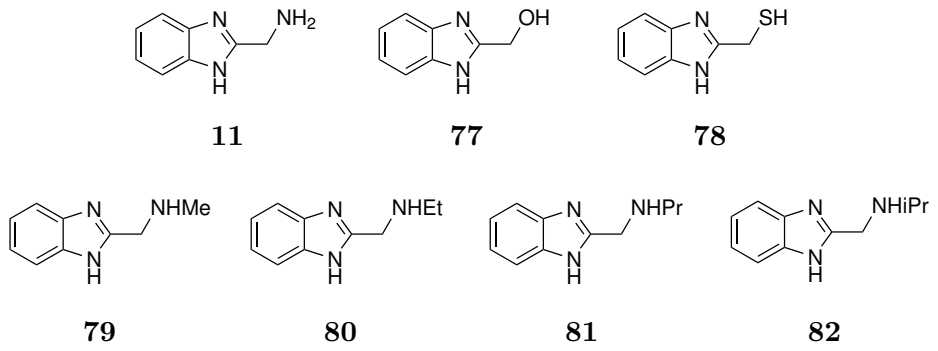

Figure 8.6 Family of small molecules prepared to study the influence of nucleophile type upon small molecule intrinsic lipidation.

Benzimidazoles **11** and **77** are readily available, however other members of reactivity family four require synthetic preparation prior to study. Secondary amines **79**, **80**, **81**, and **82** can be prepared using a single generic methodology depicted in Scheme 8.2. Chlorinated intermediate **83** was prepared using analogous methodology to that developed for the synthesis of acylated standard **67**, refluxing *o*-phenylenediamine with chloroacetic acid.[313,314] Product **83** was collected by precipitation following addition of aqueous ammonium hydroxide, and purified by recrystallisation from hexane. Bulk chlorinated intermediate **83** was then split into portions, and each reacted with the relevant alkyl amine, to yield benzimidazoles **79**, **80**, **81**, and **82**.[315,316] Products were purified as oils by Kugelrohr distillation.

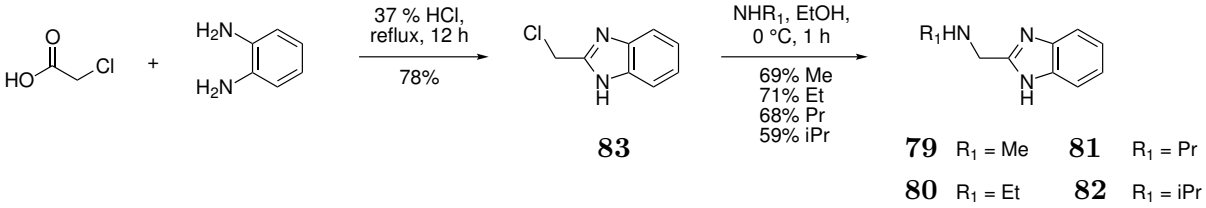

Scheme 8.2 Synthetic protocol for preparation of secondary amine containing benzimidazoles **79**, **80**, **81**, and **82**.

Preparation of thiol **78** follows the same methodology utilised during the synthesis of chlorinated intermediate **83**, and acylated standard **67**, as depicted in Scheme 8.3. *o*-phenylenediamine was refluxed with 2.4 equivalents of thioglycolic acid in 37 % HCl until TLC indicated full product conversion after 15 hours.[178,317] Benzimidazole **78** was isolated as the HCl salt following removal of water and recystallisation from methanol, minimising potential disulphide bond formation.

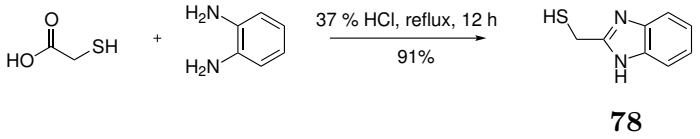

Scheme 8.3 Synthetic protocol for the preparation of benzimidazole **78** containing a thiol nucleophile.

Reactivity family members were incubated under physiological conditions for 72 hours in triplicate with three liposomal membrane models, eukaryotic (DOPC), viral (DOPC:DOPS 4:1), and prokaryotic (DOPE:DOPG 3:1). Following addition of 1.25 µL of acylated standard **67** stock solution, samples were analysed under optimised chromatographic and ionisation conditions. Alcohol containing **77** and thiol containing **78** were not observed to undergo intrinsic lipidation irrespective of membrane composition. Their soft nucleophilic natures provide poor matches to the hard electrophile of a phospholipid ester carbonyl, disfavouring reactivity. Furthermore, despite increased membrane affinity, exemplified by logD values presented in Table 8.9, reactivity may be diminished by altered binding orientation of neutral alcohol and thiol substituted benzimidazoles, compared to the cationic amine of benzimidazole **11** at physiological pH. Subscription to an intramolecular migratory pathway of benzimidazole acylation provides further unknown implications of amine exchange for a thiol or alcohol, dependent upon relative migration rates and product stabilities.

Small Molecule	pK_a	logP	logD (pH 7.4)
11	12.24	0.87	-0.25
79	11.49	0.89	-0.06
80	11.49	1.25	0.22
81	11.49	1.77	0.61
82	11.49	1.66	0.55
77	11.19	0.57	0.56
78	12.08	1.61	1.60

Table 8.9 Calculated physicochemical properties of small molecules in reactivity family four, studied to determine the influence of aromatic ring type upon intrinsic lipidation.[262]

Benzimidazoles **81** and **82**, containing secondary amines substituted with propyl and isopropyl groups respectively, did not exhibit reactivity irrespective of membrane composition. Diminished reactivity is attributed to reduced nucleophilic reactivity of the secondary amine due to steric hindrance, despite their increased logD values promoting membrane association. Altered binding orientation to prevent hydrophobic propyl substitutions penetrating the hydrophilic bilayer region, may also contribute to an observed lack of reactivity. However, in addition to known reactivity of primary amine **11**, secondary amines **79** and **80** exhibit product formation. Methyl and ethyl substituted respectively, **79** reacts within the DOPC system, whereas **80** undergoes intrinsic lipidation across all membrane compositions. Table 8.10 summarises relevant retention time and accurate mass data for oleoylated products of molecular formulae $C_{27}H_{44}N_3O$ and $C_{28}H_{46}N_3O$ respectively. Observed error is above normal instrument levels, however given a lack of alternative molecular formulae, this is attributed to low ion abundance. This lack of abundance also prevented analysis of the species by CID MSMS in order to confirm their identities. Peak area modelling and normalisation proved impossible due to areas being less than 100, preventing reactivity comparison between species or membrane types. Comparison to primary amine **11** indicates significant reactivity reduction within secondary amines **79** and **80**, assigned to the influence of steric hindrance and modified membrane binding orientation.

Small Molecule	R.T. (min)	Observed m/z	Error (ppm)	Molecular Formula	RDB
11	5.2	412.3328	0.0	$C_{26}H_{42}N_3O$	7.5
79	5.3	426.3465	-4.5	$C_{27}H_{44}N_3O$	7.5
80	5.0	440.3606	-7.9	$C_{28}H_{46}N_3O$	7.5

Table 8.10 Analytical data corresponding to molecular ions of oleoylated benzimidazoles **11**, **79**, and **80** formed by intrinsic lipidation

8.2.3 Towards the Synthesis of a Further Family

Membrane binding orientation has consistently been determined as a key influencer of small molecule intrinsic lipidation. Even functionalities remote from the reactive nucleophile of a cationic amphiphilic small molecule can promote interactions with membrane phospholipids, ultimately determining binding orientation. Study of membrane binding orientation is challenging due to its complexity, however one final reactivity family has been designed it an attempt to better understand its relationship with intrinsic lipidation. Reactivity family five, Fig. 8.7, is designed to include small molecules containing an aniline ring core comprised of both hydrophobicity and nucleophilic activity. One of three secondary amide substitutions is also present upon each aniline ring, arranged *ortho*, *meta*, and *para* relative to the nucleophilic aniline amine. Compounds **84**, **85**, and **86** are substituted with an aromatic benzene ring, favouring hydrophobic interactions with phospholipid acyl chains. Compounds **87**, **88**, and **89** contain a saturated 16 carbon palmitoyl substitution, designed to interact favourably with the hydrophobic phospholipid tail region. Finally, compounds **90**, **91**, and **92** are substituted with a quarternary methylated glycine moiety, facilitating electrostatic interactions with the phosphate head group region of a lipid bilayer. Differences in substitution properties combined with location relative to the reactive nucleophile is expected produce different binding orientations for each family five member, altering proximity of reactive moieties and local hydration levels.

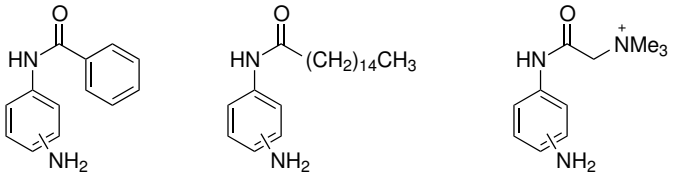

86	*ortho*	**89**	*ortho*	**92**	*ortho*
85	*meta*	**88**	*meta*	**91**	*meta*
84	*para*	**87**	*para*	**90**	*para*

Figure 8.7 Family of small molecules prepared to study the influence of membrane binding orientation upon small molecule intrinsic lipidation.

The complex nature of reactivity family five prevents purchase, instead synthetic methodologies must be designed to aid in preparation. Structural similarities within the family suggest development of a single general methodology applicable to all members to be the most efficient synthetic approach. Methodology was developed initially for compound **84**, prior to synthesis of other group members. Compound **84** excels as a method development model, due to its

para substituted ring providing favourable steric and electronic characteristics for substitution. Furthermore, benzoyl substitution requires only abundantly available commercial starting material benzoyl chloride.

Literature methodology applicable to the synthesis of compound **84** is presented in Scheme 8.4.[318] *p*-phenylenediamine reacts with benzoyl chloride in the presence of SDS, MeCN and H_2O producing a mixture of mono-substituted and di-substituted product. Isolation and purification of the desired mono-substituted product proved impossible due to poor product solubility and instability towards normal phase flash column chromatography. Modification of reaction conditions to reduce formation of di-substituted byproduct in order to simplify purification was attempted, as summarised in Table 8.11. Attempts proved unsuccessful in minimising di-substituted byproduct formation to either negligible levels or achieving complete eradication. Di-substituted byproduct formation was also observed for an alternative literature methodology reacting *p*-phenylenediamine with benzoyl chloride in the presence of NEt_3 and anhydrous DCM.[319] As a result, direct preparation of reactivity family five members from phenylenediamine precursors was not pursued further.

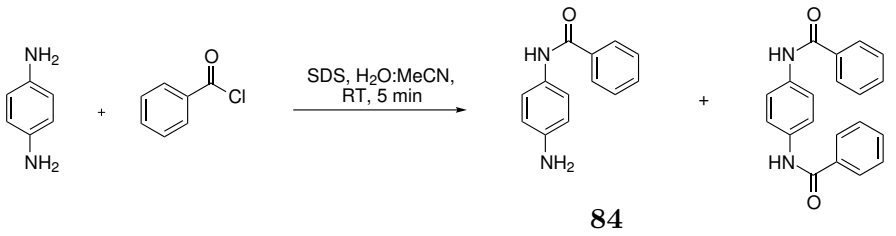

84

Scheme 8.4 Initial methodology employed for the preparation of compound **84**.

p-phenylenediamine (eq)	Reactive Carbonyl	Base	Solvent	Temp (°C)
1.0	Benzoyl Chloride	SDS	H_2O:MeCN (2:1)	20
1.0	Benzoyl Chloride	SDS	H_2O:MeCN (2:1)	0
1.0	Benzoyl Chloride	-	H_2O:MeCN (2:1)	20
1.0	Benzoic Anhydride	SDS	H_2O:MeCN (2:1)	20
1.0	Benzoic Anhydride	SDS	H_2O:MeCN (2:1)	0
1.0	Benzoic Anhydride	-	H_2O:MeCN (2:1)	20
10.0	Benzoic Anhydride	SDS	H_2O:MeCN (2:1)	20
1.0	Benzoic Anhydride	SDS	H_2O:MeCN (15:1)	20

Table 8.11 Experimental conditions tested for the preparation of compound **84** from *p*-phenylenediamine within 5 minute reaction time.

Modified methodology depicted in Scheme 8.5, was designed to avoid di-substituted byproduct formation by employing a Boc protecting group. Small scale synthetic conditions successfully produced singly Boc protected intermediate **93**, and subsequent benzolyated intermediate

94.[320] At this point, increased quantities of compound **93** stock were required for synthesis of other *para* substituted members of small molecule family five. However, scaled up preparation of Boc protected intermediate **93** proved challenging. Despite high levels of conversion, several equivalents of *p*-phenylenediamine starting material remain following reaction completion. Limited solubility of both *p*-phenylenediamine and intermediate **93** prevented successful purification by recrystallisation. Optimised normal phase flash column chromatography conditions avoiding coelution were not achieved on a large scale, resulting in inability to purify the product.

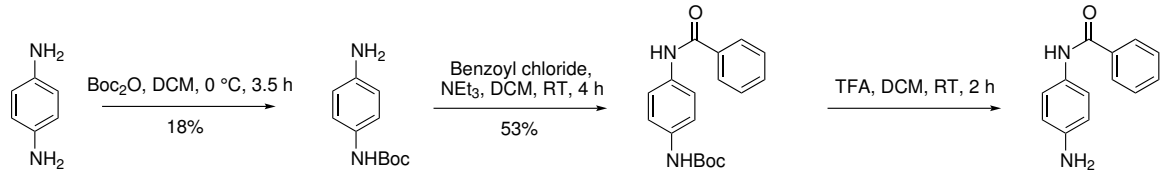

93 **94** **84**

Scheme 8.5 A second methodology designed for the preparation of compound **84**.

The third designed synthetic methodology, presented in Scheme 8.6, seeks to avoid di-substituted byproduct formation by employing *p*-nitroaniline as the starting material. Initially, *p*-nitroaniline was substituted with benzoyl chloride, resulting in isolation of intermediate **95** following recrystallisation from methanol.[321] The nitro functionality was then reduced into the desired amine moiety, successfully producing reactivity family member **84**. Three reduction methodologies were attempted in order to determine the optimum methodology.[320,321] Hydrogenation (H_2/Pd) produced the highest crude yield at 93 %, however product purification and isolation proved challenging. Several recrystallisation solvents including two phase recrystallisation failed to purify product **84**, whilst product instability upon extended silica exposure prevented use of preparative TLC or flash column chromatography. Reduction using Zn/AcOH resulted in a lower yield of 55 %, however the product did not contain impurities thus was deemed the preferred synthetic route.

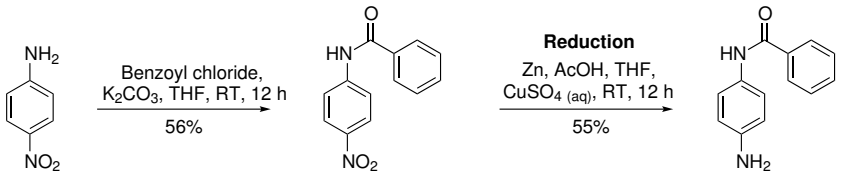

95 **84**

Scheme 8.6 The third methodology successfully designed for the synthetic preparation of compound **84**.

The successful synthetic methodology developed during the preparation of compound **84** was applied to benzoylated analogues **85** and **86**. Synthesis and subsequent purification proved

successful for both benzoylated species. *Ortho* substituted **86** exhibited lower product yields compared to *meta* and *para* analogues, attributed to steric crowding limiting amide formation in close proximity to the bulky nitro moiety. The synthetic methodology was also applied to the preparation of palmitoylated counterparts **87**, **88** and **89**. Palmitoyl chloride prepared under anhydrous conditions from palmitic acid and oxalyl chloride was utilised in place of benzoyl chloride. Successful synthesis and purification of all three species was achieved, with *ortho* analogue **89** exhibiting reducing yield due to steric hindrance.

Preparation of family members **90**, **91** and **92** using the optimised synthetic methodology proved challenging, due to the cationic quaternary glycine substitution. Initial preparation of relevant acid chloride **96** required quaternisation of glycine into betaine **97** using methyl iodide, as highlighted in Scheme 8.7.[322] Subsequent conversion of betaine **97** into acid chloride **96** proved unsuccessful due to incompatibility with standard conditions. Acid chloride alternative *N*-hydroxysuccinimide ester **98** was considered given the more favourable solvent systems required for synthetic preparation, however formation proved unsuccessful. Reactivity issues are attributed to the cationic nature of betaine **97**, therefore could be avoided by an altered order of synthetic steps, shown in Scheme 8.7. Given the zwitterionic nature of glycine, similar reactivity problems were experienced during preparation of acid chloride **99** as were observed for betaine **97**. Charge state issues were eliminated by preparation of acid chloride **100** under standard conditions from Fmoc protected glycine.[323] An additional deprotection step is therefore required as a future synthetic state, as demonstrated in Scheme 8.7.

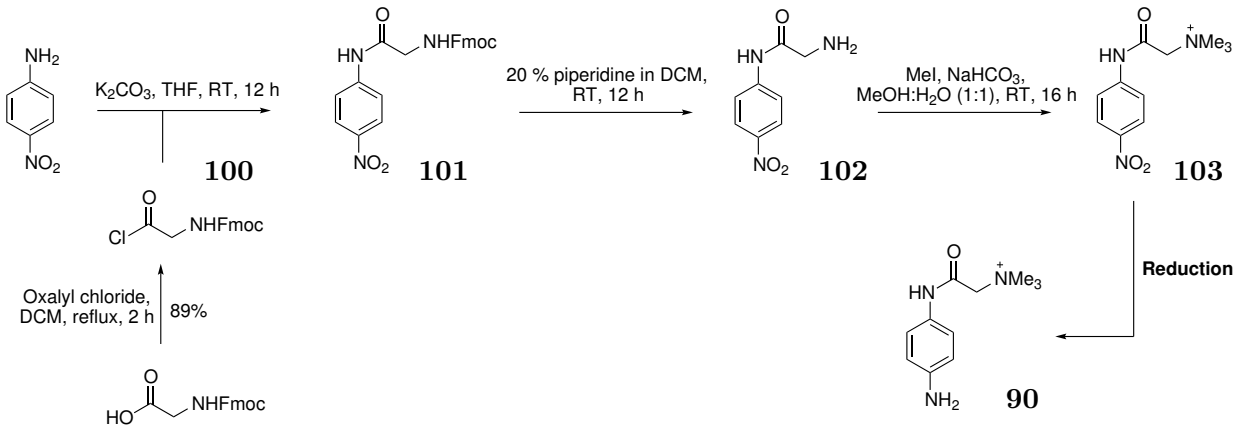

Scheme 8.7 Modified synthetic methodology proposed for the preparation of quaternary amine **90**. Analogous methodology is appropriate for preparation of *meta* and *ortho* analogues **91**, and **92**.

Acid chloride **100** was utilised during continuation of the proposed synthetic methodology depicted in Scheme 8.7, for the preparation of compounds **90**, **91**, and **92**.[321] Reactivity with *p*-nitroaniline, *m*-nitroaniline, and *o*-nitroaniline successfully yielded corresponding intermediates

101, **104**, and **105** respectively. Unfortunately due to time constraints purification and subsequent synthetic steps were not undertaken. Completion and testing of reactivity family five remains for future study of the relationship between intrinsic lipidation and small molecule membrane binding orientation.

8.3 The Phospholipidosis Link

Understanding intrinsic lipidation reactivity in relation to structural and functional small molecule features is a vital step towards incorporation into the pharmaceutical drug development process. The biological and pharmaceutical impact of reactivity is a further topic of interest for the drug development industry, considering the propensity of commercial drugs to be cationic amphiphilic and thus exhibit membrane affinity. Impacts on drug activity, efficacy, and the induction of side effects are key areas of interest. Commercial beta-blocker propranolol **1** is the sole pharmaceutical candidate studied and proved undergo intrinsic lipidation *in vitro*. In addition, propranolol **1** treatment is known to cause the phospholipid related side effect, drug induced phospholipidosis.[73–75] Phospholipidosis is a lysosomal storage disorder characterised morphologically, Fig. 8.8. Two mechanisms of action are predicted for the side effect:

1. Drug induced inhibition of phospholipase enzymes, resulting in reduced degradation and subsequent accumulation of excess phospholipids

2. Formation of an insoluble drug-phospholipid complex which proves challenging to degrade

The unclear mechanism of action leads to characterisation of drug induced phospholipidosis as a challenging drug side effect. Furthermore, inconsistencies in patient symptoms and lack of research make long term effects and treatment options for the side effect unclear.[271] Current prevention of drug induced phospholipidosis requires discontinuation of patient treatment by the pharmaceutical inducer, a problematic fact for both pharmaceutical companies and patients. Beyond propranolol **1**, over 50 FDA approved drugs are known to induce phospholipidosis, spanning a variety of classes and structures.[73] Cationic amphiphilicity is the sole unifying feature of affected drugs, highlighting the need for improved understanding.

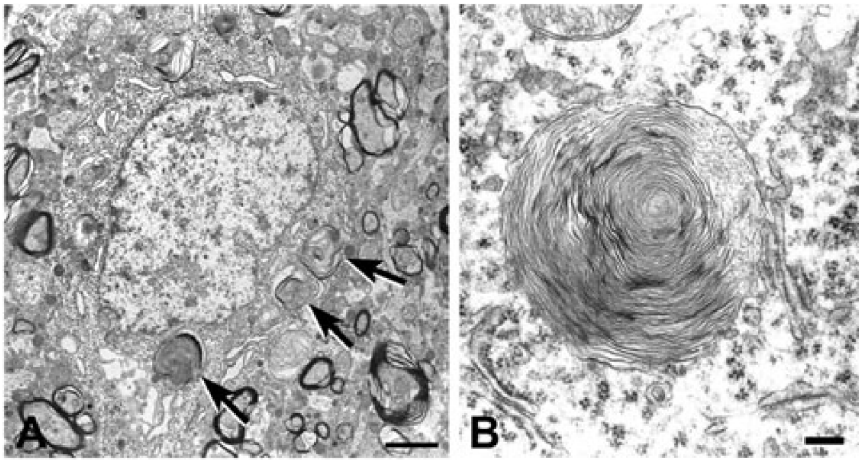

Figure 8.8 Electron micrographs of fluoxetine **106** treated cells exhibiting lysosomal bodies characteristic of drug induced phospholipidosis.[271] **A** shows several bodies highlighted with arrows (Bar = 2 µm), whereas **B** is a high powered view of a single lamellar body (Bar = 0.2 µm).

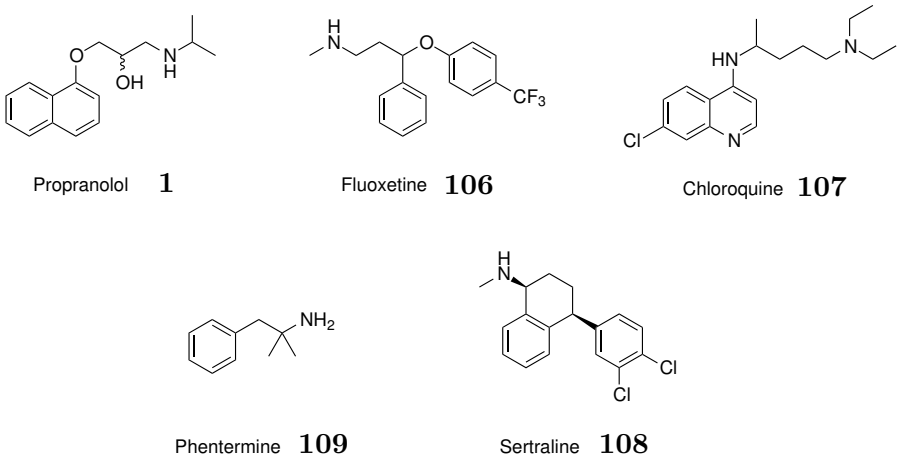

Figure 8.9 Small organic pharmaceuticals associated with the known side effect drug induced phospholipidosis.

Considering propranolol's **1** propensity towards both intrinsic lipidation and induction of phospholipidosis, a relationship between the two phospholipid derived processes may exist. Available cationic amphiphilic, phospholipidosis inducing pharmaceuticals were compiled in order to test this theory, Fig. 8.9. Pharmaceutical candidates selected span a range of classes and contain at least one nucleophilic residue primed to undergo intrinsic lipidation. Comparison of phospholipidosis induction can be achieved using NBD-PE assay EC_{50} values, the concentration of drug required to induce phospholipidosis in 50 % of cells.[324] For comparison, propranolol **1** has a measured EC_{50} value of 12.9 µM. Antimalarial chloroquine **107** exhibits low to moderate phospholipidosis induction, with an EC_{50} for phospholipidosis of 11.8 µM. Fluoxetine **106**, the active ingredient in antidepressent Prozac (Eli Lilly Ltd.), is known to

have a high EC_{50} for phospholipidosis of 4.2 µM. Antidepressant sertraline **108** is characterised as having a similarly high EC_{50} for phospholipids of 5.8 µM. Finally, appetite suppressant phentermine **109** induces phospholipidosis to a lesser extent with an EC_{50} for phospholipidosis of 314.7 µM.

Phospholipidosis inducing pharmaceuticals were incubated in 1:10 molar ratio with model liposomal membranes for 72 hours under physiological conditions. Eukaryotic DOPC, viral DOPC:DOPS (4:1), and prokaryotic DOPE:DOPG (3:1) liposomal systems were studied. Sample analysis under optimised conditions revealed a lack of reactivity for all pharmaceuticals other than propranolol **1**, irrespective of membrane system. Further analyses were conducted following 144 and 216 hour incubations, considering the relatively slow onset rate for drug induced side effect phospholipidosis, rate of intrinsic lipidation could also be slow. However, intrinsic lipidation was not observed for pharmaceuticals other than propranolol **1** at these later time points. Structural and functional complexity of the pharmaceutical candidates studied creates challenges in pinpointing underlying factors contributing to lack of reactivity. Limited information is available regarding interactions between these pharmaceuticals and membrane, including binding orientation which has proved vital in explaining observed small molecule reactivity previously.

Despite lack of acylated product formation during analysis of phospholipidosis inducing pharmaceutical species, consistently increased lysolipid levels were observed. Quantification of lysolipid concentration following 72 hours incubation of pharmaceutical small molecules with eukaryotic, viral, and prokaryotic membrane systems, was determined using a calibration curve prepared from synthetic standards. LCMS analysis was conducted in positive ionisation mode, facilitating visualisation of neutral OPC and OPE lysolipids only. Lysolipid concentrations for each membrane system are presented in Table 8.12. Lysolipid concentration variation was observed in viral and prokaryotic membranes treated with different small molecules, attributed either to differential small molecule interactions, or to analysis preventing visualisation of negatively charged lysolipids. By contrast, within the pharmaceutically relevant eukaryotic DOPC membrane, small molecules consistently increase lysolipid formation above background levels by up to 4 times. Intrinsic lipidation having been discounted for four small molecules, this observed increase in lysolipid can be attributed to phospholipid hydrolysis, a process known to be promoted in the presence of cationic amphiphilic small molecules.[28] Quantification of propranolol **1** species suggests the observed 89 pmol of OPC is above that predicted from the sum of lysolipid production as an intrinsic lipidation by-product (63 pmol) and through background hydrolysis (12 pmol). This observation further supports the theory that

pharmaceutical small molecules catalyse phospholipid hydrolysis, likely by acting as a general acid catalyst. Biologically, an alteration of membrane composition by addition of even 1 mol% lysolipid is noted to disrupt membrane stability and integrity, highlighting the relevance of this observation.[31] Additional implications are also predicted, including variation to propranolol **1** intrinsic lipidation, and potential links to drug induced phospholipidosis.

Small Molecule	DOPC (ng mL^{-1})	PC:PS (ng mL^{-1})	PE:PG (ng mL^{-1})
-	34.17	12.62	133.64
Propranolol **1**	40.49	17.49	419.04
Fluoxetine **106**	135.69	15.65	209.62
Chloroquine **107**	49.05	23.38	293.76
Sertraline **108**	104.25	10.14	90.77
Phentermine **109**	51.29	7.29	303.46

Table 8.12 Lysolipid concentrations observed upon incubation of pharmaceutical small molecules under physiological conditions for 72 hours with liposomal membrane models: (i) DOPC; (ii) DOPC:DOPS (4:1); (iii) DOPE:DOPG (3:1).

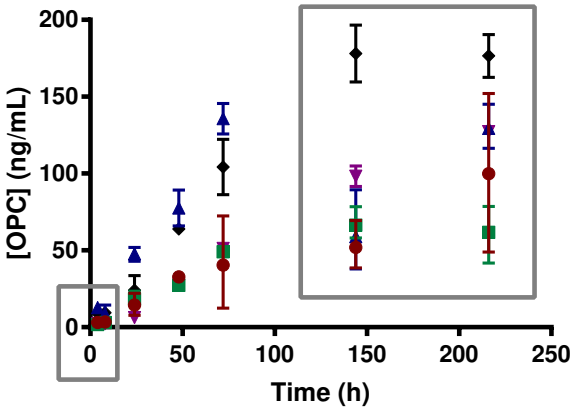

Figure 8.10 Concentration of OPC observed over 216 hour incubation of pharmaceutical small molecules with DOPC liposomes under physiological conditions, normalised by subtraction of background OPC hydrolysis in untreated DOPC liposomes: (i) propranolol **1** shown by red circles; (ii) fluoxetine **106** shown by blue triangles (iii) chloroquine **107** shown by green squares; (iv) sertraline **108** shown by purple inverse triangles; (v) phentermine **109** shown by black diamonds. Grey boxes highlight time periods exhibiting analytical challenges.

Considering the promotion of phospholipid hydrolysis observed within DOPC liposomes following 72 hours of exposure to phospholipidosis inducing small molecules, in depth study of the system was conducted. Analysis under optimised conditions was carried out at an increased number of time points, and lysolipid concentration quantified to give data presented in Fig. 8.10. Observed lysolipid concentrations in the presence of pharmaceutical small molecules are at the limit of instrument quantitation at time points up to 8 hours, preventing collection of meaningful data. Data collected at later time points 144 and 216 hours were also eliminated

from further consideration, due to data inconsistencies, combined with increased data error and differential small molecule behaviour. Furthermore, data at later time points requires caution due to loss of membrane integrity at high lysolipid concentrations, and potential reactivity between small molecules and lysolipids.

Exclusion of data prior to 8 hours and after 144 hours leaves three time points for continued study, 24, 48 and 72 hours. Lysolipid concentration is increased above background hydrolysis levels for all pharmaceutical species at these time points, however 24 hour data proves particularly interesting in relation to the study of phospholipidosis. Following 24 hour incubation, lysolipid concentration is observed to correlate with propensity of a given drug to induce phospholipidosis, as defined by its EC_{50} value. Exponential decay provides the optimum model curve for correlation of the two parameters, as shown in Fig. 8.11. Correlation provides a definitive relationship between lysolipid production and phospholipidosis consistent with literature findings.[28] Additional research is required in order to determined whether the correlation is due to direct causation or a side effect. Furthermore, the observed correlation, despite the small sample size, provides the basis for an assay predicting propensity of a drug candidate to induce phospholipidosis. Considering the unreliable and time consuming nature of current methodologies, a simplified alternative assay would aid significantly in the drug development process.

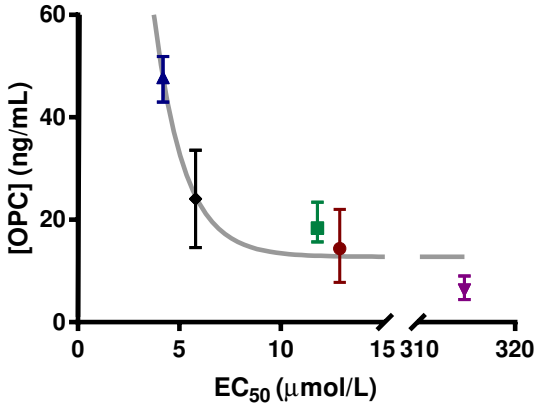

Figure 8.11 Graph correlating OPC concentration following 72 hour incubation under physiological conditions in the presences of a DOPC membrane, with EC_{50} values attributed to pharmaceutical molecules: (i) propranolol **1** shown by red circles; (ii) fluoxetine **106** shown by blue triangles (iii) chloroquine **107** shown by green squares; (iv) sertraline **108** shown by purple inverse triangles; (v) phentermine **109** shown by black diamonds. The solid grey line represents the fitted trend.

Highlighted in Fig. 8.12, phospholipidosis related lysolipids exhibit structural similarities to acylated small molecule products of intrinsic lipidation. Therefore, whilst not a requirement

for phospholipidosis induction, intrinsic lipidation products may be similarly related to the side effect. Hypothesising induction of phospholipidosis by lysolipids, acylated small molecules have the potential to adopt a similar mechanism of action, ultimately also inducing phospholipidosis. Identification of the mechanism of action for phospholipidosis induction could therefore be achieved by comparison of lysolipid and acylated small molecule properties. To further probe this theory, key properties of synthetically prepared *N*-palmitoyl propranolol **12** and *N*-oleoyl propranolol **13** were compared to those of lysolipids PPC and OPC. Lysolipids selected for study mirror common eukaryotic acyl chains present in acylated propranolol **1** analogues, incorporating a eukaryotic PC head group to ensure pharmaceutical relevance.

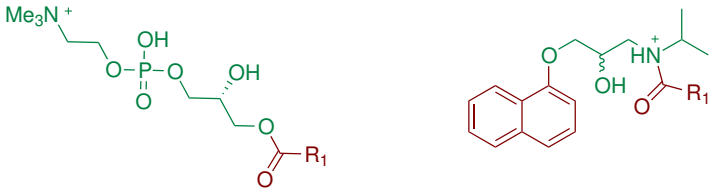

PPC R_1 = Palm

OPC R_1 = Oleo

12 R_1 = Palm

13 R_1 = Oleo

Figure 8.12 Structural and electronic similarities observed for lysolipids PPC and OPC, compared to *N*-acylated propranolol derivatives **12** and **13**. Palm represents the palmitoyl group $(CH_2)_{14}CH_3$ and oleo represents the oleoyl group $(CH_2)_7CHCH(CH_2)_7CH_3$. Hydrophobic regions are highlighted in red, and hydrophilic regions in green.

Membrane disruption is a known feature of increased lysolipid concentration, resulting in leakage of intracellular contents and, if severe, cell death. Comparison of membrane disruption properties of lysolipids and *N*-acylated propranolol species can be achieved using an 8-aminonapthalene-1,3,6 trisulfonic acid (ANTS)/*p*-xylene-bis-pyridinium bromide (DPX) assay.[325] Fluorescent ANTS and quencher DPX are trapped within a liposome, then external buffer is exchanged to remove ANTS and DPX from the medium outside vesicles. Membrane disruption, relative to positive control Tritron X-100, is measured by the observed fluorescence increase associated with ANTS leakage and dilution, removing DPX quenching. Three concentrations of each lysolipid or *N*-acylated propranolol were added to prepared liposomes, with proportions mirroring 1 %, 5 % and 100 % intrinsic lipidation product conversion. Assay data presented in Fig. 8.13, indicates that all species exhibit immediate membrane lysis and disruption of above 85 %. Comparable values are observed for both lysolipids and *N*-acylated propranolol species, and also for palmitoyl and oleoyl modifications. Increased proportion of lysolipid or *N*-acylated propranolol from 1 % to 5 % results in a corresponding increase in leakage % for all species. Further increase from 5 % to 100 % results in slightly decreased

leakage % for PPC, OPC and *N*-oleoyl propranolol **13**, attributed to competing micelle formation above species respective CMC. Membrane disruption assay results highlight the similar but significant impacts of both lysolipids and acylated small molecules upon membrane integrity. Membrane disruption therefore provides a potential mechanism of action for the induction of phospholipidosis by pharmaceutical species.

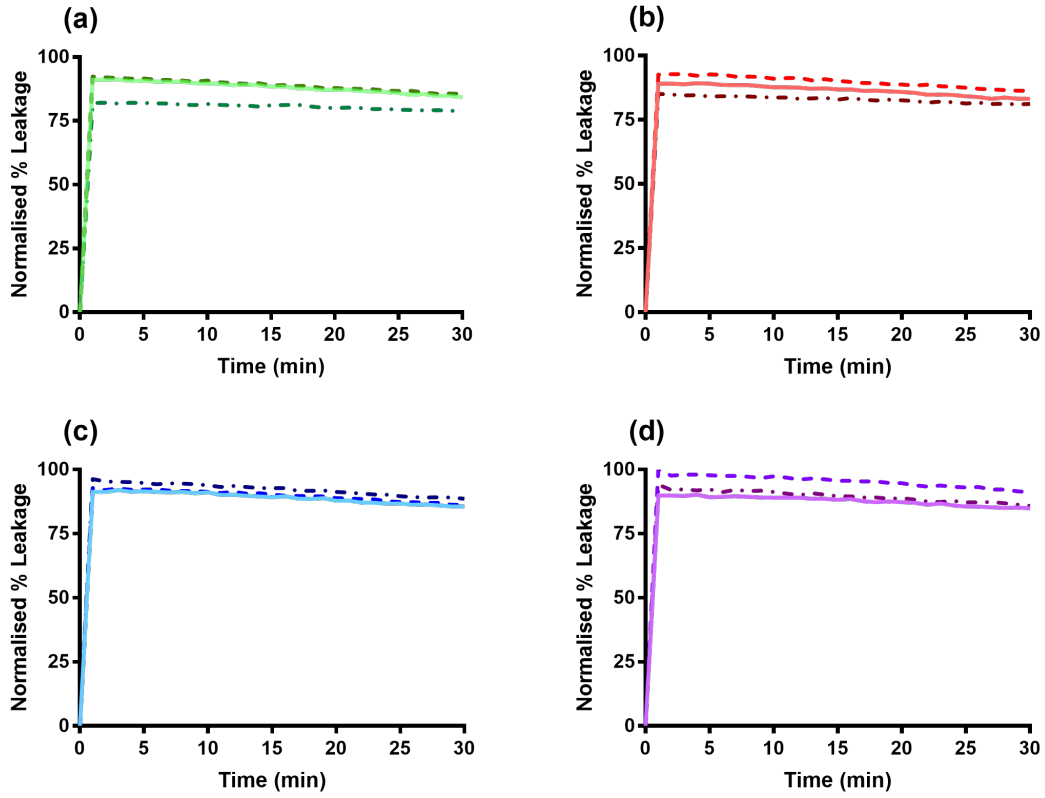

Figure 8.13 Normalised % leakage over 30 minutes for ANTS/DPX liposomes, treated under physiological conditions (pH 7.4 and 37 °C) with 1 mol% (solid lines), 5 mol% (dashed lines) and 100 mol% (dotted and dashed lines): (a) PPC; (b) OPC; (c) *N*-palmitoyl propranolol **12**; (d) *N*-oleoyl propranolol **13**.

Micelle formation is the known result of lysolipid self aggregation in aqueous solution above a CMC, and has been similarly hypothesised for *N*-acylated propranolol species. Determination of CMC, the critical concentration of molecules required for spontaneous micelle formation, can be achieved using a Rhodamine 6G assay.[326,327] Rhodamine 6G absorbs weakly at 542 nm in aqueous solution due to poor solubility, however absorption increases upon encapsulation within a hydrophobic micelle. Rhodamine 6G absorption was monitored over the concentration range 0.1 µM to 10 µM for PPC, OPC, *N*-palmitoyl propranolol **12** and *N*-oleoyl propranolol **13**. Calculated CMC values of 4 µM and 7 µM were obtained for PPC and OPC respectively, in agreement with literature values.[33,213,214] Data obtained through analogous study of *N*-

palmitoyl propranolol **12** and *N*-oleoyl propranolol **13** is presented in Fig. 8.14. Absorption increase suggests micelle formation for both species, with CMC values at graph minima determined as 10 µM and 9 µM respectively. Calculated lysolipid and acylated propranolol CMC values fall within the same concentration range, explaining their similar behaviour and providing a further mechanism of action for phospholipidosis induction.

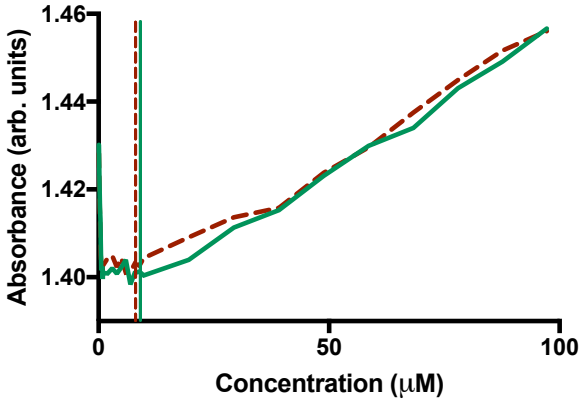

Figure 8.14 Rhodamine 6G absorbance in the presence of increasing concentrations of *N*-palmitoyl propranolol **12** (solid green line) and *N*-oleoyl propranolol **13** (red dashed line). Vertical lines indicate CMC values for each species.

8.4 Conclusions

Increased understanding of innate reactivity between membrane binding small molecules and phospholipids has been probed through study of structural and functional features of small molecules. Development or synthesis of reactivity families which differ in a single feature have facilitated study of the impact of that sole feature upon intrinsic lipidation. Synthetic preparation of acylated standard **67** has enabled studies to be conducted in a semi quantitative manner. Modification to the hydrophobic aromatic ring portion of small molecules did not result in observed reactivity, however alterations to the hydrophilic region proved more informative. Steric and electronic features favour primary amine nucleophiles for the promotion of intrinsic lipidation. Nucleophile flexibility and localisation on the hydrophilic face of the small molecule further aid in promoting reactivity with membrane phospholipids. Observations consistently point to membrane binding orientation and subsequent proximity between reactivity residues as key features in facilitating intrinsic lipidation. Synthetic methodology has been developed for preparation of a family of small molecules designed to test this feature, however time constraints have prevented analysis. LogP, pK_a, local hydration levels and membrane composition have also been noted to influence reactivity within the

families of small molecules studied. Ultimately, multiple influencing factors creates complexity in understanding the relationship of intrinsic lipidation with structural and functional features of small molecules.

Biological and pharmaceutical impacts of small molecule reactivity have been probed through study of commercial pharmaceuticals. Research has been conducted in reference to the poorly understood drug side effect phospholipidosis, a disorder resulting in phospholipid aggregation. Propranolol **1** was the only commercial pharmaceutical studied observed to undergo intrinsic lipidation, however all species promoted phospholipid hydrolysis in eukaryotic membrane models. Quantification and monitoring of lysolipid levels revealed a correlation between lysolipid concentration following 24 hour incubation, and phospholipidosis EC_{50}. This correlation proffers the basis for an improved commercial phospholipidosis assay, and provides insight into potential mechanisms of drug induced phospholipidosis. Structural similarities between lysolipids and acylated small molecules suggest analogous mechanisms of phospholipidosis induction may be possible for intrinsic lipidation products. Work directed towards understanding the mechanism of action revealed properties shared by lysolipids PPC and OPC, and acylated small molecules *N*-palmitoyl propranolol **12** and *N*-oleoyl propranolol **13**. Properties which may influence phospholipidosis onset include membrane disruption, and micelle formation above µM CMC values.

9 | Conclusion

The cell membrane is vital for cell survival, providing cell stability, integrity, and regulation of biological pathways. Chemical reactivity is an intriguing feature of the cell membrane, characterised by non-enzymatic acyl transfer from membrane phospholipids to nucleophilic membrane bound molecules. This reactivity, termed intrinsic lipidation, has been probed within this thesis for membrane active molecules including peptides, proteins, and novel reactive species, small molecules. Focus has been upon probing reactivity, in order to increase fundamental and mechanistic understanding of intrinsic lipidation, through analytical method development and kinetics studies. In tandem, biological and pharmaceutical implications of intrinsic lipidation have been investigated by employing biophysical techniques, *in cellulo* study, and disease relevant reactive species.

Effective study of intrinsic lipidation has been facilitated through development of informative and robust analytical techniques. Solution state NMR, fluorescence spectroscopy, and TLC have been investigated for routine high throughput screening of intrinsic lipidation. TLC was identified as the optimum technique, and suitable solvent system and visualisation conditions determined in reversed and normal phase for small molecule intrinsic lipidation. Routine monitoring of peptide intrinsic lipidation proved challenging by TLC, fluorescence and solution state NMR due to concentration deficiencies. Informative intrinsic lipidation analysis provided by current LCMS methodology can be supplemented with complementary ssNMR data. Preliminary screening indicated concentration limitations, resulting in the need for isotopically labelled substrates. To this end, synthetic protocols have been developed for successful preparation of ^{15}N propranolol **1**, and ^{13}C labelled phospholipids DOPC and DPPC. Preparation of labelled palmitoyl and oleoyl moieties have been attempted, towards POPC synthesis, however further synthetic development is required due to the challenging nature of alkyl bond formation.

Biological relevance of peptide intrinsic lipidation has been probed in order to determined

the role of reactivity in natural peptide function or disease induction. Biophysical techniques were applied to four acylated derivatives of model peptide melittin, *N*-palmitoyl melittin, K23-palmitoyl melittin, *N*-oleoyl melittin, and K23-oleoyl melittin. Solution phase α-helical structure with central proline kink was attributed to all acylated melittin derivatives by CD and tryptophan fluorescence, in contrast to the random coil of solution phase melittin. Furthermore, spontaneous micelle formation is observed for *N*-palmitoyl melittin and K23-palmitoyl melittin above CMC of 1 µM and 5 µM respectively. Antimicrobial activity against *E. coli* and *S. aureus* is diminished upon acylation of melittin, particularly in the case of K23 and oleoyl modifications. Disease relevance of peptide intrinsic lipidation has been probed using amyloids amylin, amyloid β, and β2-microglobulin. Thioflavin T assays and EM confirm amyloid aggregation under standard peptide intrinsic lipidation conditions, suggesting a link between acylation and amyloid nucleation. Attempts to diminish aggregation using low salt, low temperatures, and sonication proved unsuccessful over the time period of study. Furthermore, amyloid deaggregation by formic acid, HFIP, and enzymatic digestion were explored with limited success. Further technical development is required in order to visualise intrinsically lipidated amyloids, definitively proving a link between reactivity and amyloid nucleation.

Novel reactivity at the membrane interface has been identified through small molecule intrinsic lipidation. Study, facilitated by LCMS optimised using synthetically prepared acylated standards, reveals acyl transfer to multiple cationic amphiphilic small molecules *in vitro*. Reactivity is observed across multiple membrane models, including eukaryotic, viral, and prokaryotic systems. Small molecule families, prepared to study the implications of molecular structure and functionality upon reactivity, suggest reactivity is promoted by primary amine nucleophiles on the hydrophilic small molecule face. Favourable binding orientation, promoting proximity between reactive phospholipid and small molecule moieties, is predicted to drive reactivity. However, the complex nature of intrinsic lipidation suggests multiple additional and competing factors impact reactivity, including $\mathrm{p}K_\mathrm{a}$, localised hydration levels, and nucleophile mobility.

Several current pharmaceuticals are characterised as nucleophile containing and cationic amphiphilic, suggesting a propensity towards intrinsic lipidation. Many of these molecules are also known to induce drug side effect phospholipidosis, a lysosomal storage disorder characterised by phospholipid aggregation. Study of intrinsic lipidation in five phospholipidosis inducing pharmaceuticals revealed reactivity in only one case, however heighten lysolipid formation was observed across all species. Observations suggest a correlation between lysolipid

concentration and phospholipidosis induction, potentially due to innate lysolipid properties. Biophysical techniques reveal similar structure and functionality of lysolipids and acylated small molecules, including membrane disruption and micelle formation. Similar modes of action may aid in phospholipidosis induction by both lysolipids and acylated small molecules, however further study is required in order to probe this theory.

Pharmaceutical propranolol **1**, has been extensively investigated as an interesting example of small molecule intrinsic lipidation. Synthetic preparation of acylated standards combined with CID MSMS reveal two distinct reaction products of propranolol **1** intrinsic lipidation *in vitro*, *O*-acylated propranolol and *N*-acylated propranolol. Migratory studies under physiological conditions suggest a reactivity mechanism, characterised by initial transesterification from phospholipids, followed by intramolecular *O* to *N* migration. Quantitative study of propranolol **1** intrinsic lipidation reveals preferential acyl transfer within eukaryotic model systems, and from the *sn*-1 phospholipid backbone position. Kinetics studies reveal modified product distribution and reaction rate *in vitro* as a result of temperature, pH, and membrane composition. Acyl transfer reactivity to propranolol **1** from lysolipid containing micelles has also been proved during these experiments, exhibiting preferential palmitoyl transfer despite increasingly tight packing. Propranolol **1** intrinsic lipidation has also been characterised in *E. coli* and bovine liposomes, and in Hep G2 cells, forming *O*-acylated propranolol species mirroring cellular fatty acid profile.

10 | Experimental

10.1 General Techniques

Materials

Phospholipids and lysolipids were purchased as powders from Avanti Polar Lipids (via Instruchemie B.V., The Netherlands). Isotopically labelled materials were purchased from Goss Scientific Instruments Ltd. (Cheshire, UK). Melittin (synthetic 97 % by HPLC) and amyloid peptides were purchased from Enzo Life Sciences Ltd. (Exeter, UK), and acylated melittin from Almac Group (Craigavon, UK). *sn*-glycerophosphocholine was purchased from Bachem Holding AG (Bubendorf, Switzerland). Solvents, acids, and bases were purchased from Fisher Scientific (Loughborough, UK). Solvent drying was carried out over molecular sieves, with the exception of dry DCM which was refluxed over CaH_2. All other chemicals were purchased from Sigma Aldrich (Dorset, UK), Fluorochem (Derbyshire, UK), TCI UK Ltd. (Oxford, UK), or Alfa Aesar (Lancashire, UK).

Solution State NMR

^{1}H and ^{13}C NMR were performed at 400 MHz using a Bruker-400 spectrometer. Samples were prepared in $CDCl_3$ (97 % D, Goss Scientific Instruments Ltd., Cheshire, UK), D_2O (99.9 % D, Goss Scientific Instruments Ltd., Cheshire, UK) or CD_3OD (99.8 % D, Goss Scientific Instruments Ltd., Cheshire, UK). Chemical shifts (δ) are reported in ppm and are referenced relative to the residual solvent signal (7.26 ppm for $CHCl_3/CDCl_3$; 4.80 ppm for H_2O/D_2O; 4.87 ppm for CH_3OH/CD_3OD). J values are reported in Hz.

Mass Spectrometry

Routine accurate mass characterisation was conducted on a LCT Premier XE (Waters Corp., UK) or QToF Premier (Waters Corp., UK). Positive ESI was recorded between *m/z* 50 to 2000, and PDA absorbance measurement between 210 nm and 500 nm. Where relevant, chromatography was performed on an Acquity UPLC, with 3 µL injection on to a BEH C_{18}, 1.7 µm (2.1 x 100 mm) column. Mobile phase conditions ran a linear 400 µL/ min gradient from 1 % MeCN: 99 % H_2O (0.1 % formic acid) to 99 % MeCN: 1 % H_2O (0.1 % formic acid) over 5 minutes, followed by a 4 minute organic wash.

IR Spectroscopy

IR spectroscopy was performed on a Perkin Elmer FT-IR spectrometer operating through the wavenumber range 400 cm^{-1} and 4000 cm^{-1}.

Liposome Preparation by Extrusion

Stock solutions of phospholipid in $CHCl_3$ were prepared at a concentration of 10 $mg\,mL^{-1}$ and stored at -20 °C. A 100 µL aliquot of phospholipid stock solution was added to a round-bottomed flask, and solvent removed *in vacuo* resulting in formation of a lipid film. Following overnight dessication, the phospholipid film was rehydrated in buffer solution and agitated using a vortex mixer. The dispersion was subjected to 5 freeze-thaw cycles between -196 °C and 30 °C, before 10 extrusion cycles at 50 °C using a LIPEX thermobarrel extruder under a positive pressure of nitrogen and a 100 nm Whatman Nucleopore laser-etched polycarbonate filter.

Liposome Preparation by Sonication

Stock solutions of phospholipid in $CHCl_3$ were prepared at a concentration of 10 $mg\,mL^{-1}$ and stored at -20 °C. A 100 µL aliquot of phospholipid stock solution was added to a round-bottomed flask, and solvent removed *in vacuo* resulting in formation of a lipid film. Following overnight dessication, the phospholipid film was rehydrated in buffer solution and agitated using a vortex mixer. The dispersion was subjected to 5 freeze-thaw cycles between -196 °C and 30 °C, before bath sonication for 20 min at room temperature.

Peptide Buffer pH 7.41

90 mM NaCl and 10 mM $NaHCO_3$ were fully dissolved in H_2O. pH was measured and adjusted to a value of 7.41 using HCl.

Peptide Stock Solutions

Peptides were dissolved in H_2O (melittin) or HFIP (amyloids) at approximate concentration 1 mg mL^{-1}. Accurate concentrations were determined by measuring absorbance from 200 nm to 400 nm at 21 °C using a CARY100 UV-Visible spectrophotometer with Cary WinUV Scan Software 3.00(182). Absorbance was measured in triplicate following addition of 5 µL, 10 µL, 15 µL and 20 µL aliquots of peptide stock solution to a 1 mm quartz cuvette containing H_2O (1 mL). Following dilution correction, concentrations were calculated using the Beer-Lambert Law, with relevant physical parameters given in Table 10.1.

Peptide	Absorbance Wavelength (nm)	Extinction Coefficient ($M^{-1}\,cm^{-1}$)
Melittin	280	5600
Acylated Melittin	280	5600
Amyloid β	274	1400
Amylin	257	200
β-2 Microglobulin	280	19600

Table 10.1 Extinction coefficients and absorbance wavelengths used for the measurement of amyloid concentrations

Small Molecule Buffer pH 7.41

10 mM NH_4HCO_3 was fully dissolved in H_2O. pH was measured and adjusted to a value of 7.41 using formic acid.[98]

Small Molecule Stock Solutions

Small molecule stock solution were prepared at concentration 1.27 mM in H_2O or H_2O:EtOH depending upon solubility.

Small Molecule Incubation

1.27 mM liposomes in buffer of desired pH were added in 1:10 molar ratio to 1.27 mM small molecule stock solution. Samples were incubated at the desired temperature for the relevant time period prior to analysis.

Optimised Small Molecule LCMS *in vitro*

Samples were diluted in MeCN:H_2O (1:1) to small molecule concentration 1 µg mL^{-1}. LCMS analyses were conducted on a Synapt G2-S (Waters Corp., UK) recording ESI ions between *m/z* 50 to 2000, and PDA absorbance measurement between 210 nm and 500 nm. Optimised chromatography was conducted by 3 µL injection on to an Acquity UPLC with BEH Phenyl 1.7 µm (2.1 x 50 mm) column. Mobile phase conditions are summaried in Table 10.2 positive ESI ionisation parameters are presented in Table 10.3.

Time (min)	Flow Rate (mL/ min)	% H_2O (0.1 % FA)	% MeCN (0.1 % FA)	Curve
0.00	0.4	95	5	6
0.50	0.4	95	5	6
7.50	0.4	5	95	6
8.80	0.4	5	95	6
8.90	0.4	95	5	6
10.00	0.4	95	5	6

Table 10.2 Optimised chromatography gradient for small molecule LCMS.

Parameter	Optimised Value
Capillary Voltage (kV)	1.0
Source Temperature (°C)	150.0
Sampling Cone Voltage (V)	50.0
Source Offset Voltage (V)	30.0
Desolvation Temperature (°C)	350.0
Cone Gas Flow (L h^{-1})	60.0
Desolvation Gas Flow (L h^{-1})	600.0
Nebuliser Gas Flow (Bar)	6.0

Table 10.3 Optimised positive ESI parameters for small molecule LCMS.

Small Molecule CID MSMS

CD MSMS was carried out in the trap region of a Synapt G2-S (Waters Ltd., UK). Desired precursor ions were isolated in the quadrapole, and subsequently underwent CID fragmentation ramping from 30 V to 50 V.

Data Processing

Data was processed using MassLynx software version 4.1. In built elemental composition software was applied to the determination of error and RDB values. Peak area calculations were determined from EIC of desired m/z using Microsoft Excel 2013 Solver. Error calculations were determined based upon peak area variation between triplicate samples identically prepared and analysed.

10.2 Chapter 3

Fluorescence Spectroscopy

Fluorescence spectroscopy was carried out on a PerkinElmer LS 55 Fluorescence Spectrometer using a tryptophan excitation wavelength of 280 nm and a detection range of 300 nm to 450 nm. Slit widths were selected as 10 nm for excitation and 50 nm for emission, and the scan speed was 100 nm min^{-1}. Melittin stock solution (20 µL) and H_2O (1 mL) were added to a quartz cuvette with 1 mL insert and analysed as a background control. Acylated melittin stock solution was then added in sequential amounts from 1 mol% up to 20 mol%, and emission recorded in triplicate to account for instrument error.

NP/RP TLC Stains

- UV (254 nm UV lamp)
- PMA (6.25 g PMA, 2.50 g $Ce(SO_4)_2$, 15 mL H_2SO_4, 230 mL H_2O)
- Ninhydrin (0.50 g ninhydrin, 10 mL EtOH, 1 mL AcOH)
- Coomassie (0.03 % brilliant blue, 20 % MeOH, 80 % H_2O)

- *p*-Anisaldehyde (4 mL *p*-anisaldehyde, 5 mL H_2SO_4, 2 mL AcOH, 150 mL EtOH)
- I_2 (crystals of elemental iodine)
- $KMnO_4$ (3.00 g $KMnO_4$, 10.00 g K_2CO_3 in 300 mL H_2O)

Small Molecule NP TLC

1 µL of 1.27 mM stock solutions of propranolol **1**, *N*-palmitoyl propranolol **12**, and *N*-oleoyl propranolol **13** were spotted onto a NP TLC plate (Fisher Scientific Loughborough, UK). Preliminary staining was conducted with NP TLC stains. Reaction mixture concentration solutions of propranolol **1** (127 nM), *N*-palmitoyl propranolol **12** (1.27 nM), and *N*-oleoyl propranolol **13** (1.27 nM) were prepared. 1 µL to 20 µL of reaction mixture solutions were spotted on to a NP TLC plate and dried under a flow of compressed air using 1 µL graduated TLC spotters (Sigma Aldrich Dorset, UK). Sensitivity staining was conducted with relevant NP TLC stains. Solvent system optimisation was carried out using 1.27 mM stock solutions of propranolol **1**, *N*-palmitoyl propranolol **12**, and *N*-oleoyl propranolol **13**, and 12.7 mM stock solutions of POPC, PPC, and OPC. 1 µL of each was spotted on to a NP TLC plate, exposed to solvent conditions, and visualised using PMA.

Peptide RP TLC

1 µL of melittin and acylated melittin stock solutions (approximately 1 mg mL^{-1}) were spotted onto a RP TLC plate (Fisher Scientific Loughborough, UK). Preliminary staining was conducted with NP TLC stains. Reaction mixture concentration solutions (approximately 50 µg mL^{-1}) of melittin and acylated analogues were applied to RP TLC plate using 1 µL graduated TLC spotters (Sigma Aldrich Dorset, UK). Sensitivity staining was conducted with relevant RP TLC stains. Solvent system optimisation was not pursed due to insufficient TLC plate hydrophobicity.

High Performance RP TLC Stains

- PMA (6.25 g PMA, 100 mL EtOH)
- Ninhydrin (0.20 g ninhydrin, 100 mL EtOH)

- Ninhydrin (0.20 g ninhydrin, 100 mL IPA)
- Ninhydrin (0.20 g ninhydrin, 100 mL *t*-BuOH)

Peptide High Performance RP TLC

1 µL of melittin and acylated melittin stock solutions (approximately 1 mg mL^{-1}) were spotted onto a high performance RP TLC plate (Fisher Scientific Loughborough, UK). Preliminary staining was conducted with high performance RP TLC stains. Reaction mixture concentration solutions (approximately 50 µg mL^{-1}) of melittin and acylated analogues were applied to RP TLC plate using 1 µL graduated TLC spotters (Sigma Aldrich Dorset, UK). Sensitivity staining was conducted with PMA in EtOH only. Solvent system optimisation was not pursed due to insufficient visualisation sensitivity.

Small Molecule High Performance RP TLC

1 µL of 1.27 mM stock solutions of propranolol **1**, *N*-palmitoyl propranolol **12**, and *N*-oleoyl propranolol **13** were spotted onto a high performance RP TLC plate (Fisher Scientific Loughborough, UK). Preliminary staining was conducted with high performance RP TLC stains. Reaction mixture concentration solutions of propranolol **1** (127 nM), *N*-palmitoyl propranolol **12** (1.27 nM), and *N*-oleoyl propranolol **13** (1.27 nM) were prepared. 1 µL to 20 µL of reaction mixture solutions were spotted on to a high performance RP TLC plate and dried under a flow of compressed air using 1 µL graduated TLC spotters (Sigma Aldrich Dorset, UK). Sensitivity staining was conducted using PMA in EtOH. Solvent system optimisation was carried out using 1.27 mM stock solutions of propranolol **1**, *N*-palmitoyl propranolol **12**, and *N*-oleoyl propranolol **13**, and 12.7 mM stock solutions of POPC, PPC, and OPC. 1 µL of each was spotted on to a high performance RP TLC plate, exposed to solvent conditions, and visualised using PMA in EtOH.

Solid State NMR

DPPC liposomes were prepared by extrusion and sonication methodologies at a concentration of 0.2 mg mL^{-1} in D_2O. ssNMR analysis revealed insufficient sample concentration for detection. DPPC liposomes at concentration 2.0 mg mL^{-1} in D_2O were prepared by sonication. ^{31}P ssNMR was successfully carried out over 12 hours on a Bruker Avance III HD spectrometer

with 9.4 T magnet and 4 mm HX MAS probe. Analysis was repeated using 2.0 mg mL^{-1} DPPC liposomes D_2O containing 5 mol% lysolipid PPC.

Synthesis of 1-chloro-3-(1-naphthoxy)-2-propanol 14

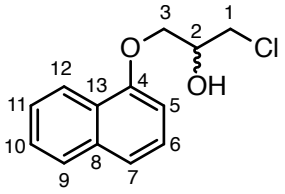

1-Naphthol (1.00 g, 6.94 mmol), epichlorohydrin (2.69 mL, 34.68 mmol) and pyridine (0.06 mL, 0.69 mmol) were stirred at 35 °C for 24 hours. Excess epichlorohydrin was removed by distillation under reduced pressure using a Kugelrohr. Product was redissolved in $CHCl_3$ (0.750 mL) and 37 % $HCl_{(aq)}$ (0.375 mL) and stirred for 1 hour at 5 °C. Mixture was diluted in $CHCl_3$, washed with H_2O three times, dried over $MgSO_4$ and solvent removed *in vacuo*. Product **14** was obtained as a dark oil (1.49 g, 91 %): ^{1}H (400 MHz; $CDCl_3$) δ 2.86 (s, 1H, OH), 3.85 (d, J = 5.5 Hz, 2H, H_1), 4.23 (m, 2H, H_3), 4.35 (m, 1H, H_2), 6.82 (d, J = 7.5 Hz, 1H, H_5), 7.36 (t, J = 7.9 Hz, 1H, H_6), 7.44-7.54 (m, 3H, $H_{7,10,11}$), 7.80 (d, J = 6.9 Hz, 1H, H_9), 8.18 (d, J = 7.1 Hz, 1H, H_{12}); ^{13}C (100 MHz; $CDCl_3$) δ 46.5 (C_1), 68.8 (C_2), 70.1 (C_3), 105.2 (C_5), 121.2 (C_7), 121.7 (C_{12}), 125.5 (C_4), 125.7 (C_{11}), 125.9 (C_6), 126.7 (C_{10}), 127.7 (C_9), 134.6 (C_8), 153.9 (C_{13}); IR (neat) υ_{max}/cm^{-1} 3485; LRMS (ASAP) *m/z* 237.1 [M+H]$^+$; HRMS (ASAP) calculated for $C_{13}H_{14}O_2Cl$ [M+H]$^+$ 237.0682, found 237.0686.[174]

Synthesis of *N*-Isopropylphthalimide 15 - Method 1

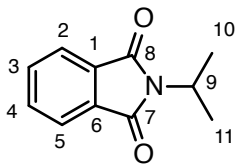

2-Bromopropane (0.40 mL, 2.48 mmol) and potassium phthalimide (0.55 mg, 2.98 mmol in dry DMF (3 mL) were stirred under argon for 12 hours. TLC analysis did not indicate product formation.[175,176]

Synthesis of *N*-Isopropylphthalimide 15 - Method 2

2-Bromopropane (0.40 mL, 2.48 mmol), potassium phthalimide (0.23 mg, 1.24 mmol) and potassium carbonate (0.34 mg, 2.48 mmol) in dry DMF (3 mL) were stirred under argon at 40 °C for 18 hours. Reaction mixture was poured on to H_2O (30 mL) and the resulting white solid **15** collected by Büchner filtration (0.12 g, 26 %): ^{1}H (400 MHz; DMSO-d6) δ 1.48 (d, J = 7.2 Hz, 6H, $H_{10,11}$), 4.47-4.57 (m, 1H, H_9), 7.79 (m, 4H, $H_{2,3,4,5}$); ^{13}C (100 MHz; DMSO-d6) δ 20.1 ($C_{10,11}$), 43.0 (C_9), 123.0 ($C_{3,4}$), 132.1 ($C_{2,5}$), 133.8 ($C_{1,6}$), 168.4 ($C_{7,8}$); IR (neat) υ_{max}/cm^{-1} 1692, 2981; LRMS (ASAP) m/z 190.1 $[M+H]^+$; HRMS (ASAP) calculated for $C_{11}H_{12}NO_2$ $[M+H]^+$ 190.0868, found 190.0858; m.p. = 83-84 °C.[175,176]

Synthesis of ^{15}*N*-Isopropylphthalimide 15

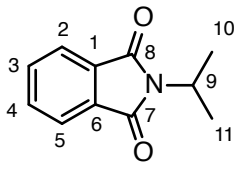

2-Bromopropane (0.40 mL, 2.48 mmol), ^{15}*N*-potassium phthalimide (0.23 mg, 1.24 mmol) and K_2CO_3 (0.34 mg, 2.48 mmol) in dry DMF (3 mL) were stirred under argon at 40 °C for 18 hours. Reaction mixture was poured on to H_2O (30 mL) and the resulting white solid ^{15}N **15** collected by Büchner filtration (0.16 g, 34 %): ^{1}H (400 MHz; DMSO-d6) δ 1.48 (d, J = 7.2 Hz, 6H, $H_{10,11}$), 4.47-4.57 (m, 1H, H_9), 7.79 (m, 4H, $H_{2,3,4,5}$); ^{13}C (100 MHz; DMSO-d6) δ 20.1 ($C_{10,11}$), 43.0 (C_9), 123.0 ($C_{3,4}$), 132.1 ($C_{2,5}$), 133.8 ($C_{1,6}$), 168.4 ($C_{7,8}$); IR (neat) υ_{max}/cm^{-1} 1692, 2981; LRMS (ASAP) m/z 191.1 $[M+H]^+$; HRMS (ASAP) calculated for $C_{11}H_{12}{}^{15}NO_2$ $[M+H]^+$ 191.0833, found 191.0838; m.p. = 83-84 °C.[175,176]

Synthesis of Isopropylamine 16 - Method 1

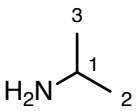

N-Isopropylphthalimide (0.50 g, 2.65 mmol) was refluxed for 2 hours in 37 % $HCl_{(aq)}$ (10 mL), cooled to allow crystallisation of phthalic acid, and refluxed for a further 2 hours. Upon

cooling phthalic acid was removed by filtration, and the remaining aqueous solution freeze-dried to yield white solid **16**. Product characterisation proved challenging due to limited conversion.[175,176]

Synthesis of Isopropylamine 16 - Method 2

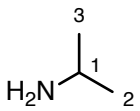

N-Isopropylphthalimide (1.26 g, 8.66 mmol) was refluxed for 1 hour in the presence of hydrazine hydrate (1.01 g, 20.16 mmol) and MeOH (1.8 mL). The mixture was filtered and solvent removed *in vacuo* to yield white solid product **16** as the HCl salt (0.41 g, 81 %): ^{1}H (400 MHz; D_2O) δ 1.31 (d, J = 7.0 Hz, 6H, $H_{2,3}$), 3.51 (sept, J = 7.0 Hz, 1H, H_1); ^{13}C (100 MHz; D_2O) δ 25.8 ($C_{2,3}$), 42.1 (C_1); IR (neat) υ_{max}/cm^{-1} 3421; LRMS (EI) *m/z* 60.1 $[M+H]^+$; m.p. = 151-152 °C.[175,176]

Synthesis of ^{15}*N*-Isopropylamine 16

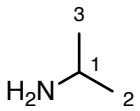

^{15}*N*-Isopropylphthalimide (1.26 g, 8.66 mmol) was refluxed for 1 hour in the presence of hydrazine hydrate (1.01 g, 20.16 mmol) and MeOH (1.8 mL). The mixture was filtered and solvent removed *in vacuo* to yield white solid product ^{15}N **16** as the HCl salt (0.40 g, 77 %): ^{1}H (400 MHz; D_2O) δ 1.31 (d, J = 7.0 Hz, 6H, $H_{2,3}$), 3.51 (sept, J = 7.0 Hz, 1H, H_1); ^{13}C (100 MHz; D_2O) δ 25.8 ($C_{2,3}$), 42.1 (C_1); IR (neat) υ_{max}/cm^{-1} 3405; LRMS (EI) *m/z* 61.1 $[M+H]^+$; m.p. = 151-152 °C.[175,176]

Synthesis of Propranolol 1

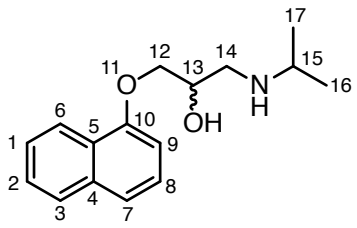

Isopropylamine HCl salt **16** (1.03 g, 10.73 mmol) was dissolved in 20 % NaOH solution (2.30 mL) to pH 14. 1-chloro-3-(1-naphthoxy)-2-propanol **14** (0.10 mL, 0.53 mmol) in IPA (2.30 mL) was added, and the mixture stirred for 16 hours. Excess isopropylamine was removed by distillation under reduced pressure using a Kugelrohr. Remaining aqueous mixture was washed with DCM, dried under $MgSO_4$, and solvent removed *in vacuo*. Purification by silica gel chromatography using EtOAc:MeOH:H_2O (98:1:1) eluent yielded a racemic mixture of propranolol **1** as a white solid (0.12 g, 85 %): ^{1}H (400 MHz; $CDCl_3$) δ 1.36 (d, J = 6.0 Hz, 6H, $H_{16,17}$), 3.11-3.17 (m, 1H, H_{14}), 3.27-3.31 (m, 1H, H_{15}), 3.32-3.38 (m, 1H, H_{14}), 3.97-4.02 (m, 1H, H_{12}), 4.05-4.12 (m, 1H, H_{12}), 4.68-4.77 (m, 1H, H_{13}), 5.42 (s, 1H, OH), 6.49-6.55 (m, 1H, H_9), 7.10-7.19 (m, 1H, H_8), 7.24-7.33 (m, 3H, $H_{1,2,7}$), 7.61-7.67 (m, 1H, H_3), 8.10-8.14 (m, 1H, H_6), 8.50 (s, 1H, NH), 9.62 (s, 1H, NH); ^{13}C (100 MHz; $CDCl_3$) δ 23.1 ($C_{16,17}$), 48.9 (C_{15}), 68.1 (C_{14}), 68.9 (C_{12}), 70.7 (C_{13}) 104.9 (C_9) 120.6 (C_7), 121.9 (C_6), 125.3 (C_5), 125.6 (C_1), 125.8 (C_8), 126.4 (C_2), 127.3 (C_3), 134.6 (C_4), 154.4 (C_{10}); IR (neat) υ_{max}/cm^{-1} 1572, 1581, 2842, 2990, 3260, 3286; LRMS (ESI) *m/z* 260.2 $[M+H]^+$; HRMS (ESI) calculated for $C_{16}H_{22}NO_2$ $[M+H]^+$ 260.1651, found 260.1649; m.p. = 91-92 °C.[174]

Synthesis of ^{15}N-Propranolol 1

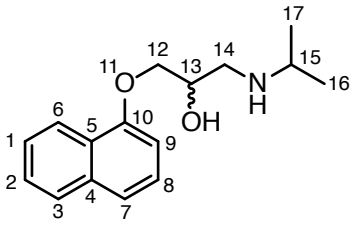

^{15}N-Isopropylamine HCl salt **16** (1.03 g, 10.73 mmol) was dissolved in 20 % NaOH solution (2.30 mL) to pH 14. 1-chloro-3-(1-naphthoxy)-2-propanol **14** (0.10 mL, 0.53 mmol) in IPA (2.30 mL) was added, and the mixture stirred for 16 hours. Excess isopropylamine was removed by distillation under reduced pressure using a Kugelrohr. Remaining aqueous mixture was washed with DCM, dried under $MgSO_4$, and solvent removed *in vacuo*. Purification by silica gel chromatography using EtOAc:MeOH:H_2O (98:1:1) eluent yielded yielded a racemic mixture of ^{15}N propranolol **1** as a white solid (0.12 g, 84 %): ^{1}H (400 MHz; $CDCl_3$) δ 1.36 (d, J = 6.0 Hz, 6H, $H_{16,17}$), 3.11-3.17 (m, 1H, H_{14}), 3.27-3.31 (m, 1H, H_{15}), 3.32-3.38 (m, 1H, H_{14}), 3.97-4.02 (m, 1H, H_{12}), 4.05-4.12 (m, 1H, H_{12}), 4.68-4.77 (m, 1H, H_{13}), 5.42 (s, 1H, OH), 6.49-6.55 (m, 1H, H_9), 7.10-7.19 (m, 1H, H_8), 7.24-7.33 (m, 3H, $H_{1,2,7}$), 7.61-7.67 (m, 1H, H_3), 8.10-8.14 (m, 1H, H_6), 8.50 (s, 1H, NH), 9.62 (s, 1H, NH); ^{13}C (100 MHz; $CDCl_3$) δ

23.1 ($C_{16,17}$), 48.9 (C_{15}), 68.1 (C_{14}), 68.9 (C_{12}), 70.7 (C_{13}) 104.9 (C_9) 120.6 (C_7), 121.9 (C_6), 125.3 (C_5), 125.6 (C_1), 125.8 (C_8), 126.4 (C_2), 127.3 (C_3), 134.6 (C_4), 154.4 (C_{10}); IR (neat) υ_{max}/cm^{-1} 1572, 1581, 2842, 2990, 3260, 3286; LRMS (ESI) *m/z* 261.2 $[M+H]^+$; HRMS (ESI) calculated for $C_{16}H_{22}{}^{15}NO_2$ $[M+H]^+$ 261.1621, found 261.1617; m.p. = 91-92 °C.[174]

Synthesis of 2-Aminomethylbenzimidazole 11 - Method 1

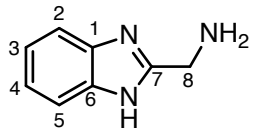

o-Phenylenediamine (1.08 g, 10.00 mmol) and glycine (1.50 g, 20.00 mmol) were refluxed in 37 % HCl (4 mL) for 5 days until NMR indicated full conversion. After cooling, the resulting solid was isolated by filtration and combined with the solid obtained by freeze drying the reaction mixture. Purification by recrystallisation from MeOH yielded the HCl salt of compound **11** as a tan solid (2.06 g, 94 %): ^1H (400 MHz; DMSO-d6) δ 3.54 (t, J = 5.7 Hz, 2H, H_8), 4.48 (t, J = 5.7 Hz, 2H, NH_2), 7.43-7.48 (m, 2H, $H_{3,4}$), 7.77-7.81 (m, 2H, $H_{2,5}$), 9.08 (s, 1H, NH); ^{13}C (100 MHz; DMSO-d6) δ 39.2 (C_8), 116.8 ($C_{2,5}$), 125.4 ($C_{3,4}$), 136.4 ($C_{1,6}$), 148.7 (C_7); IR (neat) υ_{max}/cm^{-1} 1581, 1605, 2930, 3021, 3248, 3360, 3387; LRMS (ESI) *m/z* 148.1 $[M+H]^+$; HRMS (ESI) calculated for $C_8H_{10}N_3$ $[M+H]^+$ 148.0875, found 148.0872; m.p. = 269-270 °C.[177,178]

Synthesis of 2-Aminomethylbenzimidazole 11 - Method 2

o-Phenylenediamine (1.08 g, 10.00 mmol) and glycine (0.90 g, 12.00 mmol) were refluxed in 37 % HCl (4 mL) for 5 days until NMR indicated full conversion. After cooling, the resulting solid was isolated by filtration and combined with the solid obtained by freeze drying the reaction mixture. Purification by recrystallisation from MeOH yielded the HCl salt of compound **11** as a tan solid (0.26 g, 12 %): ^1H (400 MHz; DMSO-d6) δ 3.54 (t, J = 5.7 Hz, 2H, H_8), 4.48 (t, J = 5.7 Hz, 2H, NH_2), 7.43-7.48 (m, 2H, $H_{3,4}$), 7.77-7.81 (m, 2H, $H_{2,5}$), 9.08 (s, 1H, NH); ^{13}C (100 MHz; DMSO-d6) δ 39.2 (C_8), 116.8 ($C_{2,5}$), 125.4 ($C_{3,4}$), 136.4 ($C_{1,6}$), 148.7 (C_7); IR (neat) υ_{max}/cm^{-1} 1581, 1605, 2930, 3021, 3248, 3360, 3387; LRMS (ESI) *m/z* 148.1 $[M+H]^+$; HRMS (ESI) calculated for $C_8H_{10}N_3$ $[M+H]^+$ 148.0875, found 148.0872; m.p. = 269-270 °C.[177,178]

Synthesis of ^{15}N 2-Aminomethylbenzimidazole 11

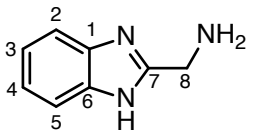

o-Phenylenediamine (1.08 g, 10.00 mmol) and glycine (0.90 g, 12.00 mmol) were refluxed in 37 % HCl (4 mL) for 5 days until NMR indicated full conversion. After cooling, the resulting solid was isolated by filtration and combined with the solid obtained by freeze drying the reaction mixture. Product formation was not observed under experimental conditions.[177,178]

Synthesis of Palmitoyl Chloride 18

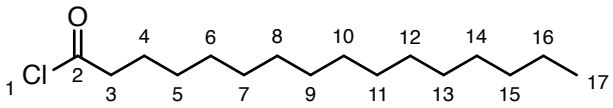

To palmitic acid (0.05 g, 0.19 mmol) in dry DCM (8 mL) under argon was added oxalyl chloride (0.03 mL, 0.38 mmol) and the mixture refluxed for 2 hours. Solvent was removed *in vacuo* to give yellow oil (0.03 g, 65 %): ^{1}H (400 MHz; $CDCl_3$) δ 0.88 (t, J = 8.0 Hz, 3H, H_{17}), 1.26 (br, 24H, H_{Alkyl}), 1.70 (quint, J = 24.0 Hz, 2H, H_4), 2.87 (q, J = 12.0 Hz, 2H, H_3); ^{13}C (100 MHz; $CDCl_3$) δ 14.3 (C_{17}), 22.9 (C_{Alkyl}), 25.2 (C_{Alkyl}), 28.7 (C_{Alkyl}), 29.3 (C_{Alkyl}), 29.5 (C_{Alkyl}), 29.6 (C_{Alkyl}), 29.7 (C_{Alkyl}), 29.8 (C_{Alkyl}), 29.9 (C_{Alkyl}), 29.9 (C_{Alkyl}), 32.1 (C_4), 48.5 (C_3), 173.8 C_2); IR (neat) υ_{max}/cm^{-1} 1473, 1800, 2861, 2931.[179]

Synthesis of Palmitic Anhydride 17

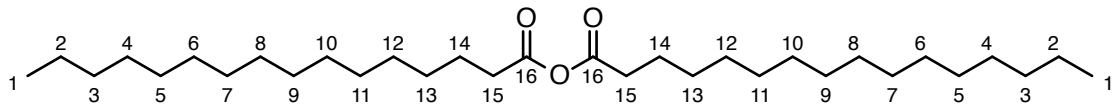

To NBu_4Br (0.01 g, 0.01 mmol) in toluene (0.1 mL) at -10 °C was added 20 % NaOH solution (0.6 mL) followed by palmitoyl chloride (0.03 g, 0.12 mmol) in toluene (0.3 mL) over 20 minutes. After stirring for 3.5 hours the reaction was allowed to warm to room temperature, washed with brine, the organic layer dried over $MgSO_4$ and solvent removed *in vacuo* to yield white powder **17** (0.02 g, 35 %): ^{1}H (400 MHz; $CDCl_3$) δ 0.88 (t, J = 8.0 Hz, 6H, H_1), 1.25 (br, 48H, H_{Alkyl}), 1.61-1.71 (m, 4H, H_{14}), 2.45 (t, J = 8.0 Hz, 4H, H_{15}); ^{13}C (100 MHz; $CDCl_3$)

δ 14.3 (C_1), 22.0 (C_2), 22.9 (C_3), 29.3-29.9 (C_{Alkyl}), 32.1 (C_{14}), 34.9 (C_{15}), 169.8 C_{16}); IR (neat) υ_{max}/cm^{-1} 1745, 1803, 2961, 3011; m.p. 60-62 °C.[180,181]

Synthesis of GPC-$CdCl_2$ Complex 110

To *sn*-glycero-3-phosphocholine (0.50 g, 1.67 mmol) in MeOH (3.5 mL) at 0 °C was added $CdCl_2$ (0.44 g, 2.40 mmol) in cold H_2O (1.5 mL) and stirred for 4 hours. The resulting precipitate was collected by fitration and lyophilised to dryness yielding a white powder carried forward without further purification (0.71 g, 88 %).[183,184]

Synthesis of DPPC - Method 1

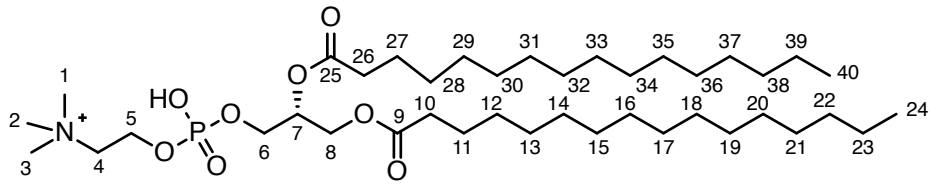

To *sn*-glycero-3-phosphocholine (0.003 g, 0.01 mmol) in pyridine (0.5 mL) was added palmitic anhydride **17** (0.018 g, 0.03 mmol) and stirred for 7 days. The reaction mixture was poured into crushed ice (0.5 g), extracted with EtOAc three times, dried over $MgSO_4$ and solvent removed *in vacuo*. Product formation was not observed.[182]

Synthesis of DPPC - Method 2

To *sn*-glycero-3-phosphocholine (0.003 g, 0.01 mmol) in dry DCM (0.1 mL) under argon was added palmitic anhydride **17** (0.002 g, 0.01 mmol) and DMAP (0.001 g, 0.01 mmol). Stirring continued for 72 hours with exclusion of light, prior to solvent removal *in vacuo*. Product formation was not observed.[182]

Synthesis of DPPC - Method 3

To palmitic acid (0.10 g, 0.39 mmol) in dry DCM (3 mL) under argon was added GCP-$CdCl_2$ **110** (0.05 g, 0.10 mmol), DMAP (0.03 g, 0.20 mmol) and DIC (0.105 mL, 0.68 mmol) in dry DCM (1 mL) and stirred for 72 hours. Solid was removed by filtration and DOWEX added to dislodge Cd. After stirring for 0.5 hours the mixture was filtered, and solvent removed

in vacuo to yield a white powder. DPPC was purified by trituration with ethyl acetate, acetone and water (0.05 g, 65%): ^{1}H (400 MHz; $CDCl_3$) δ 0.89 (t, J = 6.6 Hz, 6H, $H_{24,40}$), 1.27 (s, 48H, H_{Alkyl}), 1.54-1.67 (m, 4H, $H_{11,27}$), 2.25-2.37 (m, 4H, $H_{10,26}$), 3.31 (s, 9H, $H_{1,2,3}$), 3.62–3.70 (m, 2H, H_4), 4.00-4.06 (m, 2H, H_6), 4.24–4.36 (m, 2H, H_5), 4.41-4.48 (m, 2H, H_8), 5.25 (m, 1H, H_7); ^{13}C (100 MHz; $CDCl_3$) *delta* 13.9 ($C_{24,40}$), 22.8 ($C_{23,39}$), 25.1 (C_{Alkyl}), 29.2 (C_{Alkyl}), 29.5 (C_{Alkyl}), 29.8 (C_{Alkyl}), 32.2 (C_{Alkyl}), 34.2 (C_{Alkyl}), 35.4 (C_{Alkyl}), 54.2 ($C_{1,2,3}$), 60.1 (C_4), 63.7 (C_8), 65.1 (C_5), 67.7 (C_6), 70.3 (C_7), 173.9 ($C_{9,25}$); IR (neat) υ_{max}/cm^{-1} 1737, 2897, 2951, 2981; LRMS (ESI) *m/z* 734.6 $[M+H]^+$; HRMS (ESI) calculated for $C_{40}H_{81}NO_8P$ $[M+H]^+$ 734.5700, found 734.5701.[183,184]

Synthesis of DPPC - Method 4

To palmitic acid (0.13 g, 0.51 mmol) in dry DCM (3 mL) under argon was added GCP-$CdCl_2$ **110** (0.09 g, 0.20 mmol), DMAP (0.05 g, 0.40 mmol) and DIC (0.210 mL, 1.36 mmol) in dry DCM (1 mL) and stirred for 72 hours. Solid was removed by filtration and DOWEX added to dislodge Cd. After stirring for 0.5 hours the mixture was filtered, and solvent removed *in vacuo* to yield a white powder. DPPC was purified by trituration with ethyl acetate, acetone and water (0.02 g, 11 %): ^{1}H (400 MHz; $CDCl_3$) δ 0.89 (t, J = 6.6 Hz, 6H, $H_{24,40}$), 1.27 (s, 48H, H_{Alkyl}), 1.54-1.67 (m, 4H, $H_{11,27}$), 2.25-2.37 (m, 4H, $H_{10,26}$), 3.31 (s, 9H, $H_{1,2,3}$), 3.62–3.70 (m, 2H, H_4), 4.00-4.06 (m, 2H, H_6), 4.24–4.36 (m, 2H, H_5), 4.41-4.48 (m, 2H, H_8), 5.25 (m, 1H, H_7); ^{13}C (100 MHz; $CDCl_3$) *delta* 13.9 ($C_{24,40}$), 22.8 ($C_{23,39}$), 25.1 (C_{Alkyl}), 29.2 (C_{Alkyl}), 29.5 (C_{Alkyl}), 29.8 (C_{Alkyl}), 32.2 (C_{Alkyl}), 34.2 (C_{Alkyl}), 35.4 (C_{Alkyl}), 54.2 ($C_{1,2,3}$), 60.1 (C_4), 63.7 (C_8), 65.1 (C_5), 67.7 (C_6), 70.3 (C_7), 173.9 ($C_{9,25}$); IR (neat) υ_{max}/cm^{-1} 1737, 2897, 2951, 2981; LRMS (ESI) *m/z* 734.6 $[M+H]^+$; HRMS (ESI) calculated for $C_{40}H_{81}NO_8P$ $[M+H]^+$ 734.5700, found 734.5701.[183,184]

Synthesis of ^{13}C DPPC

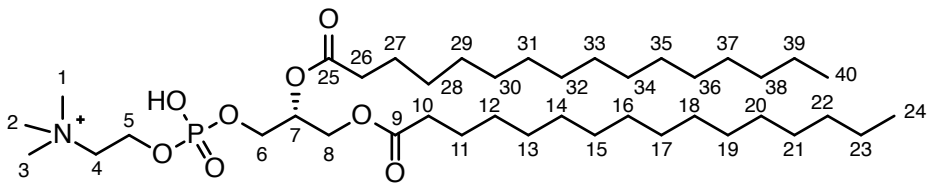

To ^{13}C palmitic acid (0.10 g, 0.39 mmol) in dry DCM (3 mL) under argon was added GCP-$CdCl_2$ **110** (0.05 g, 0.10 mmol), DMAP (0.03 g, 0.20 mmol) and DIC (0.105 mL, 0.68 mmol)

in dry DCM (1 mL) and stirred for 72 hours. Solid was removed by filtration and DOWEX added to dislodge Cd. After stirring for 0.5 hour the mixture was filtered, and solvent removed *in vacuo* to yield a white powder. ^{13}C DPPC was purified by trituration with ethyl acetate, acetone and water (0.03 g, 41 %): ^{1}H (400 MHz; $CDCl_3$) δ 0.89 (t, J = 6.6 Hz, 6H, $H_{24,40}$), 1.27 (s, 48H, H_{Alkyl}), 1.54-1.67 (m, 4H, $H_{11,27}$), 2.25-2.37 (m, 4H, $H_{10,26}$), 3.31 (s, 9H, $H_{1,2,3}$), 3.62–3.70 (m, 2H, H_4), 4.00-4.06 (m, 2H, H_6), 4.24–4.36 (m, 2H, H_5), 4.41-4.48 (m, 2H, H_8), 5.25 (m, 1H, H_7); ^{13}C (100 MHz; $CDCl_3$) *delta* 13.9 ($C_{24,40}$), 22.8 ($C_{23,39}$), 25.1 (C_{Alkyl}), 29.2 (C_{Alkyl}), 29.5 (C_{Alkyl}), 29.8 (C_{Alkyl}), 32.2 (C_{Alkyl}), 34.2 (C_{Alkyl}), 35.4 (C_{Alkyl}), 54.2 ($C_{1,2,3}$), 60.1 (C_4), 63.7 (C_8), 65.1 (C_5), 67.7 (C_6), 70.3 (C_7), 173.9 ($C_{9,25}$); IR (neat) υ_{max}/cm^{-1} 1739, 2897, 2951, 2981; LRMS (ESI) *m/z* 736.6 $[M+H]^+$; HRMS (ESI) calculated for $C_{48}{}^{13}C_2H_{81}NO_8P$ $[M+H]^+$ 736.5767, found 734.5750.[183,184]

Synthesis of DOPC

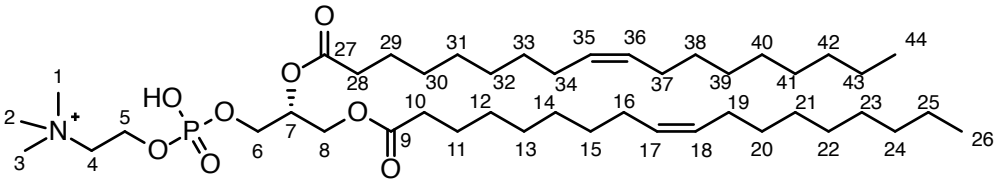

To oleic acid (0.11 g, 0.39 mmol) in dry DCM (3 mL) under argon was added GCP-$CdCl_2$ **110** (0.05 g, 0.10 mmol), DMAP (0.03 g, 0.20 mmol) and DIC (0.105 mL, 0.68 mmol) in dry DCM (1 mL) and stirred for 72 hours. Solid was removed by filtration and DOWEX added to dislodge Cd. After stirring for 0.5 hours the mixture was filtered, and solvent removed *in vacuo* to yield a white powder. DOPC was purified by trituration with ethyl acetate, acetone and water (0.02 g, 57 %): ^{1}H (400 MHz; $CDCl_3$) δ 0.87 (t, J = 7.0 Hz, 6H, $H_{26,44}$), 1.07-1.31 (m, 16H, H_{Alkyl}), 1.57-1.53 (m, 4H, $H_{11,29}$), 1.93-2.01 (m, 8H, $H_{16,19,34,37}$), 2.18-2.27 (m, 4H, $H_{10,28}$), 3.32 (s, 9H, $H_{1,2,3}$), 3.59–3.66 (m, 2H, H_4), 4.01-4.07 (m, 2H, H_6), 4.30–4.39 (m, 2H, H_5), 4.40-4.48 (m, 2H, H_8), 5.26 (m, 1H, H_7), 5.30-5.40 (m, 4H, $H_{17,18,35,36}$); ^{13}C (100 MHz; $CDCl_3$) *delta* 14.7 ($C_{26,44}$), 23.3 ($C_{25,43}$), 32.8 ($C_{24,42}$), 25.8 ($C_{11,29}$), 28.1 ($C_{16,19,34,37}$),30.0-30.4 (C_{Alkyl}), 34.6 ($C_{10,28}$), 54.6 ($C_{1,2,3}$), 60.2 (C_4), 63.5 (C_8), 67.0 (C_6), 71.4 (C_7), 130.2 ($C_{17,18,35,36}$, 175.2 ($C_{9,27}$); IR (neat) υ_{max}/cm^{-1} 1738, 2850, 2920; LRMS (ESI) *m/z* 786.6 $[M+H]^+$; HRMS (ESI) calculated for $C_{44}H_{85}NO_8P$ $[M+H]^+$ 786.6013, found 786.6025.[183,184]

Synthesis of ^{13}C DOPC

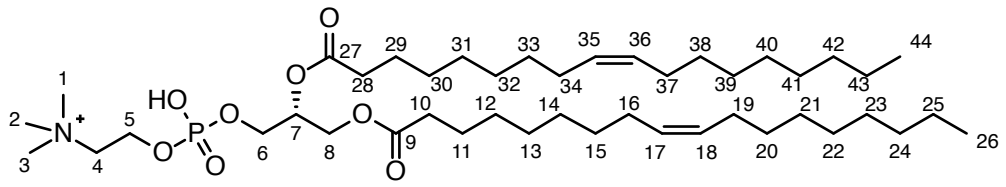

To ^{13}C oleic acid (0.11 g, 0.39 mmol) in dry DCM (3 mL) under argon was added GCP-$CdCl_2$ **110** (0.05 g, 0.10 mmol), DMAP (0.03 g, 0.20 mmol) and DIC (0.105 mL, 0.68 mmol) in dry DCM (1 mL) and stirred for 72 hours. Solid was removed by filtration and DOWEX added to dislodge Cd. After stirring for 0.5 hours the mixture was filtered, and solvent removed *in vacuo* to yield a white powder. ^{13}C DOPC was identified by MS, however low abundance prevented successful purification and characterisation: LRMS (ESI) *m/z* 788.6 $[M+H]^+$; HRMS (ESI) calculated for $C_{42}{}^{13}C_2H_{85}NO_8P$ $[M+H]^+$ 788.6080, found 788.6097.[183,184]

Synthesis of PPC

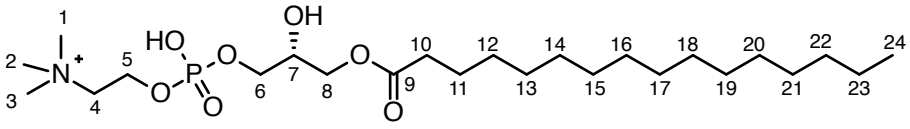

sn-glycero-3-phosphocholine (0.01 g, 0.05 mmol) and dibutyltin oxide (0.01 g, 0.05 mmol) were suspended in anhydrous IPA (1 mL) and refluxed under argon for 1 hour. After cooling, NEt_3 (0.014 mL, 0.10 mmol) and palmitoyl chloride **18** (0.029 mL, 0.10 mmol) were added. Following stirring for 1 further hour H_2O (2 mL) was added to the reaction and washed with hexane (5 mL) three times. Alcohol was removed *in vacuo* and water by lyophilisation to yield a off-white solid. PPC was purified by trituration with acetone, ethyl acetate and hexane although excess tin remained (0.06 g, 97 %): ^{1}H (400 MHz; $CDCl_3$) δ 0.88 (t, 3H, J = 8.0 Hz, H_{24}), 1.25 (s, 24H, H_{Alkyl}), 1.55-1.57 (m, 2H, H_8), 2.30 (t, 2H, J = 8.0 Hz, H_{10}), 3.29 (s, 9H, $H_{1,2,3}$), 3.71-3.76 (m, 2H, H_4), 3.79-3.85 (m, 2H, H_6), 3.90-3.99 (m, 1H, H_7), 4.19-4.23 (m, 2H, H_5), 4.32-4.40 (m, 2H, H_8); LRMS (ESI) *m/z* 496.3 $[M+H]^+$; HRMS (ESI) calculated for $C_{24}H_{51}NO_7P$ $[M+H]^+$ 496.3403, found 496.3396.[185,186]

Synthesis of Oleoyl Chloride 20

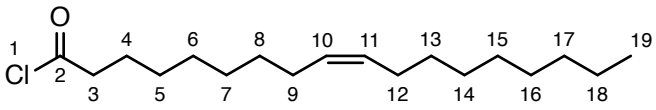

To oleic acid (0.25 g, 0.89 mmol) in dry DCM (40 mL) under argon was added oxalyl chloride (0.585 mL, 1.70 mmol) and the mixture refluxed for 2 hours. Solvent was removed *in vacuo* to yield oleoyl chloride **20** as a yellow oil (0.24 g, 89 %): ^{1}H (400 MHz; $CDCl_3$) δ 0.88 (t, 3H, J = 8.0 Hz, H_{19}), 1.23-1.28 (m, 20H, H_{Alkyl}), 1.70 (quin, 2H, J = 12.0 Hz, H_4), 2.18-2.21 (m, 4H, $H_{9,12}$), 2.88 (t, 2H, J = 8.0 Hz, H_3), 5.29-5.39 (m, 2H, $H_{10,11}$); ^{13}C (100 MHz; $CDCl_3$) δ 14.1 (C_{19}), 22.8 (C_{18}), 25.0 (C_{Alkyl}), 28.7 (C_{Alkyl}), 29.3 (C_{Alkyl}), 29.5 (C_{Alkyl}), 29.6 (C_{Alkyl}), 29.7 (C_{Alkyl}), 29.8 (C_{Alkyl}), 29.9 (C_{Alkyl}), 31.1 (C_{Alkyl}), 46.5 (C_3), 130.5 (C_{10}), 130.7 (C_{11}), 172.4 (C_2); IR (neat) υ_{max}/cm^{-1} 1801, 2845, 2926, 3002.[244,245]

Synthesis of POPC - Method 1

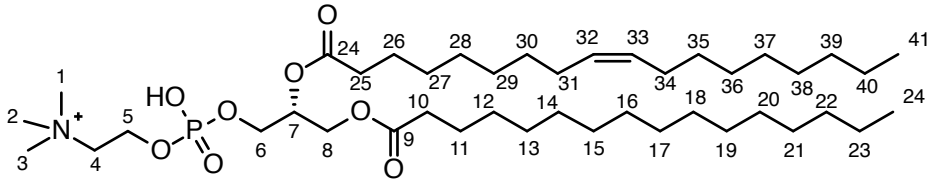

To PPC (0.06 g, 0.12 mmol) in dry DCM (1 mL) was added oleic acid (0.07 g, 0.24 mmol), DIC (0.036 mL, 0.24 mmol) and DMAP (0.02 g, 0.14 mmol). The mixture was stirred with exclusion of light for 48 hours. DCM was removed *in vacuo* and the resulting white solid triturated with water, acetone and ethyl acetate. POPC formation was unsuccessful due to excess tin remaining in PPC.[185,186]

Synthesis of POPC - Method 2

sn-glycero-3-phosphocholine (0.10 g, 0.39 mmol) and dibutyltin oxide (0.1 g, 0.39 mmol) were suspended in IPA (4 mL) and refluxed for 1 hour. After cooling the reaction mixture was treated with NEt_3 (0.098 mL, 0.70 mmol) and palmitoyl chloride **18** (0.19 g, 0.70 mmol), and stirred for 0.5 hour. Oleoyl chloride **20** (0.21 g, 0.70 mmol) and NEt_3 (0.098 mL, 0.70 mmol) were added and stirring continued for 48 hours. Solvent was removed *in vacuo*, and the resulting solid was triturated with water, acetone, ethyl acetate and hexane. POPC formation

was successful, however excess tin prevented complete characterisation (0.15 g, 49 %): ^{1}H (400 MHz; $CDCl_3$) δ 0.90 (t, 6H, J = 8.0 Hz, $H_{24,41}$), 1.24-1.30 (m, 44H, H_{Alkyl}), 1.58-1.60 (m, 4H, $H_{11,26}$), 2.29-2.34 (m, 4H, $H_{31,34}$), 3.37-3.40 (m, 4H, $H_{10,25}$), 3.86 (s, 9H, $H_{1,2,3}$), 3.92-3.98 (m, 2H, H_4), 4.11-4.16 (m, 2H, H_6), 4.24–4.36 (m, 2H, H_5), 4.35-4.41 (m, 2H, H_8), 5.37 (m, 1H, H_7), 5.38-5.43 (m, 2H, $H_{32,33}$); LRMS (ESI) *m/z* 760.6 $[M+H]^+$; HRMS (ESI) calculated for $C_{42}H_{83}NO_8P$ $[M+H]^+$ 760.5856, found 760.5851.[183,185,186]

Synthesis of Ethyl Bromoacetate 22 - Method 1

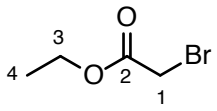

Bromoacetic acid (0.25 g, 1.80 mmol) was suspended in EtOH (5 mL) and H_2SO_4 (0.1 mL), and refluxed for 12 hours. The reaction was diluted with ether, washed with water three times, dried over $MgSO_4$ and solvent removed *in vacuo*. Product formation was not observed.[189]

Synthesis of Ethyl Bromoacetate 22 - Method 2

Bromoacetic acid (0.25 g, 1.80 mmol) and oxalyl chloride (0.282 mL, 2.70 mmol) in dry DCM (2 mL) was stirred at room temperature under argon for 30 minutes. Dry EtOH (1 mL) was added and stirring continued for a further 30 minutes. Solvent was removed *in vacuo* to give yellow oil **22** along with oxalic acid ethyl ester which proved problematic to separate.[189]

Synthesis of Ethyl Bromoacetate 22 - Method 3

Bromoacetic acid (0.25 g, 1.80 mmol) and oxalyl chloride (0.282 mL, 2.70 mmol) in dry DCM (2 mL) was stirred at room temperature under argon for 1 hour. Solvent was removed *in vacuo*, dry EtOH (1 mL) added, and stirring continued for 30 minutes. Solvent was removed *in vacuo* to yield ethyl bromoacetate **22** as a yellow oil (0.29 g, 98 %): ^{1}H (400 MHz; $CDCl_3$) δ 1.29 (t, J = 7.1 Hz, 3H, H_4), 3.84 (s, 2H, H_1), 4.25 (q, J = 7.1 Hz, 2H, H_3); ^{13}C (100 MHz; $CDCl_3$) δ 14.1 (C_4), 25.0 (C_3), 62.3 (C_1), 168.6 (C_2); IR (neat) ν_{max}/cm^{-1} 1735, 2980; LRMS (ASAP) *m/z* 167.0 $[M+H]^+$; HRMS (ASAP) calculated for $C_4H_8BrO_2$ $[M+H]^+$ 166.9708, found 166.9716.[189]

Synthesis of ^{13}C Ethyl Bromoacetate 22

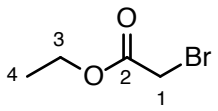

^{13}C bromoacetic acid (0.25 g, 1.80 mmol) and oxalyl chloride (0.282 mL, 2.70 mmol) in dry DCM (2 mL) was stirred at room temperature under argon for 1 hour. Solvent was removed *in vacuo*, dry EtOH (1 mL) added, and stirring continued for 30 minutes. Solvent was removed *in vacuo* to yield ^{13}C ethyl bromoacetate **22** as a yellow oil (0.20 g, 94 %): ^{1}H (400 MHz; $CDCl_3$) δ 1.29 (t, J = 7.1 Hz, 3H, H_4), 3.84 (s, 2H, H_1), 4.25 (q, J = 7.1 Hz, 2H, H_3); ^{13}C (100 MHz; $CDCl_3$) δ 14.1 (C_4), 25.0 (C_3), 62.3 (C_1), 168.6 (C_2); IR (neat) υ_{max}/cm^{-1} 1743, 2981; LRMS (ASAP) *m/z* 168.0 $[M+H]^+$; HRMS (ASAP) calculated for $C_3{}^{13}CH_8BrO_2$ $[M+H]^+$ 167.9741, found 167.9731.[189]

Synthesis of *N,N'*-Bis(*p*-toluenesulfonyl)hydrazine 24

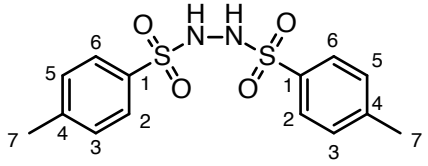

p-Toluenesulfonyl hydrazide (0.93 g, 5.00 mmol) and *p*-toluenesulfonyl chloride (1.43 g, 7.50 mmol) were combined under argon in dry DCM (5 mL). Pyridine (0.60 mL, 7.5 mmol) was added dropwise over 1 minute, and the solution stirred for 1.5 hours. Ether (20 mL) and H_2O (10 mL) were added, and the solution stirred at 0 °C for a further 15 minutes. Solid was collected by Büchner filtration and washed with cold ether. Recrystallisation from MeOH yielded catalyst **24** (1.49 g, 88 %): ^{1}H (400 MHz; DMSO-d6) δ 2.39 (s, 6H, H_7), 7.37–7.40 (m, 4H, $H_{3,5}$), 7.62–7.70 (m, 4H, $H_{2,6}$), 9.59 (s, 2H, NH); ^{13}C (100 MHz; DMSO-d6) δ 21.8 (C_7), 127.8 ($C_{3,5}$), 130.0 ($C_{2,6}$), 136.1 (C_4), 143.7 (C_1); IR (neat) υ_{max}/cm^{-1} 1590, 3202, 3235; LRMS (ASAP) *m/z* 341.1 $[M+H]^+$; HRMS (ASAP) calculated for $C_{14}H_{17}N_2O_4S_2$ $[M+H]^+$ 341.0629, found 341.0616; m.p. = 225-226 °C.[190]

Synthesis of Diazoacetic Acid Ethyl Ester 25

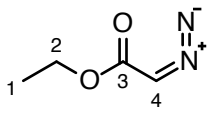

Ethyl bromoacetate **22** (0.11 g, 1.00 mmol) was added to *N,N'*-Bis(*p*-toluenesulfonyl)hydrazine **24** (0.68 g, 2.00 mmol) at 0 °C in THF (5 mL). DBU (0.75 mL, 5.00 mmol) was added dropwise over 5 minutes, and the mixture stirred for a further 0.5 hours. Ether was added, washed with saturated $NaHCO_3$ solution, dried over $MgSO_4$, and solvent removed *in vacuo*. Product formation proved unsuccessful.[187,188]

Synthesis of 1-bromo-7-hexadecyne 27

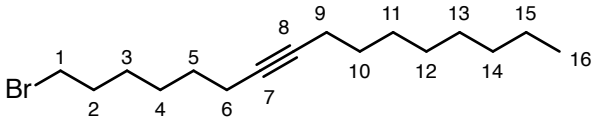

1-decyne (0.02 g, 0.14 mmol) in dry THF (1 mL) under argon was cooled to -78 °C for dropwise addition of *n*-BuLi (0.06 mL, 0.14 mmol). After 1 hour 1,6-dibromohexane (0.18 g, 0.73 mmol) was added and the reaction refluxed for 44 hour. THF was removed *in vacuo* to yield a yellow oil which was redissolved in hexane, washed with water and brine, dried over $MgSO_4$ and solvent removed *in vacuo*. Distillation purified 1-bromo-7-hexadecyne **27** as a yellow oil (0.04 g, 85 %): ^{1}H (400 MHz; $CDCl_3$) δ 0.87 (t, J = 8.0 Hz, 3H, H_{16}), 1.27-1.48 (m, 18H, H_{Alkyl}), 1.86 (quin, 2H, J = 16 Hz, H_2), 2.14 (m, 4H, $H_{6,9}$), 3.40 (t, J = 8.0 Hz, 2H, H_1); ^{13}C (100 MHz; $CDCl_3$) δ 14.1 (C_{16}), 18.8 (C_{15}), 19.0 (C_{14}), 23.0 (C_{Alkyl}), 28.2 (C_{Alkyl}), 28.3 (C_{Alkyl}), 29.1 (C_{Alkyl}), 29.3 (C_{Alkyl}), 29.5-29.7 (C_{Alkyl}), 32.1 (C_{Alkyl}), 33.3 (C_2), 33.8 (C_1), 79.9 (C_8), 80.2 (C_7); IR (neat) υ_{max}/cm^{-1} 1458, 2160, 2854, 2925; LRMS (ASAP) *m/z* 299.1 $[M+H]^+$; HRMS (ASAP) calculated for $C_{16}H_{28}Br$ $[M+H]^+$ 299.1374, found 299.1355.[328]

Synthesis of 1-pinacolborane-7-hexadecyne 29

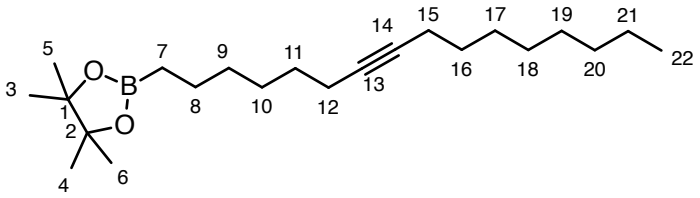

A flask containing CuI (0.002 g, 0.01 mmol), KO*t*Bu (0.012 g, 0.13 mmol), NBu_4I (0.024 g, 0.07 mmol) and bis(pinacolato)diboron (0.025 g, 0.10 mmol) was evacuated and filled with argon three times. Dry THF (1 mL) and 1-bromo-7-hexadecyne **27** (0.02 g, 0.07 mmol) were added and stirred. After 24 hours the reaction mixture was diluted with EtOAc, washed with $H_2O$and brine, dried over $MgSO_4$, and solvent removed *in vacuo*. Further purification of crude oil **29** was not conducted (0.02 g, 82 %): ^{1}H (400 MHz; $CDCl_3$) δ 0.87 (t, J = 8.0 Hz, 3H, H_{22}), 1.06 (s, 12H, $H_{3,4,5,6}$), 1.27-1.48 (m, 32H, H_{Alkyl}), 2.13 (m, 4H, $H_{13,14}$); ^{11}B (400 MHz; $CDCl_3$) δ 22.4; IR (neat) υ_{max}/cm^{-1} 1462, 1632, 2858, 2922.[193]

Synthesis of Octadec-9-ynoic Acid Ethyl Ester 28 - Method 1

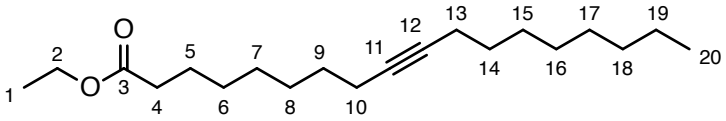

Dried zinc dust (0.005 g, 0.08 mmol) and ethyl bromoacetate **22** (0.011 g, 0.07 mmol) in toluene (0.8 mL) and ether (0.2 mL) was stirred with gentle warming until the start of a reaction. After 15 minutes 1-bromo-7-hexadecyne **27** (0.020 g, 0.07 mmol) in toluene (0.4 mL) and ether (0.1 mL) was added slowly, and the reaction brought to reflux. After 30 minutes the reaction mixture was filtered and washed with H_2O three times to remove zinc byproducts. Product formation was not observed.[329,330]

Synthesis of Octadec-9-ynoic Acid Ethyl Ester 28 - Method 2

Zinc dust (0.005 g, 0.08 mmol) was stirred with 10 % HCl solution (0.25 mL) for 2 minutes, filtered and washed with H_2O, EtOH and ether. To activated zinc in toluene (0.8 mL) and ether (0.2 mL) under argon was added ethyl bromoacetate **22** (0.011 g, 0.07 mmol) dropwise and refluxed for 1 hour. In a second flask, 1-bromo-7-hexadecyne **27** (0.020 g, 0.07 mmol) and $n-Bu_4NI$ (0.049 g, 0.13 mmol) were stirred in toluene (0.4 mL) and ether (0.1 mL) for 1 hour. The contents of the two flasks were combined and stirred for 12 hours before solvent removal *in vacuo*. The resulting oil was redissolved in toluene, washed with H_2O three times, dried over $MgSO_4$ and solvent removed *in vacuo*. Product formation was not observed.[329,330]

Synthesis of Octadec-9-ynoic Acid Ethyl Ester 28 - Method 3

Zinc dust (0.005 g, 0.08 mmol) was stirred with 10 % HCl solution (0.25 mL) for 2 minutes, filtered and washed with H_2O, EtOH and ether. To activated zinc in toluene (1.2 mL) and ether (0.3 mL) was added 1-bromo-7-hexadecyne **27** (0.020 g, 0.07 mmol) and brought to reflux. After 1 hour the reaction was cooled, ethyl bromoacetate **22** (0.011 g, 0.07 mmol) was added and stirring continued for 12 hour before solvent removal *in vacuo*. The resulting oil was redissolved in toluene, washed with H_2O three times, dried over $MgSO_4$ and solvent removed *in vacuo*. Product formation was not observed.[329,330]

Synthesis of Octadec-9-ynoic Acid Ethyl Ester 28 - Method 4

1-bromo-7-hexadecyne **27** (0.020 g, 0.07 mmol) was cooled to -78 °C in dry THF (0.7 mL) under argon. 1.6 M *n*-BuLi in hexanes (0.825 mL, 0.13 mmol) was added, and the mixture stirred for 0.5 hour. 99-Borabicyclo[3.3.1]nonane dimer (0.008 g, 0.04 mmol) was added and the reaction allowed to warm to room temperature with stirring. After 12 hours the contents of the flask were added to a second flask containing $Pd(OAc)_2$ (0.001 g, 0.01 mmol), PCy_3 (0.001 g, 0.01 mmol), $K_3PO_4 \cdot H_2O$ (0.015 g, 0.07 mmol) and ethyl bromoacetate **22** (0.008 g, 0.05 mmol) which hasd been purged with argon for 15 minutes. Stirring continued for 24 hours before dilution with ether, filtration through celite, washing with H_2O three times, drying over $MgSO_4$ and solvent remove *in vacuo*. Product formation was not observed.[192,193]

Synthesis of Octadec-9-ynoic Acid Ethyl Ester 28 - Method 5

A flask containing $Pd(OAc)_2$ (0.001 g, 0.01 mmol), PCy_3 (0.001 g, 0.01 mmol), K_3PO_4 (0.014 g, 0.07 mmol) and H_2O (0.001 g, 0.07 mmol) was purged with argon for 15 minutes. To this was added crude 1-pinacolborane-7-hexadecyne **29** (0.024 g, 0.07 mmol), ethyl bromoacetate **22** (0.008 g, 0.05 mmol), and dry THF (1.5 mL). Stirring continued for 24 hours before dilution of the reaction mixture with ether, washing with H_2O three times, filtration through a silica plug, drying over $MgSO_4$ and solvent removal *in vacuo*. Synthesis proved unsuccessful.[193]

Synthesis of Octadec-9-ynoic Acid Ethyl Ester 28 - Method 6

A flask containing $Pd(OAc)_2$ (0.001 g, 0.01 mmol), PCy_3 (0.001 g, 0.01 mmol), K_3PO_4 (0.014 g, 0.07 mmol) was purged with argon for 15 minutes. To this was added crude 1-pinacolborane-7-hexadecyne **29** (0.024 g, 0.07 mmol), ethyl bromoacetate **22** (0.008 g, 0.05 mmol), and dry THF (1.5 mL). Stirring continued for 24 hours before dilution of the reaction mixture with ether, washing with H_2O three times, filtration through a silica plug, drying over $MgSO_4$ and solvent removal *in vacuo*. Synthesis proved unsuccessful.[193]

Synthesis of Octadec-9-ynoic Acid Ethyl Ester 28 - Method 7

Ethyl bromoacetate **22** (0.010 g, 0.06 mmol), crude 1-pinacolborane-7-hexadecyne **29** (0.024 g, 0.07 mmol), $Pd(OAc)_2$ (0.001 g, 0.01 mmol), and PPh_3 (0.008 g, 0.03 mmol) in dry THF (1 mL) was deoxygenated. Under argon, KOtBu (0.014 g, 0.12 mmol) was added, and the reaction brought to reflux. After 36 hours the reaction was diluted with ether, washed with H_2O three times, brine once, dried over $MgSO_4$ and solvent removed *in vacuo*. Purification by silica gel chromatography with hexane:DCM (8:2) eluent, washing with ethanolamine, and by vacuum distillation yielded yellow oil **28** (0.007 g, 32 %): ^1H (400 MHz; $CDCl_3$) δ 0.88 (t, J = 8.0 Hz, 3H, H_{20}), 1.20-1.28 (m, 20H, H_{Alkyl}), 2.04-2.15 (m, 7H, $H_{1,4,5}$), 4.04 (t, J = 4.0 Hz, 2H, H_2); LRMS (EI) m/z 308.3 $[M]^+$.[331]

Synthesis of Oleic Acid Ethyl Ester 30 - Method 1

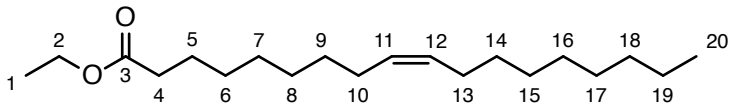

Octadec-9-ynoic Acid Ethyl Ester **28** (0.007 g, 0.01 mmol) and Lindlar's catalyst (0.001 g) were prepared in hexane:EtOH (1:1) (2 mL). The reaction mixture was degassed using freeze thaw methodology three times, and left under an atmosphere of H_2 for 36 hours. Product formation proved unsuccessful.[195,196]

Synthesis of Oleic Acid Ethyl Ester 30 - Method 2

Octadec-9-ynoic Acid Ethyl Ester (0.007 g, 0.01 mmol) and Lindlar's catalyst (0.001 g) were prepared in EtOAc (2 mL). The reaction mixture was degassed using freeze thaw methodology three times and left under an atmosphere of H_2 for 36 hours. Product formation proved unsuccessful.[195,196]

10.3 Chapter 4

Circular Dichroism of Acylated Melittin

CD analysis was performed on a JASCO J-810 Spectropolarimeter at 21 °C using a 2 mm quartz cuvette. Background scattering was determined through analysis of a blank sample containing (0.5 mL) buffer solution (90 mM NaCl, 10 mM $NaHCO_3$ in H_2O at pH 7.41). Peptide (20 µL) of approximate concentration 1×10^{-6} M was added, and the spectrum collected over a range of 180 nm to 300 nm at a continuous scanning speed of 50 nm/ min for 8 accumulations. Each peptide was analysed in triplicate in order to determine instrument error. Data was processed with in-built JASCO software, Spectra Manager version 1.53.05

Acylated Melittin Emission

Emission spectroscopy was carried out on a PerkinElmer LS 55 Fluorescence Spectrometer using a tryptophan excitation wavelength of 280 nm and a detection range of 300 nm to 450 nm. Slit widths were selected as 10 nm for excitation and 50 nm for emission, and the scan speed was 100 nm min^{-1}. H_2O (1 mL) was added to a quartz cuvette with 1 mL insert and analysed as a blank control. Peptide stock solution was then added in sequential amounts 5 µL, 10 µL, 15 µL and 20 µL, and spectra recorded. Peptide samples were analysed in triplicate in order to account for instrument error.

CMC Determination for Acylated Melittin

Rhodamine 6G stock solution (250 µM) prepared in H_2O was diluted 330 fold to 0.08 µM for use. Rhodamine 6G (45 µL) was added to a 40 µL ultra-micro quartz cuvette, excited with a wavelength of 480 nm and the emission recorded between 500 nm to 600 nm. Analysis was

repeated upon sequential addition of peptide stock solution (approximately $1\,\mathrm{mg\,mL^{-1}}$) over the concentration range 1×10^{-6} M to 1×10^{-4} M. Absorbance at 550 nm was corrected for dilution.

Antimicrobial Activity of Acylated Melittin

Bacterial cultures were prepared by streaking strains of *Staphylococcus aureus* (Oxford) and *Escherichia coli* (W3110) onto agar plates with inoculation loop. Following overnight incubation at 37 °C a colony was selected, placed into iso-sensitest broth (5 mL) and shaken at 37 °C overnight. Into iso-sensitest broth (1 mL) was added overnight culture (50 µL) and growth continued at 37 °C with shaking until exhibiting absorbance of 0.07 at 650 nm relative to a control. Inoculum was then diluted ten-fold with iso-sensitest broth prior to use. Into the 96 well plate was placed five controls of each of iso-sensitest broth (100 µL) and iso-sensitest broth (50 µL):inoculum (50 µL). Peptide stock solutions (32 µM) were serially diluted to cover the concentration range 32 µM to 0.5 µM. Inoculum (50 µL) and peptide solution of relevant concentration (50 µL) were added and incubated at 37 °C with shaking for 16 hours. Optical density was measured on Synergy H4 Plate Reader (BioTek, UK) to approximate bacterial growth.[216]

Amyloid Incubation

Amyloid stock solution in HFIP (approximately $1\,\mathrm{mg\,mL^{-1}}$) was combined with POPC:SLPS (4:1) extruded liposomes in 1:10 peptide:lipid molar ratio. Samples were diluted to 100 µL with buffer (90 mM NaCl, 10 mM $NaHCO_3$ in H_2O at pH 7.41), and incubated at 37 °C for 72 hours.

MALDI Mass Spectrometry

MALDI MS was carried out on an Autoflex II Tof/ToF (Bruker Daltonics Ltd., UK) equipped with 337 nm nitrogen laser used in both linear and reflectron mode. α-cyano-4-hydroxy-cinnamic acid matrix (9 µL) and vortexed amyloid incubation sample (1 µL) were mixed and applied (1 µL) to a MALDI target for analysis.

Thioflavin T Assay

Thioflavin T stock solution (0.8 µg mL^{-1}) was prepared in buffer (150 mM NaCl, 10 mM $NaHCO_3$ in H_2O at pH 7.4) and stored with exclusion of light. Ten-fold diluted Thioflavin T stock (150 µL) was added to amyloid incubation sample (50 µL) for analysis. Emission at 482 nm was measured on a Synergy H4 Plate Reader (BioTek, UK) following excitation at 437 nm.

Electron Microscopy

Electron microscopy was carried out on a Hitachi H7600 TEM. Amyloid incubation sample (3 µL) was added to a TEM grid and excess liquid removed. Staining solution containing 2 % uranyl acetate in water (3 µL) was also added and allowed to completely dry. Samples were analysed at high and low magnification.

Low Salt Amyloid Incubation

Amyloid stock solution in HFIP (approximately 1 mg mL^{-1}) was combined with POPC:SLPS (4:1) extruded liposomes in 1:10 peptide:lipid molar ratio. Samples were diluted to 100 µL with buffer (10 mM $NaHCO_3$ in H_2O at pH 7.41), and incubated at 37 °C for 72 hours.

Low Temperature Amyloid Incubation

Amyloid stock solution in HFIP (approximately 1 mg mL^{-1}) was combined with POPC:SLPS (4:1) extruded liposomes in 1:10 peptide:lipid molar ratio. Samples were diluted to 100 µL with buffer (90 mM NaCl, 10 mM $NaHCO_3$ in H_2O at pH 7.41), and incubated at 4 °C for 72 hours.

Sonicated Amyloid Incubation

Amyloid stock solution in HFIP (approximately 1 mg mL^{-1}) was combined with POPC:SLPS (4:1) extruded liposomes in 1:10 peptide:lipid molar ratio. Samples were diluted to 100 µL with buffer (90 mM NaCl, 10 mM $NaHCO_3$ in H_2O at pH 7.41), and incubated at 37 °C for

72 hours. Vortexed samples were sonicated at 40 °C within a bath for 20 minutes prior to MALDI analysis.

Amyloid Depolymerisation with HFIP

Amyloid incubation samples were centrifuged at 45000 rpm for 45 minutes, aqueous liquid decanted, and replaced with HFIP (100 µL). Samples were incubated for 12 hours at 37 °C prior to MALDI analysis.

Amyloid Depolymerisation with Formic Acid

Amyloid incubation samples (100 µL) were diluted with formic acid (900 µL) and acidic pH confirmed. Samples were incubated at 37 °C for 12 hours (β2-Microglobulin) or 3 hours (Amyloid-β and Amylin) prior to MALDI analysis.

β2-Microglobulin Digestion

Experimental protocol varied during optimisation as described in Table 10.4. β2-Microglobulin stock solution (10 µL at 1 mg mL^{-1}) was diluted 1:1 with relevant NH_4CO_3 buffer (10 µL). When employing IAA, DTT (3 µL at 15 mg mL^{-1}) was added and incubated at 65 °C for 10 minutes. Upon cooling, IAA (5 µL at 100 mM) was added and further incubated at room temperature with light exclusion for 30 minutes. Following on, or in the absence of IAA, DTT (2 µL at 15 mg mL^{-1}) and enzyme (1 µL at 0.2 mg mL^{-1} for 1:40 ratio) were added. Incubation at 37 °C continued for the relevant time period defined in Table 10.4.

Enzyme	Enzyme:Protein	Time	NH_4HCO_3 Buffer	DTT	IAA
Trypsin	1:40	24 hours	25 mM	Yes	No
Pepsin	1:40	24 hours	25 mM	Yes	No
Trypsin:Lys C	1:40	24 hours	25 mM	Yes	No
Trypsin:Lys C	1:40	24 hours	25 mM	Yes	Yes
Trypsin:Lys C	1:40	3 hours	50 mM	No	No
Trypsin:Lys C	1:40	5 hours	50 mM	No	No
Trypsin:Lys C	1:40	3 hours	50 mM	Yes	No
Trypsin:Lys C	1:40	3 hours	50 mM	Yes	Yes
Trypsin:Lys C	1:40	3 hours	100 mM	No	No
Trypsin:Lys C	1:20	3 hours	50 mM	Yes	No

Table 10.4 Enzymatic digestion conditions for β2-microglobulin, and resulting sequence coverage

Optimised Digestion

Amyloid stock solution (10 µL at 1 mg mL^{-1}) was diluted 1:1 with NH_4CO_3 buffer (10 µL at 50 mM). DTT (2 µL at 15 mg mL^{-1}) and trypsin:lys C (1 µL at 0.2 mg mL^{-1}) were added. Samples were incubated at 37 °C for 3 hours prior to analysis.

Amyloid Digestion LCMS

Amyloid digestions were diluted with H_2O to final concentration 2 pmol µL^{-1} for LCMS analysis. LCMS analyses were conducted on a Synapt G2-S (Waters Corp., UK) recording ESI ions between m/z 50 to 2000, and PDA absorbance measurement between 210 nm and 500 nm. Chromatography was conducted by 5 µL injection on to an Acquity UPLC with Xbridge C_{18} 1.7 µm (2.1 x 100 mm) column. Mobile phase conditions are summaried in Table 10.5. Positive mode ESI parameters are summarised in Table 10.6

Time (min)	Flow Rate (mL/ min)	% H_2O (0.1 % FA)	% MeCN (0.1 % FA)	Curve
0.00	0.4	95	5	6
8.00	0.4	5	95	6
10.00	0.4	5	95	6
12.00	0.4	95	5	6

Table 10.5 Chromatography gradient for amyloid digestion LCMS.

Parameter	Optimised Value
Capillary Voltage (kV)	1.0
Source Temperature (°C)	150.0
Sampling Cone Voltage (V)	20.0
Source Offset Voltage (V)	40.0
Desolvation Temperature (°C)	300.0
Cone Gas Flow ($L\,h^{-1}$)	60.0
Desolvation Gas Flow ($L\,h^{-1}$)	450.0
Nebuliser Gas Flow (Bar)	6.0

Table 10.6 Positive ESI parameters for amyloid digestion LCMS.

10.4 Chapter 5

Preliminary Small Molecule LCMS

Preliminary small molecule LCMS was conducted on a QToF Premier (Waters Corp., UK) with positive ions recorded between *m/z* 50-1500 and PDA absorbance measurement between 210 nm and 500 nm. Chromatography was performed with an Acquity UPLC BEH C_{18}, 1.7 µm (2.1 x 100 mm) column using a 3 µL injection volume. Mobile phase gradient ran at 400 µL/ min from H_2O (0.1 % formic acid):MeOH (99:1) to H_2O (0.1 % formic acid):MeOH (1:99) over 5 minutes, followed by a 4 minute organic wash at H_2O (0.1 % formic acid):MeOH (1:99).

Synthesis of Palmitoyl Procaine 35

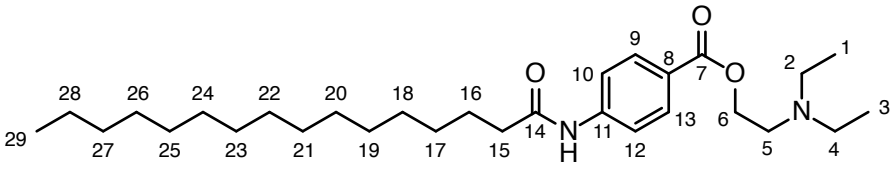

To procaine **2** (0.050 g, 0.18 mmol) in dry DCM (4 mL) was added pyridine (0.016 mL, 0.20 mmol) and palmitoyl chloride **18** (0.061 mL, 0.20 mmol). The mixture was stirred for 12 hours at room temperature, diluted with DCM and washed three times with saturated NH_4Cl solution. The organic layer was dried over $MgSO_4$ and solvent removed *in vacuo*. Purification by silica gel chromatography using eluent EtOAc:MeOH:$NH_{3\,14\%\ aq}$ (98:1:1) yielded palmitoyl procaine **35** as a white solid (0.065 g, 76 %): ^1H (400 MHz; $CDCl_3$) δ 0.89 (t, J = 8.0 Hz, 3H,

H_{29}), 1.22-1.45 (m, H, H_{Alkyl}), 1.75 (quin, J = 24.0 Hz, 2H, H_{16}), 2.49 (q, J = 12.0 Hz, 2H, H_{15}), 3.00-3.10 (m, 4H, $H_{2,4}$), 3.21-3.28 (m, 2, H_5), 4.69-4.72 (m, 2H, H_6), 7.71 (d, J = 8.5 Hz, 2H, $H_{9,13}$), 7.96 (d, J = 8.5 Hz, 2H, $H_{10,12}$); ^{13}C (100 MHz; $CDCl_3$) δ 12.2 ($C_{1,3}$), 14.3 (C_{28}), 22.9 (C_{Alkyl}), 25.2 ((C_{Alkyl}), 28.7 (C_{Alkyl}), 29.3 (C_{Alkyl}), 29.5 (C_{Alkyl}), 29.6 (C_{Alkyl}), 29.7 (C_{Alkyl}), 29.8 (C_{Alkyl}), 29.9 (C_{Alkyl}), 29.9 (C_{Alkyl}), 32.1 (C_{16}), 47.9 ($C_{2,4}$), 48.5 (C_{15}), 51.4 (C_5), 62.7 (C_6), 113.8 ($C_{10,12}$), 119.9 (C_8), 131.5 ($C_{9,13}$), 155.0 (C_{11}), 166.7 (C_7), 174.0 C_{14}); IR (neat) υ_{max}/cm^{-1} 1598, 1602, 1720, 2855, 2925, 2985; LRMS (ESI) m/z 475.4 $[M+H]^+$; HRMS (ESI) calculated for $C_{29}H_{51}N_2O_3$ $[M+H]^+$ 475.3900, found 475.3900.[242,243,246]

Synthesis of Oleoyl Procaine 36

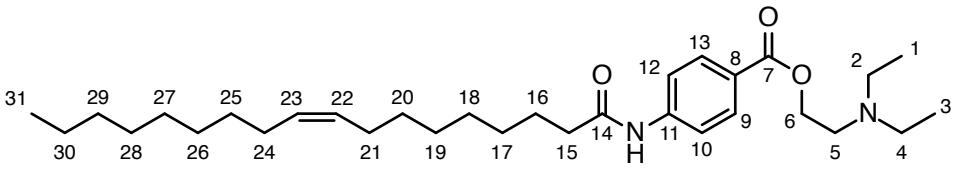

To procaine **2** (0.050 g, 0.18 mmol) in dry DCM (4 mL) was added pyridine (0.016 mL, 0.20 mmol) and oleoyl chloride **20** (0.061 mL, 0.20 mmol). The mixture was stirred for 12 hours at room temperature, diluted with DCM and washed three times with saturated NH_4Cl solution. The organic layer was dried over $MgSO_4$ and solvent removed *in vacuo*. Purification by silica gel chromatography using eluent EtOAc:MeOH:$NH_{3\,14\%\ aq}$ (98:1:1) yielded oleoyl procaine **36** as a yellow oil (0.063 g, 70 %): ^{1}H (400 MHz; $CDCl_3$) δ 0.87 (t, J = 8.0 Hz, 3H, H_{29}), 1.20-1.42 (m, H, 20H_{Alkyl}), 1.71 (quin, 2H, J = 12.0 Hz, H_{16}), 2.18-2.24 (m, 4H, $H_{21,24}$), 2.90 (t, 2H, J = 8.0 Hz, H_{15}), 3.00-3.10 (m, 4H, $H_{2,4}$), 3.20-3.25 (m, 2, H_5), 4.69-4.73 (m, 2H, H_6), 5.20-5.25 (m, 2H, $H_{22,23}$), 7.75 (d, J = 8.5 Hz, 2H, $H_{9,13}$), 8.0 (d, J = 8.5 Hz, 2H, $H_{10,12}$); ^{13}C (100 MHz; $CDCl_3$) δ 12.5 ($C_{1,3}$), 14.0 (C_{31}), 22.8 (C_{30}), 25.6 (C_{Alkyl}), 28.9 (C_{Alkyl}), 29.2 (C_{Alkyl}), 29.5 (C_{Alkyl}), 29.6 (C_{Alkyl}), 29.8 (C_{Alkyl}), 29.9 (C_{Alkyl}), 30.0 (C_{Alkyl}), 32.1 (C_{16}), 47.9 ($C_{2,4}$), 48.0 (C_{15}), 51.4 (C_5), 62.7 (C_6), 113.8 ($C_{10,12}$), 119.9 (C_8), 130.2 (C_{22}), 130.5 (C_{23}) 131.5 ($C_{9,13}$), 155.0 (C_{11}), 166.7 (C_7), 179.2 C_{14}); IR (neat) υ_{max}/cm^{-1} 1598, 1602, 1720, 2855, 2925, 2985, 3010; LRMS (ESI) m/z 501.4 $[M+H]^+$; HRMS (ESI) calculated for $C_{31}H_{53}N_2O_3$ $[M+H]^+$ 501.4056, found 501.4051.[242,243,246]

Synthesis of Palmitoyl Tetracaine 37

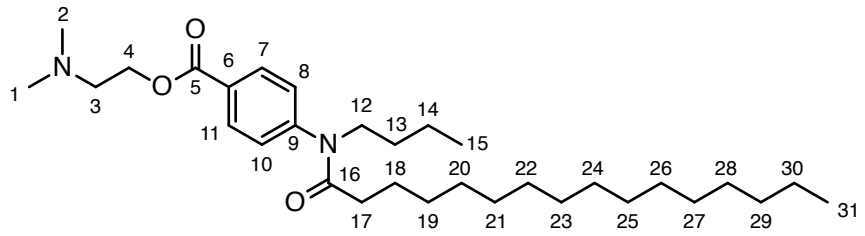

To tetracaine **3** (0.050 g, 0.16 mmol) in dry DCM (4 mL) was added pyridine (0.015 mL, 0.18 mmol) and palmitoyl chloride **18** (0.055 mL, 0.18 mmol). The mixture was stirred for 12 hours at room temperature, diluted with DCM and washed three times with saturated NH_4Cl solution. The organic layer was dried over $MgSO_4$ and solvent removed *in vacuo*. Purification by silica gel chromatography using eluent EtOAc:MeOH:$NH_{3\,14\%\ aq}$ (98:1:1) yielded palmitoyl tetracaine **37** as a white solid (0.058 g, 72 %): ^{1}H (400 MHz; $CDCl_3$) δ 0.88 (t, J = 8.0 Hz, 3H, H_{15}), 0.98 (t, J = 8.0 Hz, 3H, H_{31}), 1.13-1.35 (m, 26H, H_{Alkyl}), 1.40-1.49 (m, 2H, H_{13}), 1.51-1.60 (m, 2H, H_{18}), 2.91 (m, 2H, H_{17}), 2.93 (s, 6H, $H_{1,2}$), 3.46 (m, 2H, H_{12}), 3.71 (t, J = 6.0 Hz, 2H, H_3), 4.85 (m, 2H, H_4), 7.28 (d, J = 8.0 Hz, 2H, $H_{7,11}$), 8.18 (d, J = 8.0 Hz, 2H, $H_{8,10}$); ^{13}C (100 MHz; $CDCl_3$) δ 13.7 (C_{15}), 14.3 (C_{31}), 19.7 (C_{Alkyl}), 22.4 (C_{Alkyl}), 22.6 (C_{Alkyl}), 25.5 (C_{Alkyl}), 27.8 (C_{Alkyl}), 28.9 (C_{Alkyl}), 29.3 (C_{Alkyl}), 29.4 (C_{Alkyl}), 29.5 (C_{Alkyl}), 29.6 (C_{Alkyl}), 29.8 (C_{Alkyl}), 31.8 (C_{13}), 32.7 (C_{18}), 43.7 (C_3), 45.5 ($C_{1,2}$), 48.5 (C_{17}), 53.6 (C_{12}), 58.9 (C_4), 131.7 ($C_{8,10}$), 139.2 ($C_{7,11}$), 144.0 (C_9), 151.3 (C_6), 174.0 (C_5) 177.6 (C_{16}); IR (neat) ν_{max}/cm^{-1} 1606, 1728, 2902, 2915, 2927; LRMS (ESI) m/z 503.4 $[M+H]^+$; HRMS (ESI) calculated for $C_{31}H_{55}N_2O_3$ $[M+H]^+$ 503.4213, found 503.4214.[242,243,246]

Synthesis of Oleoyl Tetracaine 38

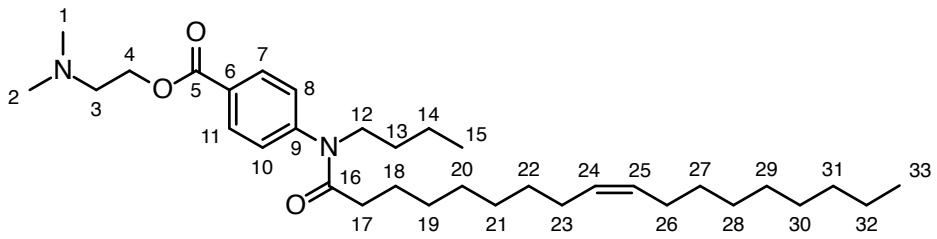

To tetracaine **3** (0.050 g, 0.16 mmol) in dry DCM (4 mL) was added pyridine (0.015 mL, 0.18 mmol) and oleoyl chloride **20** (0.055 mL, 0.18 mmol). The mixture was stirred for 12 hours at room temperature, diluted with DCM and washed three times with saturated NH_4Cl

solution. The organic layer was dried over $MgSO_4$ and solvent removed *in vacuo*. Purification by silica gel chromatography using eluent EtOAc:MeOH:$NH_{3\,14\%\ aq}$ (98:1:1) yielded oleoyl tetracaine **38** as a yellow oil (0.056 g, 66 %): ^{1}H (400 MHz; $CDCl_3$) δ 0.87 (t, J = 8.0 Hz, 3H, H_{15}), 0.96 (t, J = 8.0 Hz, 3H, H_{33}), 1.15-1.33 (m, 22H, H_{Alkyl}), 1.38-1.50 (m, 2H, H_{13}), 1.53-1.63 (m, 2H, H_{18}), 1.94-2.20 (m, 4H $H_{23,26}$) 2.73 (m, 2H, H_{17}), 2.82 (s, 6H, $H_{1,2}$), 3.32-3.36 (m, 2H, H_{12}), 3.71 (t, J = 8.0 Hz, 2H, H_3), 4.67-4.77 (m, 2H, H_4), 5.26-5.34 (m, 2H, $H_{24,25}$), 7.23 (d, J = 8.0 Hz, 2H, $H_{7,11}$), 8.13 (d, J = 8.0 Hz, 2H, $H_{8,10}$); ^{13}C (100 MHz; $CDCl_3$) δ 13.8 (C_{15}), 14.1 (C_{33}), 20.0 (C_{Alkyl}), 22.7 (C_{Alkyl}), 25.5 (C_{Alkyl}), 27.2 (C_{Alkyl}), 29.1 (C_{Alkyl}), 29.3 (C_{Alkyl}), 29.5 (C_{Alkyl}), 29.7 (C_{Alkyl}), 31.3 (C_{13}), 31.9 (C_{18}), 43.0 (C_3), 43.6 ($C_{1,2}$), 44.2 (C_{17}), 53.4 (C_{12}), 58.6 (C_4), 129.7 (C_{25}), 129.8 (C_{24}), 131.3 ($C_{8,10}$), 131.9 ($C_{7,11}$), 147.7 (C_9), 152.7 (C_6), 165.3 (C_5), 172.4 (C_{16}); IR (neat) υ_{max}/cm^{-1} 1606, 1726, 2840, 2915, 2931; LRMS (ESI) m/z 529.4 $[M+H]^+$; HRMS (ESI) calculated for $C_{33}H_{57}N_2O_3$ $[M+H]^+$ 529.4369, found 529.4371.[242,243,246]

Synthesis of Diacetyl Propanolol 39

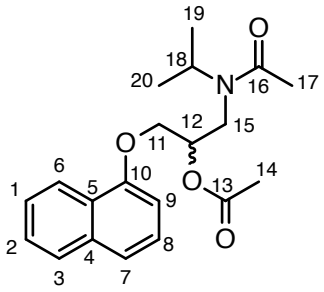

To propranolol **1** (0.100 g, 0.34 mmol) in dry DCM (8 mL) was added pyridine (0.030 mL, 0.36 mmol) and acetyl chloride (0.029 g, 0.37 mmol). The mixture was stirred for 12 hours at room temperature, diluted with DCM and washed three times with saturated NH_4Cl solution. The organic layer was dried over $MgSO_4$ and solvent removed *in vacuo*. Purification by silica gel chromatography using eluent EtOAc:MeOH:$NH_{3\,14\%\ aq}$ (98:1:1) yielded diacetyl propranolol **39** as a yellow oil (0.103 g, 88 %): ^{1}H (400 MHz; $CDCl_3$) δ 1.22–1.26 (m, 3.75H, $H_{19,20}$), 1.31 (d, J = 6.8 Hz, 2.25H, $H_{19,20}$), 2.08 (s, 2.25H, H_{17}), 2.11 (s, 0.75H, H_{17}), 2.16 (s, 2.25H, H_{14}), 2.23 (s, 0.75H, H_{14}), 3.41 (dd, J = 6.9, 14.3 Hz, 0.75 H, H_{15}), 3.64 (dd, J = 4.0, 15.8 Hz, 0.25 H, H_{15}), 3.82 (dd, J = 5.3, 14.3 Hz, 1H, H_{15}), 4.03–4.07 (m, 0.75H, H_{18}), 4.23–4.38 (m, 2H, H_{11}), 4.48–4.52 (m, 0.25H, H_{18}), 5.47–5.50 (m, 0.25H, H_{12}), 5.57–5.62 (m, 0.75H, H_{12}), 6.79-6.82 (m, 1H, H_9), 7.34-7.38 (m, 1H, H_8), 7.43 (d, J = 8.0 Hz, 1H, H_7), 7.46–7.55 (m, 2H, $H_{1,2}$), 7.78–7.83 (m, 1H, H_3), 8.18–8.23 (m, 1H, H_6); ^{13}C (100 MHz; $CDCl_3$) δ 20.2 ($C_{19,20}$),

20.6 (C_{14}), 21.0 ($C_{19,20}$), 21.2 ($C_{19,20}$), 21.7 (C_{14}), 22.1 (C_{17}), 22.7 (C_{17}), 41.4 (C_{15}), 45.5 (C_{15}), 47.2 (C_{18}), 49.5 (C_{18}), 66.9 (C_{11}), 68.4 (C_{11}), 71.0 (C_{12}), 71.6 (C_{12}), 104.8 (C_9), 104.9 (C_9), 120.6 (C_7), 121.2 (C_7), 121.4 (C_6), 121.8 (C_6), 125.3 (C_5), 125.4 (C_5), 125.5 (C_1), 125.7 (C_1), 125.8 (C_8), 126.4 (C_2), 126.6 (C_8), 127.4 (C_4), 127.6 (C_2), 128.2 (C_4), 134.5 (C_4), 134.6 (C_4), 153.7 (C_{10}), 154.2 (C_{10}), 170.2 (C_{16}), 170.5 (C_{16}), 171.3 (C_{13}); IR (neat) υ_{max}/cm^{-1} 1645, 1743, 2940, 2992, 3147; LRMS (ESI) *m/z* 344.2 $[M+H]^+$; HRMS (ESI) calculated for $C_{20}H_{26}O_4N$ $[M+H]^+$ 344.1862, found 344.1852.[247]

Synthesis of *N*-Acetyl Propranolol 40

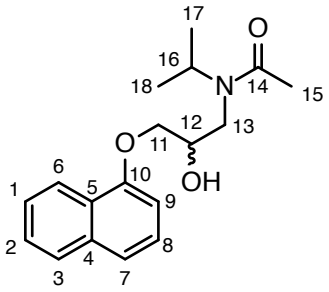

Diacetyl propranolol **39** (0.050 g, 0.14 mmol) and K_2CO_3 (0.059 g, 0.43 mmol) were stirred in MeOH (1.5 mL) for 2 hours prior to solvent removal *in vacuo*. Purification by silica gel chromatography using eluent EtOAc:MeOH:$NH_{3\,14\%\ aq}$ (98:1:1) yielded *N*-acetyl propranolol **40** as a white solid (0.032 g, 76 %): ^1H (400 MHz; $CDCl_3$) δ 1.22 (d, J = 6.6 Hz, 3H, $H_{17,18}$), 1.36 (d, J = 6.6 Hz, 3H, $H_{17,18}$), 2.25 (s, 3H, H_{15}), 3.52 (dd, J = 1.5, 14.6 Hz, 1H, H_{13}), 3.79 (dd, J = 8.4, 14.6 Hz, 1H, H_{13}), 4.04-4.29 (m, 4H, $H_{11,12,16}$), 5.74 (s, 1H, OH), 6.82-6.88 (m, 1H, H_9), 7.38-7.43 (m, 1H, H_8), 7.46–7.59 (m, 3H, $H_{1,2,7}$), 7.81–7.87 (m, 1H, H_3), 8.21–8.28 (m, 1H, H_6); ^{13}C (100 MHz; $CDCl_3$) δ 20.7 ($C_{17,18}$), 21.3 ($C_{17,18}$), 22.0 (C_{15}), 46.1 (C_{13}), 50.3 (C_{16}), 69.8 (C_{11}), 72.5 (C_{12}), 104.8 (C_9), 120.7 (C_7), 121.5 (C_6), 125.2 (C_5), 125.4 (C_1), 126.0 (C_8), 126.3 (C_2), 127.7 (C_3), 134.5 (C_4), 154.0 (C_{10}), 173.9 (C_{14}); IR (neat) υ_{max}/cm^{-1} 1619, 2916, 2986, 3000, 3403; LRMS (ESI) *m/z* 302.2 $[M+H]^+$; HRMS (ESI) calculated for $C_{18}H_{24}O_3N$ $[M+H]^+$ 302.1756, found 302.1758.[246,247]

Synthesis of Dipalmitoyl Propanolol 41

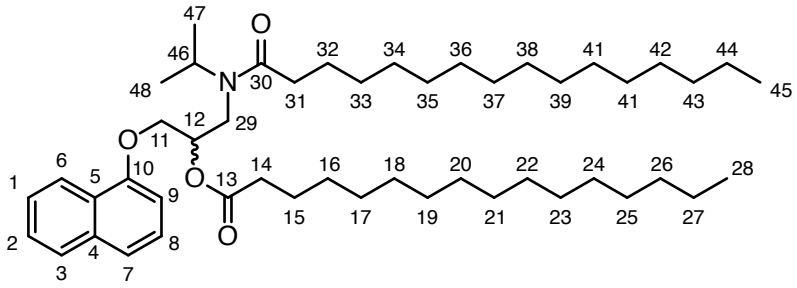

To propranolol **1** (0.050 g, 0.17 mmol) in dry DCM (4 mL) was added pyridine (0.015 mL, 0.19 mmol) and palmitoyl chloride **18** (0.112 mL, 0.37 mmol). The mixture was stirred for 12 hours at room temperature, diluted with DCM and washed three times with saturated NH_4Cl solution. The organic layer was dried over $MgSO_4$ and solvent removed *in vacuo*. Purification by silica gel chromatography using eluent EtOAc:MeOH:$NH_{3\,14\%\ aq}$ (98:1:1) yielded dipalmitoyl propranolol **41** as a yellow oil (0.105 g, 84 %): ^{1}H (400 MHz; $CDCl_3$) δ 0.87 (t, J = 7.0 Hz, 6H, $H_{28,45}$), 1.11-1.36 (m, 54H, H_{Alkyl}), 1.57-1.65 (m, 4H, $H_{15,32}$), 2.29-2.41 (m, 6H, $H_{14,31}$), 3.42 (dd, J = 6.9, 14.3 Hz, 0.75 H, H_{29}), 3.62 (dd, J = 4.0, 15.8 Hz, 0.25 H, H_{29}), 3.82 (dd, J = 5.3, 14.3 Hz, 1H, H_{29}), 4.08–4.15 (m, 0.75H, H_{46}), 4.22–4.32 (m, 2H, H_{11}), 4.42–4.47 (m, 0.25H, H_{46}), 5.42–5.47 (m, 0.25H, H_{12}), 5.52–5.58 (m, 0.75H, H_{12}), 6.79-6.82 (m, 1H, H_9), 7.33-7.38 (m, 1H, H_8), 7.43 (d, J = 8.0 Hz, 1H, H_7), 7.44–7.50 (m, 2H, $H_{1,2}$), 7.75–7.82 (m, 1H, H_3), 8.18–8.21 (m, 1H, H_6); ^{13}C (100 MHz; $CDCl_3$) δ 14.1 ($C_{28,45}$), 20.3 (C_{Alkyl}), 20.7 (C_{Alkyl}), 21.1 (C_{Alkyl}), 21.9 (C_{Alkyl}), 22.7 (C_{Alkyl}), 24.7 (C_{Alkyl}), 25.0 (C_{Alkyl}), 25.5 (C_{Alkyl}), 29.0 (C_{Alkyl}), 29.3 (C_{Alkyl}), 29.6 (C_{Alkyl}), 31.9 (C_{Alkyl}), 33.9 ($C_{14,31}$), 34.4 ($C_{14,31}$), 41.3 (C_{15}), 48.5 (C_{46}), 68.5 (C_{11}), 70.7 (C_{11}), 71.6 (C_{12}), 72.5 (C_{12}), 104.8 (C_9), 120.5 (C_7), 121.4 (C_6), 121.9 (C_6), 125.1 (C_5), 125.2 (C_5), 125.6 (C_1), 125.5 (C_1), 125.6 (C_8), 125.8 (C_2), 125.9 (C_8), 126.3 (C_4), 127.4 (C_2), 127.6 (C_4), 134.4 (C_4), 154.3 (C_{10}), 173.4 (C_{30}), 173.9 (C_{13}); IR (neat) υ_{max}/cm^{-1} 1676, 1745, 2855, 2926; LRMS (ESI) m/z 736.6 [M+H]$^+$; HRMS (ESI) calculated for $C_{48}H_{82}NO_4$ [M+H]$^+$ 736.6244, found 736.6256.[247]

Synthesis of *N*-Palmitoyl Propanolol 12

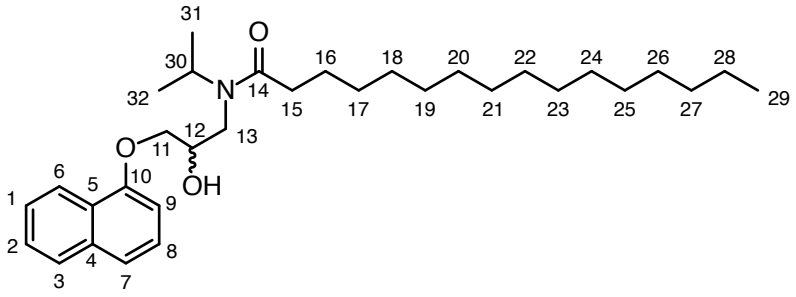

Dipalmitoyl propranolol **41** (0.050 g, 0.14 mmol) and K_2CO_3 (0.059 g, 0.43 mmol) were stirred in MeOH (1.5 mL) for 2 hours prior to solvent removal *in vacuo*. Solid was resuspended in MeOH (6 mL) and H_2SO_4 (0.12 mL), and refluxed for 1 hour to methylate excess fatty acid. The solution was diluted with DCM, washed with saturated $NaHCO_3$ solution until neutral, dried over $MgSO_4$, and solvent removed *in vacuo*. Purification by silica gel chromatography using eluent EtOAc:MeOH:$NH_{3\,14\%\ aq}$ (98:1:1) yielded *N*-palmitoyl propranolol **12** as a white solid (0.049 g, 70 %): ^{1}H (400 MHz; $CDCl_3$) δ 0.87 (t, J = 7.0 Hz, 3H, H_{29}), 1.11-1.36 (m, 54H, H_{Alkyl}), 1.59-1.65 (m, 2H, H_{16}), 2.32-2.38 (m, 2H, H_{15}), 3.51 (dd, J = 1.5, 14.6 Hz, 1H, H_{13}), 3.81 (dd, J = 8.4, 14.6 Hz, 1H, H_{13}), 4.04-4.29 (m, 4H, $H_{11,12,30}$), 5.74 (s, 1H, OH), 6.82-6.88 (m, 1H, H_9), 7.38-7.43 (m, 1H, H_8), 7.46–7.59 (m, 3H, $H_{1,2,7}$), 7.81–7.87 (m, 1H, H_3), 8.21–8.28 (m, 1H, H_6); ^{13}C (100 MHz; $CDCl_3$) δ 14.4 (C_{29}), 20.3 (C_{Alkyl}), 20.7 (C_{Alkyl}), 21.3 (C_{Alkyl}), 21.7 (C_{Alkyl}), 21.8 (C_{Alkyl}), 22.7 (C_{Alkyl}), 24.7 (C_{Alkyl}), 25.0 (C_{Alkyl}), 25.3 (C_{Alkyl}), 25.6 (C_{Alkyl}), 29.1 (C_{Alkyl}), 29.2 (C_{Alkyl}), 30.3 (C_{15}), 46.1 (C_{13}), 50.3 (C_{30}), 69.8 (C_{11}), 72.5 (C_{12}), 104.8 (C_9), 120.7 (C_7), 121.5 (C_6), 125.2 (C_5), 125.4 (C_1), 126.0 (C_8), 126.3 (C_2), 127.7 (C_3), 134.5 (C_4), 154.07 (C_{10}), 176.9 (C_{14}); IR (neat) υ_{max}/cm^{-1} 1745, 2914, 2926, 3391; LRMS (ESI) *m/z* 498.4 [M+H]$^+$; HRMS (ESI) calculated for $C_{32}H_{52}NO_3$ [M+H]$^+$ 498.3947, found 498.3943.[246,247]

Synthesis of Dioleoyl Propanolol 42

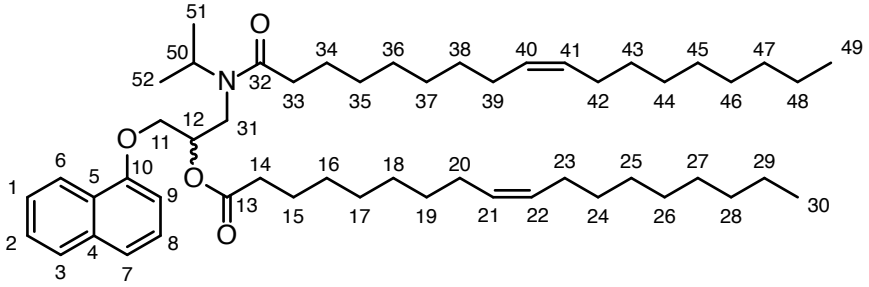

To propranolol **1** (0.050 g, 0.17 mmol) in dry DCM (4 mL) was added pyridine (0.015 mL, 0.19 mmol) and oleoyl chloride **20** (0.112 mL, 0.37 mmol). The mixture was stirred for 12 hours at room temperature, diluted with DCM and washed three times with saturated NH_4Cl solution. The organic layer was dried over $MgSO_4$ and solvent removed *in vacuo*. Purification by silica gel chromatography using eluent EtOAc:MeOH:$NH_{3\,14\%\ aq}$ (98:1:1) yielded dioleoyl propranolol **42** as a yellow oil (0.110 g, 82 %): ^{1}H (400 MHz; $CDCl_3$) δ 0.88 (t, 6H, J = 8.0 Hz, $H_{30,49}$), 1.13-1.37 (m, 46H, H_{Alkyl}), 1.55-1.67 (m, 4H, $H_{15,34}$), 1.97-2.03 (m, 8H, $H_{20,23,39,42}$), 2.31-2.51 (m, 4H, $H_{14,33}$), 3.38 (dd, J = 6.9, 14.3 Hz, 0.75 H, H_{31}), 3.66 (dd, J = 4.0, 15.8 Hz, 0.25 H, H_{31}), 3.85 (dd, J = 5.3, 14.3 Hz, 1H, H_{31}), 4.08–4.17 (m, 0.75H, H_{50}), 4.24–4.34 (m, 2H, H_{11}), 4.48–4.52 (m, 0.25H, H_{50}), 5.27-5.37 (m, 4H, $H_{21,22,40,41}$), 5.42–5.47 (m, 0.25H, H_{12}), 5.55–5.58 (m, 0.75H, H_{12}), 6.79-6.88 (m, 1H, H_9), 7.33-7.38 (m, 1H, H_8), 7.40–7.53 (m, 3H, $H_{1,2,7}$), 7.77–7.83 (m, 1H, H_3), 8.19–8.22 (m, 1H, H_6); ^{13}C (100 MHz; $CDCl_3$) δ 14.1 ($C_{30,49}$), 21.1 (C_{Alkyl}), 22.7 (C_{Alkyl}), 25.5 (C_{Alkyl}), 27.1 (C_{Alkyl}), 27.2 (C_{Alkyl}), 29.9 (C_{Alkyl}), 29.1 (C_{Alkyl}), 29.2 (C_{Alkyl}), 29.4 (C_{Alkyl}), 29.7 (C_{Alkyl}), 29.8 (C_{Alkyl}), 41.3 (C_{31}), 48.4 (C_{50}), 49. (C_{50}), 53.4 ($C_{14,33}$), 68.5 (C_{11}), 70.7 (C_{12}), 71.7 (C_{12}), 72.5 ($C_{21,22,40,41}$), 104.7 (C_9), 104.8 (C_9), 120.5 (C_7), 121.2 (C_7), 121.5 (C_6), 121.9 (C_6), 125.1 (C_5), 125.5 (C_1), 125.8 (C_8), 126.3 (C_2), 126.6 (C_8), 127.4 (C_4), 127.6 (C_2), 129.8 (C_4), 129.9 (C_4), 134.4 (C_4), 154.3 (C_{10}), 173.3 (C_{32}), 173.9 (C_{13}); IR (neat) υ_{max}/cm^{-1} 1652, 1746, 2915, 2986, 2930; LRMS (ESI) *m/z* 788.7 [M+H]$^+$; HRMS (ESI) calculater for $C_{52}H_{86}NO_4$ [M+H]$^+$ 788.6557, found 788.6573.[247]

Synthesis of *N*-Oleoyl Propanolol 13

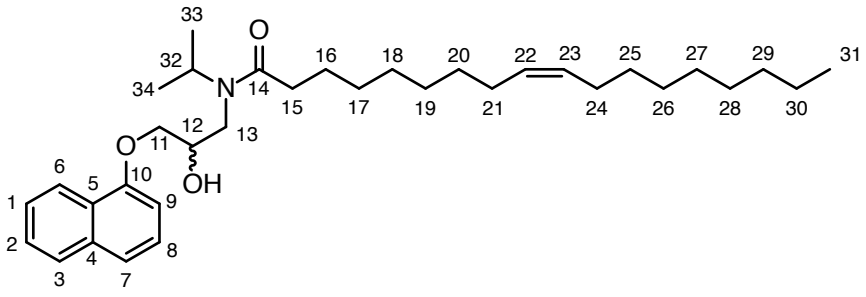

Dioleoyl propranolol **42** (0.050 g, 0.14 mmol) and K_2CO_3 (0.059 g, 0.43 mmol) were stirred in MeOH (1.5 mL) for 2 hours prior to solvent removal *in vacuo*. Solid was resuspended in MeOH (6 mL) and H_2SO_4 (0.12 mL), and refluxed for 1 hour to methylate excess fatty acid. The solution was diluted with DCM, washed with saturated $NaHCO_3$ solution until neutral, dried over $MgSO_4$, and solvent removed *in vacuo*. Purification by silica gel chromatography using eluent EtOAc:MeOH:$NH_{3\,14\%\ aq}$ (98:1:1) yielded *N*-oleoyl propranolol **13** as a yellow oil

(0.051 g, 70 %): ^{1}H (400 MHz; $CDCl_3$) δ 0.88 (t, 3H, J = 8.0 Hz, H_{31}), 1.09 (d, J = 6.6 Hz, 6H, $H_{33,34}$), 1.19-1.39 (m, 20H, H_{Alkyl}), 1.59-1.72 (m, 2H, H_{16}), 194-2.08 (m, 4H, $H_{21,24}$), 2.86 (quin, J = 20.0 Hz, 0.75H, H_{15}), 3.05 (quin, J = 20.0 Hz, 1.25H, H_{15}), 3.54 (dd, J = 1.5, 14.6 Hz, 1H, H_{13}), 3.75 (dd, J = 8.4, 14.6 Hz, 1H, H_{13}), 4.11-4.35 (m, 4H, $H_{11,12,32}$), 5.27-5.57 (m, 2H, $H_{22,23}$); 5.74 (s, 1H, OH), 6.80-6.87 (m, 1H, H_9), 7.37-7.40 (m, 1H, H_8), 7.40–7.51 (m, 3H, $H_{1,2,7}$), 7.79–7.83 (m, 1H, H_3), 8.20 (d, J = 6.0 Hz, 1H, H_6); ^{13}C (100 MHz; $CDCl_3$) δ 14.1 (C_{31}), 20.7 (C_{Alkyl}), 21.5 (C_{Alkyl}), 22.7 (C_{Alkyl}), 23.0 (C_{Alkyl}), 25.0 (C_{Alkyl}), 25.4 (C_{Alkyl}), 27.2 (C_{Alkyl}), 29.0 (C_{Alkyl}), 29.1 (C_{Alkyl}), 29.2 (C_{Alkyl}), 29.3 (C_{Alkyl}), 29.5 (C_{Alkyl}), 29.7 (C_{Alkyl}), 31.9(C_{Alkyl}), 33.8 (C_{Alkyl}), 34.0 (C_{Alkyl}), 46.2 (C_{13}), 47.3 (C_{13}), 48.6 (C_{32}), 49.1 (C_{32}), 67.8 (C_{11}), 69.9 (C_{11}), 71.7 (C_{12}), 72.5 (C_{12}), 104.8 (C_9), 120.6 (C_7), 121.6 (C_7), 121.9 (C_6), 125.2 (C_6), 125.4 (C_5), 125.7 (C_1), 125.9 (C_8), 126.3 (C_2), 127.4 (C_8), 127.6 (C_2), 129.7 (C_3), 130.0 ($C_{22,23}$), 134.5 (C_4), 154.0 (C_{10}), 173.6 (C_{14}), 176.4 (C_{14}); IR (neat) υ_{max}/cm^{-1} 1628, 2858, 2930, 3415; LRMS (ESI) m/z 524.4 $[M+H]^+$; HRMS (ESI) calculated for $C_{34}H_{54}NO_3$ $[M+H]^+$ 524.4104, found 524.4103.[246,247]

Ionisation Optimisation

Palmitoyl procaine **35** (0.5 µg mL^{-1}) in H_2O:MeCN (1:1) was direct infused into the ESI source of the Synapt G2-S (Waters Corp., UK) at a constant flow rate of 5 µL/ min using a syringe pump. Full scan data was collected in positive mode over m/z range 50-2000 for one minute. Ionisation parameters were varied as desired. Conditions tested are summarised in Table 10.7, with source temperature (150 °C), desolvation temperature (350 °C), cone gas flow (60 L h^{-1}), and desolvation gas flow (600 L h^{-1}) kept consistent.

Capillary Voltage (kV)	Sampling Cone Voltage (V)	Source Offset Voltage (V)
0.5	50	30
1.0	50	30
1.5	50	30
2.0	50	30
2.5	50	30
1.0	30	30
1.0	40	30
1.0	60	30
1.0	70	30
1.0	50	20
1.0	50	40

Table 10.7 Positive ESI parameters tested during optimisation for small molecule LCMS.

Chromatographic Optimisation

Chromatographic optimisation was conducted on a Synapt G2-S (Waters Corp., UK) recording ESI ions between *m/z* 50 to 2000, and PDA absorbance measurement between 210 nm and 500 nm. Full scan data was collected in positive mode, with optimised ionisation conditions employed throughout. Stock solutions (0.5 µg mL^{-1}) of procaine **2**, palmitoyl procaine **35**, and OPC were prepared in H_2O:MeCN (1:1). 3 µL was injected on to each stationary phase of interest, summarised in Table 10.8. Varied mobile phases were applied to each column in order to determine optimum mobile phase conditions, including: (i) linear 9 minute gradient shown in Table 10.9; (ii) modified gradient one shown in Table 10.10; (iii) modified gradient two shown in Table 10.11.

Column Type
Acquity BEH C_{18}
Acquity CSH C_{18}
Acquity BEH Phenyl
Acquity BEH Shield RP18
Acquity BEH C_8

Table 10.8 Stationary phases tested.

Time (min)	Flow Rate (mL/ min)	% H_2O (0.1 % FA)	% Mobile Phase B	Curve
0.00	0.4	95	5	6
0.50	0.4	95	5	6
7.00	0.4	5	95	6
8.30	0.4	5	95	6
8.40	0.4	95	5	6
9.00	0.4	95	5	6

Table 10.9 Linear gradient employed on column types listed in Table 10.8 during optimisation of small molecule intrinsic lipidation chromatography. Mobile phase B was either MeCN (0.1 % formic acid) or MeOH.

Time (min)	Flow Rate (mL/ min)	% H_2O (0.1 % FA)	% MeCN (0.1 % FA)	Curve
0.00	0.4	95	5	6
0.50	0.4	95	5	6
4.00	0.4	30	70	6
7.00	0.4	5	95	6
8.00	0.4	5	95	6
8.50	0.4	95	5	6
9.00	0.4	95	5	6

Table 10.10 Modified gradient one employed during optimisation of small molecule intrinsic lipidation chromatography.

Time (min)	Flow Rate (mL/ min)	% H_2O (0.1 % FA)	% MeCN (0.1 % FA)	Curve
0.00	0.4	95	5	6
0.50	0.4	95	5	6
3.00	0.4	30	70	6
7.00	0.4	5	95	6
8.00	0.4	5	95	6
8.50	0.4	95	5	6
9.00	0.4	95	5	6

Table 10.11 Modified gradient two employed during optimisation of small molecule intrinsic lipidation chromatography.

10.5 Chapter 6

Synthesis of *N*-Boc Propanolol 63

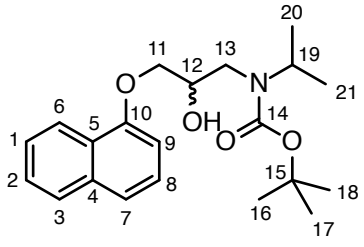

To propanolol **1** (0.048 g, 0.18 mmol) and NEt_3 (0.127 mL, 0.92 mmol) in DCM (2 mg) was added Boc_2O (0.080 mg, 0.37 mmol) and stirred for 12 hours. The mixture was diluted with DCM, washed three times with saturated NH_4Cl solution, dried over $MgSO_4$ and solvent removed *in vacuo*. Product **63** was isolated as a yellow oil by Kugelrohr distillation (0.051 g, 79 %): ^1H (400 MHz; $CDCl_3$) δ 1.23 (d, J = 5.8 Hz, 6H, $H_{20,21}$), 1.57 (s, 9H, $H_{16,17,18}$),

3.50-3.55 (m, 2H, H_{13}), 4.01-4.09 (m, 1H, H_{19}), 4.17-4.21 (m, 2H, $H_{11,12}$), 4.24-29 (m, 1H, H_{11}), 5.13 (s, 1H, OH), 6.86 (d, J = 8.0 Hz, 1H, H_9), 7.33-7.38 (m, 1H, H_8), 7.43-7.45 (m, 1H, H_7), 7.47-7.51 (m, 2H, $H_{1,2}$), 7.80 (d, J = 8.0 Hz, 1H, H_3), 8.22 (d, J = 8.0 Hz, 1H, H_6); ^{13}C (100 MHz; $CDCl_3$) δ 20.5 ($C_{20,21}$), 28.5 ($C_{16,17,18}$, 47.1 (C_{13}), 48.8 (C_{19}), 69.9 (C_{11}), 72.1 (C_{12}), 80.9 (C_{15}), 104.9 (C_9) 120.6 (C_7), 121.6 (C_6), 125.1 (C_5), 125.4 (C_1), 125.9 (C_8), 126.4 (C_2), 127.6 (C_3), 134.5 (C_4), 154.3 (C_{10}), 158.8 (C_{14}); IR (neat) υ_{max}/cm^{-1} 1692, 2953, 2983, 3476; LRMS (ESI) m/z 360.2 $[M+H]^+$; HRMS (ESI) calculated for $C_{21}H_{30}NO_4$ $[M+H]^+$ 360.2175, found 360.2168.[272]

Synthesis of *O*-Palmitoyl *N*-Boc Protected Propanolol 64

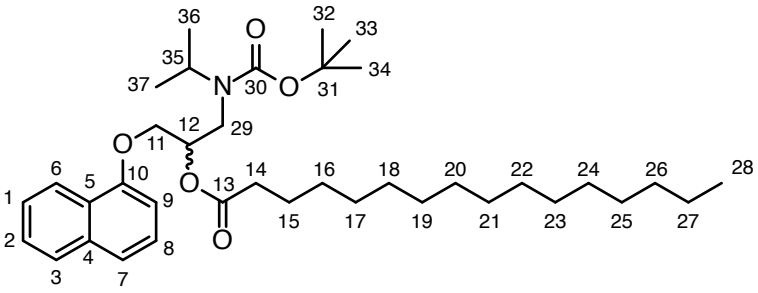

To *N*-Boc propanolol **63** (0.031 g, 0.09 mmol) in dry DCM (2 mL) was added pyridine (0.008 mL, 0.10 mmol) and palmitoyl chloride **18** (0.029 mL, 0.10 mmol). The mixture was stirred for 12 hours at room temperature, diluted with DCM and washed three time with saturated NH_4Cl solution. The organic layer was dried over $MgSO_4$ and solvent removed *in vacuo*. Purification by silica gel chromatography with eluent EtOAc:MeOH:$NH_{3(14\ \%\ aq)}$ (98:1:1) yielded **64** as a yellow oil (0.035 g, 65 %): ^{1}H (400 MHz; $CDCl_3$) δ 0.88 (t, J = 8.0 Hz, 3H, H_{28}), 1.11-1.33 (m, 30H, H_{Alkyl}), 1.51 (s, 9H, $H_{32,33,34}$), 1.61 (quint, J = 24.0 Hz, 2H, H_{15}), 2.32 (q, J = 12.0 Hz, 2H, H_{14}), 3.39-3.52 (m, 2H, H_{29}), 3.58-3.66 (m, 1H, H_{35}), 4.19-4.22 (m, 2H, $H_{11,12}$), 4.28-4.33 (m, 1H, H_{11}), 6.78 (d, J = 8.0 Hz, 1H, H_9), 7.34 (t, J = 8.0 Hz, 1H, H_8), 7.41-7.44 (m, 1H, H_7), 7.45-7.51 (m, 2H, $H_{1,2}$), 7.79 (d, J = 8.0 Hz, 1H, H_3), 8.21 (d, J = 8.0 Hz, 1H, H_6); ^{13}C (100 MHz; $CDCl_3$) δ 14.1 (C_{28}), 22.7 (C_{Alkyl}), 24.9 (C_{Alkyl}), 28.4 (C_{Alkyl}), 29.1 (C_{Alkyl}), 29.2 (C_{Alkyl}), 29.3 (C_{Alkyl}), 29.6 (C_{Alkyl}), 29.7 (C_{Alkyl}), 31.9 (C_{Alkyl}), 34.3 (C_{Alkyl}), 47.1 (C_{29}), 48.8 (C_{35}), 68.1 (C_{11}), 72.8 (C_{12}), 80.0 (C_{31}), 104.6 (C_9) 120.6 (C_7), 121.9 (C_6), 125.4 (C_5), 125.5 (C_1), 125.7(C_8), 126.4 (C_2), 127.4 (C_3), 134.5 (C_4), 154.3 (C_{10}), 173.4 (C_{30}), 178.8 (C_{13}); IR (neat) υ_{max}/cm^{-1} 1600, 1715, 2916, 2998; LRMS (ESI) m/z 598.4 $[M+H]^+$; HRMS (ESI) calculated for $C_{37}H_{60}NO_5$ $[M+H]^+$ 598.4471, found 598.4571.[242,243]

Synthesis of *O*-Oleoyl *N*-Boc Protected Propanolol 65

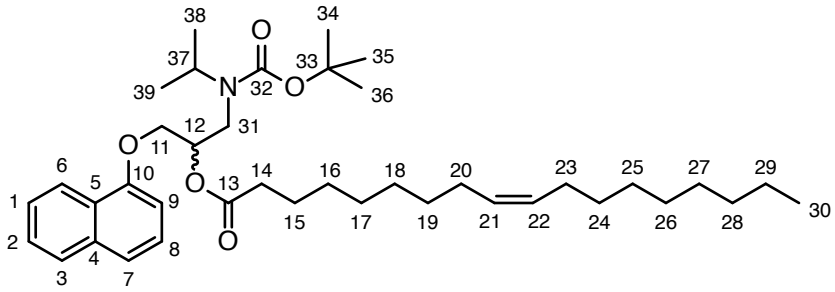

To *N*-Boc propanolol **63** (0.031 g, 0.09 mmol) in dry DCM (2 mL) was added pyridine (0.008 mL, 0.10 mmol) and oleoyl chloride **20** (0.029 mL, 0.10 mmol). The mixture was stirred for 12 hours at room temperature, diluted with DCM and washed three time with saturated NH_4Cl solution. The organic layer was dried over $MgSO_4$ and solvent removed *in vacuo*. Purification by silica gel chromatography with eluent EtOAc:MeOH:$NH_{3(14\ \%\ aq)}$ (98:1:1) yielded **65** as a yellow oil (0.035 g, 63 %): ^{1}H (400 MHz; $CDCl_3$) δ 0.88 (t, J = 8.0 Hz, 3H, H_{30}), 1.18-1.36 (m, 24H, H_{Alkyl}), 1.51 (s, 9H, $H_{34,35,36}$), 1.97-2.01 (m, 4H, $H_{20,23}$), 2.15 (q, J = 12.0 Hz, 2H, H_{15}), 2.88 (t, 2H, J = 8.0 Hz, H_{14}), 3.39-3.52 (m, 2H, H_{31}), 3.58-3.66 (m, 1H, H_{37}), 4.19-4.22 (m, 2H, $H_{11,12}$), 4.28-4.33 (m, 1H, H_{11}), 5.30-5.35 (m, 2H, $H_{21,22}$), 6.78 (d, J = 8.0 Hz, 1H, H_9), 7.36 (t, J = 8.0 Hz, 1H, H_8), 7.42-7.44 (m, 1H, H_7), 7.45-7.51 (m, 2H, $H_{1,2}$), 7.80 (d, J = 8.0 Hz, 1H, H_3), 8.22 (d, J = 8.0 Hz, 1H, H_6); ^{13}C (100 MHz; $CDCl_3$) δ 14.1 (C_{30}), 22.7 (C_{Alkyl}), 24.9 (C_{Alkyl}), 28.4 (C_{Alkyl}), 29.1 (C_{Alkyl}), 29.2 (C_{Alkyl}), 29.3 (C_{Alkyl}), 29.6 (C_{Alkyl}), 29.7 (C_{Alkyl}), 31.9 (C_{Alkyl}), 34.3 (C_{Alkyl}), 47.1 (C_{31}), 48.8 (C_{37}), 68.1 (C_{11}), 72.8 (C_{12}), 80.0 (C_{33}), 104.6 (C_9) 120.6 (C_7), 121.9 (C_6), 125.4 (C_5), 125.5 (C_1), 125.7(C_8), 126.4 (C_2), 127.4 (C_3), 130.5 (C_{21}), 130.7 (C_{22}), 134.5 (C_4), 154.3 (C_{10}), 173.9 (C_{32}), 178.8 (C_{13}); IR (neat) υ_{max}/cm^{-1} 1598, 1741, 2915, 2929; LRMS (ESI) m/z 624.5 [M+H]$^+$; HRMS (ESI) calculated for $C_{39}H_{62}NO_5$ [M+H]$^+$ 624.4628, found 624.4710.[242,243]

Synthesis of *O*-Palmitoyl Propranolol 62 - Method 1

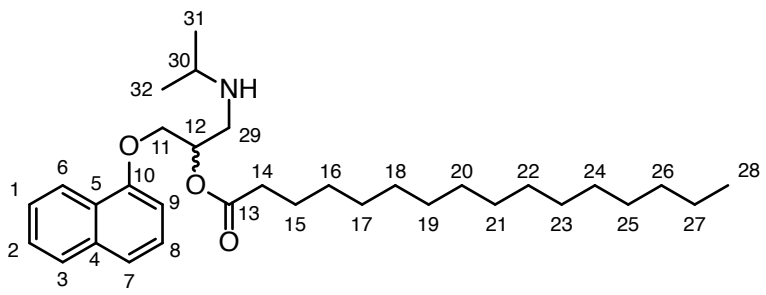

TFA (0.4 mL) was added dropwise to *O*-palmitoyl *N*-Boc propranolol **64** (0.05 g, 0.09 mmol) in DCM (0.4 mL) and stirred for 2 hours. Solvent and impurities were removed *in vacuo* to yield the TFA salt of **62** (0.044 g, 98 %): ^{1}H (400 MHz; $CDCl_3$) δ 0.88 (t, J = 8.0 Hz, 3H, H_{28}), 1.11-1.33 (m, 30H, H_{Alkyl}), 1.61 (quint, J = 24.0 Hz, 2H, H_{15}), 2.32 (q, J = 12.0 Hz, 2H, H_{14}), 3.39-3.52 (m, 2H, H_{29}), 3.58-3.66 (m, 1H, H_{30}), 4.19-4.22 (m, 2H, $H_{11,12}$), 4.28-4.33 (m, 1H, H_{11}), 6.78 (d, J = 8.0 Hz, 1H, H_9), 7.34 (t, J = 8.0 Hz, 1H, H_8), 7.41-7.44 (m, 1H, H_7), 7.45-7.51 (m, 2H, $H_{1,2}$), 7.79 (d, J = 8.0 Hz, 1H, H_3), 8.21 (d, J = 8.0 Hz, 1H, H_6), 9.70 (s, 1H, NH); ^{13}C (100 MHz; $CDCl_3$) δ 14.1 (C_{28}), 22.7 (C_{Alkyl}), 24.9 (C_{Alkyl}), 28.4 (C_{Alkyl}), 29.1 (C_{Alkyl}), 29.2 (C_{Alkyl}), 29.3 (C_{Alkyl}), 29.6 (C_{Alkyl}), 29.7 (C_{Alkyl}), 31.9 (C_{Alkyl}), 34.3 (C_{Alkyl}), 47.1 (C_{29}), 48.8 (C_{30}), 68.1 (C_{11}), 72.8 (C_{12}), 104.6 (C_9) 120.6 (C_7), 121.9 (C_6), 125.4 (C_5), 125.5 (C_1), 125.7(C_8), 126.4 (C_2), 127.4 (C_3), 134.5 (C_4), 154.3 (C_{10}), 173.4 (C_{13}); IR (neat) υ_{max}/cm^{-1} 1745, 2856, 2924; LRMS (ESI) m/z 498.4 $[M+H]^+$; HRMS (ESI) calculated for $C_{32}H_{52}NO_3$ $[M+H]^+$ 498.3947, found 498.3943.[272]

Synthesis of *O*-Palmitoyl Propranolol 62 - Method 2

37 % $HCl_{(aq)}$ (0.1 mL) was added dropwise to *O*-palmitoyl *N*-Boc propranolol **64** (0.05 g, 0.09 mmol) in EtOAc (0.9 mL) and stirred for 1.5 hours. The mixture was diluted with EtOAc, washed with 5 % HCl solution, and dried over $MgSO_4$. Solvent removal *in vacuo* yielded the *N*-acylated migration product only.[272]

Synthesis of *O*-Palmitoyl Propranolol 62 - Method 3

37 % $HCl_{(aq)}$ (0.6 mL) was added dropwise to *O*-palmitoyl *N*-Boc propranolol **64** (0.06 g, 0.09 mmol) in DCM (0.6 mL) and stirred for 1.5 hours. Solvent and impurities were removed *in vacuo* to yield the HCl salt of **62** (0.044 g, 98 %): ^{1}H (400 MHz; $CDCl_3$) δ 0.88 (t, J = 8.0 Hz, 3H, H_{28}), 1.11-1.33 (m, 30H, H_{Alkyl}), 1.61 (quint, J = 24.0 Hz, 2H, H_{15}), 2.32 (q, J = 12.0 Hz, 2H, H_{14}), 3.39-3.52 (m, 2H, H_{29}), 3.58-3.66 (m, 1H, H_{30}), 4.19-4.22 (m, 2H, $H_{11,12}$), 4.28-4.33 (m, 1H, H_{11}), 6.78 (d, J = 8.0 Hz, 1H, H_9), 7.34 (t, J = 8.0 Hz, 1H, H_8), 7.41-7.44 (m, 1H, H_7), 7.45-7.51 (m, 2H, $H_{1,2}$), 7.79 (d, J = 8.0 Hz, 1H, H_3), 8.21 (d, J = 8.0 Hz, 1H, H_6), 9.70 (s, 1H, NH); ^{13}C (100 MHz; $CDCl_3$) δ 14.1 (C_{28}), 22.7 (C_{Alkyl}), 24.9 (C_{Alkyl}), 28.4 (C_{Alkyl}), 29.1 (C_{Alkyl}), 29.2 (C_{Alkyl}), 29.3 (C_{Alkyl}), 29.6 (C_{Alkyl}), 29.7 (C_{Alkyl}), 31.9 (C_{Alkyl}), 34.3 (C_{Alkyl}), 47.1 (C_{29}), 48.8 (C_{30}), 68.1 (C_{11}), 72.8 (C_{12}), 104.6 (C_9) 120.6 (C_7), 121.9 (C_6), 125.4 (C_5), 125.5 (C_1), 125.7(C_8), 126.4 (C_2), 127.4 (C_3), 134.5 (C_4), 154.3

(C_{10}), 173.4 (C_{13}); IR (neat) υ_{max}/cm^{-1} 1745, 2856, 2924; LRMS (ESI) *m/z* 498.4 $[M+H]^+$; HRMS (ESI) calculated for $C_{32}H_{52}NO_3$ $[M+H]^+$ 498.3947, found 498.3943.[272]

Synthesis of *O*-Oleoyl Propranolol 47 - Method 1

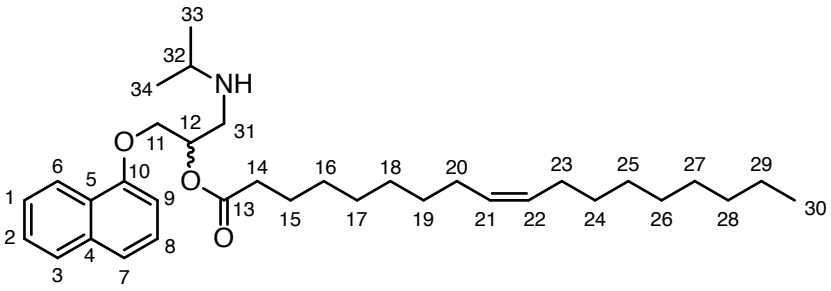

TFA (0.4 mL) was added dropwise to *O*-oleoyl *N*-Boc propranolol **65** (0.05 g, 0.08 mmol) in DCM (0.4 mL) and stirred for 2 hours. Solvent and impurities were removed *in vacuo* to yield the TFA salt of **47** (0.045 g, 96 %): ^1H (400 MHz; $CDCl_3$) δ 0.88 (t, J = 8.0 Hz, 3H, H_{30}), 1.18-1.36 (m, 24H, H_{Alkyl}), 1.97-2.01 (m, 4H, $H_{20,23}$), 2.15 (q, J = 12.0 Hz, 2H, H_{15}), 2.88 (t, 2H, J = 8.0 Hz, H_{14}), 3.39-3.52 (m, 2H, H_{31}), 3.58-3.66 (m, 1H, H_{32}), 4.19-4.22 (m, 2H, $H_{11,12}$), 4.28-4.33 (m, 1H, H_{11}), 5.30-5.35 (m, 2H, $H_{21,22}$), 6.78 (d, J = 8.0 Hz, 1H, H_9), 7.36 (t, J = 8.0 Hz, 1H, H_8), 7.42-7.44 (m, 1H, H_7), 7.45-7.51 (m, 2H, $H_{1,2}$), 7.80 (d, J = 8.0 Hz, 1H, H_3), 8.22 (d, J = 8.0 Hz, 1H, H_6), 9.58 (s, 1H, NH); ^{13}C (100 MHz; $CDCl_3$) δ 14.1 (C_{30}), 22.7 (C_{Alkyl}), 24.9 (C_{Alkyl}), 28.4 (C_{Alkyl}), 29.1 (C_{Alkyl}), 29.2 (C_{Alkyl}), 29.3 (C_{Alkyl}), 29.6 (C_{Alkyl}), 29.7 (C_{Alkyl}), 31.9 (C_{Alkyl}), 34.3 (C_{Alkyl}), 47.1 (C_{31}), 48.8 (C_{32}), 68.1 (C_{11}), 72.8 (C_{12}), 104.6 (C_9) 120.6 (C_7), 121.9 (C_6), 125.4 (C_5), 125.5 (C_1), 125.7(C_8), 126.4 (C_2), 127.4 (C_3), 130.5 (C_{21}), 130.7 (C_{22}), 134.5 (C_4), 154.3 (C_{10}), 175.2 (C_{13}); IR (neat) υ_{max}/cm^{-1} 1744, 2859, 2930; LRMS (ESI) *m/z* 524.4 $[M+H]^+$; HRMS (ESI) calculated for $C_{34}H_{54}NO_3$ $[M+H]^+$ 524.4104, found 524.4103.[272]

Synthesis of *O*-Oleoyl Propranolol 47 - Method 2

37 % $HCl_{(aq)}$ (0.1 mL) was added dropwise to *O*-oleoyl *N*-Boc propranolol **65** (0.05 g, 0.08 mmol) in EtOAc (0.9 mL) and stirred for 1.5 hours. The mixture was diluted with EtOAc, washed with 5 % HCl solution, and dried over $MgSO_4$. Solvent removal *in vacuo* yielded the *N*-acylated migration product only.[272]

Synthesis of *O*-Oleoyl Propranolol 47 - Method 3

37 % $HCl_{(aq)}$ (0.6 mL) was added dropwise to *O*-oleoyl *N*-Boc propranolol **65** (0.06 g, 0.09 mmol) in DCM (0.6 mL) and stirred for 1.5 hours. Solvent and impurities were removed *in vacuo* to yield the HCl salt of **47** (0.045 g, 96 %): ^{1}H (400 MHz; $CDCl_3$) δ 0.88 (t, J = 8.0 Hz, 3H, H_{30}), 1.18-1.36 (m, 24H, H_{Alkyl}), 1.97-2.01 (m, 4H, $H_{20,23}$), 2.15 (q, J = 12.0 Hz, 2H, H_{15}), 2.88 (t, 2H, J = 8.0 Hz, H_{14}), 3.39-3.52 (m, 2H, H_{31}), 3.58-3.66 (m, 1H, H_{32}), 4.19-4.22 (m, 2H, $H_{11,12}$), 4.28-4.33 (m, 1H, H_{11}), 5.30-5.35 (m, 2H, $H_{21,22}$), 6.78 (d, J = 8.0 Hz, 1H, H_9), 7.36 (t, J = 8.0 Hz, 1H, H_8), 7.42-7.44 (m, 1H, H_7), 7.45-7.51 (m, 2H, $H_{1,2}$), 7.80 (d, J = 8.0 Hz, 1H, H_3), 8.22 (d, J = 8.0 Hz, 1H, H_6), 9.58 (s, 1H, NH); ^{13}C (100 MHz; $CDCl_3$) δ 14.1 (C_{30}), 22.7 (C_{Alkyl}), 24.9 (C_{Alkyl}), 28.4 (C_{Alkyl}), 29.1 (C_{Alkyl}), 29.2 (C_{Alkyl}), 29.3 (C_{Alkyl}), 29.6 (C_{Alkyl}), 29.7 (C_{Alkyl}), 31.9 (C_{Alkyl}), 34.3 (C_{Alkyl}), 47.1 (C_{31}), 48.8 (C_{32}), 68.1 (C_{11}), 72.8 (C_{12}), 104.6 (C_9) 120.6 (C_7), 121.9 (C_6), 125.4 (C_5), 125.5 (C_1), 125.7(C_8), 126.4 (C_2), 127.4 (C_3), 130.5 (C_{21}), 130.7 (C_{22}), 134.5 (C_4), 154.3 (C_{10}), 175.2 (C_{13}); IR (neat) υ_{max}/cm^{-1} 1744, 2859, 2930; LRMS (ESI) *m/z* 524.4 $[M+H]^+$; HRMS (ESI) calculated for $C_{34}H_{54}NO_3$ $[M+H]^+$ 524.4104, found 524.4103.[272]

Solvation of Diacylated Propranolol

Dipalmitoyl propranolol **41** and dioleoyl propranolol **42** were dissolved in solvent mixtures listed in Table 10.12 at concentration 1 µg mL^{-1}. Each sample was then analysed according to optimised small molecule LCMS conditions.

Solvent System
MeCN
MeCN:H_2O (9:1)
MeCN:H_2O (1:1)
MeCN:DCM (10:0.01)
MeCN:H_2O:DCM (9:1:0.01)
MeCN:H_2O:DCM (1:1:0.01)
MeCN:DCM (10:0.1)
MeCN:H_2O:DCM (9:1:0.1)
MeCN:H_2O:DCM (1:1:0.1)

Table 10.12 Solvent systems applied to analysis of dipalmitoyl propranolol **41** and dioleoyl propranolol **42**

Diacylated Propranolol Chromatographic Optimisation

Chromatographic optimisation was conducted on a Synapt G2-S (Waters Corp., UK) recording ESI ions between m/z 50 to 2000, and PDA absorbance measurement between 210 nm and 500 nm. Full scan data was collected in positive mode, with optimised ionisation conditions employed throughout. Stock solutions (0.5 µg mL^{-1}) of dipalmitoyl propranolol **41** and dioleoyl propranolol **42** were injected at volume 3 µL on to a BEH Phenyl stationary phase (Waters Corp., UK). Mobile phases were applied to each column in order to determine optimum mobile phase conditions, including: (i) linear 9 minute gradient shown in Table 10.13; (ii) extended ten minute gradient shown in Table 10.14.

Time (min)	Flow Rate (mL/ min)	% H_2O (0.1 % FA)	% MeCN (0.1 % FA)	Curve
0.00	0.4	95	5	6
0.50	0.4	95	5	6
7.00	0.4	5	95	6
8.00	0.4	5	95	6
8.50	0.4	95	5	6
9.00	0.4	95	5	6

Table 10.13 Initial gradient optimised for small molecule LCMS in Chapter 5, and applied to the separation of diacylated propranolol species on a BEH Phenyl column (Waters Corp., UK).

Time (min)	Flow Rate (mL/ min)	% H_2O (0.1 % FA)	% MeCN (0.1 % FA)	Curve
0.00	0.4	95	5	6
0.50	0.4	95	5	6
7.50	0.4	5	95	6
8.80	0.4	5	95	6
8.90	0.4	95	5	6
10.00	0.4	95	5	6

Table 10.14 Extended gradient applied to separation of diacylated propranolol species of a BEH Phenyl column (Waters Corp., UK) and taken forwards as the optimised chromatography gradient for small molecule LCMS *in vitro*.

Quantitative Mass Spectrometry

Stock solutions of small molecules were prepared in H_2O:MeCN (1:1) at concentration 1 mg mL^{-1} . A 1 µL aliquot was further diluted into H_2O:MeCN (1:1) to final concentration 1 µg mL^{-1}. Serial dilution (1:1) in H_2O:MeCN (1:1) was carried out down to concentration

7.8 ng mL^{-1}. Each concentration was prepared in triplicate and analysed under optimised small molecule LCMS conditions. Peak areas were modelled for each concentration, and averaged in order to produce a calibration curve for the species.

O to *N* Intramolecular Migration Rate - Method 1

Synthetic *O*-palmitoyl propranolol **62** and *O*-oleoyl propranolol **47** stock solutions were prepared in H_2O:MeCN at 1.27 mM. Small molecule stock solution (3 µL) was added to extruded liposomes (30 µL) containing DOPC or DPPC in a 1:10 small molecule:lipid ratio. Samples were incubated under physiological conditions (pH 7.41 and 37 °C), and analysed at relevant time points by optimised small molecule LCMS.

O to *N* Intramolecular Migration Rate - Method 2

Synthetic *O*-palmitoyl propranolol **62** and *O*-oleoyl propranolol **47** stock solutions were prepared in MeCN at 1.27 mM. Small molecule stock was combined with DOPC or DPPC stock solutions in $CHCl_3$ in 1:10 small molecule:lipid ratio, and solvent removed *in vacuo* creating a thin film. Mixed small molecule and phospholipid liposomes were prepared from this film by applying extrusion methodology. Samples were incubated under physiological conditions (pH 7.41 and 37 °C), and analysed at relevant time points by optimised small molecule LCMS.

Small Molecule Buffer pH 4.30

10 mM NH_4HCO_3 was fully dissolved in H_2O. pH was measured and adjusted to a value of 4.30 using formic acid.

Small Molecule Buffer pH 10.40

10 mM NH_4HCO_3 was fully dissolved in H_2O. pH was measured and adjusted to a value of 10.40 using $NH_4OH_{(aq)}$.

Micelle Preparation

Stock solutions of lysolipid in $CHCl_3$:MeOH (2:1) were prepared at a concentration of $10\,mg\,mL^{-1}$ and stored at -20 °C. A 100 µL aliquot of lysolipid stock solution was added to a round-bottomed flask, and solvent removed *in vacuo* resulting in formation of a lipid film. Following overnight dessication, the lysolipid film was rehydrated in buffer solution and agitated using a vortex mixer creating micelles

10.6 Chapter 7

Positive Ionisation Optimisation

POPC ($0.5\,\mu g\,mL^{-1}$) in IPA:H_2O:MeCN (2:1:1) was direct infused into the ESI source of the Synapt G2-S (Waters Corp., UK) at a constant flow rate of 5 µL/ min using a syringe pump. Full scan data was collected in positive mode over *m/z* range 50-2000 for one minute. Ionisation parameters were varied as desired. Conditions tested are summarised in Table 10.15, with source temperature (150 °C), desolvation temperature (350 °C), cone gas flow ($60\,L\,h^{-1}$), and desolvation gas flow ($600\,L\,h^{-1}$) kept consistent.

Capillary Voltage (kV)	Sampling Cone Voltage (V)	Source Offset Voltage (V)
1.0	50	30
1.5	50	30
2.0	50	30
2.5	50	30
3.0	50	30
2.0	30	30
2.0	70	30
2.0	50	20
2.0	50	40

Table 10.15 Positive ESI parameters tested during optimisation for POPC LCMS.

Negative Ionisation Optimisation

POPS ($0.5\,\mu g\,mL^{-1}$) in IPA:H_2O:MeCN (2:1:1) was direct infused into the ESI source of the Synapt G2-S (Waters Corp., UK) at a constant flow rate of 5 µL/ min using a syringe pump. Full scan data was collected in positive mode over *m/z* range 50-2000 for one minute.

Ionisation parameters were varied as desired. Conditions tested are summarised in Table 10.16, with source temperature (150 °C), desolvation temperature (350 °C), cone gas flow ($60\,\mathrm{L\,h^{-1}}$), and desolvation gas flow ($600\,\mathrm{L\,h^{-1}}$) kept consistent.

Capillary Voltage (kV)	Sampling Cone Voltage (V)	Source Offset Voltage (V)
1.0	50	30
1.5	50	30
2.0	50	30
2.5	50	30
3.0	50	30
2.5	20	30
2.5	30	30
2.5	40	30
2.5	30	20
2.5	30	40

Table 10.16 Positive ESI parameters tested during optimisation for small molecule LCMS.

Chromatographic Optimisation

Chromatographic optimisation was conducted on a Synapt G2-S (Waters Corp., UK) recording ESI ions between *m/z* 50 to 2000, and PDA absorbance measurement between 210 nm and 500 nm. Full scan data was collected in positive and negative mode, with optimised ionisation conditions employed throughout. Lipid mixture was prepared containing components listed in Table 10.17 at concentration $0.5\,\mathrm{\mu g\,mL^{-1}}$ in IPA:H_2O:MeCN (2:1:1). 3 µL was injected on to Acquity CSH C_{18} 1.7 µm (2.1 x 150 mm) column at 60 °C. Varied gradients of mobile phases A (H_2O:MeCN 4:6 with 10 mM NH_4HCO_2 and 0.1 % formic acid) and B (MeCN:IPA 1:9 with 10 mM NH_4HCO_2 and 0.1 % formic acid) were applied to each column in order to determine optimum mobile phase conditions.

Lipid
PPC
OPC
OPE
OPG
DOPC
POPC
OPPC
DOPE
DOPG
SLPG
DOPS
POPS

Table 10.17 Components of lipid mix prepared for chromatography optimisation.

Optimised Small Molecule LCMS *in cellulo*

Samples were diluted in MeCN:H_2O (1:1) to small molecule concentration 1 µg mL^{-1}. LCMS analyses were conducted on a Synapt G2-S (Waters Corp., UK) recording ESI ions between *m/z* 50 to 2000, and PDA absorbance measurement between 210 nm and 500 nm. Optimised chromatography was conducted by 3 µL injection on to an Acquity UPLC with CSH C_{18} 1.7 µm (2.1 x 150 mm) column at 60 °C. Mobile phase conditions are summarised in Table 10.18 positive ESI ionisation parameters are presented in Table 10.19.

Time (min)	Flow Rate (mL/ min)	% A	% B	Curve
0.00	0.4	60	40	6
2.00	0.4	57	43	6
2.10	0.4	50	50	6
12.00	0.4	46	54	6
12.10	0.4	30	70	6
18.00	0.4	1	99	6
18.10	0.4	60	40	6
20.0	0.4	60	40	6

Table 10.18 Optimised chromatography gradient for small molecule LCMS *in cellulo*. Mobile phase A is H_2O:MeCN 4:6 (10 mM NH_4HCO_2 and 0.1 % formic acid), and B is MeCN:IPA 1:9 (10 mM NH_4HCO_2 and 0.1 % formic acid).

Parameter	Positive Mode	Negative Mode
Capillary Voltage (kV)	2.5	2.0
Source Temperature (°C)	150.0	150.0
Sampling Cone Voltage (V)	50.0	30.0
Source Offset Voltage (V)	30.0	30.0
Desolvation Temperature (°C)	350.0	350.0
Cone Gas Flow ($L\,h^{-1}$)	60.0	60.0
Desolvation Gas Flow ($L\,h^{-1}$)	600.0	600.0
Nebuliser Gas Flow (Bar)	6.0	6.0

Table 10.19 Optimised ESI parameters for small molecule LCMS *in cellulo*.

$CHCL_3$ Extraction

Small molecule incubations were prepared under standard conditions containing propranolol **1** (3 µL at 1.27 mM) and POPC (30 µL at 1.27 mM). Following 72 hour incubation under physiological conditions, $CHCl_3$ (33 µL) was added and vortexed to mix. Layer separation occurred, and an aliquot was removed from the lower organic layer for LCMS analysis.

$CHCL_3$:MeOH Extraction

Small molecule incubations were prepared under standard conditions containing propranolol **1** (3 µL at 1.27 mM) and POPC (30 µL at 1.27 mM). Following 72 hour incubation under physiological conditions, $CHCl_3$:MeOH (2:1) (33 µL) was added and vortexed to mix. Layer separation occurred, and an aliquot was removed from the lower organic layer for LCMS analysis.

MTBE Extraction

Small molecule incubations were prepared under standard conditions containing propranolol **1** (3 µL at 1.27 mM) and POPC (30 µL at 1.27 mM). Following 72 hour incubation under physiological conditions, MTBE (33 µL) was added and vortexed to mix. Layer separation occurred, and an aliquot was removed from the lower organic layer for LCMS analysis.

Hep G2 Cell Growth

Hep G2 cells were grown at 37 °C, 5 % CO_2, and 95 % humidity in Dulbecco's modified Eagle medium supplemented with foetal bovine medium (10 % v/v). Media was removed from confluent cells, washed with PBS solution, and Triplex (1 mL) added to facilitate cell detachment. Following 10 minutes further incubation, media (10 mL) was added to the cloudy solution. Solution (10 µL) was removed to determine cell number using a haemocytometer, and concentration adjusted accordingly.[332,333]

Hep G2 Concentration Test

Hep G2 cells (50 µL equal to 2×10^4) were added to each well of a 95 well plate and incubated at 37 °C, 5 % CO_2, and 95 % humidity for 5 hours to adhere. Sterilised propranolol **1** stock solution at concentration 60 µM in H_2O was serially diluted (1:1) down to concentration 117 nM. Propranolol **1** (50 µL) at desired concentration was added to cells in triplicate, and incubated at 37 °C, 5 % CO_2, and 95 % humidity. Cell growth was examined by light microscopy following 72 hours.

Intrinsic Lipidation in Hep G2 Cells

Hep G2 cells (1×10^6) were added to each of four T-75 flasks and incubated at 37 °C, 5 % CO_2, and 95 % humidity overnight to adhere. Media was removed and replaced with either fresh media (5 mL) for two controls, or medium containing 30 µM propranolol **1** (5 mL). Following 72 hour incubation, media was removed from flasks and replaced with PBS (5 mL). Cells were removed from surface by manual scraping, and washed three times with PBS. Solid cells were collected by 10 minute centrifugation at 1000 g, and decanted into a glass tube for extraction. $CHCl_3$:MeOH (2:1) (3 mL) was added, shaken for 30 minutes, and centrifuged to isolate remaining solid. The $CHCl_3$:MeOH (2:1) solution was washed with H_2O (0.6 mL), isolated, and solvent removed *in vacuo*. Samples were resuspended in IPA:MeCN:H_2O (2:1:1) for analysis by optimised *in cellulo* LCMS.

10.7 Chapter 8

Synthesis of 2-Aminomethylbenzimidazole 11 - Method 1

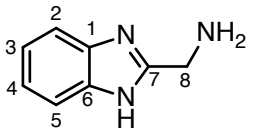

o-Phenylenediamine (1.080 g, 10.00 mmol) and glycine (1.060 g, 14.00 mmol) were refluxed in toluene (20 mL) for 9 hours. After cooling the resulting solid was collected by filtration but revealed only starting material.[309]

Synthesis of 2-Aminomethylbenzimidazole 11 - Method 2

o-Phenylenediamine (1.08 g, 10.00 mmol) and glycine (0.90 g, 20.00 mmol) were refluxed in 37 % HCl (4 mL) for 5 days until NMR indicated full conversion. After cooling, the resulting solid was isolated by filtration and combined with the solid obtained by freeze drying the reaction mixture. Purification by recrystallisation from MeOH yielded compound **11** as a tan solid (2.06 g, 94 %): ^{1}H (400 MHz; DMSO-d6) δ 3.54 (t, J = 5.7 Hz, 2H, H_8), 4.48 (t, J = 5.7 Hz, 2H, NH_2), 7.43-7.48 (m, 2H, $H_{3,4}$), 7.77-7.81 (m, 2H, $H_{2,5}$), 9.08 (s, 1H, NH); ^{13}C (100 MHz; DMSO-d6) δ 39.2 (C_8), 116.8 ($C_{2,5}$), 125.4 ($C_{3,4}$), 136.4 ($C_{1,6}$), 148.7 (C_7); IR (neat) ν_{max}/cm^{-1} 1581, 1605, 2930, 3021, 3248, 3360, 3387; LRMS (ESI) m/z 148.1 $[M+H]^+$; HRMS (ESI) calculated for $C_8H_{10}N_3$ $[M+H]^+$ 148.0875, found 148.0872; m.p. = 269-270 °C.[177,178]

Synthesis of *N*-Oleoyl 2-Aminomethylbenzimidazole 67

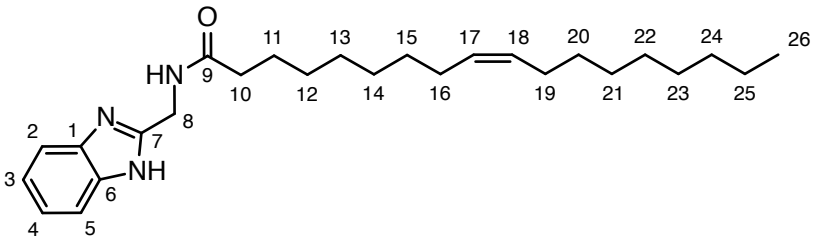

2-Aminomethylbenzimidazole **11** (0.15 g), 1.02 mmol), pyridine (0.09 mL), 1.12 mmol), and oleoyl chloride **20** (0.37 mL), 1.12 mmol) were stirred in dry DCM (10 mL) under argon for

12 hours. The organic phase was washed with saturated NH_4Cl solution three times, dried over $MgSO_4$, and solvent removed *in vacuo*. Purification by Kugelrohr distillation yielded compound **67** as a yellow oil (0.26 g, 61 %): ^{1}H (400 MHz; DMSO-d6) δ 0.87 (t, 3H, J = 8.0 Hz, H_{26}), 1.23-1.28 (m, 20H, H_{Alkyl}), 1.63 (quin, 2H, J = 12.0 Hz, H_{11}), 1.95-2.01 (m, 4H, $H_{16,19}$), 2.27 (t, 2H, J = 8.0 Hz, H_{10}), 4.58 (m, 2H, H_8), 5.28-5.37 (m, 2H, $H_{17,18}$), 7.43-7.48 (m, 2H, $H_{3,4}$), 7.77-7.81 (m, 2H, $H_{2,5}$); ^{13}C (100 MHz; DMSO-d6) δ 14.1 (C_{26}), 22.6 (C_{Alkyl}), 25.6 (C_{Alkyl}), 27.1 (C_{Alkyl}), 27.2 (C_{Alkyl}), 29.1 (C_{Alkyl}), 29.2 (C_{Alkyl}), 29.3 (C_{Alkyl}), 29.5 (C_{Alkyl}), 29.7 (C_{Alkyl}), 31.9 (C_{Alkyl}), 36.3 (C_{10}), 37.9 (C_8), 122.7 ($C_{2,5}$), 129.6 ($C_{3,4}$), 129.8 ($C_{1,6}$), 130.0 ($C_{17,18}$), 152.0 (C_7) 175.8 (C_9; IR (neat) υ_{max}/cm^{-1} 1635, 2930, 2995, 3347; LRMS (ESI) *m/z* 412.3 $[M+H]^+$; HRMS (ESI) calculated for $C_{26}H_{42}N_3O$ $[M+H]^+$ 412.3328, found 412.3325.[310]

Semi Quantitative Mass Spectrometry

Small molecules were incubated *in vitro* under standard conditions. Samples were diluted with H_2O:MeCN (1:1) to approximate concentration 1 µg mL^{-1} of small molecule. Acylated standard **67** stock solution (1.25 µL at 1 µg mL^{-1} in H_2O) was added into MS sample prior to analysis under optimised LCMS conditions. Acylated standard **67** peak areas were determined and utilised to normalise data between samples.

Synthesis of 2-Chloromethyl-1H-benzimidazole 83

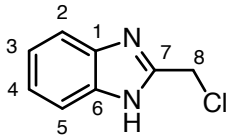

Monochloroacetic acid (3.75 g, 0.04 mol), and *o*-phenylenediamine (3.79 g, 0.04 mol) were refluxed in 37 % $HCl_{(aq)}$ (30 mL) for 12 hours. Upon cooling to 5 °C, the solution was neutralised with $NH_4OH_{(aq)}$ and the resulting precipitate collected. Hexane recyrstallisation yielded orange solid **83** (5.18 g, 78 %): ^{1}H (400 MHz; DMSO-d6) δ 4.53 (s, 2H, H_8), 7.25-7.31 (m, 2H, $H_{3,4}$), 7.50-7.56 (m, 2H, $H_{2,5}$), 12.21 (s, 1H, NH); ^{13}C (100 MHz; DMSO-d6) δ 42.1 (C_8), 116.5 ($C_{2,5}$), 124.1 ($C_{3,4}$), 138.4 ($C_{1,6}$), 150.0 (C_7); IR (neat) υ_{max}/cm^{-1} 1626, 2916, 3000, 3177; LRMS (ESI) *m/z* 167.0 $[M+H]^+$; HRMS (ESI) calculated for $C_8H_8ClN_2$ $[M+H]^+$ 167.0376, found 167.0375; m.p. = 153-155 °C.[313,314]

Synthesis of 2-(Methylaminomethyl)benzimidazole 79 - Method 1

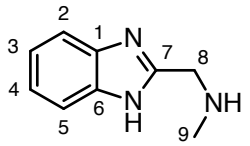

To 33 % methylamine in EtOH (1.23 mL, 10.00 mmol), and K_2CO_3 (0.92 g, 6.00 mmol) in MeOH (3.3 mL) was added 2-chloromethyl-1H-benzimidazole **83** (0.55 g, 3.00 mmol) in MeOH (8 mL) dropwise. Reaction mixture was stirred for 30 minutes, and solvent removed *in vacuo*. Product formation was not observed.[315,316]

Synthesis of 2-(Methylaminomethyl)benzimidazole 79 - Method 2

Finely powdered 2-chloromethyl-1H-benzimidazole **83** (0.46 g, 1.64 mmol) was added to 33 % methylamine in EtOH (9 mL at 0 °C. Stirring continued at 0 °C for 45 minutes, then the reaction mixture was allowed to warm to room temperature over 15 minutes. Reaction mixture was diluted with H_2O, extracted with DCM three times, dried over $MgSO_4$, and solvent removed *in vacuo*. Kugelrohr distillation under reduced pressure yielded compound **79** as a yellow oil (0.18 g, 69 %): ^{1}H (400 MHz; DMSO-d6) δ 2.38 (s, 3H, H_9), 4.03 (s, 2H, H_8), 7.19-7.22 (m, 2H, $H_{3,4}$), 7.50-7.56 (m, 2H, $H_{2,5}$), 12.13 (s, 1H, NH); ^{13}C (100 MHz; DMSO-d6) δ 34.8 (C_9), 48.1 (C_8), 114.8 ($C_{2,5}$), 123.0 ($C_{3,4}$), 138.1 ($C_{1,6}$), 151.3 (C_7); IR (neat) υ_{max}/cm^{-1} 1626, 2855, 2999, 3065; LRMS (ASAP) *m/z* 162.1 $[M+H]^+$; HRMS (ASAP) calculated for $C_9H_{12}N_3$ $[M+H]^+$ 162.1031, found 162.1027.[315,316]

Synthesis of 2-(Ethylaminomethyl)benzimidazole 80

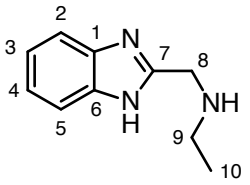

Finely powdered 2-chloromethyl-1H-benzimidazole **83** (0.46 g, 1.64 mmol) was added to ethylamine (3 mL in EtOH (6 mL at 0 °C. Stirring continued at 0 °C for 45 minutes, then the reaction mixture was allowed to warm to room temperature over 15 minutes. Reaction mixture was diluted with H_2O, extracted with DCM three times, dried over $MgSO_4$, and

solvent removed *in vacuo*. Kugelrohr distillation under reduced pressure yielded compound **80** as a yellow oil (0.20 g, 71 %): ^{1}H (400 MHz; DMSO-d6) δ 1.32 (t, J = 8.0 Hz, 3H, H_{10}), 2.68 (q, J = 8.0 Hz, 2H, H_9), 4.04 (s, 2H, H_8), 7.21-7.24 (m, 2H, $H_{3,4}$), 7.50-7.55 (m, 2H, $H_{2,5}$), 12.13 (s, 1H, NH); ^{13}C (100 MHz; DMSO-d6) δ 14.0 (C_{10}), 42.3 (C_9), 47.9 (C_8), 115.3 ($C_{2,5}$), 123.0 ($C_{3,4}$), 138.2 ($C_{1,6}$), 149.3 (C_7); IR (neat) υ_{max}/cm^{-1} 1626, 2858, 3000, 3065; LRMS (ESI) m/z 176.1 [M+H]$^+$; HRMS (ESI) calculated for $C_{10}H_{14}N_3$ [M+H]$^+$ 176.1188, found 176.1186.[315,316]

Synthesis of 2-(Propylaminomethyl)benzimidazole 81

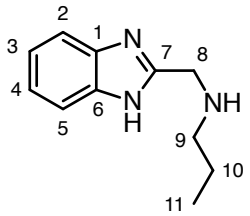

Finely powdered 2-chloromethyl-1H-benzimidazole **83** (0.46 g, 1.64 mmol) was added to propylamine (3 mL in EtOH (6 mL at 0 °C. Stirring continued at 0 °C for 45 minutes, then the reaction mixture was allowed to warm to room temperature over 15 minutes. Reaction mixture was diluted with H_2O, extracted with DCM three times, dried over $MgSO_4$, and solvent removed *in vacuo*. Kugelrohr distillation under reduced pressure yielded compound **81** as a yellow oil (0.21 g, 68 %): ^{1}H (400 MHz; DMSO-d6) δ 1.29 (t, J = 8.0 Hz, 3H, H_{11}), 1.49-1.58 (m, 2H, H_{10}), 2.75 (t, J = 8.0 Hz, 2H, H_9), 4.01 (s, 2H, H_8), 7.15-7.19 (m, 2H, $H_{3,4}$), 7.52-7.58 (m, 2H, $H_{2,5}$), 12.29 (s, 1H, NH); ^{13}C (100 MHz; DMSO-d6) δ 14.1 (C_{11}), 29.8 (C_{10}), 42.3 (C_9), 47.8 (C_8), 115.3 ($C_{2,5}$), 122.0 ($C_{3,4}$), 138.2 ($C_{1,6}$), 149.3 (C_7); IR (neat) υ_{max}/cm^{-1} 1630, 2853, 3017, 3078; LRMS (ASAP) m/z 190.1 [M+H]$^+$; HRMS (ASAP) calculated for $C_{11}H_{16}N_3$ [M+H]$^+$ 190.1344, found 190.1343.[315,316]

Synthesis of 2-(*iso*-Propylaminomethyl)benzimidazole 82

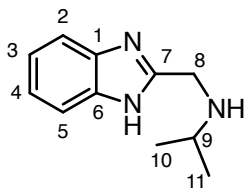

Finely powdered 2-chloromethyl-1H-benzimidazole **83** (0.46 g, 1.64 mmol) was added to *iso*-propylamine (3 mL in EtOH (6 mL at 0 °C. Stirring continued at 0 °C for 45 minutes, then the reaction mixture was allowed to warm to room temperature over 15 minutes. Reaction mixture was diluted with H_2O, extracted with DCM three times, dried over $MgSO_4$, and solvent removed *in vacuo*. Kugelrohr distillation under reduced pressure yielded compound **82** as a yellow oil (0.18 g, 59 %): ^{1}H (400 MHz; DMSO-d6) δ 1.27 (d, J = 8.0 Hz, 6H, $H_{10,11}$), 2.78 (sept, J = 8.0 Hz, 1H, H_9), 4.01 (s, 2H, H_8), 7.15-7.20 (m, 2H, $H_{3,4}$), 7.52-7.58 (m, 2H, $H_{2,5}$), 12.29 (s, 1H, NH); ^{13}C (100 MHz; DMSO-d6) δ 15.0 ($C_{10,11}$), 42.3 (C_9), 47.8 (C_8), 115.3 ($C_{2,5}$), 122.0 ($C_{3,4}$), 138.2 ($C_{1,6}$), 149.3 (C_7); IR (neat) υ_{max}/cm^{-1} 1631, 2855, 3008, 3077; LRMS (ASAP) *m/z* 190.1 $[M+H]^+$; HRMS (ASAP) calculated for $C_{11}H_{16}N_3$ $[M+H]^+$ 190.1344, found 190.1343.[315,316]

Synthesis of (1H-benzimidazol-2-yl)methanethiol 78

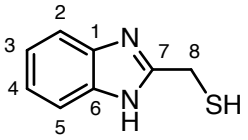

Thioglycolic acid (1.40 mL, 20.00 mmol) and *o*-phenylenediamine (1.89 g, 17.50 mmol) were refluxed in 37 % $HCl_{(aq)}$ (15 mL) for 12 hours. Aqeous solvent was removed by freeze drying, and MeOH recrystallisation yielded the HCl salt of compound **78** as a white powder (2.61 g, 91 %): ^{1}H (400 MHz; DMSO-d6) δ 4.18 (s, 2H, H_8), 7.19 (dd, J = 3.2, 5.9 Hz, 2H, $H_{3,4}$), 7.53 (dd, J = 3.2, 5.9 Hz, 2H, $H_{2,5}$); ^{13}C (100 MHz; DMSO-d6) δ 36.1 (C_8), 115.4 ($C_{2,5}$), 122.3 ($C_{3,4}$), 139.7 ($C_{1,6}$), 151.0 (C_7); IR (neat) υ_{max}/cm^{-1} 1624, 2879, 2946, 2995, 3155; LRMS (ESI) *m/z* 165.0 $[M+H]^+$; HRMS (ESI) calculated for $C_8H_9N_2S$ $[M+H]^+$ 165.0486, found 165.0474.[178,317]

Synthesis of *N*-Boc-1,4-Phenylenediamine 93

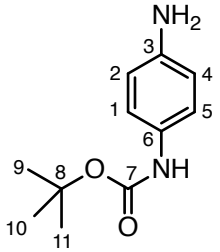

p-phenylenediamine (0.100 g, 0.92 mmol) in DCM (5 mL) was added dropwise at 0 °C to Boc_2O (0.039 g, 0.18 mmol) in DCM (1 mL). Following stirring at 0 °C for 3.5 hours, solvent was removed *in vacuo* to yield a white powder. Purification by silica gel chromatography using DCM:Acetone (4:1) as eluent yielded white powder **93** (0.035 g, 18 %): ^{1}H (400 MHz; $CDCl_3$) δ 1.52 (s, 9H, $H_{9,10,11}$), 3.55 (s, 2H, NH_2), 6.29 (s, 1H, NH), 6.67 (d, J = 8.0 Hz, 2H, $H_{2,4}$), 7.12 (d, J = 8.0 Hz, 2H, $H_{1,5}$; ^{13}C (100 MHz; DMSO-d6) δ 28.1 ($C_{9,10,11}$), 77.6 (C_8), 114.0 ($C_{2,4}$), 120.6 ($C_{1,5}$), 128.6 (C_3), 144.1 (C_6), 153.1 (C_7).[320]

Synthesis of *t*-Butyl(4-Benzamidophenyl)Carbamate 94

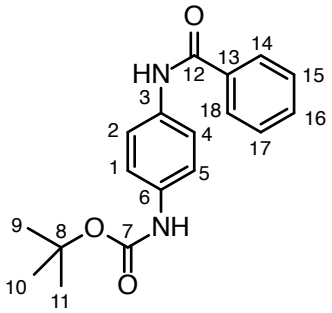

To *N*-Boc-1,4-phenylenediamine **93** (0.035 g, 0.17 mmol) in DCM (3 mL) at 0 °C was added dropwise NEt_3 (0.020 g, 0.20 mmol) and benzoyl chloride (0.028 g, 0.20 mmol). The reaction mixture was allowed to warm to room termperature and stirred for 4 hours. Solvent removal *in vacuo* yielded white powder **94** however low abunadance and problematic large scale purification prevented complete characterisation (0.028 g, 53 %): ^{1}H (400 MHz; $CDCl_3$) δ 1.52 (s, 9H, $H_{9,10,11}$), 7.38 (d, J = 8.0 Hz, 1H, H_2), 7.47-7.59 (m, 4H, $H_{1,4,5,17}$), 7.68 (t, J = 8.0 Hz, 1H, H_{15}), 7.86 (d, J = 8.0 Hz, 1H, H_{16}), 8.17 (d, J = 8.0 Hz, 2H, $H_{14,18}$).[320]

Synthesis of *p*-Nitrobenzanilide 95

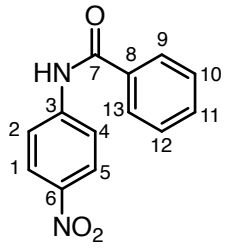

p-nitroaniline (0.100 g, 0.72 mmol) in dry THF (2.4 mL) under argon was treated with K_2CO_3 (0.200 g, 1.45 mmol) and benzoyl chloride (0.110 g, 0.76 mmol). After 12 hours, the reaction

mixture was poured on to 10 % $HCl_{(aq)}$ (2.0 mL) and the resulting precipitate collected. Following washing with H_2O and hexane, MeOH recrystallisation yielded compound **95** (0.097 g, 56 %): ^{1}H (400 MHz; DMSO-d6) δ 7.54 (t, J = 7.9 Hz, 2H, $H_{12,10}$), 7.61 (t, J = 7.4 Hz, 1H, H_{11}), 7.96 (d, J = 8.3 Hz, 2H, $H_{9,13}$), 8.05 (d, J = 9.3 Hz, 2H, $H_{1,5}$), 8.25 (d, J = 9.3 Hz, 2H, $H_{2,4}$) 10.78 (br s, 1H, NH); ^{13}C (100 MHz; DMSO-d6) δ 120.3 ($C_{2,4}$), 125.2 ($C_{1,5}$), 128.4 ($C_{9,13}$), 129.0 ($C_{10,12}$), 132.6 (C_{11}), 134.7 (C_8), 142.9 (C_6), 145.9 (C_3), 166.7 (C_7); IR (neat) υ_{max}/cm^{-1} 1341, 1502, 3332; LRMS (ASAP) m/z 243.1 $[M+H]^+$; HRMS (ASAP) calculated for $C_{13}H_{11}N_2O_3$ $[M+H]^+$ 243.0769, found 243.0762.[321]

Synthesis of *N*-(4-Aminophenyl)Benzamide 84 - Method 1

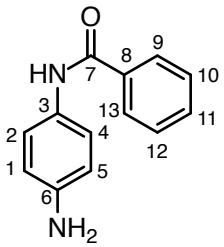

p-Phenylenediamine (0.100 g, 0.92 mmol) and SDS (0.040 g, 0.14 mmol) were warmed in H_2O (2 mL) until a clear solution formed. Benzoyl chloride (0.129 g, 0.92 mmol) in MeCN (1 mL) was added and the reaction mixture stirred for 5 minutes. MeCN was removed *in vacuo*, and the remaining aqueous solution neutralised with $NaHCO_3$ solution. The resulting white precipitate collected by Büchner filtration was determined to be an inseparable mixture of monosubstituted and disubstituted product.[318]

Synthesis of *N*-(4-Aminophenyl)Benzamide 84 - Method 2

p-Phenylenediamine (0.100 g, 0.92 mmol) and SDS (0.040 g, 0.14 mmol) were warmed in H_2O (2 mL) until a clear solution formed. Reaction mixture was cooled to 0 °C, benzoyl chloride (0.129 g, 0.92 mmol) in MeCN (1 mL) was added and the reaction mixture stirred at 0 °C for 5 minutes. MeCN was removed *in vacuo*, and the remaining aqueous solution neutralised with $NaHCO_3$ solution. The resulting white precipitate collected by Büchner filtration was determined to be an inseparable mixture of monosubstituted and disubstituted product.[318]

Synthesis of *N*-(4-Aminophenyl)Benzamide 84 - Method 3

p-Phenylenediamine (0.100 g, 0.92 mmol) was warmed in H_2O (2 mL) until a clear solution formed. Benzoyl chloride (0.129 g, 0.92 mmol) in MeCN (1 mL) was added and the reaction mixture stirred for 5 minutes. MeCN was removed *in vacuo*, and the remaining aqueous solution neutralised with $NaHCO_3$ solution. The resulting white precipitate collected by Büchner filtration was determined to be an inseparable mixture of monosubstituted and disubstituted product.[318]

Synthesis of *N*-(4-Aminophenyl)Benzamide 84 - Method 4

p-Phenylenediamine (0.100 g, 0.92 mmol) and SDS (0.040 g, 0.14 mmol) were warmed in H_2O (2 mL) until a clear solution formed. Benzoic anhydride (0.218 g, 0.92 mmol) in MeCN (1 mL) was added and the reaction mixture stirred for 5 minutes. MeCN was removed *in vacuo*, and the remaining aqueous solution neutralised with $NaHCO_3$ solution. The resulting white precipitate collected by Büchner filtration was determined to be an inseparable mixture of monosubstituted and disubstituted product.[318]

Synthesis of *N*-(4-Aminophenyl)Benzamide 84 - Method 5

p-Phenylenediamine (0.100 g, 0.92 mmol) and SDS (0.040 g, 0.14 mmol) were warmed in H_2O (2 mL) until a clear solution formed. Reaction mixture was cooled to 0 °C, benzoic anhydride (0.218 g, 0.92 mmol) in MeCN (1 mL) was added and the reaction mixture stirred at 0 °C for 5 minutes. MeCN was removed *in vacuo*, and the remaining aqueous solution neutralised with $NaHCO_3$ solution. The resulting white precipitate collected by Büchner filtration was determined to be an inseparable mixture of monosubstituted and disubstituted product.[318]

Synthesis of *N*-(4-Aminophenyl)Benzamide 84 - Method 6

p-Phenylenediamine (0.100 g, 0.92 mmol) was warmed in H_2O (2 mL) until a clear solution formed. Benzoic anhydride (0.218 g, 0.92 mmol) in MeCN (1 mL) was added and the reaction mixture stirred for 5 minutes. MeCN was removed *in vacuo*, and the remaining aqueous solution neutralised with $NaHCO_3$ solution. The resulting white precipitate collected by

Büchner filtration was determined to be an inseparable mixture of monosubstituted and disubstituted product.[318]

Synthesis of *N*-(4-Aminophenyl)Benzamide 84 - Method 7

p-Phenylenediamine (1.000 g, 9.20 mmol) and SDS (0.040 g, 0.14 mmol) were warmed in H_2O (2 mL) until a clear solution formed. Benzoic anhydride (0.218 g, 0.92 mmol) in MeCN (1 mL) was added and the reaction mixture stirred for 5 minutes. MeCN was removed *in vacuo*, and the remaining aqueous solution neutralised with $NaHCO_3$ solution. The resulting white precipitate collected by Büchner filtration was determined to be an inseparable mixture of monosubstituted and disubstituted product.[318]

Synthesis of *N*-(4-Aminophenyl)Benzamide 84 - Method 8

p-Phenylenediamine (0.100 g, 0.92 mmol) and SDS (0.040 g, 0.14 mmol) were warmed in H_2O (15 mL) until a clear solution formed. Benzoic anhydride (0.218 g, 0.92 mmol) in MeCN (1 mL) was added and the reaction mixture stirred for 5 minutes. MeCN was removed *in vacuo*, and the remaining aqueous solution neutralised with $NaHCO_3$ solution. The resulting white precipitate collected by Büchner filtration was determined to be an inseparable mixture of monosubstituted and disubstituted product.[318]

Synthesis of *N*-(4-Aminophenyl)Benzamide 84 - Method 9

To *p*-phenylenediamine (0.100 g, 0.92 mmol) in dry DCM (4 mL) under argon was added benzoyl chloride (0.037 g, 0.26 mmol) and NEt_3 (0.044 mL, 0.32 mmol). Th reaction mixture was tirred at room temperature for 2 hours. The resulting white precipitate collected by Büchner filtration and washed with DCM, was determined to be an inseparable mixture of monosubstituted and disubstituted product.[319]

Synthesis of *N*-(4-Aminophenyl)Benzamide 84 - Method 10

$SnCl_2$ (0.117 g, 0.62 mmol) in 37 % HCl (2.0 mL) was added dropwise to *p*-nitrobenzanilide **95** (0.050 g, 0.21 mmol) in EtOH (2.5 mL). The reaction mixture was stirred with gentle warming for 1 hour, and the resulting precipitate removed by filtration. Remaining aqueous solution

was neutralised with saturated $NaHCO_3$ solution, yielding a white flocculation isolated by centrifugation. Reduction proved unsuccessful, with starting material only retained.[320]

Synthesis of *N*-(4-Aminophenyl)Benzamide 84 - Method 11

p-Nitrobenzanilide **95** (0.100 g, 0.42 mmol) and 10 % Pd on charcoal (0.010 g, 10% w/w) in EtOAc (2.0 mL) was degassed under an environment of H_2, and stirred for 12 hours. Excess Pd was removed by celite filtration, and solvent removed *in vacuo* to yield impure compound **84** (0.083 g, 93 %): ^{1}H (400 MHz; DMSO-d6) δ 4.93 (s, 2H, NH_2), 6.55 (d, J = 8.8 Hz, 2H, $H_{1,5}$), 7.37 (d, J = 8.4 Hz, 2H, $H_{2,4}$), 7.48-7.60 (m, 3H, $H_{10,11,12}$), 7.92 (d, J = 7.6 Hz, 2H, $H_{9,13}$), 9.87 (s, 1H, NH); ^{13}C (100 MHz; DMSO-d6) δ 113.6 ($C_{1,5}$), 122.3 ($C_{2,4}$), 127.4 (C_6), 128.3 ($C_{9,13}$), 128.8 ($C_{10,12}$), 131.6 (C_{11}), 135.3 (C_8), 145.4 (C_3), 164.7 (C_7); IR (neat) υ_{max}/cm^{-1} 1322, 1521, 1637, 3332; LRMS (ASAP) *m/z* 213.1 $[M+H]^+$; HRMS (ASAP) calculated for $C_{13}H_{13}N_2O$ $[M+H]^+$ 213.1028, found 213.1016.[321]

Synthesis of *N*-(4-Aminophenyl)Benzamide 84 - Method 12

To *p*-nitrobenzanilide **95** (0.100 g, 0.42 mmol) and zinc dust (0.546 g, 8.35 mmol) in THF:AcOH (1:1) (5 mL), saturated $CuSO_4$ solution (0.8 mL) was added dropwise at 0 °C. After warming to room temperature the reaction mixture was stirred for 12 hours, then filtered through celite, diluted with EtOAc, washed twice with saturated $NaHCO_3$ solution, and once with brine. The organic phase was dried over $MgSO_4$, and solvent removed *in vacuo* to yield compoundcmpd:HB7 (0.049 g, 55 %): ^{1}H (400 MHz; DMSO-d6) δ 4.93 (s, 2H, NH_2), 6.55 (d, J = 8.8 Hz, 2H, $H_{1,5}$), 7.37 (d, J = 8.4 Hz, 2H, $H_{2,4}$), 7.48-7.60 (m, 3H, $H_{10,11,12}$), 7.92 (d, J = 7.6 Hz, 2H, $H_{9,13}$), 9.87 (s, 1H, NH); ^{13}C (100 MHz; DMSO-d6) δ 113.6 ($C_{1,5}$), 122.3 ($C_{2,4}$), 127.4 (C_6), 128.3 ($C_{9,13}$), 128.8 ($C_{10,12}$), 131.6 (C_{11}), 135.3 (C_8), 145.4 (C_3), 164.7 (C_7); IR (neat) υ_{max}/cm^{-1} 1322, 1521, 1637, 3332; LRMS (ASAP) *m/z* 213.1 $[M+H]^+$; HRMS (ASAP) calculated for $C_{13}H_{13}N_2O$ $[M+H]^+$ 213.1028, found 213.1016.[320]

Synthesis of *m*-Nitrobenzanilide 111

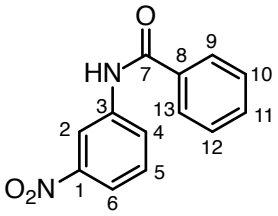

m-nitroaniline (0.100 g, 0.72 mmol) in dry THF (2.4 mL) under argon was treated with K_2CO_3 (0.200 g, 1.45 mmol) and benzoyl chloride (0.110 g, 0.76 mmol). After 12 hours, the reaction mixture was poured on to 10 % $HCl_{(aq)}$ (2.0 mL) and the resulting precipitate collected. Following washing with H_2O and hexane, MeOH recrystallisation yielded compound **111** (0.124 g, 71 %): ^{1}H (400 MHz; DMSO-d6) δ 7.55-7.69 (m, 4H, $H_{5,10,11,12}$), 7.98-7.80 (m, 3H, $H_{4,9,13}$), 8.19-8.22 (m, 1H, H_6), 8.82-8.84 (m, 1H, H_2), 10.72 (s, 1H, NH); ^{13}C (100 MHz; DMSO-d6) δ 114.8 (C_2), 118.6 (C_6), 126.6 (C_4), 128.2 ($C_{9,13}$), 129.0 ($C_{10,12}$), 130.5 (C_5), 132.5 (C_{11}), 134.7 (C_8), 140.8 (C_1), 148.4 (C_3), 166.5 (C_7); IR (neat) υ_{max}/cm^{-1} 1351, 1521, 3362; LRMS (ASAP) *m/z* 243.1 $[M+H]^+$; HRMS (ASAP) calculated for $C_{13}H_{11}N_2O_3$ $[M+H]^+$ 243.0769, found 243.0762.[321]

Synthesis of *N*-(3-Aminophenyl)Benzamide 85

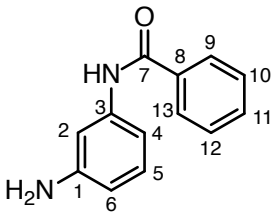

To *m*-nitrobenzanilide **111** (0.100 g, 0.42 mmol) and zinc dust (0.546 g, 8.35 mmol) in THF:AcOH (1:1) (5 mL), saturated $CuSO_4$ solution (0.8 mL) was added dropwise at 0 °C. After warming to room temperature the reaction mixture was stirred for 12 hours, then filtered through celite, diluted with EtOAc, washed twice with saturated $NaHCO_3$ solution, and once with brine. The organic phase was dried over $MgSO_4$, and solvent removed *in vacuo* to yield compoundcmpd:HB47 (0.050 g, 56 %): ^{1}H (400 MHz; DMSO-d6) δ 5.09 (s, 2H, NH_2), 6.31 (d, J = 11.1 Hz, 1H, H_2), 6.86 (d, J = 8.0 Hz, 1H, H_5), 6.96 (t, J = 8.0 Hz, 1H, H_6), 7.11 (t, J = 2.0 Hz, 1H, $4H_4$), 7.47-7.63 (m, 3H, $H_{10,11,12}$), 7.92 (d, J = 6.9 Hz, 2H, $H_{9,13}$), 9.96 (s, 1H, NH); ^{13}C (100 MHz; DMSO-d6) δ 106.6 (C_6), 108.8 (C_5), 110.2 (C_4), 128.1 (C_1), 128.8

($C_{9,13}$), 129.3 ($C_{10,12}$), 131.8 (C_{11}), 135.8 (C_8), 140.2 (C_2), 149.4 (C_3), 165.7 (C_7); IR (neat) v_{max}/cm^{-1} 1320, 1538, 1636, 3329; LRMS (ASAP) *m/z* 213.2016 $[M+H]^+$; HRMS (ASAP) calculated for $C_{13}H_{13}N_2O$ $[M+H]^+$ 213.1028, found 213.2016.[320]

Synthesis of *o*-Nitrobenzanilide 112

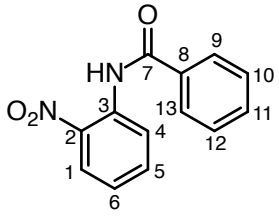

o-nitroaniline (0.100 g, 0.72 mmol) in dry THF (2.4 mL) under argon was treated with K_2CO_3 (0.200 g, 1.45 mmol) and benzoyl chloride (0.110 g, 0.76 mmol). After 12 hours, the reaction mixture was poured on to 10 % $HCl_{(aq)}$ (2.0 mL) and the resulting precipitate collected. Following washing with H_2O and hexane, MeOH recrystallisation yielded compound **112** (0.075 g, 43 %): ^1H (400 MHz; DMSO-d6) δ 7.34-7.38 (m, 1H, H_6), 7.64 (tt, J = 1.3, 7.3 Hz, 1H, H_5), 7.70-7.74 (m, 3H, $H_{5,10,12}$), 8.00-8.02 (m, 2H, $H_{9,13}$), 8.21 (dd, J = 1.5, 8.4 Hz, 1H, H_4), 8.42 (dd, J = 1.5, 8.4 Hz, 1H, H_1), 10.23 (br s, 1H, NH); ^{13}C (100 MHz; DMSO-d6) δ 125.0 (C_1), 125.5 (C_4), 125.9 (C_5), 127.8 (C_6), 128.8 ($C_{9,13}$), 131.6 ($C_{10,12}$), 132.5 (C_{11}), 133.6 (C_3), 134.0 (C_8), 142.8 (C_2), 166.0 (C_7); IR (neat) v_{max}/cm^{-1} 1341, 1596, 1685, 3366; LRMS (ASAP) *m/z* 243.1 $[M+H]^+$; HRMS (ASAP) calculated for $C_{13}H_{11}N_2O_3$ $[M+H]^+$ 243.0769, found 243.0762.[321]

Synthesis of *N*-(2-Aminophenyl)Benzamide 86

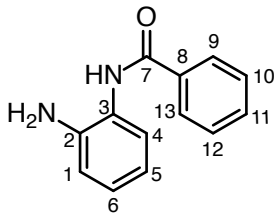

To *o*-nitrobenzanilide **112** (0.100 g, 0.42 mmol) and zinc dust (0.546 g, 8.35 mmol) in THF:AcOH (1:1) (5 mL), saturated $CuSO_4$ solution (0.8 mL) was added dropwise at 0 °C. After warming to room temperature the reaction mixture was stirred for 12 hours, then filtered through celite, diluted with EtOAc, washed twice with saturated $NaHCO_3$ solution, and once with

brine. The organic phase was dried over $MgSO_4$, and solvent removed *in vacuo* to yield compoundcmpd:HB13 (0.064 g, 72 %): ^{1}H (400 MHz; DMSO-d6) δ 4.91 (s, 2H, NH_2), 6.60 (t, J = 7.6 Hz, 1H, H_5), 6.79 (d, J = 8.0 Hz, 1H, H_1), 6.98 (t, J = 8.8 Hz, 1H, H_6), 7.17 (d, J = 7.0 Hz, 1H, H_4), 7.48-7.62 (m, 3H, $H_{10,11,12}$), 7.99 (d, J = 7.1 Hz, 2H, $H_{9,13}$), 9.68 (s, 1H, NH); ^{13}C (100 MHz; DMSO-d6) δ 116.6 (C_1), 116.7 (C_4), 123.8 (C_5), 127.0 (C_6), 127.2 ($C_{9,13}$), 128.2 ($C_{10,12}$), 128.7 (C_{11}), 131.8 (C_3), 135.1 (C_8), 143.6 (C_2), 165.8 (C_7); IR (neat) υ_{max}/cm^{-1} 1336, 1564, 1637, 3395; LRMS (ASAP) m/z 213.1 $[M+H]^+$; HRMS (ASAP) calculated for $C_{13}H_{13}N_2O$ $[M+H]^+$ 213.1028, found 213.1022.[318,320]

Synthesis of *p*-Nitropalmanilide 113

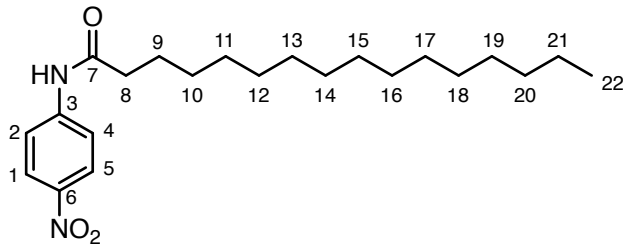

p-nitroaniline (0.100 g, 0.72 mmol) in dry THF (2.4 mL) under argon was treated with K_2CO_3 (0.200 g, 1.45 mmol) and palmitoyl chloride **18** (0.209 g, 0.76 mmol). After 12 hours, the reaction mixture was poured on to 10 % $HCl_{(aq)}$ (2.0 mL) and the resulting precipitate collected. Following washing with H_2O and hexane, IPA recrystallisation yielded compound **113** (0.157 g, 58 %): ^{1}H (400 MHz; DMSO-d6) δ 0.87 (t, J = 8.0 Hz, 3H, H_{22}), 1.17-1.39 (m, 24H, H_{Alkyl}), 1.73 (quin, J = 15.0 Hz, 2H, H_8), 2.41 (t, J = 7.3 Hz, 2H, H_8), 7.60 (s, 1H, NH), 7.72 (d, J = 9.2 Hz, 2H, $H_{2,4}$), 8.20 (d, J = 9.2 Hz, 2H, $H_{1,5}$); ^{13}C (100 MHz; DMSO-d6) δ 14.1 (C_{22}), 22.7 (C_{Alkyl}), 25.3 (C_{Alkyl}), 29.2 (C_{Alkyl}), 29.3 (C_{Alkyl}), 29.4 (C_{Alkyl}), 29.6 (C_{Alkyl}), 29.7 (C_{Alkyl}), 31.9 (C_9), 37.9 (C_8), 118.9 ($C_{1,5}$), 125.1 ($C_{2,4}$), 143.4 (C_3), 143.8 (C_6), 171.8 (C_7); IR (neat) υ_{max}/cm^{-1} 1670, 2852, 2921, 3355; LRMS (ASAP) m/z 377.3 $[M+H]^+$; HRMS (ASAP) calculated for $C_{22}H_{37}N_2O_3$ $[M+H]^+$ 377.2804, found 377.2797.[321]

Synthesis of *N*-(4-Aminophenyl)Palmamide 87

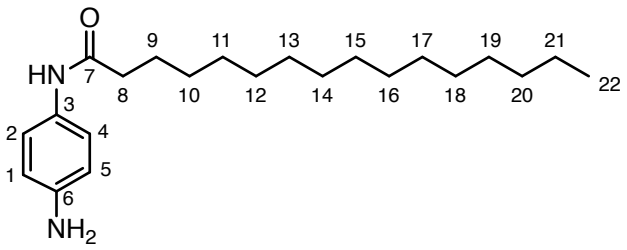

To *p*-nitropalmanilide **113** (0.050 g, 0.21 mmol) and zinc dust (0.273 g, 4.18 mmol) in THF:AcOH (1:1) (2.5 mL), saturated $CuSO_4$ solution (0.4 mL) was added dropwise at 0 °C. After warming to room temperature the reaction mixture was stirred for 12 hours, then filtered through celite, diluted with EtOAc, washed twice with saturated $NaHCO_3$ solution, and once with brine. The organic phase was dried over $MgSO_4$, and solvent removed *in vacuo* to yield compoundcmpd:HB65 (0.045 g, 62 %): ^{1}H (400 MHz; DMSO-d6) δ 0.87 (t, J = 8.0 Hz, 3H, H_{22}), 1.18-1.37 (m, 24H, H_{Alkyl}), 1.46-1.60 (m, 2H, H_8), 2.20 (t, J = 7.3 Hz, 2H, H_8), 4.90 (s, 2H, NH_2, 6.48 (d, J = 8.8 Hz, 2H, $H_{1,5}$), 7.20 (d, J = 8.8 Hz, 2H, $H_{2,4}$), 9.41 (s, 1H, NH); ^{13}C (100 MHz; DMSO-d6) δ 14.4 (C_{22}), 22.6 (C_{Alkyl}), 25.8 (C_{Alkyl}), 29.2 (C_{Alkyl}), 29.3 (C_{Alkyl}), 29.6 (C_{Alkyl}), 29.7 (C_{Alkyl}), 31.8 (C_9), 36.8 (C_8), 114.3 ($C_{1,5}$), 121.3 ($C_{2,4}$), 136.5 (C_3), 143.3 (C_6), 162.0 (C_7); IR (neat) υ_{max}/cm^{-1} 1660, 2913, 2920, 3300; LRMS (ASAP) *m/z* 347.3 $[M+H]^+$; HRMS (ASAP) calculated for $C_{22}H_{39}N_2O$ $[M+H]^+$ 347.3062, found 347.4066.[320]

Synthesis of *m*-Nitropalmanilide 114

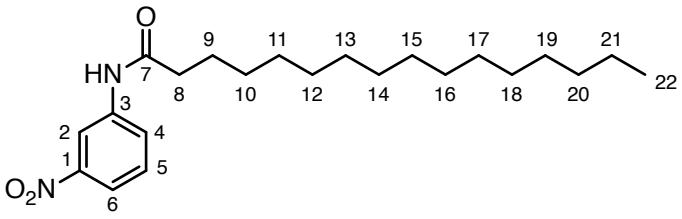

m-nitroaniline (0.100 g, 0.72 mmol) in dry THF (2.4 mL) under argon was treated with K_2CO_3 (0.200 g, 1.45 mmol) and palmitoyl chloride **18** (0.209 g, 0.76 mmol). After 12 hours, the reaction mixture was poured on to 10 % $HCl_{(aq)}$ (2.0 mL) and the resulting precipitate collected. Following washing with H_2O and hexane, IPA recrystallisation yielded compound **114** (0.171 g, 63 %): ^{1}H (400 MHz; DMSO-d6) δ 0.88 (t, J = 8.0 Hz, 3H, H_{22}), 1.20-1.44 (m, 24H, H_{Alkyl}), 1.74 (quin, J = 15.0 Hz, 2H, H_8), 2.40 (t, J = 7.3 Hz, 2H, H_8), 7.35 (s, 1H, NH),

7.49 (t, J = 4.7 Hz, 1H, H_5), 7.93-7.97 (m, 2H, $H_{4,6}$), 8.34-8.37 (m, 1H, H_2); ^{13}C (100 MHz; DMSO-d6) δ 14.1 (C_{22}), 22.7 (C_{Alkyl}), 25.4 (C_{Alkyl}), 29.2 (C_{Alkyl}), 29.3 (C_{Alkyl}), 29.4 (C_{Alkyl}), 29.6 (C_{Alkyl}), 29.7 (C_{Alkyl}), 31.9 (C_9), 37.7 (C_8), 114.3 (C_2), 118.7 (C_6), 125.3 (C_4), 129.8 (C_5), 139.0 (C_3), 148.5 (C_1), 175.7 (C_7); IR (neat) υ_{max}/cm^{-1} 1668, 2851, 2934, 3358; LRMS (ASAP) m/z 377.3 [M+H]$^+$; HRMS (ASAP) calculated for $C_{22}H_{37}N_2O_3$ [M+H]$^+$ 377.2804, found 377.2779.[321]

Synthesis of *N*-(3-Aminophenyl)Palmamide 88

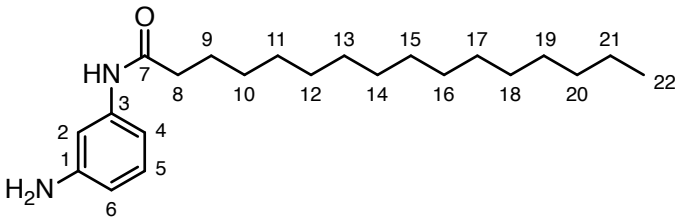

To *m*-nitropalmanilide **114** (0.050 g, 0.21 mmol) and zinc dust (0.273 g, 4.18 mmol) in THF:AcOH (1:1) (2.5 mL), saturated $CuSO_4$ solution (0.4 mL) was added dropwise at 0 °C. After warming to room temperature the reaction mixture was stirred for 12 hours, then filtered through celite, diluted with EtOAc, washed twice with saturated $NaHCO_3$ solution, and once with brine. The organic phase was dried over $MgSO_4$, and solvent removed *in vacuo* to yield compoundcmpd:HB49 (0.049 g, 67 %): ^{1}H (400 MHz; DMSO-d6) δ 0.86 (t, J = 8.0 Hz, 3H, H_{22}), 1.17-1.32 (m, 24H, H_{Alkyl}), 1.51-1.59 (m, 2H, H_8), 2.24 (t, J = 7.3 Hz, 2H, H_8), 5.10 (s, 2H, NH_2, 6.23 (d, J = 10.0 Hz, 1H, H_6), 6.67 (d, J = 1.0 Hz, 1H, H_4), 6.89 (t, J = 8.0 Hz, 1H, H_5), 6.94 (s, 1H, H_2), 9.53 (s, 1H, NH); ^{13}C (100 MHz; DMSO-d6) δ 14.4 (C_{22}), 22.6 (C_{Alkyl}), 25.8 (C_{Alkyl}), 29.2 (C_{Alkyl}), 29.3 (C_{Alkyl}), 29.6 (C_{Alkyl}), 29.7 (C_{Alkyl}), 31.8 (C_9), 36.9 (C_8), 117.6 ($C_{2,6}$), 124.1 (C_4), 129.3 (C_5), 137.8 (C_3), 140.4 (C_1), 171.4 (C_7); IR (neat) υ_{max}/cm^{-1} 1658, 2915, 2927, 3298; LRMS (ASAP) m/z 347.3 [M+H]$^+$; HRMS (ASAP) calculated for $C_{22}H_{39}N_2O$ [M+H]$^+$ 347.3062, found 347.3070.[320]

Synthesis of *o*-Nitropalmanilide 115

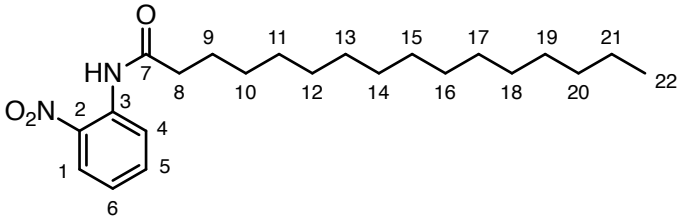

o-nitroaniline (0.100 g, 0.72 mmol) in dry THF (2.4 mL) under argon was treated with K_2CO_3 (0.200 g, 1.45 mmol) and palmitoyl chloride **18** (0.209 g, 0.76 mmol). After 12 hours, the reaction mixture was poured on to 10 % $HCl_{(aq)}$ (2.0 mL) and the resulting precipitate collected. Following washing with H_2O and hexane, IPA recrystallisation yielded compound **115** (0.141 g, 52 %): ^{1}H (400 MHz; DMSO-d6) δ 0.88 (t, J = 8.0 Hz, 3H, H_{22}), 1.18-1.40 (m, 24H, H_{Alkyl}), 1.69-1.73 (m, 2H, H_8), 2.42 (t, J = 7.3 Hz, 2H, H_8), 7.31 (s, 1H, NH), 7.12–7.15 (m, 1H, H_6), 7.57–7.61 (m, 1H, H_4), 8.17 (dd, J = 1.5, 8.5 Hz, 1H, H_5), 8.79 (dd, J = 1.5, 8.6 Hz, 1H, H_1); ^{13}C (100 MHz; $CDCl_3$) δ 14.2 (C_{22}), 22.7 (C_{Alkyl}), 25.4 (C_{Alkyl}), 29.2 (C_{Alkyl}), 29.3 (C_{Alkyl}), 29.4 (C_{Alkyl}), 29.6 (C_{Alkyl}), 29.7 (C_{Alkyl}), 31.8 (C_9), 38.2 (C_8), 122.3 (C_1), 123.1 (C_4), 125.8 (C_5), 135.2 (C_6), 136.0 (C_3), 136.3 (C_2), 172.3 (C_7); IR (neat) υ_{max}/cm^{-1} 1662, 2854, 2927, 3352; LRMS (ASAP) *m/z* 377.3 $[M+H]^+$; HRMS (ASAP) calculated for $C_{22}H_{37}N_2O_3$ $[M+H]^+$ 377.2804, found 377.2800.[321]

Synthesis of *N*-(2-Aminophenyl)Palmamide 89

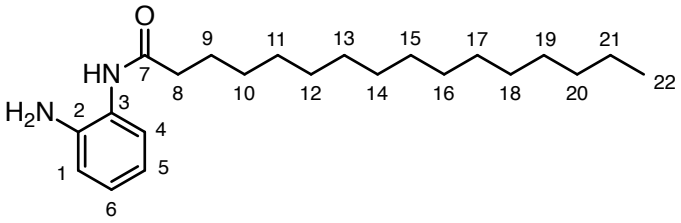

To *m*-nitropalmanilide **115** (0.050 g, 0.21 mmol) and zinc dust (0.273 g, 4.18 mmol) in THF:AcOH (1:1) (2.5 mL), saturated $CuSO_4$ solution (0.4 mL) was added dropwise at 0 °C. After warming to room temperature the reaction mixture was stirred for 12 hours, then filtered through celite, diluted with EtOAc, washed twice with saturated $NaHCO_3$ solution, and once with brine. The organic phase was dried over $MgSO_4$, and solvent removed *in vacuo* to yield compoundcmpd:HB48 (0.047 g, 64 %): ^{1}H (400 MHz; DMSO-d6) δ 0.86 (t, J = 8.0 Hz, 3H, H_{22}), 1.19-1.35 (m, 24H, H_{Alkyl}), 1.54-1.62 (m, 2H, H_8), 2.30 (t, J = 7.3 Hz, 2H, H_8), 4.81 (s, 2H, NH_2), 6.53 (td, J = 1.4, 7.9 Hz, 1H, H_5), 6.71 (dd, J = 1.4, 8.0 Hz, 1H, H_1), 6.89 (td, J = 1.5, 7.9 Hz, 1H, H_6), 7.08-7.18 (m, 1H, H_4), 9.09 (s, 1H, NH); ^{13}C (100 MHz; DMSO-d6) δ 14.2 (C_{22}), 22.6 (C_{Alkyl}), 25.8 (C_{Alkyl}), 29.1 (C_{Alkyl}), 29.3 (C_{Alkyl}), 29.6 (C_{Alkyl}), 29.8 (C_{Alkyl}), 31.9 (C_9), 36.7 (C_8), 115.6 (C_1), 118.7 (C_4), 122.9 (C_5), 129.7 (C_6), 134.5 (C_3), 138.9 (C_2), 173.8 (C_7); IR (neat) υ_{max}/cm^{-1} 1649, 2913, 2926, 3304; LRMS (ASAP) *m/z* 347.3 $[M+H]^+$; HRMS (ASAP) calculated for $C_{22}H_{39}N_2O$ $[M+H]^+$ 347.3062, found 347.3049.[320]

Synthesis of Betaine 97

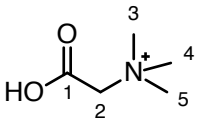

MeI (3.025 g, 21.31 mmol) was added dropwise to glycine (0.100 g, 1.33 mmol) and $NaHCO_3$ (1.330 g, 15.83 mmol) in MeOH:H_2O (1:1) (20 mL). Following 16 hours with exclusion of light, solvent was removed *in vacuo*. EtOH was added, filtered to remove excess salt, and solvent removed *in vacuo* yielding betaine **97** as a white solid (0.128 g, 82 %): ^{1}H (400 MHz; DMSO-d6) δ 3.14 (s, 9H, $H_{3,4,5}$), 3.56 (s, 2H, H_2); ^{13}C (100 MHz; $CDCl_3$) δ 52.5 ($C_{3,4,5}$), 66.7 (C_2), 164.9 (C_1); IR (neat) υ_{max}/cm^{-1} 1557, 1597, 2853, 3386; LRMS (ASAP) *m/z* 118.1 $[M+H]^+$; HRMS (ASAP) calculated for $C_5H_{12}NO_2$ $[M+H]^+$ 118.0868, found 118.0867; m.p. = 293-294 °C.[322]

Synthesis of Betainyl Chloride 96

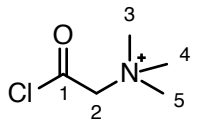

Betaine **97** (0.050 g, 0.85 mmol) and oxalyl chloride (0.073 mL, 1.70 mmol) in dry DCM (10 mL) were refluxed under argon for 2 hours. Solvent was removed *in vacuo*, however product formation was not observed.

Synthesis of Betaine-*N*-Hydroxysuccinimide Ester 98 - Method 1

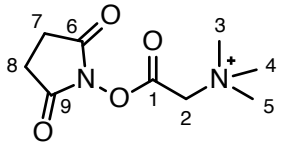

To betaine **97** (0.050 g, 0.85 mmol) and *N*-hydroxysuccinimide (0.040 g, 0.43 mmol) in dry DMF (3.5 mL) was added DIC (0.071 g, 0.55 mmol). Stirring continued for 12 hours, however product formation was not observed.

Synthesis of Betaine-*N*-Hydroxysuccinimide Ester 98 - Method 2

To betaine **97** (0.050 g, 0.85 mmol) and *N*-hydroxysuccinimide (0.080 g, 0.86 mmol) in dry DMF (3.5 mL) was added DIC (0.142 g, 1.10 mmol). Stirring continued for 12 hours at 65 °C, however product formation was not observed.

Synthesis of Glycinyl Chloride 99 - Method 1

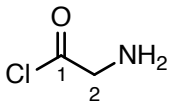

Glycine (0.071 g, 0.95 mmol) and oxalyl chloride (0.165 mL, 1.90 mmol) in dry DCM (40 mL) were refluxed under argon for 2 hours. Solvent was removed *in vacuo*, however product formation was not observed.

Synthesis of Glycinyl Chloride 99 - Method 2

Glycine (0.071 g, 0.95 mmol) and oxalyl chloride (0.165 mL, 1.90 mmol) in dry DCM:DMF (19:1) (40 mL) were refluxed under argon for 2 hours. Solvent was removed *in vacuo*, however product formation was not observed.

Synthesis of Fmoc Glycinyl Chloride 100

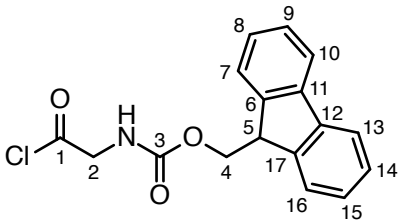

Fmoc glycine (0.200 g, 0.67 mmol) was dissolved in a combination of dry DCM (1.0 mL), dry DMF (6.0 µL) and dry THF (0.2 mL). Oxalyl chloride (0.117 mL, 1.35 mmol) was added dropwise, and the mixture refluxed for 1.5 hours. Solvent removal *in vacuo* yielded compound-cmpd:HB76 as a pale yellow solid (0.188 g, 89 %): ^{1}H (400 MHz; DMSO-d6) δ 3.65 (d, J = 5.6 Hz, 2H, H_2), 4.21-4.28 (m, 3H, $H_{4,5}$), 7.33 (t, J = 7.2 Hz, 2H, $H_{8,15}$), 7.41 (t, J = 7.3 Hz,

2H, $H_{9,14}$), 7.72 (d, J = 7.3 Hz, 2H, $H_{7,16}$), 7.87 (d, J = 7.4 Hz, 2H, $H_{10,13}$); ^{13}C (100 MHz; DMSO-d6) δ 42.1 (C_2), 46.6 (C_5), 66.3 (C_4), 120.1 ($C_{10,13}$), 125.2 ($C_{7,16}$), 127.1 ($C_{8,15}$), 127.6 ($C_{9,14}$), 140.7 ($C_{11,12}$), 143.8 ($C_{6,17}$), 156.5 (C_3), 174.7 (C_1); IR (neat) υ_{max}/cm^{-1} 1689, 1701, 1742, 2916, 2955.[323]

Synthesis of *p*-NitroFmocglycylanilide 101

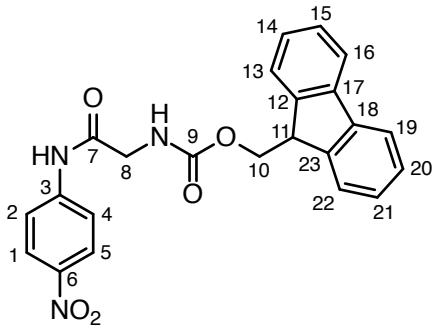

p-nitroaniline (0.100 g, 0.72 mmol) in dry THF (2.4 mL) under argon was treated with K_2CO_3 (0.200 g, 1.45 mmol) and acid chloride **100** (0.182 mL, 0.76 mmol). After 12 hours, the reaction mixture was poured on to 10 % $HCl_{(aq)}$ (2.0 mL) and the resulting precipitate compound **101** collected however time constraints prevented charactersation.[321]

Synthesis of *m*-NitroFmocglycylanilide 104

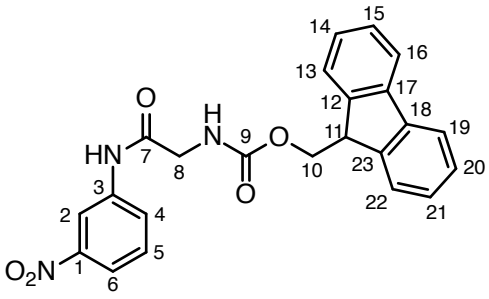

m-nitroaniline (0.050 g, 0.36 mmol) in dry THF (1.2 mL) under argon was treated with K_2CO_3 (0.100 g, 0.73 mmol) and acid chloride **100** (0.091 mL, 0.38 mmol). After 12 hours, the reaction mixture was poured on to 10 % $HCl_{(aq)}$ (1.0 mL) and the resulting precipitate compound **104** collected however time constraints prevented charactersation.[321]

Synthesis of *o*-NitroFmocglycylanilide 105

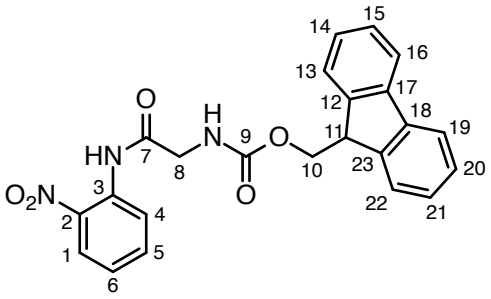

o-nitroaniline (0.050 g, 0.36 mmol) in dry THF (1.2 mL) under argon was treated with K_2CO_3 (0.100 g, 0.73 mmol) and acid chloride **100** (0.091 mL, 0.38 mmol). After 12 hours, the reaction mixture was poured on to 10 % $HCl_{(aq)}$ (1.0 mL) and the resulting precipitate compound **105** collected however time constraints prevented charactersation.[321]

Marker Release Assay

Stock solutions of phospholipid in $CHCl_3$ were prepared at a concentration of 10 mg mL^{-1} and stored at -20 °C. A 100 µL aliquot of phospholipid stock solution was added to a round-bottomed flask, and solvent removed *in vacuo* resulting in formation of a lipid film. Following overnight dessication, the phospholipid film was rehydrated in 12.5 mM ANTS and 45.0 mM DPX solution, and agitated using a vortex mixer. The dispersion was subjected to 5 freeze-thaw cycles between -196 °C and 30 °C, before 10 extrusion cycles at 50 °C using a LIPEX thermobarrel extruder under a positive pressure of nitrogen and a 100 nm Whatman Nucleopore laser-etched polycarbonate filter. External buffer was exchanged for osmotically equivalent buffer (10 mM NH_4HCO_3 in H_2O at pH 7.4) using a PD-10 desalting column. Liposomes (100 µL) were added to each well of a 96 well plate, along with substrate (10 µL) of interest. Emission at 530 nm was measured at one minute intervals following excitation at 360 nm using a Synergy H4 Plate Reader (BioTek, UK). Data was normalised to a positive control of 20 % Triton X.[325]

CMC Determination for Acylated Propranolol

Stock solution of Rhodamine 6G was prepared in H_2O at 20 mg mL^{-1}. Stock (1 mL) was added to a 1 mL cuvette, and absorbance measured over the range 520 nm to 560 nm at 21 °C using a CARY100 UV-Visible spectrophotometer with Cary WinUV Scan Software 3.00(182). 100 µM

solution of desired substrate in H_2O was added in 1 µL portions over the total concentration range 0.1 µM to 100 µM, and absorbance measurements repeated. Data was corrected for dilution.[326,327]

Bibliography

[1] G. L. Nicolson, *Biochim. Biophys. Acta Biomembr.*, 2014, **1838**, 1451–1466.

[2] M. R. Salton, *Annu. Rev. Microbiol.*, 1967, **21**, 417–442.

[3] S. J. Singer and G. Nicolson, *Science*, 1972, **175**, 720–731.

[4] J. R. Silvius, *Lipid-Protein Interactions*, Wiley, New York, 1982.

[5] W. P. Heal and E. W. Tate, *Org. Biomol. Chem.*, 2010, **8**, 731–738.

[6] G. Triola, H. Waldmann and C. Hedberg, *ACS Chem. Biol.*, 2012, **7**, 87–99.

[7] S. L. Veatch and S. L. Keller, *Phys. Rev. Lett.*, 2002, **89**, 1–4.

[8] N. P. Barrera, M. Zhou and C. V. Robinson, *Trends Cell Biol.*, 2013, **23**, 1–8.

[9] D. Huang, T. Zhao, W. Xu, T. Yang and P. S. Cremer, *Anal. Chem.*, 2013, **85**, 10240–10248.

[10] C. J. Pridmore, J. A. Mosely, A. Rodger and J. M. Sanderson, *Chem. Commun.*, 2011, **47**, 1422–4.

[11] R. H. Dods, J. A. Mosely and J. M. Sanderson, *Biophys. J.*, 2012, **102**, 491–492.

[12] J. Arnhold, A. N. Osipov, H. Spalteholz, O. M. Panasenko and J. Schiller, *Biochim. Biophys. Acta*, 2002, **1572**, 91–100.

[13] E. D. Korn, *J. Gen. Physiol.*, 1968, **52**, 257–278.

[14] A. J. Morris, *Trends Pharmacol. Sci.*, 1999, **20**, 393–395.

[15] A. J. Morris, M. Panchatcharam, H. Y. Cheng, L. Federico, Z. Fulkerson, S. Selim, S. Miriyala, D. Escalante-Alcalde and S. S. Smyth, *J. Thromb. Haemost.*, 2009, **7**, 38–43.

[16] T. Koklic and J. Štrancar, *BMC Res. Notes*, 2012, **5**, 179.

[17] B. Banno, L. M. Ickenstein, G. N. C. Chui, M. B. Bally, J. Thewalt, E. Brief and E. K. Wasan, *J. Pharm. Sci.*, 2010, **99**, 2295–2308.

[18] H. Lodish, A. Berk, C. A. Kaiser, M. Krieger, M. P. Scott, A. Bretscher, H. Ploegh and P. Matsudaira, *Molecular Cell Biology*, W. H. Freeman and Company, New York, 6th edn., 2007.

[19] J. Singh and R. Ranganathan, *J. Lipid Res.*, 2012, **53**, 1993–2001.

[20] N. J. Zuidam and D. J. Crommelin, *J. Pharm. Sci.*, 1995, **84**, 1113–1119.

[21] A. J. De Koning and K. B. McMullan, *Biochim. Biophys. Acta*, 1965, **106**, 519–526.

[22] H. Brockerhoff, *J. Lipid Res.*, 1962, **4**, 96–99.

[23] C. R. Kepsil and E. A. Dennis, *Biochem.*, 1981, **20**, 6079–6085.

[24] M. Grit and D. J. Crommelin, *Chem. Phys. Lipids*, 1993, **64**, 3–18.

[25] J. Olley and J. A. Lovern, *J. Sci. Food Agric.*, 1960, **11**, 644–652.

[26] H. Takamura, H. Narita, H. J. Park, K. Tanaka, T. Matsuura and M. Kito, *J. Biol. Chem.*, 1987, **262**, 2262–2269.

[27] D. R. Casey, S. C. Sebai, G. C. Shearman, O. Ces, R. V. Law, R. H. Templer and A. D. Gee, *Ind. Eng. Chem. Res.*, 2008, **47**, 650–655.

[28] D. Casey, K. Charalambous, A. Gee, R. V. Law and O. Ces, *J. R. Soc. Interface*, 2014, **11**, 20131062.

[29] M. Baciu, S. C. Sebai, O. Ces, X. Mulet, J. A. Clarke, G. C. Shearman, R. V. Law, R. H. Templer, C. Plisson, C. A. Parker and A. Gee, *Phil. Trans. R. Soc. A*, 2006, **364**, 2597–2614.

[30] A. Arouri and O. G. Mouritsen, *Prog. Lipid Res.*, 2013, **52**, 130–140.

[31] J. R. Henriksen, T. L. Andresen, L. N. Feldborg, L. Duelund and J. H. Ipsen, *Biophys. J.*, 2010, **98**, 2199–2205.

[32] C. J. A. Van Echteld, B. De Kruijff, J. G. Mandersloot and J. De Gier, *Biochim. Biophys. Acta*, 1981, **649**, 211–220.

[33] P. O. Eriksson, G. Lindblom and G. Arvidsori, *J. Phys. Chem.*, 1987, **91**, 846–853.

[34] N. Fuller and R. P. Rand, *Biophys. J.*, 2001, **81**, 243–254.

[35] D. V. Zhelev, *Biophys. J.*, 1998, **75**, 321–330.

[36] S. Blaskovic, M. Blanc and F. G. Van Der Goot, *FEBS J.*, 2013, **280**, 2766–2774.

[37] R. N. Hannoush and J. Sun, *Nat. Chem. Biol.*, 2010, **6**, 498–506.

[38] D. Brown and G. L. Waneck, *J. Am. Soc. Nephrol.*, 1992, **3**, 895–906.

[39] R. H. Dods, B. Bechinger, J. A. Mosely and J. M. Sanderson, *J. Mol. Biol.*, 2013, **425**, 4379–4387.

[40] V. S. Ismail, *Probing Lipidation of Membrane Active Peptides and Integral Membrane Proteins by Liquid Chromatography Mass Spectrometry and Ion Mobility Separation Mass Spectrometry*, Durham University Ph.D. Thesis, 2017.

[41] C. J. Pridmore, *Analytical Methods for the Study of Membranes and Peptide-Membrane Interactions*, Durham University Ph.D. Thesis, 2010.

[42] P. L. Urban, *Phil. Trans. R. Soc. A*, 2016, **374**, 20150382.

[43] S. P. Markey, *Biomed. Mass Spectrom.*, 1981, **8**, 426–420.

[44] R. H. Dods, J. A. Mosely and J. M. Sanderson, *Org. Biomol. Chem.*, 2012, **10**, 5371–5378.

[45] H. Raghuraman and A. Chattopadhyay, *Biophys. J.*, 2004, **87**, 2419–2432.

[46] C. Dempsey, M. Bitbol and A. Watts, *Biochem.*, 1989, **1**, 6590–6596.

[47] P. Roepstorff and J. Fohlman, *Biomed. Mass Spectrom.*, 1984, **11**, 601–601.

[48] F. W. McLafferty, E. K. Fridriksson, D. M. Horn, M. A. Lewis and R. A. Zubarev, *Science*, 1999, **284**, 1289–1290.

[49] K. Biemann, *Annu. Rev. Biochem.*, 1992, **61**, 977–1010.

[50] M. Zasloff, *Proc. Natl. Acad. Sci. USA*, 1987, **84**, 5449–5453.

[51] R. Cruciani and J. Barker, *Eur. J. Pharmacol.*, 1992, **226**, 287–296.

[52] B. Bechinger, M. Zasloff and S. J. Opella, *Biophys. J.*, 1992, **62**, 12–14.

[53] M. Bodanszky and M. Fink, *J. Org. Chem.*, 1977, **42**, 149–152.

[54] T. Wieprecht, O. Apostolov, M. Beyermann and J. Seelig, *Biochem.*, 2000, **39**, 442–452.

[55] G. Beschiaschvili and J. Seelig, *Biochem.*, 1990, **29**, 52–58.

[56] M. Monette and M. Lafleur, *Biophys. J.*, 1995, **68**, 187–95.

[57] M. Lafleur, J. Faucon, J. Dufourcq and M. Pézolet, *Biochim. Biophys. Acta*, 1989, **980**, 85–92.

[58] M. Salton and K.-S. Kim, *Medical Microbiology*, University of Texas Medical Branch, 4th edn., 1996.

[59] H. M. Britt, *Lipidation of Membrane-Active Peptides*, Durham University MSci Thesis, 2014.

[60] D. Recktenwald and H. McConnell, *Biochem.*, 1981, 4505–4510.

[61] A. Andersson, H. Biverståhl, J. Nordin, J. Danielsson, E. Lindahl and L. Mäler, *Biochim. Biophys. Acta*, 2007, **1768**, 115–121.

[62] I. Constantinescu and M. Lafleur, *Biochim. Biophys. Acta*, 2004, **1667**, 26–37.

[63] L. R. McLean and M. C. Phillips, *Biochim. Biophys. Acta*, 1984, **776**, 21–26.

[64] O. A. Bizzozero, *Methods Enzymol.*, 1995, **250**, 361–379.

[65] G. Blaser, J. M. Sanderson and M. R. Wilson, *Org. Biomol. Chem.*, 2009, **7**, 5119–5128.

[66] E. H. Clark, J. M. East and A. G. Lee, *Biochem.*, 2003, **42**, 11065–11073.

[67] J. M. Sanderson and E. J. Whelan, *Phys. Chem.*, 2004, **6**, 1012–1017.

[68] H. A. Scheidt and D. Huster, *Acta Pharmacol. Sin.*, 2008, **29**, 35–49.

[69] J. Hoque, P. Akkapeddi, V. Yarlagadda, D. S. Uppu, P. Kumar and J. Haldar, *Langmuir*, 2012, **28**, 12225–12234.

[70] C. Ghosh, G. B. Manjunath, M. M. Konai, D. S. Uppu, K. Paramanandham, B. R. Shome, R. Ravikumar and J. Haldar, *ACS Infect. Dis.*, 2016, **2**, 111–122.

[71] M. Avadisian and P. T. Gunning, *Mol. Biosys.*, 2013, **9**, 2179–88.

[72] L. Zhang and G. Bulaj, *Curr. Med. Chem.*, 2012, **19**, 1602–1618.

[73] W. H. Halliwell, *Toxicol. Pathol.*, 1997, **25**, 53–60.

[74] N. Anderson and J. Borlak, *FEBS Letters*, 2006, **580**, 5533–5540.

[75] L. A. Chatman, D. Morton, T. O. Johnson and S. D. Anway, *Toxicol. Pathol.*, 2009, **37**, 997–1005.

[76] S. Appleby, *Small Molecule Lipidation in Membranes*, Durham University MChem Thesis, 2015.

[77] A. S. Prakash, J. A. Mosely and J. M. Sanderson, *Membrane-Reactive Small Molecules*, DSTL Report, 2014.

[78] J. M. Andrews, *J. Antimicrob. Chemother.*, 2001, **48**, 5–16.

[79] J. J. Thomson, *Proc. R. Soc. Lond. A*, 1913, **89**, 1–20.

[80] F. W. McLafferty, *Annu. Rev. Anal. Chem.*, 2011, **4**, 1–22.

[81] E. de Hoffmann and V. Stroobant, *Mass Spectrometry: Principles and Applications*, John Wiley & Sons Ltd., 2007.

[82] J. B. Fenn, *J. Am. Soc. Mass Spectrom.*, 1993, **4**, 524–535.

[83] J. B. Fenn, M. Mann, C. K. A. I. Meng, S. F. Wong and C. M. Whitehouse, *Science*, 1989, **246**, 64–71.

[84] C. M. Whitehouse, R. N. Dreyer, M. Yamashita and J. B. Fenn, *Anal. Chem.*, 1985, **57**, 675–679.

[85] M. Yamashita and J. B. Fenn, *J. Phys. Chem.*, 1984, **88**, 4451–4459.

[86] K. Tanaka, H. Waki, Y. Ido, S. Akita, Y. Yoshida, T. Yoshida and T. Matsuo, *Rapid Comm. Mass Spectrom.*, 1988, **2**, 151–153.

[87] R. Abate, A. Ballistreri, G. Montaudo, D. Garozzo, G. Impallomeni, G. Critchley and K. Tanaka, *Rapid Comm. Mass Spectrom.*, 1993, **7**, 1033–1036.

[88] W. Paul, *Angew. Chem. Int. Ed.*, 1990, **29**, 739–748.

[89] H. Dehmelt, *Physica Scripta*, 1988, **T22**, 102–110.

[90] A. G. Marshall, *Int. J. Mass Spectrom.*, 2000, **200**, 331–356.

[91] Q. Hu, R. J. Noll, H. Li, A. Makarov, M. Hardman and R. G. Cooks, *J. Mass Spectrom.*, 2005, **40**, 430–443.

[92] F. W. McLafferty, *Science*, 1981, **214**, 280–287.

[93] A. B. Kanu, P. Dwivedi, M. Tam, L. Matz and H. H. Hill, *J. Mass Spectrom.*, 2008, **43**, 1–22.

[94] F. Lanucara, S. W. Holman, C. J. Gray and C. E. Eyers, *Nature Chem.*, 2014, **6**, 281–294.

[95] S. J. Lehotay, *J. Chromatogr. A*, 2003, **1000**, 153–180.

[96] R. E. Ardrey, *Liquid Chromatography - Mass Spectrometry: An Introduction*, Wiley, New York, 2003.

[97] K. Shimbo, *Agric. Biol. Chem.*, 1986, **50**, 2643–2645.

[98] A. Espada and A. Rivera-Sagredo, *J. Chromatogr. A*, 2003, **987**, 211–220.

[99] Waters Corporation, *Waters Columns and Analytical Standards and Reagents Selection Guide*, `http://www.waters.com/webassets/cms/library/docs/720002241en.pdf`.

[100] C. S. Ho, C. W. K. Lam, M. H. M. Chan, R. C. K. Cheung, L. K. Law, L. C. W. Lit, K. F. Ng, M. W. M. Suen and H. L. Tai, *Clin. Biochem.*, 2003, **24**, 3–12.

[101] S. J. Gaskell, *J. Mass Spectrom.*, 1997, **32**, 677 – 688.

[102] M. Holcapek, R. Jirasko and M. Lisa, *J. Chromatogr. A*, 2010, **1217**, 3908–3921.

[103] M. Yamashita and B. J. Fenn, *J. Phys.Chem.*, 1984, **88**, 4671–4675.

[104] P. Kebarle and L. Tang, *Anal. Chem.*, 1993, **65**, 972A–986A.

[105] P. Kebarle and U. H. Verkerk, *Mass Spectrom. Rev.*, 2009, **28**, 898– 917.

[106] L. Konermann, E. Ahadi, A. D. Rodriguez and S. Vahidi, *Anal. Chem.*, 2013, **85**, 2–9.

[107] M. J. P. Smith, *Applications of New Mass Spectrometric Technologies for the Structural Characterisation of Synthetic Polymers*, Durham University Ph.D. Thesis, 2013.

[108] M. Karas and F. Hillenkamp, *Anal. Chem.*, 1988, **60**, 2299–2301.

[109] F. Hillenkamp and J. Peter-Katalinic, *MALDI MS: A Practical Guide to Instrumentation, Methods and Applications*, Wiley-Blackwell, 2nd edn., 2013.

[110] T. E. Itina, L. V. Zhigilei and B. J. Garrison, *Nucl. Instr. Meth. Phys. Res. B*, 2001, **180**, 238–244.

[111] T. E. Itina, L. V. Zhigilei, B. J. Garrison, T. Hall, V. Uni and V. Charlottes, *J. Phys. Chem. B*, 2002, **106**, 303–310.

[112] A. W. Bristow, *Mass Spectrom. Rev.*, 2006, **25**, 99–111.

[113] E. Mathieson and T. J. Harris, *Am. J. Phys.*, 1969, **37**, 1054–1059.

[114] F. W. McLafferty, *Int. J. Mass Spectrom.*, 2001, **212**, 81–87.

[115] W. C. Wiley and I. H. McLaren, *Rev. Sci. Instrum.*, 1955, **26**, 1150–1157.

[116] B. A. Mamyrin, *Int. J. Mass Spectrom.*, 2001, **206**, 251–266.

[117] R. J. Cotter, *Anal. Chem.*, 1992, **64**, 1027–1039.

[118] M. Guilhaus, *J. Mass Spectrom.*, 1995, **30**, 1519–1532.

[119] H. R. Morris, T. Paxton, A. Dell, J. Langhorne, M. Berg, R. S. Bordoli, J. Hoyes and R. H. Bateman, *Rapid Comm. Mass Spectrom.*, 1996, **10**, 889–896.

[120] M. Guilhaus, D. Selby and V. Mlynski, *Mass Spectrom. Rev.*, 2000, **19**, 65–107.

[121] L. Sleno and D. A. Volmer, *J. Mass Spectrom.*, 2004, **39**, 1091–1112.

[122] K. Giles, S. D. Pringle, K. R. Worthington, D. Little, J. L. Wildgoose and R. H. Bateman, *Rapid Comm. Mass Spectrom.*, 2004, **18**, 2401–2414.

[123] A. K. Shukla and J. H. Futrell, *J. Mass Spectrom.*, 2000, **35**, 1069–1090.

[124] K. Biemann, *Biomed. Environ. Mass Spectrom.*, 1988, **16**, 99–111.

[125] J. A. Loo, C. G. Edmonds and R. D. Smith, *Anal. Chem.*, 1991, **63**, 2488–2499.

[126] R. D. Smith, J. A. Loo, C. J. Barinaga, C. G. Edmonds and H. R. Udseth, *J. Am. Soc. Mass Spectrom.*, 1990, **1**, 53–65.

[127] K. M. Downard and K. Biemann, *J. Am. Soc. Mass Spectrom.*, 1994, **5**, 966–975.

[128] W. M. A. Niessen, *Mass Spectrom. Rev.*, 2011, **30**, 626–663.

[129] B. A. Wolucka and E. de Hoffmann, *J. Biol. Chem*, 1995, **270**, 20151–20155.

[130] F. W. McLafferty, *Org. Mass Spectrom.*, 1980, **15**, 114–121.

[131] K. Levsen, H.-M. Schiebel, J. K. Terlouw, K. J. Jobst, M. Elend, A. Preib, H. Thiele and A. Ingendoh, *J. Mass Spectrom.*, 2007, **42**, 1024–1044.

[132] M. Karni and A. Mandelbaum, *Org. Mass Spectrom.*, 1980, **15**, 53–64.

[133] R. Cumeras, E. Figueras, C. E. Davis, J. I. Baumbach and I. Gràcia, *Analyst*, 2015, **140**, 1376–1390.

[134] C. Lapthorn, F. Pullen and B. Z. Chowdhry, *Mass Spectrom. Rev.*, 2013, **32**, 43–71.

[135] J. Hofmann, H. S. Hahm, P. H. Seeberger and K. Pagel, *Nature*, 2015, **526**, 241–244.

[136] L. Ahonen, M. Fasciotti, G. B. af Gennäs, T. Kotiaho, R. J. Daroda, M. Eberlin and R. Kostiainen, *J. Chromatogr. A*, 2013, **1310**, 133–137.

[137] G. Paglia and G. Astarita, *Nat. Protoc.*, 2017, **12**, 797–813.

[138] K. M. Hines, J. C. May, J. A. McLean and L. Xu, *Anal. Chem.*, 2016, **88**, 7329–7336.

[139] J. Ujma, K. Giles, M. Morris and P. E. Barran, *Anal. Chem.*, 2016, **88**, 9469–9478.

[140] A. Shvartsburg and R. Smith, *Anal. Chem.*, 2008, **80**, 9689–9699.

[141] G. Paglia, P. Angel, J. P. Williams, K. Richardson, H. J. Olivos, J. W. Thompson, L. Menikarachchi, S. Lai, C. Walsh, A. Moseley, R. S. Plumb, D. F. Grant, B. O. Palsson, J. Langridge, S. Geromanos and G. Astarita, *Anal. Chem.*, 2015, **87**, 1137–1144.

[142] G. Paglia, M. Kliman, E. Claude, S. Geromanos and G. Astarita, *Anal. Bioanal. Chem.*, 2015, **407**, 4995–5007.

[143] J. E. Kyle, X. Zhang, K. K. Weitz, M. E. Monroe, Y. M. Ibrahim, R. J. Moore, J. Cha, X. Sun, E. S. Lovelace, J. Wagoner, S. J. Polyak, T. O. Metz, S. K. Dey, R. D. Smith, K. E. Burnum-Johnson and E. S. Baker, *Analyst*, 2016, **141**, 1649–1659.

[144] M. Groessl, S. Graf and R. Knochenmuss, *Analyst*, 2015, **140**, 6904–6911.

[145] Y. Sun, S. Vahidi, M. A. Sowole and L. Konermann, *J. Am. Soc. Mass Spectrom.*, 2016, **27**, 31–40.

[146] A. Laganowsky, E. Reading, T. M. Allison, M. B. Ulmschneider, M. T. Degiacomi, A. J. Baldwin and C. V. Robinson, *Nature*, 2014, **510**, 172–175.

[147] K. M. Hines, D. H. Ross, K. L. Davidson, M. F. Bush and L. Xu, *Anal. Chem.*, 2017, **89**, 9023–9030.

[148] M. A. Bernstein, *Magn. Reson. Chem.*, 2016, **54**, 422.

[149] B. Meyer, T. Weimar and T. Peters, *Eur. J. Biochem.*, 1997, **246**, 705–709.

[150] D. Marion, *Mol. Cell. Proteomics*, 2013, **12**, 3006–3025.

[151] M. Billeter, G. Wagner and Kurt Wüthrich, *J. Biomol. NMR*, 2008, **42**, 155–158.

[152] P. R. L. Markwick, T. Malliavin and M. Nilges, *PLOS Comput. Biol.*, 2008, **4**, 1–7.

[153] V. Lyne, *Partition Coefficients of Membrane Active Compounds*, Durham University MChem Thesis, 2017, pp. 1–61.

[154] A. Cruz, L. Vázquez, M. Vélez and J. Pérez-Gil, *Langmuir*, 2005, **21**, 5349–5355.

[155] H. Bouvrais, T. Pott, L. A. Bagatolli, J. H. Ipsen and P. Méléard, *Biochim. Biophys. Acta Biomembr.*, 2010, **1798**, 1333–1337.

[156] E. K. Esbjörner, C. E. B. Caesar, B. Albinsson, P. Lincoln and B. Nordén, *Biochem. Biophys. Res. Commun.*, 2007, **361**, 645–650.

[157] J. Dachary-Prigent, J. Dufourcq, C. Lussan and M. Boisseau, *Thromb. Res.*, 1979, **14**, 15–22.

[158] C. Pereira-Leite, C. Carneiro, J. X. Soares, C. Afonso, C. Nunes, M. Lúcio and S. Reis, *Eur. J. Pharm. Biopharm.*, 2013, **84**, 183–191.

[159] C. D. Tran and G. S. Beddard, *Eur. Biophys. J.*, 1985, **13**, 59–64.

[160] M. van Veen, G. N. Georgiou, A. F. Drake and R. J. Cherry, *Biochem. J.*, 1995, **305**, 785–90.

[161] E. Lederer and M. Lederer, *Chromatography: A Review of Principles and Applications*, Elsevier Publishing Company, 1955.

[162] E. Stahl, *Thin-Layer Chromatography*, Springer-Verlag, New York, 2nd edn., 1960.

[163] J. Sherman and B. Fried, *Handbook of Thin-Layer Chromatography*, Marcel Dekker, Ney York, 1st edn., 1991.

[164] A. Fagerström, M. Nilsson, U. Berg and R. Isaksson, *Organic & biomolecular chemistry*, 2006, **4**, 3067–3076.

[165] H. Foster, *TLC and ASAP: A Combined Approach for the Qualitative Analysis of Lipidomic Changes During Viral Infection*, Durham University MChem. Thesis, 2011.

[166] M. Attimarad, K. Mueen Ahmed, B. E. Aldhubaib and S. Harsha, *Pharm. Methods*, 2011, **2**, 71–75.

[167] P. Zarzycki, M. Bartoszuk and A. Radziwon, *J. Planar. Chromatogr. - Mod. TLC*, 2006, **19**, 52–57.

[168] P. Henne, R. Thiericke, S. Grabley, K. Hütter, J. Wink, E. Jurkiewicz and A. Zeeck, *Liebigs Ann. Chem.*, 1993, **1993**, 565–571.

[169] B. Fuchs, R. Süß, K. Teuber, M. Eibisch and J. Schiller, *J. Chromatogr. A*, 2011, **1218**, 2754–2774.

[170] D. Apperley, R. Harris and P. Hodgkinson, *Solid State NMR: Basic Principles and Practice*, Momentum Press, New York, 1st edn., 2012.

[171] D. D. Laws, H.-M. L. Bitter and A. Jerschow, *Angew. Chem. Int. Ed.*, 2002, **41**, 3096–3129.

[172] A. Watts, *Nat. Rev. Drug Discov.*, 2005, **4**, 555–568.

[173] S. P. Bhamidipati and J. a. Hamilton, *Biochem.*, 1995, **34**, 5666–5677.

[174] H. S. Bevinakatti and A. A. Banerji, *J. Org. Chem.*, 1991, **56**, 5372–5375.

[175] Y. C. Yuan, R. Kamaraj, C. Bruneau, T. Labasque, T. Roisnel and R. Gramage-Doria, *Org. Lett.*, 2017, **19**, 6404–6407.

[176] K. Sun, C. Fang, W. Yang, Z. Xu, H. Wang, W. Sun, Y. Luo and Y. Xu, *J. Labelled Comp. Radiopharm.*, 2016, **59**, 552–556.

[177] C. Chen, H. Liu, B. Zhang, Y. Wang, K. Cai, Y. Tan, C. Gao, H. Liu, C. Tan and Y. Jiang, *Tetrahedron*, 2016, **72**, 3980–3985.

[178] F. Alasmary, A. Snelling, M. Zain, A. Alafeefy, A. Awaad and N. Karodia, *Molecules*, 2015, **20**, 15206–15223.

[179] M. Pal and S. L. Bearne, *Org. Biomol. Chem.*, 2014, **12**, 9760–9763.

[180] D. Plusquellec, F. Roulleau and M. Lefeuvre, *Tetrahedron*, 1988, **44**, 0–5.

[181] Y. Kita, S. Akai, N. Ajimura, M. Yoshigi, T. Tsugoshi, H. Yasuda and Y. Tamura, *J. Org. Chem.*, 1986, **51**, 4150.

[182] C. M. Gupta, R. Radhakrishnan and H. G. Khorana, *Proc. Natl. Acad. Sci. USA*, 1977, **74**, 4315–4319.

[183] N. Niezgoda, P. Mitula, K. Kempinska, J. Wietrzyk and C. Wawrzenczyk, *Aust. J. Chem.*, 2013, **66**, 354–361.

[184] D. a. Smuga, M. Smuga, A. Świzdor, A. Panek and C. Wawrzeńczyk, *Steroids*, 2010, **75**, 1146–1152.

[185] P. D'Arrigo, E. Fasoli, G. Pedrocchi-Fantoni, C. Rossi, C. Saraceno, D. Tessaro and S. Servi, *Chem. Phys. Lipids*, 2007, **147**, 113–118.

[186] E. Fasoli, A. Arnone, A. Caligiuri, P. D'Arrigo, L. de Ferra and S. Servi, *Org. Biomol. Chem.*, 2006, **4**, 2974–2978.

[187] C. Matheis, T. Krause, V. Bragoni and L. J. Goossen, *Chem. Eur. J.*, 2016, **22**, 12270–12273.

[188] A. Suárez and G. C. Fu, *Angew. Chem. Int. Ed.*, 2004, **43**, 3580–3582.

[189] A. F. Creemers and J. Lugtenburg, *J. Am. Chem. Soc.*, 2002, **124**, 6324–6334.

[190] T. Torna, J. Shimokawa and T. Fukuyama, *Org. Lett.*, 2007, **9**, 3195–3197.

[191] R. Ocampo and W. R. Dolbier, *Tetrahedron*, 2004, **60**, 9325–9374.

[192] S. Bunnai and G. C. Fu, *J. Am. Chem. Soc.*, 2007, **129**, 9602–9603.

[193] J. H. Delcamp, *Tetrahedron*, 2005, **3**, 1–5.

[194] K. C. Nicolaou, P. G. Bulger and D. Sarlah, *Angew. Chem. Int. Ed.*, 2005, **44**, 4442–4489.

[195] D. E. Ames and R. E. Bowman, *J. Chem. Soc*, 1952, **0**, 677–680.

[196] E. J. Whittle, A. E. Tremblay, P. H. Buist and J. Shanklin, *Proc. Natl. Acad. Sci. USA*, 2008, **105**, 14738–14743.

[197] H. C. Hang and M. E. Linder, *Chem. Rev.*, 2011, **111**, 6341–58.

[198] H. Raghuraman and A. Chattopadhyay, *Biosci. Rep.*, 2007, **27**, 189–223.

[199] W. Zhang, J. Song, R. Liang, X. Zheng, J. Chen, G. Li, B. Zhang, X. Yan and R. Wang, *Bioconjugate Chem.*, 2013, **24**, 1805–1812.

[200] T. C. Terwilliger, L. Weissman and D. Eisenberg, *Biophys. J.*, 1982, **37**, 353–359.

[201] D. Eisenberg, T. C. Terwilliger, F. Tsui and M. Biology, *Biophys. J.*, 1980, **32**, 252–254.

[202] D. Anderson, T. C. Terwilliger, W. Wickner, D. Eisenberg, D. Anderson, T. C. Terwilliger, W. Wickner and D. Eisenberg, *J. Biol. Chem.*, 1980, **255**, 2578–2582.

[203] J. T. Pelton, *Science*, 2001, **291**, 2175–2176.

[204] S. M. Kelly, T. J. Jess and N. C. Price, *Biochim. Biophys. Acta*, 2005, **1751**, 119–139.

[205] H. Vogel and F. Jaehnig, *Biophys. J.*, 1986, **50**, 573–582.

[206] Y. Lam, S. R. Wassall, C. J. Morton, R. Smith and F. Separovic, *Biophys. J.*, 2001, **81**, 2752–2761.

[207] D. T. Hickman, M. P. Lopez-Deber, D. M. Ndao, A. B. Silva, D. Nand, M. Pihlgren, V. Giriens, R. Madani, A. St-Pierre, H. Karastaneva, L. Nagel-Steger, D. Willbold, D. Riesner, C. Nicolau, M. Baldus, A. Pfeifer and A. Muhs, *J. Biol. Chem.*, 2011, **286**, 13966–13976.

[208] C. Tanfordl and C. Tanford, *J. Phys. Chem.*, 1972, **76**, 3020–3024.

[209] T. Janek, A. Krasowska, A. Radwańska and M. Łukaszewicz, *PLoS ONE*, 2013, **8**, 1–9.

[210] M. Morikawa, H. Daido, T. Takao, S. Murata, Y. Shimonishi and T. Imanaka, *J. Bacteriol.*, 1993, **175**, 6459–6466.

[211] E. D. Vendittis, G. Palumbo, G. Parlato and V. Bocchini, *Anal. Biochem.*, 1981, **115**, 278–286.

[212] F. M. Zehentbauer, C. Moretto, R. Stephen, T. Thevara, J. R. Gilchrist, D. Pokrajac, K. L. Richard and J. Kiefer, *Spectrochim. Acta A*, 2014, **121**, 147–151.

[213] R. E. Stafford, T. Fanni and E. a. Dennis, *Biochem.*, 1989, **28**, 5113–5120.

[214] L. J. Chen, S. Y. Lin and C. C. Huang, *J. Phys. Chem. B*, 1998, **102**, 4350–4356.

[215] R. Saravanan, A. Bhunia and S. Bhattacharjya, *Biochim. Biophys. Acta*, 2010, **1798**, 128–139.

[216] J. M. Andrews, *J. Antimicrob. Chemother.*, 2001, **48**, 5–16.

[217] M. Stefani and S. Rigacci, *Int. J. Mol. Sci.*, 2013, **14**, 12411–57.

[218] J. V. Rushworth and N. M. Hooper, *Int. J. Alzheimers Dis.*, 2010, **2011**, 603052.

[219] S. Mankar, A. Anoop, S. Sen and S. K. Maji, *Nano Rev.*, 2011, **2**, 1–12.

[220] A. Nagarathinam, P. Höflinger, A. Bühler, C. Schäfer, G. McGovern, M. Jeffrey, M. Staufenbiel, M. Jucker and F. Baumann, *J. Neurosci.*, 2013, **33**, 19284–91924.

[221] M. P. L. Deber, D. T. Hickman, D. Nand, M. Baldus, A. Pfeifer and A. Muhs, *PLoS ONE*, 2014, **9**, 1–10.

[222] W. Qiang, W. M. Yau and J. Schulte, *Biochim. Biophys. Acta*, 2015, **1848**, 266–276.

[223] C. L. Masters and D. J. Selkoe, *Cold Spring Harb. Perspect. Med.*, 2012, **2**, 1–24.

[224] C. L. Masters, G. Simms, N. A. Weinman, G. Multhaup, B. L. McDonald and K. Beyreuther, *Proc. Natl. Acad. Sci. USA*, 1985, **82**, 4245–9.

[225] O. Schmitz, B. Brock and J. Rungby, *Diabetes*, 2004, **53**, 233–238.

[226] T. Miyata, S. Taneda, R. Kawai, Y. Ueda, S. Horiuchi, M. Hara, K. Maeda and V. M. Monnier, *Proc. Natl. Acad. Sci. USA*, 1996, **93**, 2353–2358.

[227] V. Castillo and S. Ventura, *PLOS Comput. Biol.*, 2009, **5**, 1–16.

[228] T. M. Ryan, J. Caine, H. D. Mertens, N. Kirby, J. Nigro, K. Breheney, L. J. Waddington, V. A. Streltsov, C. Curtain, C. L. Masters and B. R. Roberts, *PeerJ*, 2013, **1**, e73.

[229] M. Winter, A. Tholey, A. Kristen and C. Röcken, *Proteomics*, 2017, **17**, 1–35.

[230] M. Stoeckli, R. Knochenmuss, G. McCombie, D. Mueller, T. Rohner, D. Staab and K. H. Wiederhold, *Methods Enzymol.*, 2006, **412**, 94–106.

[231] M. R. Nilsson, *Methods*, 2004, **34**, 151–160.

[232] S. A. Hudson, H. Ecroyd, T. W. Kee and J. A. Carver, *FEBS J.*, 2009, **276**, 5960–5972.

[233] R. Khurana, C. Coleman, C. Ionescu-Zanetti, S. A. Carter, V. Krishna, R. K. Grover, R. Roy and S. Singh, *J. Struct. Biol.*, 2005, **151**, 229–238.

[234] H. LeVine, *Methods in Enzymol.*, 1999, **309**, 274–284.

[235] S. Inoue, M. Kuroiwa, M. J. Saraiva, A. Guimaraes and R. Kisilevsky, *J. Struct. Biol.*, 1998, **124**, 1–12.

[236] C. Goldsbury, K. Goldie, J. Pellaud, J. Seelig, P. Frey, S. A. Müller, J. Kistler, G. J. Cooper and U. Aebi, *J. Struct. Biol.*, 2000, **130**, 352–362.

[237] H. A. Lashuel, D. M. Hartley, B. M. Petre, J. S. Wall, M. N. Simon, T. Walz and P. T. Lansbury, *J. Mol. Biol.*, 2003, **332**, 795–808.

[238] M. R. R. de Planque, V. Raussens, S. A. Contera, D. T. S. Rijkers, R. M. J. Liskamp, J. M. Ruysschaert, J. F. Ryan, F. Separovic and A. Watts, *J. Mol. Biol.*, 2007, **368**, 982–997.

[239] K. Numata and D. L. Kaplan, *Biochem.*, 2010, **49**, 3254–3260.

[240] A. E. Ashcroft, *J. Am. Soc. Mass Spectrom.*, 2010, **21**, 1087–1096.

[241] G. Sessa and G. Weissmann, *J. Lipid Res.*, 1968, **9**, 310–318.

[242] C. S. Chen, D. M. Gou, W. R. Shieh and Y. C. Liu, *Tetrahedron*, 1993, **49**, 3281–3290.

[243] A. M. Escorcia, D. Molina, M. C. Daza and M. Doerr, *J. Mol. Catal. B Enzym.*, 2013, **98**, 21–29.

[244] S. Laurichesse, C. Huillet and L. Avérous, *Green Chem.*, 2014, **16**, 3958–3970.

[245] F. Mainini, A. Contini, D. Nava, P. A. Corsetto, A. M. Rizzo, E. Agradi and E. Pini, *J. Am. Oil Chem. Soc*, 2013, **90**, 1751–1759.

[246] W. L. Nelson and R. B. Walker, *Res. Commun. Chem. Pathol. Pharmacol.*, 1978, **22**, 435–445.

[247] K. Uwai, M. Tani, Y. Ohtake, S. Abe, A. Maruko, T. Chiba, Y. Hamaya, Y. Ohkubo and M. Takeshita, *Life Sciences*, 2005, **78**, 357–365.

[248] L. Liu, *J. Am. Oil Chem. Soc*, 2004, **81**, 331–337.

[249] J. A. Aguilar, A. T. Ball, C. R. Coxon, A. M. Kenwright, R. W. Lancaster, J. A. Mosely and M. A. Mutton, *J. Pharm. Sci.*, 2016, **105**, 3073–3078.

[250] R. B. Cole, *Electrospray and MALDI Mass Spectrometry*, Wiley, New York, 2nd edn., 2010.

[251] A. Furey, M. Moriarty, V. Bane, B. Kinsella and M. Lehane, *Talanta*, 2012, **115**, 104–122.

[252] R. S. Plumb and P. D. Rainville, *Simplifying Qual/Quan Analysis in Discovery DMPK Using UPLC and Xevo TQ MS*, Waters Corporation Technical Report, 2009.

[253] A. L. Upthagrove, M. Hackett and W. L. Nelson, *Rapid Comm. Mass Spectrom.*, 1999, **13**, 1671–1679.

[254] K. Murzyn, T. Róg and M. Pasenkiewicz-Gierula, *Biophys. J.*, 2005, **88**, 1091–1103.

[255] A. Avdeef, K. J. Box, J. E. Comer, C. Hibbert and K. Y. Tam, *Pharm. Res.*, 1998, **15**, 209–215.

[256] P. A. Zapata-Morin, F. J. Sierra-Valdez and J. C. Ruiz-Suárez, *J. Mol. Graph. Model.*, 2014, **53**, 200–205.

[257] *DrugBank Database*, `https://www.drugbank.ca/`.

[258] Y. Boulanger, S. Schreier, L. C. Leitch and I. C. P. Smith, *Can. J. Biochem.*, 1980, **58**, 986–995.

[259] E. C. Kelusky and I. C. Smith, *Biochem.*, 1983, **22**, 6011–6017.

[260] L. B. Johansson and G. Lindblom, *Biophys. J.*, 1981, **36**, 735–741.

[261] S. S. Efimova, R. Y. Medvedev, L. V. Schagina and O. S. Ostroumova, *Cell Tissue Biol.*, 2016, **10**, 324–331.

[262] *ChemAxon*, `https://chemaxon.com/`.

[263] V. Gerskowitch, R. A. Hull and N. P. Shankley, *Trends Pharmacol. Sci.*, 1988, **91**, 435–437.

[264] M. P. Stapleton, *Tex. Heart Inst. J.*, 1997, **24**, 336–42.

[265] World Health Organisation, *WHO Model List of Essential Medicines*, `http://www.who.int/medicines/publications/essentialmedicines/en/`.

[266] G. Först, L. Cwiklik, P. Jurkiewicz, R. Schubert and H. Martin, *Eur. J. Pharm. Biopharm.*, 2014, **87**, 559–569.

[267] L. Herbette, A. M. Katz and J. M. Sturtevant, *Mol. Pharmacol.*, 1983, **24**, 259–269.

[268] G. Mangiapia, M. Gvaramia, L. Kuhrts, J. Teixeira, A. Koutsioubas, O. Soltwedel and H. Frielinghaus, *Phys. Chem. Chem. Phys.*,, 2017, **19**, 32057–32071.

[269] C. A. Lipinski, F. Lombardo, B. W. Dominy and P. J. Feeney, *Adv. Drug Deliv. Rev.*, 2001, **46**, 3–26.

[270] W. K. Surewicz and W. Leyko, *Biochim. Biophys. Acta*, 1981, **643**, 387–397.

[271] T. Nonoyama and R. Fukuda, *J. Toxicol. Pathol.*, 2008, **21**, 9–24.

[272] A. M. Kawamoto and M. Wills, *J. Chem. Soc. Perkin Trans. 1*, 2001, 1916–1928.

[273] R. A. Klein, *J. Lipid Res.*, 1971, **12**, 123–131.

[274] W. J. Irwin and K. A. Belaid, *Int. J. Pharm.*, 1988, **46**, 57–67.

[275] D. A. Dougherty, *Science*, 1996, **271**, 163–168.

[276] R. K. Chitta and M. L. Gross, *Biophys. J.*, 2004, **86**, 473–479.

[277] R. D. Smith and K. J. Lightwahl, *Biol. Mass Spectrom.*, 1993, **22**, 493–501.

[278] J. M. Quigley, C. G. M. Jordan and R. F. Timoney, *Int. J. Pharm.*, 1994, **101**, 145–163.

[279] M. Baidya and A. K. Das, *Orient. J. Chem*, 2011, **27**, 173–178.

[280] A. Buur, H. Bundgaard and V. H. Lee, *Int. J. Pharm.*, 1988, **42**, 51–60.

[281] W. J. Irwin and K. A. Belaid, *Drug Dev. Ind. Pharm.*, 1987, **13**, 2033–2045.

[282] W. Rawicz, K. C. Olbrich, T. McIntosh, D. Needham and E. Evans, *Biophys. J.*, 2000, **79**, 328–39.

[283] B. Fadeel and D. Xue, *Crit. Rev. Biochem. Mol. Biol.*, 2009, **44**, 264–277.

[284] M. Ikeda, A. Kihara and Y. Igarashi, *Biol. Pharm. Bull.*, 2006, **29**, 1542–1546.

[285] V. T. Pham, T. Q. Nguyen, U. P. Dao and T. T. Nguyen, *Spectrochim. Acta A*, 2018, **191**, 50–61.

[286] Waters Corporation, *Waters Mobile Phase Preparation Guidelines*, `http://www.waters.com/webassets/cms/library/docs/xterra132-133.pdf`.

[287] D. Y. Leung, X. Wu and M. K. Leung, *Appl. Energy*, 2010, **87**, 1083–1095.

[288] A. G. De Oliveira and H. Chaimovich, *J. Pharm. Pharmacol.*, 1993, **45**, 850–861.

[289] R. H. Bisby, S. W. Botchway, A. G. Crisostomo, J. Karolin, A. W. Parker and L. Schröder, *Spectroscopy*, 2010, **24**, 137–142.

[290] D. Needham and D. V. Zhelev, *Ann. Biomed. Eng.*, 1995, **23**, 287–298.

[291] H. Y. Y. Kim, T. C. L. C. Wang and Y. C. C. Ma, *Anal. Chem.*, 1994, **66**, 3977–3982.

[292] M. Pulfer and R. C. Murphy, *Mass Spectrom. Rev.*, 2003, **22**, 332–364.

[293] Waters Corporation, *Background Ion List for ESI*, `https://www.waters.com/webassets/cms/support/docs/bkgrnd{_}ion{_}mstr{_}list.pdf`.

[294] Waters Corporation, *Lipid Separtion using UPLC with Charged Surface Hybrid Technology*, http://www.waters.com/webassets/cms/library/docs/720004107en.pdf.

[295] Avanti Polar Lipids Inc., *E. coli Extract Polar*, https://avantilipids.com/product/100600/.

[296] *Lipid MAPS Lipidomics Gateway*, http://www.lipidmaps.org/.

[297] T. K. Lind, H. Wacklin, J. Schiller, M. Moulin, M. Haertlein, T. G. Pomorski and M. Cárdenas, *PLoS ONE*, 2015, **10**, 1–16.

[298] B. Fuchs, A. Bischoff, R. Sü, K. Teuber, M. Schürenberg, D. Suckau and J. Schiller, *Anal. Bioanal. Chem.*, 2009, **395**, 2479–2487.

[299] L. J. Stuart, J. P. Buck, A. E. Tremblay and P. H. Buist, *Org. Lett.*, 2006, **8**, 79–81.

[300] N. Rozes, S. Garbay, M. Denayrolles and A. Lonvaud-Funel, *Lett. Appl. Microbiol*, 1993, **17**, 126–131.

[301] N. E. Braverman and A. B. Moser, *Biochim. Biophys. Acta*, 2012, **1822**, 1442–1452.

[302] G. F. White, K. I. Racher, A. Lipski, F. R. Hallett and J. M. Wood, *Biochim. Biophys. Acta Biomembr.*, 2000, **1468**, 175–186.

[303] Avanti Polar Lipids Inc., *Liver Extract Polar*, https://avantilipids.com/product/181108/.

[304] J. Folch, M. Lees and G. H. Sloane Stanley, *J. Biol. Chem.*, 1957, **226**, 497–509.

[305] V. Matyash, G. Liebisch, T. V. Kurzchalia, A. Shevchenko and D. Schwudke, *J. Lipid Res.*, 2008, **49**, 1137–1146.

[306] S. R. Wang, M. Pessah, J. Infante, D. Catala, C. Salvat and R. Infante, *Biochim. Biophys. Acta*, 1988, **961**, 351–363.

[307] M. Skoog, M. Berggren-Soderlund, P. Nilsson-Ehle and N. Xu, *Lipids Health Dis.*, 2010, **9**, 1–6.

[308] C. Angeletti and M. J. de Alaniz, *Mol. Cell. Biochem.*, 1995, **143**, 99–105.

[309] O. O. Ajani, D. V. Aderohunmu, S. J. Olorunshola, C. O. Ikpo and I. O. Olanrewaju, *Orient. J. Chem.*, 2016, **32**, 109–120.

[310] H. Elshihawy, M. A. Helal, M. Said and M. A. Hammad, *Bioorg. Med. Chem.*, 2014, **22**, 550–558.

[311] J. B. Wright, *Chem. Rev.*, 1951, **48**, 397–541.

[312] R. Rastogi and S. Sharma, *Synthesis*, 1983, **11**, 861–882.

[313] Y. B. Bai, A. L. Zhang, J. J. Tang and J. M. Gao, *J. Agric. Food Chem.*, 2013, **61**, 2789–2795.

[314] M. Raban, H. Chang and L. Craine, *J. Org. Chem.*, 1985, **50**, 2205–2210.

[315] J. A. Butera, N. Marcopulos, J. F. Bagli, W. Spinelli, R. W. Parsons, I. F. Moubarak, C. Cullinan, V. Anantharaman and C. Cullinan, *J. Med. Chem.*, 1991, **34**, 3212–3228.

[316] K. F. Ansari, C. Lal and D. L. Parmar, *Synth. Commun.*, 2012, **42**, 3553–3568.

[317] S. A. Galal, A. S. Abdelsamie, H. Tokuda, N. Suzuki, A. Lida, M. M. Elhefnawi, R. A. Ramadan, M. H. Atta and H. I. El Diwani, *Eur. J. Med. Chem.*, 2011, **46**, 327–340.

[318] S. Naik, G. Bhattacharjya, B. Talukdar and B. K. Patel, *Eur. J. Org. Chem.*, 2004, 1254–1260.

[319] M. L. Brown, W. Aaron, R. J. Austin, A. Chong, T. Huang, B. Jiang, J. a. Kaizerman, G. Lee, B. S. Lucas, D. L. McMinn, J. Orf, M. Rong, M. M. Toteva, G. Xu, Q. Ye, W. Zhong, M. R. Degraffenreid, D. Wickramasinghe, J. P. Powers, R. Hungate and M. G. Johnson, *Bioorg. Med. Chem. Lett.*, 2011, **21**, 5206–5209.

[320] D. Best, S. Kujawa and H. W. Lam, *J. Am. Chem. Soc.*, 2012, **134**, 18193–18196.

[321] H. Kakuta, X. Zheng, H. Oda, S. Harada, Y. Sugimoto, K. Sasaki and A. Tai, *J. Med. Chem.*, 2008, **51**, 2400–2411.

[322] V. Naresh Chary, C. Dinesh Kumar, M. Vairamani and S. Prabhakar, *J. Mass Spectrom.*, 2012, **47**, 79–88.

[323] R. Braslau, J. R. Axon and B. Lee, *Org. Lett.*, 2000, **2**, 1399–1401.

[324] J. K. Morelli, M. Buehrle, F. Pognan, L. R. Barone, W. Fieles and P. J. Ciaccio, *Cell Biol. Toxicol.*, 2006, **22**, 15–27.

[325] A. S. Ladokhin, W. C. Wimley and S. H. White, *Biophys. J.*, 1995, **69**, 1964–1971.

[326] P. P. Bonsen, G. H. de Haas, W. A. Pieterson and L. L. Van Deenen, *Biochim. Biophys. Acta*, 1972, **270**, 364–382.

[327] P. Becher, *J. Phys. Chem.*, 1962, **66**, 374–375.

[328] M. J. Kates and J. H. Schauble, *J. Org. Chem.*, 1996, **61**, 4164–4167.

[329] M. Gaudemer, *Tetrahedron Lett.*, 1983, **24**, 2749–2752.

[330] M. Mineno, Y. Sawai, K. Kanno, N. Sawada and H. Mizufune, *Tetrahedron*, 2013, **69**, 10921–10926.

[331] H. Doucet, *Eur. J. Org. Chem.*, 2008, **12**, 2013–2030.

[332] J. R. Masters and G. N. Stacey, *Nat. Protoc.*, 2007, **2**, 2276–2284.

[333] R. Hamid, Y. Rotshteyn, L. Rabadi, R. Parikh and P. Bullock, *Toxicol. In Vitro*, 2004, **18**, 703–710.